Title

Development and Mechanistic Explorations of Novel Rhodium-Catalyzed Hydrothiolations and Hydroacylations

Author

Kuker, Erin Louise

Publication Date

2024

Peer reviewed|Thesis/dissertation

UNIVERSITY OF CALIFORNIA,
IRVINE

Development and Mechanistic Explorations of Novel Rhodium-Catalyzed Hydrothiolations and Hydroacylations

DISSERTATION

submitted in partial satisfaction of the requirements
for the degree of

DOCTOR OF PHILOSOPHY

in Chemistry

by

Erin Louise Kuker

Dissertation Committee:
Professor Vy M. Dong, Chair
Professor Suzanne A. Blum
Professor Elizabeth R. Jarvo

2024

TABLE OF CONTENTS

LIST OF FIGURES

LIST OF TABLES

ACKNOWLEDGEMENTS

I would like to thank my advisor, Professor Vy Dong, for giving me the opportunity to explore research in her lab. You encouraged me to have confidence in myself and trusted me throughout the process. I appreciate all the time and effort you dedicated to helping me prepare for a future in chemistry. I am beyond excited to take what I have learned and apply it to my future endeavors.

I would like to thank my committee members, Professor Suzanne Blum and Professor Elizabeth Jarvo, for their support throughout graduate school. I learned so many important fundamentals in the courses you both taught in my first year. Additionally, I am extremely grateful for the support and encouragement from both of you after my candidacy exam. I had so much doubt in myself at that point, and you both encouraged me that I was on the right track and in the right place. I will forever be grateful for the support.

I would like to thank all the past Dong lab members that I have had the chance to work with. Dr. Alex Lu, Dr. Ryan Davison, Dr. Alex Jiu, Dr. Shaozhen Nie, Dr. Xiaohui Yang, Dr. Jihye Park, and Dr. Patrick Parker were all my first mentors when arriving in Irvine. I was intimidated by this group of intelligent people, but they all showed me so much kindness. Lu, I deeply appreciate your friendship and time. I always felt comfortable coming to you with questions and trusting you would try your hardest to give me a thoughtful answer. You were a friend to me when I felt the most alone in graduate school. Ryan, you brought so much joy and laughter to the lab. I felt immediately welcomed into the group by you. Jiu, it was hard to be bored with you around. I appreciate all the crazy debates and conversations you were willing to have with me. Shaozhen, I am so grateful you invited me to join the cyclopropene project. It was extremely motivating working with someone as tenacious as you. Xiaohui and Jihye, you brought so much knowledge,

peace, and stability to the group. And finally, Patrick, I am so grateful for your friendship. You spent hours on the phone with me during the pandemic quarantine, let me stay in your apartment when mine was infested with fleas, and gave me a million reasons to laugh and feel joy when graduate school felt hard and lonely. I love you and am so excited to live close to you soon!

I would also like to thank all the present lab members. Dr. Hannah Slocumb and Dr. Xintong Hou were the best possible cohort. Hannah and Xintong, I love and appreciate you both so much. I truly don't know if I could have done it without you both by my side. I can't wait to see what all you accomplish! Kirsten Ruud, I always looked forward to being greeted by you in the morning and debriefing all that life threw at us over the past four years. Minghao Wang, your presence in the lab is so calm and encouraging, and you are secretly a comedic genius. I am looking forward to watching you both graduate over the next year! Antoinette Antonucci, I wish we could have been bay mates earlier. I am glad you are no longer scared of me, because you make me smile a lot throughout the day. Camryn Wallace, I am grateful for all the hard work you put into the azetine project. I know it must have been frustrating working with me at times. I hope in the end it was as rewarding for you as it was for me. I am also happy we have become friends. I hope the friendship continues! Dr. Lori Digal, it has been really nice to have a lab and gym buddy. You have been a great friend and listener. Alice de Vos, I am grateful for your friendship and hard work on the azetine project. You should have all the confidence that you will accomplish great things! To Brian Daniels, Sophia Xu, Bryan Blackburn, Kara Greene, and Silas Scibner, I appreciate the kindness you have all shown me and look forward to seeing all that you accomplish in the future.

I would also like to thank the undergraduate students that I had the opportunity to mentor, Kevin Pham and Jonathan Vu. Kevin, you had the unfortunate pleasure of being the first undergraduate I mentored. I am sure it was not the most smooth and enjoyable experience, but you

always showed up ready to work and listen. You are intelligent, kind, and hardworking. It was a pleasure to work with you. I hope you keep growing in confidence! Jonathan, you have impressed me so much! You came into the lab with very little experience and knowledge, but you didn't let that stop you from getting things done and getting to where you wanted to go. I know I was a very grumpy person at the time you joined, but you managed to make me laugh and enjoy my time in lab again. Keep working hard and making people laugh!

I would especially like to thank the people who encouraged me to apply and attend graduate school. Professor Kevin Brown was my undergraduate research advisor at Indiana University. I would have never thought to pursue a career in chemistry if it weren't for my time in his lab. Dr. Brown, I could never thank you enough for that experience and the support you have shown me since day one. Dr. Allison Pearson, you helped me get started in undergraduate research and supported me as a friend and mentor throughout. Dr. Stephen Sardini, you played such an integral role in getting me excited about chemistry and research. Beyond research, you have been a friend and encourager. It's incredibly cool to have a friend I can talk to about complex chemistry topics, stupid internet memes, or anything at all in life. Professor Johannes Wahl (Jojo), looking back I am shocked to think about how incredibly kind and generous you were to a random undergrad while you were working as a postdoc in a new country. You are one of the kindest and coolest humans I know. I wish you didn't live across an ocean, but I am sure you are making an incredible impact as a professor.

Dr. Erin Hancock deserves an award for all the patience she had to mentor me in undergrad. I truly knew nothing when I joined the lab. Erin, you taught me practically every lab skill I have. You spent countless hours showing me techniques, answering my questions, and teaching me to be an independent researcher. You also showed me how to be a whole, unserious person while

exploring complex chemistry problems. I will never forget one of the very first interactions I had with you. I walked into lab with you, terrified, and you pointed at a chemical structure and asked me what I thought that molecule would say if it could talk. How funny and amazing you are. I am so grateful to have you as a mentor and friend in life.

My parents are some of the coolest people I know. From extremely early on, they trusted me to be the one in charge of my own life. Without that trust and infinite confidence and love, I would not be where I am today. I could write a whole book about all the love you have both shown me. My brother John, and his wife, Gloria, are the best siblings. I hope I will get to see you all more often now that this is done. I am so excited to become an aunt to Eliane.

I have two of the best friends in the world, Caroline and Ella. Caroline, you have been by my side since the day I was born. I feel so loved and at peace when I get to be with you. Ella, when I was at one of my lowest points in graduate school you got on a plane and flew to be with me that very day. I have leaned on you for so much support throughout everything. I think very few people have friends as amazing as both of you. I love you both so much.

There are so many people who have loved me and encouraged me. I am grateful for Sumbul Haider, Anna Greene, Gabriella Altchek, Sam Booth, Josh and Bridget Eggold, Sonya and Thomas Eggold, Maddie Ripke, Brendan Keen, Carl and Becky Lottman, and so many, many more people. Finally, I am grateful for my two cats, Earl and Professor Snail.

Chapter 1 is adapted with permission from Nie, S.; Lu, A.; Kuker, E. L.; Dong, V. M. "Enantioselective Hydrothiolation: Diverging Cyclopropenes Through Ligand Control" *J. Am. Chem. Soc.* **2021**, *143*, 6176– 6184. © 2021 American Chemical Society

VITA

Erin Louise Kuker

EDUCATION

University of California, Department of Chemistry, Irvine, CA — 2019 – present
Ph.D. in Chemistry — GPA 3.97/4.00
Advisor: Professor Vy Dong

Indiana University, College of Arts and Sciences, Bloomington, IN — 2015 – 2019
Bachelor of Arts in Chemistry, Hutton Honors Notation — GPA 3.86/4.00
Advisor: Professor Kevin Brown

RESEARCH EXPERIENCE

Dong Lab at University of California, Irvine, CA — January 2020 – present
Graduate Researcher

- Studied a carbon-sulfur bond formation via a Rh-catalyzed hydrothiolation of cyclopropenes
- Designed and implemented a selective hydroacylation of azetines
- Completed comprehensive mechanistic studies via kinetic analysis, isotope labeling, and NMR experimentation

Brown Lab at Indiana University, Bloomington, IN — May 2017 – May 2019
Undergraduate Researcher

- Contributed to an enantioselective synthesis of Pentacycloanammoxic Acid, a ladderane natural product isolated from bacteria
- Optimized the setup and purification of large scale [2+2] cycloadditions
- Pursued the synthesis of oxazaborolidine catalysts and studied their applications

Indiana University School of Medicine, Fort Wayne, IN — May 2016 – August 2016
Student Researcher through Midwest Alliance for Health Education

- Worked with Cardiovascular Surgeon Dr. Grey on retrospective lung cancer screening study
- Reviewed patient charts and performed statistical analysis on findings
- Received training in biomedical and social research

PUBLICATIONS

1) **Kuker, E. L.**; Wallace, C.; de Vos, A. E.; Vu, J.; Dong, V. M. "Enantio- and Regioselective Hydroacylations of Azetines" *Manuscript in preparation.*
2) Ferrer, M. J.; **Kuker, E. L.**; Semenova, E.; Gangano, A. J.; Lapak, M. P.; Grenning, A. J.; Dong, V. M.; Bowers, C. R. "Adiabatic Passage through Level Anticrossings in Systems of Chemically Inequivalent Protons Incorporating Parahydrogen: Theory, Experiment, and Prospective Applications" *J. Am. Chem. Soc.* **2022**, *144*, 20847–20853.
3) Nie, S.; Lu, A.; **Kuker, E. L.**; Dong, V. M. "Enantioselective Hydrothiolation: Diverging Cyclopropenes Through Ligand Control" *J. Am. Chem. Soc.* **2021**, *143*, 6176– 6184.
4) Davison, R. T.; **Kuker, E. L.**; Dong, V. M. "Teaching Aldehydes New Tricks Using Rhodium- and Cobalt-Hydride Catalysis" *Acc. Chem. Res*. **2021**, *54*, 1236–1250.
5) Hancock, E. N.; **Kuker, E. L.**; Tantillo, D.; Brown, M. K. "Lessons in Strain and Stability: An Enantioselective Synthesis of (+)-[5]-Ladderanoic Acid" *Angew. Chem. Int. Ed*. **2020**, *59*, 436–441.

ABSTRACT OF THE DISSERTATION

Development and Mechanistic Explorations of Novel Rhodium-Catalyzed Hydrothiolations and Hydroacylations

By

Erin Louise Kuker

Doctor of Philosophy in Chemistry

University of California, Irvine, 2024

Professor Vy M. Dong, Chair

My Ph.D. research has spanned several areas of synthetic organic chemistry, including divergent hydrothiolations of cyclopropenes, dynamic kinetic resolutions of aldehydes via hydroacylations, and regiodivergent hydroacylations of azetines. I developed catalysts and methodologies to synthesize a variety of chemical motifs and performed mechanistic experiments to gain useful insight on how the reactions proceed.

Chapter 1 is focused on the divergent hydrothiolation of cyclopropenes. Given the prevalence of sulfur in biologically relevant organic molecules, inventing methods to forge C–S bonds remains a worthwhile pursuit. We sought to develop a hydrothiolation that could take advantage of cyclopropene strain energy to provide diverse sulfide motifs from the same readily available materials. Through our investigation, we discovered that divergent reactivity could be obtained by altering the electronics of the bisphosphine ligands on a rhodium catalyst. Rh-catalysts with electron-rich Josiphos ligands afford cyclopropyl sulfides exclusively, whereas slightly less electron-rich ligands, such as DTBM-BINAP, afford allylic sulfides exclusively. A variety of mechanistic experiments were performed to elucidate the divergence in the mechanisms.

Chapter 2 is focused on the dynamic kinetic resolution of aldehydes via hydroacylation. Dynamic kinetic resolution (DKR) is a compelling method used to prepare enantiopure materials from racemic starting materials with no limit in the theoretical yield. In this example, we have combined an intermolecular hydroacylation of acrylamides with the DKR of racemic aldehydes. Through this C– C bond formation the synthesis of 1,4-ketoamides is achieved with high enantio- and diastereoselectivity. In-depth mechanistic explorations in tandem with computations have allowed for the proposed catalytic cycle to be explored in this chapter.

Chapter 3 is focused on the regiodivergent hydroacylation of azetines. Azetidines are four-membered cyclic amines that are found in both natural products and pharmaceutical candidates, and azetines are their unsaturated counterparts. Inspired by the biological activity of these structures and the limited exploration of azetine reactivity, I imagined developing a hydroacylation of azetines to construct novel azetidines. I found an exciting and compelling lead result where electron-rich Josiphos ligands yield the chiral isomer selectively. Alternatively, the achiral regioisomer can be obtained with several different biaryl bisphosphine ligands, including dppe. In addition to optimization and scope exploration, several derivatizations of the hydroacylation azetidine products are demonstrated. Initial studies on the divergent mechanisms are included in the chapter.

CHAPTER 1 – Enantioselective Hydrothiolation: Diverging Cyclopropenes Through Ligand Control

1.1 Introduction

Given the prevalence of sulfur in biologically relevant organic molecules,[1] inventing methods to forge C–S bonds remains a worthwhile pursuit.[2] Hydrothiolation, the addition of a thiol across a degree of unsaturation, represents a straightforward and atom economical[3] way of building molecules with sulfide functional groups.[4] In previous communications,[4c,4d] our laboratory disclosed highly regioselective hydrothiolations of conjugated dienes, where regiocontrol was achieved through careful selection of the counterion associated with the Rh-catalyst (Figure 1.1A). Using a non-coordinating counterion, such as SbF_6^-, allows the conjugated diene to bind the catalyst in an η^4 fashion en route to allylic sulfide products.[4c] Using a coordinating counterion, such as Cl^-, forces the conjugated diene to bind the catalyst in an η^2 fashion en route to homoallylic sulfide products.[4d] The switch in regioselectivity was achieved by having chloride occupy a coordination site on the catalyst.

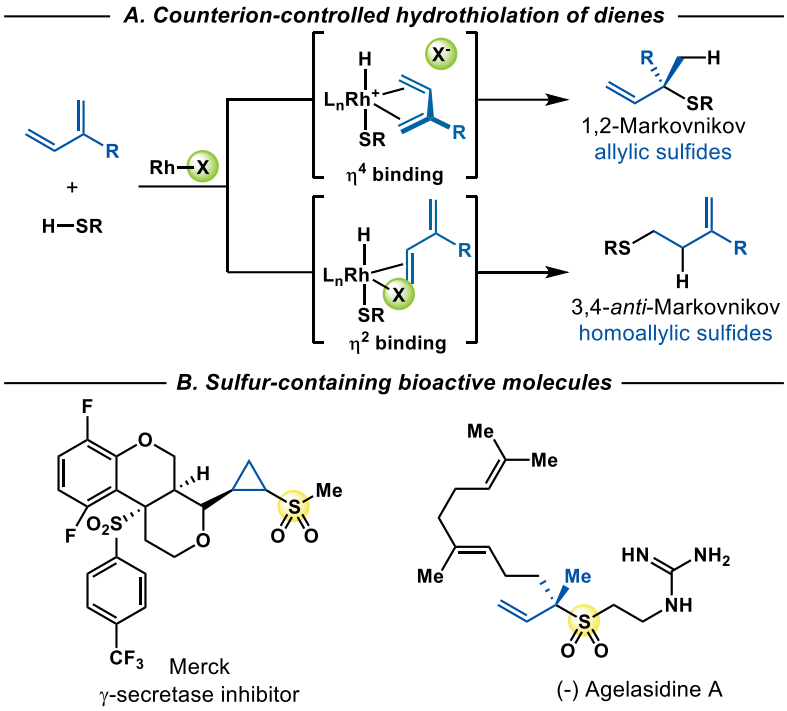

Figure 1.1 Extending hydrothiolation to cyclopropenes

In this article, we focus on the hydrothiolation of cyclopropenes. In contrast to our previous study, the appropriate choice of ligand enables divergent pathways to yield either the cyclopropyl or allylic sulfide motifs, both architectures germane to natural products and biologically active molecules (Figure 1.1B).

Since their synthesis in 1922,[5] cyclopropenes have captivated chemists due to their strained structures and high reactivity.[6] Cyclopropene, the smallest possible unsaturated carbocycle, owes its unique reactivity to 54.1 kcal/mol of strain energy.[7] Releasing the strain energy enables cyclopropenes to undergo cycloadditions and hydrofunctionalizations that are challenging for simpler alkenes and alkynes. In contrast to less strained alkenes, however, there exists a unique challenge in controlling the diverse modes of reactivity (Figure 1.2A). Additions to cyclopropenes are known to occur with ring-retention to yield cyclopropyl products,[8] as well as with ring-opening to yield allylic products.[9] In general, ring-retentive hydrofunctionalizations require softer nucleophiles, such as boranes, stannanes, and carbon nucleophiles.[10,11] Ring opening hydrofunctionalizations require harder nucleophiles, such as amines,

alcohols, or phosphonates.[12] However, there are exceptions to this trend, including Hou's ring-retentive hydroamination[10f] and Yamamoto's ring-opening addition of carbon nucleophiles.[12a]

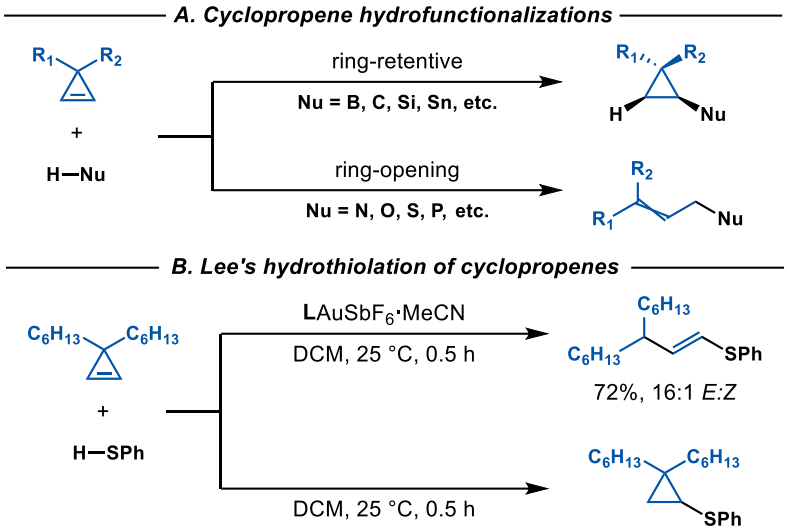

Figure 1.2 Diverse reactivity of cyclopropenes

Lee demonstrated that both modes of reactivity are possible for thiol nucleophiles, depending on the choice of conditions (Figure 1.2B).[13] The Au-catalyst opens the cyclopropene through C–C bond activation. The regioselectivity of the subsequent hydrothiolation depends on the choice of thiol or thioacid as the nucleophile. While the reactivity is novel, only racemic mixtures of the allylic sulfide are obtained when coupling unsymmetrical cyclopropenes to thiols. In the absence of a Au-catalyst, cyclopropyl sulfide products are observed.[14] Rendering either variant of Lee's cyclopropene hydrothiolation asymmetric would be difficult: the enantio-determining step of ring-opening hydrothiolation is protonation, while the ring-retentive hydrothiolation proceeds in the absence of catalyst.

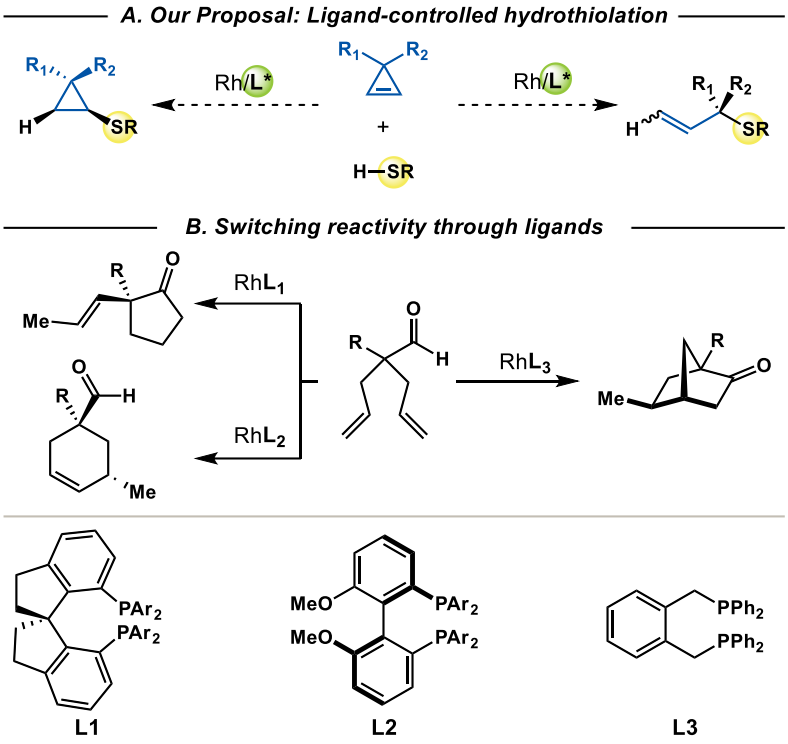

Figure 1.3 Enabling divergent reactivity through ligand control

To address this challenge, we hypothesized that Rh-catalysis, along with careful selection of the bisphosphine ligand, would enable access to both ring-opening and ring-retentive hydrothiolations of cyclopropenes (Figure 1.3A). Controlling the reactivity of the cyclopropene through ligands would enable us to select for products that are chiral, thus offering an opportunity to render the transformations enantioselective. Identifying ligands that can override the native reactivity of substrates is challenging. However, there are several examples in the literature of ligands enabling the divergent synthesis of constitutional isomers.[15,16] Ligand-control is established primarily through governing the regioselectivity[15] or chemoselectivity[16c,16d] of the transformation. Our group has studied the reactivity of bisallylaldehydes under Rh-catalyzed hydroacylation (Figure 1.3B). Through the choice of bisphosphine ligand, we can alter the steps of the catalytic cycle and obtain different carbocycles from the same bisallylaldehyde starting material.[16a,16b,17] Encouraged that transition metals can catalyze reactions with thiols,[2] we focused on studying Rh-catalysts to explore how different bisphosphine ligands diverge the reactivity of cyclopropenes.

1.2 Reaction Discovery and Optimization

To test our hypothesis, we attempted to couple cyclopropene **1a** and thiophenol **2a** using a variety of achiral bisphosphine ligands with $[Rh(cod)Cl]_2$. Gratifyingly, we observed a correlation between **3aa**:**4aa** and the bite angle of the bisphosphine ligands (Figure 1.4A). Bisphoshines with smaller bite angles (dppm, dppe) give exclusively cyclopropyl sulfide (±)-**4aa** (76% and 82%, >20:1 *dr*), while ligands with larger bite angles (*rac*-BINAP) form allylic sulfide (±)-**3aa** exclusively (80%, >20:1 *rr*). Bisphosphine ligands with intermediate bite angles furnish mixtures of **3aa** and **4aa**. The 1,1-dialkysubstituted cyclopropene (3,3-dihexylcycloprop-1-ene) has been shown to undergo addition with thiols in the absence of any catalysts (Figure 1.2B).[13] In contrast, control experiments with cyclopropene **1a** show that neither product is obtained in the absence of Rh-precursor or ligand, indicating that the selectivity is ligand-controlled. Next, we optimized for asymmetric variants of the transformation to access **3aa** or **4aa** with high enantioselectivity (Figure 1.4B). Ligands from the Josiphos family bearing alkyl substituents (**L5**, **L6**) afforded **3aa**. Ultimately, using **L5** with MeCN as solvent afforded the best yield and selectivity for **3aa** (90%. 95:5 *er*, >20:1 *dr*) after 6 h. Hydrothiolations promoted with axially chiral ligands bearing DTBM (3,5-di-tert-butyl-4-methoxyphenyl) substituents (**L7**, **L8**) afford allylic sulfide **4aa** with good yields (86–87%, >20:1 *rr*) when conducted at 0 °C for 30 min. The best enantioselectivity for **4aa** was achieved when using bisphosphine **L8** (96:4 *er*).[18] Given the structural differences between chiral bisphosphines **3aa** and **4aa**, both steric and electronic parameters must influence selectivity.

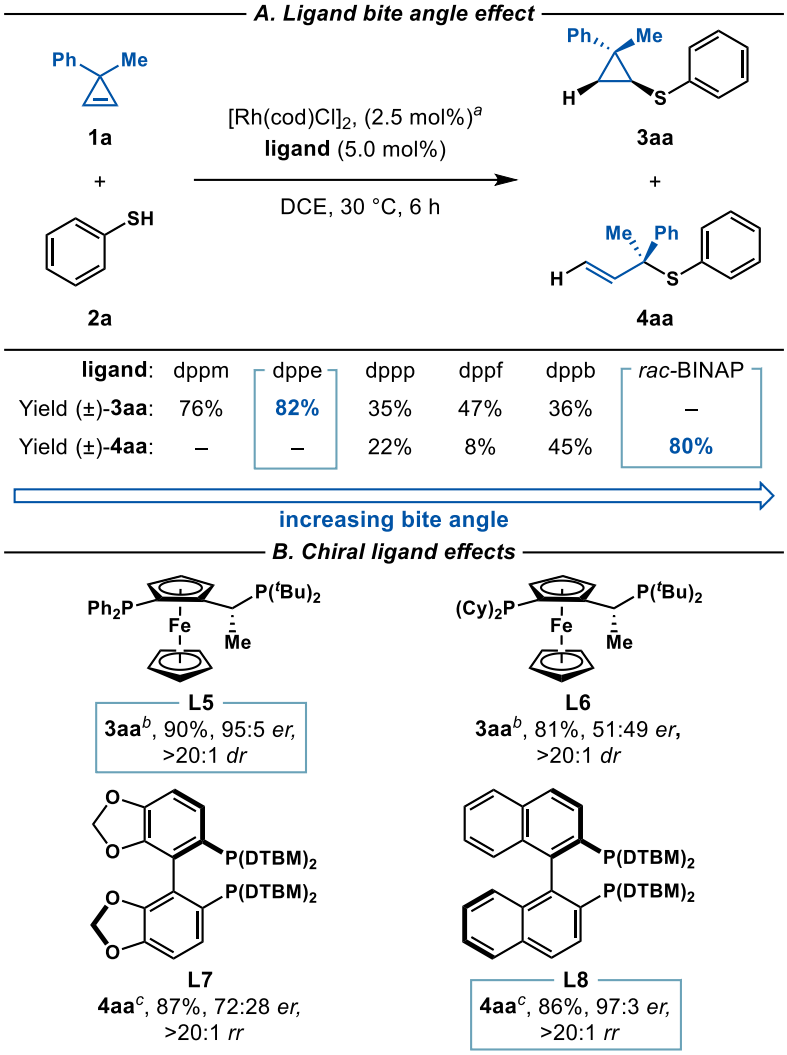

Figure 1.4 Reaction optimization using various bisphosphine ligands.

[a]Reaction conditions: **1** (0.12 mmol, **2** (0.10 mmol), $[Rh(cod)Cl]_2$ (2.5 mol%), ligand (5.0 mol%), 0.6 mL DCE, 30 °C, 6 h. Yields of isolated products are given. [b]Reaction performed using MeCN for 6 h. [c]Reaction performed at 0 °C for 30 min. DTBM: 3,5-di(tert-butyl)-4-methoxyphenyl.

1.3 Substrate Scope

With these conditions in hand, we evaluated the scope of the ring-retentive hydrothiolation (Table 1.1). High reactivity and enantioselectivity (91:9–95:5 *er*) are observed with aromatic thiol partners (**3ab**–**3ag**). However, aliphatic thiols are unreactive under these conditions (**3ap** and **3aq**). This result most likely stems from the differences in their ability to bind Rh (vide infra). Thus, further tuning of the bisphospine

Table 1.1 Ring-retentive hydrothiolation of cyclopropenes

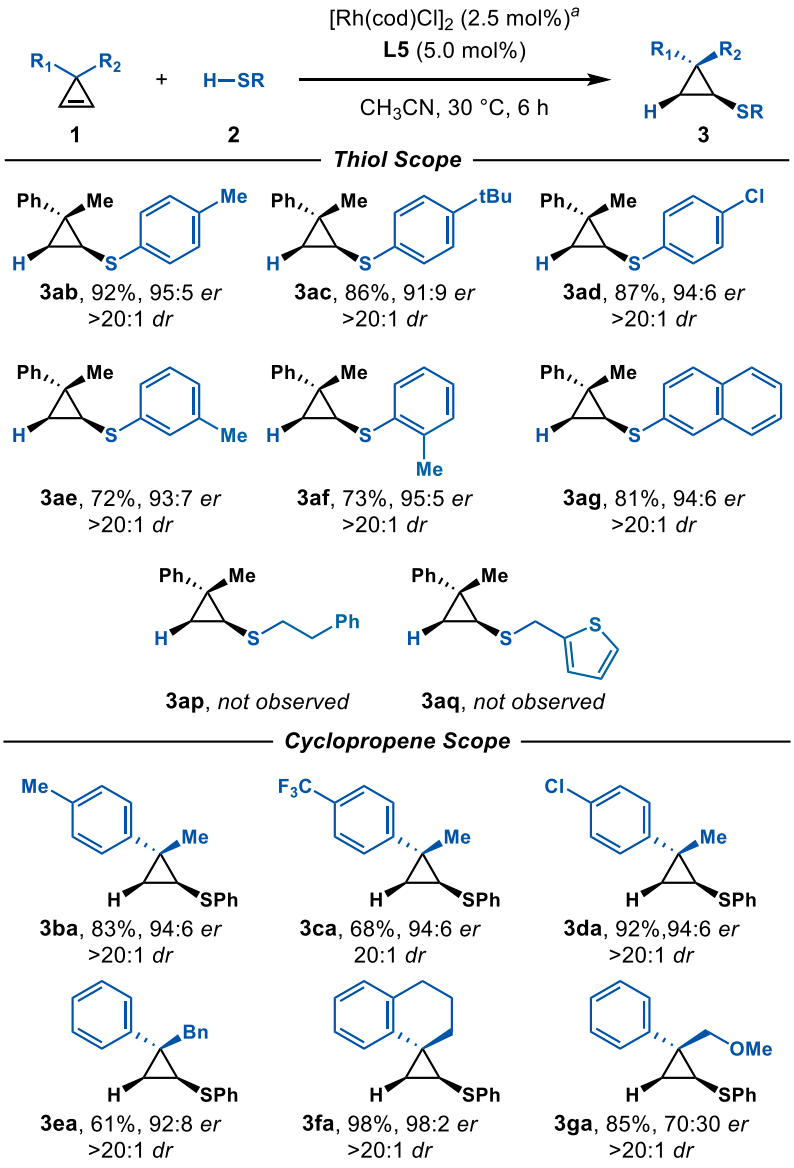

[a]**Reaction conditions: 1** (0.12 mmol, **2** (0.10 mmol), $[Rh(cod)Cl]_2$ (2.5 mol%), **L5** (5.0 mol%), 0.6 mL MeCN, 30 °C, 6 h. Yields of isolated products are given. Diastereomeric ratios (*dr*) were determined from ^1H NMR analysis of the unpurified reaction mixture. Enantiomeric ratios (*er*) were determined by SFC analysis on a chiral stationary phase.

ligand will be necessary to obtain reactivity using alkyl thiols. On the other hand, aromatic thiols bearing halogens transform well (**3ad**, 87%, >20:1 *dr*, 94:6 *er*). Sterically hindered thiophenols with *ortho* substituents display good reactivity and high selectivity (**3af,** 73%, >20:1 *dr*, 95:5 *er*). Withdrawing functional groups on aromatic thiols (such as 4-(trifluoromethyl)thiophenol) give mixtures of both

cyclopropyl and allylic sulfide products. Aromatic thiols with extended π-systems couple to **1a** with 81% yield and 94:6 *er* (**3ag**).

Cyclopropenes bearing different aromatic groups are all suitable coupling partners for the transformation (**3ba–3da**). Cyclopropenes with electron rich aromatic groups (**3ba**) show excellent reactivity (83%) and selectivity (>20:1 *dr*, 94:6 *er*).[19] The hydrothiolation occurs even with the addition of electron withdrawing substituents on the cyclopropene (**3ca** and **3da**, 68–92%, ≥20:1 *dr*, 94:6 *er*). The methyl substituent can be replaced with a bulkier benzyl substituent (**3ea**, 61%, >20:1 *dr*, 92:8 *er*). There are many spirocyclic natural products containing quaternary carbons, and these quaternary centers are difficult to set in a stereoselective manner.[20] Through a desymmetrization of the corresponding spirocyclic cyclopropene, sulfide **3fa** is obtained in excellent yield and stereoselectivity. Cyclopropenes containing a methyl ether can also undergo hydrothiolation (**3ga**).

Next, we explored the scope for obtaining allylic sulfides (Table 1.2). The hydrothiolation of **1a** was carried out with structurally and electronically different thiols. Both aryl (**4ab**–**4ao**) and alkyl thiols (**4ap**, **4aq**) add to cyclopropene **1a**.

In general, the ring-opened allylic sulfides are obtained with excellent regioselectivity (>20:1 *rr*).[21] Electron rich thiophenols couple to **1a** with high reactivity and good selectivities (**4ab**, **4ac**, **4ah**, 85%–90%, 92:8–96:4 *er*). Electron deficient thiophenols undergo addition with good selectivities (**4ai**–**4al**, 82%–89%, 91:9–95:5 *er*). Allylic sulfide **4al** was originally obtained as a mixture with **3al**. However, raising the reaction temperature allows for the exclusive formation of **4al**. Sterically hindered thiophenols react with high enantioselectivities (**4af** and **4ao**, >99:1 *er* and 95:5 *er*). Alkyl thiols couple, albeit with moderate yields and selectivities (**4ap** and **4aq**, 63–71%, 74:26 *er*).

Most of the cyclopropenes that react under the ring-retentive conditions also react under the ring-opened hydrothiolation conditions. Cyclopropenes with either electron rich (**4ba**) or electron poor (**4ca** and **4da**) aryl substituents can couple to **2a** (58%–83%, 85:15–97:3 *er*). Cyclopropenes bearing larger

Table 1.2 Ring-opened hydrothiolaton of cyclopropenes

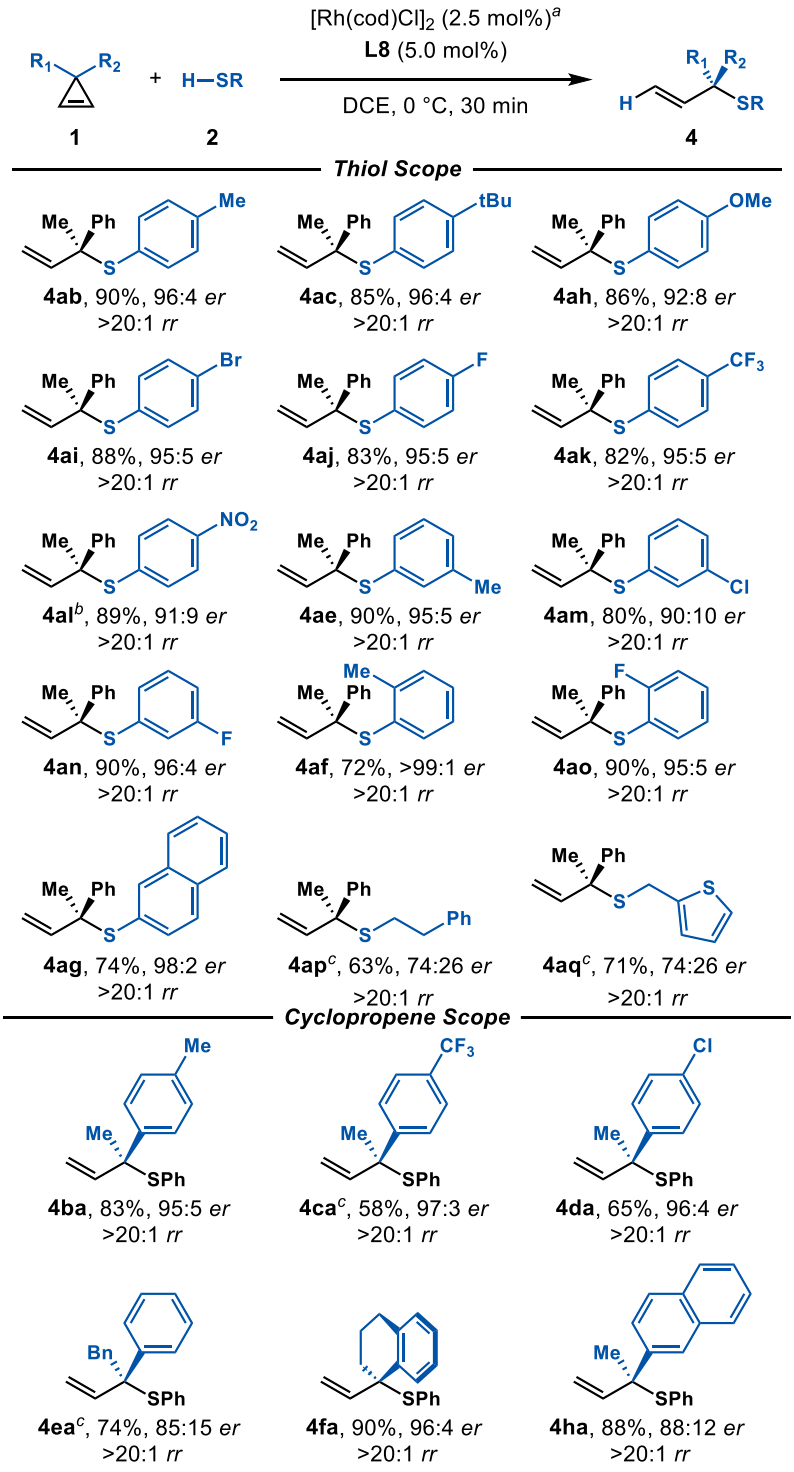

[a]**Reaction conditions: 1** (0.12 mmol), **2** (0.1 mmol), $[Rh(cod)Cl]_2$ (2.5 mol%), **L8** (5.0 mol%), 0.4 mL DCE, 0 °C, 30 min. Yields of isolated products are given. Regioisomeric ratios (*rr*) were determined from ^1H NMR analysis of the unpurified reaction mixture. Enantiomeric ratios (*er*) were determined by SFC analysis on a chiral stationary phase. [b]Reaction performed at 30 °C. [c]Reaction performed with **L7** at 30 °C.

substituents, such as benzyl (**4ea**) or naphthyl (**4ha**) also show good reactivity, albeit with less selectivity (74%–88%, 85:15–88:12 *er*). Allylic sulfides **4ap**, **4aq**, **4ca**, and **4ea** are obtained as mixtures with their ring-retentive counterparts under the standard conditions. However, raising the temperature to 30 °C and switching the bisphosphine ligand from **L8** to **L7** gives exclusively the ring-opened allylic sulfide.

1.4 Mechanistic Insights

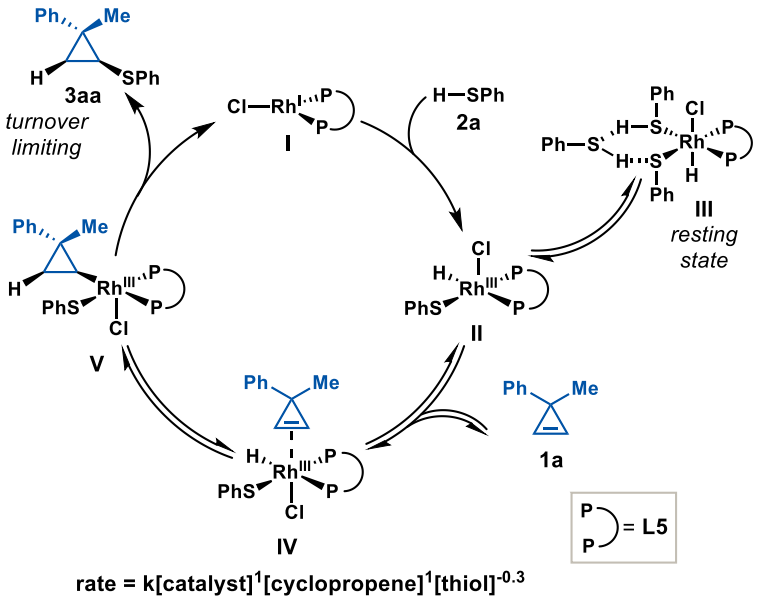

Figure 1.5 Proposed catalytic cycle for ring-retentive hydrothiolation.

Based on both literature precedent and our own observations, we propose the following mechanism for ring-retentive hydrothiolation of cyclopropenes (Figure 1.5). The catalyst resting state is an off-cycle species **III**, with multiple thiols bound. Upon dissociation of thiols to enter the catalytic cycle, the Rh-catalyst (**I**) undergoes oxidative addition to **2a** to generate **II**. Following coordination, cyclopropene **1a** inserts into the Rh–H bond to afford cyclopropyl-Rh(III) **V**. The turnover limiting step is reductive elimination to form the C–S bond, which furnishes **3aa** and regenerates the Rh-catalyst **I**. The mechanistic experiments that led to this proposed mechanism are discussed below.

Through studies of the initial reaction rates, we determined that the hydrothiolation was first order with regards to Rh-catalyst and **1a**, and a negative fractional order with regards to thiol **2a**. A negative order

in thiol has been observed in our group's previous report on the hydrothiolation of dienes,[4d] leading us to propose an off-cycle resting state where multiple thiols are coordinated through a hydrogen-bonding network (**III**).[22] The proposed resting state **III** is further supported by the presence of a metal hydride resonance at -15.9 ppm when using ^{1}H NMR spectroscopy to monitor experiments using stoichometric amounts of $[Rh(cod)Cl]_2$, dppe, and **2a**.[23]

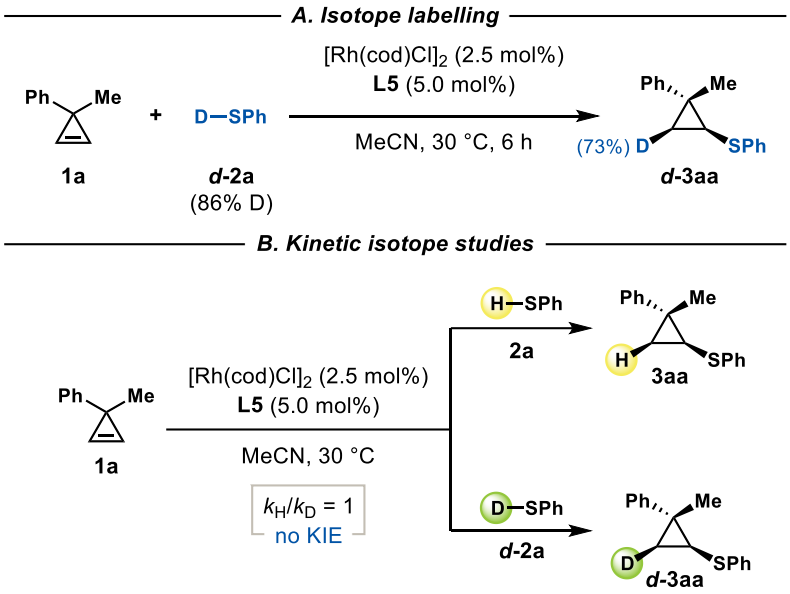

Figure 1.6 Mechanistic experiments for ring-retentive hydrothiolation using ***d*-2a**.

An isotopic labelling experiment was performed with the ring-retentive conditions using deuterated thiophenol ***d*-2a** (Figure 1.6A). Analysis of ***d*-3aa** shows that the deuterium is incorporated exclusively *syn* relative to the sulfide. This result suggests a *syn* hydrorhodation operates in the catalytic cycle. No kinetic isotope effect (KIE) is observed when running hydrothiolations with **2a** and ***d*-2a** in parallel (Figure 1.6B). The empirical rate law and lack of KIE support reductive elimination as the turnover-limiting step.[24]

Based on both literature precedent and our own observations, we propose the catalytic cycle for the ring-opening hydrothiolation depicted in Figure 1.7. After formation of Rh-catalyst **I**, oxidative addition into **2a** occurs to form **II**, the catalyst resting state. Coordination of **1a** and its subsequent insertion into the Rh–H bond forms cyclopropyl-Rh(III) intermediate **V**. The *syn* hydrorhodation to form **V** is the

turnover-limiting step. Ring-opening occurs, forming Rh-π-allyl complex **VI**. Reductive elimination forms the C–S bond of **4aa** and regenerates catalyst **I**. Reductive elimination for C–S bond formation is favored over outer-sphere attack of **2a** due to its high acidity (6.62 in H_2O).[25,26]

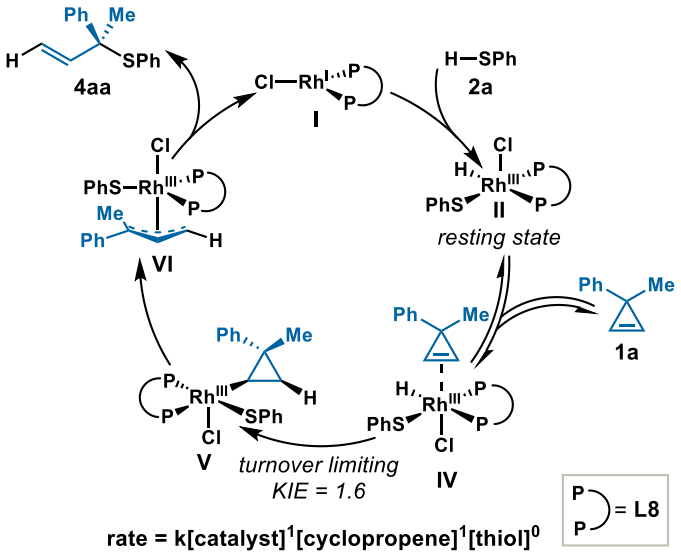

Figure 1.7 Proposed catalytic cycle for ring-opening hydrothiolation of cyclopropenes.

There are two main pathways that are proposed for cyclopropene ring opening. One pathway is through direct activation of the σ_{C-C} bond (eq. 1).[9f] However, in a few cases, it is proposed that hydrometallation occurs first to generate a cyclopropyl-metal species.[12a,12c] Ring-opening of the cyclopropyl metal species then occurs to afford a metal-π-allyl intermediate (eq. 2). Our proposed mechanism is based on the ring-opening pathway outlined in equation 2. The observations and mechanistic experiments that led to this proposed mechanism are discussed below.

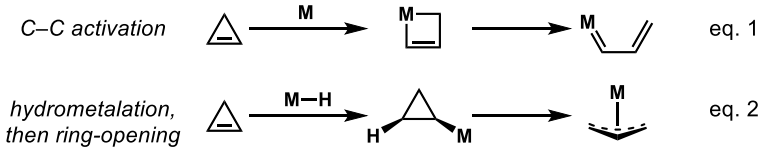

Mixtures of **3aa** and **4aa** are obtained when certain bisphosphine ligands are used for the hydrothiolation (Figure 1.4A). However, in a crossover study where **3aa** is subjected to the standard ring-opening hydrothiolation conditions, only **3aa** is recovered (Figure 1.8A). This demonstrates that **3aa** is

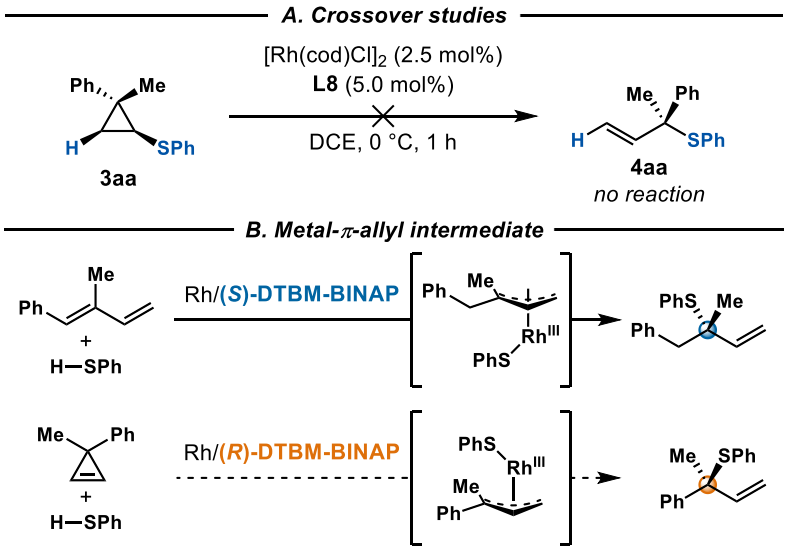

Figure 1.8 Determining the operative pathway for ring-opening

not converted into **4aa** during catalysis. One explanation for these results is that the ring-retentive and ring-opened pathways share a common intermediate, cyclopropyl-Rh(III) **V** (Figure 1.5). Allylic sulfide **4aa,** the product obtained under ring opening conditions, is similar to the products obtained from Rh-catalyzed hydrothiolation of 1,3-dienes (Figure 1.8B).[4c] Rh-π-allyl species generally form the branched product upon interception with a nucleophile.[27] Additionally, the correlation between the enantiomer of DTBM-BINAP and absolute configuration of the branched allylic sulfide product is in agreement between these two previous examples. The highly regioselective formation of **4aa** and its absolute configuration support the intermediacy of Rh-π-allyl **VI.**

The reactivity of cyclopropene **1g** provides additional mechanistic support for the proposed isomerization of cyclopropyl-Rh(III) **V** into Rh-π-allyl complex **VI**. While **1g** was able to couple to **2a** in a ring-retentive fashion to access **3ga** (Table 1.1), no reactivity was observed with **1g** under ring-opening hydrothiolation conditions (Figure 1.9A). One explanation for the observed reactivity could be that ring-opening requires an additional coordination site on the metal. The cyclopropyl group only occupies one coordination site, whereas the corresponding π-allyl ligand requires two. The methyl ether of **1g** could occupy the coordination site needed for ring-opening, thus halting the reaction. Similar reactivity is observed for cyclopropyl metal complexes prepared by the Puddephatt and Bergman groups.[28] For these

Rh and Pt complexes, abstraction of the halide ligand is required to induce isomerization into metal-π-allyl complexes (Figure 1.9B).[28a–c]

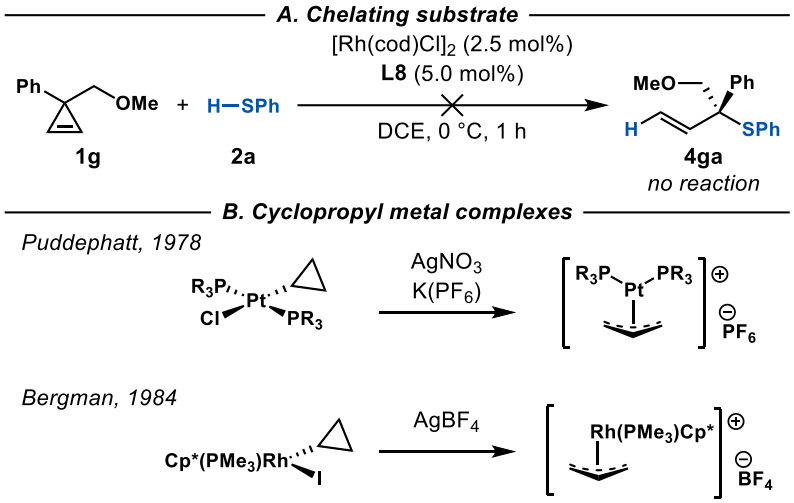

Figure 1.9 Ring-opening of prepared cyclopropyl metal complexes.

Additional kinetic and isotope labelling experiments were carried out to gain further mechanistic insights. Initial rate studies show that this process is first order with regards to Rh-catalyst and cyclopropene **1a**, and zeroth order with regards to thiol **2a**. The saturation kinetics observed with **2a** support complex **II** as the catalyst resting state. The deuterium is incorporated into the terminal carbon of the olefin in ***d*-4aa**, with most of the deuterium incorporated *trans* relative to the rest of the molecule (Figure 1.10A). Additionally, a primary KIE of 1.6 is observed when ring opening hydrothiolations with **2a** and ***d*-2a** were carried out in parallel (Figure 1.10B). The first order dependence in **1a** and primary KIE of 1.6 suggest that migratory insertion to form **V** from **IV** is the turnover-limiting step.

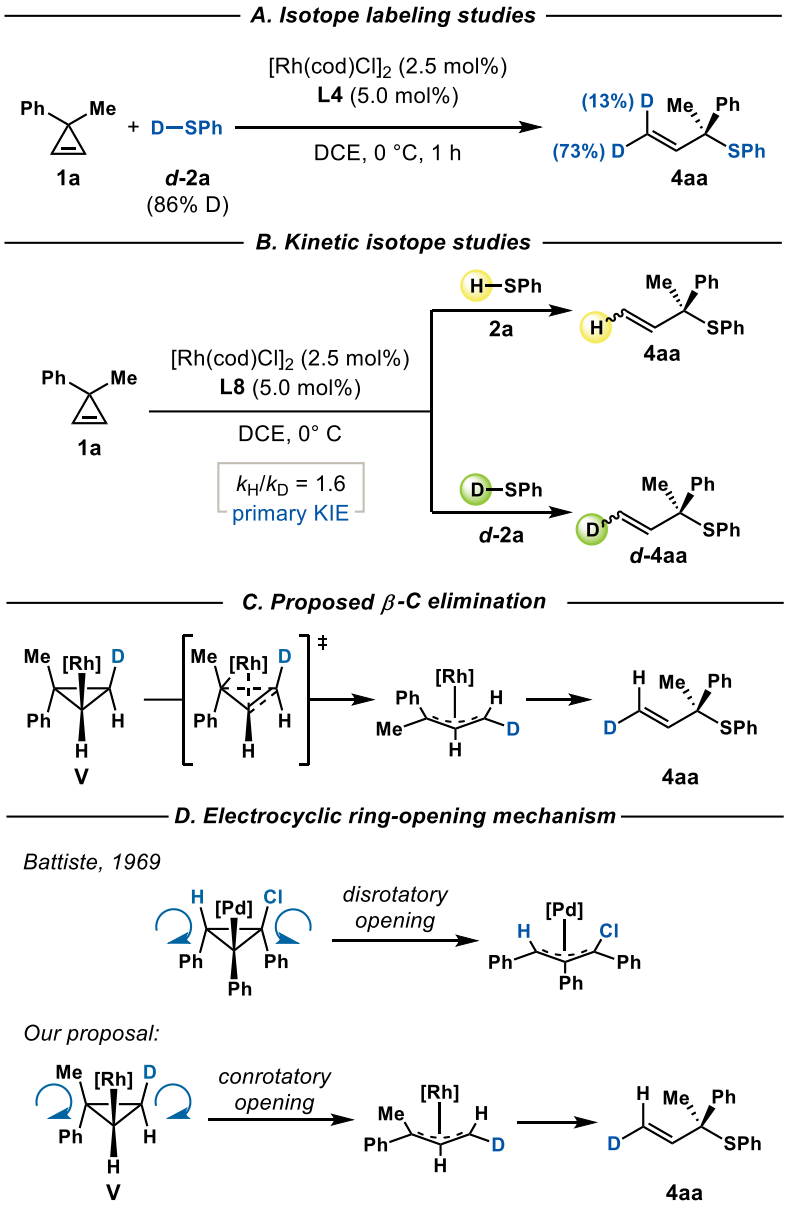

Figure 1.10 Deuterium labeling studies for ring-opening hydrothiolation

There are a few possible explanations for the primarily *trans* incorporation of deuterium. Considering proposals from previous ring-opening hydrofunctionalizations, the ring-opening process might be through β-C elimination.[12a,12c] The *trans*-selectivity would result from a bond rotation to align the σ_{C-C} bond of the cyclopropane with the Rh–C bond in a *syn*-coplanar conformation to enable the β-elimination (Figure 1.10C). Studies on the isomerization of cyclopropyl metal species into metal-π-allyl complexes have also been likened to the ring-opening process to electrocyclic ring-opening.[28d] Based on Woodward-Hoffman

rules, if cyclopropyl-Rh(III) **V** is treated like a cyclopropyl-anion, conrotatory electrocyclic ring-opening could also explain the *trans*-selectivity for deuterium incorporation (Figure 1.10D).[29]

1.5 Conclusion

While the reactivity of cyclopropenes has been extensively studied, there has yet to be a catalyst that takes advantage of both modes of reactivity cyclopropenes offer. Through choice of ligand on the Rh-catalyst, thiols add to cyclopropenes, resulting in cyclopropyl sulfides or allylic sulfides. This divergent reactivity allows cyclopropenes to act as versatile building blocks that enables access to a diverse chemical space. Either hydrothiolation product can be obtained with high yield and stereocontrol. Mechanistic experiments suggest that the ring opening from a cyclopropyl-Rh(III) intermediate is the key step for achieving divergent reactivity. For the ring-retentive process, the Rh-catalyst with smaller bite-angle ligands and chiral ligand **L5** promote reductive elimination to forge the C–S bond of the cyclopropyl sulfide product. For the ring-opening process, the Rh-catalyst with larger bite angle ligands and chiral ligand **L8** promote ring-opening, isomerizing the cyclopropane ring to form allylic sulfide products. Initially, the ligand bite angle effect seems contradictory, given that wider bite angle ligands are known to accelerate reductive elimination. However, given the faster reaction rate of the ring-opening hydrothiolation, the wider bite angle ligands might accelerate the ring-opening process to a greater extent than reductive elimination. These studies provide experimental support for a mechanism that has only previously been proposed. Further computational studies are warranted to provide additional insight into the more elusive aspects, such as nuances in the ring-opening of cyclopropyl-Rh(III) **V**.[30] Mechanistic insights from this study pave the way for divergent hydrofunctionalizations of cyclopropenes with a wide array of nucleophiles.

1.6 Author Contributions

Shaozhen Nie (S.N.) and Professor Vy M. Dong (V.M.D.) conceived of the project idea discussed in Chapter 1. S.N. identified the optimal conditions for the transformation (Figure 1.4). S.N. and A.L. explored the scope of the mechanism. E.L.K synthesized and characterized compounds 1e, 3ea, and 4ea. E.L.K. explored the mechanistic insights for the ring-retained and ring-opened transformations. All authors analyzed the experimental results, contributed to the supporting information, and edited the manuscript.

1.7 References

(1) For sulfur compounds, see: (a) McGrath, N. A.; Brichacek, M.; Njardarson, J. T. A Graphical Journey of Innovative Organic Architectures That Have Improved Our Lives. *J. Chem. Educ.* **2010**, *87*, 1348. (b) Feng, M.; Tang, B.; Liang, S. H.; Jiang, X. Sulfur Containing Scaffolds in Drugs: Synthesis and Application in Medicinal Chemistry. *Curr. Top. Med. Chem*. **2016**, *16*, 1200−1216. (c) Scott, K. A.; Njardarson, J. T. Analysis of US FDA-Approved Drugs Containing Sulfur Atoms. *Top. Curr. Chem.* **2018**, *376 (5)*, 1−34.

(2) For reviews on C−S bond formation, see: (a) Kondo, T.; Mitsudo, T.-A. Metal-Catalyzed Carbon−Sulfur Bond Formation. *Chem. Rev.* **2000**, *100*, 3205−3220. (b) Arisawa, M.; Yamaguchi, M. Transition-metal-catalyzed synthesis of organosulfur compounds. *Pure Appl. Chem*. **2008**, *80*, 993−1003. (c) Chauhan, P.; Mahajan, S.; Enders, D. Organocatalytic Carbon−Sulfur Bond-Forming Reactions. *Chem. Rev.* **2014**, *114*, 8807−8864. (d) Shen, C.; Zhang, P.; Sun, Q.; Bai, S.; Hor, T. S. A.; Liu, X. Recent advances in C−S bond formation via C−H bond functionalization and decarboxylation. *Chem. Soc. Rev*. **2015**, *44*, 291−314. (e) Yu, J.-S.; Huang, H.-M.; Ding, P.-G.; Hu, X.- S.; Zhou, F.; Zhou, J. Catalytic Enantioselective Construction of Sulfur-Containing Tetrasubstituted Carbon Stereocenters. *ACS Catal*. **2016**, *6*, 5319−5344. (f) Qian, Z.; Jiang, X. Recent developments in sulfur−carbon bond formation reaction involving thiosulfates. *Org. Biomol. Chem*. **2017**, *15*, 1942−1946. For a review on enzymatic C−S bond formation, see: (g) Dunbar, K. L.; Scharf, D. H.; Litomska, A.; Hertweck, C. Enzymatic Carbon−Sulfur Bond Formation in Natural Product Biosynthesis. *Chem. Rev.* **2017**, *117*, 5521−5577. (h) Kawaguchi, S. I.; Yamamoto, Y.; Ogawa, A. Catalytic synthesis of sulfur and phosphorus compounds via atom-economic reactions. *Mendeleev Commun.* **2020**, *30*, 129−138.

(3) Trost, B. M. The Atom Economy–A Search for Synthetic Efficiency. *Science* **1991**, *254*, 1471–1477.

(4) For select catalytic methods for accessing chiral sulfur compounds, see: (a) Pritzius, A. B.; Breit, B. Asymmetric Rhodium-Catalyzed Addition of Thiols to Allenes: Synthesis of Branched Allylic Thioethers and Sulfones. *Angew. Chem., Int. Ed*. **2015**, *54*, 3121− 3125. (b) Pritzius, A. B.; Breit, B. Z-Selective Hydrothiolation of Racemic 1,3-Disubstituted Allenes: An Atom-Economic Rhodium Catalyzed Dynamic Kinetic Resolution. *Angew. Chem., Int. Ed*. **2015**, *54*, 15818−15822. (c) Yang, X.-H.; Davison, R. T.; Dong, V. M. Catalytic Hydrothiolation: Regio- and Enantioselective Coupling of Thiols and Dienes. *J. Am. Chem. Soc.* **2018**, *140*, 10443−10446. (d) Yang, X.-H.; Davison, R.; Nie, S.-Z.; Cruz, F. A.; McGinnis, T. M.; Dong, V. M. Catalytic Hydrothiolation: Counterion-Controlled

Regioselectivity. *J. Am. Chem. Soc*. **2019**, *141*, 3006−3013. (e) Khan, A.; Zhao, H.; Zhang, M.; Khan, S.; Zhao, D. Regio- and enantioselective synthesis of sulfone-bearing quaternary carbon stereocenters by pd-catalyzed allylic substitution. *Angew. Chem., Int. Ed.* **2020**, *59*, 1340−1345. (f) Li, M.-M.; Cheng, L.; Xiao, L.-J.; Xie, J.-H.; Zhou, Q.-L. Palladium-Catalyzed Asymmetric Hydrosulfonylation of 1,3-Dienes with Sulfonyl Hydrazides. *Angew. Chem., Int. Ed*. **2020**, *59*, 1−5. (g) Zhang, Q.-L.; Dong, D.-F.; Zi, W.-W. Palladium-Catalyzed Regio- and Enantioselective Hydrosulfonylation of 1,3-Dienes with Sulfinic Acids: Scope, Mechanism, and Origin of Selectivity. *J. Am. Chem. Soc*. **2020**, *142*, 15860−15869.

(5) (a) Demjanov, N. Y.; Doyarenko, M. N. Cyclopropene. *Bull. Acad. Sci. Russ*. **1922**, *16*, 297−304. (b) Demjanow, N. J.; Dojarenko, M. Cyclopropene. *Ber. Dtsch. Chem. Ges. B*. **1923**, *56*, 2200−2207.

(6) For reviews on cyclopropenes, see: (a) Carter, F. L.; Frampton, V. L. Review of the chemistry of cyclopropene compounds. *Chem. Rev.* **1964**, *64*, 497–525. (b) Closs, G. L. Cyclopropenes. *Adv. Alicyclic Chem.* **1966**, *1*, 53–127. (c) Baird, M. S. Thermally induced cyclopropene-carbene rearrangements: an overview. *Chem. Rev.* **2003**, *103*, 1271−1294. (d) Walsh, R. The cyclopropene pyrolysis story. *Chem. Soc. Rev*. **2005**, *34*, 714−732. (e) Rubin, M.; Rubina, M.; Gevorgyan, V. Recent advances in cyclopropene chemistry. *Synthesis* **2006**, *8*, 1221–1245. (f) Rubin, M.; Rubina, M.; Gevorgyan, V. Transition metal chemistry of cyclopropenes and cyclopropanes. *Chem. Rev.* **2007**, *107*, 3117−3179. (g) Zhu, Z.-B.; Wei, Y.; Shi, M. Recent developments of cyclopropene chemistry. *Chem. Soc. Rev.* **2011**, *40*, 5534−5563. (h) Vicente, R. Recent progresses towards the strengthening of cyclopropene chemistry. *Synthesis* **2016**, *48*, 2343–2360. (i) Raiguru, B. P.; Nayak, S.; Mishra, D. R.; Das, T.; Mohapatra, S.; Mishra, N. P. Synthetic Applications of Cyclopropene and Cyclopropenone: Recent Progress and Developments. *Asian J. Org. Chem*. **2020**, *9*, 1088–1132. (j) Li, P.-H.; Zhang, X.-Y.; Shi, M. Recent developments in cyclopropene chemistry. *Chem. Commun.* **2020**, *56*, 5457–5471.

(7) Bach, R. D.; Dmitrenko, O. Strain Energy of Small Ring Hydrocarbons. Influence of C−H Bond Dissociation Energies. *J. Am. Chem. Soc.* **2004**, *126*, 4444−4452.

(8) Dian, L.-Y.; Marek, I. Asymmetric Preparation of Polysubstituted Cyclopropanes Based on Direct Functionalization of Achiral Three-Membered Carbocycles. *Chem. Rev*. **2018**, *118*, 8415−8434.

(9) For reviews on ring-opening of cyclopropenes, see: (a) Phun, L. H.; Aponte-Guzman, J.; France, S. Acid-catalyzed ring-opening isomerizations of cyclopropenes. *Synlett* **2012**, *23(19)*, 2723−2728. (b) Archambeau, A.; Miege, F.; Meyer, C.; Cossy, J. Intramolecular Cyclopropanation and C−H Insertion Reactions with Metal Carbenoids Generated from Cyclopropenes. *Acc. Chem. Res*. **2015**, *48*, 1021−1031. (c) Fumagalli, G.; Stanton, S.; Bower, J. F. Recent Methodologies That Exploit C−C Single-Bond Cleavage of Strained Ring Systems by Transition Metal Complexes. *Chem. Rev*. **2017**, *117*, 9404−9432. (d) Azizollahi, H.; García-López, J. A. Recent advances on synthetic methodology merging C-H functionalization and C-C cleavage. *Molecules* **2020**, *25*, 5900. (e) Li, D.-Y.; Zang, W.-Q.; Bird, M. J.; Hyland, C. J. T.; Shi, M. Gold-catalyzed conversion of highly strained compounds. *Chem. Rev.* **2020**, DOI: 10.1021/acs.chemrev.0c00624. (f) Vicente, R. C−C Bond Cleavages of Cyclopropenes: Operating for Selective Ring Opening Reactions. *Chem. Rev*. **2021**, *121*, 162–226.

(10) For select ring-retentive hydrofunctionalizations of cyclopropenes, see: (a) Rubina, M.; Rubin, M.; Gevorgyan, V. Catalytic Enantioselective Hydroboration of Cyclopropenes. *J. Am. Chem. Soc.* **2003**, *125*, 7198–7199. (b) Rubina, M.; Rubin, M.; Gevorgyan, V. Catalytic Enantioselective Hydrostannation of Cyclopropenes. *J. Am. Chem. Soc.* **2004**, *126*, 3688–3689. (c) Sherrill, W. M.; Rubin, M. Rhodium-Catalyzed Hydroformylation of Cyclopropenes. *J. Am. Chem. Soc*. **2008**, *130*, 13804–13809. (d) Phan, D. H. T.; Kou, K. G. M.; Dong, V. M. Enantioselective Desymmetrization of Cyclopropenes by Hydroacylation. *J. Am. Chem. Soc*. **2010**, *132*, 16354–16355. (e) Liu, F.; Bugaut, X.; Schedler, M.; Fröhlich, R.; Glorius, F. Designing N-Heterocyclic Carbenes: Simultaneous Enhancement of Reactivity and Enantioselectivity in the Asymmetric Hydroacylation of

Cyclopropenes. *Angew. Chem., Int. Ed.* **2011**, *50*, 12626–12630. (f) Teng, H.-L.; Luo, Y.; Wang, B.; Zhang, L.; Nishiura, M.; Hou, Z. Synthesis of Chiral Aminocyclopropanes by Rare-Earth-Metal-Catalyzed Cyclopropene Hydroamination. *Angew. Chem., Int. Ed*. **2016**, *55*, 15406–15410. (g) Parra, A.; Amenós, L.; Guisán-Ceinos, M.; López, A.; Ruano, J. L. G.; Tortosa, M. Copper-Catalyzed Diastereo- and Enantioselective Desymmetrization of Cyclopropenes: Synthesis of Cyclopropylboronates. *J. Am. Chem. Soc*. **2014**, *136*, 15833–15836. (h) Li, Z.; Zhao, J.; Sun, B.; Zhou, T.; Liu, M.; Liu, S.; Zhang, M.; Zhang, Q. Asymmetric Nitrone Synthesis via Ligand-Enabled Copper-Catalyzed Cope-Type Hydroamination of Cyclopropene with Oxime. *J. Am. Chem. Soc*. **2017**, *139*, 11702–11705. (i) Luo, Y.; Teng, H.-L.; Nishiura, M.; Hou, Z. Asymmetric Yttrium-Catalyzed C(sp3)–H Addition of 2-Methyl Azaarenes to Cyclopropenes. *Angew. Chem., Int. Ed.* **2017**, **56**, 9207–9210. (j) Dian, L.; Marek, I. Rhodium-Catalyzed Arylation of Cyclopropenes Based on Asymmetric Direct Functionalization of Three-Membered Carbocycles. *Angew. Chem. Int. Ed.* **2018**, *57*, 3682–3686. (k) Zhang, H.; Huang, W.; Wang, T.; Meng, F.-K. Cobalt-Catalyzed Diastereo- and Enantioselective Hydroalkenylation of Cyclopropenes with Alkenylboronic Acids. *Angew. Chem. Int. Ed.* **2019**, *58*, 11049–11053. (l) Zheng, G.-F.; Zhou, Z.; Zhu, G.-X.; Zhai, S.-L.; Xu, H.-Y.; Duan, X.-J.; Yi, W.; Li, X.-W. Rhodium(III)-Catalyzed Enantio- and Diastereoselective C–H Cyclopropylation of N-Phenoxylsulfonamides: Combined Experimental and Computational Studies. *Angew. Chem. Int. Ed.* **2020**, *59*, 2890–2896. (m) Huang, W.; Meng, F.-K. Cobalt-Catalyzed Diastereo- and Enantioselective Hydroalkylation of Cyclopropenes with Cobalt Homoenolates. *Angew. Chem. Int. Ed.* **2020**, *59*, 1–6. (n) Dian, L.; Marek, I. Cobalt-Catalyzed Diastereoselective and Enantioselective Hydrosilylation of Achiral Cyclopropenes. *Org. Lett*. **2020**, *22*, 4914–4918.

(11) For select ring-retentive functionalizations of cyclopropenes through carbometallation, see: (a) Cohen, Y.; Marek, I. Regio- and Diastereoselective Copper-Catalyzed Carbometallation of Cyclopropenylsilanes. *Org. Lett.* **2019**, *21*, 9162–9165. (b) Simaan, M.; Marek, I. Diastereo- and Enantioselective Preparation of Cyclopropanol and Cyclopropylamine Derivatives. Beilstein *J. Org. Chem.* **2019**, *15*, 752–760.

(12) For select ring-opening hydrofunctionalizations of cyclopropenes, see: (a) Nakamura, I.; Bajracharya, G. B.; Yamamoto, Y. Palladium-Catalyzed Hydrocarbonation and Hydroamination of 3,3-Dihexylcyclopropene with Pronucleophiles. *J. Org. Chem.* **2003**, *68*, 2297–2299. (b) Phan, D. T. H.; Dong, V. M. Silver-catalyzed ring-opening of cyclopropenes: preparation of tertiary α-branched allylic amines. *Tetrahedron,* **2013**, *69*, 5726–5731. (c) Li, Z.; Peng. G.; Zhao, J.; Zhang, Q. Catalytically Generated Allyl Cu(I) Intermediate via Cyclopropene Ring-Opening Coupling en Route to Allylphosphonates. *Org. Lett.* **2016**, *18*, 4840–4843. (d) Hadfield, M. S.; Bauer, J. T.; Glen, P. E.; Lee, A.-L. Gold(I)-catalyzed alcohol additions to cyclopropenes. *Org. Biomol. Chem*. **2010**, *8*, 4090–4095.

(13) Mudd, R. J.; Young, P. C.; Jordan-Hore, J. A.; Rosair, G. M.; Lee, A.-L. Gold(I)-Catalyzed Addition of Thiols and Thioacids to 3,3-Disustituted Cyclopropenes. *J. Org. Chem*. **2012**, *77*, 7633−7639.

(14) Gritsenko, E. I.; Butenko, G. G.; Plemenkov, V. V.; Bolesov, I. G. Synthesis of cyclopropyl sulfide and cyclopropyl sulfone derivatives by the nucleophilic addition of thiols to 3,3-disubstituted cyclopropenes. *J. Gen. Chem. USSR*. **1986**, *56*, 796–800.

(15) For select examples of ligand-controlled regiodivergence, see: (a) Wu, J. Y.; Stanzl, B. N.; Ritter, T. A Strategy for the Synthesis of Well-Defined Iron Catalysts and Application to Regioselective Diene Hydrosilylation. *J. Am. Chem. Soc*. **2010**, *132*, 13214−13216. (b) Parker, S. E.; Börgel, J.; Ritter, T. 1,2-Selective Hydrosilylation of Conjugated Dienes. *J. Am. Chem. Soc*. **2014**, *136*, 4857−4860. (c) Kennemur, J. L.; Kortman, G. D.; Hull, K. L. Rhodium-Catalyzed Regiodivergent Hydrothiolation of Allyl Amines and Imines. *J. Am. Chem. Soc.* **2016**, *138*, 11914−11919. (d) Li, Z.-Q.; Fu, Y.; Deng, R.; Tran, V. T.; Gao, Y.; Liu, P.; Engle, K. M. Ligand-Controlled Regiodivergence in Nickel-Catalyzed Hydroarylation and Hydroalkenylation of Alkenyl Carboxylic Acids. *Angew. Chem Int. Ed.*

2020, *59*, 23306–23312. (e) Debrauwer, V.; Turlik, A.; Rummler, L.; Prescimone, A.; Blanchard, N.; Houk, K. N.; Bizet, V. Ligand-Controlled Regiodivergent Palladium-Catalyzed Hydrogermylation of Ynamides. *J. Am. Chem. Soc.* **2020**, *142*, 11153–11164. (f) Wang, G.; Khan, R.; Liu, H.; Shen, G.; Yang, F.; Chen, J.; Zhou, Y.; Fan, B. Cobalt-Catalyzed Ligand-Controlled Divergent Regioselective Reactions of 1,6-Enynes with Thiols. *Organometallics* **2020**, *39*, 2037–2042.

(16) For other examples of ligand-controlled synthesis of constitutional isomers, see: (a) Park, J.-W.; Kou, K. G. M.; Kim, D. K.; Dong, V. M. Rh-catalyzed desymmetrization of α-quaternary centers by isomerization-hydroacylation. *Chem. Sci.* **2015**, *6*, 4479−4483. (b) Park, J. W.; Chen, Z.-W.; Dong, V. M. Rhodium-Catalyzed Enantioselective Cycloisomerization to Cyclohexenes Bearing Quaternary Carbon Centers. *J. Am. Chem. Soc*. **2016**, *138*, 3310−3313. (c) Santhoshkumar, R.; Mannathan, S.; Cheng, C.-H. Ligand-Controlled Divergent C–H Functionalization of Aldehydes with Enynes by Cobalt Catalysts. *J. Am. Chem. Soc*. **2015**, *137*, 16116–16120. (d) Littke, A. F.; Dai, C.; Fu, G. C. Versatile Catalysts for the Suzuki Cross-Coupling of Arylboronic Acids with Aryl and Vinyl Halides and Triflates under Mild Conditions. *J. Am. Chem. Soc*. **2000**, *122*, 4020–4028.

(17) The same bisallylaldehyde can be converted into cyclobutanones. This requires changing both the metal center and bisphosphine ligand. See: Kim, D. K.; Riedel, J.; Kim, R. S.; Dong, V. D. Cobalt catalysis for enantioselective cyclobutanone construction. *J. Am. Chem. Soc*. **2017**, *139*, 10208−10211.

(18) The absolute configuration of allylic sulfides 4 is assigned based on the optical rotation data obtained during our synthesis of (–)-agelasidine A. See reference 4d.

(19) Deposition number 2038552 for 3ba contains the supplementary crystallographic data for this paper. This data is provided free of charge by the joint Cambridge Crystallographic Data Centre and Fachinformationszentrum Karlsruhe Access Structures service www.ccdc.cam.ac.uk/structures. The absolute configurations of the remaining cyclopropyl sulfides 3 are assigned by analogy.

(20) For reviews on enantioselective construction of spiro quaternary carbon centers, see: (a) Xu, P.-W. ; Yu, J.-S.; Chen, C.; Cao, Z.-Y.; Zhou, F.; Zhou, J. Catalytic Enantioselective Construction of Spiro Quaternary Carbon Stereocenters. *ACS Catal*. **2019**, *9*, 1820–1882. (b) Rios, R. Enantioselective methodologies for the synthesis of spiro compounds. *Chem. Soc. Rev*. **2012**, *41*, 1060–1074.

(21) Some alkyl thiols (not included in this table) give mixtures of regioisomers. Isolated branched allylic thiols 4 can slowly isomerize to the achiral linear regioisomer over time. To prevent this process, the sulfides can be oxidized to the corresponding sulfones with an m-CPBA workup, see ref 4a.

(22) Wang, Y.; Huang, Z.; Leng, X.; Zhu, H.; Liu, G.; Huang, Z. Transfer Hydrogenation of Alkenes using Ethanol Catalyzed by a NCP Pincer Iridium Complex: Scope and Mechanism. *J. Am. Chem. Soc.* **2018**, *140*, 4417–4429.

(23) See Appendix 1.

(24) The mechanistic experiments do not rule out the possibility of migratory insertion of the cyclopropene into the Rh–S bond. A mechanism where there is a turnover-limiting of migratory insertion of the cyclopropene into the Rh–S bond, followed by C–H forming reductive elimination also fits the kinetic data. For examples of migratory insertions into M–S bonds, see ref 14c and: (a) Ogawa, A.; Ikeda, T.; Kimura, K.; Hirao, T. Highly Regio- and Stereocontrolled Synthesis of Vinyl Sulfides via Transition-Metal-Catalyzed Hydrothiolation of Alkynes with Thiols. *J. Am. Chem. Soc.* **1999**, *121*, 5108–5114. (b) Di Giuseppe, A.; Castarlenas, R.; Perez-Torrente, J. J.; Crucianelli, M.; Polo, V.; Sancho, R.; Lahoz, F. J.; Oro, L. A. Ligand-Controlled Regioselectivity in the Hydrothiolation of Alkynes by Rhodium N-Heterocyclic Carbene Catalysts. *J. Am. Chem. Soc.* **2012**, *134*, 8171–8183. (c) Shoai, S.; Bichler, P.; Kang, B.; Buckley, H.; Love, J. A. Catalytic Alkyne Hydrothiolation with Alkanethiols using Wilkinson's Catalyst. *Organometallics* **2007**, *26*, 5778–5781.

(25)Trost, B. M.; Thaisrivongs, D. A. Strategy for Employing Unstabilized Nucleophiles in Palladium-Catalyzed Asymmetric Allylic Alkylations. *J. Am. Chem. Soc*. **2008**, *130*, 14092–14293.

(26) Serjeant, E. P.; Dempsy, B. Ionisation Constants of Organic Acids in Aqueous Solution (IUPAC chemical data series). Pergamon: New York, 1979, p 165.
(27) For Rh and Ir catalysts forming branched allylic products, see: (a) Evans, P. A.; Leahy, D. K. Regio- and Enantiospecific Rhodium-Catalyzed Allylic Etherification Reactions Using Copper(I) Alkoxides: Influence of the Copper Halide Salt on Selectivity. *J. Am. Chem. Soc*. **2002**, *124*, 7882–7883. (b) Koschker, P.; Breit, B. Branching Out: Rhodium-Catalyzed Allylation with Alkynes and Allenes. *Acc. Chem. Res.* **2016**, *49*, 1524–1536. (c) Madrahimov, S. T.; Li, Q.; Sharma, A.; Hartwig, J. F. Origins of Regioselectivity in Iridium Catalyzed Allylic Substitution. *J. Am. Chem. Soc*. **2015**, *137*, 14968–14981.
(28) For formation of metal-π-allyl species from cyclopropyl metal complexes, see: (a) Periana, R. A.; Bergman, R. G. C–C Activation of Organic Small Ring Compounds by Rearrangement of Cycloalkylhydridorhodium Complexes to Rhodacycloalkanes. Synthesis of Metallacyclobutanes, Including One with a Tertiary M–C bond, by Nucleophilic Addition to π-Allyl Complexes. *J. Am. Chem. Soc.* **1986**, *108*, 7346–7355. (b) Periana, R. A.; Bergman, R. G. Rapid Intramolecular Rearrangement of Hydridocyclopropylrhodium Complex to a Rhodacyclobutane. Independent Synthesis of the Metallacycle by Addition of Hydride to the Central Carbon Atom of a Cationic Rhodium π-Allyl Complex. *J. Am. Chem. Soc*. **1984**, *106*, 7272–7273. (c) Philips, R. L.; Puddephatt, R. J. Some Cyclopropylplatinum Complexes. *J. Chem. Soc., Dalton Trans*. **1978**, 1732–1735. (d) Mushak, P.; Battiste, M. A. The reaction of 1,2,3-triphenylcyclopropene with palladium(II) chloride. A novel ring-opening reaction in the cyclopropene series. *J. Organometal. Chem*. **1969**, *17*, 46–48.
(29) Woodward, R. B.; Hoffman, R. Stereochemistry of Electrocyclic Reactions. *J. Am. Chem. Soc.* **1965**, *87*, 395–397.
(30) Chen, J.; Guo, W.; Xia, Y. Computational Revisit to the β-Carbon Elimination Step in Rh(III)-Catalyzed C–H Activation/Cycloaddition Reactions of N-Phenoxyacetamide and Cyclopropenes. *J. Org. Chem.* **2016**, *81*, 2635–2638.

CHAPTER 2 – Dynamic Kinetic Resolution of Aldehydes via Intermolecular Hydroacylation

2.1 Introduction

While biosynthetic pathways leverage the natural polarization of molecules, chemists can develop alternative strategies to access elusive architectures. Specifically, 1,4-dicarbonyls have inspired creative

approaches for their construction. Methods to prepare this versatile motif include oxidative enolate cross-couplings[1] and umpolung transformations via enolates,[2,3] acyl radicals,[4–6] or acyl anions[7–9] (Figure 2.1A). Despite significant progress in asymmetric variants,[10–14] an opportunity exists to provide complementary patterns via stereoconvergent catalysis.[15–17] Dynamic kinetic resolutions (DKR) and dynamic kinetic asymmetric transformations (DyKAT) have proven efficiency in accessing pharmaceuticals.[18–21] The full potential of these catalytic approaches remains untapped in umpolung transformations. Motivated by this gap, we imagined transforming racemic aldehydes into enantioenriched 1,4-dicarbonyl motifs through a hydroacylation featuring DKR. If successful, this intermolecular C–C bond formation reaction would construct relatively remote (1,4-stereogenic) centers in a single operation.

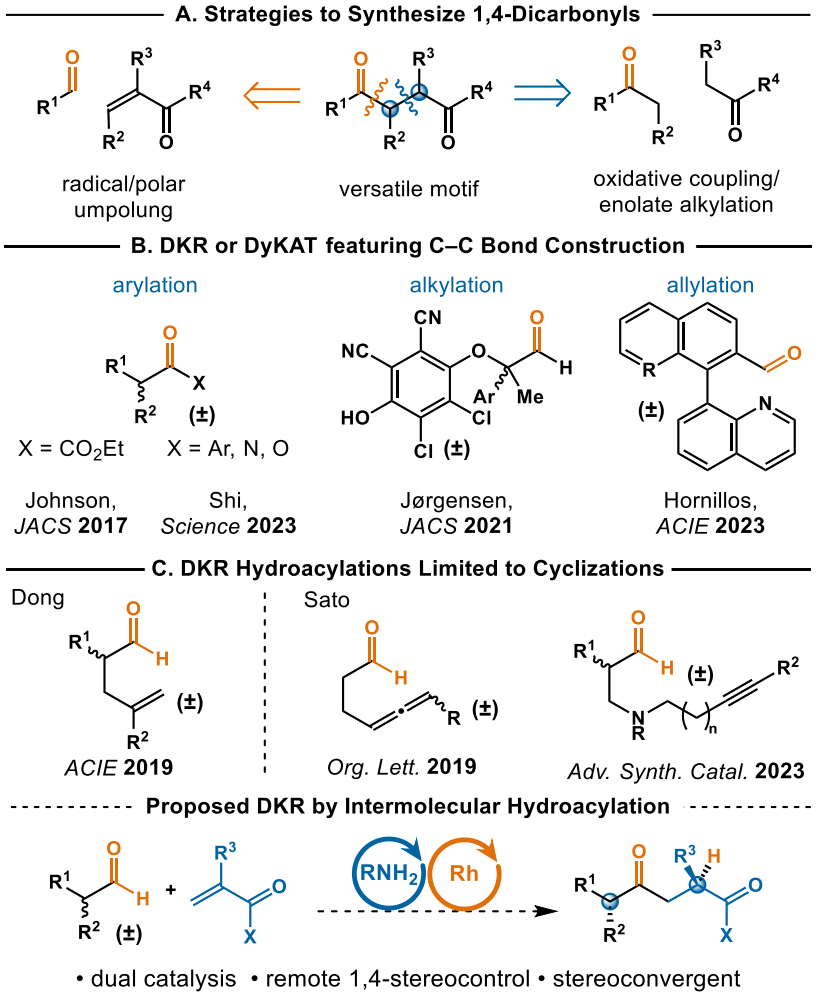

Figure 2.1 A. Creative strategies to 1,4-dicarbonyls. B. Stereoconvergent catalysis to construct carbonyl α-stereocenters through C–C bond formations. C. State-of-the-art in DKR hydroacylation.

Compared to hydrogenations[22–25] or alcohol acylations,[26–29] DKR's that feature C–C bond construction are less explored.[30–34] Exciting breakthroughs in the DKR or DyKAT of ketoesters, ketones and aldehydes have been achieved via arylations, vinylations, alkylations and aldol reactions (Figure 2.1B).[35–39] Transition-metal catalyzed hydroacylation[40–42] represents an attractive method to make ketones and esters through aldehyde C–H bond activation and functionalization.[43] In 2008, Willis and co-workers disclosed a DyKAT via an intermolecular hydroacylation with sulfur-directed aldehydes and racemic allenes.[44] Our lab developed a DKR of racemic aldehydes by intramolecular hydroacylation in 2019.[45] With α,ɣ-disubstituted cyclopentanones prepared, we proposed that the amine-catalyst facilitated epimerization while the Rh-catalyst activated the aldehyde. Since then, the Sato group has reported intramolecular hydroacylations with allenals[46] and alkynes.[47] While promising, these approaches have been limited to intramolecular variants to make cyclic ketones (Figure 2.1C).

Through the use of chelating substrates and an appropriate catalyst, intermolecular hydroacylations that overcome competitive decarbonylation[41,48] have been achieved. The additional coordinating group (e.g., phenol, sulfide, or ether) potentially blocks open coordination sites required for decarbonylation while promoting hydroacylation by decreasing the entropic cost through chelation.[40] We chose Tanaka's intermolecular hydroacylation of acrylamides (**2a**) using achiral, aliphatic aldehydes[49] as an attractive platform for proof-of-concept. Achieving a DKR variant would allow the resolution of chiral, α-substituted aldehydes and generate 1,4-ketoamides with the concomitant formation of 1,4-stereogenic centers. Thus, we set out to develop a dual catalytic system[50–54] using Rh and amine that would (1) allow fast epimerization of the aldehyde reagents in preference to the ketone products, (2) enable high enantio- and diastereoselectivity, and (3) disfavor the formation of Rh-amine adduct and deactivation of the Rh-catalyst.[55]

2.2 Results and Discussion

Our model system focused on the addition of racemic α-branched aldehyde **1a** to acrylamide **2a** (Table 2.1). We first evaluated cationic Rh catalysts on the basis of Tanaka's report[49] and identified a promising catalyst generated by hydrogenation of $Rh(nbd)_2BF_4$. The achiral bisphosphine ligand, dppb (**L1**), provided ketoamide **3aa** in 67% yield and 2:1 *dr* (entry 1) at 80 °C, suggesting an inherent diastereoselectivity of this hydroacylation. In our previous DKR, [45] bulky 1-adamantylamine ($1\text{-}AdNH_2$) was key to both diastereo- and enantiocontrol, presumably facilitating chemoselective racemization of the aldehyde starting material over the ketone product.

Table 2.1 Optimization for DKR via intermolecular hydroacylation

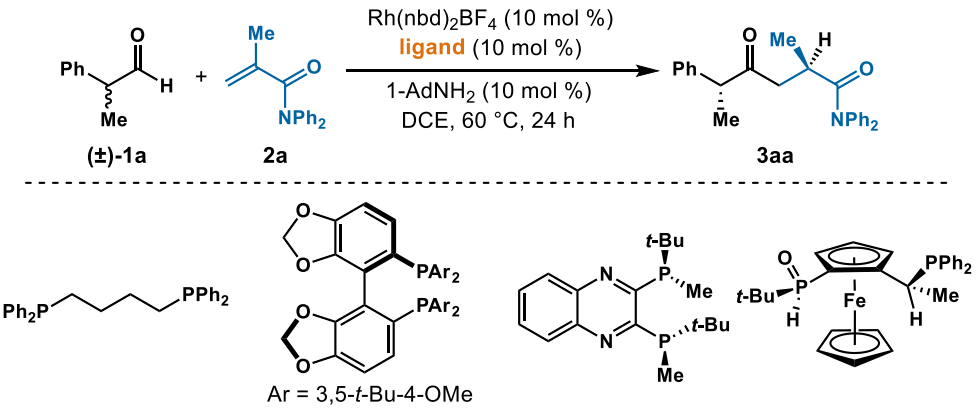

entry	ligand	deviation	yield (%)[b]	*dr*[c]	*ee* (%)[d]
1	**L1**	no $1\text{-}AdNH_2$, 80 °C	67	2:1	-
2	**L2**	none	n.r.	-	-
3	**L3**	80 °C	37	6:1	98
4	**L4**	no $1\text{-}AdNH_2$	70	4:1	99
5	**L4**	2,6-diethylaniline instead of $1\text{-}AdNH_2$	66	6:1	99
6	**L4**	diphenylmethanamine instead of $1\text{-}AdNH_2$	53	7:1	>99
7	**L4**	40 °C	42	14:1	>99
8	**L4**	none	92	12:1	>99

[a] Reaction conditions: **1a** (0.3 mmol, 1.5 equiv), **2a** (0.2 mmol, 1.0 equiv), $Rh(nbd)_2BF_4$ (10 mol %), ligand (10 mol %), amine (10 mol %), DCE (0.4 mL). [b] Isolated yields. [c] Diastereoselectivities (*dr*) were determined by ^1H NMR analysis of unpurified reaction mixture. [c] Enantioselectivities (*ee*) were determined by chiral SFC analysis.

We reason that these dual catalysts act as a "frustrated lewis pair"[55] because the steric bulk of the amine co-catalyst hinders the coordination to the Rh-catalyst. To develop an asymmetric version, we examined chiral bisphosphine ligands with 1-AdNH_2 as the co-catalyst. The (*R*)-DTBM-SegPhos ligand (**L2**) was effective for the intramolecular hydroacylation of alkyl aldehydes;[45] however, it showed no reactivity in the proposed intermolecular hydroacylation (entry 2). The (*R,R*)-QuinoxP* ligand (**L3**), reported by the Tanaka group,[49] was unsuccessful at 60 °C, but at an elevated temperature (80 °C) furnished **3aa** in 37% yield and 6:1 *dr* (entry 3). After a more comprehensive ligand survey, we discovered that JoSPOphos (**L4**) gave **3aa** in 92% yield and >99% *ee*, and enhanced *dr* (12:1) (entry 8). Omitting the amine led to a decreased *dr* (4:1) (entry 4). Other bulky amines were investigated and resulted in diminished yields and diastereoselectivities (entry 5-6). At lower temperatures, we observed 42% yield with 14:1 *dr* (entry 7). The absolute configuration of the 1,4-stereocenters for **3aa** was established as (*R, R*) by X-ray crystallography (see appendix 2).

With a protocol in hand, we examined aldehydes **1** bearing different α-aryl substituents (Table 2.2). Aldehydes with para-substituted methoxy and halogens underwent DKR smoothly; ketoamides **3ba**–**3da** can be prepared with moderate to high yields (65–94%) and stereoselectivites (10:1–13:1 *dr*, >99% *ee*). In addition, a strong electron-withdrawing trifluoromethyl substituted α-aryl aldehyde was tolerated (**3ea**, 93% yield, 11:1 *dr*, >99% *ee*). Both electron-donating and -withdrawing groups could be incorporated at the meta-position to provide ketoamides **3fa** (78% yield, 10:1 *dr*, >99% *ee*) and **3ga** (92% yield, 11:1 *dr*, >99% *ee*). The introduction of a sterically hindered ortho-methyl substituent led to a drop in both reactivity (39% yield) and stereocontrol (5:1 *dr*, 97% *ee*) in forming ketoamide **3ha**. Ketoamides **3ia** bearing a napthyl group (86% yield, 13:1 *dr*, >99% *ee*) and **3ja** with an acetal moiety (82% yield, 8:1 *dr*, >99% *ee*) were both accessible. Additional steric bulk at the alkyl substitution or removal of the aromatic substitution was not tolerated, as no reactivity was observed when using an α-isopropyl-substituted

aldehyde **1k** or an α, α-dialkyl aldehyde **1l**. Overall, these results showcase the first DKR's of aldehydes by intermolecular hydroacylation with excellent stereocontrol.

Table 2.2 Hydroacylation aldehye scope

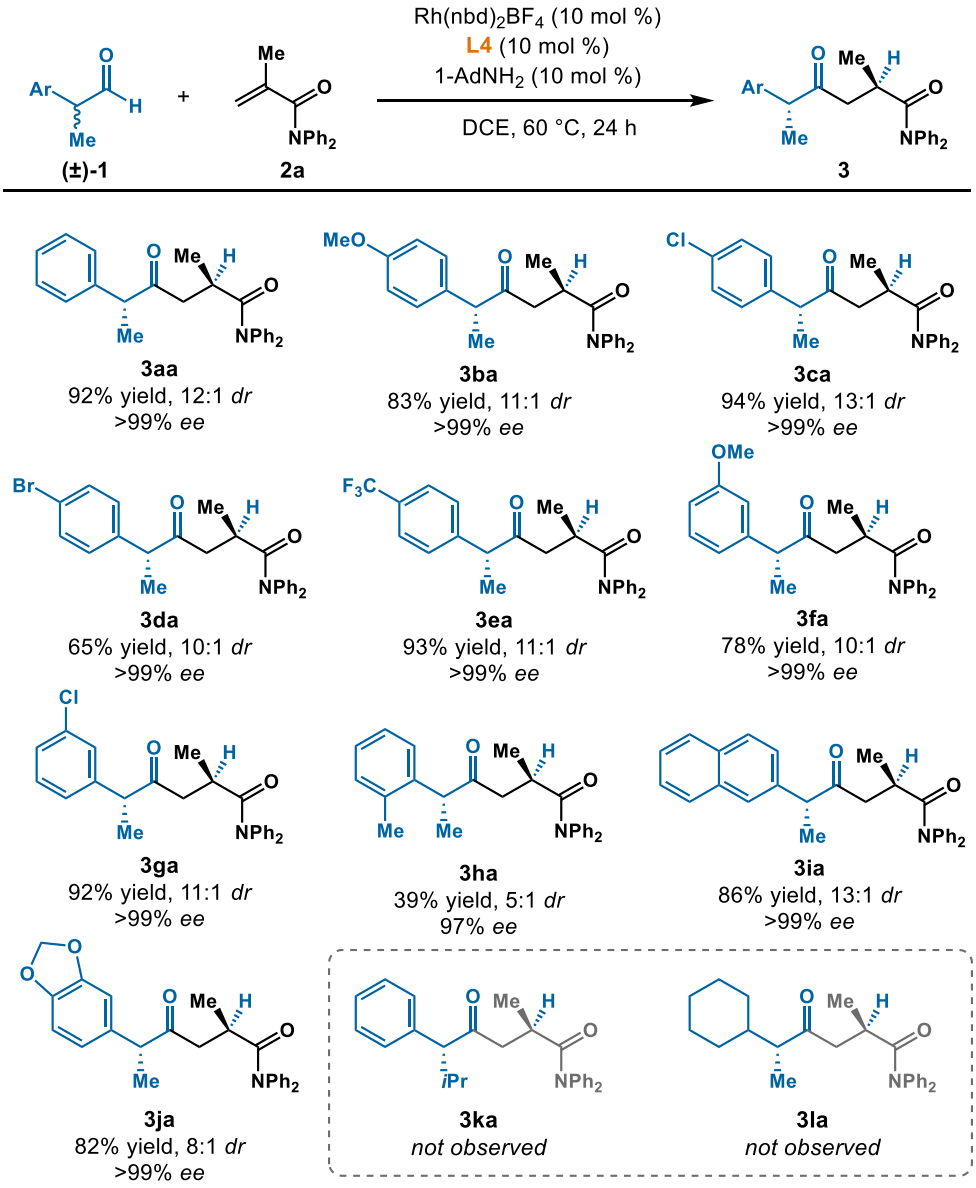

[a] Reaction conditions: **1a** (0.3 mmol, 1.5 equiv), **2a** (0.2 mmol, 1.0 equiv), $Rh(nbd)_2BF_4$ (10 mol %), **L4** (10 mol %), 1-$AdNH_2$ (10 mol %), DCE (0.4 mL). Diastereoselectivities (*dr*) were determined by ^1H NMR analysis of unpurified reaction mixture. Enantioselectivities (*ee*) were determined by chiral SFC analysis.

Next, we investigated the acrylamide scope (Table 2.3). The 1,1-disubstituted acrylamides gave ketoamides **3ab** (83% yield, 9:1 *dr*, >99% *ee*) and **3ac** (91% yield, 9:1 *dr*, >99% *ee*). An unsubstituted acrylamide **2d** provided **3ad** (45% yield, 79% *ee*). The diminished yield is presumably due to competitive

polymerization.[56,57] In place of Tanaka's diphenyl acrylamide substrate,[49] we prepared acrylamides derived from morpholine (**2e**), *N*,*N*-dibenzylamine (**2f**) and aniline (**2g**). While **3ae** was produced with 11:1 *dr*, selectivities for the less sterically hindered substrates were considerably lower (**3af** and **3ag**, 8:1 and 6:1 *dr*). The Weinreb amide **3ah** was prepared (65% yield, 9:1 *dr*, >99% *ee*). This amide provides a convenient handle for further elaboration.[58]

Table 2.3 Hydroacylation acrylamide scope

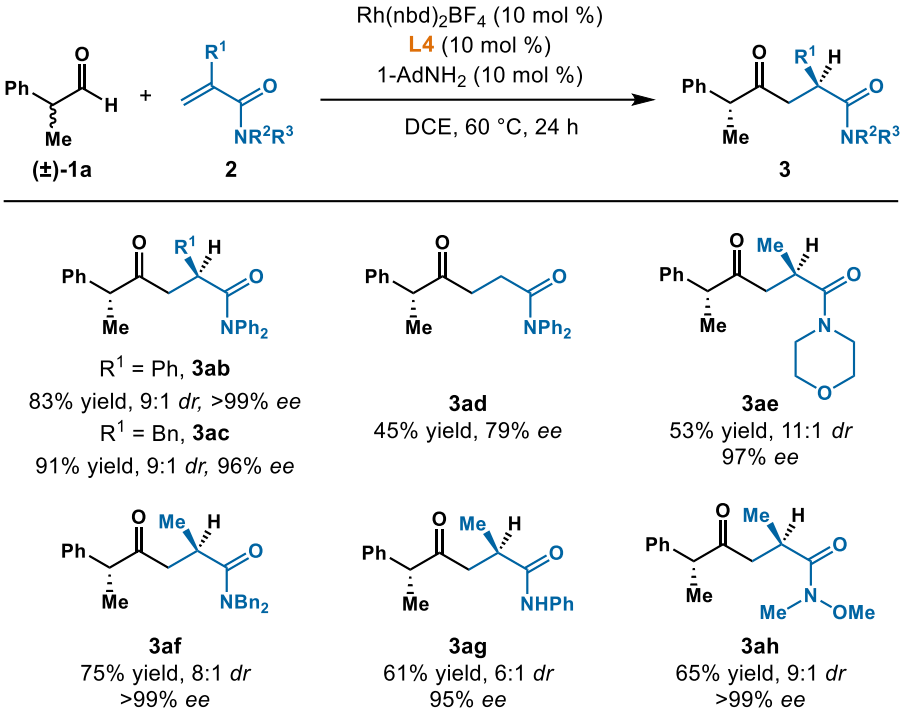

[a] Reaction conditions: **1a** (0.3 mmol, 1.5 equiv), **2a** (0.2 mmol, 1.0 equiv), $Rh(nbd)_2BF_4$ (10 mol %), **L4** (10 mol %), 1-$AdNH_2$ (10 mol %), DCE (0.4 mL). Diastereoselectivities (*dr*) were determined by ^1H NMR analysis of unpurified reaction mixture. Enantioselectivities (*ee*) were determined by chiral SFC analysis.

To inspect the tolerance of different heterocycles in this DKR, we conducted a compatibility test[59] using the model reaction (Table 2.4). Reactivities and enantioselectivities were not significantly affected by addition of pyrrole (93% yield, 99% *ee*) or thiophene (96% yield, 99% *ee*), but the diastereocontrol was less effective (both 8:1 *dr*). Furan decreased the yield (42%), but stereoselectivity was maintained (10:1 *dr*, >99% *ee*). Pyridine completely inhibited the reactivity,

Table 2.4 Examining functional group compatibility

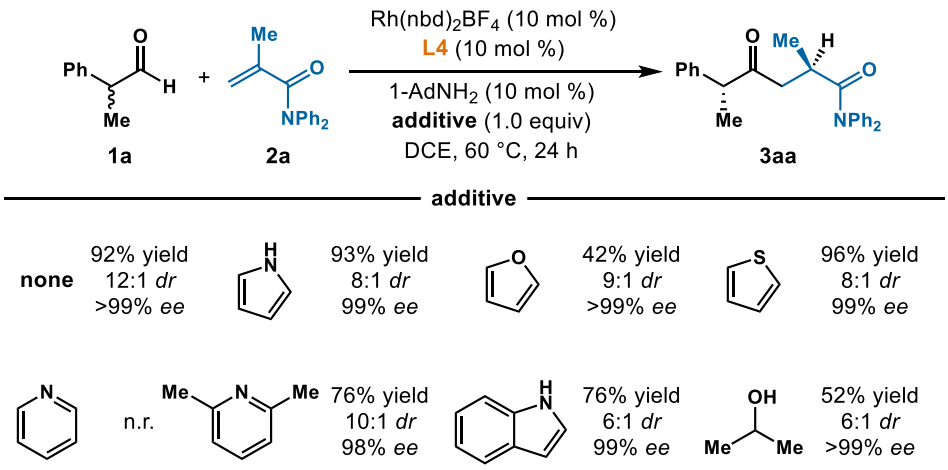

[a] Reaction conditions: **1a** (0.3 mmol, 1.5 equiv), **2a** (0.2 mmol, 1.0 equiv), $Rh(nbd)_2BF_4$ (10 mol %), **L4** (10 mol%), 1-$AdNH_2$ (10 mol %), additive (0.2 mmol, 1.0 equiv), DCE (0.4 mL). Diastereoselectivities (*dr*) were determined by ^1H NMR analysis of unpurified reaction mixture. Enantioselectivities (*ee*) were determined by chiral SFC analysis.

presumably due to strong binding to the Rh catalyst. The presence of sterically hindered 2,6-lutidine was tolerated; **3aa** was isolated in 76% yield with comparable *dr* (10:1). Compared to other heterocycles, indole had the biggest impact on lowering diastereoselectivity (6:1 *dr*). The use of isopropanol led to a lower yield (52%), as the aldehyde **1a** was consumed by a competitive pathway (based on nuclear magnetic resonance (NMR) spectroscopy of the unpurified mixture). \

2.3 Mechanistic Studies

On the basis of literature precedence[40,42] and our own observations, we propose the following catalytic cycle for the formation of the major diastereomer (2*R*,5*R*)-**3** (Figure 2.2). The active Rh catalyst **I** is formed upon coordination of **L4** to the precatalyst. Acrylamide **2** chelates to complex **I**. Then, oxidative addition of **II** to the C–H bond of aldehyde **1** generates Rh complex **III**, which is coordinatively saturated and less likely to undergo undesired decarbonylation. The

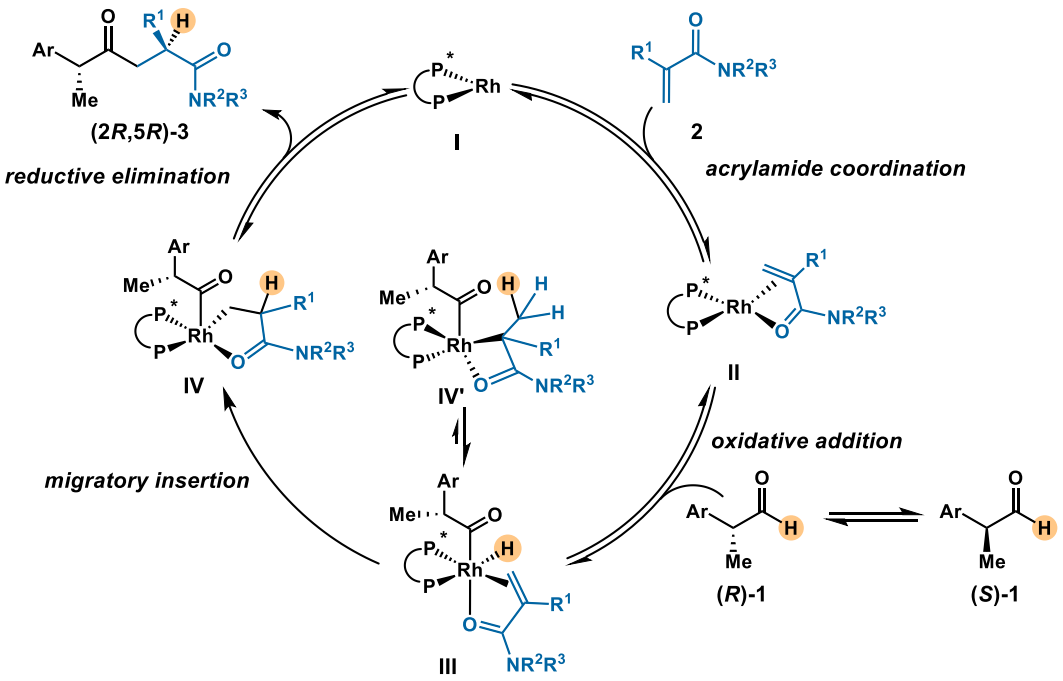

Figure 2.2 Proposed hydroacylation mechanism

aldehyde undergoes rapid isomerization; the matched enantiomer, (*R*)-**1**, reacts faster in hydroacylation leading to the observed configuration of the ketone's a-chiral center. Subsequent migratory insertion gives the hydrorhodation product **IV**, where the facial selectivity determines the amide stereocenter configuration. Finally, reductive elimination releases (2*R*,5*R*)-**3** and regenerate the catalyst. Because the epimerization of **3** with the bulky 1-AdNH_2 is highly unfavorable, high diastereoselectivity can be preserved.

While the general mechanism of hydroacylation has been investigated, the turnover-limiting step depends on the substrate and catalyst. To probe mechanistic detail for our transformation, we performed deuterium labeling and kinetic isotope effect (KIE) studies. With deuterated aldehyde ***d*-1a**, ketoamide ***d*-3aa** was formed in 83% yield under standard conditions (Figure 2.3A). Analysis of ***d*-3aa** using deuterium NMR spectroscopy revealed an incorporation at the α-position of the amide, as well as 14% deuterium incorporation at the cis β-position. In addition, NMR analysis of the unpurified reaction mixture confirmed H/D exchange and deuterium

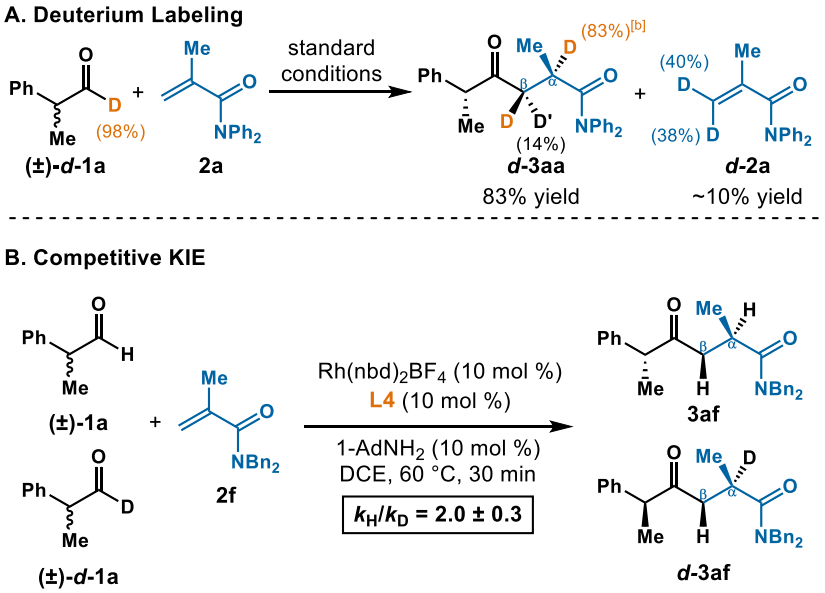

Figure 2.3 Isotopic labeling and KIE experiments. Reaction conditions: 1a (0.15 mmol, 0.75 equiv), d-1a (0.15 mmol, 0.75 equiv), 2a (0.2 mmol, 1.0 equiv), Rh(nbd)2BF4 (10 mol %), L4 (10 mol %), 1-AdNH2 (10 mol %), DCE (0.4 mL). [a] Isolated yields. [b] Due to the overlap of α-proton and the trans β-proton, 83% represents the total percent of deuterium incorporation of both positions (orange); 14% refers to the percent of deuterium incorporation of the cis α-position (black).

scrambling of unreacted ***d*-1a** at the α-position, indicating that oxidative addition is reversible. Deuterium incorporation into the residual acrylamide **2a** was also observed. Although ***d*-1a** was not isolable, 39% deuterium incorporation at the terminal position of the olefin was found in recovered ***d*-2a**. The result suggests a competing pathway where Rh inserts to the more hindered internal site, forming a four-membered intermediate **IV'** (Figure 2.2)**.** Reversible β-hydride elimination leads to **III** and aldehyde hydride could be exchanged to the acrylamide **2**. The deuterium incorporation of both protons could be explained by the geminal proton scrambling in hydroacylation or the reversibility of migratory insertion to **IV'**. We therefore conclude that acrylamide coordination and oxidative addition are not turnover-limiting.

Competitive KIE experiments using a 1:1 mixture of **1a** and ***d*-1a** were conducted to further elucidate probe the turnover-limiting step (Figure 2.3B). A primary k_H/k_D of 2.0 $\pm$ 0.3 suggests that C–H bond cleavage is involved in the turnover-limiting step for the aldehyde.[60] Given the reversibility of

oxidative addition based on deuterium labeling results, we propose that migratory insertion to **IV** is turnover-limiting.

Although the isomerization of **1a** with primary amines has been studied,[61] the role of Rh on this racemization had yet to be explored. As shown in figure 2.4, we examined the transformation in the absence of 1-$AdNH_2$. In these experiments, we recovered unreacted **1a** at

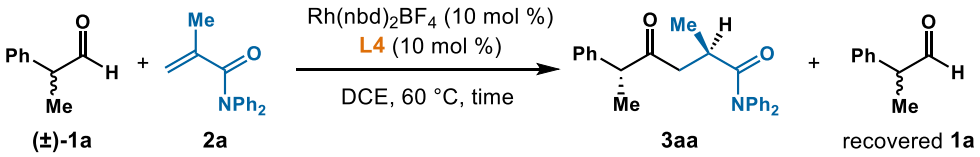

entry	time	deviation	yield (%)[b]	*dr*[b]	theoretical *ee* of 1a for KR (%)[c]	observed 1a *ee* (%)[d]
1	5 min	none	24	9:1	15	12
2	1 h	none	70	8:1	68	38
3	4 h	none	96	3.5:1	>99	42
4	1 h	with 1-$AdNH_2$[a]	53	10:1	82	14

Figure 2.4 Racemization studies. Reaction conditions: **1a** (0.3 mmol, 1.5 equiv), **2a** (0.2 mmol, 1.0 equiv), $Rh(nbd)_2BF_4$ (10 mol %), **L4** (10 mol %), DCE (0.4 mL). [a] 10 mol %. [b] Yields and diastereoselectivities of **3aa** were determined by ^1H NMR analysis of a portion of unpurified reaction mixture using 1,3,5-trimethoxybenzne an internal standard. The other portion of reaction mixtures was quenched using $NaBH_4$ (>20 equiv) in MeOH. [c] Theoretical *ee* of recovered **1a** for kinetic resolution was calculated based on equivalence of **1a** and yields and *dr* of **3aa** assuming there was no racemization on a highly selective transformation. [d] **1a** was recovered as the alcohol for determination of enantiomeric excess (*ee*), which was performed by SFC analysis on a chiral stationary phase.

various time points and measured their *ee*. This observed value was compared to the expected *ee* of the aldehyde, in a theoretical case where there was no aldehyde racemization occurring (in other words, a simple and not dynamic kinetic resolution). When the experiment was quenched at 5 min (by addition of $NaBH_4$ to reduce the aldehyde), minimal racemization of the starting aldehyde **1a** was observed (observed 12% *ee*, vs. expected 15% *ee*, entry 1). At the 1 h time point, aldehyde **1a** was recovered in 38% *ee* (expected 68% *ee*, entry 2). At 4 h, ketoamide **3aa** was formed in 96% NMR yield with 4:1 *dr*. In a kinetic resolution, this result would indicate a depletion of the matched enantiomer. However, instead of a highly

enantioenriched **1a** (>99% *ee*), we recovered **1a** in 42% *ee* (entry 3). These results indicated that isomerization of the aldehyde occurs with Rh, in the absence of the amine co-catalyst. This conclusion was further supported by an observed decrease in *ee* of enantioenriched **1a** when subjected to active Rh catalyst without acrylamide. Throughout the hydroacylation, (*S*)-**1a** became the major recovered enantiomer, which aligned with the proposal that (*R*)-**1a** is the matched substrate.

Various possible mechanisms for the racemization of **1a** were explored using density functional theory (DFT) calculations performed at B3LYP-D3/6-311+G** LANL2DZ (Rh, Fe) PCM (DCE) // B3LYP-D3/6-31G* LANL2DZ (Rh, Fe) level of theory,[62,63] as implemented in Gaussian 16. We modeled the deprotonation of the Lewis acid (Rh) activated **1a**[64,65] by 1-AdNH$_2$ to form the Rh-bound enolate as a pathway for racemization. (Figure 2.5, Pathway A). Alternatively, Rh could also racemize **1a** through a β-hydride elimination pathway (Figure 2.5, Pathway B), similar to the mechanism recently proposed by Shi for the Ni-catalyzed epimerization of α-substituted ketones.[36] Rh has also been implicated in the epimerization of aminophosphine ligands.[66] In a previous study, we demonstrated that Rh can play a dual role in racemization and asymmetric hydrogenation in the DyKAT of chiral sulfoxides.[67]

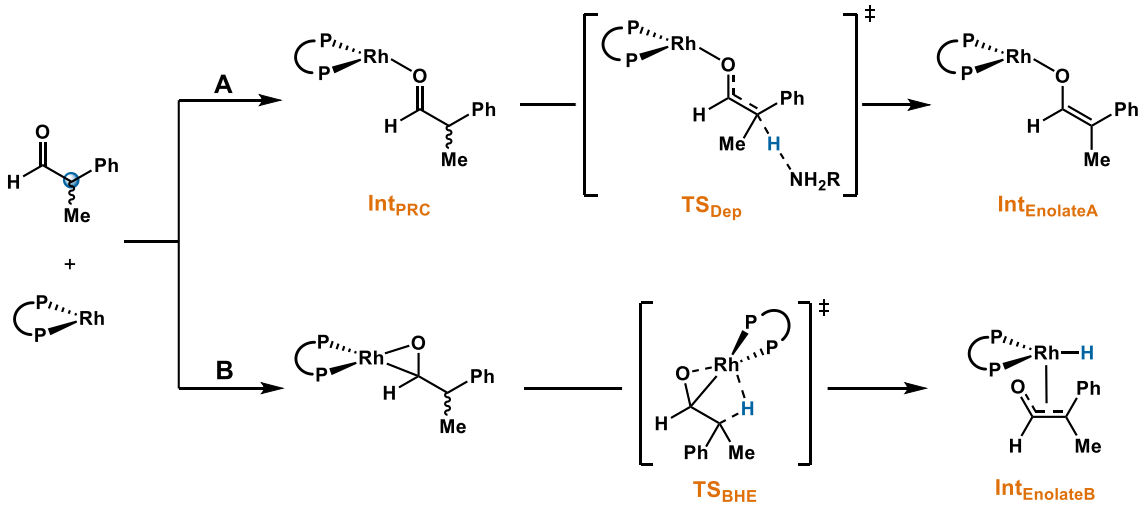

Figure 2.5 Proposed mechanisms for Rh-catalyzed epimerization of **1a**

The potential energy surface (PES) (Figure 2.6) follows the Curtin-Hammett principle; the equilibration of starting material enantiomers (*R*)-**1a** and (*S*)-**1a** through racemization pathways described

(*vide supra*) are lower in energy relative to the likely turnover-limiting migratory insertion step in the catalytic cycle (Figure 2.6, **$TS_{MI\text{-}R}$** leads to the major enantiomer of product and **$TI_{MI\text{-}S}$** leads to the minor enantiomer). The calculated PES aligns with the experimentally observed racemization of recovered aldehyde (Figure 2.4, **1a**), consistent with a dynamic kinetic resolution (i.e. the rate of racemization > rate of product formation).

Transition state structures (TSs) for the racemization proceeding through Pathway A, for the deprotonation of the Lewis acid Rh complex via external base (1-$AdNH_2$) are lowest in energy and lie 13.2 (**TS_{DepR}**) and 13.7 (**TS_{DepS}**) kcal/mol above the stable Rh bound enolate intermediate **$Int_{EnolateA}$** (which was arbitrarily standardized to 0.0 kcal/mol). The TSs calculated for the alternative β-hydride elimination mechanism (Pathway B) are **$TS_{BHE\text{-}S}$** and **$TS_{BHE\text{-}S}$**, which are 14.4 and 16.3 kcal/mol, respectively, above **$Int_{EnolateA}$**. We also calculated transition structures for the racemization pathways involving p-coordinated acrylamide (**2a**) which are slightly higher in energy for both Pathways A and B, due to the more sterically hindered catalyst environment. Importantly, the calculated racemization pathways proceeding through *both base deprotonation and β-hydride elimination mechanisms are accessible* with respect to migratory insertion, consistent with the racemization of starting material aldehyde (**1a**) via several operative pathways prior to entering the catalytic cycle.

While there is an unexpected pathway for racemization involving Rh alone, the addition of 1-AdNH$_2$ has a strong influence on the diastereocontrol. At 1 h, there was an increase in diastereoselectivity for the generation of ketoamide **3aa** in comparison to the experiment performed without amine co-catalyst (10:1 vs. 8:1) and a decrease in enantioenrichment of recovered **1a** (14% *ee* vs. 38% *ee*) (entry 4).

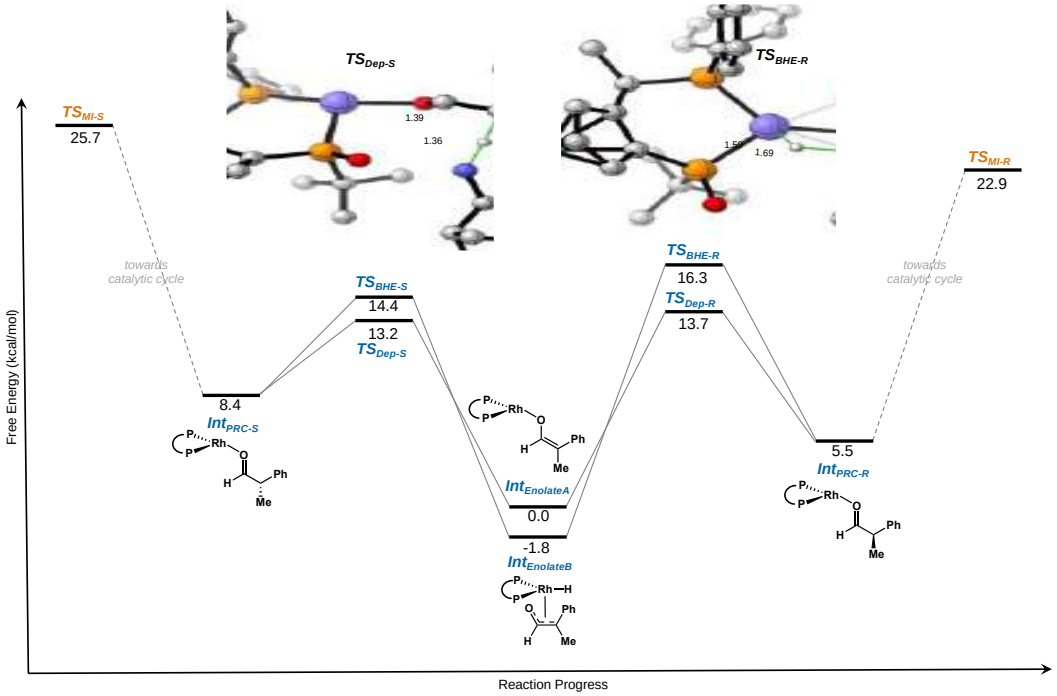

Figure 2.6 Free energy surface comparing the potential racemization pathways of (R)-1a and (S)-1a. Key transition state structures for deprotonation by 1-ADNH2 (TSDep-S) and β-hydride elimination by Rh (TSBHE-S) are highlighted. DFT calculations were performed at B3LYP-D3/6-311+G** LANL2DZ (Rh, Fe) PCM (DCE) // B3LYP-D3/6-31G* LANL2DZ (Rh, Fe) level of theory.

The amine can act as a simple base in the racemization; however, we observed enamine formation (when **1a** is treated with 1-AdNH$_2$) by NMR spectroscopy which suggests a condensation mechanism (Figure 2.6). The *E*-enamine was generated using a catalytic amount of 1-AdNH$_2$ and it is the thermodynamically more favorable isomer on the basis of steric strain. The hydroacylation proceeded less efficiently with the addition of amine (Figure 2.4, 53% vs. 70% NMR yield at 1h); this difference may be due to Rh-amine coordination or the presence of water generated by imine condensation. Thus, the amine

could play multiple roles in enhancing the *relative rate* of racemization over hydroacylation, a key parameter for high selectivity in DKR's.

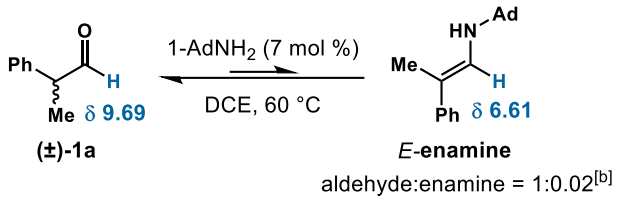

Figure 2.7 Enamine formation studies. [a] Reaction conditions: 1a (0.15 mmol, 1.0 equiv), 1-AdNH2 (7 mol % or 1.0 equiv), DCE (0.2 mL). [b] Ratio determined by 1H NMR analysis of a portion of unpurified reaction mixture. With 1.0 equiv of 1-AdNH2, aldehyde: enamine = 1:1.7.

2.4 Conclusion

In summary, we have developed a DKR using intermolecular hydroacylation by leveraging the chemoselective racemization of an aldehyde starting material over the ketone product with a bulky 1-$AdNH_2$ co-catalyst. Various ketoamides can be obtained with high control for remote 1,4-stereocenters. Mechanistic studies point to racemization pathways involving both Rh and amine. While this initial study was limited in scope to acrylamides, we expect these insights and strategies described will aid in the 44development of future DKR's that feature C–C bond construction.

2.5 Author Contributions

Alexander Lu (A.L.) and Professor Vy M. Dong (V.M.D.) conceived of the project idea discussed in Chapter 2. A.L., E.L.K, and J.M.W. identified the optimal conditions for the transformation. E.L.K explored alternative catalyst syntheses and reaction robustness. J.M.W. and M.X. explored the scope of transformation. E.L.K synthesized acrylamide **2h**. M.X. explored the mechanistic insights. Jennifer Hirschi (J.H.) and Stephanie A. Corio (S.A.C.) completed the computational studies. All authors analyzed the experimental results, contributed to the supporting information, and edited the manuscript.

2.6 References

(1) DeMartino, M. P.; Chen, K.; Baran, P. S. Intermolecular Enolate Heterocoupling: Scope, Mechanism, and Application. *J. Am. Chem. Soc.* **2008**, *130* (34), 11546–11560. https://doi.org/10.1021/ja804159y.

(2) Yasuda, M.; Tsuji, S.; Shigeyoshi, Y.; Baba, A. Cross-Coupling Reaction of α-Chloroketones and Organotin Enolates Catalyzed by Zinc Halides for Synthesis of γ-Diketones. *J. Am. Chem. Soc.* **2002**, *124* (25), 7440–7447. https://doi.org/10.1021/ja0258172.

(3) Chan, C.-K.; Chan, Y.-L.; Tsai, Y.-L.; Chang, M.-Y. One-Pot Synthesis of 2-Cyano-1,4-Diketones: Applications to Synthesis of Cyanosubstituted Furans, Pyrroles, and Dihydropyridazines. *J. Org. Chem.* **2016**, *81* (17), 8112–8120. https://doi.org/10.1021/acs.joc.6b01672.

(4) Banerjee, A.; Lei, Z.; Ngai, M.-Y. Acyl Radical Chemistry via Visible-Light Photoredox Catalysis. *Synthesis* **2019**, *51* (02), 303–333. https://doi.org/10.1055/s-0037-1610329.

(5) Li, S.; Shu, H.; Wang, S.; Yang, W.; Tang, F.; Li, X.-X.; Fan, S.; Feng, Y.-S. Cooperative NHC and Photoredox Catalysis for the Synthesis of 1,4-Dicarbonyl Compounds via Diacylation of Alkenes. *Org. Lett.* **2022**, *24* (31), 5710–5714. https://doi.org/10.1021/acs.orglett.2c02108.

(6) Liu, Y.-L.; Ouyang, Y.-J.; Zheng, H.; Liu, H.; Wei, W.-T. Recent Advances in Acyl Radical Enabled Reactions between Aldehydes and Alkenes. *Chem. Commun.* **2021**, *57* (50), 6111–6120. https://doi.org/10.1039/D1CC02112E.

(7) Heravi, M. M.; Zadsirjan, V.; Kafshdarzadeh, K.; Amiri, Z. Recent Advances in Stetter Reaction and Related Chemistry: An Update. *Asian J. Org. Chem.* **2020**, *9* (12), 1999–2034. https://doi.org/10.1002/ajoc.202000378.

(8) Murry, J. A.; Frantz, D. E.; Soheili, A.; Tillyer, R.; Grabowski, E. J. J.; Reider, P. J. Synthesis of α-Amido Ketones via Organic Catalysis: Thiazolium-Catalyzed Cross-Coupling of Aldehydes with Acylimines. *J. Am. Chem. Soc.* **2001**, *123* (39), 9696–9697. https://doi.org/10.1021/ja0165943.

(9) Myers, M. C.; Bharadwaj, A. R.; Milgram, B. C.; Scheidt, K. A. Catalytic Conjugate Additions of Carbonyl Anions under Neutral Aqueous Conditions. *J. Am. Chem. Soc.* **2005**, *127* (42), 14675–14680. https://doi.org/10.1021/ja0520161.

(10) Lemmerer, M.; Schupp, M.; Kaiser, D.; Maulide, N. Synthetic Approaches to 1,4-Dicarbonyl Compounds. *Nat. Synth.* **2022**, *1* (12), 923–935. https://doi.org/10.1038/s44160-022-00179-1.

(11) Baran, P. S.; DeMartino, M. P. Intermolecular Oxidative Enolate Heterocoupling. *Angew. Chem. Int. Ed.* **2006**, *45* (42), 7083–7086. https://doi.org/10.1002/anie.200603024.

(12) Robinson, E. E.; Thomson, R. J. A Strategy for the Convergent and Stereoselective Assembly of Polycyclic Molecules. *J. Am. Chem. Soc.* **2018**, *140* (5), 1956–1965. https://doi.org/10.1021/jacs.7b13234.

(13) Wurz, N. E.; Daniliuc, C. G.; Glorius, F. Highly Enantioselective Intermolecular Stetter Reaction of Simple Acrylates: Synthesis of α-Chiral γ-Ketoesters. *Chem. – Eur. J.* **2012**, *18* (51), 16297–16301. https://doi.org/10.1002/chem.201202432.

(14) De Alaniz, J. R.; Kerr, M. S.; Moore, J. L.; Rovis, T. Scope of the Asymmetric Intramolecular Stetter Reaction Catalyzed by Chiral Nucleophilic Triazolinylidene Carbenes. *J. Org. Chem.* **2008**, *73* (6), 2033–2040. https://doi.org/10.1021/jo702313f.

(15) Bhat, V.; Welin, E. R.; Guo, X.; Stoltz, B. M. Advances in Stereoconvergent Catalysis from 2005 to 2015: Transition-Metal-Mediated Stereoablative Reactions, Dynamic Kinetic Resolutions, and Dynamic Kinetic Asymmetric Transformations. *Chem. Rev.* **2017**, *117* (5), 4528–4561. https://doi.org/10.1021/acs.chemrev.6b00731.

(16) Yang, L.-C.; Deng, H.; Renata, H. Recent Progress and Developments in Chemoenzymatic and Biocatalytic Dynamic Kinetic Resolution. *Org. Process Res. Dev.* **2022**, *26* (7), 1925–1943. https://doi.org/10.1021/acs.oprd.1c00463.

(17) Verho, O.; Bäckvall, J.-E. Chemoenzymatic Dynamic Kinetic Resolution: A Powerful Tool for the

Preparation of Enantiomerically Pure Alcohols and Amines. *J. Am. Chem. Soc.* **2015**, *137* (12), 3996–4009. https://doi.org/10.1021/jacs.5b01031.

(18) Chen, C.; Frey, L. F.; Shultz, S.; Wallace, D. J.; Marcantonio, K.; Payack, J. F.; Vazquez, E.; Springfield, S. A.; Zhou, G.; Liu, P.; Kieczykowski, G. R.; Chen, A. M.; Phenix, B. D.; Singh, U.; Strine, J.; Izzo, B.; Krska, S. W. Catalytic, Enantioselective Synthesis of Taranabant, a Novel, Acyclic Cannabinoid-1 Receptor Inverse Agonist for the Treatment of Obesity. *Org. Process Res. Dev.* **2007**, *11* (3), 616–623. https://doi.org/10.1021/op700026n.

(19) Rew, Y.; Sun, D.; Yan, X.; Beck, H. P.; Canon, J.; Chen, A.; Duquette, J.; Eksterowicz, J.; Fox, B. M.; Fu, J.; Gonzalez, A. Z.; Houze, J.; Huang, X.; Jiang, M.; Jin, L.; Li, Y.; Li, Z.; Ling, Y.; Lo, M.-C.; Long, A. M.; McGee, L. R.; McIntosh, J.; Oliner, J. D.; Osgood, T.; Saiki, A. Y.; Shaffer, P.; Wang, Y. C.; Wortman, S.; Yakowec, P.; Ye, Q.; Yu, D.; Zhao, X.; Zhou, J.; Medina, J. C.; Olson, S. H. Discovery of AM-7209, a Potent and Selective 4-Amidobenzoic Acid Inhibitor of the MDM2–P53 Interaction. *J. Med. Chem.* **2014**, *57* (24), 10499–10511. https://doi.org/10.1021/jm501550p.

(20) Lall, M. S.; Hoge, G.; Tran, T. P.; Kissel, W.; Murphy, S. T.; Taylor, C.; Hutchings, K.; Samas, B.; Ellsworth, E. L.; Curran, T.; Showalter, H. D. H. Stereoselective Synthesis of (*S*)-3-(Methylamino)-3-((*R*)-Pyrrolidin-3-Yl)Propanenitrile. *J. Org. Chem.* **2012**, *77* (10), 4732–4739. https://doi.org/10.1021/jo3004716.

(21) Träff, A.; Lihammar, R.; Bäckvall, J.-E. A Chemoenzymatic Dynamic Kinetic Resolution Approach to Enantiomerically Pure (*R*)- and (*S*)-Duloxetine. *J. Org. Chem.* **2011**, *76* (10), 3917–3921. https://doi.org/10.1021/jo2003665.

(22) Chen, T.; Liu, W.; Gu, W.; Niu, S.; Lan, S.; Zhao, Z.; Gong, F.; Liu, J.; Yang, S.; Cotman, A. E.; Song, J.; Fang, X. Dynamic Kinetic Resolution of β-Substituted α-Diketones via Asymmetric Transfer Hydrogenation. *J. Am. Chem. Soc.* **2023**, *145* (1), 585–599. https://doi.org/10.1021/jacs.2c11149.

(23) Wang, F.; Yang, T.; Wu, T.; Zheng, L.-S.; Yin, C.; Shi, Y.; Ye, X.-Y.; Chen, G.-Q.; Zhang, X. Asymmetric Transfer Hydrogenation of α-Substituted-β-Keto Carbonitriles via Dynamic Kinetic Resolution. *J. Am. Chem. Soc.* **2021**, *143* (6), 2477–2483. https://doi.org/10.1021/jacs.0c13273.

(24) Liu, J.; Krajangsri, S.; Yang, J.; Li, J.-Q.; Andersson, P. G. Iridium-Catalysed Asymmetric Hydrogenation of Allylic Alcohols via Dynamic Kinetic Resolution. *Nat. Catal.* **2018**, *1* (6), 438–443. https://doi.org/10.1038/s41929-018-0070-0.

(25) Steward, K. M.; Gentry, E. C.; Johnson, J. S. Dynamic Kinetic Resolution of α-Keto Esters via Asymmetric Transfer Hydrogenation. *J. Am. Chem. Soc.* **2012**, *134* (17), 7329–7332. https://doi.org/10.1021/ja3027136.

(26) Zhou, M.; Gridneva, T.; Zhang, Z.; He, E.; Liu, Y.; Zhang, W. Chiral Bicyclic Imidazole-Catalyzed Acylative Dynamic Kinetic Resolution for the Synthesis of Chiral Phthalidyl Esters. *Angew. Chem. Int. Ed.* **2021**, *60* (3), 1641–1645. https://doi.org/10.1002/anie.202012445.

(27) Kühn, F.; Katsuragi, S.; Oki, Y.; Scholz, C.; Akai, S.; Gröger, H. Dynamic Kinetic Resolution of a Tertiary Alcohol. *Chem. Commun.* **2020**, *56* (19), 2885–2888. https://doi.org/10.1039/C9CC09103C.

(28) Piotrowski, D. W.; Kamlet, A. S.; Dechert-Schmitt, A.-M. R.; Yan, J.; Brandt, T. A.; Xiao, J.; Wei, L.; Barrila, M. T. Regio- and Enantioselective Synthesis of Azole Hemiaminal Esters by Lewis Base Catalyzed Dynamic Kinetic Resolution. *J. Am. Chem. Soc.* **2016**, *138* (14), 4818–4823. https://doi.org/10.1021/jacs.6b00207.

(29) Lee, S. Y.; Murphy, J. M.; Ukai, A.; Fu, G. C. Nonenzymatic Dynamic Kinetic Resolution of Secondary Alcohols via Enantioselective Acylation: Synthetic and Mechanistic Studies. *J. Am. Chem. Soc.* **2012**, *134* (36), 15149–15153. https://doi.org/10.1021/ja307425g.

(30) Bartlett, S. L.; Johnson, J. S. Synthesis of Complex Glycolates by Enantioconvergent Addition Reactions. *Acc. Chem. Res.* **2017**, *50* (9), 2284–2296. https://doi.org/10.1021/acs.accounts.7b00263.

(31) Yang, K.; Mao, Y.; Zhang, Z.; Xu, J.; Wang, H.; He, Y.; Yu, P.; Song, Q. Construction of C-B Axial Chirality via Dynamic Kinetic Asymmetric Cross-Coupling Mediated by Tetracoordinate Boron. *Nat.*

Commun. **2023**, *14* (1), 4438. https://doi.org/10.1038/s41467-023-40164-6.
(32) Han, Y.; Qin, A.; Zhang, Q.; Zhang, X.; Qian, H.; Ma, S. Rhodium-Catalyzed Dynamic Kinetic [4+2] Cycloaddition of Allene-1,3-Dienes. *Angew. Chem. Int. Ed.* **2022**, *61* (47), e202211635. https://doi.org/10.1002/anie.202211635.
(33) Lim, K. M.-H.; Hayashi, T. Dynamic Kinetic Resolution in Rhodium-Catalyzed Asymmetric Arylation of Phospholene Oxides. *J. Am. Chem. Soc.* **2017**, *139* (24), 8122–8125. https://doi.org/10.1021/jacs.7b04570.
(34) Yan, Y.; Li, W.-C.; Meng, H.; Chen, S.; Ming, J.; Hayashi, T. Rhodium-Catalyzed Asymmetric Conjugate Addition to γ-Substituted α,β-Unsaturated γ-Lactams through Dynamic Kinetic Resolution: Asymmetric Synthesis of *Trans* -β,γ-Disubstituted γ-Lactams. *ACS Catal.* **2023**, *13* (10), 6603–6609. https://doi.org/10.1021/acscatal.3c01413.
(35) Bartlett, S. L.; Keiter, K. M.; Johnson, J. S. Synthesis of Complex Tertiary Glycolates by Enantioconvergent Arylation of Stereochemically Labile α-Keto Esters. *J. Am. Chem. Soc.* **2017**, *139* (10), 3911–3916. https://doi.org/10.1021/jacs.7b00943.
(36) Ruan, L.-X.; Sun, B.; Liu, J.-M.; Shi, S.-L. Dynamic Kinetic Asymmetric Arylation and Alkenylation of Ketones. *Science* **2023**, *379* (6633), 662–670. https://doi.org/10.1126/science.ade0760.
(37) Rezayee, N. M.; Enemærke, V. J.; Linde, S. T.; Lamhauge, J. N.; Reyes-Rodríguez, G. J.; Jørgensen, K. A.; Lu, C.; Houk, K. N. An Asymmetric S_N2 Dynamic Kinetic Resolution. *J. Am. Chem. Soc.* **2021**, *143* (19), 7509–7520. https://doi.org/10.1021/jacs.1c02193.
(38) Carmona, J. A.; Rodríguez-Salamanca, P.; Fernández, R.; Lassaletta, J. M.; Hornillos, V. Dynamic Kinetic Resolution of 2-(Quinolin-8-yl)Benzaldehydes: Atroposelective Iridium-Catalyzed Transfer Hydrogenative Allylation. *Angew. Chem. Int. Ed.* **2023**, *62* (35), e202306981. https://doi.org/10.1002/anie.202306981.
(39) Rodríguez-Franco, C.; Ros, A.; Merino, P.; Fernández, R.; Lassaletta, J. M.; Hornillos, V. Dynamic Kinetic Resolution of Indole-Based Sulfenylated Heterobiaryls by Rhodium-Catalyzed Atroposelective Reductive Aldol Reaction. *ACS Catal.* **2023**, *13* (18), 12134–12141. https://doi.org/10.1021/acscatal.3c03422.
(40) Davison, R. T.; Kuker, E. L.; Dong, V. M. Teaching Aldehydes New Tricks Using Rhodium- and Cobalt-Hydride Catalysis. *Acc. Chem. Res.* **2021**, *54* (5), 1236–1250. https://doi.org/10.1021/acs.accounts.0c00771.
(41) Willis, M. C. Transition Metal Catalyzed Alkene and Alkyne Hydroacylation. *Chem. Rev.* **2010**, *110* (2), 725–748. https://doi.org/10.1021/cr900096x.
(42) Murphy, S. K.; Dong, V. M. Enantioselective Hydroacylation of Olefins with Rhodium Catalysts. *Chem Commun* **2014**, *50* (89), 13645–13649. https://doi.org/10.1039/C4CC02276A.
(43) Biju, A. T.; Kuhl, N.; Glorius, F. Extending NHC-Catalysis: Coupling Aldehydes with Unconventional Reaction Partners. *Acc. Chem. Res.* **2011**, *44* (11), 1182–1195. https://doi.org/10.1021/ar2000716.
(44) Osborne, J. D.; Randell-Sly, H. E.; Currie, G. S.; Cowley, A. R.; Willis, M. C. Catalytic Enantioselective Intermolecular Hydroacylation: Rhodium-Catalyzed Combination of β- *S* -Aldehydes and 1,3-Disubstituted Allenes. *J. Am. Chem. Soc.* **2008**, *130* (51), 17232–17233. https://doi.org/10.1021/ja8069133.
(45) Chen, Z.; Aota, Y.; Nguyen, H. M. H.; Dong, V. M. Dynamic Kinetic Resolution of Aldehydes by Hydroacylation. *Angew. Chem. Int. Ed.* **2019**, *58* (14), 4705–4709. https://doi.org/10.1002/anie.201900545.
(46) Oonishi, Y.; Hosotani, A.; Yokoe, T.; Sato, Y. Rhodium(I)-Catalyzed Enantioselective Hydroacylation of Racemic Allenals via Dynamic Kinetic Resolution. *Org. Lett.* **2019**, *21* (11), 4120–4123. https://doi.org/10.1021/acs.orglett.9b01307.
(47) Oonishi, Y.; Takagishi, K.; Liu, Y.; Sato, Y. Enantioselective Intramolecular Hydroacylation of

Alkynes by Rhodium Catalysis through Dynamic Kinetic Resolution. *Adv. Synth. Catal.* **2023**, *365* (20), 3432–3437. https://doi.org/10.1002/adsc.202300206.
(48) Jun, C.; Jo, E.; Park, J. Intermolecular Hydroacylation by Transition-Metal Complexes. *Eur. J. Org. Chem.* **2007**, *2007* (12), 1869–1881. https://doi.org/10.1002/ejoc.200600846.
(49) Shibata, Y.; Tanaka, K. Rhodium-Catalyzed Highly Enantioselective Direct Intermolecular Hydroacylation of 1,1-Disubstituted Alkenes with Unfunctionalized Aldehydes. *J. Am. Chem. Soc.* **2009**, *131* (35), 12552–12553. https://doi.org/10.1021/ja905908z.
(50) Malakar, C. C.; Dell'Amico, L.; Zhang, W. Dual Catalysis in Organic Synthesis: Current Challenges and New Trends. *Eur. J. Org. Chem.* **2023**, *26* (1), e202201114. https://doi.org/10.1002/ejoc.202201114.
(51) Skubi, K. L.; Blum, T. R.; Yoon, T. P. Dual Catalysis Strategies in Photochemical Synthesis. *Chem. Rev.* **2016**, *116* (17), 10035–10074. https://doi.org/10.1021/acs.chemrev.6b00018.
(52) Venugopalan Nair, V.; Arunprasath, D.; Pandidurai, S.; Sekar, G. Synergistic Dual Amine/Transition Metal Catalysis: Recent Advances. *Eur. J. Org. Chem.* **2022**, *2022* (23), e202200244. https://doi.org/10.1002/ejoc.202200244.
(53) Xu, M.-M.; Wang, H.-Q.; Mao, Y.-J.; Mei, G.-J.; Wang, S.-L.; Shi, F. Cooperative Catalysis-Enabled Asymmetric α-Arylation of Aldehydes Using 2-Indolylmethanols as Arylation Reagents. *J. Org. Chem.* **2018**, *83* (9), 5027–5034. https://doi.org/10.1021/acs.joc.8b00228.
(54) Mukherjee, S.; List, B. Chiral Counteranions in Asymmetric Transition-Metal Catalysis: Highly Enantioselective Pd/Brønsted Acid-Catalyzed Direct α-Allylation of Aldehydes. *J. Am. Chem. Soc.* **2007**, *129* (37), 11336–11337. https://doi.org/10.1021/ja074678r.
(55) Stephan, D. W. Frustrated Lewis Pairs. *J. Am. Chem. Soc.* **2015**, *137* (32), 10018–10032. https://doi.org/10.1021/jacs.5b06794.
(56) Miyake, G. M.; Mariott, W. R.; Chen, E. Y.-X. Asymmetric Coordination Polymerization of Acrylamides by Enantiomeric Metallocenium Ester Enolate Catalysts. *J. Am. Chem. Soc.* **2007**, *129* (21), 6724–6725. https://doi.org/10.1021/ja072073p.
(57) Okamoto, Y.; Hayashida, H.; Hatada, K. Asymmetric Polymerization of N,N-Disubstituted Acrylamides. *Polym. J.* **1989**, *21* (7), 543–549. https://doi.org/10.1295/polymj.21.543.
(58) Nahm, S.; Weinreb, S. M. N-Methoxy-n-Methylamides as Effective Acylating Agents. *Tetrahedron Lett.* **1981**, *22* (39), 3815–3818. https://doi.org/10.1016/S0040-4039(01)91316-4.
(59) Collins, K. D.; Glorius, F. A Robustness Screen for the Rapid Assessment of Chemical Reactions. *Nat. Chem.* **2013**, *5* (7), 597–601. https://doi.org/10.1038/nchem.1669.
(60) Simmons, E. M.; Hartwig, J. F. On the Interpretation of Deuterium Kinetic Isotope Effects in C□H Bond Functionalizations by Transition-Metal Complexes. *Angew. Chem. Int. Ed.* **2012**, *51* (13), 3066–3072. https://doi.org/10.1002/anie.201107334.
(61) Huang, M.; Zhang, L.; Pan, T.; Luo, S. Deracemization through Photochemical *E* / *Z* Isomerization of Enamines. *Science* **2022**, *375* (6583), 869–874. https://doi.org/10.1126/science.abl4922.
(62) Miertuš, S.; Scrocco, E.; Tomasi, J. Electrostatic Interaction of a Solute with a Continuum. A Direct Utilizaion of AB Initio Molecular Potentials for the Prevision of Solvent Effects. *Chem. Phys.* **1981**, *55* (1), 117–129. https://doi.org/10.1016/0301-0104(81)85090-2.
(63) Tomasi, J.; Mennucci, B.; Cammi, R. Quantum Mechanical Continuum Solvation Models. *Chem. Rev.* **2005**, *105* (8), 2999–3094. https://doi.org/10.1021/cr9904009.
(64) Gao, H.; Zhang, J. Cationic Rhodium(I)-Catalyzed Regioselective Tandem Heterocyclization/[3+2] Cycloaddition of 2-(1-Alkynyl)-2-alken-1-ones with Alkynes. *Chem. – Eur. J.* **2012**, *18* (10), 2777–2782. https://doi.org/10.1002/chem.201103924.
(65) Carmona, D.; Lamata, M. P.; Viguri, F.; Rodríguez, R.; Oro, L. A.; Balana, A. I.; Lahoz, F. J.; Tejero, T.; Merino, P.; Franco, S.; Montesa, I. The Complete Characterization of a Rhodium Lewis Acid−Dipolarophile Complex as an Intermediate for the Enantioselective Catalytic 1,3-Dipolar

Cycloaddition of *C* , *N* -Diphenylnitrone to Methacrolein. *J. Am. Chem. Soc.* **2004**, *126* (9), 2716–2717. https://doi.org/10.1021/ja031995z.
(66) Andrieu, J.; Camus, J.-M.; Poli, R.; Richard, P. New Chiral α-Aminophosphine Oxides and Sulfides: An Unprecedented Rhodium-Catalyzed Ligand Epimerization. *New J. Chem.* **2001**, *25* (8), 1015–1023. https://doi.org/10.1039/b100217l.
(67) Dornan, P. K.; Kou, K. G. M.; Houk, K. N.; Dong, V. M. Dynamic Kinetic Resolution of Allylic Sulfoxides by Rh-Catalyzed Hydrogenation: A Combined Theoretical and Experimental Mechanistic Study. *J. Am. Chem. Soc.* **2014**, *136* (1), 291–298. https://doi.org/10.1021/ja409824b.

CHAPTER 3 – Regio- and Enantioselective Hydroacylation of Azetines

3.1 Introduction

Azetidines are four-membered cyclic amines found in pharmaceutical candidates and natural products, such as Nicotianamine, Ximelagatran, and Azelnidipine (Figure 1A).[1–6] The unique characteristics of azetidines, including high Fsp^3 character, rigidity, and basicity, have increased their synthetic interest in recent years. They possess an intermediate level of reactivity fitting nicely between unstable aziridines

and unreactive pyrrolidines.[7] Azetidines have been proposed as replacements for several functionalities in drug syntheses including piperidine, pyrrolidine, piperazine, proline, and more.[8–15] This is in part due to their potential improvements in the areas of solubility, lipophilicity, and PK. [16]

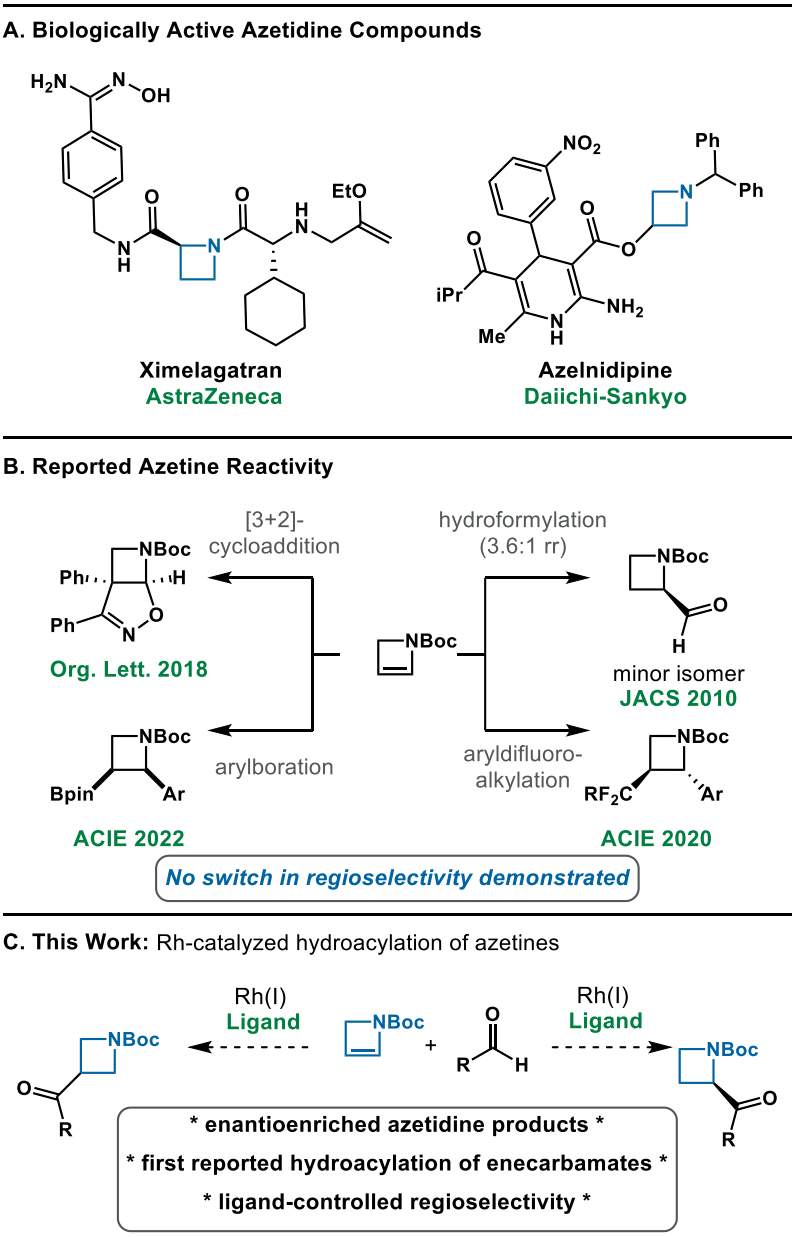

Figure 3.1 Azetine hydroacylation background and proposal

Despite the increasing interest in azetidines, current synthetic approaches are limited.[17] This is especially true for enantiopure azetidines. One such way to access enantioenriched azetidines is through the hydro- or difunctionalization of 1- and 2-azetines.[18] This area of research has been largely

underexplored. Recent examples of azetine difunctionalization include a Ni-catalyzed aryldiflouroalkylation reported by Zhang et al in 2020.[19] Additionally, a Cu/Pd dual catalytic arylboration of enecarbamates, including azetines, was reported by Brown and coworkers in 2022 (Figure 2B).[20] However, neither of the above methods afford enantioenriched azetidine scaffolds. In addition to these difunctionalizations, several cycloadditions involving azetines have been reported resulting in a range of bicyclic azetidine compounds.[21–26] The enantioselective hydroformylation of azetines has been reported by Stahl and Landis in 2010, yet only one example is shown in modest regioselectivity (1:3.6) with the chiral isomer as the minor product (Figure 2B).[27] While several other hydrofunctionalizations of enecarbamates have been reported[28–31], none have included the 4-membered azetine variant. Additionally, none of the current methods of hydro- or difunctionalizations of 2-azetines allow for a switch in regiocontrol.

With this gap in the literature noted, we hoped to develop a highly regio- and enantioselective hydroacylation of 2-azetines (Figure 1C). Previous hydroacylations of strained alkenes, such as cyclopropenes[32,33] and cyclobutenes,[34] guided our initial efforts. Furthermore, the hydroacylation of enamides to afford racemic amide scaffolds was reported by Bolm in 2011.[35] The first and only hydroacylation of enamides with enantiocontrol was published earlier this year by Li and coworkers.[36] While the resulting amide products have synthetic value, a carbamate product would allow for facile amine deprotection using well-studied and mild conditions.[37–40] Taking inspiration from Bolm and Li, we proposed the complimentary hydroacylation of enecarbamates in place of enamides. If successful, this could afford enantioenriched azetidine products that could be readily deprotected and further derivatized.

3.2 Reaction Discovery and Optimization

To probe initial reactivity, azetine **1** and salicylaldehyde **2** were subjected to various catalysts prepared *in situ*. Inspiration from previous hydroacylations of strained alkenes was used as a

Table 3.1 Optimization of azetine hydroacylation

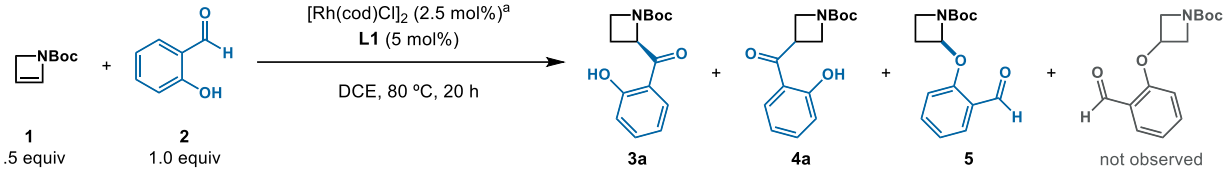

1 (1.5 equiv) + 2 (1.0 equiv) → 3a + 4a + 5 + not observed

Entry	Variation from standard conditions	3a:4a:5	Yield
1	none	>20:1:0	97% (A)
2	60 °C	>20:1:0	85% (A)
3	K_3PO_4 (10 mol%) added	>20:1:0	84% (A)
4	**L2** instead of **L1**, K_3PO_4 (10 mol%) added[b]	10:1:0	42% (A)
5	**L3** instead of **L1**[b]	>20:1:0	60% (A)
6	**L4** instead of **L1**	0:1:2	--
7	**L5** instead of **L1**	0.7:0.3:1	--
8	**L6** instead of **L1**[c]	1:>20:0	trace (B)
9	**L6** instead of **L1**, K_3PO_4 (10 mol%) added[c]	1:>20:0	53% (B)
10	**L6** instead of **L1**, K_3PO_4 (10 mol%) added, 60 °C[c]	1:>20:0	98% (B)

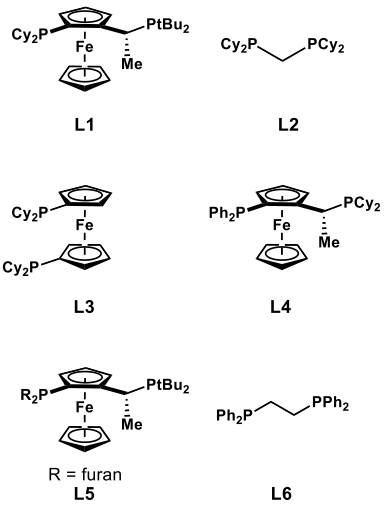

[a]**Condition change:** [b]5.0 mol% $[Rh(cod)Cl]_2$ and 10 mol% ligand. [c]10 mol% $[Rh(cod)Cl]_2$ and 20 mol% ligand

launching point for catalyst evaluation.[32] Examining a range of bisphosphine ligands with $[Rh(cod)Cl]_2$ led to electron rich Josiphos ligands as most promising for generation of 2-acylazetidine **3a** (Table 1). Use of ligand **L5** resulted in a complex mixture of azetidine isomers **3a** and **4a** as well as hydroalkoxylation product **5** (0.7:0.3:1 of A:B:C). However, slightly less electron donating **L4** resulted in a 1:2 mixture of **4a** and hydroalkoxylation product **5**. The **L1** afforded azetidine **3a** with the highest yield and selectivity (97%, >20:1 rr) at 80 °C in DCE. We reason that both the steric bulk and electronically rich nature of **L1** are crucial for high regioselectivity. The enantiopurity of **3a** was found to be high (96% ee) when **L1** was employed. Previous reports of hydroacylations with salicylaldehyde have shown that the addition of catalytic amounts of base can improve reactivity.[41,42] However, with the addition of K_3PO_4 (10 mol%) we saw a slight decrease in yield to 84%. Electronically rich achiral ligands (**L2** and **L3**) in

combination with $[Rh(cod)Cl]_2$ also result in formation of isomer **3a**. Use of **L3** selectively afforded 2-acylazetidine **3a** (60% yield, >20:1 rr).

Next, we aimed to obtain the other constitutional isomer, 3-acylazetidine **4a**. Through additional ligand evaluation, we found that biaryl bisphosphine ligands, such as **L6**, afford **4a** selectively. In the case of **4a**, the addition of K_3PO_4 (10 mol%) drastically improved reactivity to afford desired product in 53% yield with >20:1 rr. Lowering the temperature from 80 °C to 60 °C further improved the yield to 98%. The temperature effect is potentially due to the propensity for azetine to polymerize at higher temperatures. The optimized conditions for each isomer were subsequently used to explore the scope of reactivity.

3.3 Substrate Scope

A variety of salicylaldehydes were evaluated with azetine **1** (Table 2A). Using unmodified salicylaldehyde **2a** afforded the model substrate **3a** in 97% yield, 98:2 er, and >20:1 rr. Alkyl substituents on the 2, 3, and 4 positions of the salicylaldehyde were well tolerated (**3b**−**3d**) in (82%−99%), (93:7−>99:1 er), and (all >20:1 rr). 3-Methoxysalicylaldehyde gave product **3e** in slightly increased yield (99%) and maintained selectivity (98:2 er and >20:1 rr). An allyl substituted salicylaldehyde afforded **3f** (90% yield, 99:1 er, and >20:1 rr) with no observed side reactivity of the tethered alkene. We observe **3g** (88% yield, 99:1 er, and >20:1 rr) with a pinacolborane substituent due to the potential for further derivatization with the boron handle. Halogenated salicylaldehyes were well tolerated with slightly lowered reactivity. 5-Chloro and 5-bromo substituted salicylaldehyes gave **3h** (65% yield, 98:2 er, and >20:1 rr) and **3i** (69% yield, 92:8 er, and >20:1 rr), respectively. Fluorinated salicylaldehydes were subjected to standard conditions affording **3j** (67% yield, -:- er, and >20:1 rr) with a trifluoromethyl substituent at the 5

Table 3.2 2-Acylazetidine and 3-acylazetidine scope

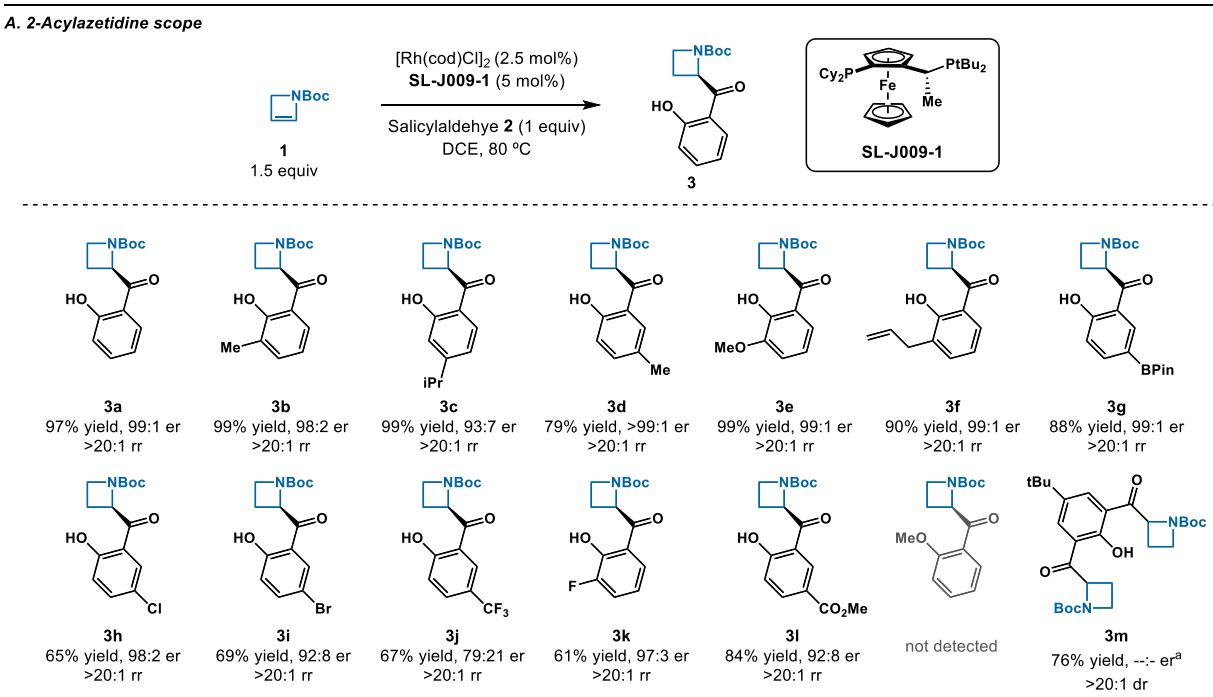

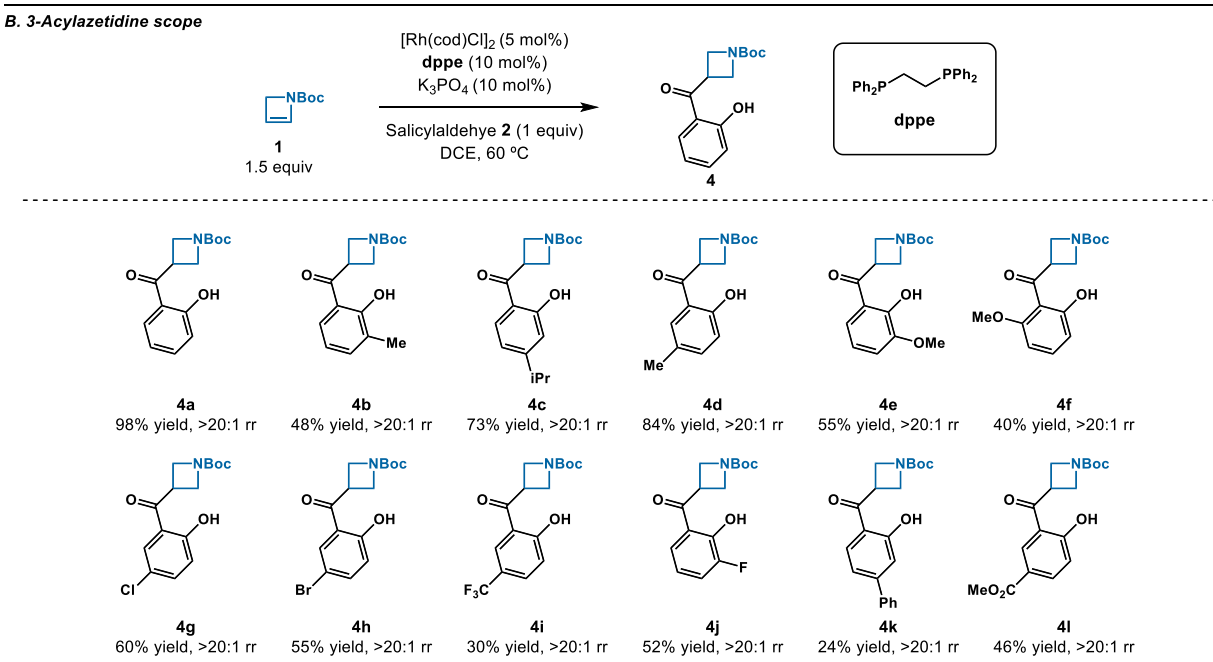

[a]Current efforts are underway to optimize chiral HPLC conditions for compound **3m**.

position and **3k** (61% yieldm 97:3 er, and >20:1 rr) with a fluoro substituent at the 3 position. The methyl ester substitution on **3l** (84% yield, 92:8 er, and >20:1 rr) could offer another potential

synthetic handle. Unfortunately, replacing the hydroxy directing group of the salicylaldehyde with a methoxy group resulted in no formation of desired product. Finally, a dialdehyde successfully underwent hydroacylation with two equivalents of azetine **1** to afford **3m** in 76% yield.

The substrate scope of the 3-acylazetidine was evaluated next (Table 2B). Unmodified salicylaldehyde **2** was again used as the model coupling partner to selectively form **4a** (98%, >20:1 rr). Alkyl substituents at various positions on salicyclaldehyde were tolerated to form **4b** (48% yield, >20:1 rr), **4c** (50% yield, >20:1 rr), and **4d** (79% yield, >20:1 rr). Methoxy substitution was tolerated at the 3 and 6 positions providing **4e** (39% yield, >20:1 rr) and **4f** (26% yield, >20:1 rr), respectively. Halogenated salicylaldehydes including 5-Chloro, 5-Bromo, 5-CF3, and 3-Fluoro were employed to give azetidines **4g**−**4j** in a range of yields (24%−52%) with high regioselectivity (all >20:1 rr). Aryl substitution was tolerated to give 4-phenyl product **4k** in 24% yield with >20:1 rr. Finally, ester substituents were shown to be tolerated when **4l** was obtained in 24% yield with >20:1 rr.

3.4 2-Acylazetidine Derivatizations and Gram-Scale Hydroacylation

A one- gram scale hydroacylation with the 2-acylazetidine conditions was completed with a catalyst loading of 1.0 mol% Rh (Figure 2A). The increase from 0.10 mmol scale to a 5.0 mmol scale with the lowered catalyst loading resulted in a 16% loss in yield. With **3d** in hand, we explored derivatizations. Alcohol **6** was obtained in high yield and diastereoselectivity (99% yield and >20:1 dr) via reduction of the ketone with $NaBH_4$. A Grignard reduction of **3d** resulted in the alkylated material **7** in 67% yield and 7:1 dr. The boc-protecting group was easily removed with the addition of HCl to afford the ammonium salt **8**. Finally, we converted **3d** to aryl triflate **9** which possesses a convenient handle for cross-coupling or reduction.[43–49]

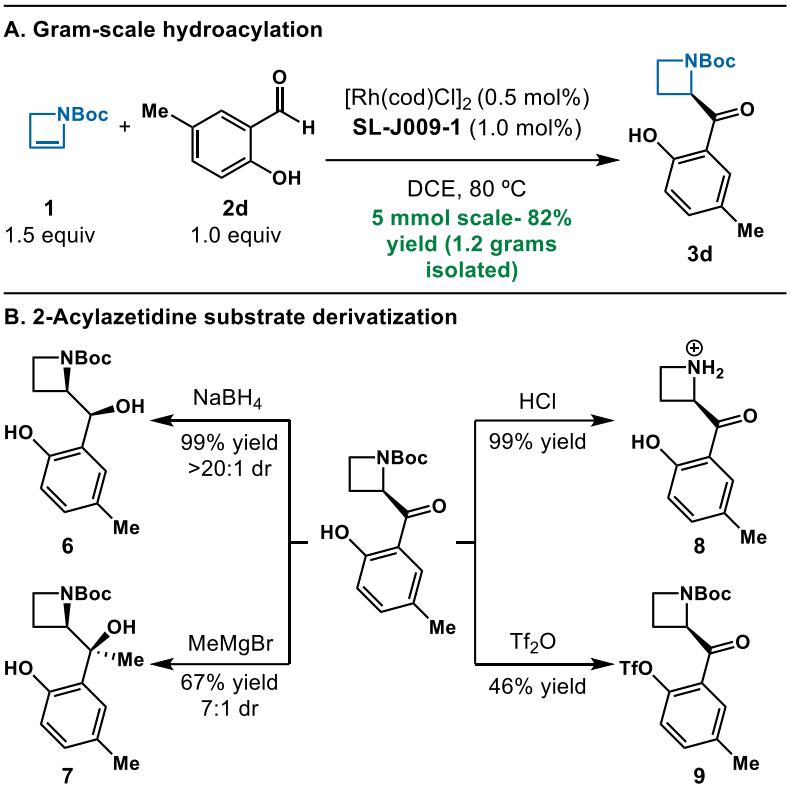

Figure 3.2 Gram-scale hydroacylation and substrate derivatization

3.5 Mechanistic Insights

On the basis of literature and our own observations, we propose the following mechanism for accessing 2-acylazetidines (Figure 3C). The steps oxidative addition (**I**) and olefin coordination (**II**) are rapid and reversible under these reaction conditions. Following coordination, the turnover limiting step is the azetine **1a** insertion in the Rh-H bond to afford azetidinyl-Rh(III) **V**. The final step is the reductive elimination to form the C-C bond, which furnishes **3a** and regenerates the Rh-catalyst **I**. The mechanistic experiments that led to this proposed mechanism are discussed below.

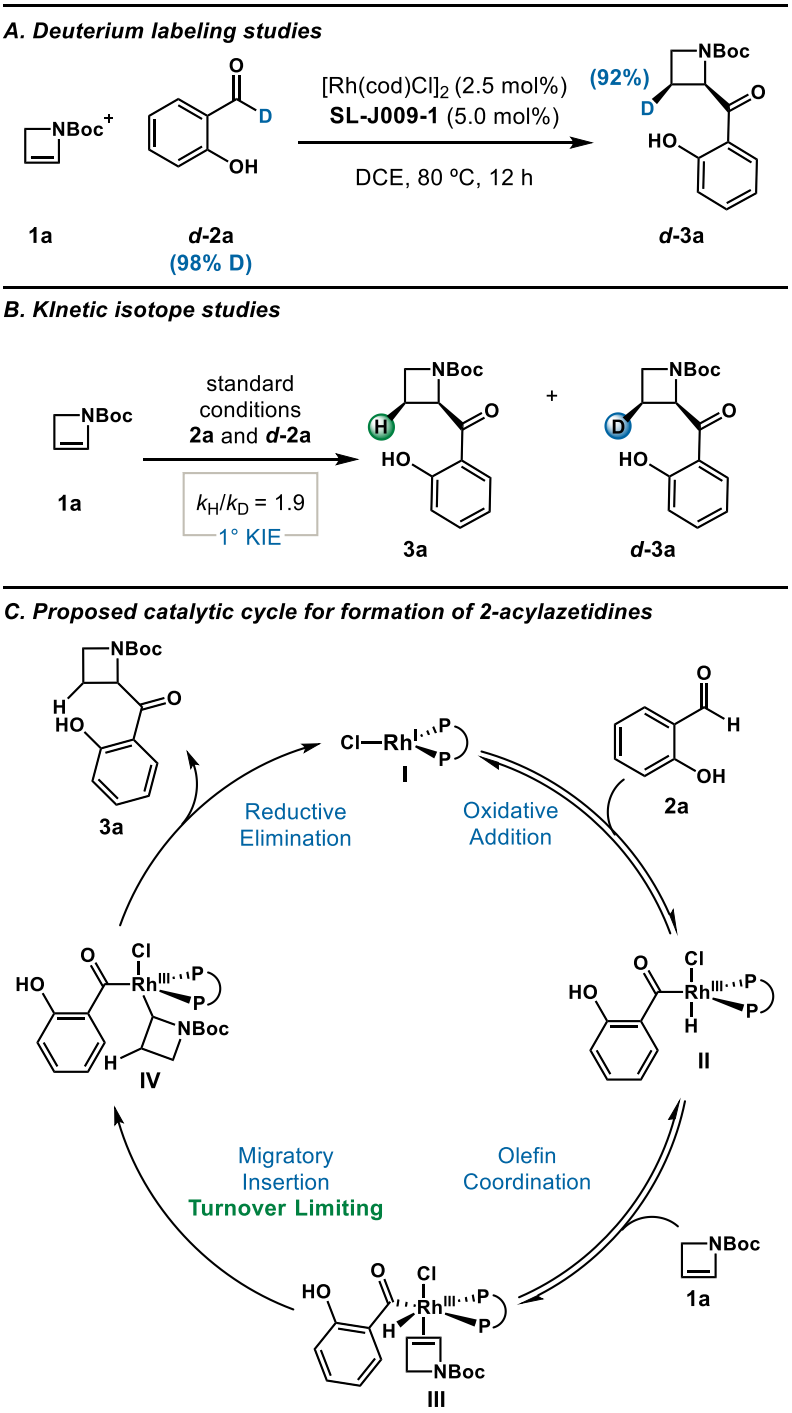

Figure 3.3 Mechanistic experiments and proposed catalytic cycle for the formation of 2-acylazetidines

We performed an isotopic labeling experiment in which we subjected deuterated salicylaldehyde (***d*-2a**) and azetine (**1a**) to the standard 2-acylazetidine reaction conditions (Figure

3A). Analysis of ***d*-3a** shows that the deuterium incorporated exclusively *syn* relative to the newly formed C-C bond. This result suggests a *syn* hydrorhodation step in the catalytic cycle. A primary kinetic isotope effect (KIE) of 1.90 is observed when running the 2-acylazetidine hydroacylation with **2a** and ***d*-2a** in competition (Figure 3B). The presence of a primary KIE supports migratory insertion as the turnover-limiting step. The mechanistic conclusions drawn from these findings are summarized in the catalytic cycle presented in Figure 3C.

On the basis of literature and our own observations, we propose the following mechanism for accessing 3-acylazetidines (Figure X). The Rh-catalyst (**I**) undergoes oxidative addition to **2a** to generate **II**. Following coordination, azetine **1a** inserts into the Rh-H bond to afford azetidinyl-Rh(III) **V**. The turnover limiting step is the reductive elimination to form the C-C bond, which furnishes **4a** and regenerates the Rh-catalyst **I**. The mechanistic experiments that led to this proposed mechanism are discussed below.

We performed an isotopic labeling experiment in which we subjected deuterated salicylaldehyde (***d*-2a**) and azetine (**1a**) to the standard 3-acylazetidine reaction conditions. No kinetic isotope effect (KIE) is observed when running the 3-acylazetidine hydroacylation with **2a** and ***d*-2a** in parallel. The lack of a KIE supports reductive elimination as the turnover-limiting step.

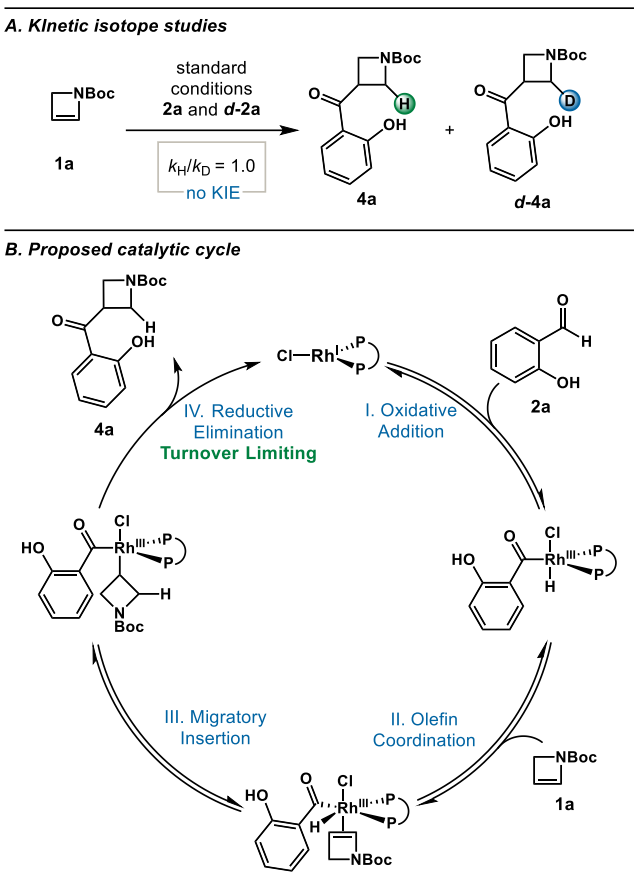

Figure 3.4 Mechanistic experiments and proposed catalytic cycle for the formation of 3-acylazetidines

3.6 Conclusion

While enzymes can diverge common building blocks into various isomers, chemists can access divergent products through tuning of the ligand on a transition metal. While exciting progress has been made in the synthesis of functionalized four-membered nitrogen heterocycles called azetidines, few stereo or regio-divergent approaches exist for their construction. Azetidines are promising motifs in natural products and medicinal chemistry due to their unique characteristics and stability.[7] Inspired by this challenge, we have developed a divergent hydroacylation of 2-azetines to selectively form 3-acylazetidines in high regiocontrol and 2-acylazetidines in high enantio- and regiocontrol. This transformation is the first reported hydroacylation of

enecarbamates. A wide range of salicylaldehyde derivatives were well tolerated as coupling partners under both optimized conditions. Alkyl, aryl, halogen, allyl, ester, and pinacolborane substituents on the salicyclaldehydes were successfully employed to synthesize novel azetidines. 2-Acylazetidine compounds were further derivatized to demonstrate potential synthetic use. Additionally, Isotope labeling experiments in conjunction with kinetic analysis helped to shed light on the divergent rhodium reactivity. Future studies will focus on expanding the scope of enecarbamate hydroacylations.

3.7 Author Contributions

Erin Louise Kuker (E.L.K) conceived of the project idea discussed in Chapter 3. E.L.K identified the optimal conditions for the transformation with the help of C.E.W. E.L.K explored the 2-acylazetidine scope. C.E.W. and Alice E. de Vos (A.E.D.V) explored the 3-acylazetidine scope. E.L.K explored the gram-scale reaction and substrate derivatizations. C.E.W. explored the mechanistic insights for the transformation. All authors analyzed the experimental results, contributed to supporting information, and edited the manuscript.

3.8 References

(1) Zheng, L.; Cheng, Z.; Ai, C.; Jiang, X.; Bei, X.; Zheng, Y.; Glahn, R. P.; Welch, R. M.; Miller, D. D.; Lei, X. G.; Shou, H. Nicotianamine, a Novel Enhancer of Rice Iron Bioavailability to Humans. *PLoS ONE* **2010**, *5* (4), e10190. https://doi.org/10.1371/journal.pone.0010190.

(2) Takahashi, M.; Terada, Y.; Nakai, I.; Nakanishi, H.; Yoshimura, E.; Mori, S.; Nishizawa, N. K. Role of Nicotianamine in the Intracellular Delivery of Metals and Plant Reproductive Development. *Plant Cell* **2003**, *15* (6), 1263–1280. https://doi.org/10.1105/tpc.010256.

(3) Schulman, S.; Wåhlander, K.; Lundström, T.; Clason, S. B.; Eriksson, H. Secondary Prevention of Venous Thromboembolism with the Oral Direct Thrombin Inhibitor Ximelagatran. *N. Engl. J. Med.* **2003**, *349* (18), 1713–1721. https://doi.org/10.1056/NEJMoa030104.

(4) Francis, C. W.; Berkowitz, S. D.; Comp, P. C.; Lieberman, J. R.; Ginsberg, J. S.; Paiement, G.; Peters, G. R.; Roth, A. W.; McElhattan, J.; Colwell, C. W. Comparison of Ximelagatran with Warfarin for the Prevention of Venous Thromboembolism after Total Knee Replacement.

N. Engl. J. Med. **2003**, *349* (18), 1703–1712. https://doi.org/10.1056/NEJMoa035162.
(5) Oizumi, K.; Nishino, H.; Koike, H.; Sada, T.; Miyamoto, M.; Kimura, T. Antihypertensive Effects of CS-905, a Novel Dihydropyridine Ca++ Channel Blocker. *Jpn. J. Pharmacol.* **1989**, *51* (1), 57–64. https://doi.org/10.1016/S0021-5198(19)40137-6.
(6) Pang, L.; Yao, D.; Gao, F.; Bian, X.; Zhang, Y.; Zhong, G. Biosyntheses of Azetidine-Containing Natural Products. *Org. Biomol. Chem.* **2023**, *21* (36), 7242–7254. https://doi.org/10.1039/D3OB01205K.
(7) Mughal, H.; Szostak, M. Recent Advances in the Synthesis and Reactivity of Azetidines: Strain-Driven Character of the Four-Membered Heterocycle. *Org. Biomol. Chem.* **2021**, *19* (15), 3274–3286. https://doi.org/10.1039/D1OB00061F.
(8) Brown, A.; Brown, T. B.; Calabrese, A.; Ellis, D.; Puhalo, N.; Ralph, M.; Watson, L. Triazole Oxytocin Antagonists: Identification of an Aryloxyazetidine Replacement for a Biaryl Substituent. *Bioorg. Med. Chem. Lett.* **2010**, *20* (2), 516–520. https://doi.org/10.1016/j.bmcl.2009.11.097.
(9) Butler, C. R.; Beck, E. M.; Harris, A.; Huang, Z.; McAllister, L. A.; am Ende, C. W.; Fennell, K.; Foley, T. L.; Fonseca, K.; Hawrylik, S. J.; Johnson, D. S.; Knafels, J. D.; Mente, S.; Noell, G. S.; Pandit, J.; Phillips, T. B.; Piro, J. R.; Rogers, B. N.; Samad, T. A.; Wang, J.; Wan, S.; Brodney, M. A. Azetidine and Piperidine Carbamates as Efficient, Covalent Inhibitors of Monoacylglycerol Lipase. *J. Med. Chem.* **2017**, *60* (23), 9860–9873. https://doi.org/10.1021/acs.jmedchem.7b01531.
(10) Burkhard, J. A.; Wagner, B.; Fischer, H.; Schuler, F.; Müller, K.; Carreira, E. M. Synthesis of Azaspirocycles and Their Evaluation in Drug Discovery. *Angew. Chem. Int. Ed.* **2010**, *49* (20), 3524–3527. https://doi.org/10.1002/anie.200907108.
(11) Burkhard, J.; Carreira, E. M. 2,6-Diazaspiro[3.3]Heptanes: Synthesis and Application in Pd-Catalyzed Aryl Amination Reactions. *Org. Lett.* **2008**, *10* (16), 3525–3526. https://doi.org/10.1021/ol801293f.
(12) Burkhard, J. A.; Guérot, C.; Knust, H.; Rogers-Evans, M.; Carreira, E. M. Synthesis and Structural Analysis of a New Class of Azaspiro[3.3]Heptanes as Building Blocks for Medicinal Chemistry. *Org. Lett.* **2010**, *12* (9), 1944–1947. https://doi.org/10.1021/ol1003302.
(13) Lowe, J. T.; Lee, M. D.; Akella, L. B.; Davoine, E.; Donckele, E. J.; Durak, L.; Duvall, J. R.; Gerard, B.; Holson, E. B.; Joliton, A.; Kesavan, S.; Lemercier, B. C.; Liu, H.; Marié, J.-C.; Mulrooney, C. A.; Muncipinto, G.; Welzel-O'Shea, M.; Panko, L. M.; Rowley, A.; Suh, B.-C.; Thomas, M.; Wagner, F. F.; Wei, J.; Foley, M. A.; Marcaurelle, L. A. Synthesis and Profiling of a Diverse Collection of Azetidine-Based Scaffolds for the Development of CNS-Focused Lead-like Libraries. *J. Org. Chem.* **2012**, *77* (17), 7187–7211. https://doi.org/10.1021/jo300974j.
(14) Johansson, A.; Löfberg, C.; Antonsson, M.; Von Unge, S.; Hayes, M. A.; Judkins, R.; Ploj, K.; Benthem, L.; Lindén, D.; Brodin, P.; Wennerberg, M.; Fredenwall, M.; Li, L.; Persson, J.; Bergman, R.; Pettersen, A.; Gennemark, P.; Hogner, A. Discovery of (3-(4-(2-Oxa-6-Azaspiro[3.3]Heptan-6-Ylmethyl)Phenoxy)Azetidin-1-Yl)(5-(4-Methoxyphenyl)-1,3,4-Oxadiazol-2-Yl)Methanone (AZD1979), a Melanin Concentrating Hormone Receptor 1 (MCHr1) Antagonist with Favorable Physicochemical Properties. *J. Med. Chem.* **2016**, *59* (6), 2497–2511. https://doi.org/10.1021/acs.jmedchem.5b01654.
(15) Jia, H.; Dai, G.; Su, W.; Xiao, K.; Weng, J.; Zhang, Z.; Wang, Q.; Yuan, T.; Shi, F.; Zhang, Z.; Chen, W.; Sai, Y.; Wang, J.; Li, X.; Cai, Y.; Yu, J.; Ren, P.; Venable, J.; Rao, T.; Edwards, J. P.; Bembenek, S. D. Discovery, Optimization, and Evaluation of Potent and Highly Selective

PI3Kγ–PI3Kδ Dual Inhibitors. *J. Med. Chem.* **2019**, *62* (10), 4936–4948. https://doi.org/10.1021/acs.jmedchem.8b02014.
(16) Bauer, M. R.; Di Fruscia, P.; Lucas, S. C. C.; Michaelides, I. N.; Nelson, J. E.; Storer, R. I.; Whitehurst, B. C. Put a Ring on It: Application of Small Aliphatic Rings in Medicinal Chemistry. *RSC Med. Chem.* **2021**, *12* (4), 448–471. https://doi.org/10.1039/D0MD00370K.
(17) Brandi, A.; Cicchi, S.; Cordero, F. M. Novel Syntheses of Azetidines and Azetidinones. *Chem. Rev.* **2008**, *108* (9), 3988–4035. https://doi.org/10.1021/cr800325e.
(18) Gatazka, M. R.; McFee, E. C.; Ng, C. H.; Wearing, E. R.; Schindler, C. S. New Strategies for the Synthesis of 1- and 2-Azetines and Their Applications as Value-Added Building Blocks. *Org. Biomol. Chem.* **2022**, *20* (46), 9052–9068. https://doi.org/10.1039/D2OB01812H.
(19) Xu, C.; Cheng, R.; Luo, Y.; Wang, M.; Zhang, X. *Trans* -Selective Aryldifluoroalkylation of Endocyclic Enecarbamates and Enamides by Nickel Catalysis. *Angew. Chem. Int. Ed.* **2020**, *59* (42), 18741–18747. https://doi.org/10.1002/anie.202008498.
(20) Trammel, G. L.; Kannangara, P. B.; Vasko, D.; Datsenko, O.; Mykhailiuk, P.; Brown, M. K. Arylboration of Enecarbamates for the Synthesis of Borylated Saturated N-Heterocycles. *Angew. Chem. Int. Ed.* **2022**, *61* (46), e202212117. https://doi.org/10.1002/anie.202212117.
(21) Engelsma, S. B.; Willems, L. I.; Van Paaschen, C. E.; Van Kasteren, S. I.; Van Der Marel, G. A.; Overkleeft, H. S.; Filippov, D. V. Acylazetine as a Dienophile in Bioorthogonal Inverse Electron-Demand Diels–Alder Ligation. *Org. Lett.* **2014**, *16* (10), 2744–2747. https://doi.org/10.1021/ol501049c.
(22) Baumann, A. N.; Reiners, F.; Juli, T.; Didier, D. Chemodivergent and Stereoselective Access to Fused Isoxazoline Azetidines and Thietanes through [3 + 2]-Cycloadditions. *Org. Lett.* **2018**, *20* (21), 6736–6740. https://doi.org/10.1021/acs.orglett.8b02848.
(23) Burtoloso, A. C. B.; Correia, C. R. D. A New Entry to the Synthesis of Substituted Azetidines: [2+2] Cycloaddition Reaction of Four-Membered Endocyclic Enamides to Ketenes. *Tetrahedron Lett.* **2006**, *47* (36), 6377–6380. https://doi.org/10.1016/j.tetlet.2006.06.174.
(24) Luheshi, A.-B. N.; Smalley, R. K.; Kennewell, P. D.; Westwood, R. 1,3-Dipolar Cycloadditions of 2-Ethoxy- and 2-(Ethylthio)-1-Azetines with Nitrilimines. *Tetrahedron Lett.* **1990**, *31* (1), 127–130. https://doi.org/10.1016/S0040-4039(00)94352-1.
(25) Hemming, K.; Khan, M. N.; O'Gorman, P. A.; Pitard, A. 1,2,4-Oxadiazoles from Cycloreversions of Oxadiazabicyclo[3.2.0]Heptenes: 1-Azetines as Thiocyanate Equivalents. *Tetrahedron* **2013**, *69* (4), 1279–1284. https://doi.org/10.1016/j.tet.2012.12.007.
(26) Dave, P. R.; Duddu, R.; Surapaneni, R.; Gilardi, R. Diels-Alder Reactions ofN-Acetyl-2-Azetine. *Tetrahedron Lett.* **1999**, *40* (3), 443–446. https://doi.org/10.1016/S0040-4039(98)02506-4.
(27) McDonald, R. I.; Wong, G. W.; Neupane, R. P.; Stahl, S. S.; Landis, C. R. Enantioselective Hydroformylation of *N* -Vinyl Carboxamides, Allyl Carbamates, and Allyl Ethers Using Chiral Diazaphospholane Ligands. *J. Am. Chem. Soc.* **2010**, *132* (40), 14027–14029. https://doi.org/10.1021/ja106674n.
(28) Gopalaiah, K.; Kagan, H. B. Use of Nonfunctionalized Enamides and Enecarbamates in Asymmetric Synthesis. *Chem. Rev.* **2011**, *111* (8), 4599–4657. https://doi.org/10.1021/cr100031f.
(29) Holmberg-Douglas, N.; Choi, Y.; Aquila, B.; Huynh, H.; Nicewicz, D. A. β-Functionalization of Saturated Aza-Heterocycles Enabled by Organic Photoredox Catalysis. *ACS Catal.* **2021**, *11* (5), 3153–3158. https://doi.org/10.1021/acscatal.1c00099.
(30) Plehiers, M.; Hootelé, C. Hydroboration of Enecarbamates and the Synthesis of β-

Hydroxypiperidine Alkaloids. *Tetrahedron Lett.* **1993**, *34* (47), 7569–7570. https://doi.org/10.1016/S0040-4039(00)60402-1.
(31) Wang, C.; Xi, Y.; Huang, W.; Qu, J.; Chen, Y. Nickel-Catalyzed Regioselective Hydroarylation of Internal Enamides. *Org. Lett.* **2020**, *22* (23), 9319–9324. https://doi.org/10.1021/acs.orglett.0c03542.
(32) Phan, D. H. T.; Kou, K. G. M.; Dong, V. M. Enantioselective Desymmetrization of Cyclopropenes by Hydroacylation. *J. Am. Chem. Soc.* **2010**, *132* (46), 16354–16355. https://doi.org/10.1021/ja107738a.
(33) Bugaut, X.; Liu, F.; Glorius, F. N-Heterocyclic Carbene (NHC)-Catalyzed Intermolecular Hydroacylation of Cyclopropenes. *J. Am. Chem. Soc.* **2011**, *133* (21), 8130–8133. https://doi.org/10.1021/ja202594g.
(34) Goetzke, F. W.; Sidera, M.; Fletcher, S. P. Catalytic Asymmetric Hydrometallation of Cyclobutenes with Salicylaldehydes. *Chem. Sci.* **2022**, *13* (1), 236–240. https://doi.org/10.1039/D1SC06035J.
(35) Zhang, H.-J.; Bolm, C. Highly Regioselective Intermolecular Hydroacylations of Enamides with Salicylaldehydes. *Org. Lett.* **2011**, *13* (15), 3900–3903. https://doi.org/10.1021/ol201431c.
(36) Sun, X.; Gao, P.-C.; Sun, Y.-W.; Li, B.-J. Amide-Directed, Rhodium-Catalyzed Regio- and Enantioselective Hydroacylation of Internal Alkenes with Unfunctionalized Aldehydes. *J. Am. Chem. Soc.* **2024**, *146* (1), 723–732. https://doi.org/10.1021/jacs.3c10609.
(37) Wuts, P. G. M.; Greene, T. W. *Greene's Protective Groups in Organic Synthesis*, 4th ed.; Wiley-Interscience: Hoboken, N.J., 2007.
(38) Gibson, F. S.; Bergmeier, S. C.; Rapoport, H. Selective Removal of an N-BOC Protecting Group in the Presence of a Tert-Butyl Ester and Other Acid-Sensitive Groups. *J. Org. Chem.* **1994**, *59* (11), 3216–3218. https://doi.org/10.1021/jo00090a045.
(39) Ashworth, I. W.; Cox, B. G.; Meyrick, B. Kinetics and Mechanism of *N* -Boc Cleavage: Evidence of a Second-Order Dependence upon Acid Concentration. *J. Org. Chem.* **2010**, *75* (23), 8117–8125. https://doi.org/10.1021/jo101767h.
(40) Jacquemard, U.; Bénéteau, V.; Lefoix, M.; Routier, S.; Mérour, J.-Y.; Coudert, G. Mild and Selective Deprotection of Carbamates with Bu4NF. *Tetrahedron* **2004**, *60* (44), 10039–10047. https://doi.org/10.1016/j.tet.2004.07.071.
(41) Coulter, M. M.; Kou, K. G. M.; Galligan, B.; Dong, V. M. Regio- and Enantioselective Intermolecular Hydroacylation: Substrate-Directed Addition of Salicylaldehydes to Homoallylic Sulfides. *J. Am. Chem. Soc.* **2010**, *132* (46), 16330–16333. https://doi.org/10.1021/ja107198e.
(42) von Delius, M.; Le, C. M.; Dong, V. M. Rhodium-Phosphoramidite Catalyzed Alkene Hydroacylation: Mechanism and Octaketide Natural Product Synthesis. *J. Am. Chem. Soc.* **2012**, *134* (36), 15022–15032. https://doi.org/10.1021/ja305593y.
(43) Ackerman, L. K. G.; Lovell, M. M.; Weix, D. J. Multimetallic Catalysed Cross-Coupling of Aryl Bromides with Aryl Triflates. *Nature* **2015**, *524* (7566), 454–457. https://doi.org/10.1038/nature14676.
(44) Huang, L.; Ackerman, L. K. G.; Kang, K.; Parsons, A. M.; Weix, D. J. LiCl-Accelerated Multimetallic Cross-Coupling of Aryl Chlorides with Aryl Triflates. *J. Am. Chem. Soc.* **2019**, *141* (28), 10978–10983. https://doi.org/10.1021/jacs.9b05461.
(45) Littke, A. F.; Dai, C.; Fu, G. C. Versatile Catalysts for the Suzuki Cross-Coupling of Arylboronic Acids with Aryl and Vinyl Halides and Triflates under Mild Conditions. *J. Am.*

Chem. Soc. **2000**, *122* (17), 4020–4028. https://doi.org/10.1021/ja0002058.
(46) Sumida, Y.; Sumida, T.; Hosoya, T. Nickel-Catalyzed Reductive Cross-Coupling of Aryl Triflates and Nonaflates with Alkyl Iodides. *Synthesis* **2017**, *49* (16), 3590–3601. https://doi.org/10.1055/s-0036-1588464.
(47) Taeufer, T.; Pospech, J. Palladium-Catalyzed Synthesis of *N* , *N*- Dimethylanilines via Buchwald–Hartwig Amination of (Hetero)Aryl Triflates. *J. Org. Chem.* **2020**, *85* (11), 7097–7111. https://doi.org/10.1021/acs.joc.0c00491.
(48) PALLADIUM-CATALYZED REDUCTION OF VINYL TRIFLUOROMETHANESULFONATES TO ALKENES: CHOLESTA-3,5-DIENE. *Org. Synth.* **1990**, *68*, 138. https://doi.org/10.15227/orgsyn.068.0138.
(49) Kotsuki, H.; Datta, P. K.; Hayakawa, H.; Suenaga, H. An Efficient Procedure for Palladium-Catalyzed Reduction of Aryl/Enol Triflates. *Synthesis* **1995**, *1995* (11), 1348–1350. https://doi.org/10.1055/s-1995-4120.

CONCLUSION

In this dissertation, I have discussed the divergent hydrothiolation of cyclopropenes, dynamic kinetic resolution of aldehydes via hydroacylations, and regiodivergent hydroacylation of azetines. The control of regio-, diastereo-, and enantioselecvity via hydrofunctionalizations has been explored throughout. In particular, the divergent reactivity of cyclopropenes and azetines was controlled through careful choice in the ligand paired with a rhodium catalyst. In chapter 1, ring-opened allylic sulfides and ring-retained cyclopropyl sulfides were selectively formed through an enantioselective hydrothiolation of cyclopropenes. In chapter 3, a controlled switch in regioselectivity allowed for the selective formation of enantioenriched 2-acylazetidines as well as achiral 3-acylazetidines via a rhodium-catalyzed hydroacylation. Chapter 2 explores another rhodium-catalyzed hydroacylation leading to the diastereo- and enantioselective formation of 1,4-ketoamides. This transformation takes advantage of the racemization of racemic aldehydes to achieve a dynamic kinetic resolution. Over the course of these projects, I developed catalysts and methodologies to synthesize a variety of chemical motifs and performed mechanistic experiments to gain useful insight on how the reactions proceed. These studies aim to provide insight into the divergent reactivity of rhodium in order to overcome future synthetic challenges with the use of rhodium-catalysis.

APPENDICES

APPENDIX 1

Supporting Information for Chapter 1

Enantioselective Hydrothiolation: Diverging Cyclopropenes Through Ligand Control

Table of Contents

1. General:

Commercial reagents were purchased from Sigma Aldrich, Strem, Alfa Aesar, Acros Organics or TCI and used without further purification. 1,2-Dichloroethane and acetonitrile were purified using an Innovative Technologies Pure Solv system, degassed by three freeze-pump-thaw cycles, and stored over 3Å MS within a N_2 filled glove box. All experiments were performed in oven-dried or flame-dried glassware. Reactions were monitored using either thin-layer chromatography (TLC) or gas chromatography using an Agilent Technologies 7890A GC system equipped with an Agilent Technologies 5975C inert XL EI/CI MSD. Visualization of the developed plates was performed

under UV light (254 nm) or $KMnO_4$ stain. Organic solutions were concentrated under reduced pressure on a Büchi rotary evaporator. Purification and isolation of products were performed via silica gel chromatography (both column and preparative thin-layer chromatography). Column chromatography was performed with Silicycle Silica-P Flash Silica Gel using glass columns. Solvent was purchased from Fisher. ^{1}H, ^{2}H, ^{13}C, and ^{19}F NMR spectra were recorded on Bruker CRYO500 or DRX400 spectrometer. ^{1}H NMR spectra were internally referenced to the residual solvent signal or TMS. ^{13}C NMR spectra were internally referenced to the residual solvent signal. Data for ^{1}H NMR are reported as follows: chemical shift (δ ppm), multiplicity (s = singlet, d = doublet, t = triplet, q = quartet, m = multiplet), coupling constant (Hz), integration. Data for ^{2}H, ^{13}C, and ^{19}F NMR are reported in terms of chemical shift (δ ppm). Infrared (IR) spectra were obtained on a Nicolet iS5 FT-IR spectrometer with an iD5 ATR and are reported in terms of frequency of absorption (cm^{-1}). High resolution mass spectra (HRMS) were obtained on a micromass 70S-250 spectrometer (EI) or an ABI/Sciex QStar Mass Spectrometer (ESI). Enantiomeric ratio for enantioselective reactions was determined by chiral SFC analysis using an Agilent Technologies HPLC (1200 series) system and Aurora A5 Fusion. Cyclopropene **1a**-**1d**, **1f**-**1h** used here were known compounds and synthesized according to reported methods.[1,2] **2a**-**2q** and all other reagents used for the synthesis of non-commercial starting materials were used without further purification from commercial sources (Sigma Aldrich, Combi-Blocks, Solvias and Alfa Aesar).

2. Cyclopropene Hydrothiolation General Procedures and Compound Characterization

2.1 Ring-Retained Hydrothiolation General Procedure and Compound Characterization

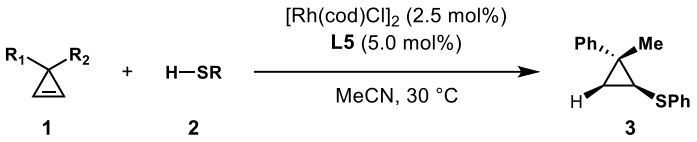

Ring-Retained General Procedure:

In a N_2-filled glove box, $[Rh(cod)Cl]_2$ (1.2 mg, 0.0025 mmol), **L5** (2.7 mg, 0.0050 mmol), and MeCN (0.50 mL) were added to a 1-dram vial containing a stir bar. The resulting mixture was stirred for 10 min. Thiol **2** (11.0 mg, 0.10 mmol) was added followed by cyclopropene **1** (0.10 mL, 1.2 M solution in MeCN, 0.12 mmol) to initiate the reaction. The mixture was held at 30 °C until no starting material was observed by TLC. The regioselectivity ratio was determined by ^{1}H NMR analysis of the unpurified reaction mixture. Isolated yields (obtained by column chromatography on silica gel or preparative thin-layer chromatography) of the title compound are reported.

((1*S*,2*R*)-2-methyl-2-phenylcyclopropyl)(phenyl)sulfane(3aa)

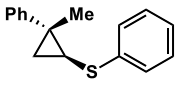

Colorless oil, 90% yield, 95:5 *er*, >20:1 *dr*, $[\alpha]^{24}_D$ = +13.7 (*c* 0.4, $CHCl_3$). **^{1}H NMR** (400 MHz, $CDCl_3$) δ 7.39 – 7.20 (m, 9H), 7.18 – 7.11 (m, 1H), 2.56 (dd, *J* = 8.7, 5.5 Hz, 1H), 1.68 (dd, *J* = 8.7, 5.4 Hz, 1H), 1.60 (s, 3H), 0.96 (t, *J* = 5.4 Hz, 1H). **^{13}C NMR** (126 MHz, $CDCl_3$) δ 145.7, 138.6, 128.9, 128.6, 126.9, 126.6, 126.3, 125.1, 28.5, 27.9, 21.9, 20.5. **IR** (ATR): 2923, 1479, 1439, 1090, 1025, 786, 763, 689 cm^{-1}. **HRMS** calculated for $C_{16}H_{16}S$ $[M]^+$ 240.0973, found 240.0982. **Chiral SFC**: 100 mm CHIRALCEL AD-H, 3% ^{i}PrOH, 2.0 mL/min, 254 nm, 44 °C, nozzle pressure = 200 bar CO_2, t_{R1} (major) = 3.6 min, t_{R2} (minor) = 2.5 min.

((1*S*,2*R*)-2-methyl-2-phenylcyclopropyl)(p-tolyl)sulfane(3ab)

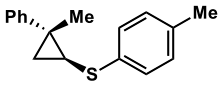

Colorless oil, 92% yield, 95:5 *er*, >20:1 *dr*, $[\alpha]^{24}_D$ = +22.7 (*c* 0.4, $CHCl_3$). **^{1}H NMR** (400 MHz, $CDCl_3$) δ 7.38 – 7.27 (m, 5H), 7.27 – 7.20 (m, 2H), 7.11 (d, *J* = 8.1 Hz, 2H), 2.56 (dd, *J* = 8.7, 5.5 Hz, 1H), 2.34 (s, 3H), 1.65 (dd, *J* = 8.7, 5.4 Hz, 1H), 1.60 (s, 3H), 0.94 (t, *J* = 5.4 Hz, 1H). **^{13}C NMR** (126 MHz, $CDCl_3$) δ 145.9, 135.2, 134.8, 129.7, 128.6, 127.6, 126.8, 126.3, 29.1, 28.1, 21.9, 21.1, 20.7. **IR** (ATR): 2922, 1601, 1492, 1445, 1115, 1090, 1029, 801, 762, 697 cm^{-1}. **HRMS** calculated for $C_{17}H_{18}S$ $[M]^+$ 254.1129, found 254.1116. **Chiral SFC**: 100 mm CHIRALCEL AD-H, 3% ^{i}PrOH, 2.0 mL/min, 254 nm, 44 °C, nozzle pressure = 200 bar CO_2, t_{R1} (major) = 5.2 min, t_{R2} (minor) = 3.3 min.

(4-(tert-butyl)phenyl)((1*S*,2*R*)-2-methyl-2-phenylcyclopropyl)sulfane(3ac)

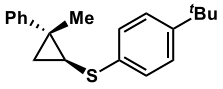

Colorless oil, 86% yield, 91:9 *er*, >20:1 *dr*, $[\alpha]^{24}_D$ = +14.7 (*c* 0.2, $CHCl_3$). **^{1}H NMR** (400 MHz, $CDCl_3$) δ 7.38 – 7.26 (m, 7H), 7.26 – 7.17 (m, 2H), 2.53 (dd, *J* = 8.7, 5.5 Hz, 1H), 1.63 (dd, *J* = 8.7, 5.5 Hz, 1H), 1.60 (s, 3H), 1.30 (s, 9H), 0.93 (t, *J* = 5.4 Hz, 1H). **^{13}C NMR** (126 MHz, $CDCl_3$) δ 148.4, 145.9, 135.0, 128.7, 126.9, 126.7, 126.3, 126.0, 34.5, 31.5, 28.9, 27.9, 22.0, 20.6. **IR** (ATR): 2960, 1496, 1445, 1268, 1121, 1012, 819, 741, 697 cm^{-1}. **HRMS** calculated for $C_{20}H_{24}S$ $[M]^+$ 296.1599, found 296.1578. **Chiral SFC**: 100 mm CHIRALCEL OJ-H, 3% ^{i}PrOH, 2.0 mL/min, 254 nm, 44 °C, nozzle pressure = 200 bar CO_2, t_{R1} (major) = 8.9 min, t_{R2} (minor) = 7.8 min.

(4-chlorophenyl)((1*S*,2*R*)-2-methyl-2-phenylcyclopropyl)sulfane (3ad)

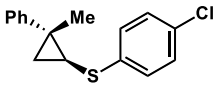

Colorless oil, 87% yield, 94:6 *er*, >20:1 *dr*, $[\alpha]^{24}_D$ = +29.4 (*c* 0.4, $CHCl_3$). **^{1}H NMR** (400 MHz, $CDCl_3$) δ 7.41 – 7.33 (m, 2H), 7.33 – 7.22 (m, 7H), 2.54 (dd,

J = 8.7, 5.4 Hz, 1H), 1.71 (dd, *J* = 8.7, 5.5 Hz, 1H), 1.60 (s, 3H), 0.97 (t, *J* = 5.4 Hz, 1H). **^{13}C NMR** (126 Hz, $CDCl_3$) δ 145.4, 137.3, 131.1, 129.0, 128.7, 128.2, 126.6, 126.5, 28.7, 28.1, 22.0, 20.5. **IR** (ATR): 2924, 1495, 1474, 1093, 1010, 810, 763, 697 cm^{-1}. **HRMS** calculated for $C_{16}H_{15}ClS$ $[M]^+$ 274.0583, found 274.0584. C**hiral SFC**: 100 mm CHIRALCEL AD-H, 3% ^{i}PrOH, 2.0 mL/min, 254 nm, 44 °C, nozzle pressure = 200 bar CO_2, t_{R1} (major) = 5.7 min, t_{R2} (minor) = 4.2 min.

((1*S*,2*R*)-2-methyl-2-phenylcyclopropyl)(m-tolyl)sulfane (3ae)

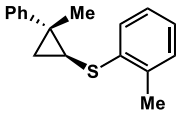

Colorless oil, 72% yield, 93:7 *er*, >20:1 *dr*, $[\alpha]^{24}_D$ = +8.9 (*c* 0.3, $CHCl_3$). **^{1}H NMR** (499 MHz, $CDCl_3$) δ 7.40 – 7.29 (m, 4H), 7.29 – 7.20 (m, 1H), 7.20 – 7.10 (m, 3H), 7.00 – 6.92 (m, 1H), 2.53 (ddd, *J* = 8.7, 5.5, 1.5 Hz, 1H), 2.31 (s, 3H), 1.69 (dd, *J* = 8.4, 5.5 Hz, 1H), 1.59 (s, 3H), 0.95 (td, *J* = 5.4, 1.6 Hz, 1H). **^{13}C NMR** (125 MHz, $CDCl_3$) δ 145.8, 138.7, 138.4, 128.8, 128.7, 127.6, 126.7, 126.3, 126.1, 123.9, 28.7, 28.0, 21.8, 21.5, 20.6. **IR** (ATR): 2922, 1592, 1495, 1444, 1083, 763, 697, 688 cm^{-1}. **HRMS** calculated for $C_{17}H_{18}S$ $[M]^+$ 254.1129, found 254.1119. **Chiral SFC**: 100 mm CHIRALCEL AD-H, 3% ^{i}PrOH, 2.0 mL/min, 254 nm, 44 °C, nozzle pressure = 200 bar CO_2, t_{R1} (major) = 4.8 min, t_{R2} (minor) = 2.3 min.

((1*S*,2*R*)-2-methyl-2-phenylcyclopropyl)(o-tolyl)sulfane (3af)

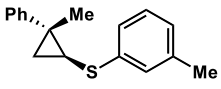

Colorless oil, 73% yield, 95:5 *er*, >20:1 *dr*, $[\alpha]^{24}_D$ = +10.8 (*c* 0.3, $CHCl_3$). **^{1}H NMR** (499 MHz, $CDCl_3$) δ 7.40 – 7.29 (m, 5H), 7.29 – 7.21 (m, 1H), 7.19 – 7.11 (m, 2H), 7.11 – 7.02 (m, 1H), 2.49 (dd, *J* = 8.6, 5.6 Hz, 1H), 2.36 (s, 3H), 1.72 (dd, *J* = 8.6, 5.4 Hz, 1H), 1.59 (s, 3H), 0.99 (t, *J* = 5.4 Hz, 1H). **^{13}C NMR** (125 MHz, $CDCl_3$) δ 145.7, 138.0, 135.2, 129. 9, 128.7, 126.6, 126.5, 126.3, 125.8, 124.8, 28.1, 27.7, 22.0, 20.3, 20.1. **IR** (ATR):

3058, 2924, 1589, 1495, 1467, 1444, 1064, 1047, 1030, 762, 742, 696 cm^{-1}. **HRMS** calculated for $C_{17}H_{18}S$ $[M]^+$ 254.1129, found 254.1122. **Chiral SFC**: 100 mm CHIRALCEL AD-H, 3% ^{i}PrOH, 2.0 mL/min, 220 nm, 44 °C, nozzle pressure = 200 bar CO_2, t_{R1} (major) = 3.2 min, t_{R2} (minor) = 2.3 min.

((1*S*,2*R*)-2-methyl-2-phenylcyclopropyl)(naphthalen-2-yl)sulfane(3ag)

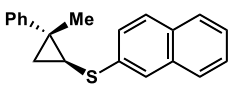

Colorless oil, 81% yield, 94:6 *er*, >20:1 *dr*, $[\alpha]^{24}_D$ = -18.2 (*c* 0.4, $CHCl_3$). **^{1}H NMR** (400 MHz, $CDCl_3$) δ 7.83 – 7.69 (m, 3H), 7.65 (d, *J* = 8.0 Hz, 1H), 7.51 – 7.32 (m, 7H), 7.31 – 7.19 (m, 1H), 2.63 (dd, *J* = 8.7, 5.5 Hz, 1H), 1.78 (dd, *J* = 8.6, 5.6 Hz, 1H), 1.62 (s, 3H), 1.02 (t, *J* = 5.5 Hz, 1H). **^{13}C NMR** (126 MHz, $CDCl_3$) δ 145.7, 136.5, 134.0, 131.5, 128.7, 128.3, 127.9, 127.0, 126.6, 126.4, 125.6, 125.3, 124.2, 28.8, 28.0, 21.8, 20.4. **IR** (ATR): 3053, 2922, 1589, 1500, 1444, 1133, 1070, 941, 812, 738, 697 cm^{-1}. **HRMS** calculated for $C_{20}H_{18}S$ $[M]^+$ 290.1124, found 290.1129. **Chiral SFC**: 100 mm CHIRALCEL AD-H, 3% ^{i}PrOH, 2.0 mL/min, 254 nm, 44 °C, nozzle pressure = 200 bar CO_2, t_{R1} (major) = 18.7 min, t_{R2} (minor) = 11.8 min.

((1*S*,2*R*)-2-methyl-2-(p-tolyl)cyclopropyl)(phenyl)sulfane(3ba)

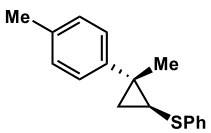

White solid, 83% yield, 94:6 *er*, >20:1 *dr*, $[\alpha]^{24}_D$ = +23.9 (*c* 0.5, $CHCl_3$). **^{1}H NMR** (400 MHz, $CDCl_3$) δ 7.38 – 7.31 (m, 2H), 7.31 – 7.24 (m, 2H), 7.24 – 7.18 (m, 2H), 7.18 – 7.10 (m, 3H), 2.53 (dd, *J* = 8.7, 5.4 Hz, 1H), 2.36 (s, 3H), 1.65 (dd, *J* = 8.7, 5.4 Hz, 1H), 1.58 (s, 3H), 0.93 (t, *J* = 5.4 Hz, 1H). **^{13}C NMR** (126 MHz, $CDCl_3$) δ 142.8, 138.8, 135.9, 129.4, 128.9, 126.9, 126.6, 125.1, 28.4, 27.7, 21.9, 21.1, 20.6. **IR** (ATR): 2922, 1478, 1438, 1116, 1085, 820, 736, 690 cm^{-1}. **HRMS** calculated for $C_{17}H_{18}S$ $[M]^+$ 254.1129, found 254.1127.

Chiral SFC: 100 mm CHIRALCEL AD-H, 3% ^{i}PrOH, 2.0 mL/min, 254 nm, 44 °C, nozzle pressure = 200 bar CO_2, t_{R1} (major) = 4.9 min, t_{R2} (minor) = 3.3 min.

((1*S*,2*R*)-2-methyl-2-(4-(trifluoromethyl)phenyl)cyclopropyl)(phenyl)sulfane (3ca)

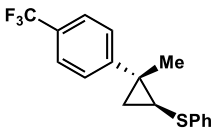

White solid, 68% yield, 94:6 *er*, >20:1 *dr*, $[\alpha]^{24}_{D}$ = +19.4 (*c* 0.9, $CHCl_3$). **^{1}H NMR** (400 MHz, $CDCl_3$) δ 7.59 (d, *J* = 8.2 Hz, 2H), 7.38 (d, *J* = 8.1 Hz, 2H), 7.35 – 7.24 (m, 4H), 7.21 – 7.11 (m, 1H), 2.57 (dd, *J* = 8.8, 5.6 Hz, 1H), 1.70 (dd, *J* = 8.7, 5.7 Hz, 1H), 1.61 (s, 3H), 1.03 (t, *J* = 5.6 Hz, 1H). **^{13}C NMR** (126 MHz, CDCl3) δ 149.8 (q, *J* = 1.3 Hz), 138.2, 129.0, 128.6 (d, *J* = 32.8 Hz), 127.2, 126.9, 125.7 (q, *J* = 3.8 Hz), 125.5, 124.4 (d, *J* = 272.2 Hz), 29.4, 27.8, 22.4, 20.1. **^{19}F NMR** (376 MHz, $CDCl_3$) δ – 62.6. **IR** (ATR): 2927, 1618, 1480, 1439, 1323, 1164, 1088, 1067, 840, 736, 700, 602. **HRMS** calculated for $C_{17}H_{15}F_3S$ $[M]^+$ 308.0847, found 308.0834. **Chiral SFC**: 100 mm CHIRALCEL OJ-H, 3% ^{i}PrOH, 2.0 mL/min, 254 nm, 44 °C, nozzle pressure = 200 bar CO_2, t_{R1} (major) = 2.3 min, t_{R2} (minor) = 2.6 min.

((1*S*,2*R*)-2-(4-chlorophenyl)-2-methylcyclopropyl)(phenyl)sulfane (3da)

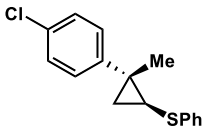

White solid, 92% yield, 94:6 *er*, >20:1 *dr*, $[\alpha]^{24}_{D}$ = +37.4 (*c* 1.3, $CHCl_3$). **^{1}H NMR** (500 MHz, $CDCl_3$) δ 7.41 – 7.30 (m, 6H), 7.30 – 7.24 (m, 2H), 7.24 – 7.18 (m, 1H), 2.57 (dd, *J* = 8.8, 5.5 Hz, 1H), 1.69 (dd, *J* = 8.7, 5.5 Hz, 1H), 1.62 (s, 3H), 1.02 (t, *J* = 5.5 Hz, 1H). **^{13}C NMR** (126 MHz, $CDCl_3$) δ 144.3, 138.4, 132.1, 131.0, 129.0, 128. 8, 128.5, 128.0, 127.1, 125.4, 28.9, 27.5, 22.1, 20.4. **IR** (ATR): 2924, 1583, 1495, 1479, 1439, 1091, 1011, 829, 734, 689. **HRMS** calculated for. $C_{16}H_{15}ClS$ $[M]^+$ 274.0583, found 274.0587. **Chiral SFC**: 100 mm CHIRALCEL AD-H, 2% ^{i}PrOH, 2.0 mL/min, 220 nm, 44 °C, nozzle pressure = 200 bar CO_2, t_{R1} (major) = 7.0 min, t_{R2} (minor) = 5.4 min.

((1*S*,2*R*)-2-benzyl-2-phenylcyclopropyl)(phenyl)sulfane (3ea)

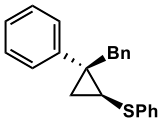

White solid, 61% yield, 92:8 *er*, >20:1 *dr*, $[\alpha]^{24}_{D}$ = -5.8 (*c* 0.6, $CHCl_3$). **^{1}H NMR** (400 MHz, $CDCl_3$) δ 7.51 – 7.40 (m, 2H), 7.40 – 7.29 (m, 2H), 7.29 – 7.08 (m, 9H), 7.00 – 6.88 (m, 2H), 3.32 (d, *J* = 14.6 Hz, 1H), 3.23 (d, *J* = 14.6 Hz, 1H), 2.63 (dd, *J* = 8.5, 5.5 Hz, 1H), 1.76 (ddd, *J* = 8.5, 5.5, 1.3 Hz, 1H), 1.15 (t, *J* = 5.5 Hz, 1H). **^{13}C NMR** (126 MHz, $CDCl_3$) δ 143.7, 139.6, 138.4, 129.6, 129.0, 128.8, 128.4, 128.0, 127.6, 126.6, 126.0, 125.6, 40.3, 34.7, 28.6, 20.1. **IR** (ATR): 3058, 2918, 1601, 1582, 1494, 1479, 1254, 1025, 767, 737, 689. **HRMS** calculated for. $C_{22}H_{21}S$ $[M+H]^+$ 317.1364, found 317.1362. **Chiral SFC**: 100 mm CHIRALCEL AD-H, 2% ^{i}PrOH, 2.0 mL/min, 220 nm, 44 °C, nozzle pressure = 200 bar CO_2, t_{R1} (major) = 6.4 min, t_{R2} (minor) = 7.1 min.

((1*S*,2*R*)-3',4'-dihydro-2'H-spiro[cyclopropane-1,1'-naphthalen]-2-yl)(phenyl)sulfane (3fa)

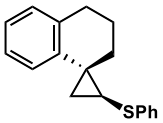

Colorless oil, 98% yield, 98:2 *er*, >20:1 *dr*, $[\alpha]^{24}_{D}$ = -30.0 (*c* 0.5, $CHCl_3$). **^{1}H NMR** (400 MHz, $CDCl_3$) δ 7.28 – 7.19 (m, 4H), 7.19 – 7.05 (m, 4H), 6.80 (d, *J* = 7.3 Hz, 1H), 2.95 – 2.76 (m, 2H), 2.64 (dd, *J* = 8.7, 5.8 Hz, 1H), 2.09 (ddd, *J* = 13.6, 7.4, 3.2 Hz, 1H), 1.97 – 1.79 (m, 2H), 1.78 – 1.65 (m, 2H), 1.01 (t, *J* = 5.7 Hz, 1H). **^{13}C NMR** (126 MHz, $CDCl_3$) δ 140.1, 138.5, 138.0, 129.2, 128.9, 126.6, 126.4, 125.6, 125.0, 121.9, 31.8, 30.7, 29.6, 26.4, 24.7, 22.5. **IR** (ATR): 2926, 1490, 1454, 1155, 1025, 759, 753, 689 cm^{-1}. **HRMS** calculated for $C_{18}H_{18}S$ $[M]^+$ 266.1129, found 266.1115. **Chiral SFC**: 100 mm CHIRALCEL AD-H, 3% ^{i}PrOH, 2.0 mL/min, 254 nm, 44 °C, nozzle pressure = 200 bar CO_2, t_{R1} (major) = 8.6 min, t_{R2} (minor) = 4.5 min.

((1*S*,2*R*)-2-(methoxymethyl)-2-phenylcyclopropyl)(phenyl)sulfane (3ga)

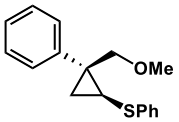

Colorless oil, 85% yield, 70:30 *er*, >20:1 *dr*, $[\alpha]^{24}_{D}$ = +14.7 (*c* 0.3, $CHCl_3$). **^{1}H NMR** (400 MHz, $CDCl_3$) δ 7.45 – 7.40 (m, 2H), 7.40 – 7.34 (m, 2H), 7.34 – 7.22 (m, 5H), 7.22 – 7.14 (m, 1H), 3.86 (d, *J* = 10.2 Hz, 1H), 3.82 (d, *J* = 10.2 Hz, 1H), 3.28 (s, 3H), 2.66 (dd, *J* = 8.2, 5.6 Hz, 1H), 1.68 (dd, *J* = 8.2, 5.6 Hz, 1H), 1.14 (t, *J* = 5.5 Hz, 1H).**^{13}C NMR** (126 MHz, $CDCl_3$) δ 142.7, 138.1, 129.0, 128.6, 128.4, 127.6, 126.9, 125.6, 76.5, 59.0, 33.2, 27.3, 20.0. **IR** (ATR): 2920, 1479, 1117, 1100, 1025, 766, 737, 689 cm^{-1}. **HRMS** calculated for. $C_{17}H_{18}OS$ $[M]^+$ 270.1078, found 270.1066. **Chiral SFC**: 100 mm CHIRALCEL AD-H, 3% ^{i}PrOH, 2.0 mL/min, 254 nm, 44 °C, nozzle pressure = 200 bar CO_2, t_{R1} (major) = 5.8 min, t_{R2} (minor) = 4.4 min.

2.2 Ring-Opened Hydrothiolation General Procedures and Compound Characterization

Ring-Opened General Procedure A:

In a N_2-filled glove box, $[Rh(cod)Cl]_2$ (1.2 mg, 0.0025 mmol), **L8** (5.9 mg, 0.0050 mmol), and DCE (0.30 mL) were added to a 1-dram vial containing a stir bar. The resulting mixture was stirred for 10 min. Thiol **2** (11.0 mg, 0.10 mmol) was added followed by cyclopropene **1** (0.10 mL, 1.2 M solution in DCE, 0.12 mmol) to initiate the reaction. The mixture was held at 0 °C until no starting material was observed by TLC. The regioselectivity ratio was determined by ^{1}H NMR analysis of the unpurified reaction mixture. Isolated yields (obtained by column chromatography on silica gel or preparative thin-layer chromatography) of the title compound are reported.

Ring-Opened General Procedure B:

In a N_2-filled glove box, $[Rh(cod)Cl]_2$ (1.2 mg, 0.0025 mmol), **L8** (5.9 mg, 0.0050 mmol), and DCE (0.30 mL) were added to a 1-dram vial containing a stir bar. The resulting mixture was stirred for 10 min. Thiol **2** (11.0 mg, 0.10 mmol) was added followed by cyclopropene **1** (0.10 mL, 1.2 M solution in DCE, 0.12 mmol) to initiate the reaction. The mixture was held at 30 °C until no starting material was observed by TLC. The regioselectivity ratio was determined by ^{1}H NMR analysis of the unpurified reaction mixture. Isolated yields (obtained by column chromatography on silica gel or preparative thin-layer chromatography) of the title compound are reported.

Ring-Opened General Procedure C:

In a N_2-filled glove box, $[Rh(cod)Cl]_2$ (1.2 mg, 0.0025 mmol), **L7** (5.9 mg, 0.0050 mmol), and DCE (0.30 mL) were added to a 1-dram vial containing a stir bar. The resulting mixture was stirred for 10 min. Thiol **2** (11.0 mg, 0.10 mmol) was added followed by cyclopropene **1** (0.10 mL, 1.2 M solution in DCE, 0.12 mmol) to initiate the reaction. The mixture was held at 30 °C until no starting material was observed by TLC. The regioselectivity ratio was determined by ^{1}H NMR analysis of the unpurified reaction mixture. Isolated yields (obtained by column chromatography on silica gel or preparative thin-layer chromatography) of the title compound are reported.

(*S*)-phenyl(2-phenylbut-3-en-2-yl)sulfane (4aa)

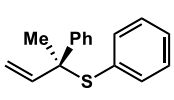

General Procedure A. Colorless oil, 86% yield, 96:4 *er*, >20:1 *rr*, $[\alpha]^{24}_D$ = -84.3 (*c* 0.4, $CHCl_3$). The characterization data is in agreement with previously reported spectral data.[3] **^{1}H NMR** (400 MHz, $CDCl_3$) δ 7.57 – 7.50 (m, 2H), 7.37 – 7.27 (m, 5H), 7.27 –

7.17 (m, 3H), 6.31 (dd, *J* = 17.3, 10.6 Hz, 1H), 5.15 (d, *J* = 10.6 Hz, 1H), 4.99 (d, *J* = 17.3 Hz, 1H), 1.69 (s, 3H). **^{13}C NMR** (125 MHz, $CDCl_3$) δ 144. 6, 143.0, 136.9, 132.6, 128.8, 128.4, 128.3, 127.4, 127.1, 113. 6, 56.7, 26.4. **IR** (ATR): 2926, 1490, 1438, 1368, 1059, 1025, 915, 747. **HRMS** calculated for $C_{16}H_{16}S$ $[M]^+$ 240.0973, found 240.0957. **Chiral SFC**: 100 mm CHIRALCEL AD-H, 3% ^{i}PrOH, 2.0 mL/min, 254 nm, 44 °C, nozzle pressure = 200 bar CO_2, t_{R1} (major) = 2.2 min, t_{R2} (minor) = 2.0 min.

(*S*)-(2-phenylbut-3-en-2-yl)(p-tolyl)sulfane (4ab)

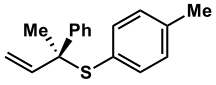

General Procedure A. Colorless oil. 90% yield. 96:4 *er*, >20:1 *rr*. $[\alpha]^{24}_D$ = -44.0 (*c* 1.0, $CHCl_3$). **^{1}H NMR** (499 MHz, $CDCl_3$) δ 7.56 (d, *J* = 7.6 Hz, 2H), 7.34 (t, *J* = 7.6 Hz, 2H), 7.27 (d, *J* = 7.0 Hz, 1H), 7.22 (d, *J* = 8.0 Hz, 2H), 7.06 (d, *J* = 7.9 Hz, 2H), 6.33 (dd, *J* = 17.3, 10.6 Hz, 1H), 5.16 (d, *J* = 10.6 Hz, 1H), 4.99 (d, *J* = 17.3 Hz, 1H), 2.34 (s, 3H), 1.70 (s, 3H). **^{13}C NMR** (125 MHz, $CDCl_3$) δ 144.7, 143.1, 139.0, 137.0, 129.2, 129.0, 128.2, 127.4, 127.0, 113.4, 56.5, 26.3, 21.4. **IR** (ATR): 3020, 2974, 2922, 1630, 1600, 1490, 1444, 1076, 1059, 914, 810, 697. **HRMS** calculated for $C_{17}H_{18}S$ $[M]^+$ 254.1129, found 254.1106. **Chiral SFC**: 100 mm CHIRALCEL OJ-H, 2% ^{i}PrOH, 2.0 mL/min, 254 nm, 44 °C, nozzle pressure = 200 bar CO_2, t_{R1} (major) = 5.8 min, t_{R2} (minor) = 7.7 min.

(*S*)-(4-(tert-butyl)phenyl)(2-phenylbut-3-en-2-yl)sulfane (4ac)

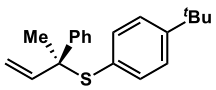

General Procedure A. Colorless oil, 85% yield, 96:4 *er*, >20:1 *rr*, $[\alpha]^{24}_D$ = -77.7 (*c* 1.0, $CHCl_3$). **^{1}H NMR** (400 MHz, $CDCl_3$) δ 7.55 (d, *J* = 7.8 Hz, 2H), 7.32 (t, *J* = 7.5 Hz, 2H), 7.29 – 7.18 (m, 5H), 6.32 (dd, *J* = 17.3, 10.6 Hz, 1H), 5.15 (d, *J* = 10.6 Hz, 1H), 4.99 (d, *J* = 17.3 Hz, 1H), 1.69 (s, 3H), 1.30 (s, 9H). **^{13}C NMR** (126 MHz, $CDCl_3$) δ 152.0, 144.7,

143.2, 136.6, 129.2, 128.2, 127.4, 127.0, 125.5, 113.4, 56.6, 34.8, 31.4, 26.4. **IR** (ATR): 2962, 2867, 1633, 1597, 1489, 1444, 1363, 1267, 1059, 1014, 914, 829, 760, 697 cm^{-1}. **HRMS** calculated for $C_{20}H_{24}S$ $[M]^+$ 296.1599, found 296.1597. **Chiral SFC**: 100 mm CHIRALCEL AD-H, 3% ^{i}PrOH, 2.0 mL/min, 220 nm, 44 °C, nozzle pressure = 200 bar CO_2, t_{R1} (major) = 3.4 min, t_{R2} (minor) = 5.6 min.

(*S*)-(4-methoxyphenyl)(2-phenylbut-3-en-2-yl)sulfane (4ah)

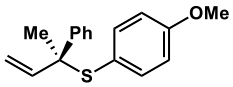

General Procedure A. Colorless oil. 86% yield. 92:8 *er*, >20:1 *rr*. $[\alpha]^{24}_D$ = -25.7 (*c* 1.4, $CHCl_3$). **^{1}H NMR** (499 MHz, $CDCl_3$) δ 7.55 (d, *J* = 7.5 Hz, 2H), 7.35 (t, *J* = 7.6 Hz, 2H), 7.31 – 7.22 (m, 3H), 6.80 (d, *J* = 8.8 Hz, 2H), 6.33 (dd, *J* = 17.3, 10.6 Hz, 1H), 5.17 (d, *J* = 10.6 Hz, 1H), 4.99 (d, *J* = 17.3 Hz, 1H), 3.82 (s, 3H), 1.70 (s, 3H). **^{13}C NMR** (125 MHz, $CDCl_3$) δ 160.5, 144.6, 143.1, 138.8, 128.2, 127.4, 127.0, 123.3, 113.9, 113.4, 56.5, 55.4, 26.1. **IR** (ATR): 3091, 2995, 1586, 1488, 1244, 1025, 905, 694. **HRMS** calculated for $C_{17}H_{18}OS$ $[M]^+$ 270.1078, found 270.1086. **Chiral SFC**: 100 mm CHIRALCEL OJ-H, 2% ^{i}PrOH, 2.0 mL/min, 254 nm, 44 °C, nozzle pressure = 200 bar CO_2, t_{R1} (major) = 9.6 min, t_{R2} (minor) = 13.2 min.

(*S*)-(4-bromophenyl)(2-phenylbut-3-en-2-yl)sulfane (4ai)

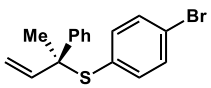

General Procedure A. Colorless oil. 88% yield. 95:5 *er*, >20:1 *rr*. $[\alpha]^{24}_D$ = -35.9 (*c* 1.1, $CHCl_3$. ^{1}H NMR (499 MHz, $CDCl_3$) δ 7.56 – 7.47 (m, 2H), 7.40 – 7.29 (m, 4H), 7.29 – 7.22 (m, 1H), 7.18 – 7.11 (m, 2H), 6.29 (dd, *J* = 17.3, 10.6 Hz, 1H), 5.18 (dd, *J* = 10.6, 0.7 Hz, 1H), 5.01 (dd, *J* = 17.3, 0.7 Hz, 1H), 1.69 (s, 3H). **^{13}C NMR** (126 MHz, $CDCl_3$) δ 144.2, 142.7, 142.7, 138.3, 131.8, 131.6, 128.4, 127.4, 127.3, 123.6, 114.0, 57.0, 26.3. **IR** (ATR):

3056, 2973, 2926, 1471, 1068, 1009, 915, 696. **HRMS** calculated for $C_{16}H_{15}BrS$ $[M]^+$ 318.0078, found 318.0087. **Chiral SFC**: 100 mm CHIRALCEL OJ-H, 5% ^{i}PrOH, 2.0 mL/min, 220 nm, 44 °C, nozzle pressure = 200 bar CO_2, t_{R1} (major) = 4.5 min, t_{R2} (minor) = 6.0 min.

(*S*)-(4-fluorophenyl)(2-phenylbut-3-en-2-yl)sulfane (4aj)

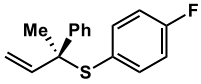

General Procedure A. Colorless oil. 83% yield. 95:5 *er*, >20:1 *rr*. $[\alpha]^{24}_D$ = -37.9 (*c* 0.7, $CHCl_3$). **^{1}H NMR** (499 MHz, $CDCl_3$) δ 7.53 (d, *J* = 7.3 Hz, 2H), 7.35 (t, *J* = 7.6 Hz, 2H), 7.32 – 7.27 (m, 3H), 6.95 (t, *J* = 8.7 Hz, 2H), 6.32 (dd, *J* = 17.3, 10.6 Hz, 1H), 5.19 (d, *J* = 10.6 Hz, 1H), 5.01 (d, *J* = 17.3 Hz, 1H), 1.70 (s, 3H). **^{13}C NMR** (126 MHz, $CDCl_3$) δ 163.5 (d, *J* = 249.0 Hz), 144.3, 142.8, 139.1 (d, *J* = 8.4 Hz), 128.3, 127.9 (d, *J* = 3.4 Hz), 127.4, 127.2, 115.5 (d, *J* = 21.6 Hz), 113.8, 56.8, 26.2. **^{19}F NMR** (376 MHz, $CDCl_3$) δ – 112.6. **IR** (ATR): 3057, 2973, 2922, 1632, 1600, 1490, 1444, 1076, 1059, 914, 810, 697. **HRMS** calculated for $C_{16}H_{15}FS$ $[M]^+$ 258.0879, found 258.0884 **Chiral SFC**: 100 mm CHIRALCEL OJ-H, 3% ^{i}PrOH, 2.0 mL/min, 220 nm, 44 °C, nozzle pressure = 200 bar CO_2, t_{R1} (major) = 4.5 min, t_{R2} (minor) = 6.6 min.

(*S*)-(2-phenylbut-3-en-2-yl)(4-(trifluoromethyl)phenyl)sulfane (4ak)

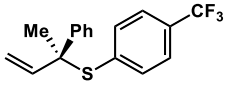

General Procedure A. Colorless oil. 82% yield. 95:5 *er*, >20:1 *rr*. $[\alpha]^{24}_D$ = -30.6 (*c* 1.0, $CHCl_3$). ^{1}H NMR (400 MHz, $CDCl_3$) δ 7.55 – 7.49 (m, 2H), 7.46 – 7.40 (m, 2H), 7.37 – 7.28 (m, 4H), 7.28 – 7.21 (m, 1H), 6.28 (dd, *J* = 17.3, 10.6 Hz, 1H), 5.18 (d, *J* = 10.6 Hz, 1H), 5.04 (d, *J* = 17.3 Hz, 1H), 1.70 (s, 3H). **^{13}C NMR** (126 MHz, $CDCl_3$) δ 144.0, 142.5, 137.9 (q, *J* = 1.7 Hz), 135.9, 130.4 (q, *J* = 32.5 Hz), 128.5, 127.4, 127.4, 125.2 (q, *J* = 3.7 Hz), 124.2 (q, *J* = 270.5 Hz), 114.3, 57.4, 26.7. **^{19}F NMR** (376 MHz, $CDCl_3$) δ – 62.9. **IR** (ATR):

3058, 2978, 2929, 1605, 1398, 1320, 1123, 1101, 1029, 836, 697. **HRMS** calculated for $C_{17}H_{15}F_3S$ $[M]^+$ 308.0847, found 308.0858. **Chiral SFC**: 100 mm CHIRALCEL OJ-H, 2% ^{i}PrOH, 2.0 mL/min, 220 nm, 44 °C, nozzle pressure = 200 bar CO_2, t_{R1} (major) = 2.0 min, t_{R2} (minor) = 2.5 min.

(*S*)-(4-nitrophenyl)(2-phenylbut-3-en-2-yl)sulfane (4al)

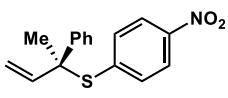

General Procedure B. Yellow oil. 89% yield. 91:9 *er*, >20:1 *rr*. $[\alpha]^{24}_D$ = -63.8 (*c* 0.7, $CHCl_3$). **^{1}H NMR** (400 MHz, $CDCl_3$) δ 7.93 (d, *J* = 8.8 Hz, 2H), 7.46 (d, *J* = 7.7 Hz, 2H), 7.31 – 7.22 (m, 4H), 7.22 – 7.16 (m, 1H), 6.24 (dd, *J* = 17.2, 10.6 Hz, 1H), 5.17 (d, *J* = 10.6 Hz, 1H), 5.06 (d, *J* = 17.2 Hz, 1H), 1.70 (s, 3H). **^{13}C NMR** (126 MHz, $CDCl_3$) δ 147.4, 143.8, 143.3, 142.2, 134.6, 128.9, 127.9, 127.5, 123.6, 115.2, 58.2, 27.3. **IR** (ATR): 2975, 1594, 1575, 1510, 1444, 1335, 1089, 911, 851, 741, 697. **HRMS** calculated for $C_{16}H_{19}N_2O_2S$ $[M+NH_4]^+$ 303.1167, found 303.1159. **Chiral SFC**: 100 mm CHIRALCEL AD-H, 3% ^{i}PrOH, 2.0 mL/min, 220 nm, 44 °C, nozzle pressure = 200 bar CO_2, t_{R1} (major) = 3.1 min, t_{R2} (minor) = 3.5 min.

(*S*)-(2-phenylbut-3-en-2-yl)(m-tolyl)sulfane (4ae)

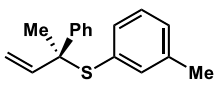

General Procedure A. Colorless oil. 90% yield. 95:5 *er*, >20:1 *rr*. $[\alpha]^{24}_D$ = -40.2 (*c* 0.9, $CHCl_3$). **^{1}H NMR** (400 MHz, $CDCl_3$) δ 7.56 – 7.47 (m, 2H), 7.36 – 7.28 (m, 2H), 7.27 – 7.18 (m, 1H), 7.15 – 7.05 (m, 4H), 6.31 (dd, *J* = 17.3, 10.6 Hz, 1H), 5.15 (d, *J* = 10.6 Hz, 1H), 5.00 (d, *J* = 17.3 Hz, 1H), 2.26 (s, 3H), 1.69 (s, 3H). **^{13}C NMR** (126 MHz, $CDCl_3$) δ 144.7, 143.1, 138.1, 137.5, 133.8, 132.3, 129.6, 128.2, 128.2, 127.5, 127.1, 113. 5, 56.6, 26.4, 21.3. **IR** (ATR): 3054, 2972, 2924, 1591, 1444, 1059, 914, 779, 760, 604. **HRMS** calculated for

$C_{17}H_{18}S$ $[M]^+$ 254.1129, found 254.1116. **Chiral SFC**: 100 mm CHIRALCEL OJ-H, 3% ^{i}PrOH, 2.0 mL/min, 220 nm, 44 °C, nozzle pressure = 200 bar CO_2, t_{R1} (major) = 5.3 min, t_{R2} (minor) = 7.3 min.

(S)-(3-chlorophenyl)(2-phenylbut-3-en-2-yl)sulfane (4am)

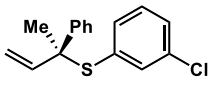

General Procedure A. Colorless oil. 80% yield. 90:10 *er*, >20:1 *rr*. $[\alpha]^{24}_D$ = -43.4 (*c* 0.8, $CHCl_3$). **^{1}H NMR** (400 MHz, $CDCl_3$) δ 7.56 – 7.48 (m, 2H), 7.38 – 7.29 (m, 2H), 7.29 – 7.22 (m, 3H), 7.20 – 7.11 (m, 2H), 6.30 (dd, *J* = 17.3, 10.6 Hz, 1H), 5.19 (d, *J* = 10.6 Hz, 1H), 5.03 (d, *J* = 17.3 Hz, 1H), 1.71 (s, 3H). **^{13}C NMR** (126 MHz, $CDCl_3$) δ 144.1, 142.6, 136.3, 134.7, 133.9, 129.4, 128.9, 128.4, 127.4, 114.0, 57.2, 26.4. **IR** (ATR): 3057, 2973, 2927, 1573, 1459, 1396, 1071, 1059, 917, 778, 697, 683. **HRMS** calculated for $C_{16}H_{15}ClS$ $[M]^+$ 274.0583, found 274.0585. **Chiral SFC**: 100 mm CHIRACEL OJ-H, 5% *i*-PrOH, 2.0 mL/min, 220 nm, 44 °C, nozzle pressure = 200 bar CO_2, t_{R1} (major) = 4.0 min, t_{R2} (minor) = 5.3 min.

(S)-(3-fluorophenyl)(2-phenylbut-3-en-2-yl)sulfane (4an)

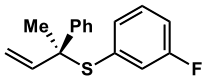

General Procedure A. Colorless oil. 90% yield. 96:4 *er*, >20:1 *rr*. $[\alpha]^{24}_D$ = -38.0 (*c* 0.9, $CHCl_3$). **^{1}H NMR** (499 MHz, $CDCl_3$) δ 7.57 – 7.46 (m, 2H), 7.38 – 7.29 (m, 2H), 7.29 – 7.20 (m, 1H), 7.20 – 7.12 (m, 1H), 7.10 – 7.01 (m, 1H), 7.01 – 6.91 (m, 2H), 6.29 (dd, *J* = 17.3, 10.6 Hz, 1H), 5.18 (d, *J* = 10.6 Hz, 1H), 5.02 (d, *J* = 17.3 Hz, 1H), 1.70 (s, 3H). **^{13}C NMR** (126 MHz, $CDCl_3$) δ 162.1 (d, *J* = 248.3 Hz), 144.2, 142.77, 134.9 (d, *J* = 7.7 Hz), 132.2 (d, *J* = 2.9 Hz), 129.5 (d, *J* = 8.3 Hz), 128.4, 127.4, 127.3, 123.0 (d, *J* = 21.3 Hz), 115.8 (d, *J* = 21.0 Hz), 114.0, 57.2, 26.5. **^{19}F NMR** (376 MHz, $CDCl_3$) δ –113.3. **IR** (ATR): 3060, 2978, 2928, 1596, 1576, 1471, 1214, 878, 781, 696, 680. **HRMS** calculated for $C_{16}H_{15}FS$ $[M]^+$ 258.0879, found

258.0887. **Chiral SFC**: 100 mm CHIRACEL AD-H, 2% *i*-PrOH, 2.0 mL/min, 220 nm, 44 °C, nozzle pressure = 200 bar CO_2, t_{R1} (major) = 2.5 min, t_{R2} (minor) = 2.1 min.

(S)-(2-phenylbut-3-en-2-yl)(o-tolyl)sulfane (4af)

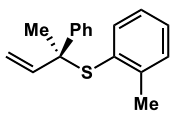

General Procedure A. Colorless oil. 72% yield. >99:1 *er*, >20:1 *rr*. $[\alpha]^{24}_D$ = -31.3 (*c* 1.0, $CHCl_3$). **^{1}H NMR** (400 MHz, $CDCl_3$) δ 7.59 – 7.49 (m, 2H), 7.38 – 7.30 (m, 2H), 7.30 – 7.18 (m, 4H), 7.08 – 6.98 (m, 1H), 6.34 (dd, *J* = 17.3, 10.6 Hz, 1H), 5.13 (d, *J* = 10.6 Hz, 1H), 4.97 (d, *J* = 17.3 Hz, 1H), 2.39 (s, 3H), 1.69 (s, 3H). **^{13}C NMR** (126 MHz, $CDCl_3$) δ 144.8, 143.6, 143.1, 137.8, 132.1, 130.4, 128.9, 128.3, 127.3, 127.1, 125.8, 113.4, 57.3, 26.2, 21.7. **IR** (ATR): 3056, 2971, 2925, 1489, 1444, 1057, 914, 750, 696. **HRMS** calculated for $C_{17}H_{18}S$ $[M]^+$ 254.1129, found 254.1122. **Chiral SFC**: 100 mm CHIRALCEL OJ-H, 2% ^{i}PrOH, 2.0 mL/min, 220 nm, 44 °C, nozzle pressure = 200 bar CO_2, t_{R1} (major) = 7.8 min.

(*S*)-(2-fluorophenyl)(2-phenylbut-3-en-2-yl)sulfane (4ao)

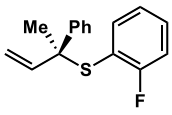

General Procedure A. Colorless oil. 90% yield. 95:5 *er*, >20:1 *rr*. $[\alpha]^{24}_D$ = -33.1 (*c* 0.7, $CHCl_3$). **^{1}H NMR** (499 MHz, $CDCl_3$) δ 7.57 – 7.48 (m, 2H), 7.35 – 7.26 (m, 3H), 7.26 – 7.18 (m, 2H), 7.04 (t, *J* = 8.5 Hz, 1H), 6.97 (t, *J* = 7.6 Hz, 1H), 6.33 (dd, *J* = 17.3, 10.7 Hz, 1H), 5.08 (d, *J* = 10.6 Hz, 1H), 4.90 (d, *J* = 17.3 Hz, 1H), 1.68 (s, 3H). **^{13}C NMR** (126 MHz, $CDCl_3$) δ 164.2 (d, *J* = 247.3 Hz), 144.1, 142.7, 139.8, 131.4 (d, *J* = 8.2 Hz), 128.3, 127.3, 127.3, 124.0 (d, *J* = 3.9 Hz), 119.7 (d, *J* = 18.4 Hz), 115.9 (d, *J* = 24.3 Hz), 113.6, 57.9, 26.3. **^{19}F NMR** (376 MHz, $CDCl_3$) δ – 104.7. **IR** (ATR): 3087, 3056, 2980, 2928, 1588, 1487, 1221, 1155, 916, 830, 696. **HRMS** calculated for $C_{16}H_{15}FS$ $[M]^+$ 258.0879, found 258.0870. **Chiral SFC**: 100 mm

CHIRALCEL AD-H, 3% ^{i}PrOH, 2.0 mL/min, 220 nm, 44 °C, nozzle pressure = 200 bar CO_2, t_{R1} (major) = 2.2 min, t_{R2} (minor) = 1.7 min.

(S)-naphthalen-2-yl(2-phenylbut-3-en-2-yl)sulfane (4ag)

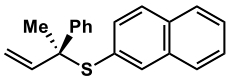

General Procedure A. Yellow solid. 74% yield. 98:2 *er*, >20:1 *rr*. $[\alpha]^{24}_{D}$ = -89.3 (*c* 0.7, $CHCl_3$). **^{1}H NMR** (499 MHz, $CDCl_3$) δ 7.77 (s, 1H), 7.75 – 7.70 (m, 1H), 7.70 – 7.65 (m, 1H), 7.61 (d, *J* = 8.5 Hz, 1H), 7.55 – 7.47 (m, 2H), 7.45 – 7.37 (m, 2H), 7.32 – 7.24 (m, 3H), 7.23 – 7.17 (m, 1H), 6.31 (dd, *J* = 17.3, 10.7 Hz, 1H), 5.10 (d, *J* = 10.6 Hz, 1H), 4.95 (d, *J* = 17.3 Hz, 1H), 1.68 (s, 3H). **^{13}C NMR** (125 MHz, $CDCl_3$) δ 144.6, 143.0, 136.6, 133.5, 133.4, 133.2, 130.1, 128.3, 128.0, 127.7, 127.5, 127.2, 126.8, 126.3, 113.7, 57.0, 26.5. **IR** (ATR): 3053, 2925, 1583, 1490, 1444, 1368, 1058, 916, 814, 742, 697. **HRMS** calculated for $C_{20}H_{18}S$ $[M]^+$ 290.1129, found 290.1124. **Chiral SFC**: 100 mm CHIRALCEL OJ-H, 4% ^{i}PrOH, 2.0 mL/min, 220 nm, 44 °C, nozzle pressure = 200 bar CO_2, t_{R1} (major) = 14.9 min, t_{R2} (minor) = 19.6 min.

(*S*)-phenethyl(2-phenylbut-3-en-2-yl)sulfane (4ap)

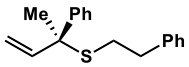

General Procedure C. Colorless oil. 63% yield. 74:26 *er*, >20:1 *rr*. $[\alpha]^{24}_{D}$ = -7.4 (*c* 0.6, $CHCl_3$). **^{1}H NMR** (499 MHz, $CDCl_3$) δ 7.57 – 7.46 (m, *J* = 7.1 Hz, 2H), 7.38 – 7.29 (m, *J* = 7.6 Hz, 2H), 7.29 – 7.21 (m, 3H), 7.21 – 7.16 (m, *J* = 13.5, 6.3 Hz, 1H), 7.16 – 7.08 (m, *J* = 7.1 Hz, 2H), 6.20 (dd, *J* = 17.2, 10.6 Hz, 1H), 5.22 (d, *J* = 10.5 Hz, 1H), 5.16 (d, *J* = 17.3 Hz, 1H), 2.76 (t, *J* = 7.9 Hz, 2H), 2.67 – 2.53 (m, 2H), 1.74 (s, 3H). **^{13}C NMR** (125 MHz, $CDCl_3$) δ 144.7, 142.8, 140.9, 128.6, 128.5, 128.4, 127.2, 127.0, 126.4, 113.4, 53.8, 36.0, 31.5, 27.2. **IR** (ATR): 3026, 2924, 1630, 1600, 1490, 1444, 1369, 1029, 915, 738, 670. **HRMS**

calculated for $C_{18}H_{20}S$ $[M]^+$ 268.1286, found 268.1277. **Chiral SFC**: 100 mm CHIRALCEL OJ-H, 3% ^{i}PrOH, 2.0 mL/min, 220 nm, 44 °C, nozzle pressure = 200 bar CO_2, t_{R1} (major) = 9.7 min, t_{R2} (minor) = 19.0 min.

(*S*)-2-(((2-phenylbut-3-en-2-yl)thio)methyl)furan (4aq)

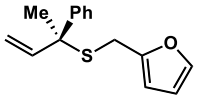

General Procedure C. Colorless oil, 71% yield, 74:26 *er*, >20:1 *rr*, $[\alpha]^{24}_D$ = -8.0 (*c* 0.7, $CHCl_3$). **^{1}H NMR** (499 MHz, $CDCl_3$) δ 7.52 (d, *J* = 7.6 Hz, 2H), 7.34 – 7.27 (m, 3H), 7.25 – 7.18 (m, 1H), 6.26 – 6.15 (m, 2H), 6.05 (d, *J* = 2.5 Hz, 1H), 5.25 (d, *J* = 10.6 Hz, 1H), 5.18 (d, *J* = 17.3 Hz, 1H), 3.58 (d, *J* = 14.1 Hz, 1H), 3.54 (d, *J* = 14.1 Hz, 1H), 1.73 (s, 3H). **^{13}C NMR** (126 MHz, $CDCl_3$) δ 151.7, 144.2, 142.6, 142.4, 142.0, 128.5, 127.2, 113.9, 110.6, 107.5, 54.4, 27.2, 27.0. **IR** (ATR): 2970, 1631, 1597, 1490, 1444, 1149, 1063, 1009, 934, 733, 697, 598. **HRMS** calculated for $C_{15}H_{16}OS$ $[M]^+$ 244.0922, found 244.0919. **Chiral SFC**: 100 mm CHIRALCEL OJ-H, 3% ^{i}PrOH, 2.0 mL/min, 220 nm, 44 °C, nozzle pressure = 200 bar CO_2, t_{R1} (major) = 5.4 min, t_{R2} (minor) = 6.7 min.

(*S*)-phenyl(2-(p-tolyl)but-3-en-2-yl)sulfane (4ba)

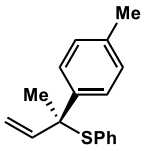

General Procedure A. Colorless oil, 83% yield, 95:5 *er*, >20:1 *rr*, $[\alpha]^{24}_D$ = -66.5 (*c* 0.9, $CHCl_3$). The characterization data is in agreement with previously reported spectral data.[3] **^{1}H NMR** (400 MHz, $CDCl_3$) δ 7.48 – 7.39 (d, *J* = 8.0 Hz, 2H), 7.39 – 7.27 (m, 3H), 7.27 – 7.20 (m, 2H), 7.18 – 7.10 (d, *J* = 7.9 Hz, 2H), 6.32 (dd, *J* = 17.3, 10.6 Hz, 1H), 5.13 (d, *J* = 10.6 Hz, 1H), 4.96 (d, *J* = 17.3 Hz, 1H), 2.36 (s, 3H), 1.68 (s, 3H). **IR** (ATR): 2922, 1583, 1515, 1479, 1438, 1112, 1024, 817, 737, 690. cm^{-1}. **HRMS** calculated for $C_{17}H_{19}S$ $[M+H]^+$ 255.1207,

found 255.1222. **Chiral SFC**: 100 mm CHIRALCEL OJ-H, 3% ^{i}PrOH, 2.0 mL/min, 220 nm, 44 °C, nozzle pressure = 200 bar CO_2, t_{R1} (major) = 7.6 min, t_{R2} (minor) = 9.9 min.

(*S*)-phenyl(2-(4-(trifluoromethyl)phenyl)but-3-en-2-yl)sulfane (4ca)

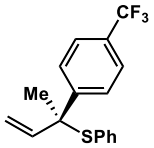

General Procedure C. Colorless oil, 58% yield, 97:3 *er*, >20:1 *rr*, $[\alpha]^{24}_{D}$ = -63.7 (*c* 0.8, $CHCl_3$). The characterization data is in agreement with previously reported spectral data.[3] **^{1}H NMR** (499 MHz, $CDCl_3$) δ 7.62 (d, *J* = 7.4 Hz, 2H), 7.56 (d, *J* = 7.7 Hz, 2H), 7.34 – 7.17 (m, 5H), 6.26 (dd, *J* = 17.3, 10.7 Hz, 1H), 5.19 (d, *J* = 10.5 Hz, 1H), 5.01 (d, *J* = 17.3 Hz, 1H), 1.69 (s, 3H). **^{19}F NMR** (376 MHz, $CDCl_3$) δ – 62.7. **IR** (ATR): 2929, 1616, 1438, 1324, 1165, 1115, 1070, 1015, 919, 842, 748, 692. cm^{-1}. **HRMS** calculated for $C_{17}H_{15}F_3S$ $[M]^+$ 308.0847, found 308.0847. **Chiral SFC**: 100 mm CHIRALCEL OJ-H, 3% ^{i}PrOH, 2.0 mL/min, 220 nm, 44 °C, nozzle pressure = 200 bar CO_2, t_{R1} (major) = 1.6 min, t_{R2} (minor) = 1.9 min.

(*S*)-(2-(4-chlorophenyl)but-3-en-2-yl)(phenyl)sulfane (4da)

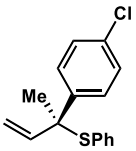

General Procedure A. Colorless oil, 65% yield, 96:4 *er*, >20:1 *rr*, $[\alpha]^{24}_{D}$ = -33.7 (*c* 1.0, $CHCl_3$). **^{1}H NMR** (499 MHz, $CDCl_3$) δ 7.57 – 7.40 (m, 2H), 7.38 – 7.28 (m, 5H), 7.28 – 7.22 (m, 2H), 6.28 (dd, *J* = 16.9, 10.9 Hz, 1H), 5.19 (d, *J* = 10.6 Hz, 1H), 5.02 (d, *J* = 17.3 Hz, 1H), 1.69 (s, 3H). **^{13}C NMR** (125 MHz, $CDCl_3$) δ 143.2, 142.6, 136.9, 132.9, 132.2, 129.0, 128.9, 128.5, 128.3, 114.0, 56.2, 26.5. **IR** (ATR): 3057, 2926, 1489, 1438, 1096, 1012, 917, 829, 748, 692. **HRMS** calculated for $C_{16}H_{15}ClS$ $[M]^+$ 274.0583, found 274.0593. **Chiral SFC**: 100 mm CHIRALCEL AD-H, 2% ^{i}PrOH, 2.0 mL/min, 220 nm, 44 °C, nozzle pressure = 200 bar CO_2, t_{R1} (major) = 3.9 min, t_{R2} (minor) = 3.5 min.

(S)-(1,2-diphenylbut-3-en-2-yl)(phenyl)sulfane (4ea)

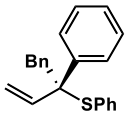

General Procedure C. Colorless oil, 74% yield, 85:15 *er*, >20:1 *rr*, $[\alpha]^{24}_D$ = +10.0 (*c* 1.0, $CHCl_3$). **^{1}H NMR** (400 MHz, $CDCl_3$) δ 7.46 – 7.36 (m, 2H), 7.32 – 7.08 (m, 11H), 6.94 – 6.83 (m, 2H), 6.15 (dd, *J* = 17.4, 10.8 Hz, 1H), 5.29 (dd, *J* = 10.8, 0.7 Hz, 1H), 5.24 (dd, *J* = 17.4, 0.7 Hz, 1H), 3.50 (d, *J* = 13.8 Hz, 1H), 3.33 (d, *J* = 13.8 Hz, 1H). **^{13}C NMR** (125 MHz, $CDCl_3$) δ 142.0, 140. 7, 136.8, 135.9, 133.1, 131.1, 128.9, 128.4, 128.2, 127. 9, 127.6, 127.1, 126.5, 116.0, 62.1, 46.7. **IR** (ATR): 3058, 3028, 1599, 1494, 1437, 1077, 1025, 911, 745, 691. **HRMS** calculated for $C_{22}H_{21}S$ $[M+H]^+$ 317.1364, found 317.1362. **Chiral SFC**: 100 mm CHIRALCEL AD-H, 3% ^{i}PrOH, 2.0 mL/min, 220 nm, 44 °C, nozzle pressure = 200 bar CO_2, t_{R1} (major) = 6.4 min, t_{R2} (minor) = 4.0 min.

(*S*)-phenyl(1-vinyl-1,2,3,4-tetrahydronaphthalen-1-yl)sulfane (4fa)

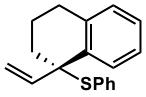

General Procedure A. Colorless oil, 90% yield, 96:4 *er*, >20:1 *rr*, $[\alpha]^{24}_D$ = -96.7 (*c* 0.2, $CHCl_3$). **^{1}H NMR** (400 MHz, $CDCl_3$) δ 7.66 (d, *J* = 7.6 Hz, 1H), 7.41 – 7.33 (m, 2H), 7.33 – 7.28 (m, 1H), 7.28 – 7.23 (m, 2H), 7.23 – 7.11 (m, 2H), 7.07 (d, *J* = 7.2 Hz, 1H), 6.24 (dd, *J* = 17.2, 10.5 Hz, 1H), 5.13 (d, *J* = 10.5 Hz, 1H), 4.79 (d, *J* = 17.2 Hz, 1H), 2.81 – 2.67 (m, 2H), 2.11 – 1.88 (m, 3H), 1.81 – 1.64 (m, 1H). **^{13}C NMR** (126 MHz, $CDCl_3$) δ 143.7, 137.9, 137.8, 136.7, 133.1, 130.1, 129.4, 128.7, 128.5, 127.0, 125.8, 115.0, 57.4, 34.4, 30.3, 19.6. **IR** (ATR): 2930, 1682, 1438, 1085, 1047, 1024, 746, 691 cm^{-1}. **HRMS** calculated for $C_{18}H_{18}S$ $[M]^+$ 266.1129, found 266.1137. **Chiral SFC**: 100 mm CHIRALCEL OJ-H, 3% ^{i}PrOH, 2.0 mL/min, 220 nm, 44 °C, nozzle pressure = 200 bar CO_2, t_{R1} (major) = 5.8 min, t_{R2} (minor) = 7.1 min.

(S)-(2-(naphthalen-2-yl)but-3-en-2-yl)(phenyl)sulfane (4ha)

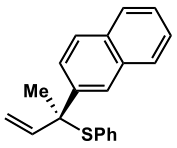

General Procedure A. White solid, 88% yield, 88:12 *er*, >20:1 *rr*, $[\alpha]^{24}_{D}$ = -36.5 (*c* 0.4, $CHCl_3$). **^{1}H NMR** (400 MHz, $CDCl_3$) δ 7.89 – 7.79 (m, 3H), 7.79 – 7.73 (m, 2H), 7.51 – 7.37 (m, 2H), 7.31 – 7.21 (m, 3H), 7.21 – 7.11 (m, 2H), 6.39 (dd, *J* = 17.3, 10.6 Hz, 1H), 5.21 (d, *J* = 10.6 Hz, 1H), 5.06 (d, *J* = 17.3 Hz, 1H), 1.79 (s, 3H). **^{13}C NMR** (126 MHz, $CDCl_3$) δ 142.9, 141.9, 136.8, 133.2, 132.5, 128.8, 128.5, 128.3, 127.9, 127.6, 126.3, 126.2, 126.1, 125.7, 113.9, 56.9, 26.4. **IR** (ATR): 3055, 1674, 1478, 1438, 1022, 818, 742, 689 cm^{-1}. **HRMS** calculated for $C_{20}H_{18}S$ $[M]^+$ 290.1129, found 290.1139. **Chiral SFC**: 100 mm CHIRALCEL OJ-H, 3% ^{i}PrOH, 2.0 mL/min, 220 nm, 44 °C, nozzle pressure = 200 bar CO_2, t_{R1} (major) = 13.1 min, t_{R2} (minor) = 16.8 min.

3. Cyclopropene synthesis

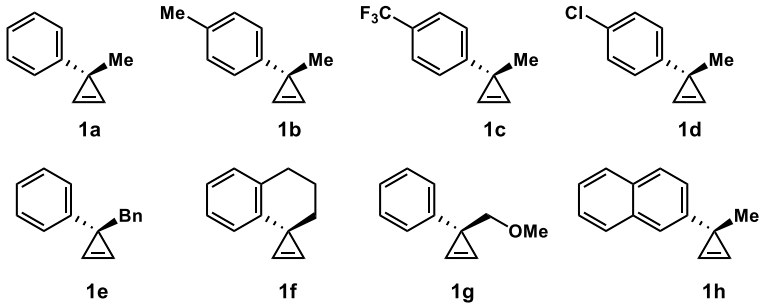

Cyclopropenes **1a**-**1d**, **1f**, and **1h** were synthesized following these reported proecdures.[1,2]

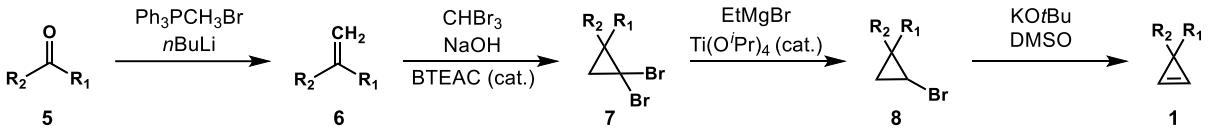

Cyclopropene **1g** was synthesized from 2-phenylacetophenone following these reported proecdures.[2]

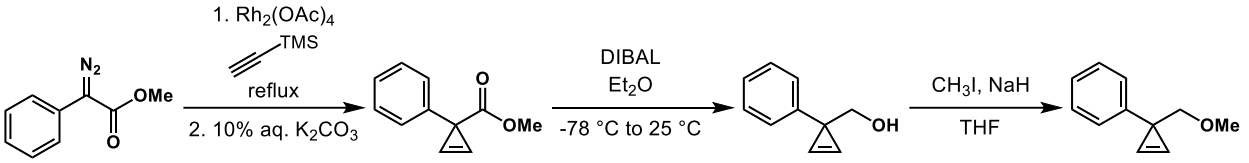

Cyclopropene **1e** was synthesized from 2-phenylacetophenone following these reported proecdures.[1,2]

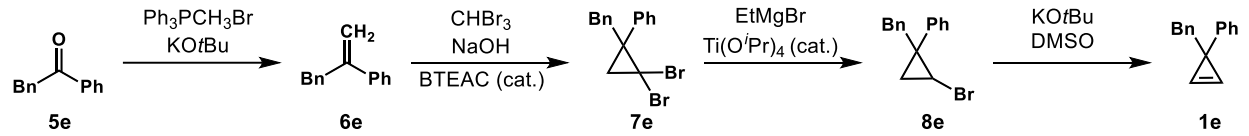

Synthesis of prop-1-en-2-ylbenzene (6e):

Methyltriphenylphoshphonium bromide (11 g, 30 mmol, 3.0 equiv) was added to a flame-dried flask under an atmosphere of N_2. Anhydrous THF (40 mL) was added and the mixture was cooled to 0 °C. KO*t*Bu (3.4 g, 30 mmol, 3.0 equiv) was added all at once and the resulting mixture was stirred for 10 min. A solution of 2-phenylacetophenone **5e** (2.0 g, 10 mmol, 1 equiv) in dry THF (10 mL) was added. The reaction was allowed to warm to room temperature and stirred overnight. The reaction was monitored by TLC for complete consumption of starting material. The mixture was quenched with sat. ammonium chloride and extracted with ethyl acetate (3x). The combined organic layers were dried with $MgSO_4$, filtered, and concentrated under reduced pressure. The crude mixture was purified by column chromatography on silica gel (hexanes) to yield the desired product. ^1H and ^{13}C NMR spectra of the product are in agreement with previously reported data.[4]

Synthesis of (2,2-dibromo-1-methylcyclopropyl)benzene (7e):

Benzyltriethylammonium chloride (0.11 g, 0.46 mmol, 0.050 equiv) was added to a flask charged with a stir bar and placed under an atmosphere of N_2. A solution of **6e** (1.8 g, 9.3 mmol, 1.0 equiv) in bromoform (3.2 mL, 37 mmol, 4.0 equiv) was added followed by dropwise addition of 50% aq. NaOH (1.5 mL, 37 mmol, 4.0 equiv). The resulting mixture was heated to 60 °C and stirred

overnight. Upon completion determined by TLC, the reaction mixture was allowed to cool to room temperature, quenched with water, and extracted with dichloromethane (3x). The combined organic layers were dried with $MgSO_4$, filtered, and concentrated under reduced pressure. The crude mixture was purified by column chromatography on silica gel (hexanes) to yield the desired product.

Synthesis of (2-bromo-1-methylcyclopropyl)benzene (8e):

A 0.74 M solution of ethylmagnesium bromide (5.7 mL, 4.2 mmol, 1.3 equiv) in Et_2O was added dropwise to a cooled solution (0 °C ice bath) of dibromide **7e** (1.2 g, 3.2 mmol, 1.0 equiv) and titanium(IV) isopropoxide (0.10 mL, 0.32 mmol, 0.10 equiv) in Et_2O (6.4 mL). The reaction mixture was stirred for 4 h at 30 °C. The reaction was monitored by TLC for complete consumption of starting material. Upon completion, the reaction mixture was quenched with 10% aq. HCl and extracted with Et_2O (3x). The combined ethereal layers were washed with brine (2x), dried with $MgSO_4$, filtered, and concentrated under reduced pressure. The crude mixture was purified by column chromatography on silica gel (hexanes) to yield the desired product.

Synthesis of (1-methylcycloprop-2-en-1-yl)benzene (1e):

A solution of bromide **8e** (0.73 g, 2.5 mmol, 1.0 equiv) in DMSO (20 mL) was added to a flask under an atmosphere of N_2. A solution of KO*t*Bu (0.43 g, 3.8 mmol, 1.5 equiv) in DMSO (5 mL) was added slowly and the resulting mixture was stirred at 30 °C overnight. The reaction was monitored by TLC for complete consumption of starting material. Upon completion, the reaction mixture was quenched with 10% aq. HCl and extracted with Et2O (3x). The combined ethereal layers were washed with brine (2x), dried with $NaSO_4$, filtered, and concentrated under reduced

pressure. The crude mixture was purified by column chromatography on silica gel (hexanes) to yield the desired product. Purified product was stored in a 1.2 M solution of DCE or MeCN at 0 °C to prevent decomposition.

(1-benzyl-2,2-dibromocyclopropyl)benzene (7e):

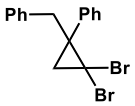

White solid. 34.8% yield. **^{1}H NMR** (500 MHz, $CDCl_3$) δ 7.25 – 7.20 (m, 3H), 7.15 – 7.10 (m, 3H), 7.09 – 7.04 (m, 2H), 6.86 – 6.80 (m, 2H), 3.49 (d, *J* = 13.8 Hz, 1H), 3.10 (d, *J* = 13.9 Hz, 1H), 2.08 (d, *J* = 7.7 Hz, 1H), 2.02 (d, *J* = 7.7 Hz, 1H). **^{13}C NMR** (126 MHz, $CDCl_3$) δ 140.4, 138.1, 129.9, 129.6, 128.2, 128.2, 127.4, 126.6, 46.3, 41.3, 36.4, 32.9. **IR** (ATR): 3084, 3061, 3023, 2958, 1494, 1454, 1013, 757, 698. **HRMS** calculated for $C_{16}H_{14}Br_2$ $[M + NH_4]^+$ 386.9799, found 386.9658.

(1-benzyl-2-bromocyclopropyl)benzene (8e):

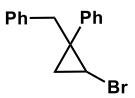

Colorless oil. 81.7% yield. **^{1}H NMR** (500 MHz, $CDCl_3$) δ 7.22 – 7.11 (m, 5H), 7.08 – 7.03 (m, 2H), 7.01 – 6.95 (m, 2H), 3.38 – 3.26 (m, 2H), 3.10 (d, *J* = 14.4 Hz, 1H), 1.68 (t, *J* = 7.2 Hz, 1H), 1.29 (t, *J* = 5.6 Hz, 1H). **^{13}C NMR** (126 MHz, $CDCl_3$) δ 142.5, 139.0, 129.6, 129.0, 128.3, 128.1, 126.8, 126.2, 43.5, 32.2, 30.2, 21.9. **IR** (ATR): 3059, 3026, 2916, 1493, 1445, 765, 697. **HRMS** calculated for $C_{16}H_{15}Br$ $[M + NH_4]^+$ 307.0714, found 307.0695.

(1-benzylcycloprop-2-en-1-yl)benzene (1e):

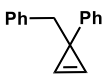

Colorless oil. 34.4% yield. **^{1}H NMR** (500 MHz, $CDCl_3$) δ 7.40 – 7.29 (m, 6H), 7.27 – 7.20 (m, 4H), 7.18 – 7.15 (m, 1H), 7.15 – 7.13 (m, 1H), 3.48 (s, 2H). **^{13}C NMR** (126 MHz, $CDCl_3$) δ 149.0, 140.3, 129.7, 128.3, 128.1, 126.6, 125.8, 125.5, 114.0, 43.2, 28.0. **IR** (ATR): 3083, 3058,

3025, 2915, 2851, 1640, 1493, 1444, 695. **HRMS** calculated for $C_{16}H_{14}$ $[M]^+$ 207.1129, found 207.1157.

4. Mechanism studies for cyclopropene hydrothiolation

4.1. Deuterium-Labeling Study

Synthesis of *d*-2a:

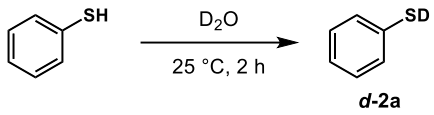

Benezenethiol **2a** (1.62 g, 15 mmol) was dissolved in D_2O (3.0 g, 150 mmol) and vigorously stirred for 2 hours at room temperature. The clear solution was concentrated *in vacuo* and resulted in ***d*-2a** with 86% D incorporation which was determined by ^{1}H NMR. Colorless oil, 84% yield. **^{1}H NMR** (400 MHz, d_6-benzene) δ 7.01 – 6.92 (m, 2H), 6.91 – 6.78 (m, 3H), 3.00 (s, 0.14H).

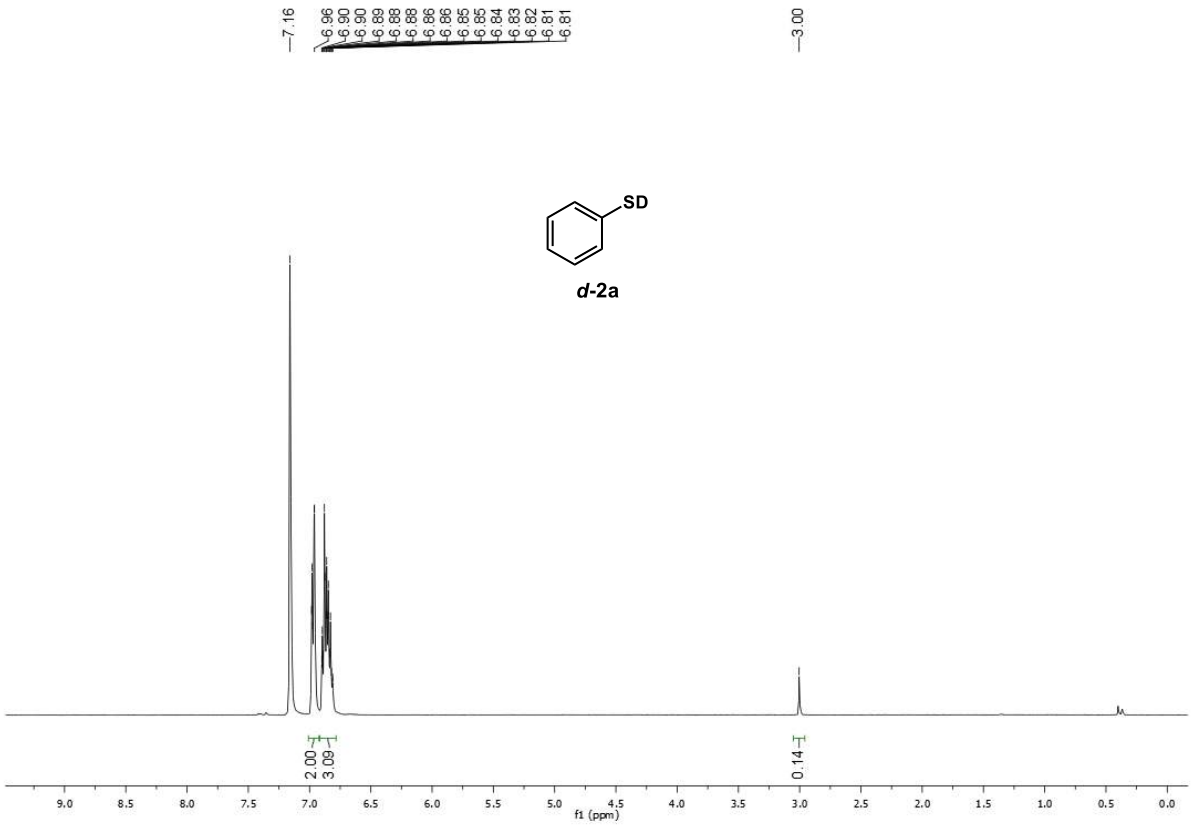

Synthesis of *d*-3aa:

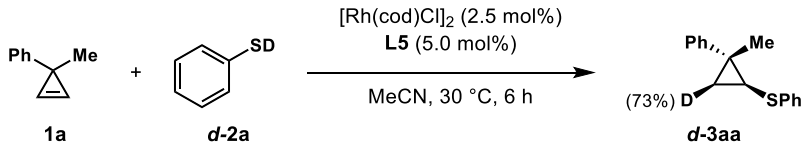

Following the **"Ring-Retained General Procedure", *d*-2a** was used as the thiol partner. Colorless oil, 81% yield, >20:1 *rr*. **^{1}H NMR** (400 MHz, $CDCl_3$) δ 7.40 – 7.29 (m, 7H), 7.28 – 7.22 (m, 2H), 7.18 – 7.11 (m, 1H), 2.55 (d, *J* = 8.4 Hz, 1H), 1.60 (s, 3H), 0.96 (t, *J* = 5.6 Hz, 0.27 H). Deuterium

incorporation was determined by ^{1}H NMR. Percent deuterium (% D) incorporation is depicted as the amount of deuterium in place of a single hydrogen atom at that site.

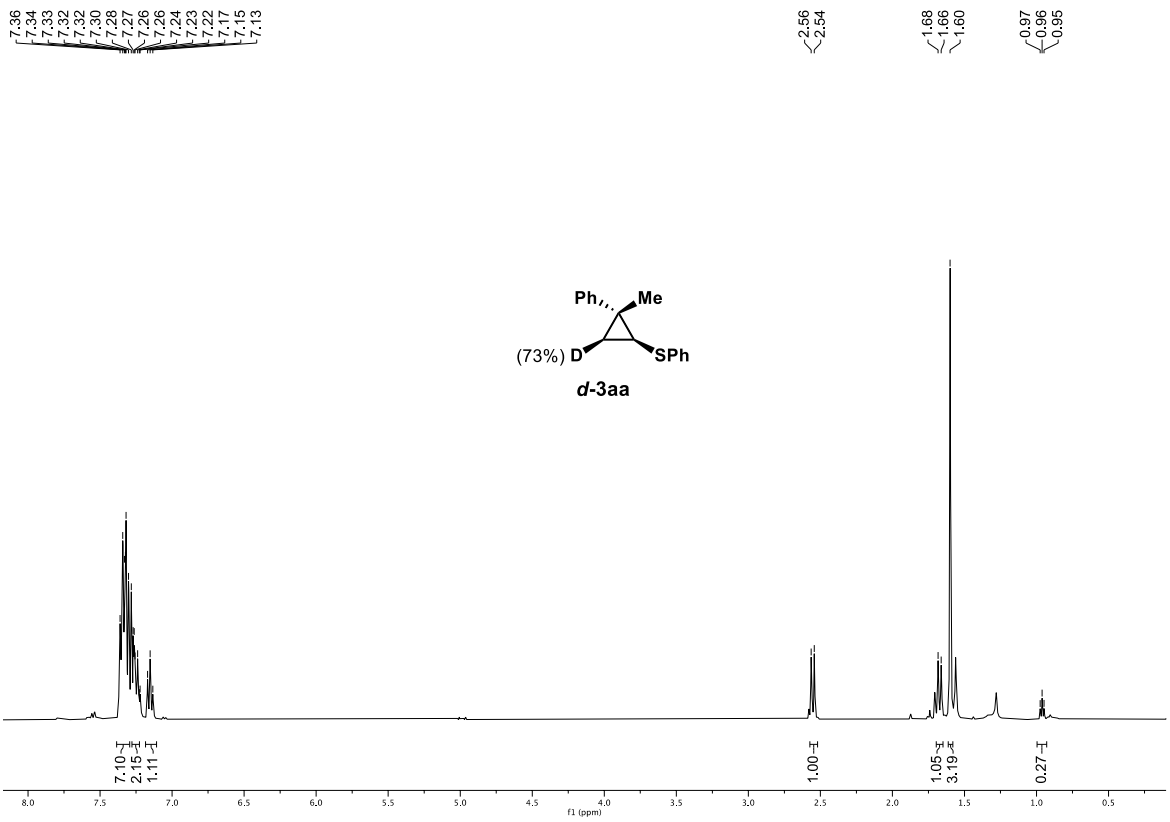

Synthesis of *d*-4aa:

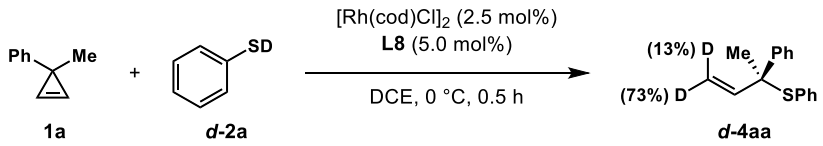

Following the **"Ring-Opened General Procedure A", *d*-2a** was used as the thiol partner. Colorless oil, 83% yield, >20:1 *rr*. **^{1}H NMR** (400 MHz, $CDCl_3$) δ 7.55 (d, *J* = 7.8 Hz, 2H), 7.37 – 7.29 (m, 5H), 7.24 (dd, *J* = 14.6, 7.2 Hz, 3H), 6.33 (d, *J* = 17.3 Hz, 1H), 5.15 (dd, *J* = 10.6, 5.8 Hz,

0.27 H), 4.99 (dd, *J* = 17.3, 5.4 Hz, 0.87 H), 1.71 (s, 3H). Deuterium incorporation was determined by ^{1}H NMR. Percent deuterium (% D) incorporation is depicted as the amount of deuterium in place of a single hydrogen atom at that site.

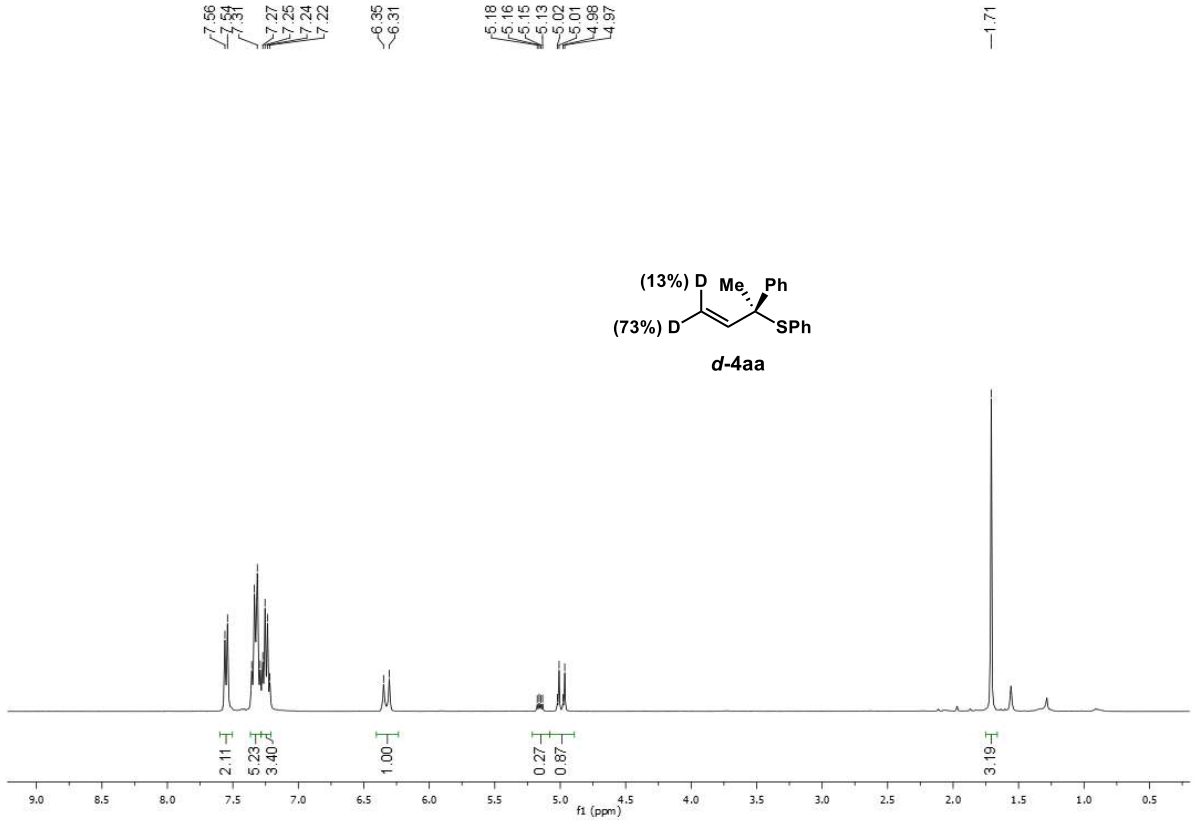

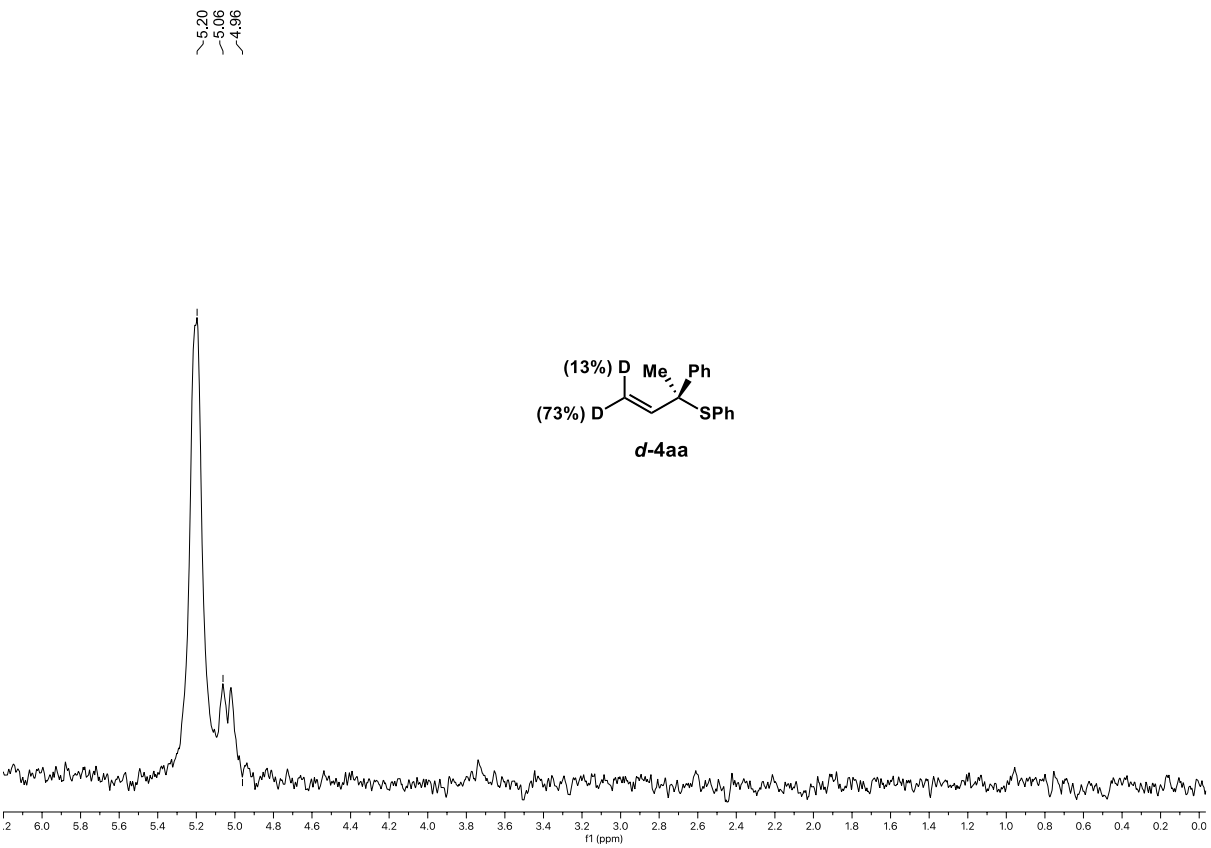

4.2 Initial rate studies

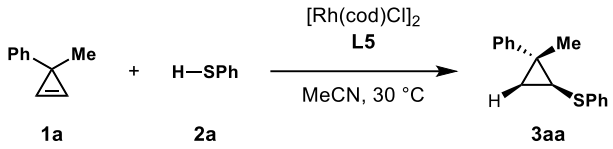

The kinetic profile of the reaction was studied by obtaining initial rates of reaction for different concentrations of (1-methylcycloprop-2-en-1-yl)benzene **1a**, benzenethiol **2a**, and Rh-catalyst.[4] No products of decomposition are observed for the system. The rates were monitored by GC-FID analysis using 1,3,5-trimethoxybenzene as an internal standard.

Determination of the reaction order in (1-methylcycloprop-2-en-1-yl)benzene 1a (entries 1-5)

Representative procedure (entry 1):

In a N_2-filled glove box, a 0.025 M solution of catalyst was prepared by combining $[Rh(cod)Cl]_2$

(7.4 mg, 0.015 mmol), **L5** (16 mg, 0.030 mmol), and MeCN (1.2 mL). The resulting mixture was stirred for 10 min. A second 0.50 M solution of thiol **2a** was prepared by combining **2a** (66 mg, 0.60 mmol) and MeCN (1.2 mL). A vial was charged with a stir bar and 1,3,5-trimethoxybenzene (3.4 mg, 0.020 mmol). Catalyst solution (0.20 mL, 5.0 mol% Rh) was added to the vial, followed by **2a** (0.20 mL, 0.10 mmol). MeCN (0.10 mL) was added so that the final reaction volume was 0.6 mL. The vial was sealed with a Teflon cap. **1a** (0.10 mL, 1.2 M solution in MeCN, 0.12 mmol) was added to the sealed vial to initiate the reaction. 20 μL aliquots were taken every 5 minutes and quenched in 2 mL of ethyl acetate. No further catalysis occurs after dilution in ethyl acetate. The appearance of **3aa** was monitored by internally referenced GC-FID analysis.

Determination of the reaction order in Rh-catalyst (entries 6-10)

Representative procedure (entry 6):

In a N_2-filled glove box, a 0.30 M solution of catalyst was prepared by combining $[Rh(cod)Cl]_2$ (9.9 mg, 0.020 mmol), **L5** (22 mg, 0.040 mmol), and MeCN (1.3 mL). The resulting mixture was stirred for 10 min. A second 0.50 M solution of thiol **2a** was prepared by combining **2a** (66 mg, 0.60 mmol) and MeCN (1.2 mL). A vial was charged with a stir bar and 1,3,5-trimethoxybenzene (2.0 mg, 0.012 mmol). Catalyst solution (0.10 mL, 3.0 mol% Rh) was added to the vial, followed by **2a** (0.20 mL, 0.10 mmol). MeCN (0.13 mL) was added so that the final reaction volume was 0.6 mL. The vial was sealed with a Teflon cap. **1a** (0.17 mL, 1.2 M solution in MeCN, 0.20 mmol) was added to the sealed vial to initiate the reaction. 20 μL aliquots were taken every 5 minutes and quenched in 2 mL of ethyl acetate. No further catalysis occurs after dilution in ethyl acetate. The appearance of **3aa** was monitored by internally referenced GC-FID analysis.

Determination of the reaction order in benzenethiol 2a (entries 11-14)

Representative procedure (entry 11):

In a N_2-filled glove box, a 0.050 M solution of catalyst was prepared by combining $[Rh(cod)Cl]_2$ (7.4 mg, 0.015 mmol), **L5** (16 mg, 0.030 mmol), and MeCN (0.60 mL). The resulting mixture was stirred for 10 min. A second 0.50 M solution of thiol **2a** was prepared by combining **2a** (77 mg, 0.70 mmol) and MeCN (1.4 mL). A vial was charged with a stir bar and 1,3,5-trimethoxybenzene (4.8 mg, 0.029 mmol). Catalyst solution (0.10 mL, 5.0 mol% Rh) was added to the vial, followed by **2a** (0.16 mL, 0.080 mmol). MeCN (0.17 mL) was added so that the final reaction volume was 0.6 mL. The vial was sealed with a Teflon cap. **1a** (0.17 mL, 1.2 M solution in MeCN, 0.20 mmol) was added to the sealed vial to initiate the reaction. 20 μL aliquots were taken every 5 minutes and quenched in 2 mL of ethyl acetate. No further catalysis occurs after dilution in ethyl acetate. The appearance of **3aa** was monitored by internally referenced GC-FID analysis.

Table S1. Kinetic Data for Ring-Retained Cyclopropene Hydrothiolation.

Entry	[1a] (M)	[Rh] (M)	[2a] (M)	Initial rate ($M \cdot min^{-1}$)
1	2.0×10^{-1}	8.3×10^{-3}	1.7×10^{-1}	$(1.1 \pm .04) \times 10^{-3}$
2	2.5×10^{-1}	8.3×10^{-3}	1.7×10^{-1}	$(1.4 \pm .03) \times 10^{-3}$
3	3.0×10^{-1}	8.3×10^{-3}	1.7×10^{-1}	$(1.6 \pm .02) \times 10^{-3}$
4	3.5×10^{-1}	8.3×10^{-3}	1.7×10^{-1}	$(1.9 \pm .04) \times 10^{-3}$
5	4.0×10^{-1}	8.3×10^{-3}	1.7×10^{-1}	$(2.2 \pm .04) \times 10^{-3}$
6	3.3×10^{-1}	5.0×10^{-3}	1.7×10^{-1}	$(9.0 \pm .19) \times 10^{-4}$
7	3.3×10^{-1}	6.7×10^{-3}	1.7×10^{-1}	$(1.2 \pm .03) \times 10^{-3}$
8	3.3×10^{-1}	8.3×10^{-3}	1.7×10^{-1}	$(1.5 \pm .03) \times 10^{-3}$
9	3.3×10^{-1}	1.0×10^{-2}	1.7×10^{-1}	$(1.8 \pm .08) \times 10^{-3}$
10	3.3×10^{-1}	1.2×10^{-2}	1.7×10^{-1}	$(2.1 \pm .05) \times 10^{-3}$
11	3.3×10^{-1}	8.3×10^{-3}	1.3×10^{-1}	$(2.3 \pm .04) \times 10^{-3}$
12	3.3×10^{-1}	8.3×10^{-3}	1.6×10^{-1}	$(2.2 \pm .02) \times 10^{-3}$
13	3.3×10^{-1}	8.3×10^{-3}	2.0×10^{-1}	$(2.1 \pm .04) \times 10^{-3}$
14	3.3×10^{-1}	8.3×10^{-3}	2.7×10^{-1}	$(1.9 \pm .04) \times 10^{-3}$

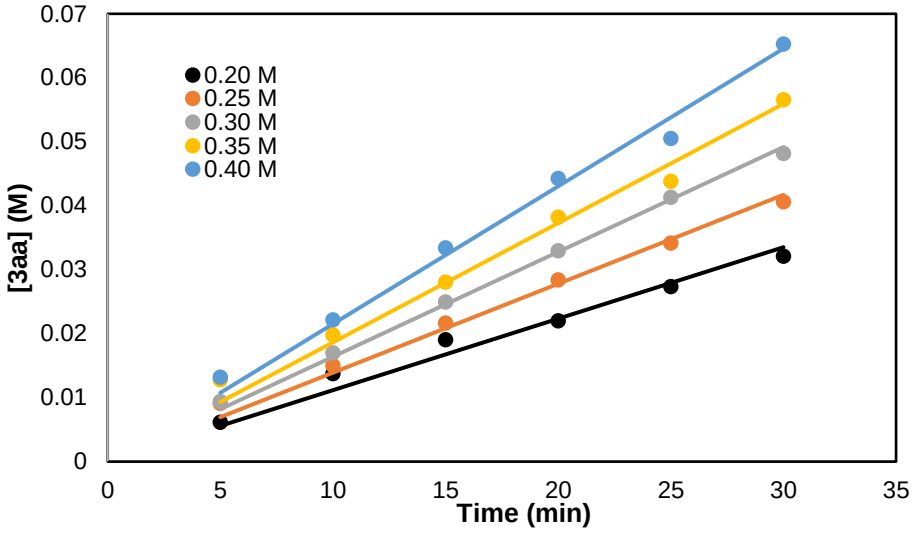

Figure S1. Plots of initial reaction rates at different concentrations of **1a**.

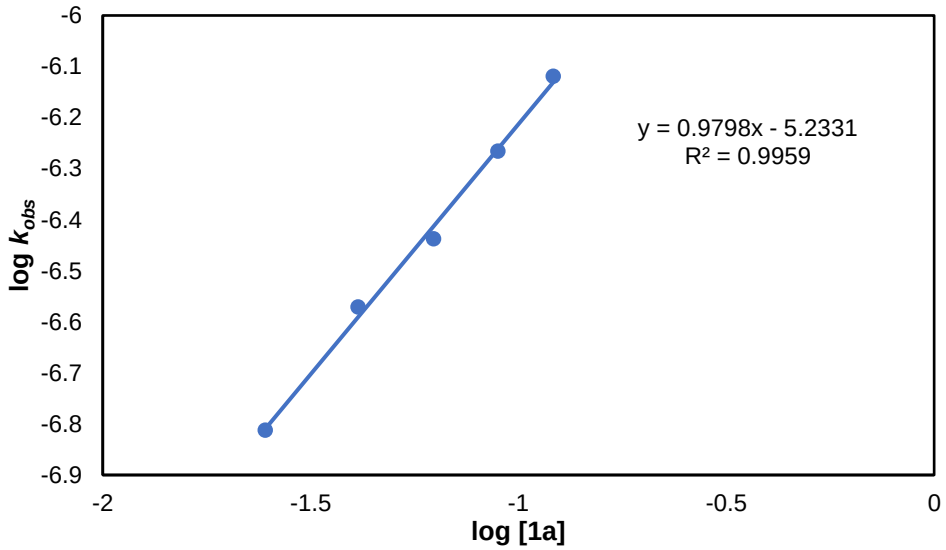

Figure S2. Plot of logk_{obs} vs log[**1a**] (slope = 0.98) for ring-retained cyclopropene hydrothiolation (first order).

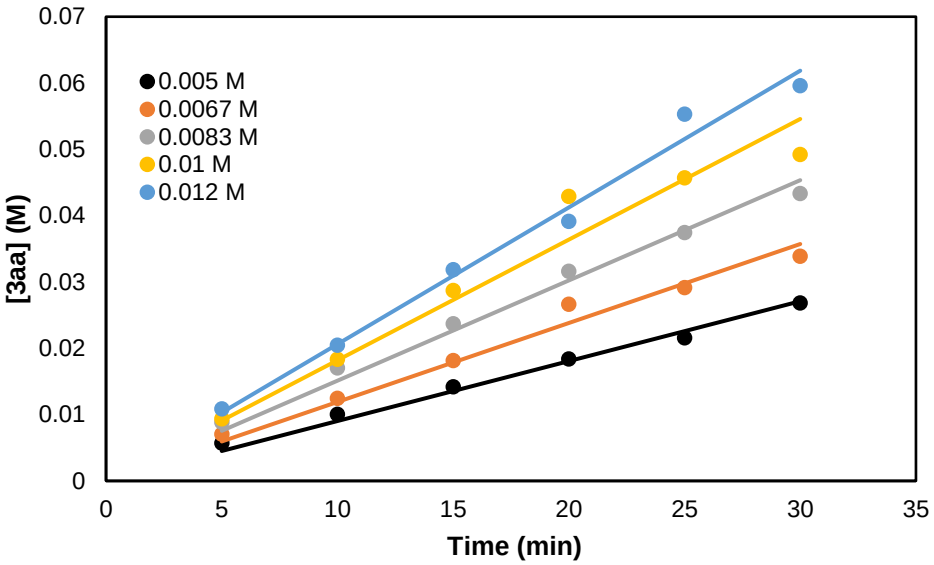

Figure S3. Plots of initial reaction rates at different concentrations of Rh.

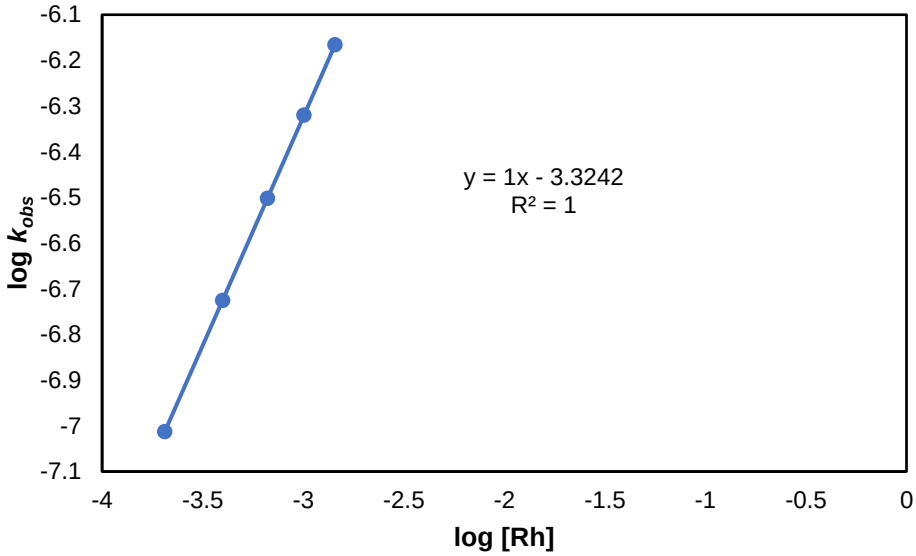

Figure S4. Plot of logk_{obs} vs log[Rh] (slope = 1.0) for ring-retained cyclopropene hydrothiolation (first order).

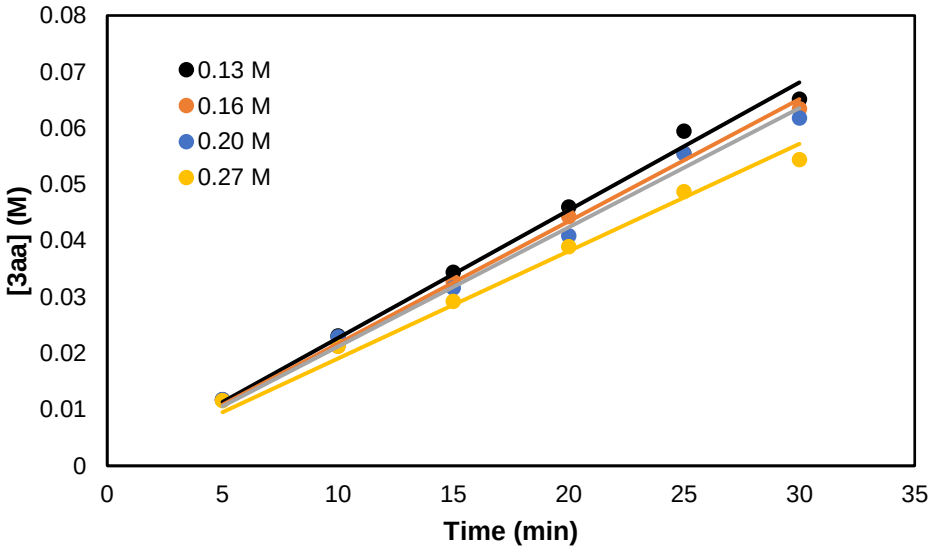

Figure S5. Plots of initial reaction rates at different concentrations of **2a**.

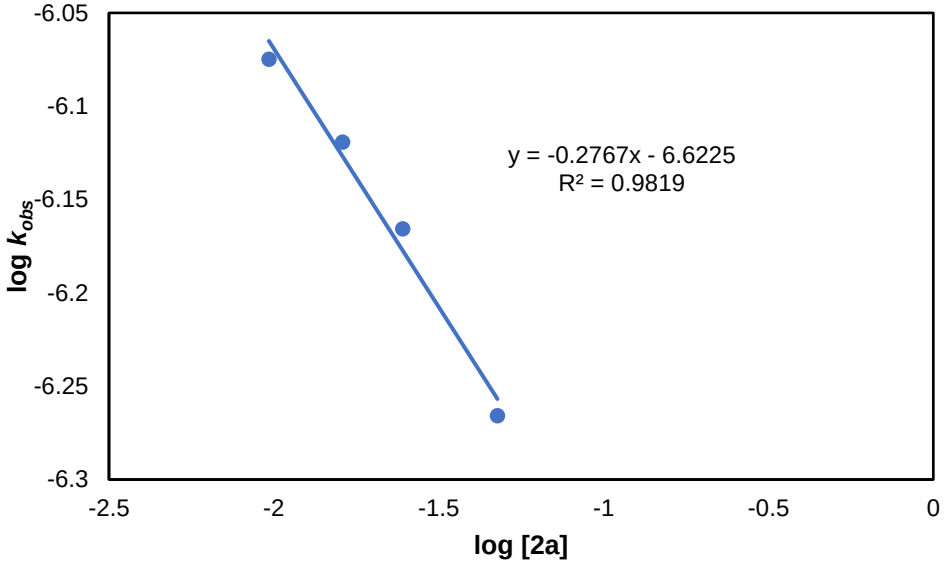

Figure S6. Plot of logk_{obs} vs log[**2a**] (slope = -0.28) for ring-retained cyclopropene hydrothiolation.

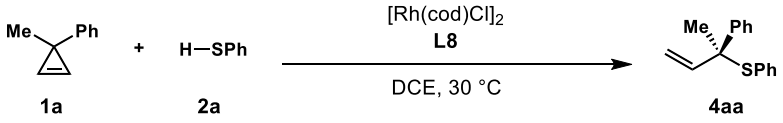

The kinetic profile of the reaction was studied by obtaining initial rates of reaction for different concentrations of (1-methylcycloprop-2-en-1-yl)benzene **1a**, benzenethiol **2a**, and Rh-catalyst. No products of decomposition are observed for the system. The rates were monitored by ^{1}H NMR analysis using 1,3,5-trimethoxybenzene as an internal standard.

Determination of the reaction order in (1-methylcycloprop-2-en-1-yl)benzene 1a (entries 1-5)

Representative procedure (entry 1):

In a N_2-filled glove box, a 0.010 M solution of catalyst was prepared by combining $[Rh(cod)Cl]_2$ (1.5 mg, 0.0030 mmol), **L8** (7.2 mg, 0.0060 mmol), and DCE-d_4 (0.60 mL). The resulting mixture was stirred for 10 min. A second 1.0 M solution of thiol **2a** was prepared by combining **2a** (66 mg, 0.60 mmol) and DCE-d_4 (0.60 mL). 1,3,5-trimethoxybenzene (2.0 mg, 0.012 mmol) was added to a J. Young NMR tube. Catalyst solution (0.10 mL, 1.0 mol% Rh) was then added to the J. Young NMR tube, followed by **2a** (0.10 mL, 0.10 mmol). DCE-d_4 (0.20 mL) was added so that the final reaction volume was 0.50 mL. The J. Young NMR tube was sealed with a Teflon cap. **1a** (0.10 mL, 1.2 M solution in DCE-d_4, 0.12 mmol) was added to the sealed tube to initiate the reaction. A ^1H NMR spectrum was taken every minute with one scan. The appearance of **4aa** was monitored by comparing the integration of one of the vinyl protons of the product (5.16 ppm) to the internal standard (3.77 ppm).

Determination of the reaction order in Rh-catalyst (entries 6-9)

Representative procedure (entry 6):

In a N_2-filled glove box, a 0.010 M solution of catalyst was prepared by combining $[Rh(cod)Cl]_2$ (1.5 mg, 0.0030 mmol), **L8** (7.2 mg, 0.0060 mmol), and DCE-d_4 (0.60 mL). The resulting mixture was stirred for 10 min. A second 1.0 M solution of thiol **2a** was prepared by combining **2a** (66 mg, 0.60 mmol) and DCE-d_4 (0.60 mL). 1,3,5-trimethoxybenzene (2.0 mg, 0.012 mmol) was added to a J. Young NMR tube. Catalyst solution (0.10 mL, 1.0 mol% Rh) was then added to the J. Young NMR tube, followed by **2a** (0.080 mL, 0.080 mmol). DCE-d_4 (0.22 mL) was added so that the

final reaction volume was 0.50 mL. The J. Young NMR tube was sealed with a Teflon cap. **1a** (0.10 mL, 1.2 M solution in DCE-d_4, 0.12 mmol) was added to the sealed tube to initiate the reaction. A ^{1}H NMR spectrum was taken every minute with one scan. The appearance of **4aa** was monitored by comparing the integration of one of the vinyl protons of the product (5.16 ppm) to the internal standard (3.77 ppm).

Determination of the reaction order in benzenethiol 2a (entries 10-13)

Representative procedure (entry 10):

In a N_2-filled glove box, a 0.050 M solution of catalyst was prepared by combining $[Rh(cod)Cl]_2$ (4.9 mg, 0.010 mmol), **L8** (7.2 mg, 0.0060 mmol), and DCE-d_4 (0.60 mL). The resulting mixture was stirred for 10 min. A second 1.0 M solution of thiol **2a** was prepared by combining **2a** (66 mg, 0.60 mmol) and DCE-d_4 (0.60 mL). 1,3,5-trimethoxybenzene (2.0 mg, 0.012 mmol) was added to a J. Young NMR tube. Catalyst solution (0.10 mL, 1.0 mol% Rh) was then added to the J. Young NMR tube, followed by **2a** (0.080 mL, 0.080 mmol). DCE-d_4 (0.22 mL) was added so that the final reaction volume was 0.50 mL. The J. Young NMR tube was sealed with a Teflon cap. **1a** (0.10 mL, 1.2 M solution in DCE-d_4, 0.12 mmol) was added to the sealed vial to initiate the reaction. A ^{1}H NMR spectrum was taken every minute with one scan. The appearance of **4aa** was monitored by comparing the integration of one of the vinyl protons of the product (5.16 ppm) to the internal standard (3.77 ppm).

Table S2. Kinetic Data for Ring-Opened Cyclopropene Hydrothiolation.

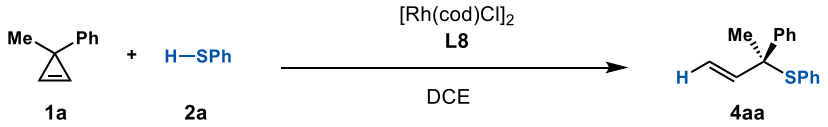

1a 2a 4aa

Entry	[1a] (M)	[Rh] (M)	[2a] (M)	Initial rate (M•min^{-1})
1	1.9 x 10^{-1}	2.0 x 10^{-3}	2.0 x 10^{-1}	(6.7 ± .3) x 10^{-3}
2	2.4 x 10^{-1}	2.0 x 10^{-3}	2.0 x 10^{-1}	(7.4 ± .4) x 10^{-3}
3	2.9 x 10^{-1}	2.0 x 10^{-3}	2.0 x 10^{-1}	(9.2 ± .2) x 10^{-3}
4	3.8 x 10^{-1}	2.0 x 10^{-3}	2.0 x 10^{-1}	(1.4 ± .02) x 10^{-2}
5	2.4 x 10^{-1}	2.0 x 10^{-3}	2.0 x 10^{-1}	(3.4 ± .3) x 10^{-3}
6	2.4 x 10^{-1}	4.0 x 10^{-3}	2.0 x 10^{-1}	(6.7 ± .4) x 10^{-3}
7	2.4 x 10^{-1}	6.0 x 10^{-3}	2.0 x 10^{-1}	(1.1 ± .04) x 10^{-2}
8	2.4 x 10^{-1}	8.0 x 10^{-3}	2.0 x 10^{-1}	(1.2 ± .04) x 10^{-2}
9	2.4 x 10^{-1}	1.0 x 10^{-2}	2.0 x 10^{-1}	(1.6 ± .08) x 10^{-2}
10	2.4 x 10^{-1}	2.0 x 10^{-3}	1.6 x 10^{-1}	(9.0 ± .7) x 10^{-3}
11	2.4 x 10^{-1}	2.0 x 10^{-3}	2.0 x 10^{-1}	(8.9 ± .5) x 10^{-3}
12	2.4 x 10^{-1}	2.0 x 10^{-3}	2.2 x 10^{-1}	(9.0 ± .6) x 10^{-3}
13	2.4 x 10^{-1}	2.0 x 10^{-3}	2.4 x 10^{-1}	(8.8 ± .5) x 10^{-3}

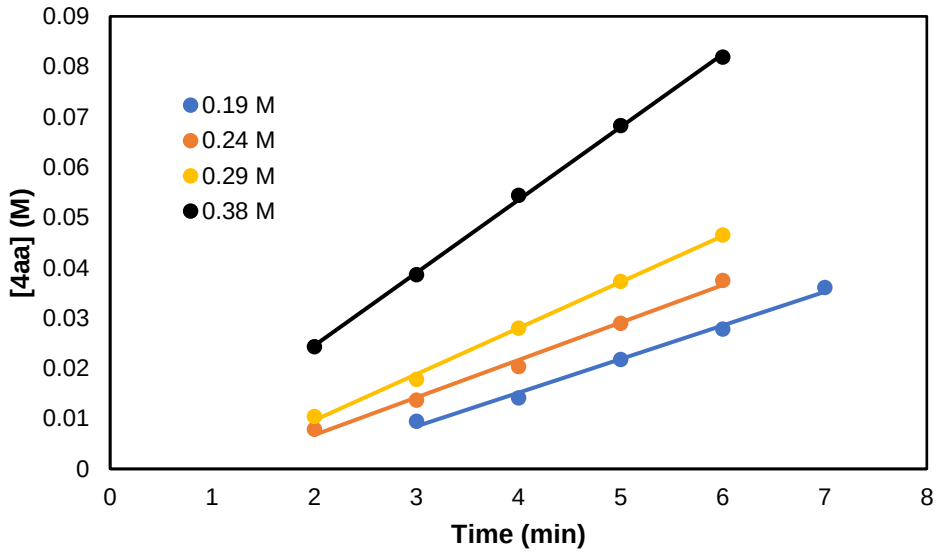

Figure S7. Plots of initial reaction rates at different concentrations of **1a**.

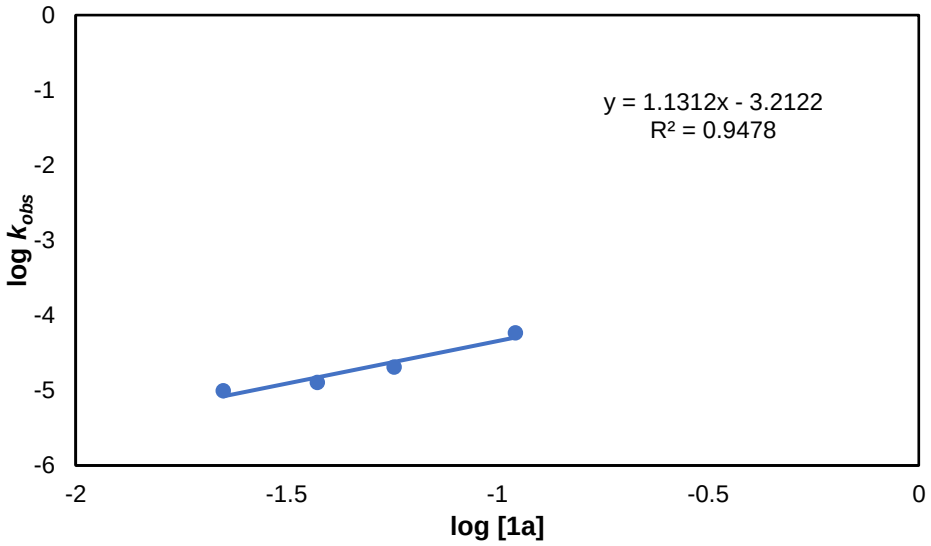

Figure S8. Plot of logk_{obs} vs log[**1a**] (slope = 1.1) for ring-opened cyclopropene hydrothiolation (first order).

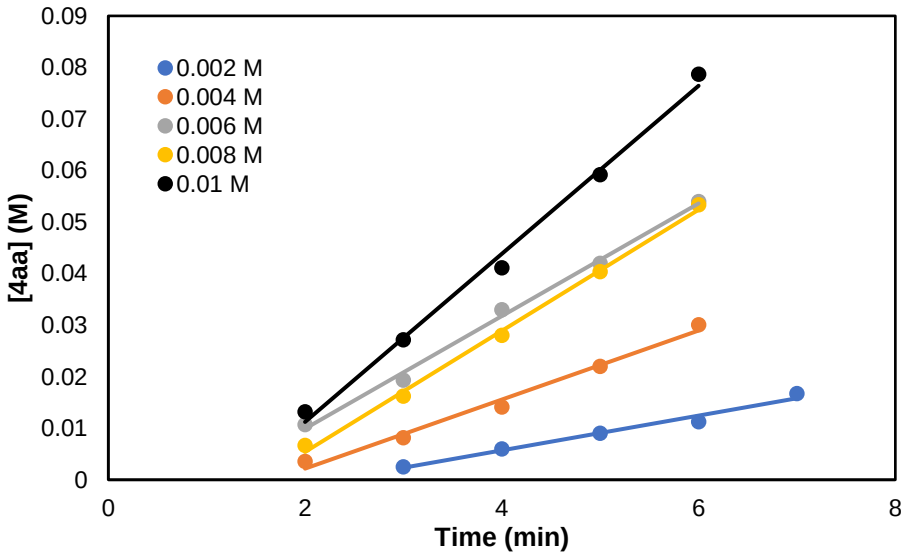

Figure S9. Plots of initial reaction rates at different concentrations of Rh.

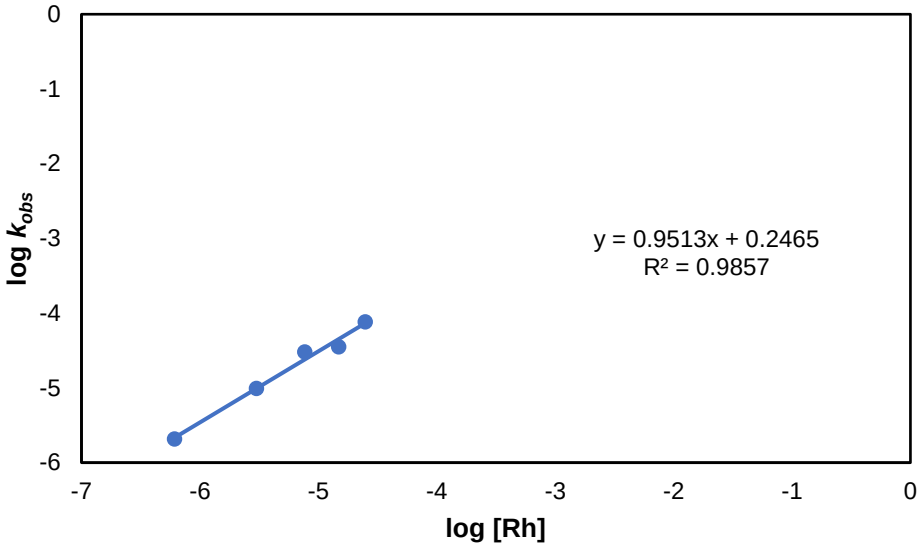

Figure S10. Plot of logk_{obs} vs log[Rh] (slope = 0.95) for ring-opened cyclopropene hydrothiolation (first order).

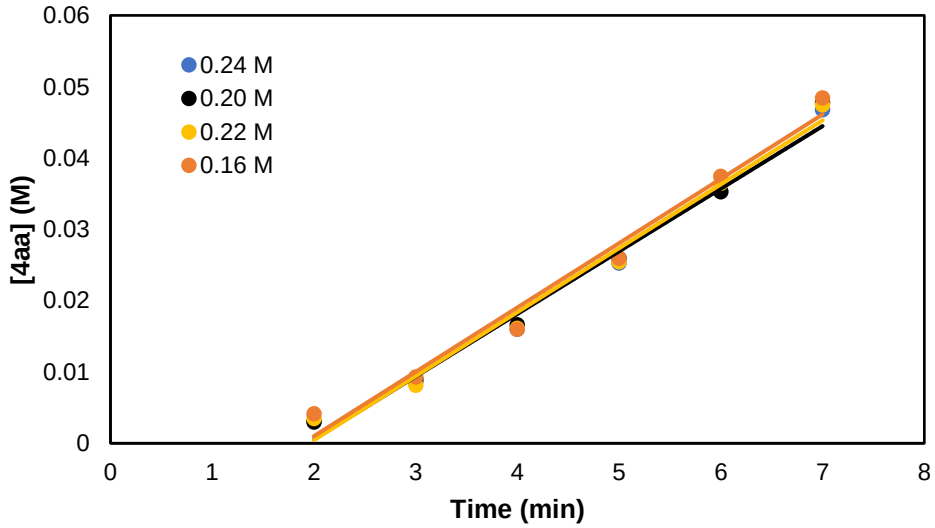

Figure S11. Plots of initial reaction rates at different concentrations of **2a**.

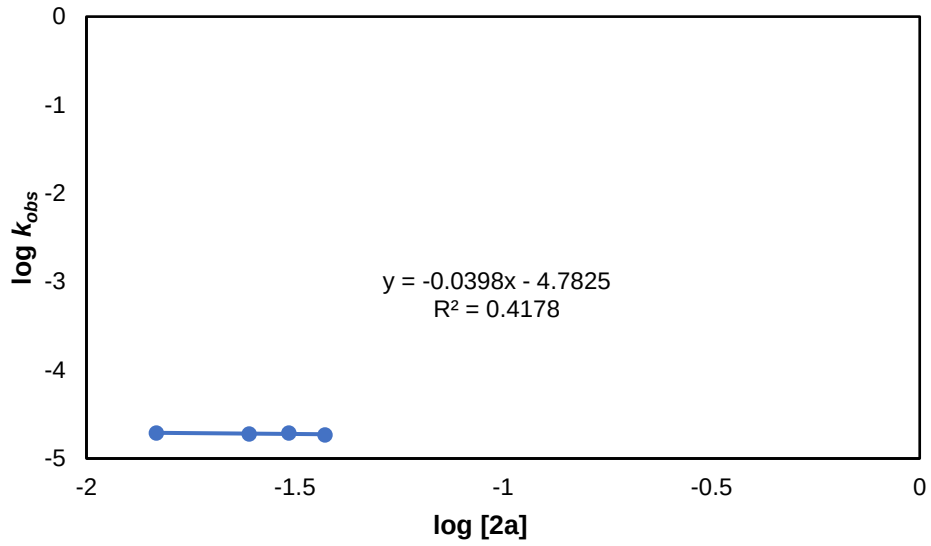

Figure S12. Plot of logk_{obs} vs log[**2a**] (slope = -0.04) for ring-opened cyclopropene hydrothiolation (zero order).

4.3 Initial rate KIE studies

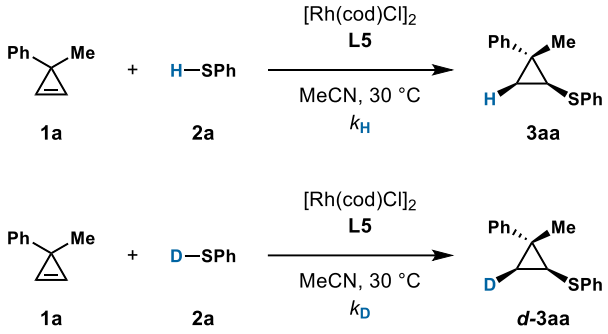

In a N_2-filled glove box, a 0.025 M solution of catalyst was prepared by combining $[Rh(cod)Cl]_2$ (3.7 mg, 0.0075 mmol), **L5** (8.1 mg, 0.015 mmol), and MeCN (0.60 mL). The resulting mixture was stirred for 10 min. A vial was charged with a stir bar and 1,3,5-trimethoxybenzene (5.1 mg, 0.030 mmol). Catalyst solution (0.20 mL, 5.0 mol% Rh) was added to the vial, followed by **2a** (11 mg, 0.10 mmol) or ***d*-2a** (11 mg, 0.10 mmol) and MeCN (0.23 mL). The vial was sealed with a Teflon cap. **1a** (0.17 mL, 1.2 M solution in MeCN, 0.20 mmol) was added to the sealed vial to initiate the reaction. 30 µL aliquots were taken every 5 minutes and quenched in 2 mL of ethyl acetate. No further catalysis occurs after dilution in ethyl acetate. The appearance of **3aa** or ***d*-3aa**

was monitored by internally referenced GC-FID analysis.[5]

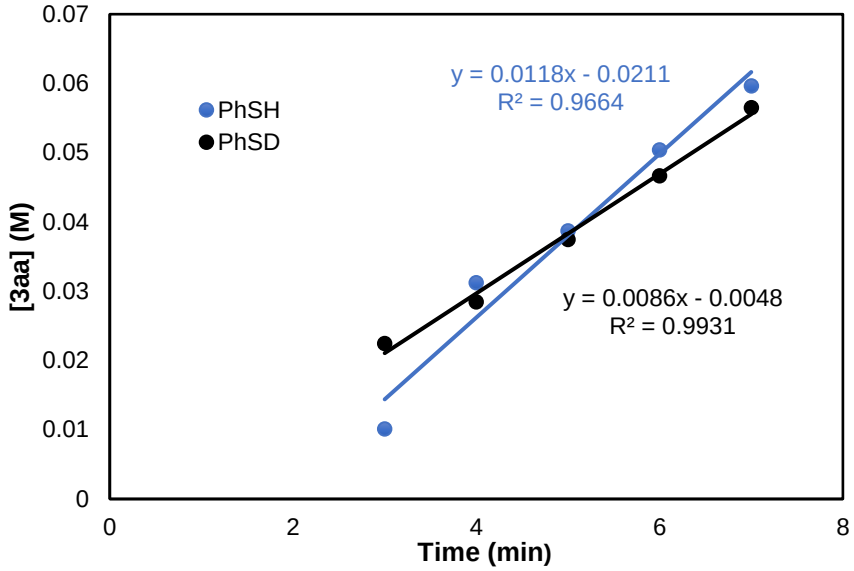

adjusted initial rate of deuterium species (considering 25% of **2a** in ***d*-2a**):

$$0.0086 = 0.75\ K_D + 0.25 \times 0.012$$

$$K_D = 0.0075$$

Calculation of KIE: $K_H/K_D = 0.012/0.0075 = 1.6$

Figure S13. Initial Rate *KIE* for ring-retained hydrothiolation

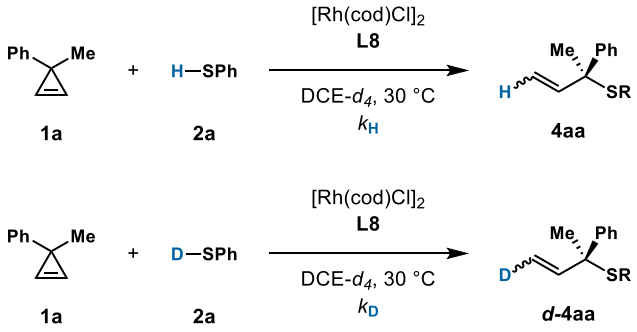

In a N_2-filled glove box, a 0.050 M solution of catalyst was prepared by combining $[Rh(cod)Cl]_2$ (3.7 mg, 0.0075 mmol), **L8** (17.9 mg, 0.015 mmol), and DCE-d_4 (0.30 mL). The resulting mixture was stirred for 10 min. 1,3,5-trimethoxybenzene (2.0 mg, 0.012 mmol) was added to a J. Young

NMR tube. Catalyst solution (0.10 mL, 5.0 mol% Rh) was then added to the J. Young NMR tube, followed by **2a** (11 mg, 0.10 mmol) or ***d*-2a** (11 mg, 0.10 mmol) and DCE-d_4 (0.30 mL). The J. Young NMR tube was sealed with a Teflon cap. **1a** (0.10 mL, 1.2 M solution in DCE-d_4, 0.12 mmol) was added to the sealed tube to initiate the reaction. A ^{1}H NMR spectrum was taken every minute with one scan. The appearance of **4aa** or ***d*-4aa** was monitored by comparing the integration of one of the vinyl protons of the product (5.16 ppm) to the internal standard (3.77 ppm).[5]

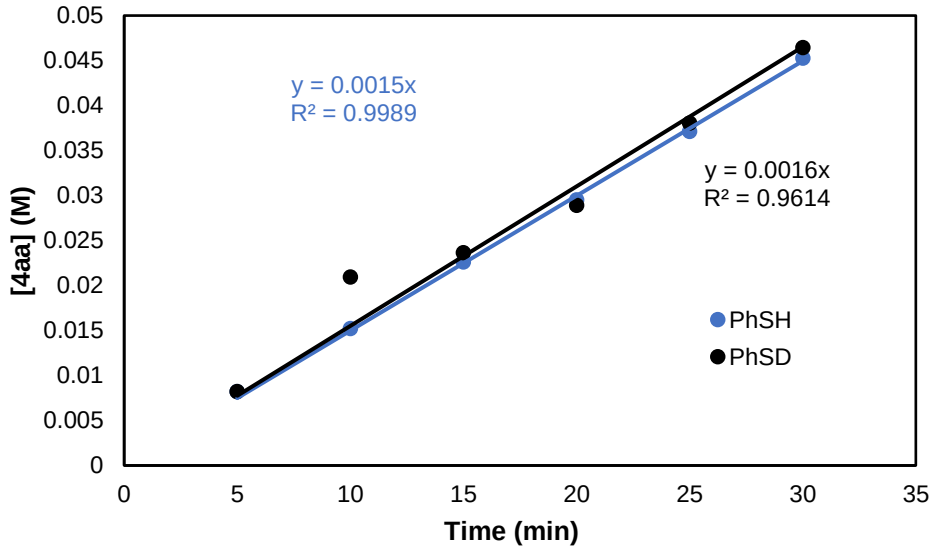

adjusted initial rate of deuterium species (considering 25% of **2a** in ***d*-2a**):

$$0.0016 = 0.75\ K_D + 0.25 \times 0.0015$$

$$K_D = 0.0016$$

Calculation of KIE: $K_H/K_D = 0.0015/0.0016 = 0.94$

Figure S14. Initial Rate *KIE* for ring-opened hydrothiolation

4.4 Cross-over studies

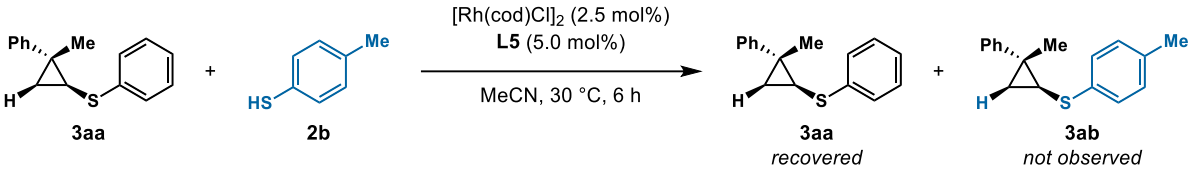

Ring-retained crossover experiment:

In a N_2-filled glove box, $[Rh(cod)Cl]_2$ (1.2 mg, 0.0025 mmol), **L5** (2.7 mg, 0.0050 mmol), and MeCN (0.60 mL) were added to a 1-dram vial containing a stir bar. The resulting mixture was stirred for 10 min. Thiol **2b** (11 mg, 0.10 mmol) was added followed by **3aa** (24 mg, 0.10 mmol). The mixture was stirred at 30 °C for 6 h. We observed no reactivity (i.e. incorporation of **2b** to form product **3ab**), but rather remaining starting materials after 6 h. Production of **3ab** was monitored by GC-FID.

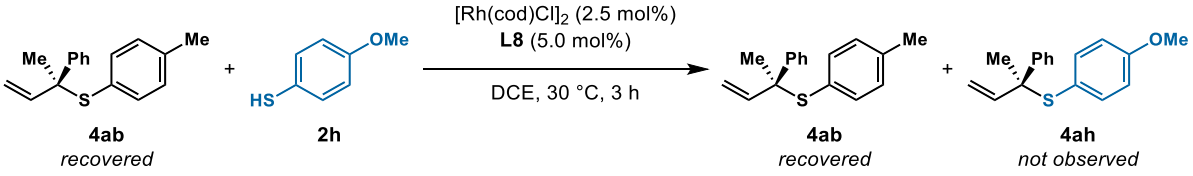

Ring-opening crossover experiment:

In a N_2-filled glove box, $[Rh(cod)Cl]_2$ (0.74 mg, 0.0015 mmol), **L8** (3.6 mg, 0.0030 mmol), and DCE (0.30 mL) were added to a 1-dram vial containing a stir bar. The resulting mixture was stirred for 10 min. Thiol **2h** (8.4 mg, 0.060 mmol) was added followed by **4ab** (15 mg, 0.060 mmol). The mixture was stirred at 30 °C for 3h. We observed no reactivity (i.e. incorporation of **2c** to form

product **4ah**), but rather remaining starting materials after 3 h. **4ab** was re-isolated after preparatory TLC (hexanes) and confirmed by ^{1}H NMR.

4.5 NMR Studies

Stoichiometric rhodium hydride experiment:

In a N_2-filled glovebox, $[Rh(cod)Cl]_2$ (4.9 mg, 0.010 mmol), dppe (8.0 mg, 0.020 mmol), and DCE-d_4 (0.x mL) were added to a 1-dram vial containing a stir bar. the resulting mixture was stirred for 10 min, followed by the addition of **2a** (11 mg, 0.10 mmol). The mixture was transferred to a J. Young NMR tube and sealed with a Young's valve. A multiplet at –15.9 ppm was observed in ^{1}H NMR spectrum (Figure S15). Based on this study and the empirical rate law, we assign **III** as the resting state.

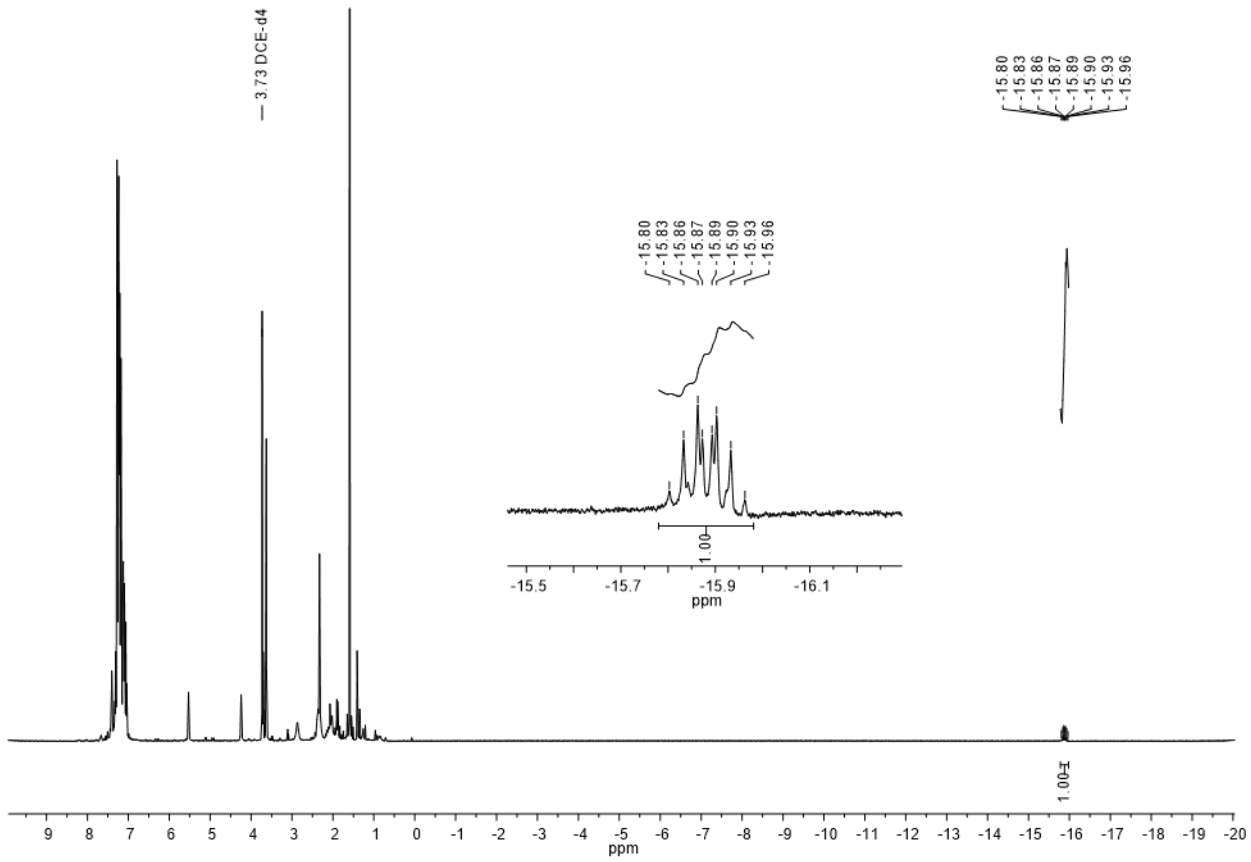

Figure S15. ^{1}H NMR (400 MHz) spectrum for a mixture of $[Rh(dppe)Cl]_2$ and **2a** in DCE-d_4 (δ 3.73 ppm).

5. References

(1). Sherill, W. M.; Kim, R.; Rubin, M. *Tetrahedron*, **2008**, *64*, 8610.

(2). Phan, D. H. T.; Kou, K. G. M.; Dong, V. M. *J. Am. Chem. Soc*. **2010**, *132*, 16354.

(3). Yang, X.-H.; Davison, R. T.; Nie, S.-Z.; Cruz, F. A.; McGinnis, T. M.; Dong, V. M. *J. Am. Chem. Soc.* **2019**, *141*, 3006.

(4). Standley, E. A.; Jamison, T. F. *J. Am. Chem. Soc.* **2013**, *135*, 1585.

(5). Simmons, E. M.; Hartwig, J. F. *Angew. Chem. Int. Ed.* **2012**, *51*, 3066.

6. NMR Spectra of Unknown Compounds

((1*S*,2*R*)-2-methyl-2-phenylcyclopropyl)(phenyl)sulfane(**3aa**)

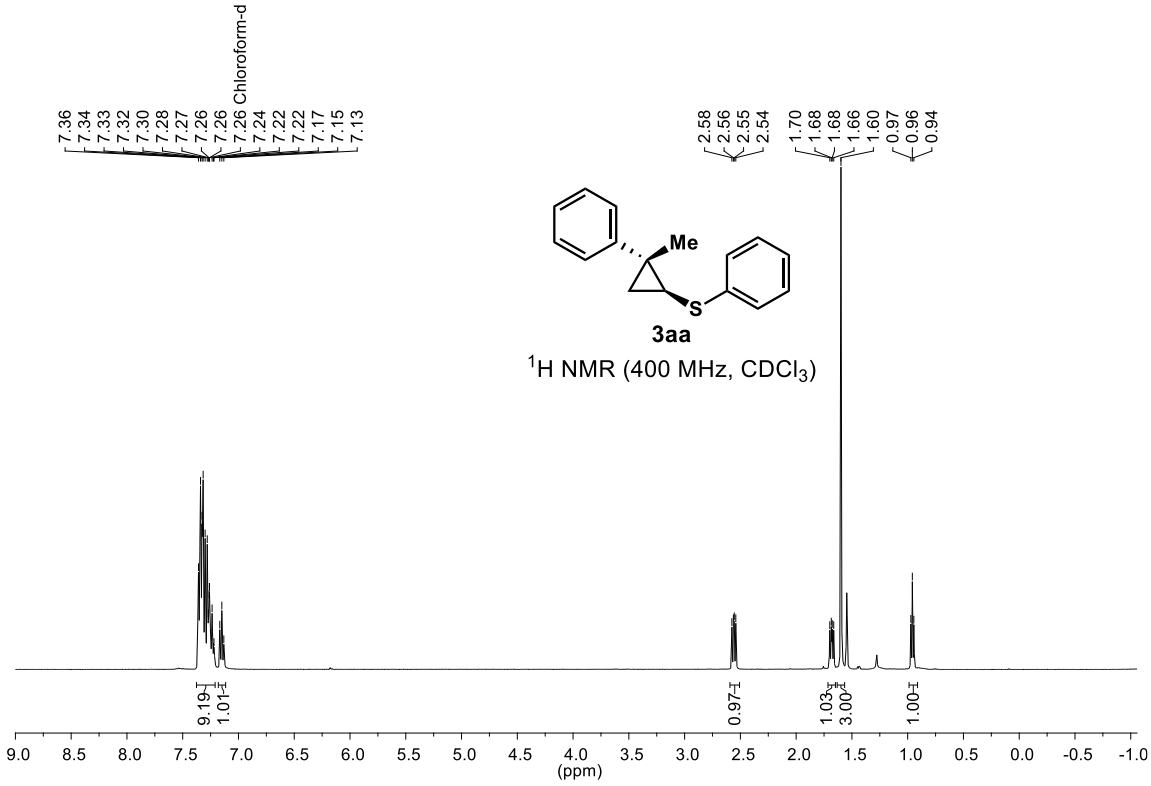

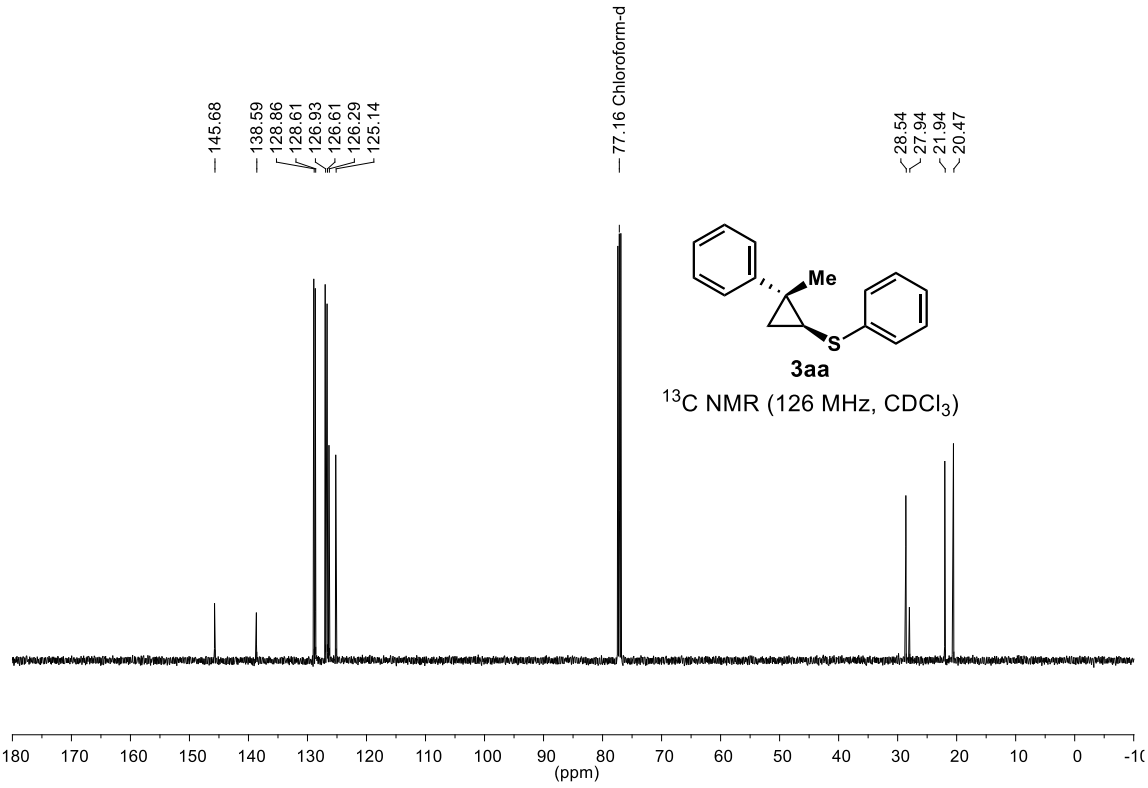

((1*S*,2*R*)-2-methyl-2-phenylcyclopropyl)(p-tolyl)sulfane(**3ab**)

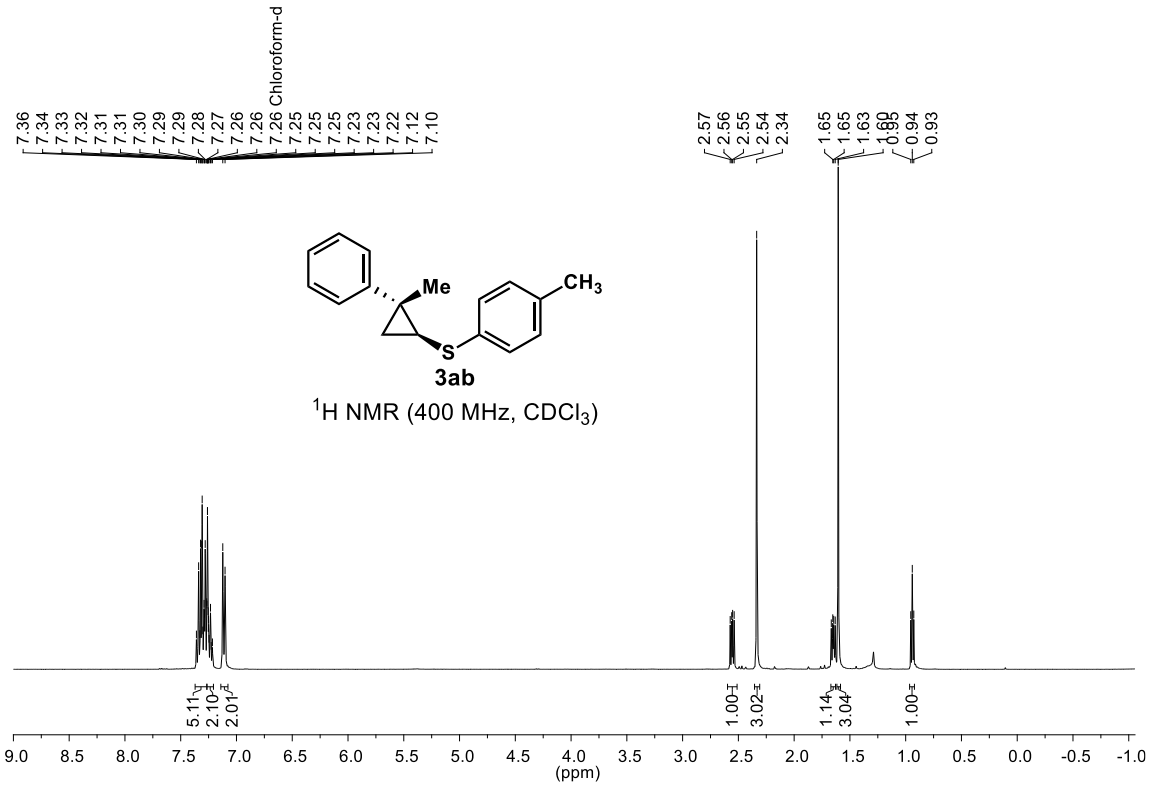

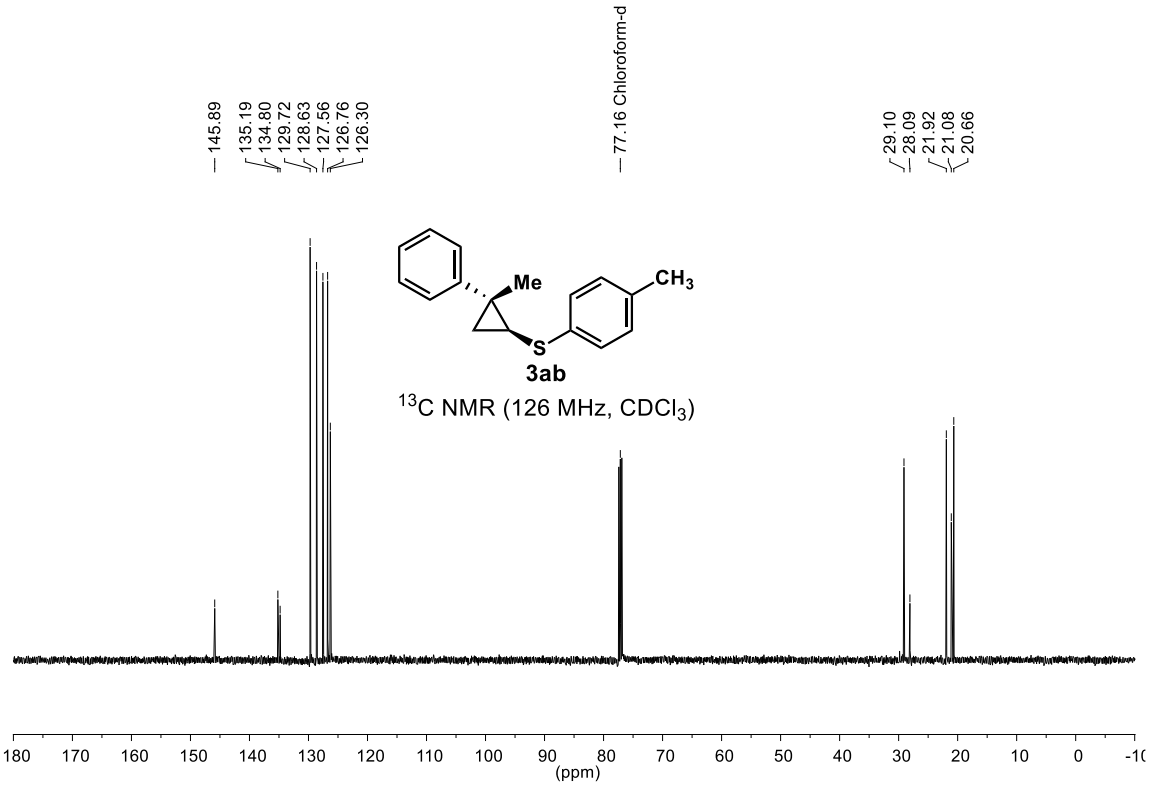

(4-(tert-butyl)phenyl)((1*S*,2*R*)-2-methyl-2-phenylcyclopropyl)sulfane(**3ac**)

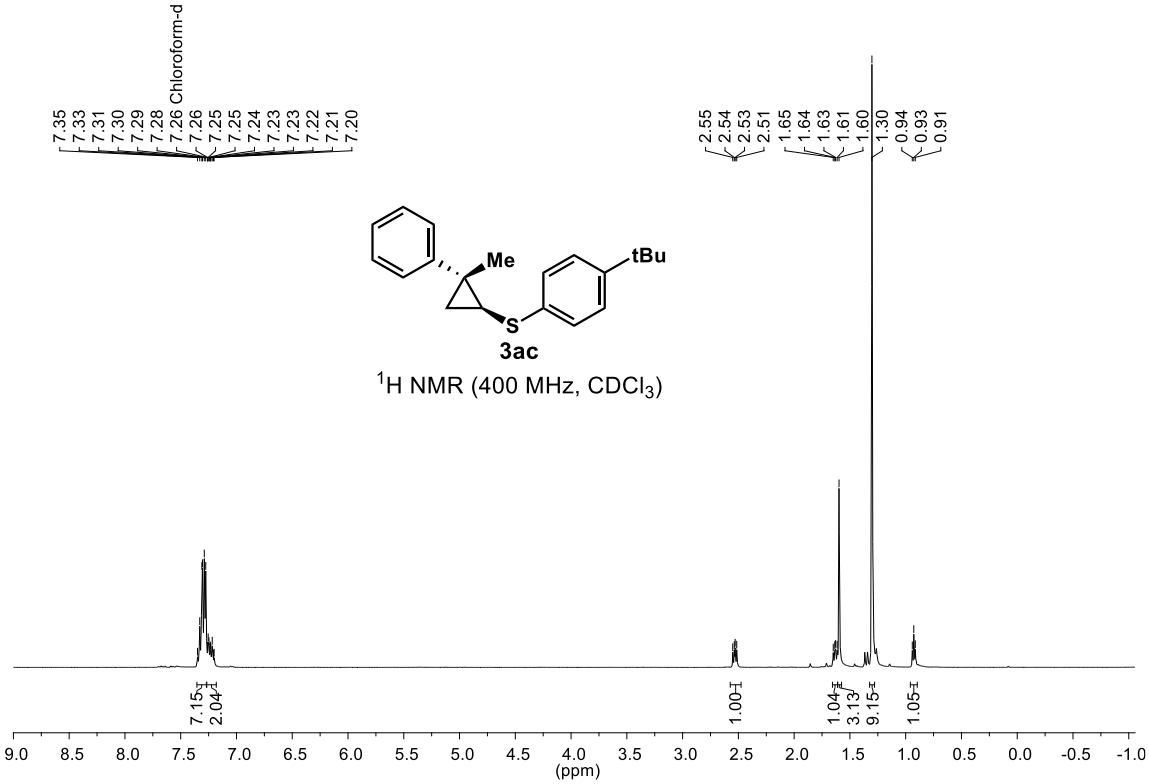

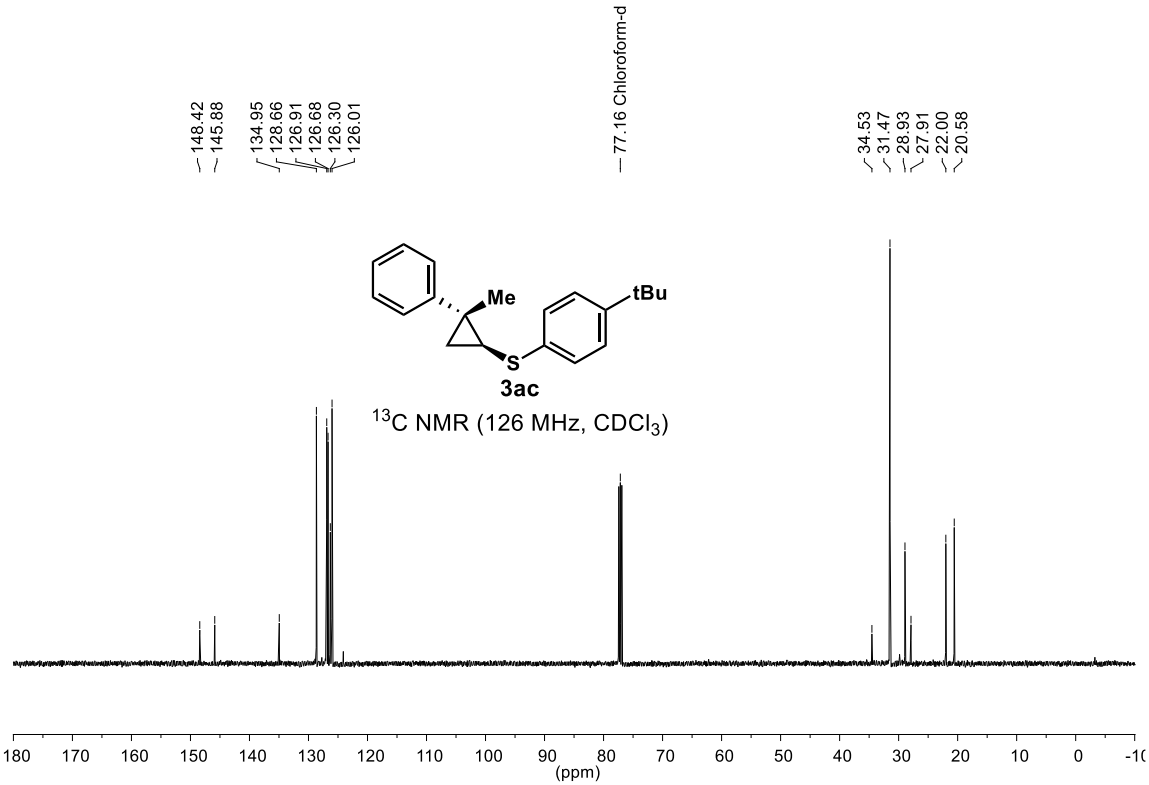

(4-chlorophenyl)((1*S*,2*R*)-2-methyl-2-phenylcyclopropyl)sulfane (**3ad**)

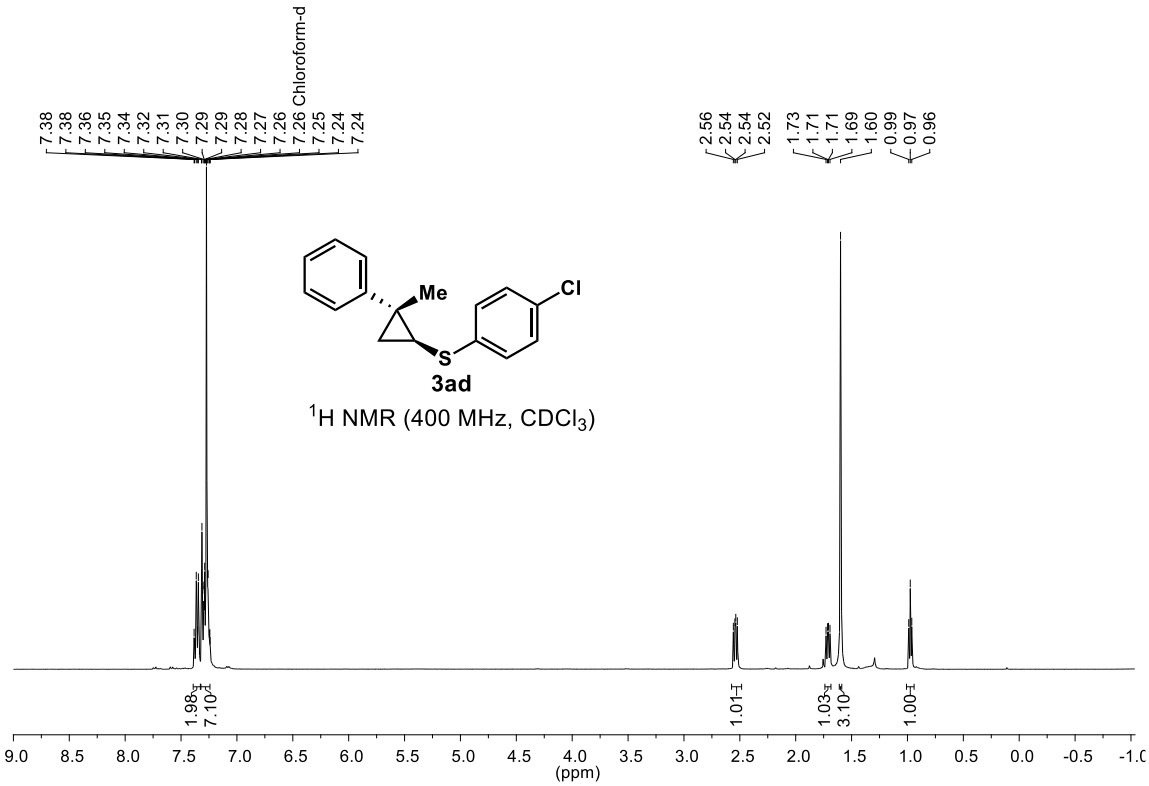

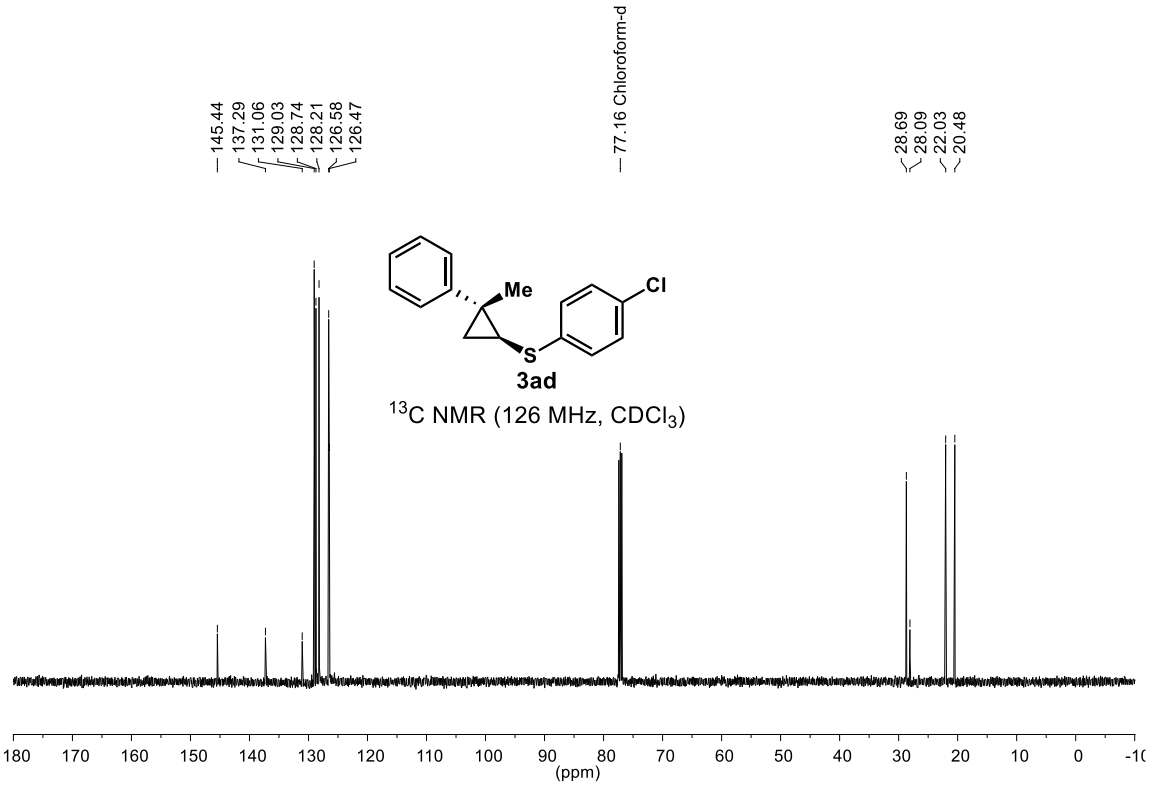

((1*S*,2*R*)-2-methyl-2-phenylcyclopropyl)(m-tolyl)sulfane (**3ae**)

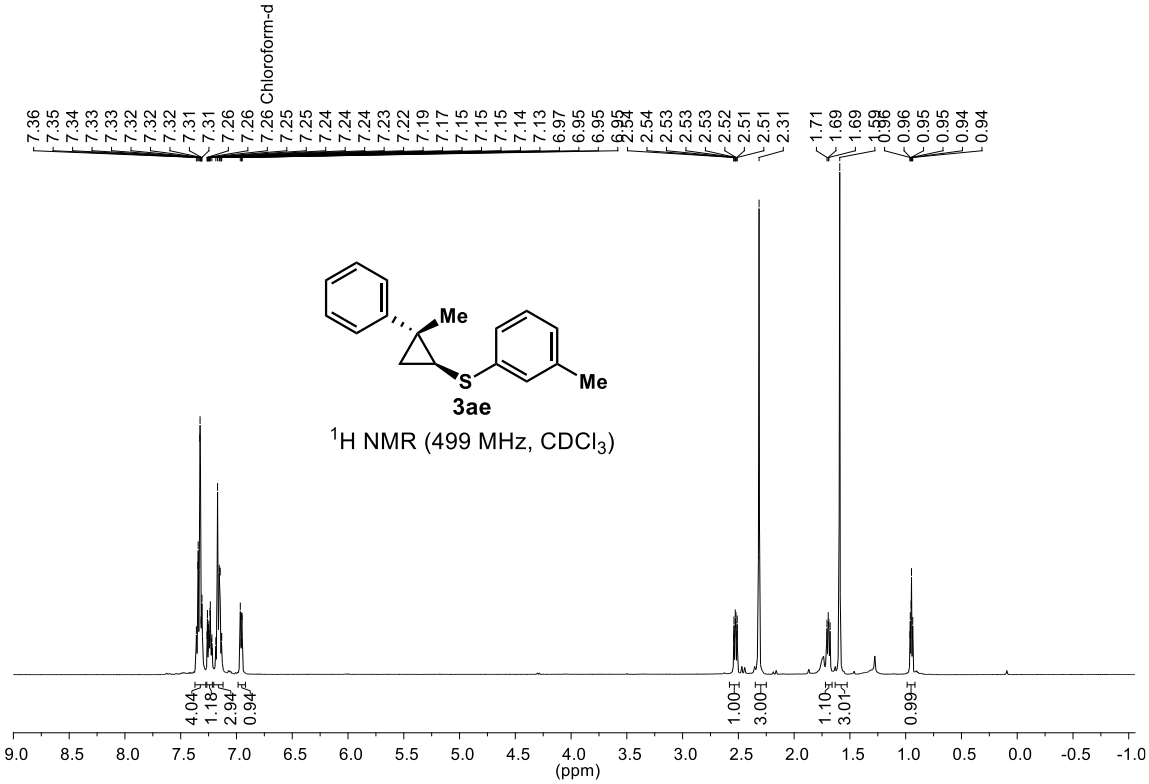

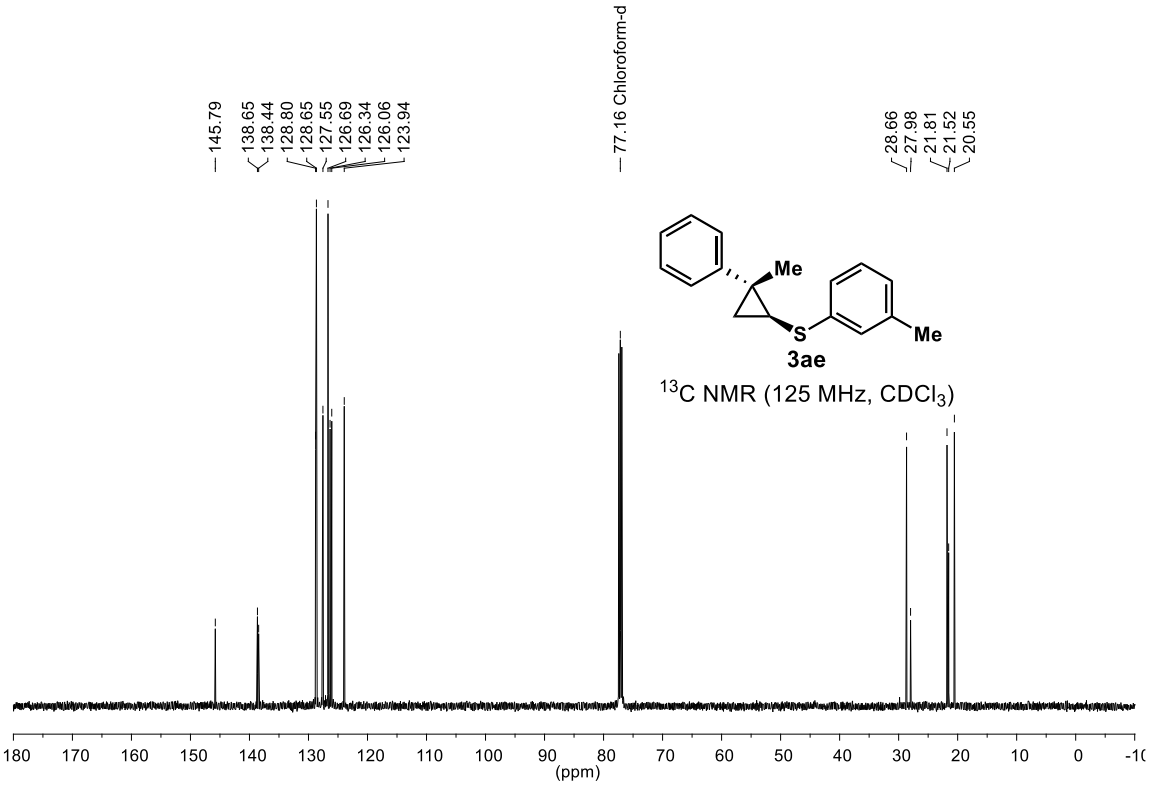

((1*S*,2*R*)-2-methyl-2-phenylcyclopropyl)(o-tolyl)sulfane (**3af**)

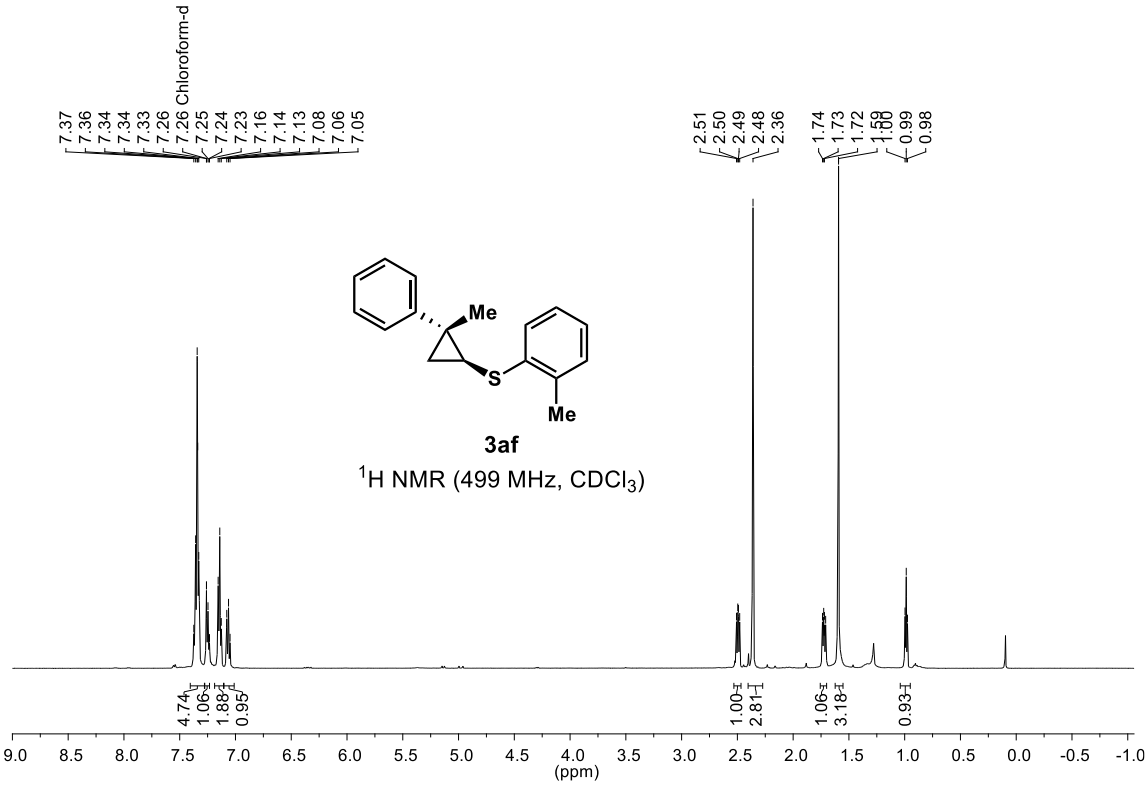

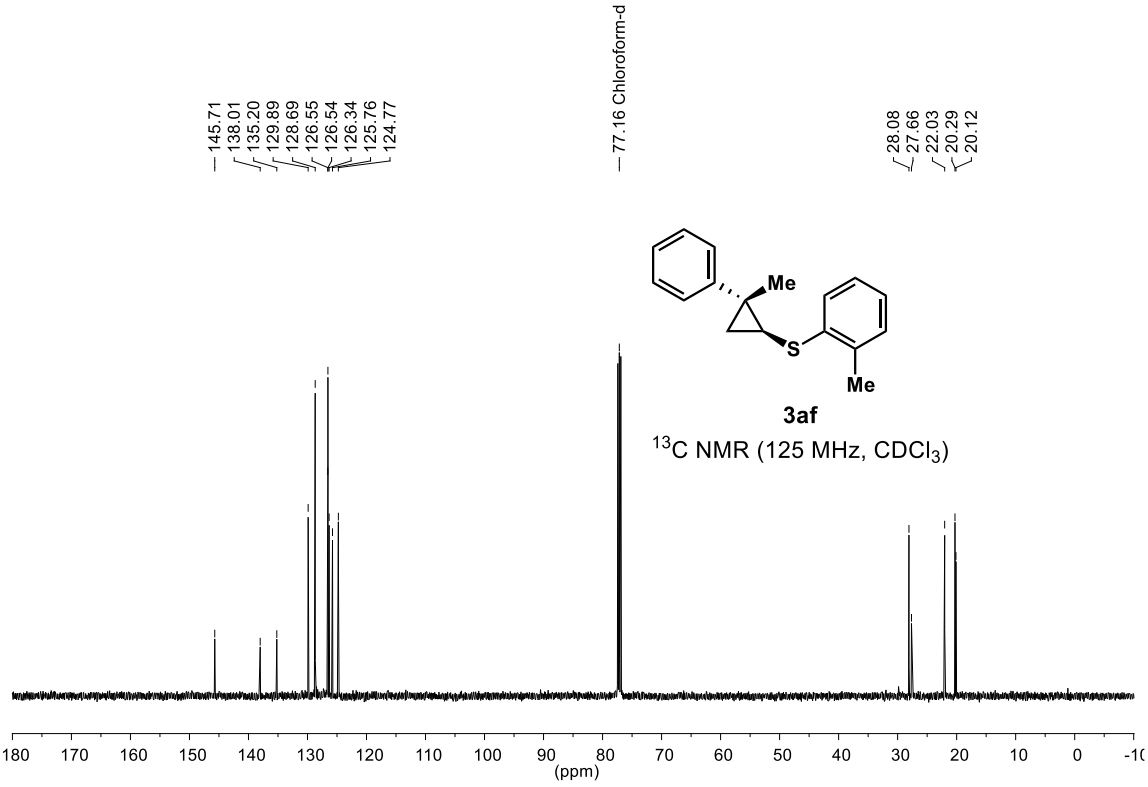

((1*S*,2*R*)-2-methyl-2-phenylcyclopropyl)(naphthalen-2-yl)sulfane(**3ag**)

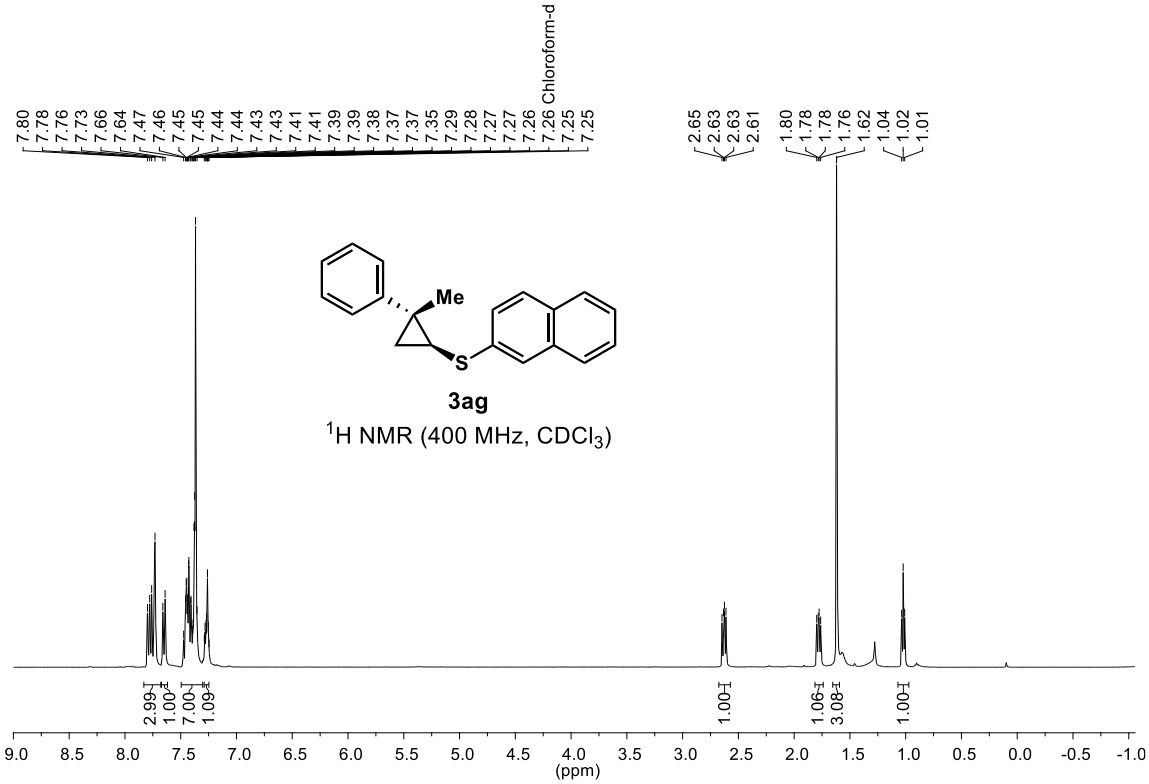

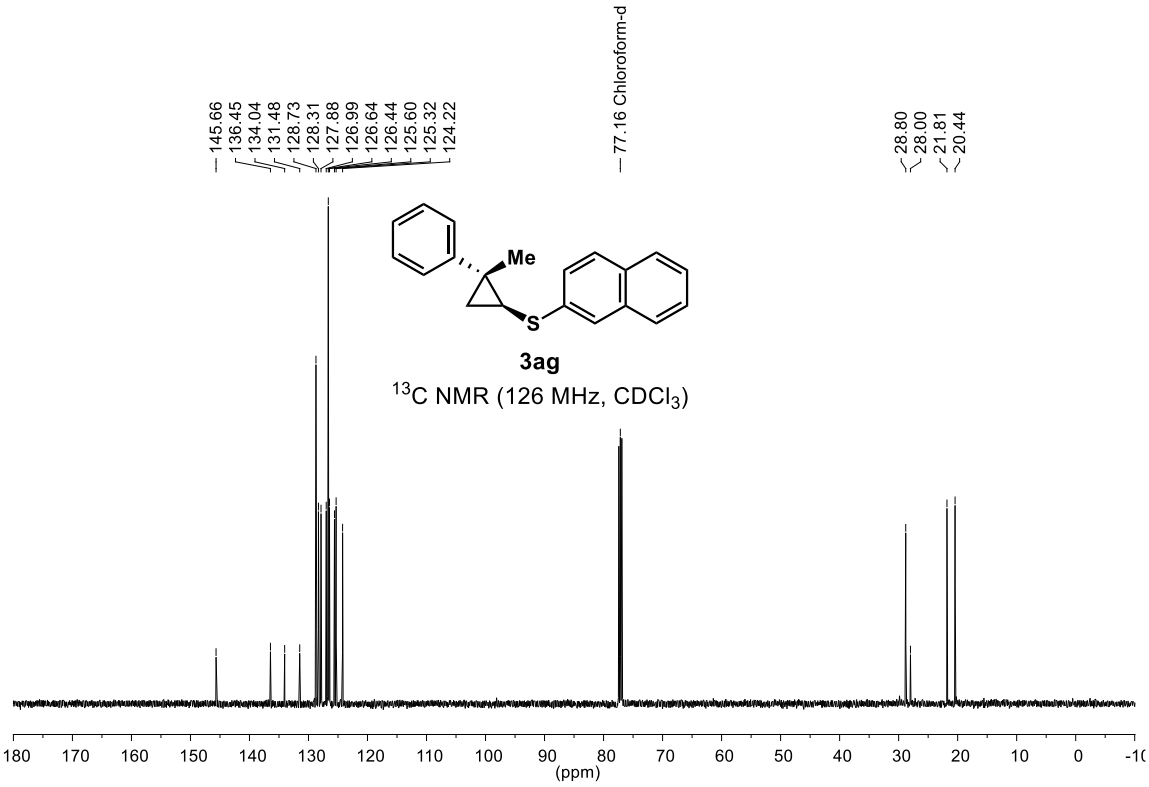

((1*S*,2*R*)-2-methyl-2-(p-tolyl)cyclopropyl)(phenyl)sulfane(**3ba**)

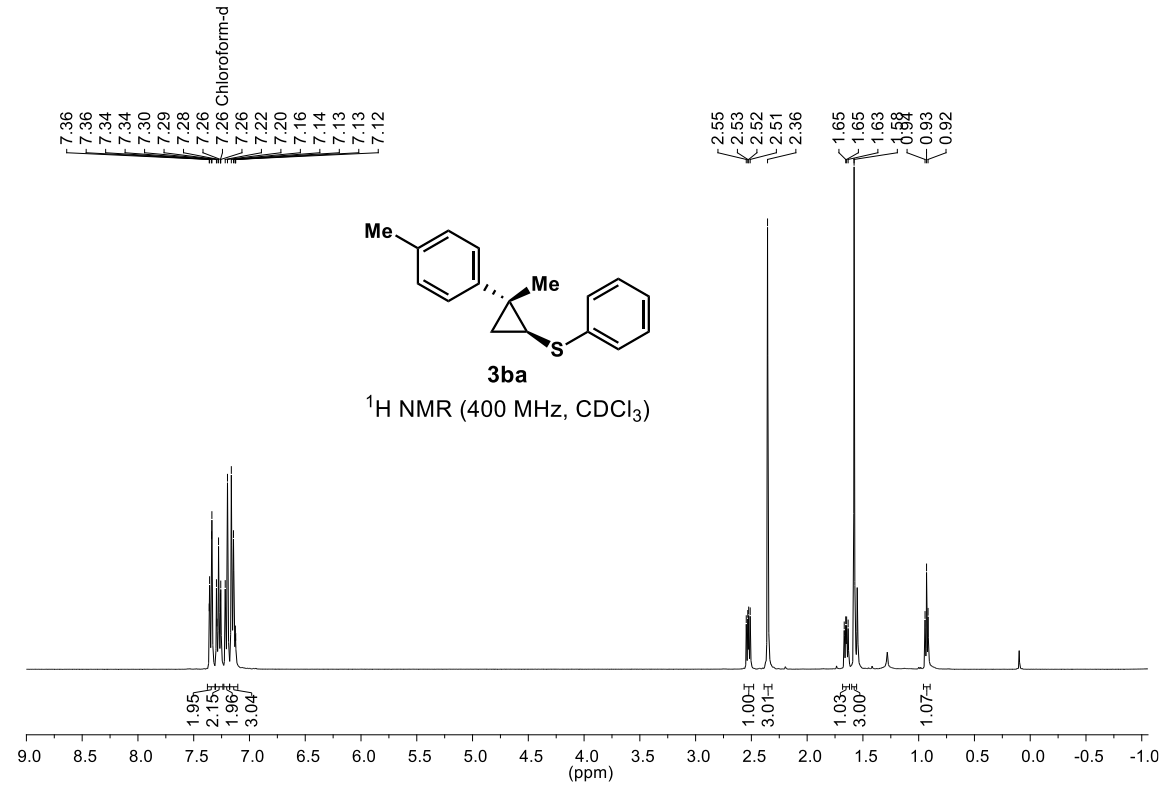

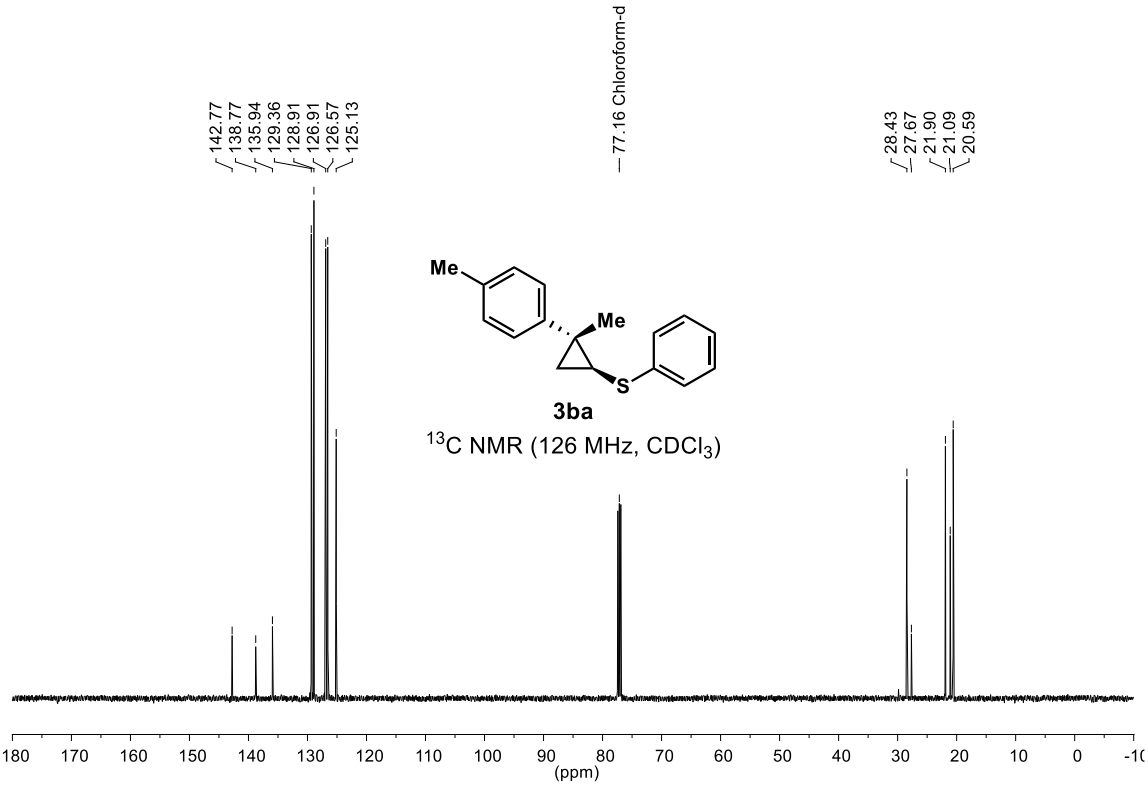

((1*S*,2*R*)-2-methyl-2-(4-(trifluoromethyl)phenyl)cyclopropyl)(phenyl)sulfane (**3ca**)

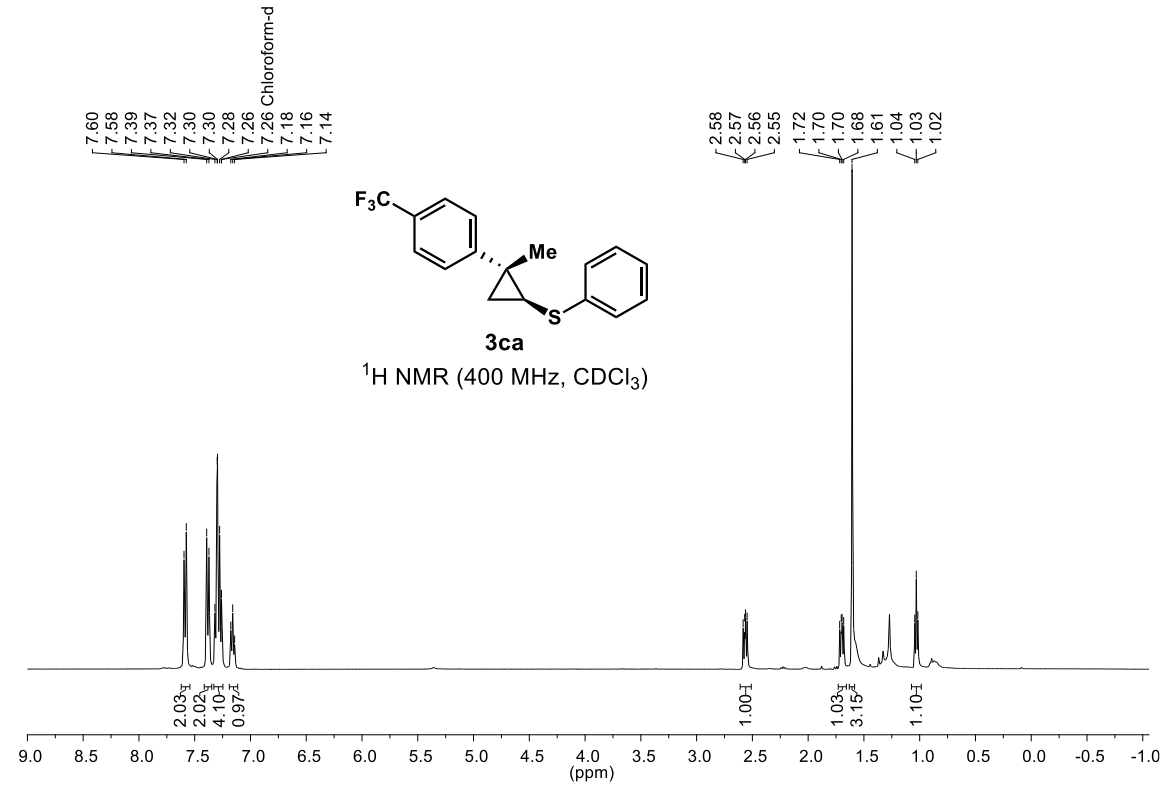

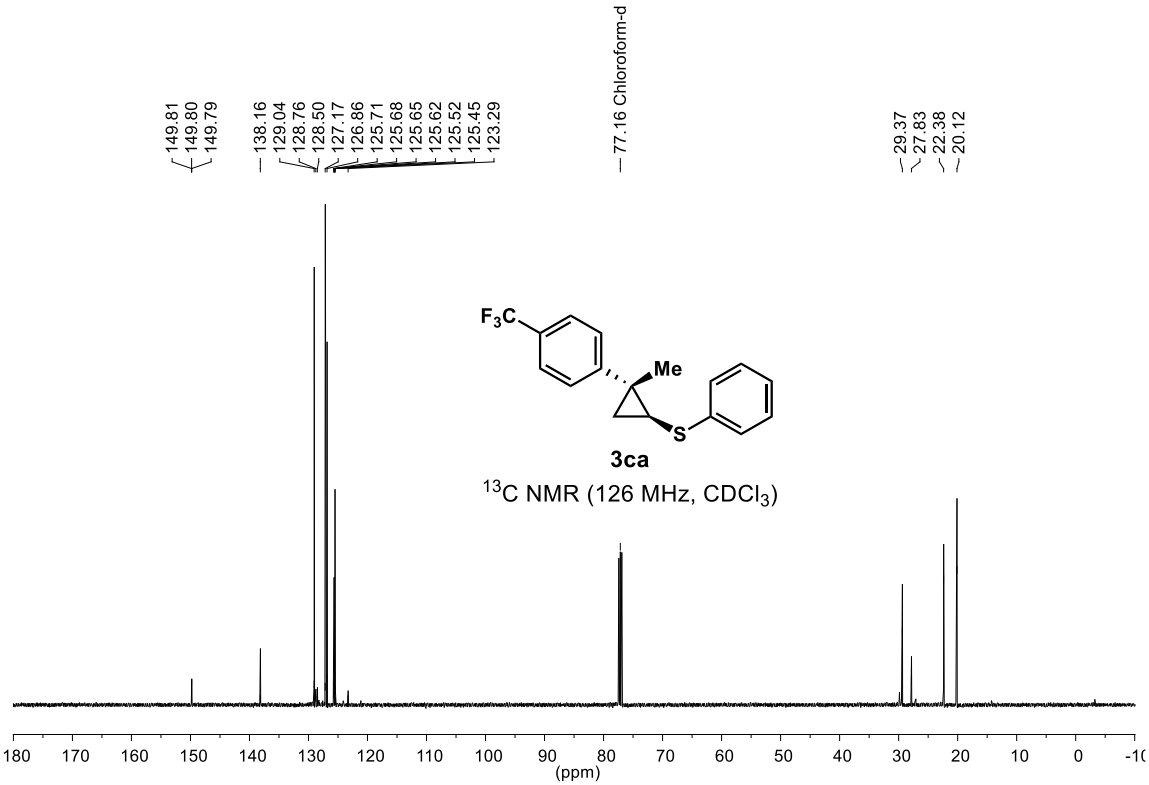

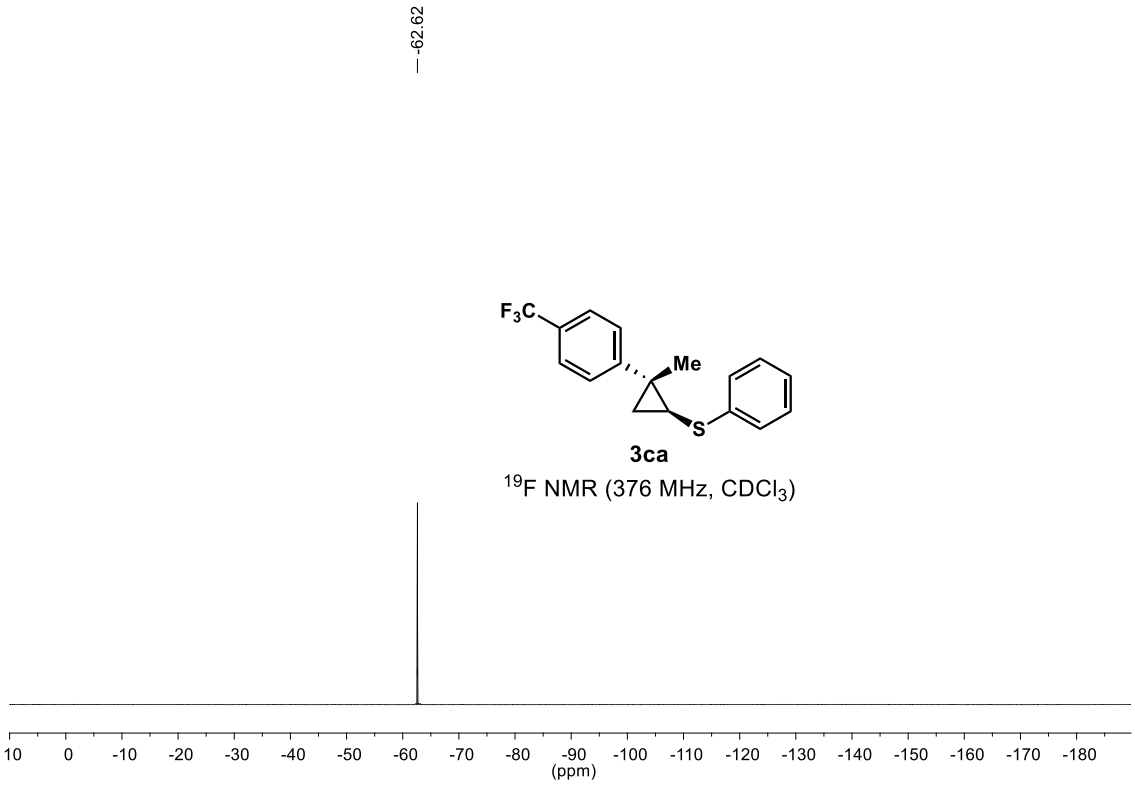

3ca

^{19}F NMR (376 MHz, $CDCl_3$)

((1*S*,2*R*)-2-(4-chlorophenyl)-2-methylcyclopropyl)(phenyl)sulfane (**3da**)

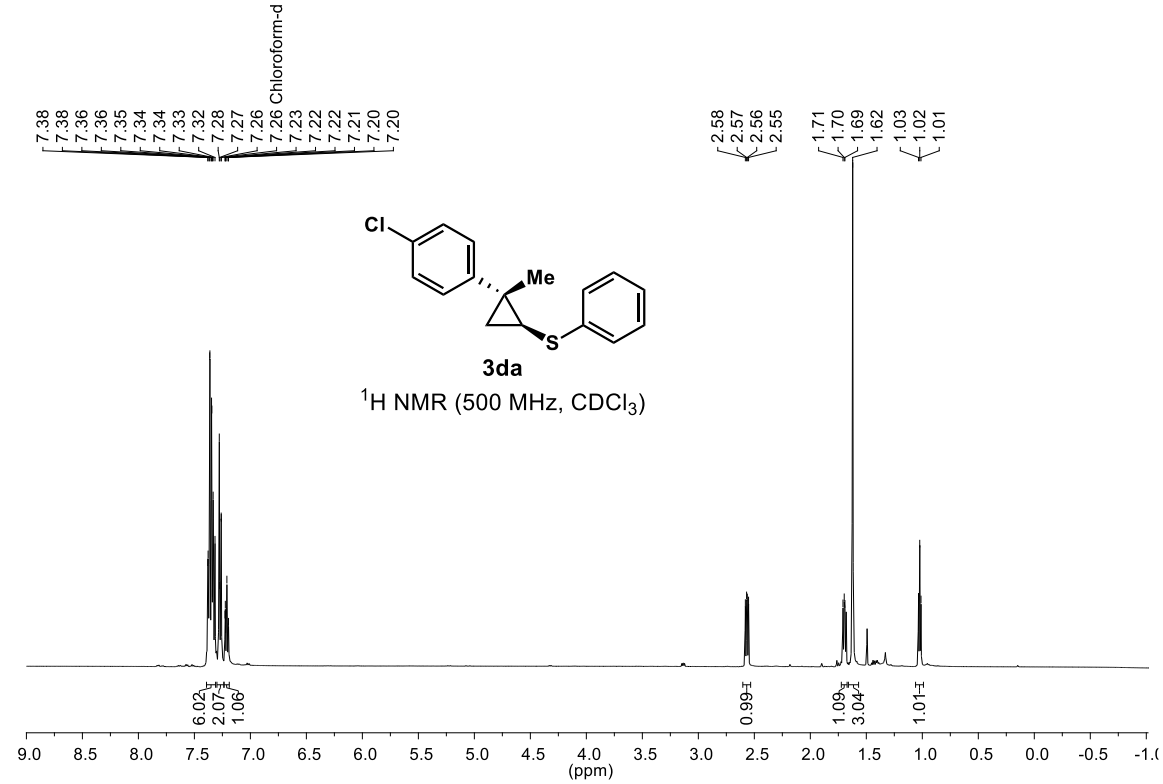

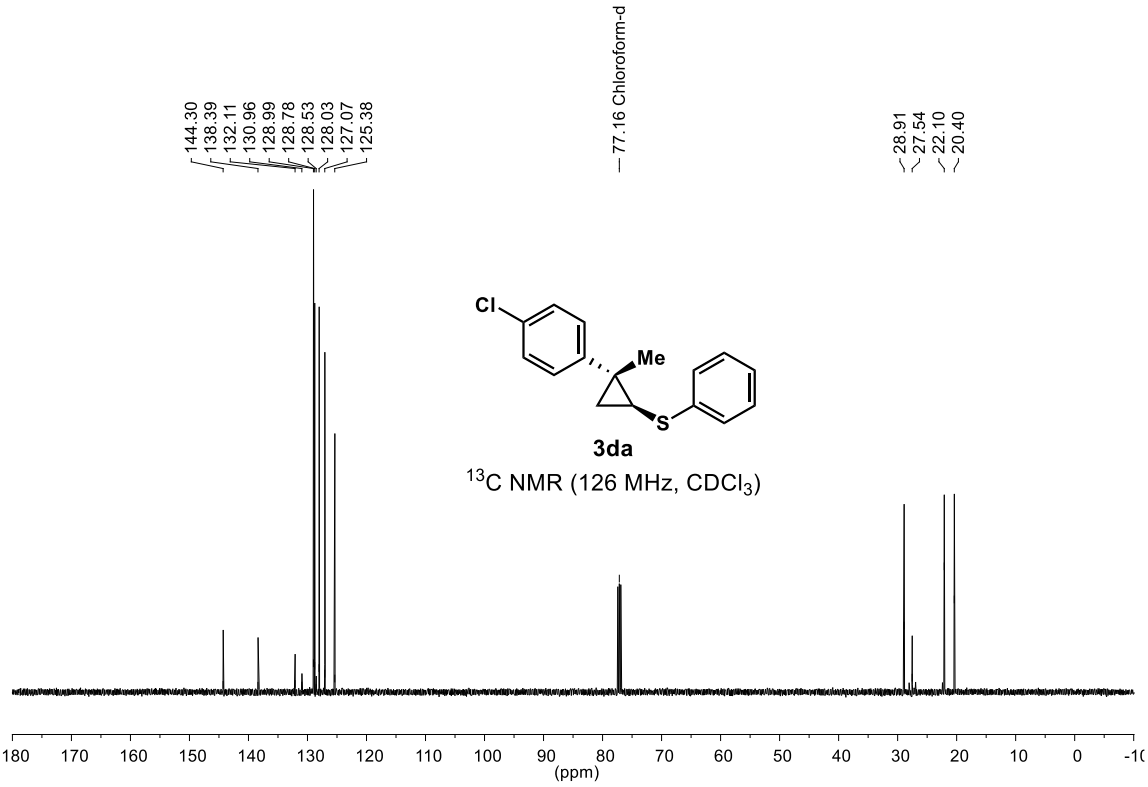

((1*S*,2*R*)-2-benzyl-2-phenylcyclopropyl)(phenyl)sulfane (**3ea**)

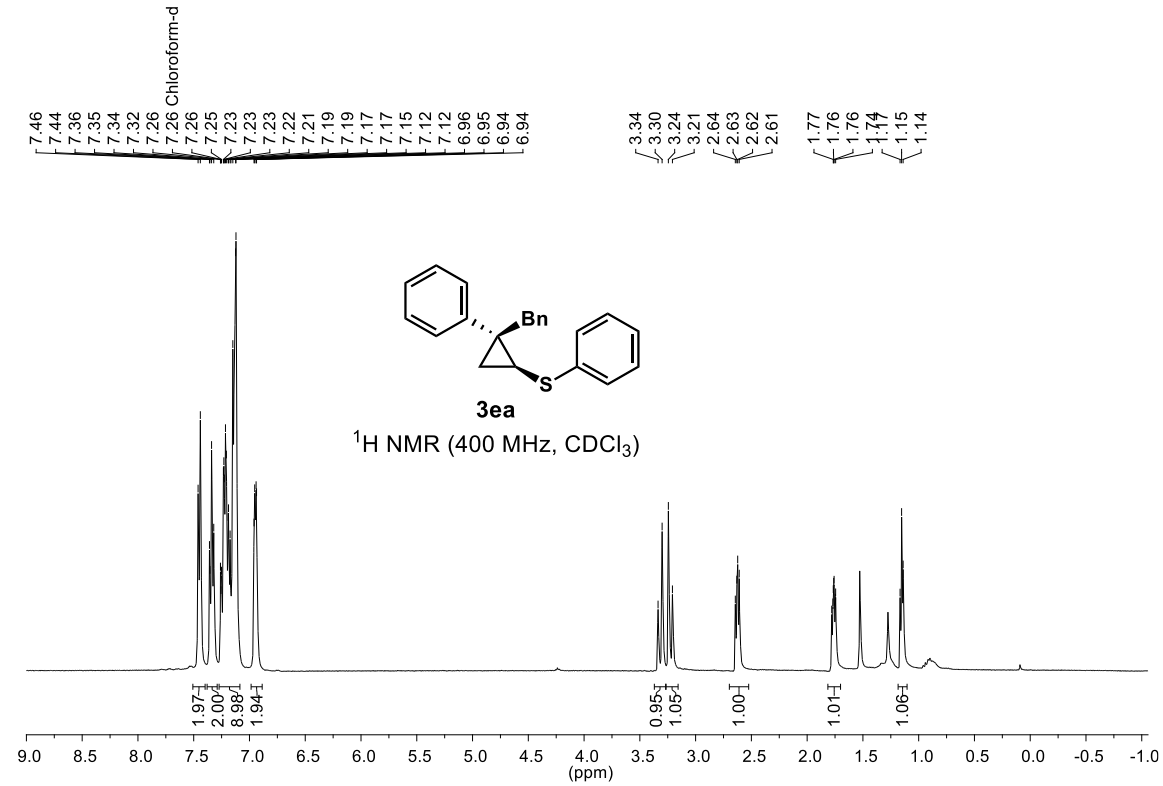

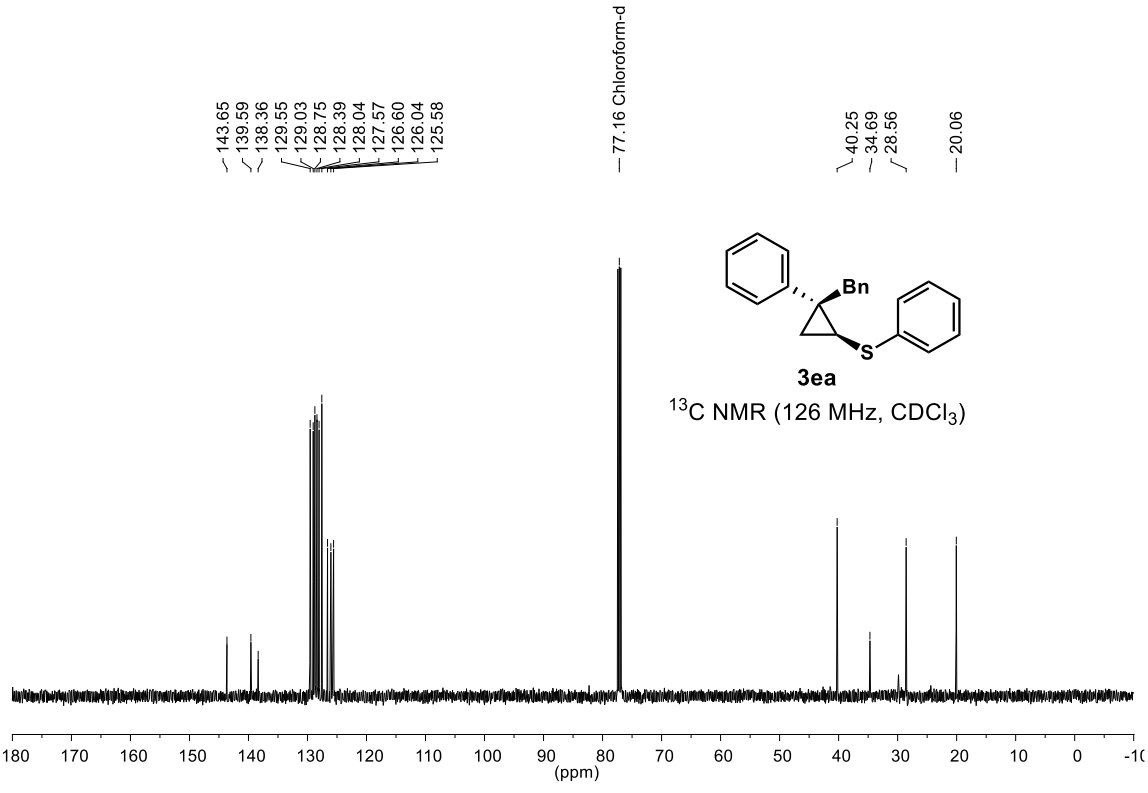

((1*S*,2*R*)-3',4'-dihydro-2'H-spiro[cyclopropane-1,1'-naphthalen]-2-yl)(phenyl)sulfane (**3fa**)

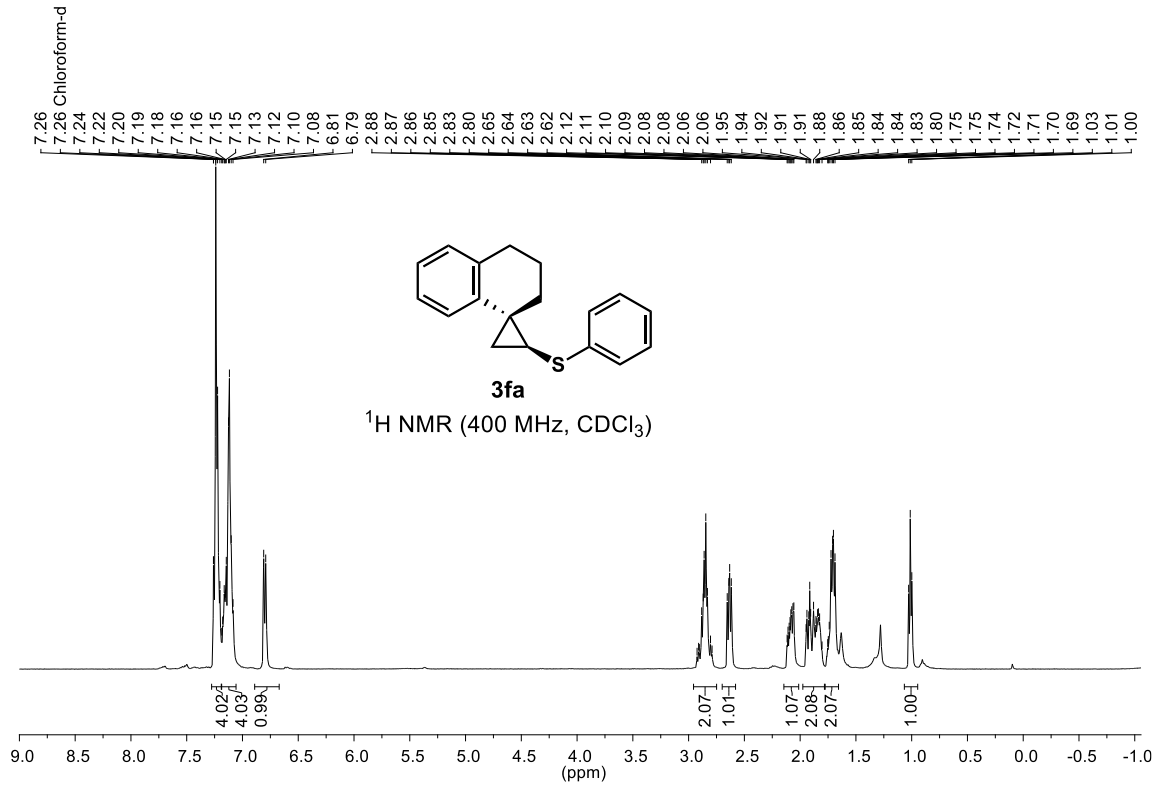

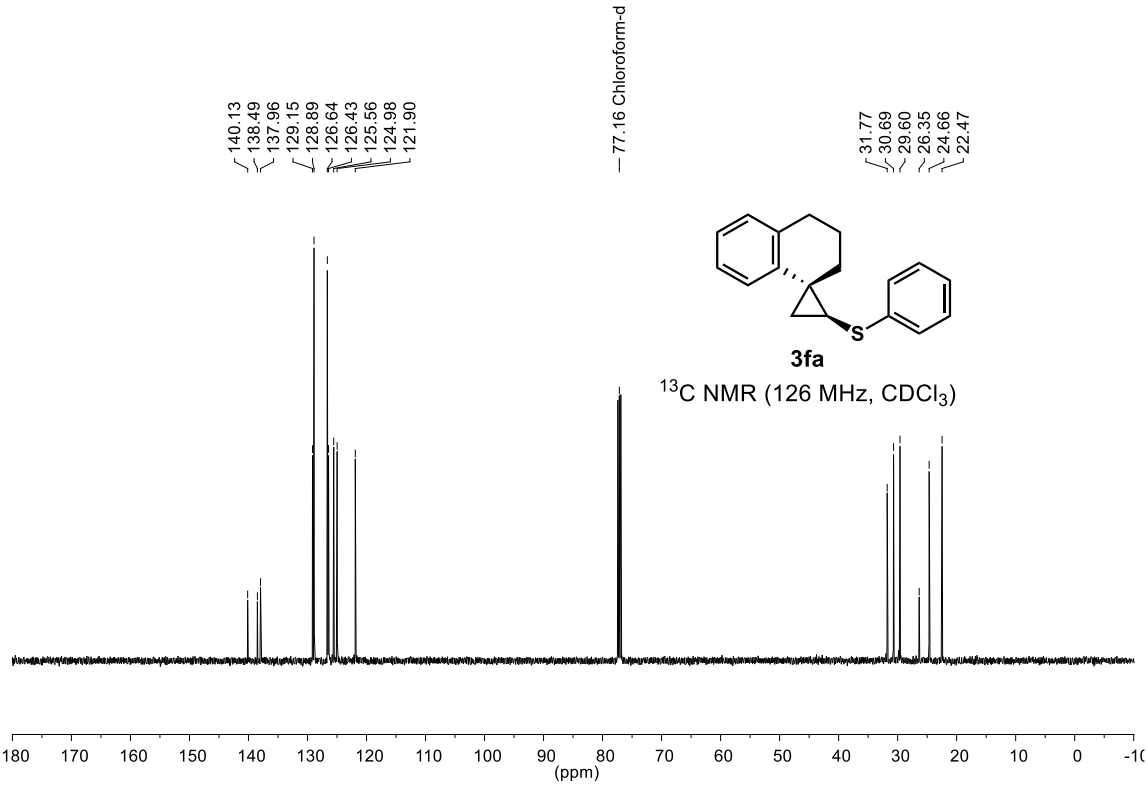

((1*S*,2*R*)-2-(methoxymethyl)-2-phenylcyclopropyl)(phenyl)sulfane (**3ga**)

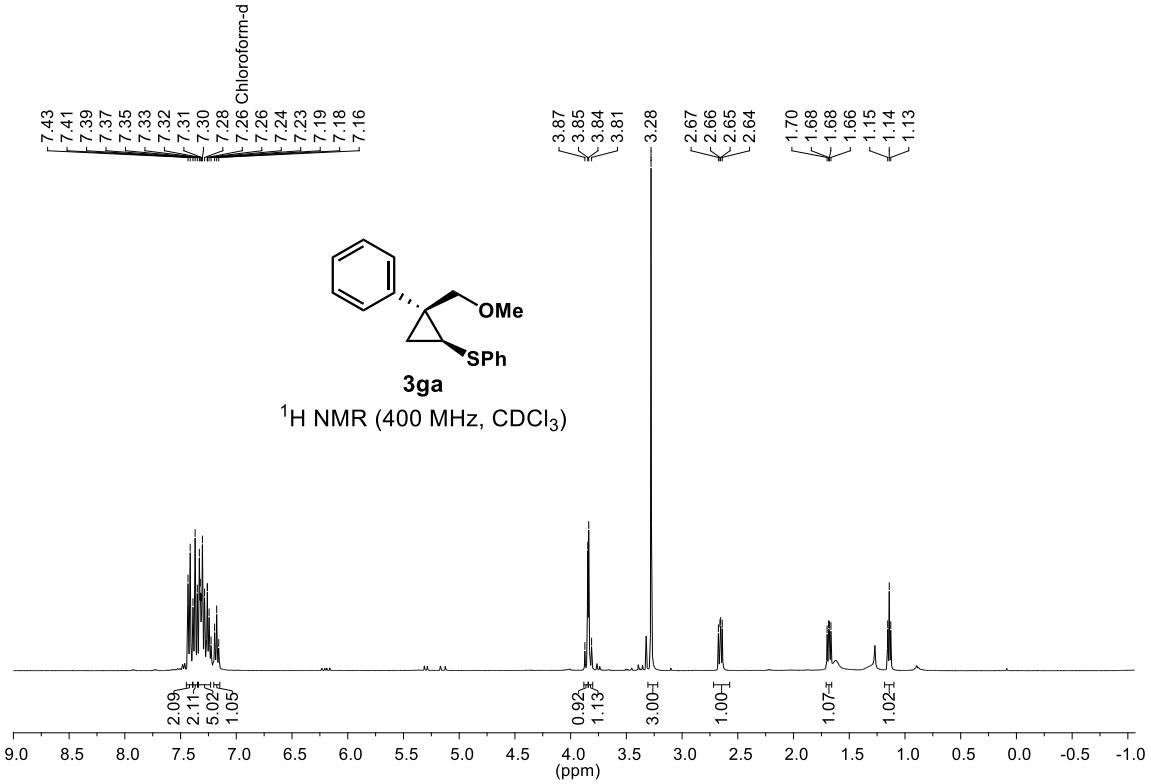

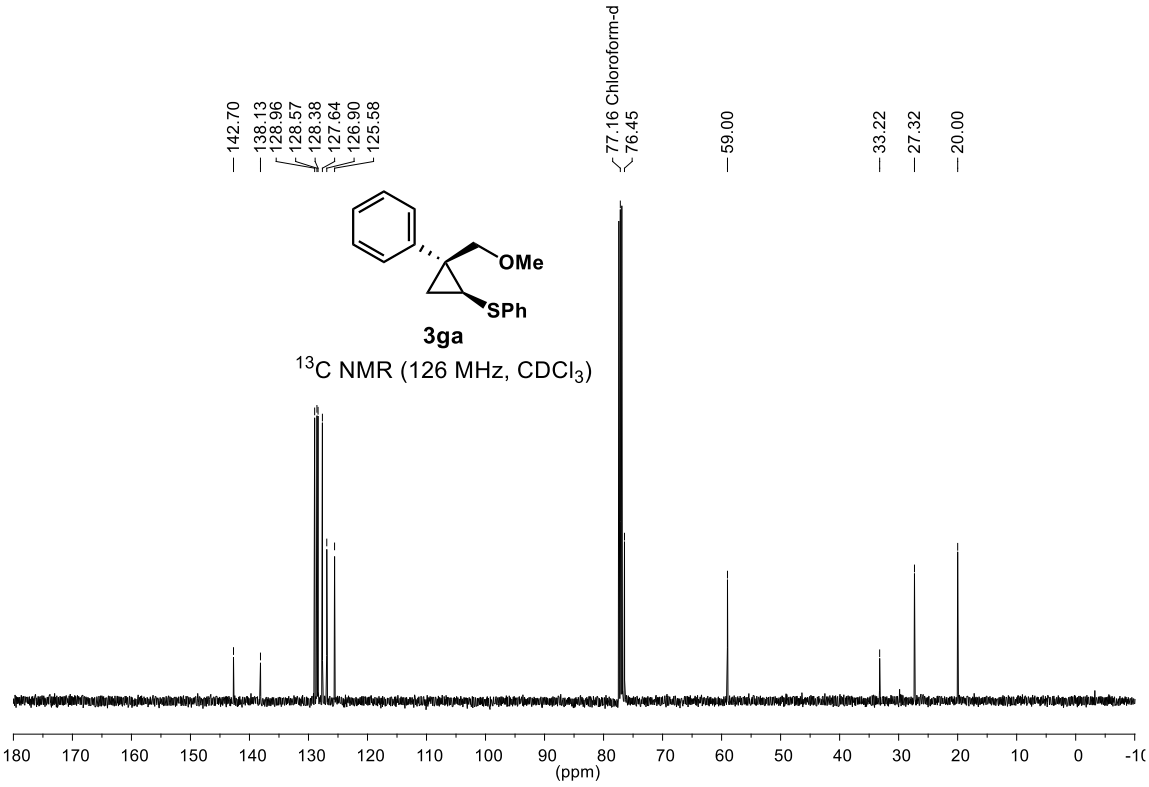

(*S*)-phenyl(2-phenylbut-3-en-2-yl)sulfane (**4aa**)

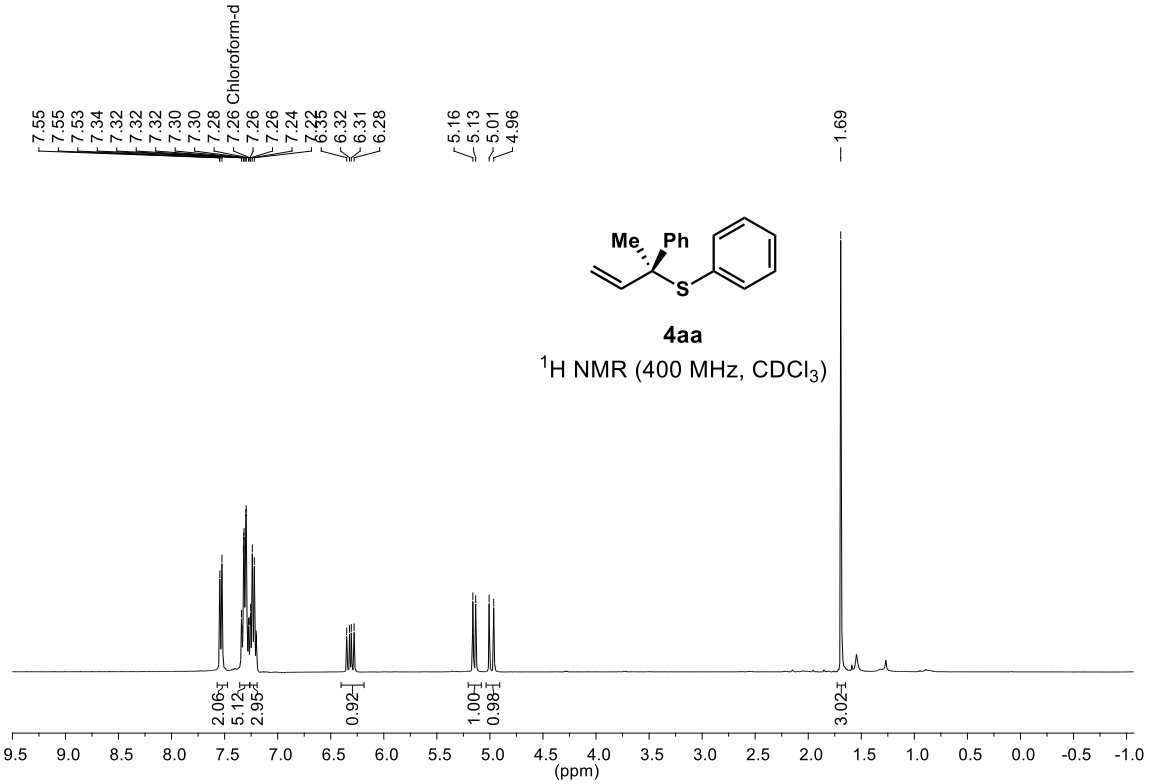

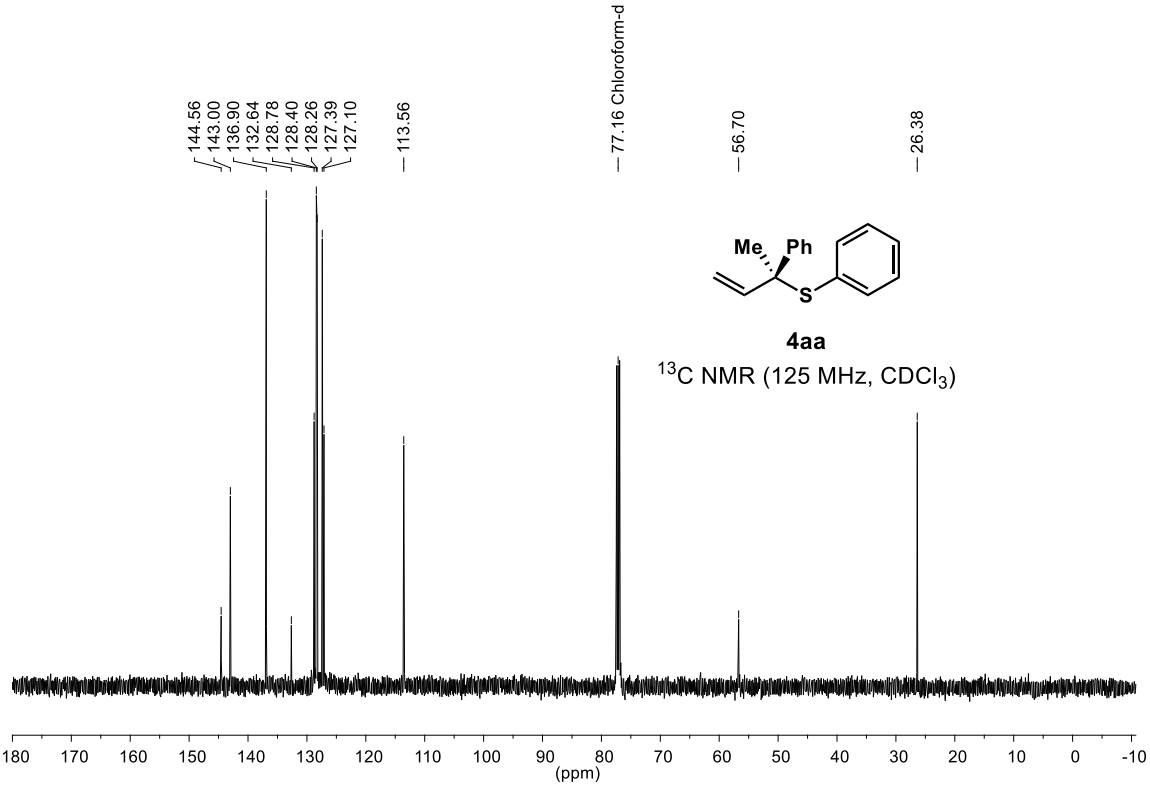

(*S*)-(2-phenylbut-3-en-2-yl)(p-tolyl)sulfane (**4ab**)

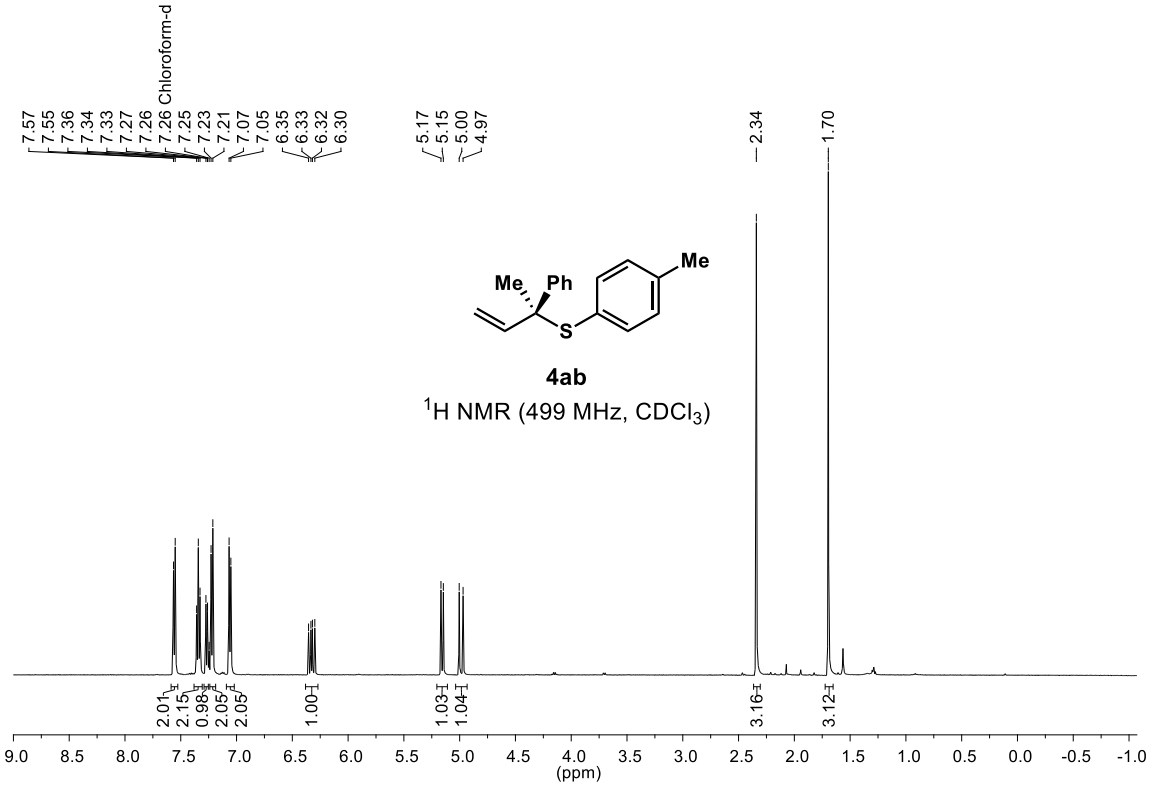

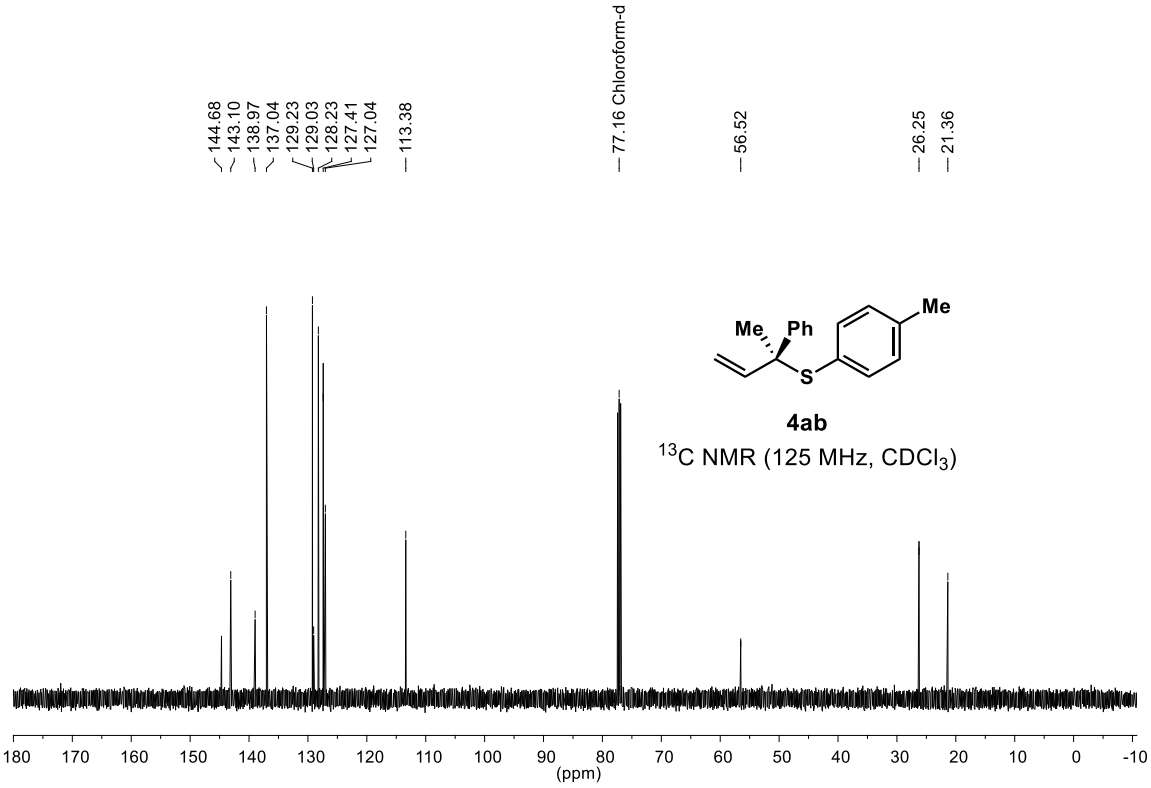

(*S*)-(4-(tert-butyl)phenyl)(2-phenylbut-3-en-2-yl)sulfane (**4ac**)

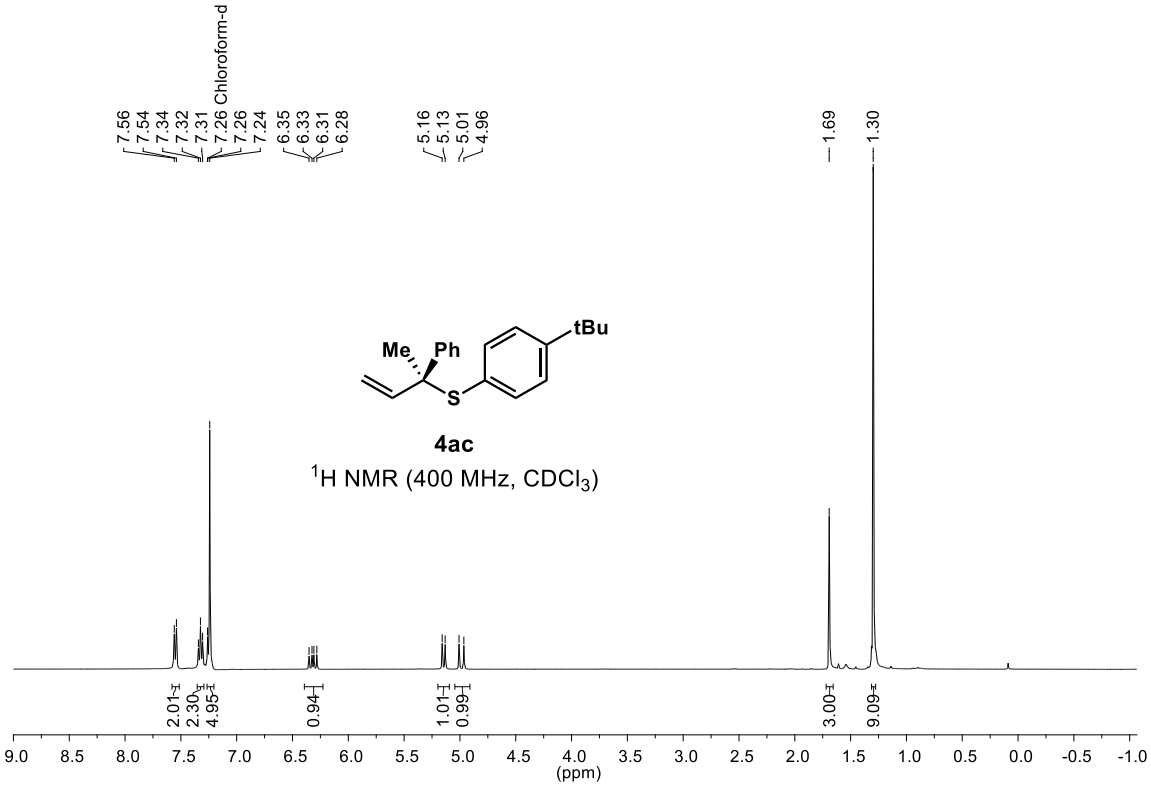

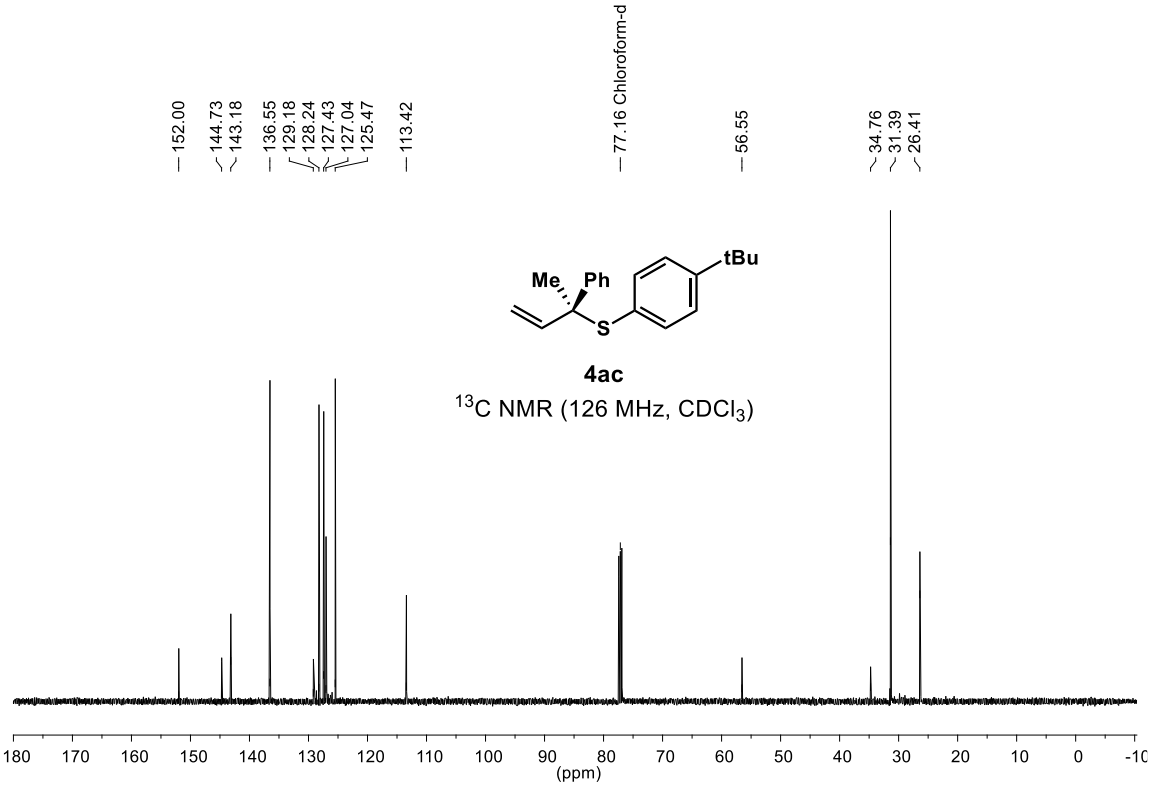

(*S*)-(4-methoxyphenyl)(2-phenylbut-3-en-2-yl)sulfane (**4ah**)

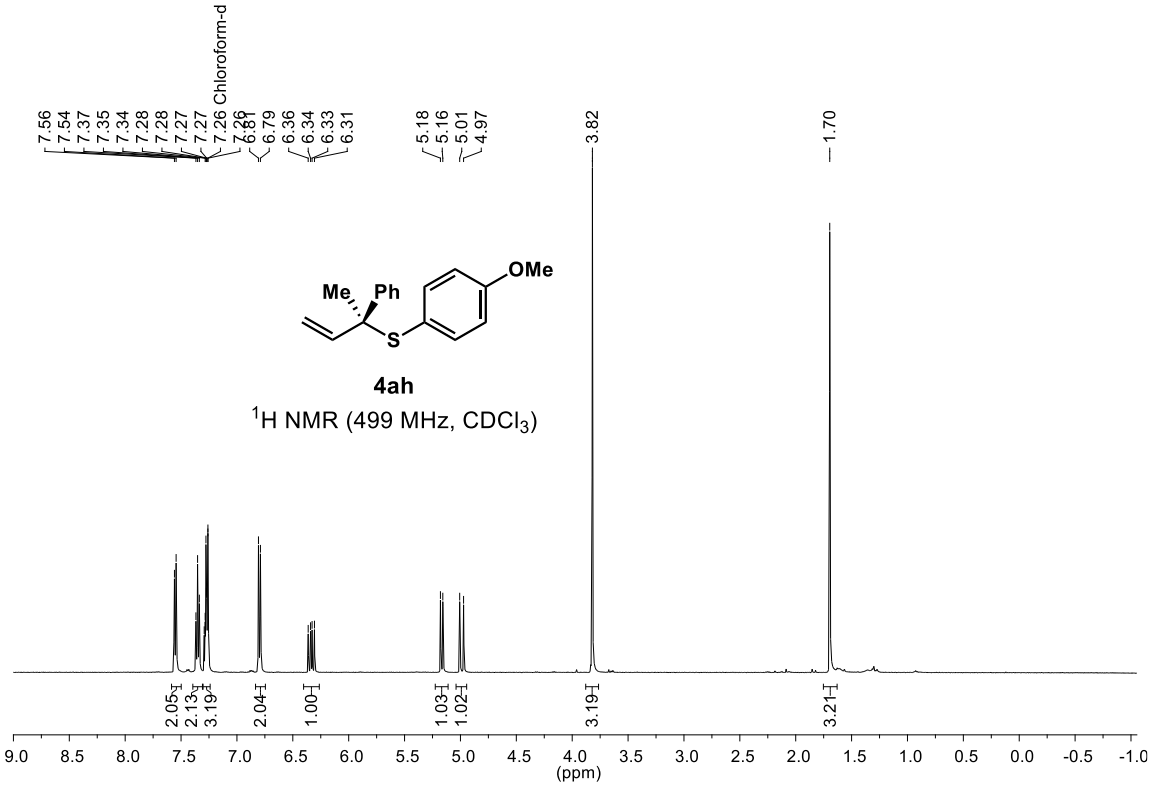

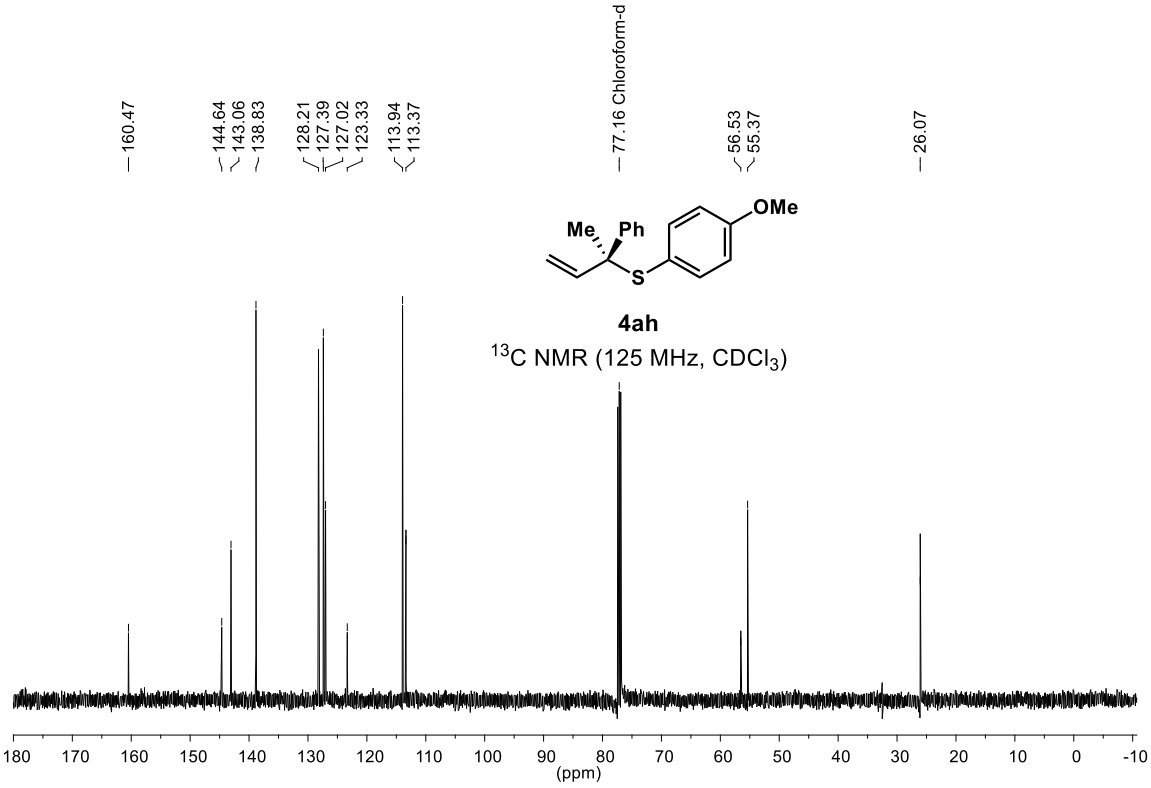

(*S*)-(4-bromophenyl)(2-phenylbut-3-en-2-yl)sulfane (**4ai**)

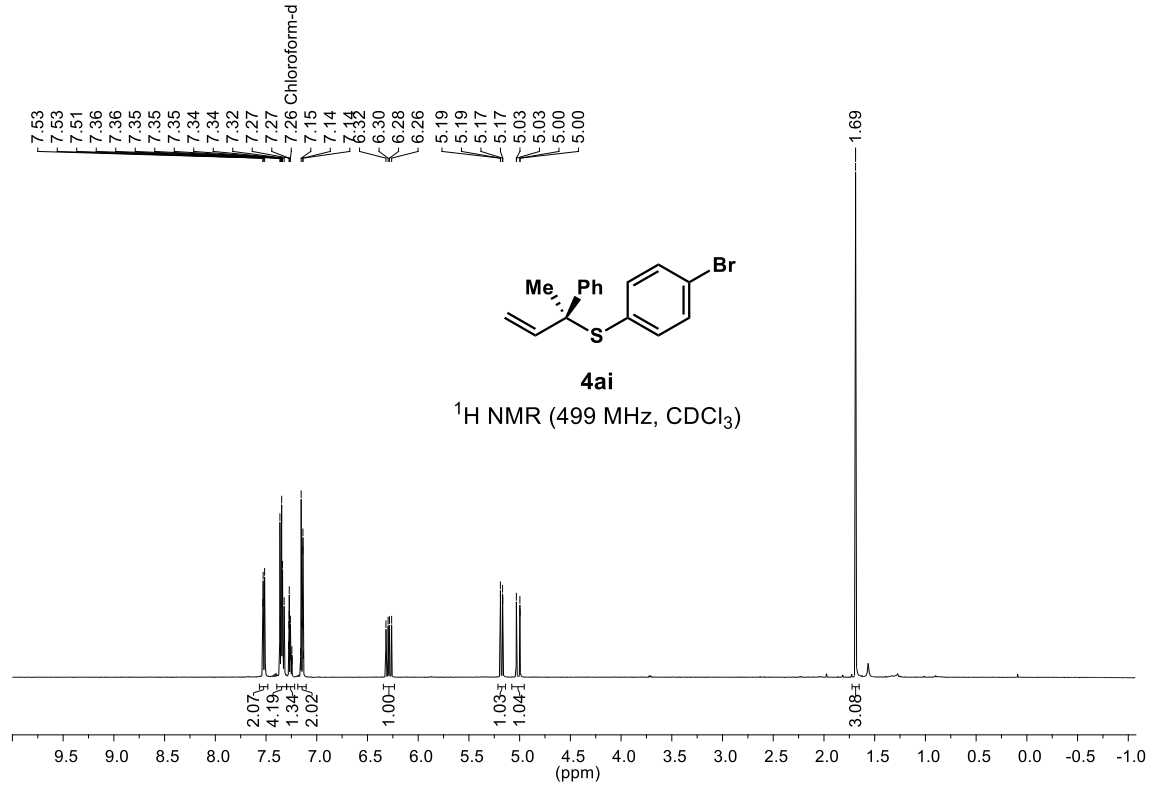

4ai

^{1}H NMR (499 MHz, $CDCl_3$)

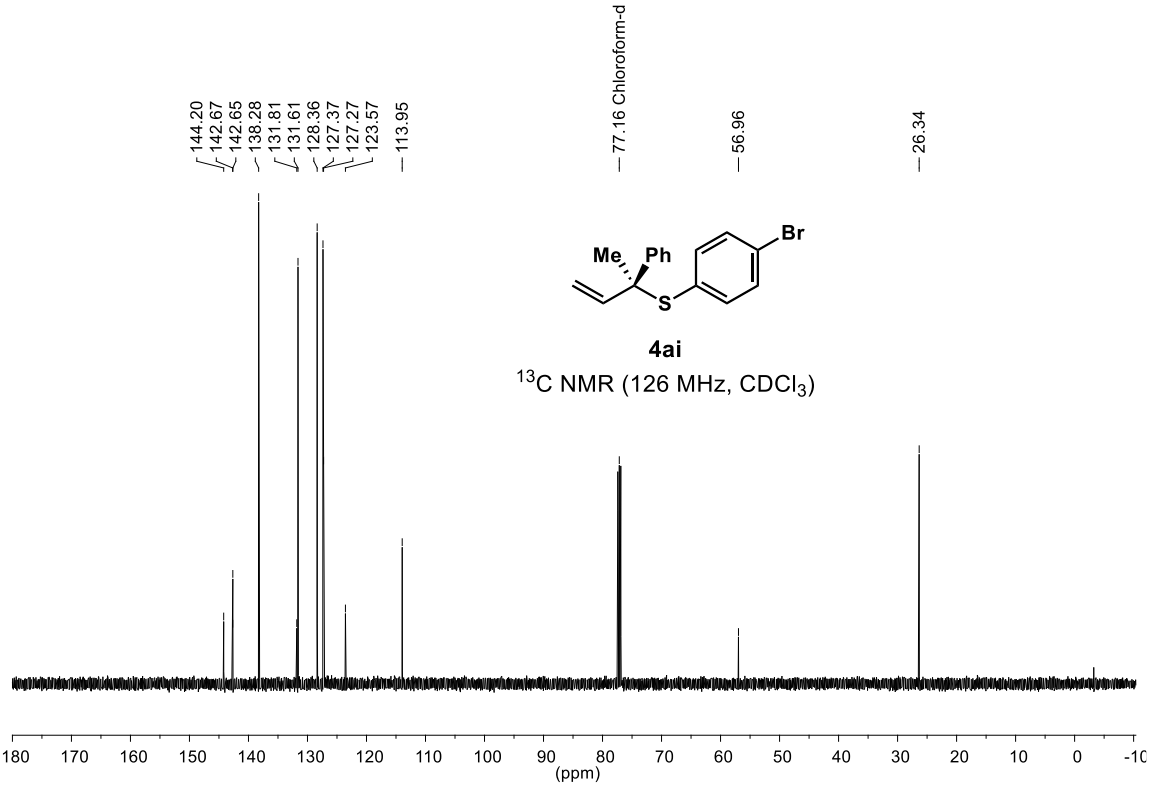

4ai

^{13}C NMR (126 MHz, $CDCl_3$)

(*S*)-(4-fluorophenyl)(2-phenylbut-3-en-2-yl)sulfane (**4aj**)

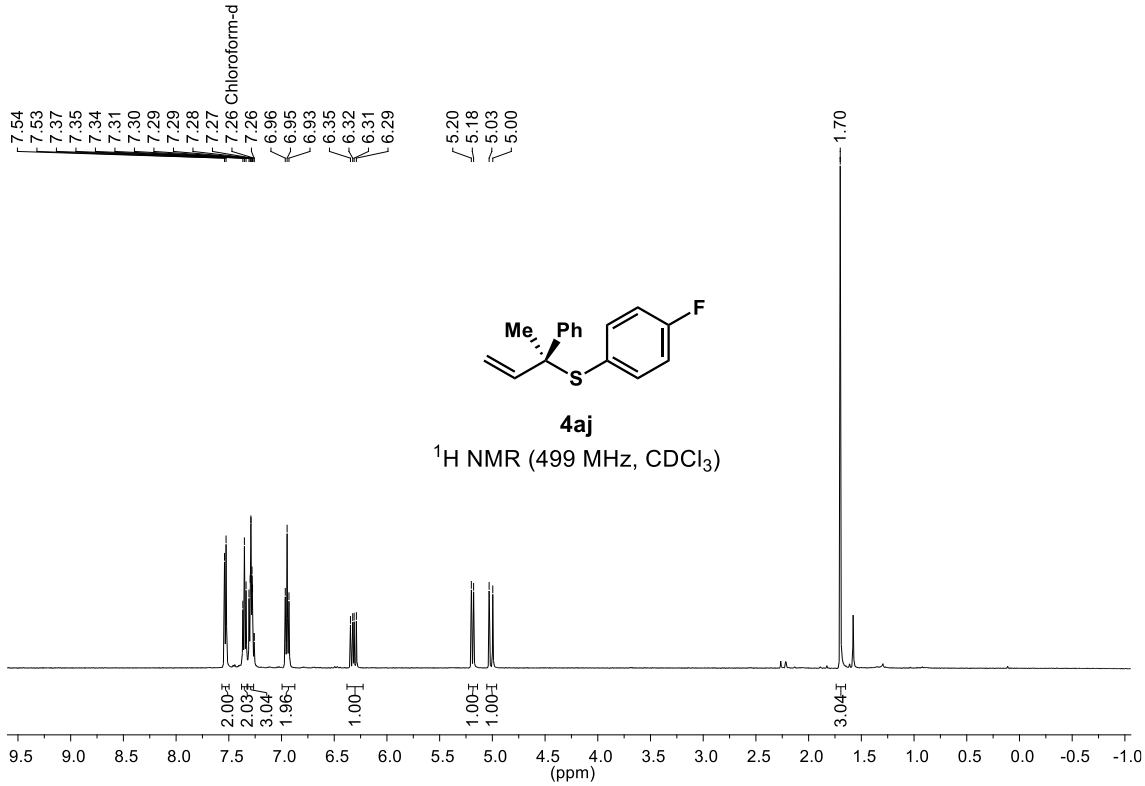

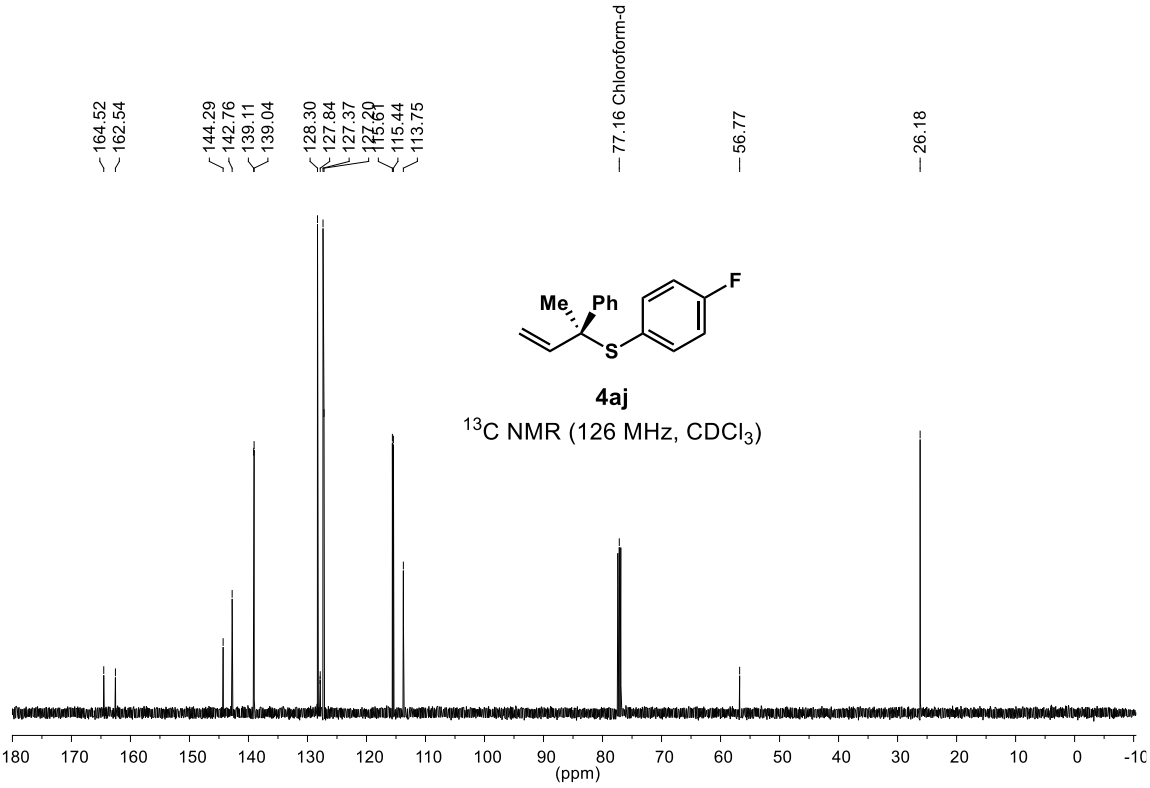

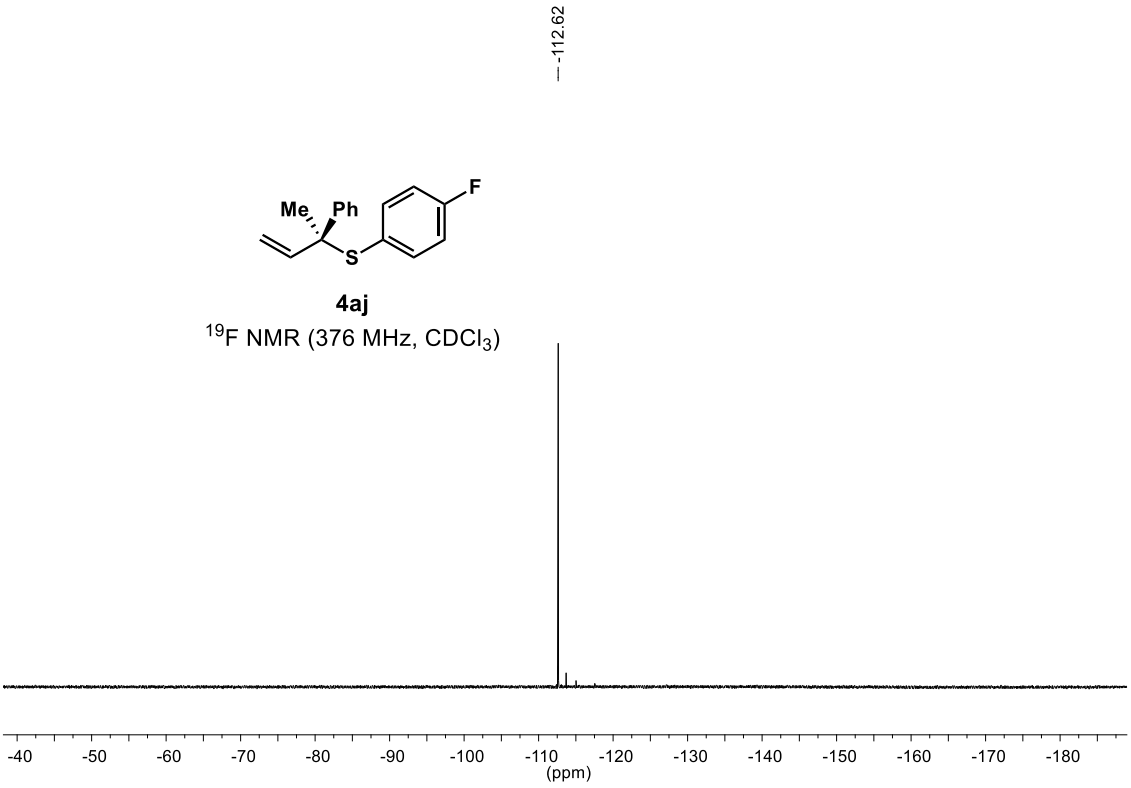

4aj

^{19}F NMR (376 MHz, $CDCl_3$)

(*S*)-(2-phenylbut-3-en-2-yl)(4-(trifluoromethyl)phenyl)sulfane (**4ak**)

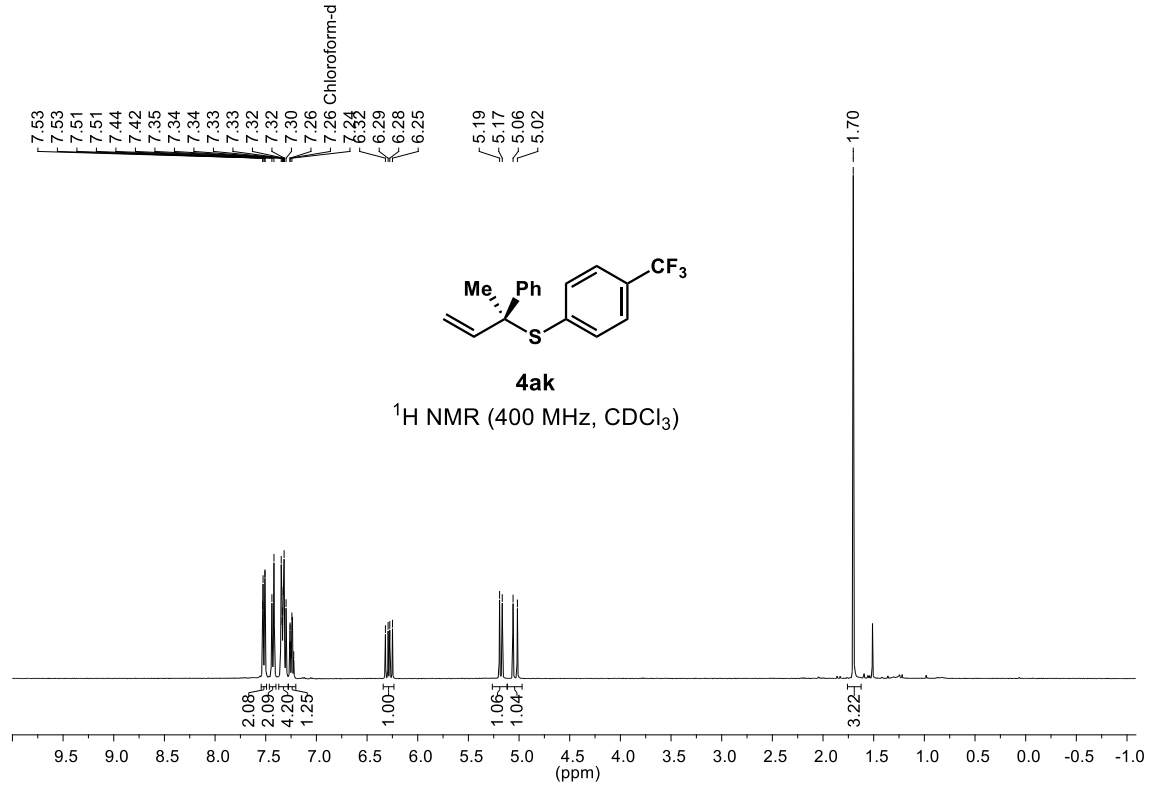

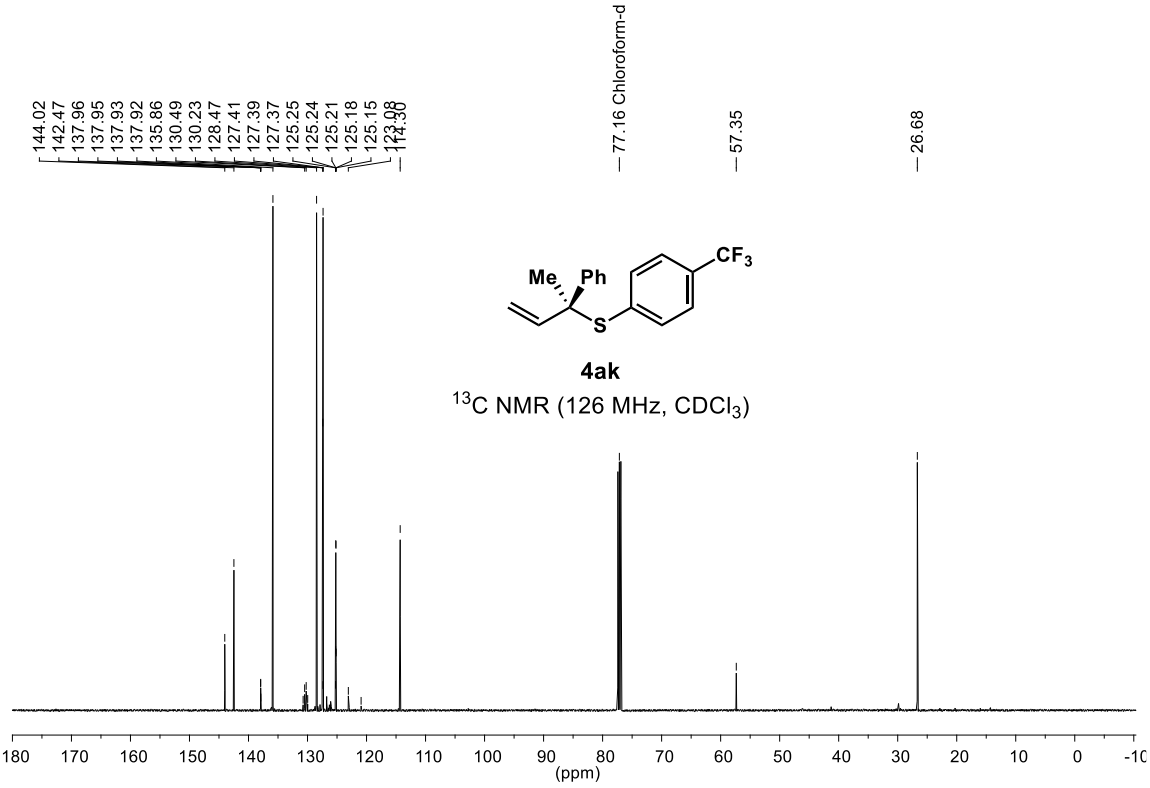

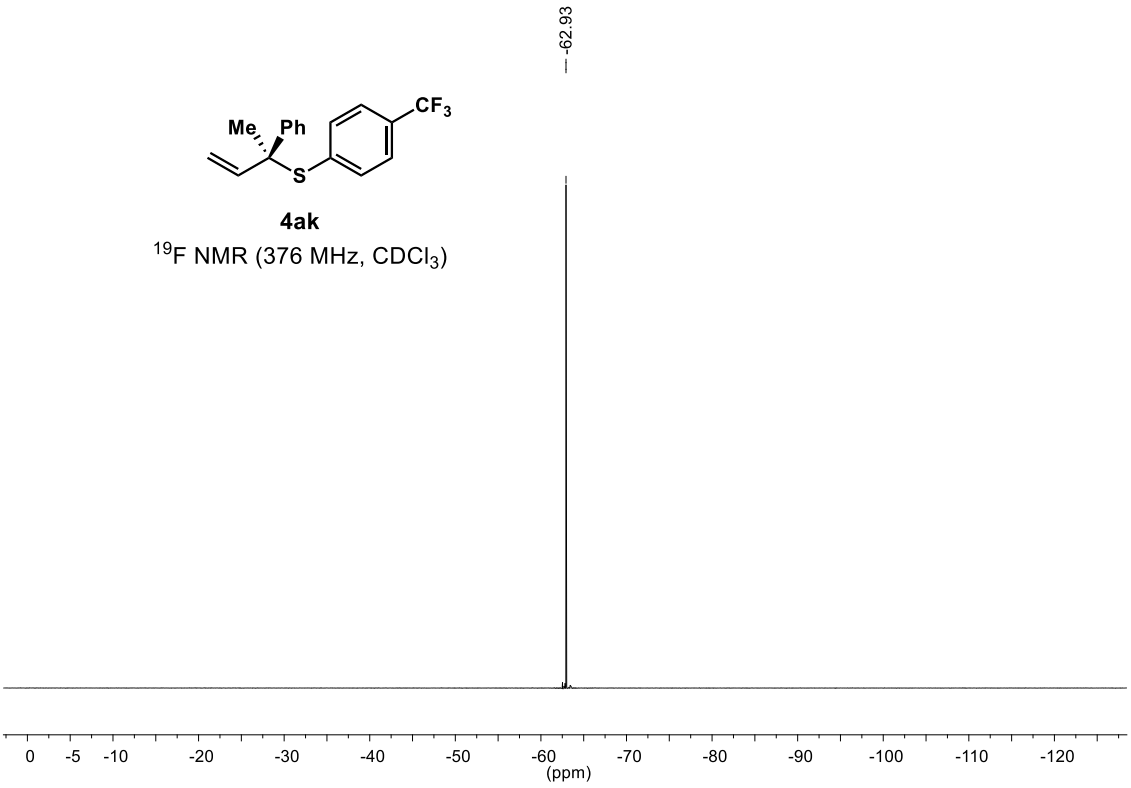

4ak

^{19}F NMR (376 MHz, $CDCl_3$)

(*S*)-(4-nitrophenyl)(2-phenylbut-3-en-2-yl)sulfane (**4al**)

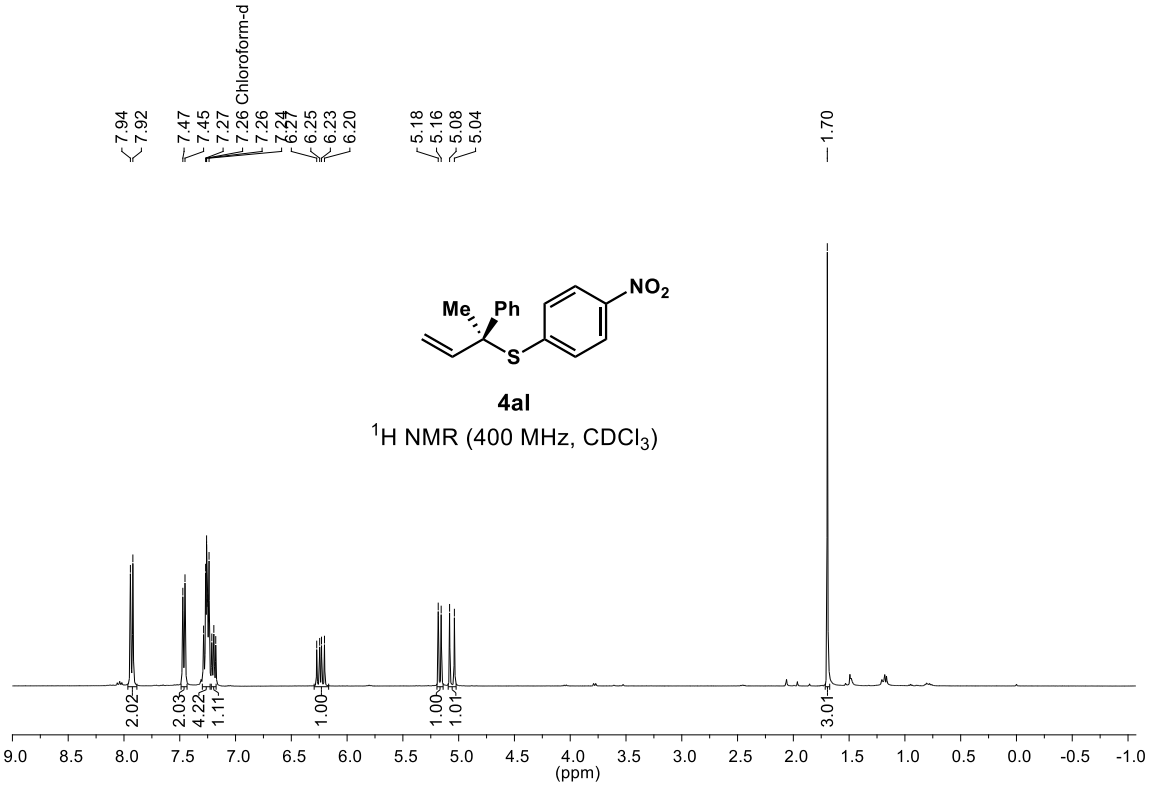

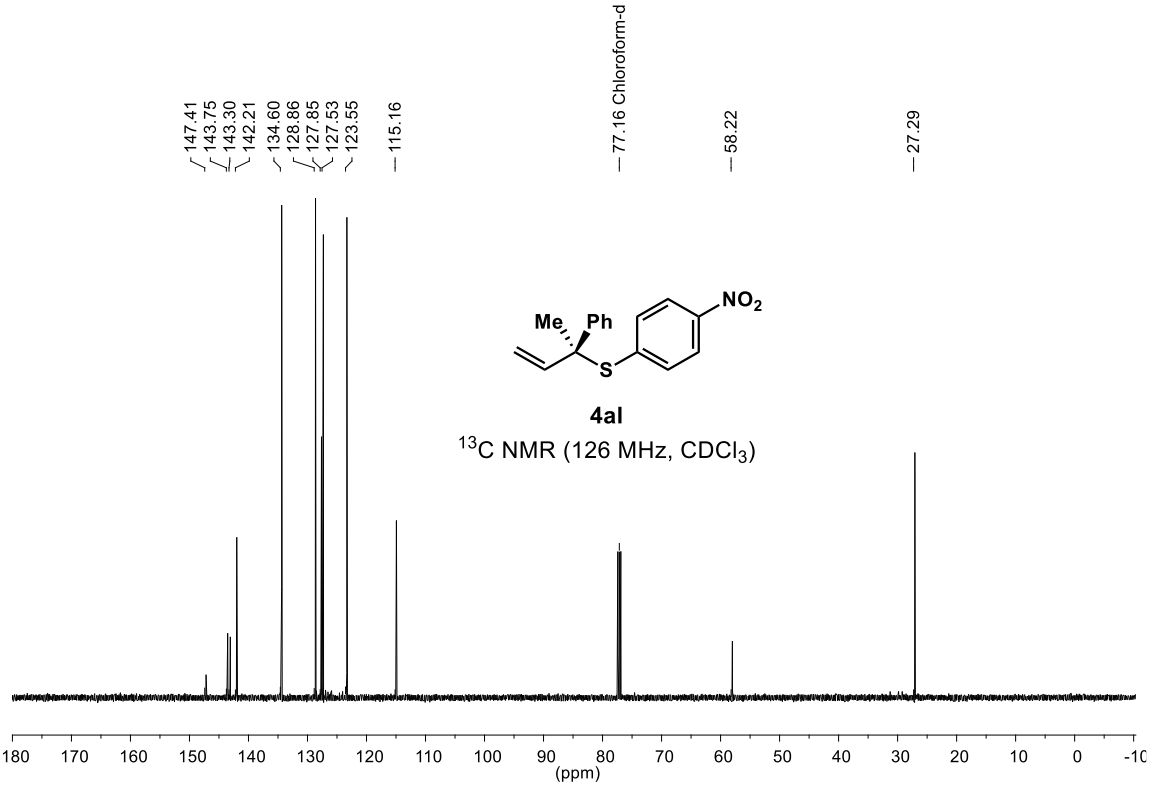

(*S*)-(2-phenylbut-3-en-2-yl)(m-tolyl)sulfane (**4ae**)

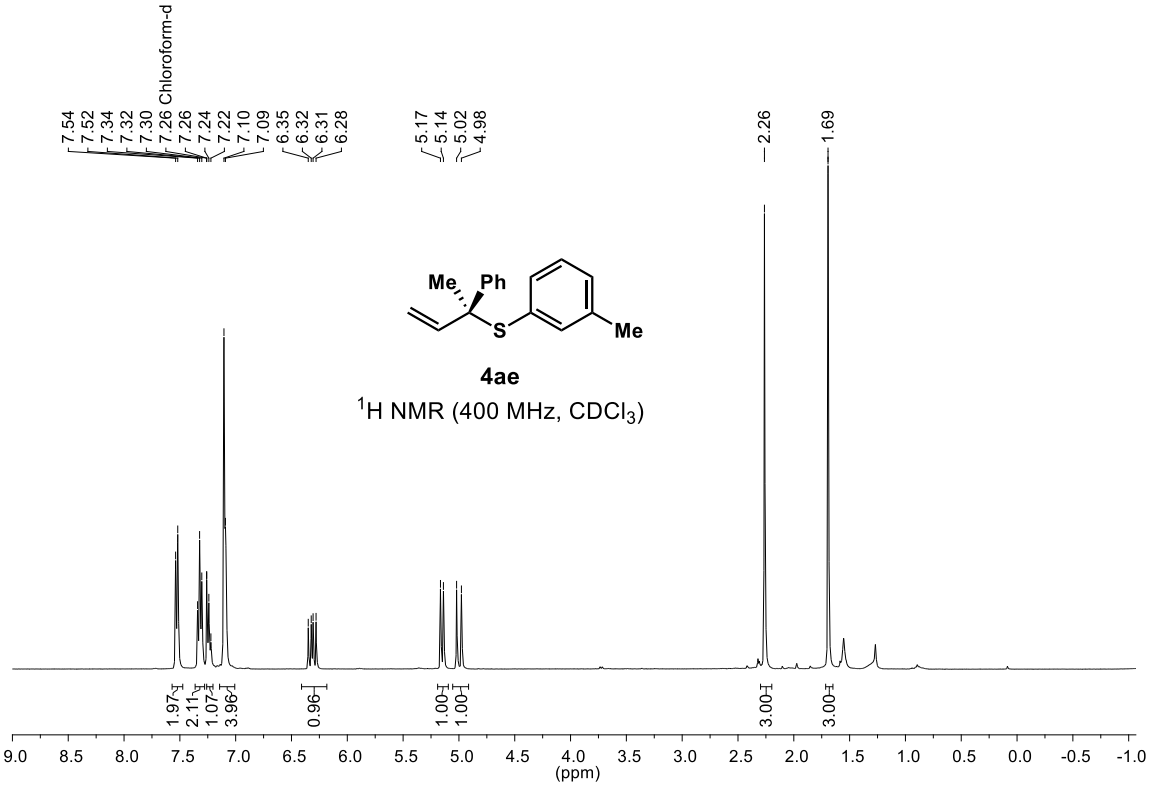

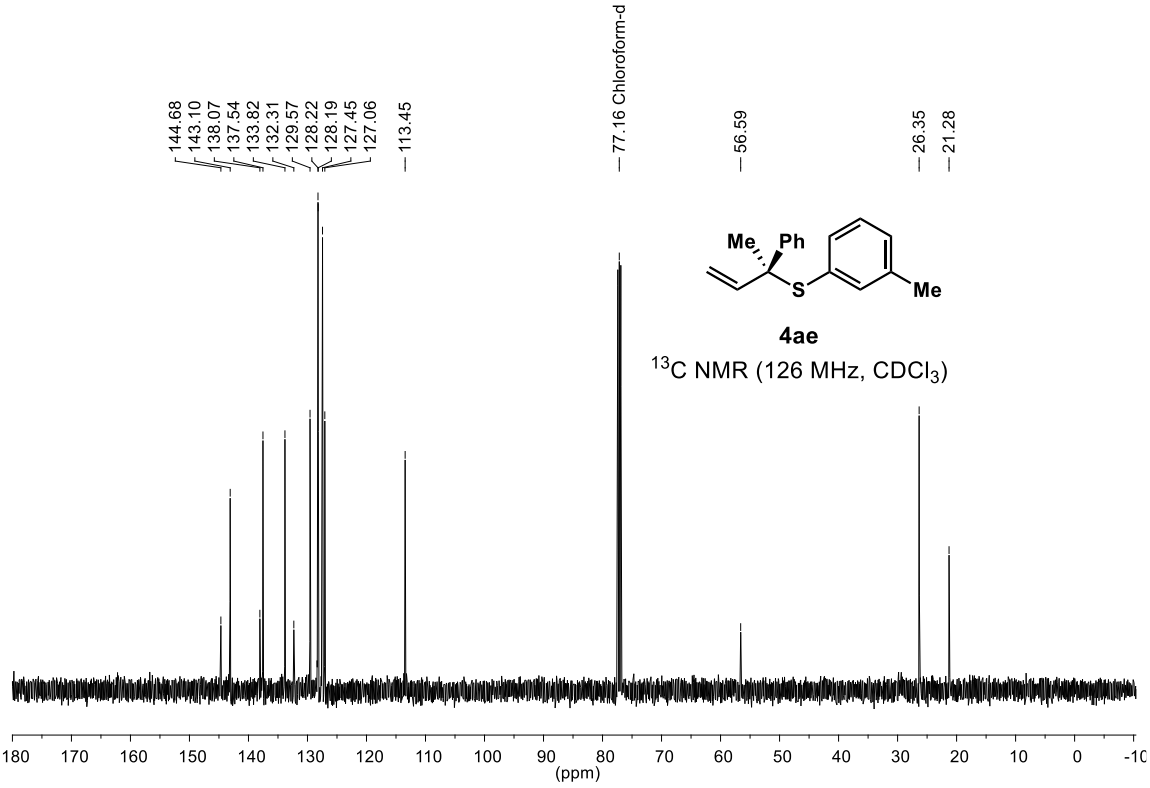

(S)-(3-chlorophenyl)(2-phenylbut-3-en-2-yl)sulfane (**4am**)

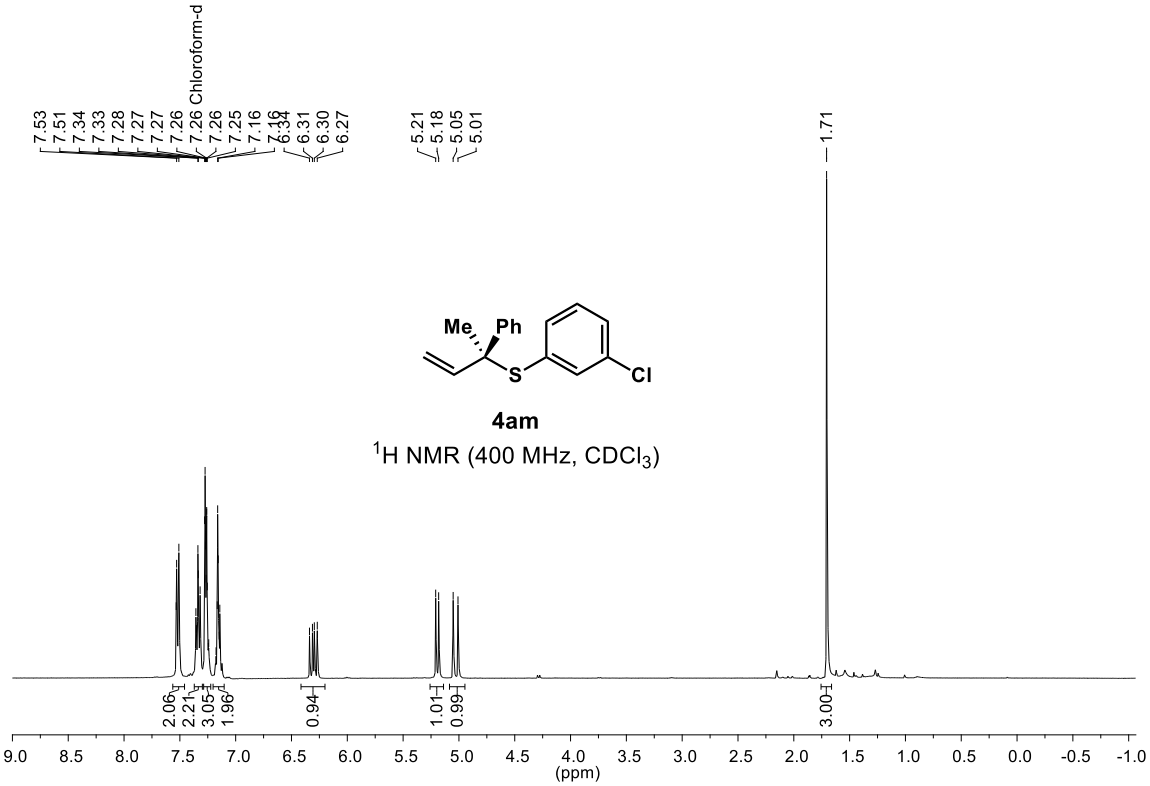

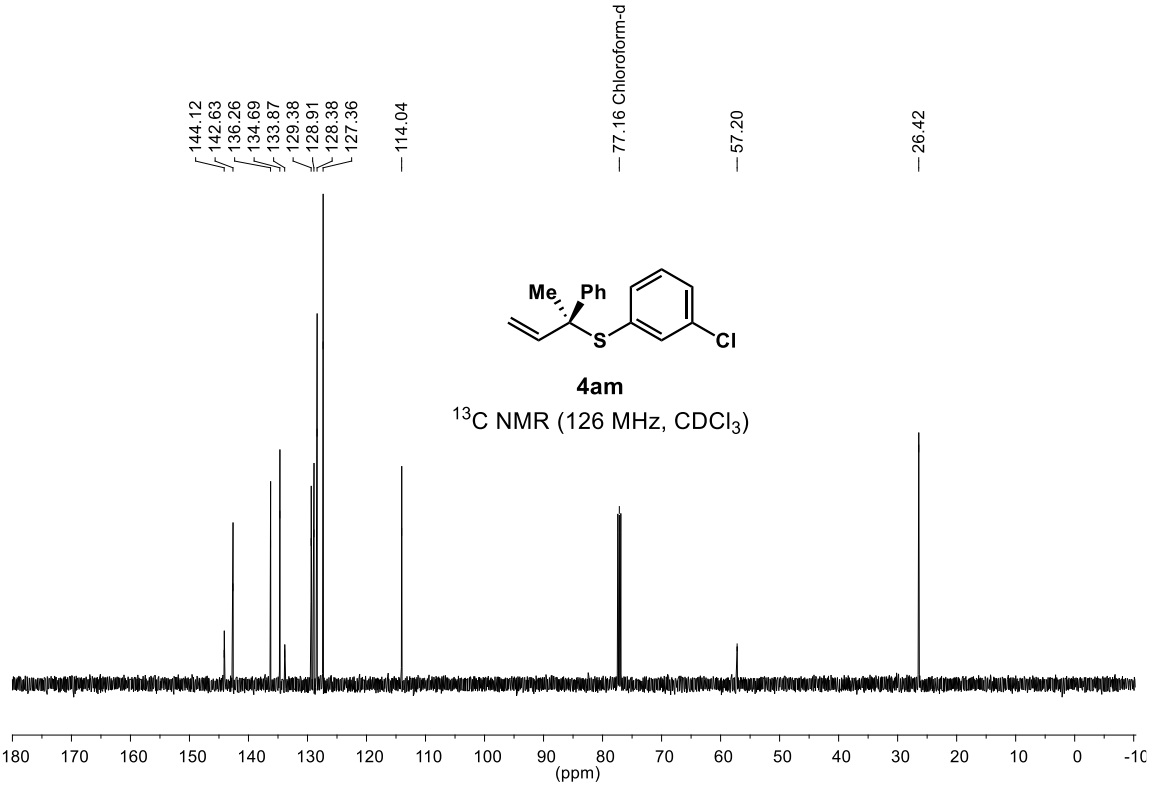

(S)-(3-fluorophenyl)(2-phenylbut-3-en-2-yl)sulfane (**4an**)

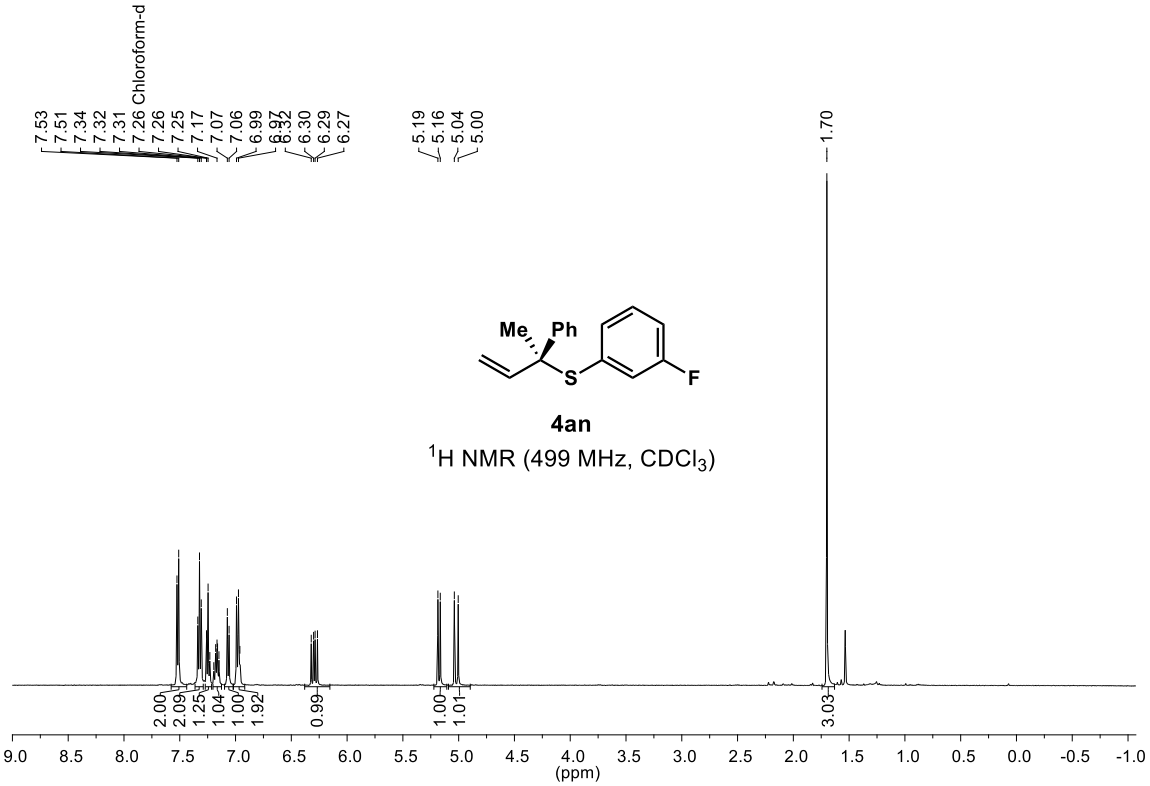

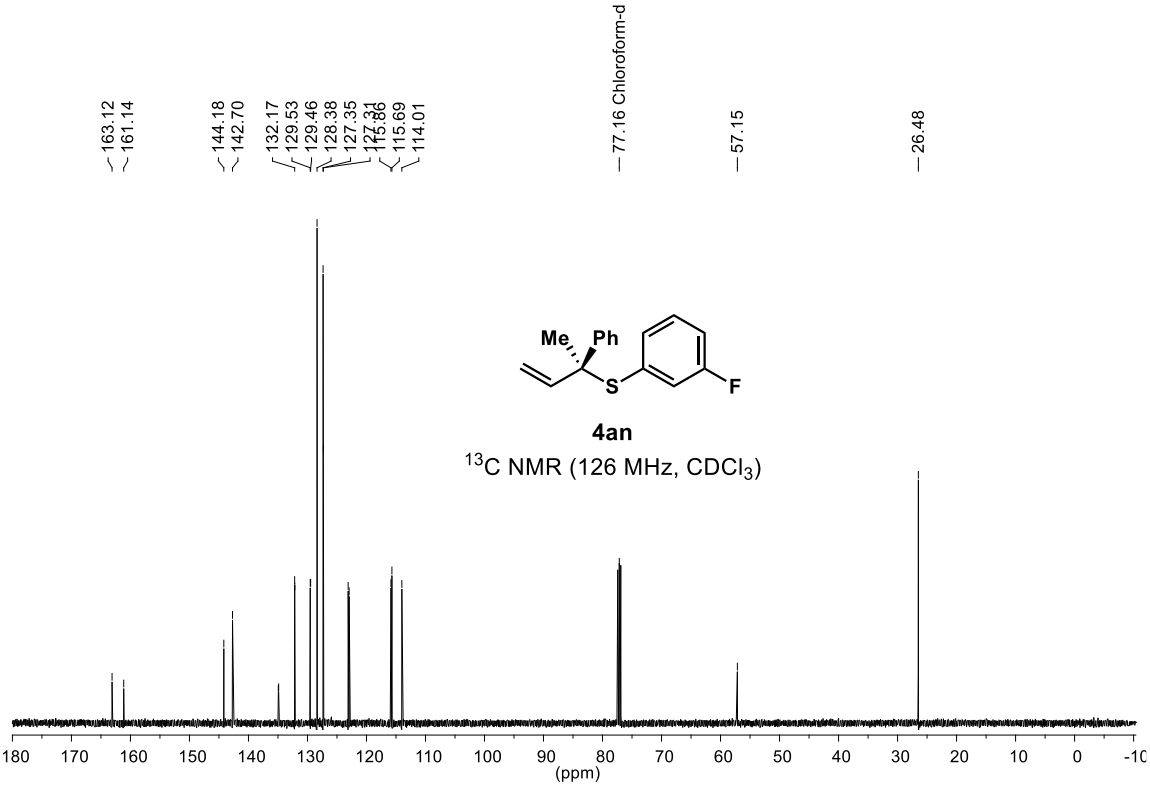

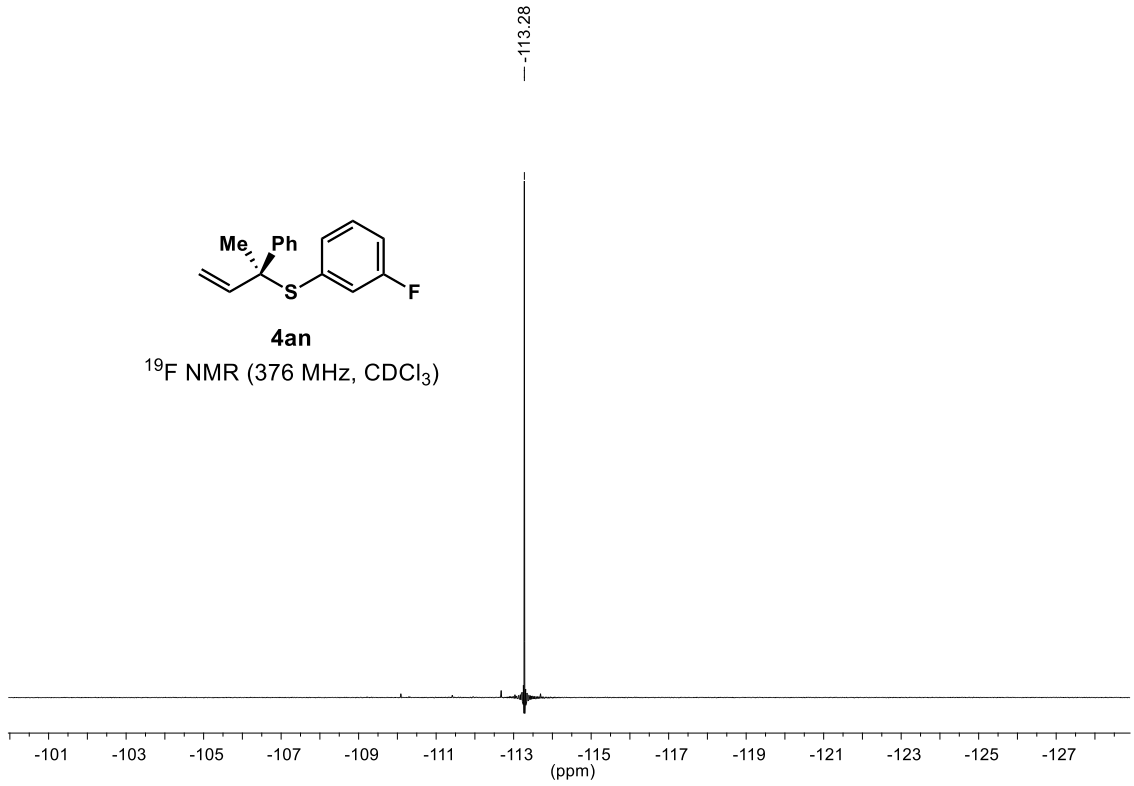

4an

^{19}F NMR (376 MHz, $CDCl_3$)

(S)-(2-phenylbut-3-en-2-yl)(o-tolyl)sulfane (**4af**)

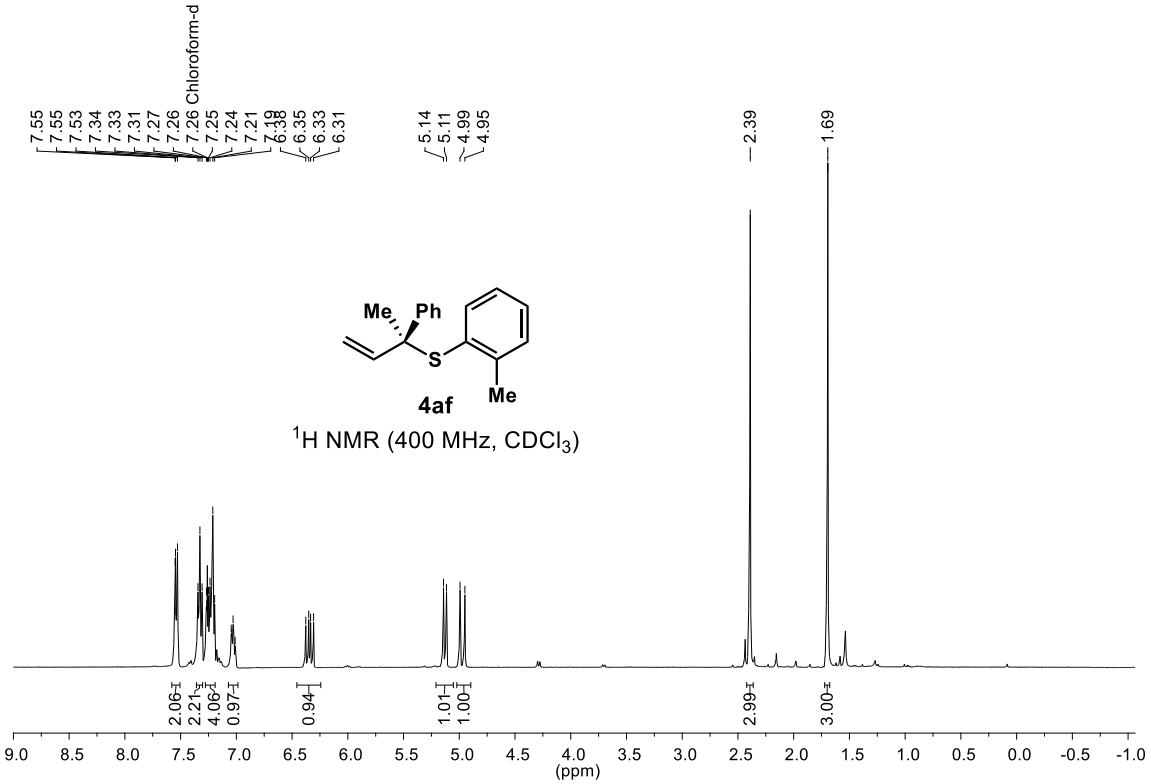

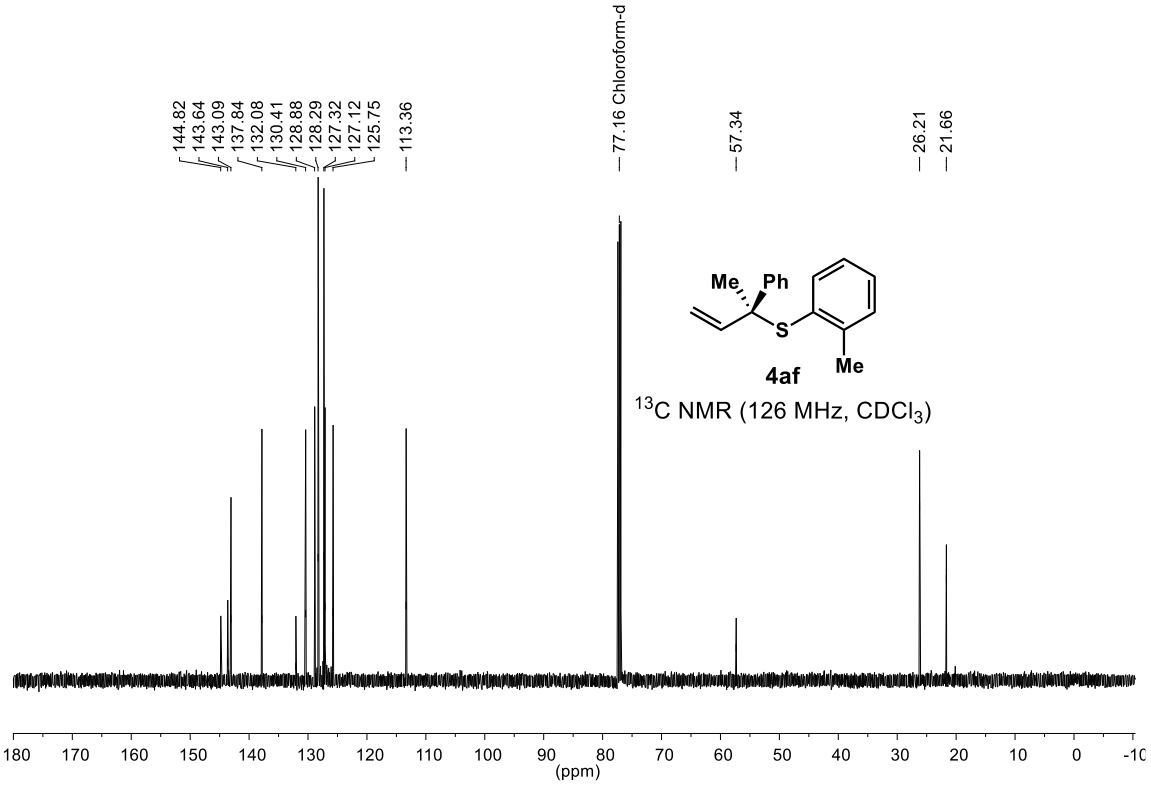

(*S*)-(2-fluorophenyl)(2-phenylbut-3-en-2-yl)sulfane (**4ao**)

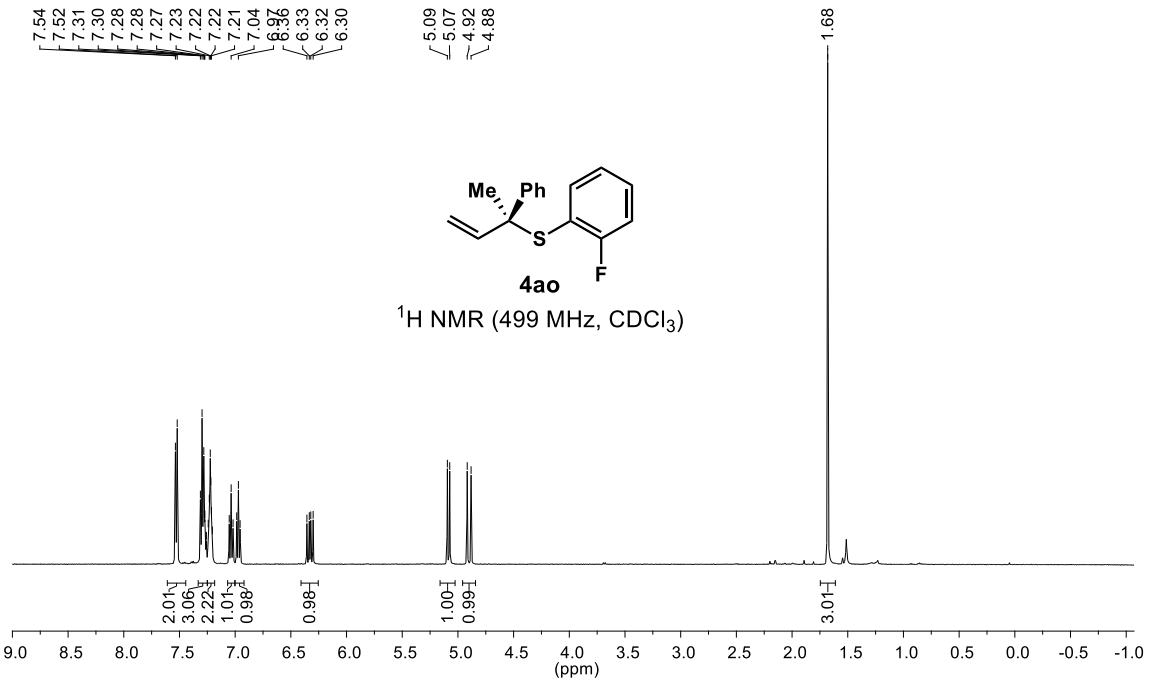

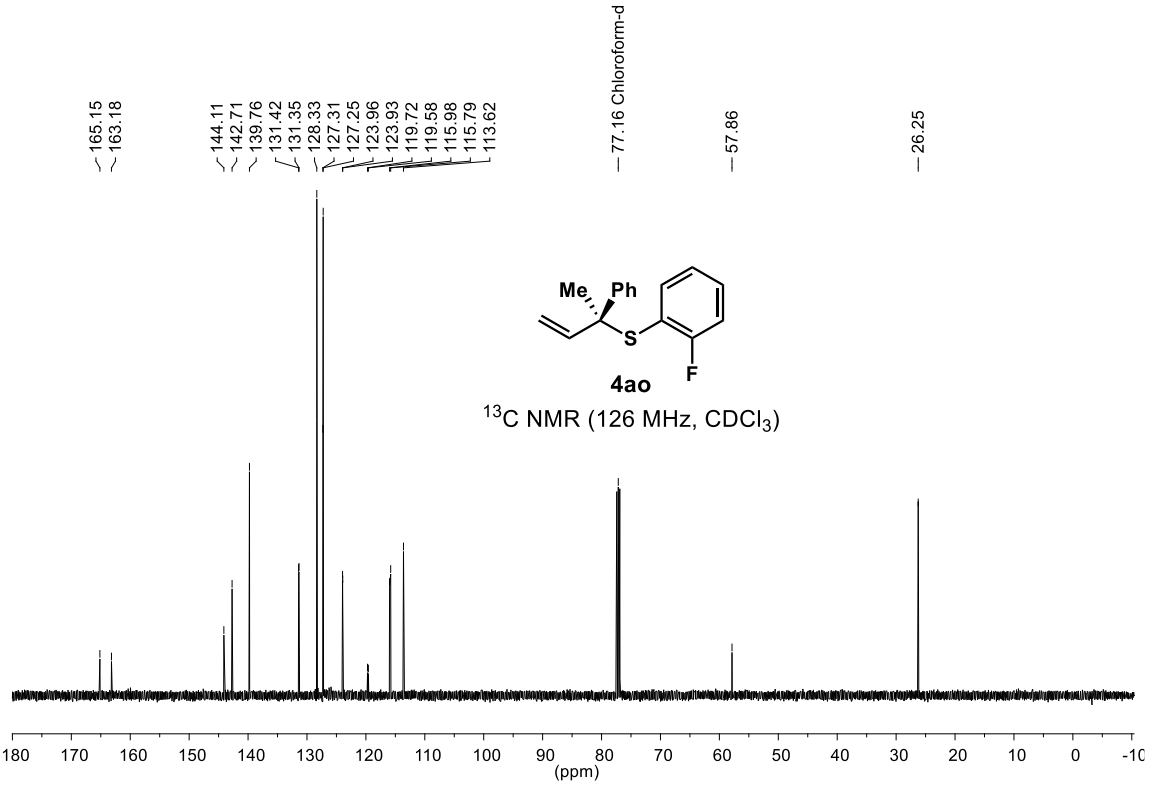

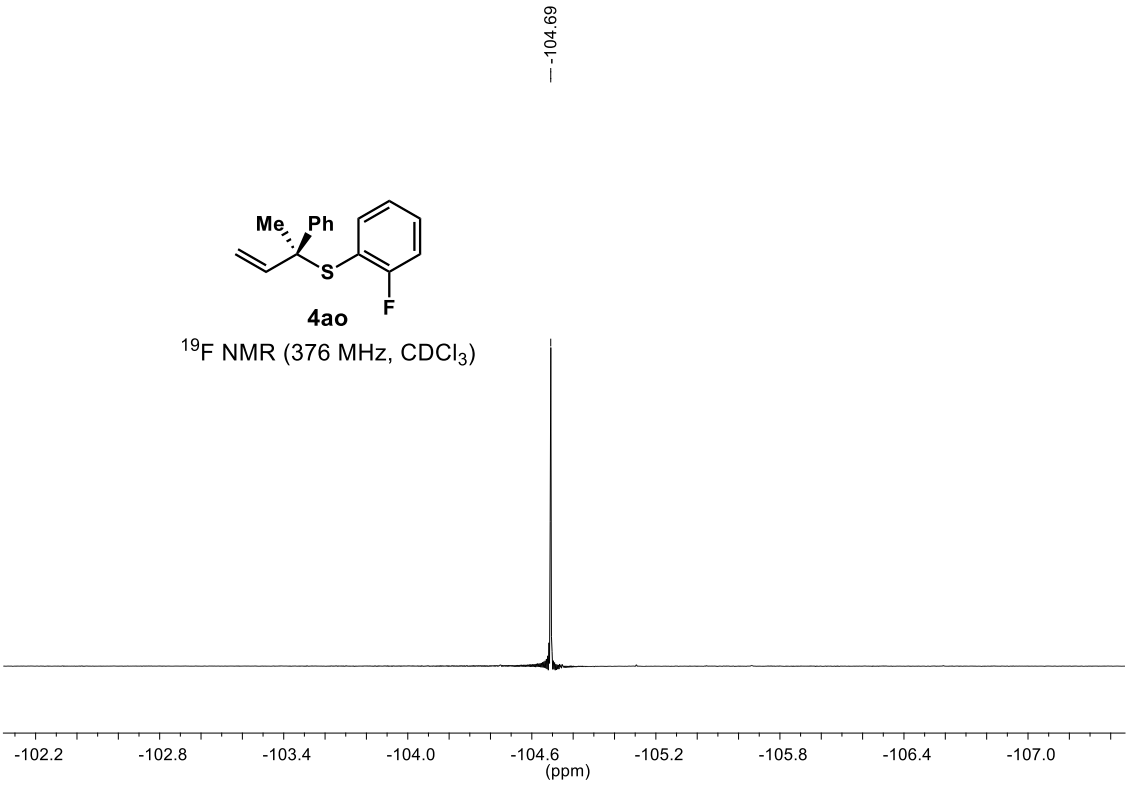

4ao

^{19}F NMR (376 MHz, $CDCl_3$)

(S)-naphthalen-2-yl(2-phenylbut-3-en-2-yl)sulfane (**4ag**)

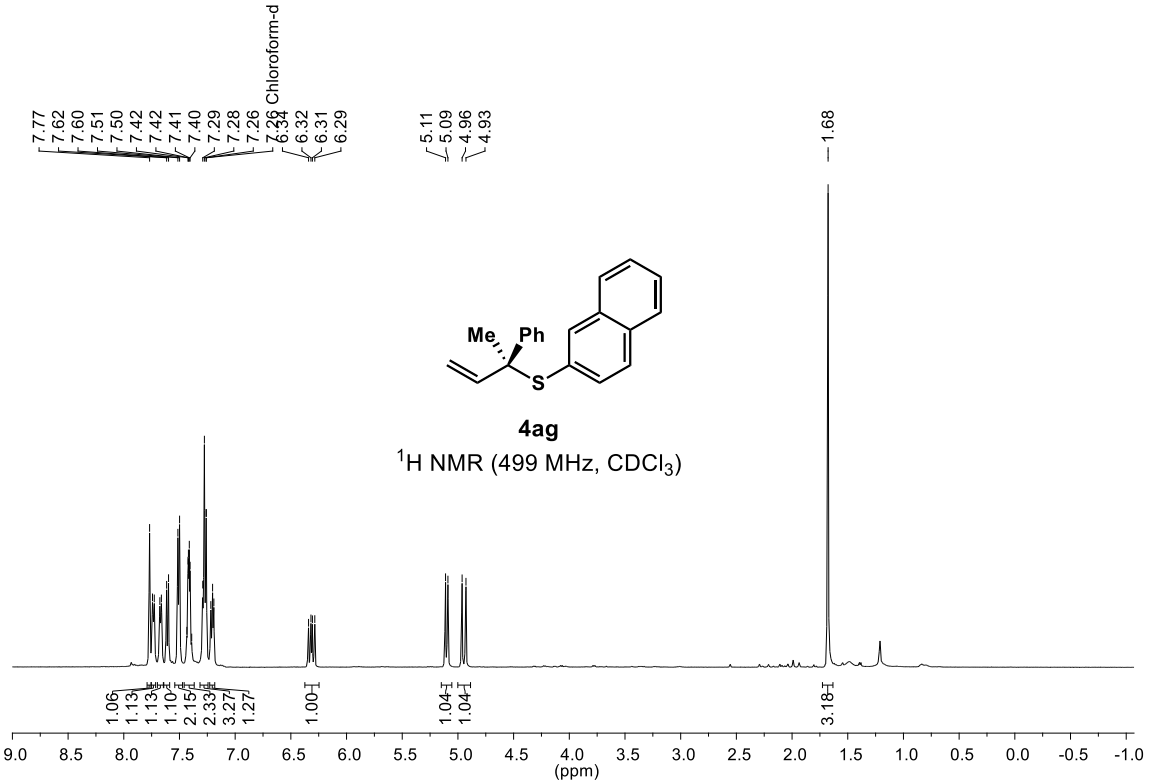

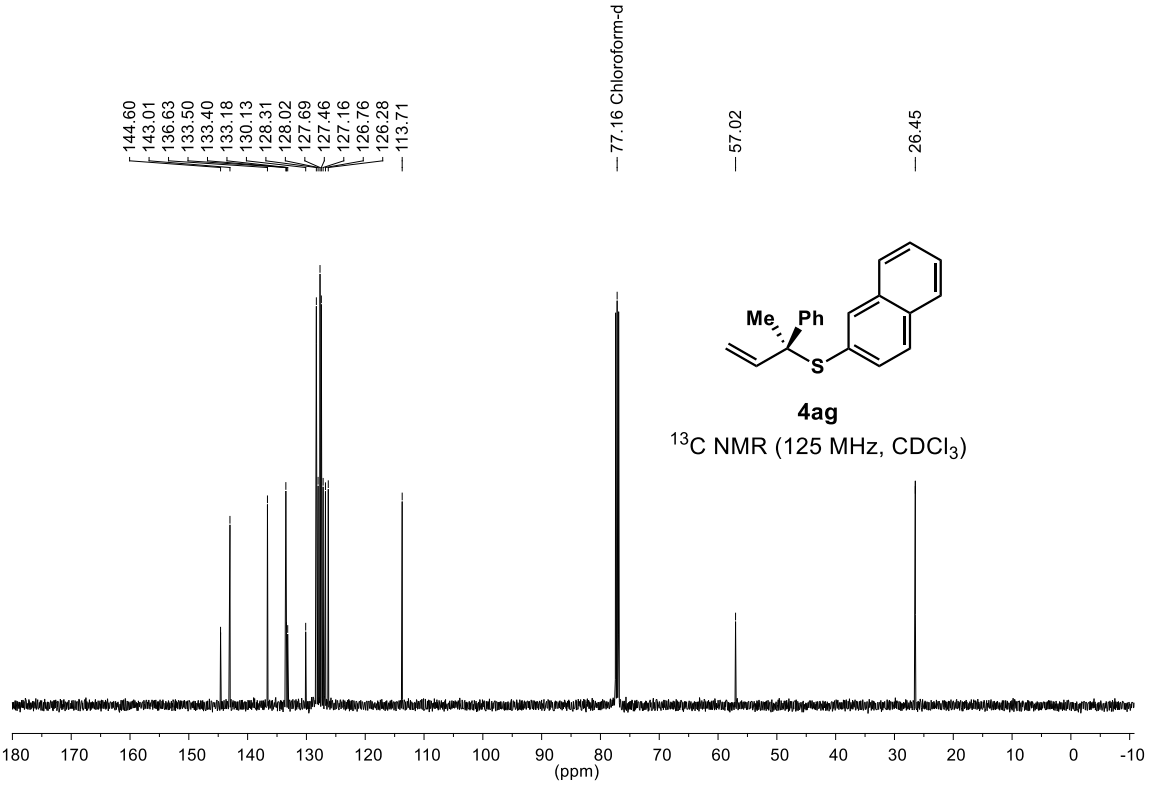

(*S*)-phenethyl(2-phenylbut-3-en-2-yl)sulfane (**4ap**)

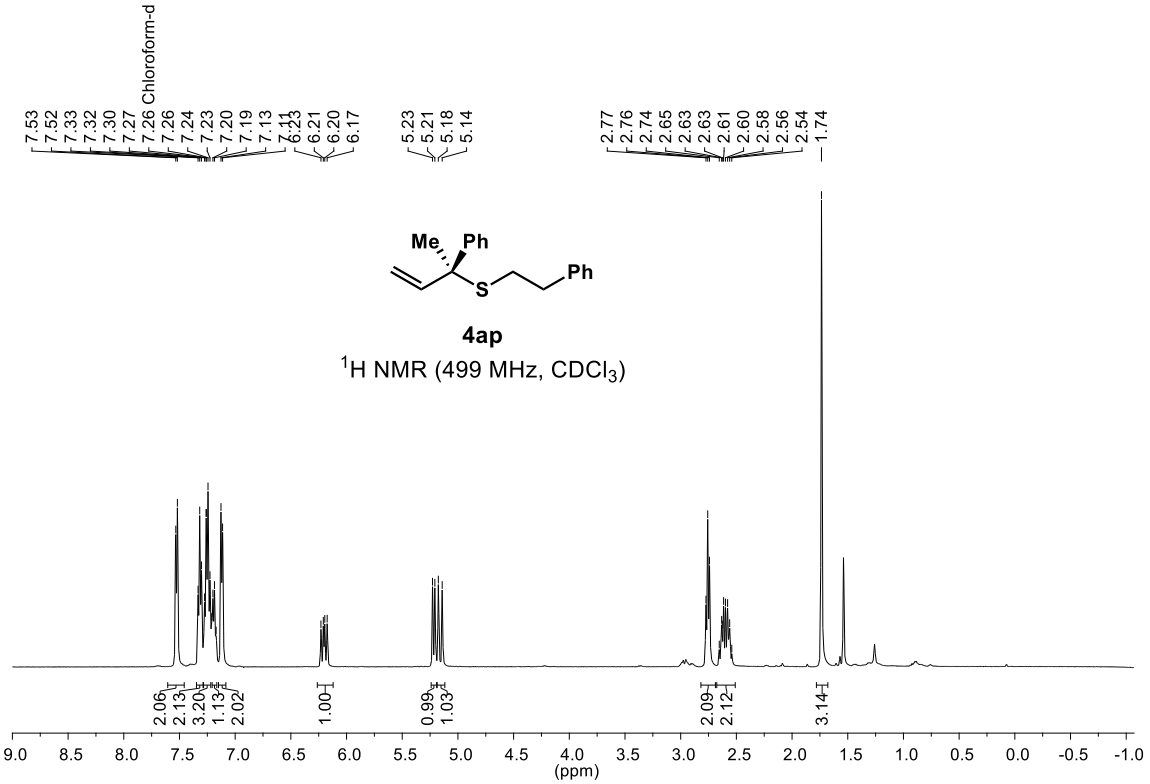

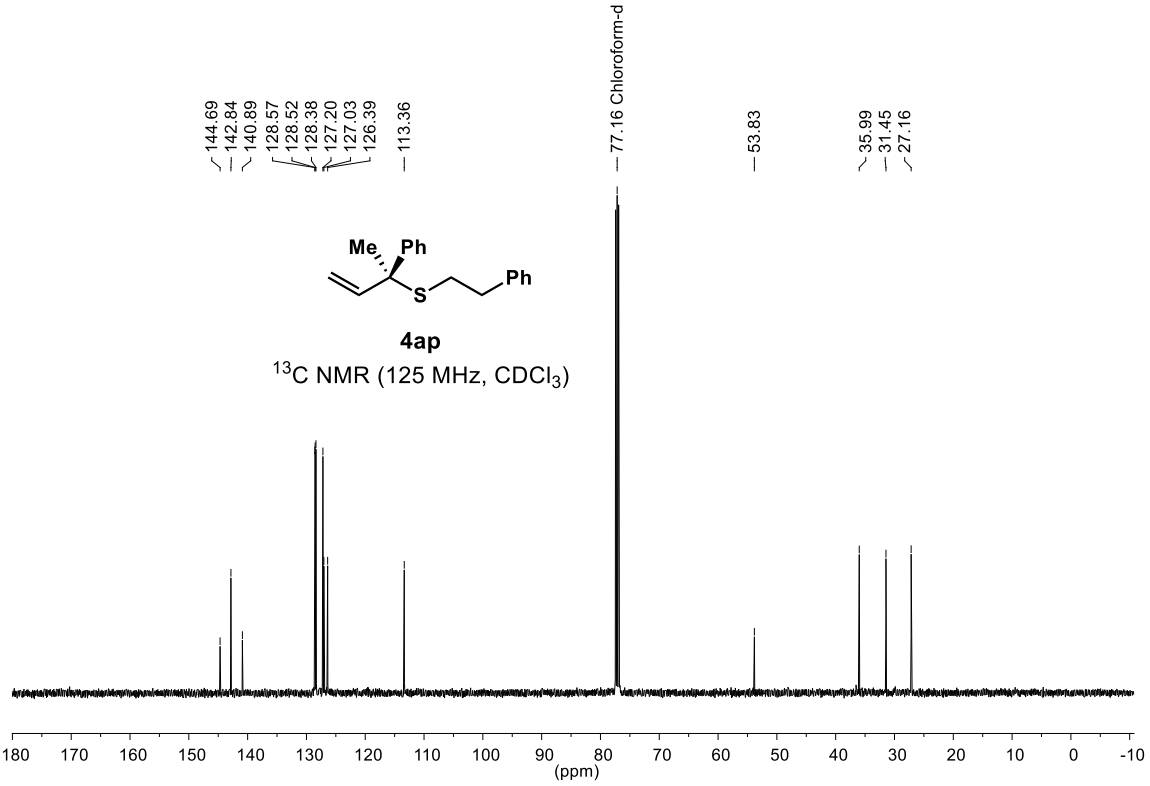

(*S*)-2-(((2-phenylbut-3-en-2-yl)thio)methyl)furan (**4aq**)

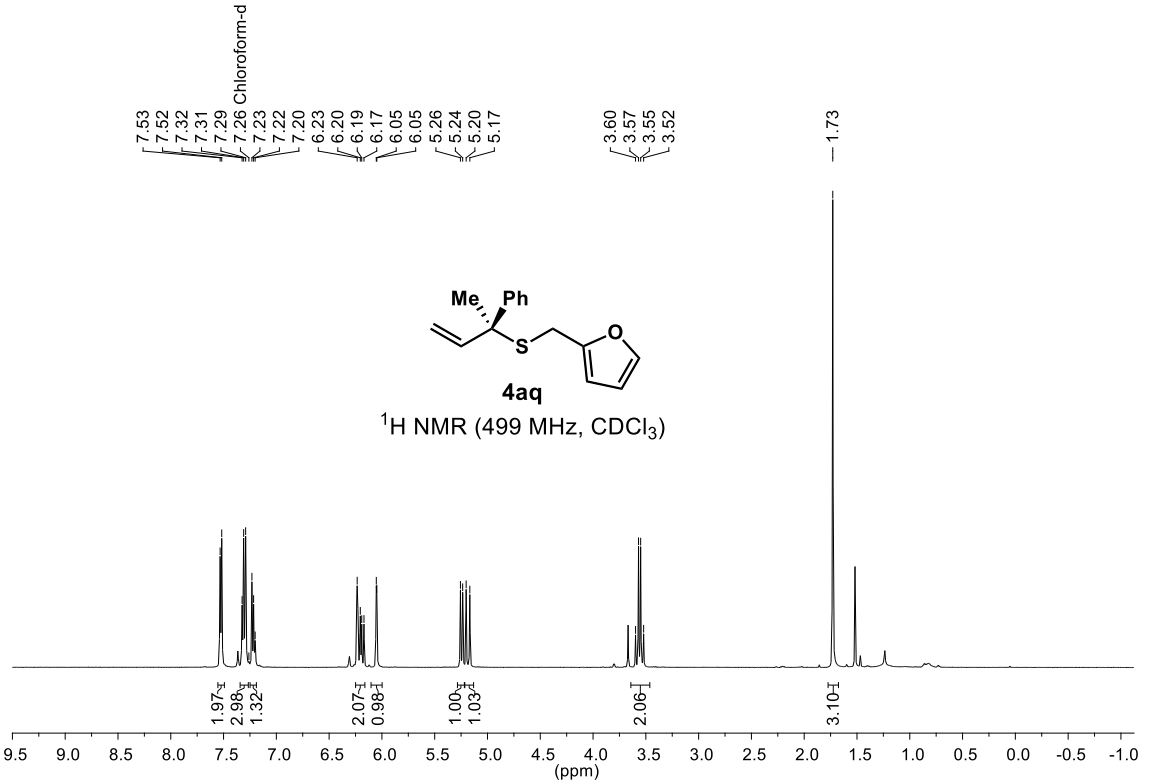

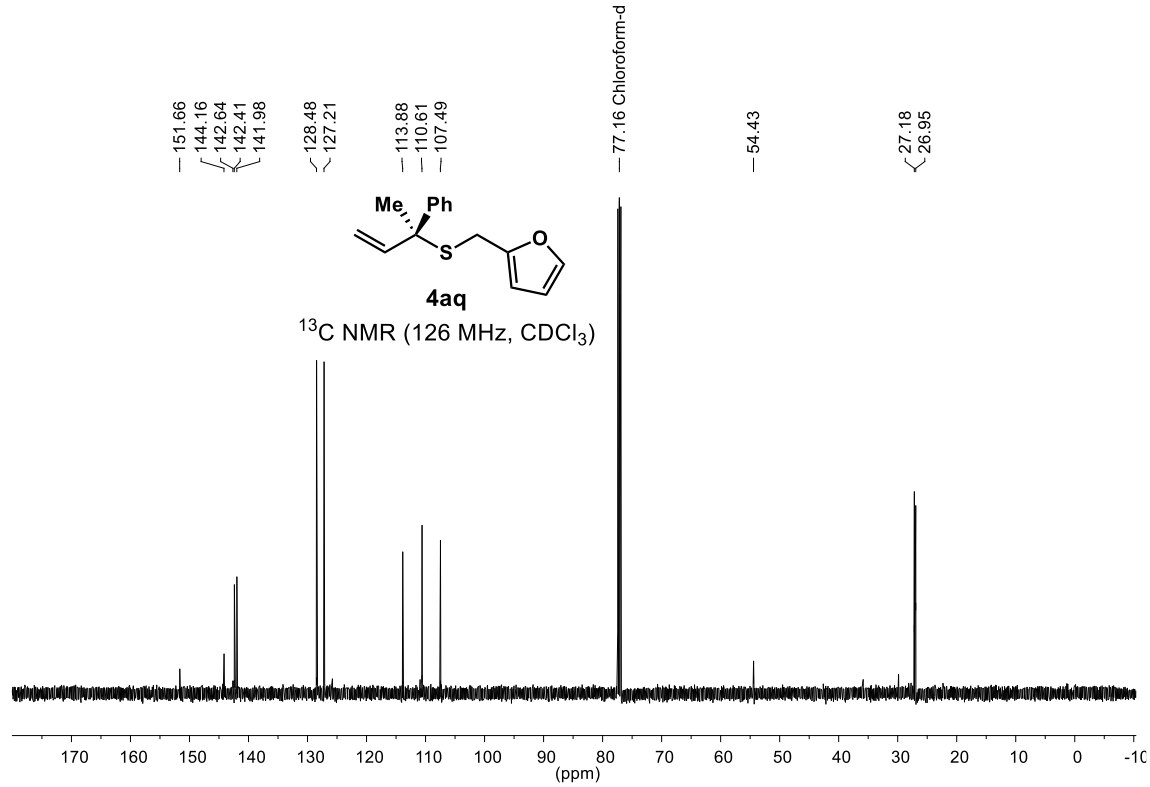

(*S*)-phenyl(2-(p-tolyl)but-3-en-2-yl)sulfane (**4ba**)

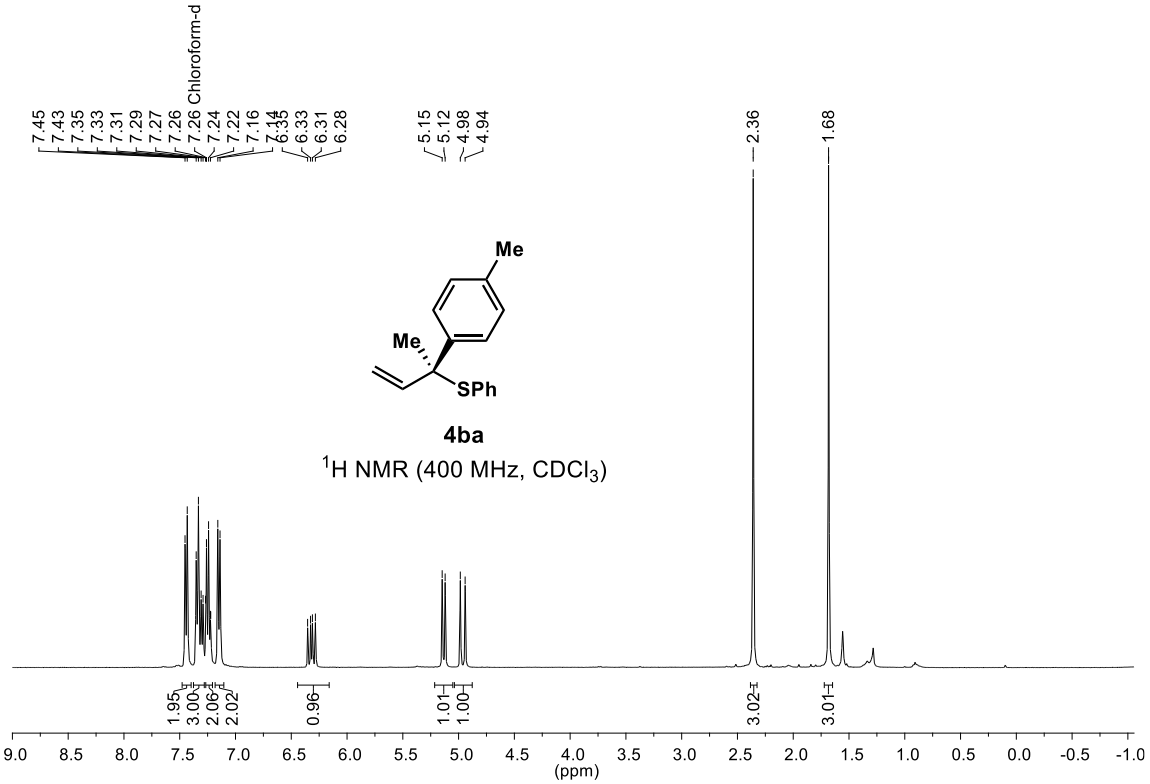

(*S*)-phenyl(2-(4-(trifluoromethyl)phenyl)but-3-en-2-yl)sulfane (**4ca**)

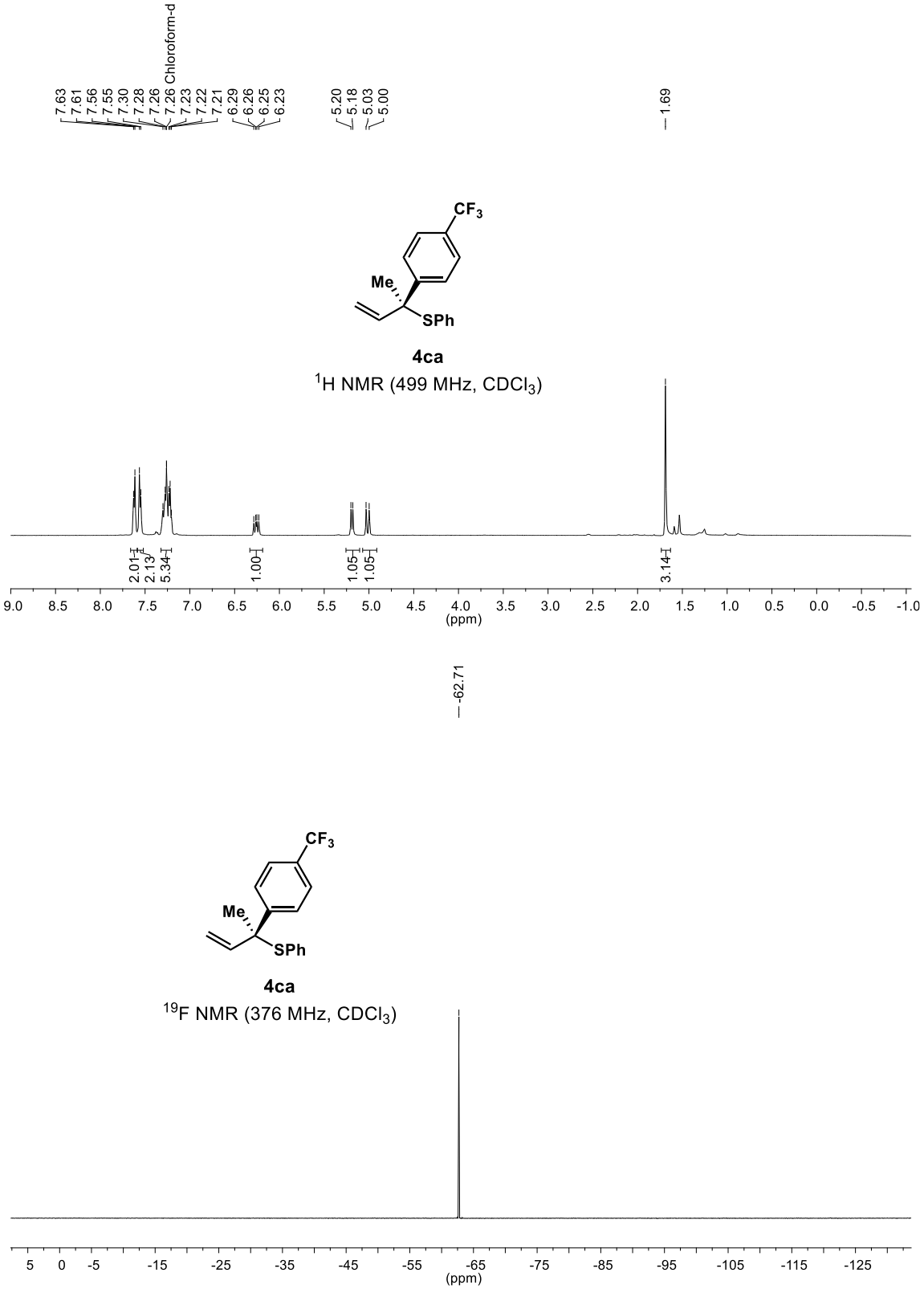

(*S*)-(2-(4-chlorophenyl)but-3-en-2-yl)(phenyl)sulfane (**4da**)

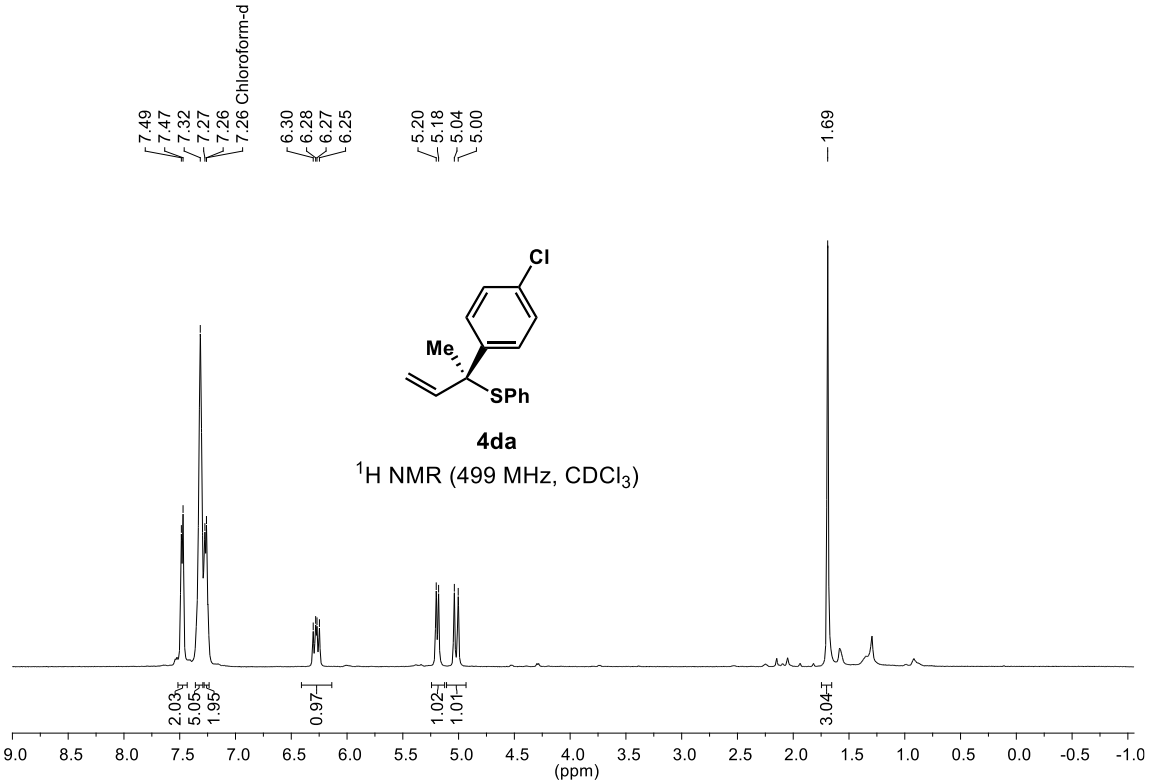

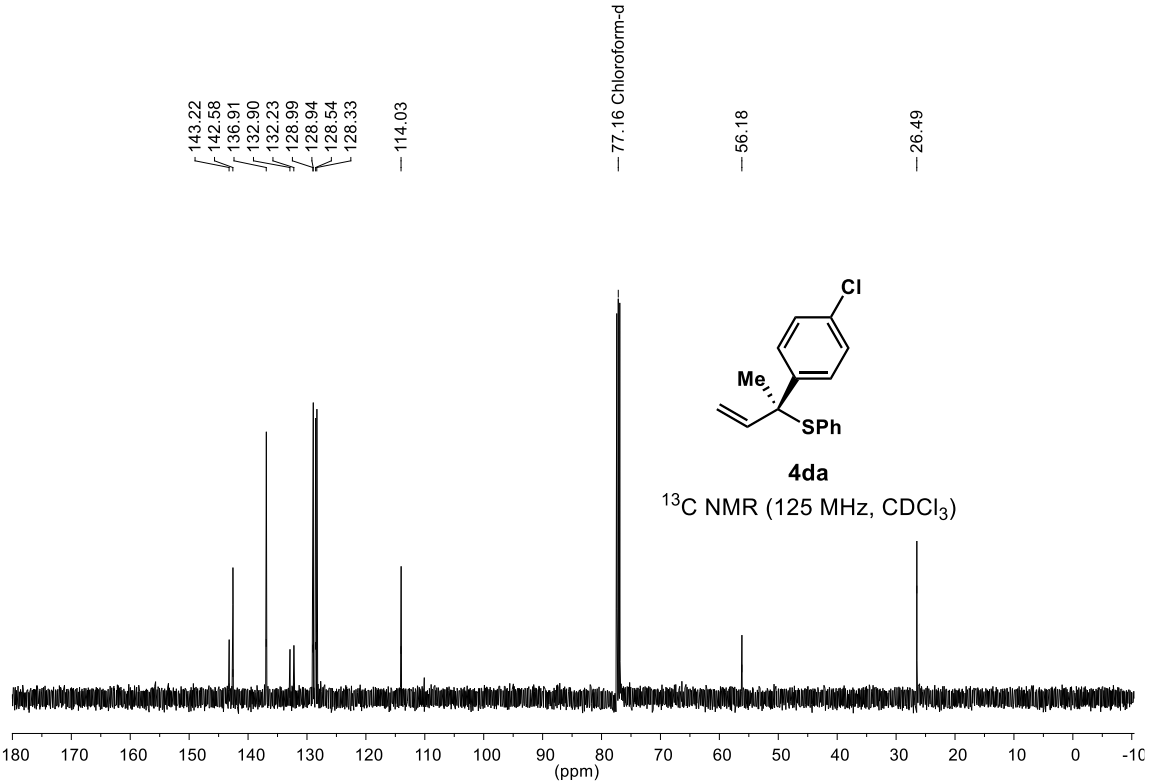

(S)-(1,2-diphenylbut-3-en-2-yl)(phenyl)sulfane (**4ea**)

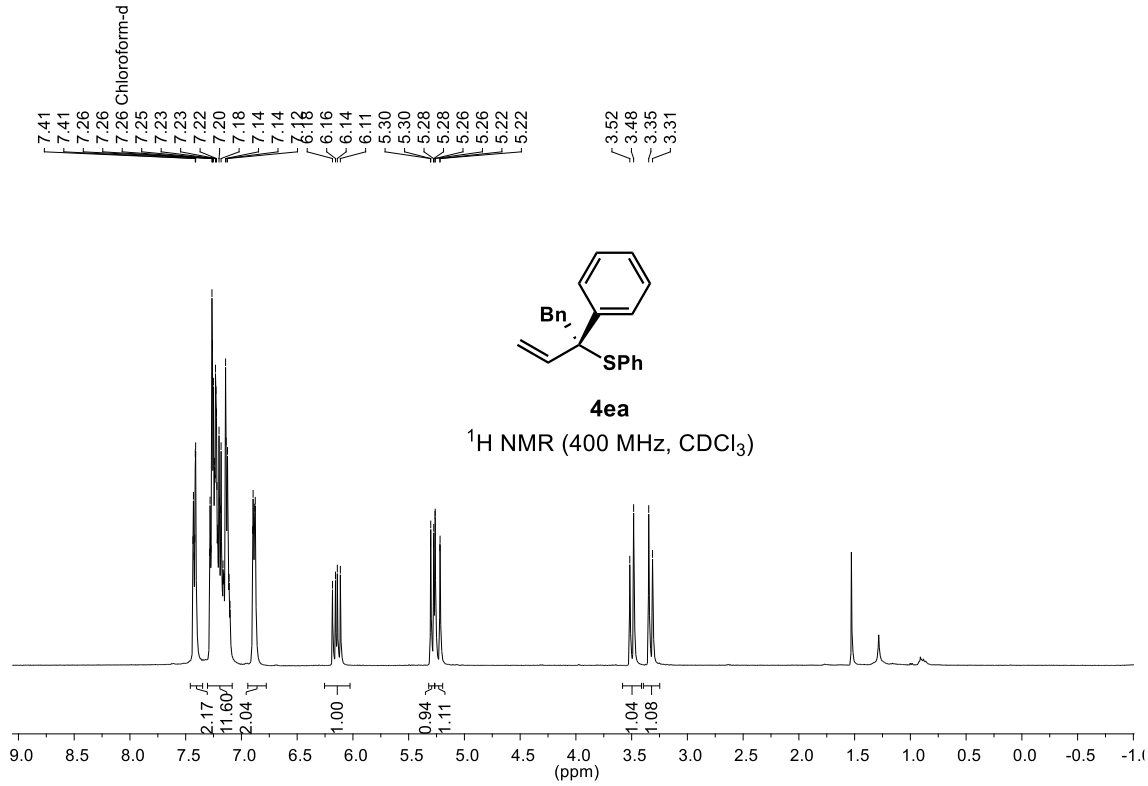

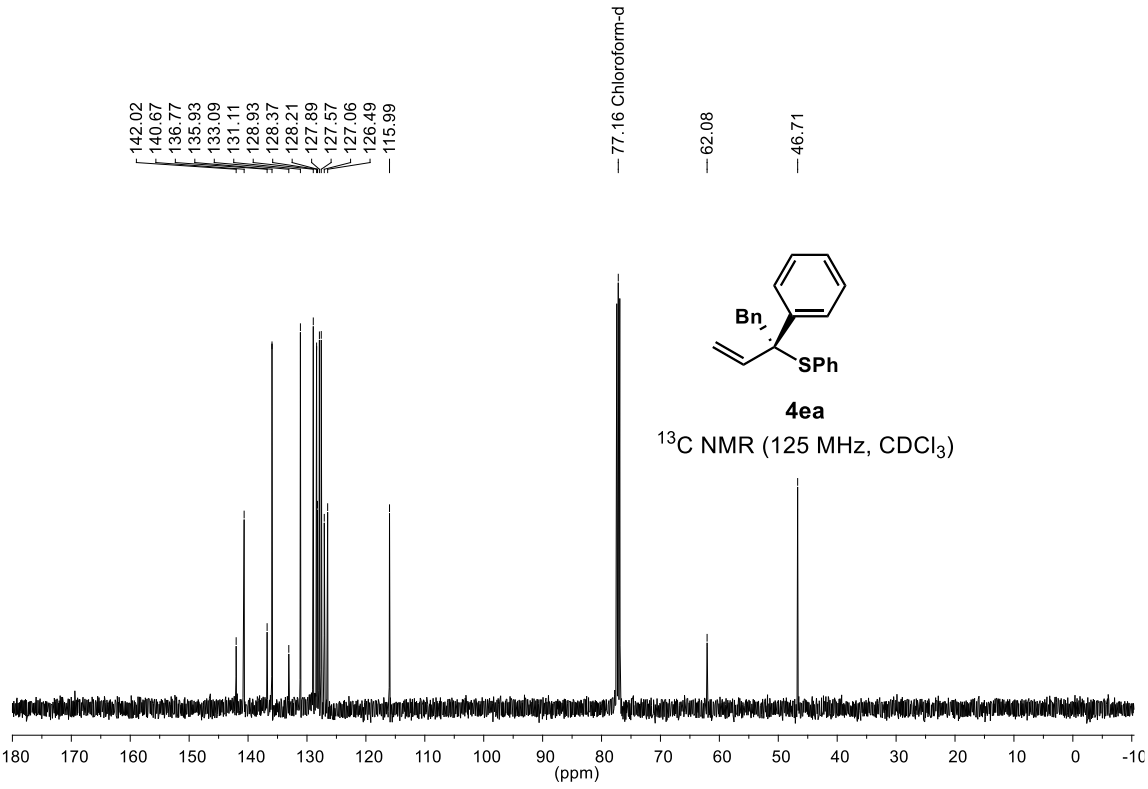

(*S*)-phenyl(1-vinyl-1,2,3,4-tetrahydronaphthalen-1-yl)sulfane (**4fa**)

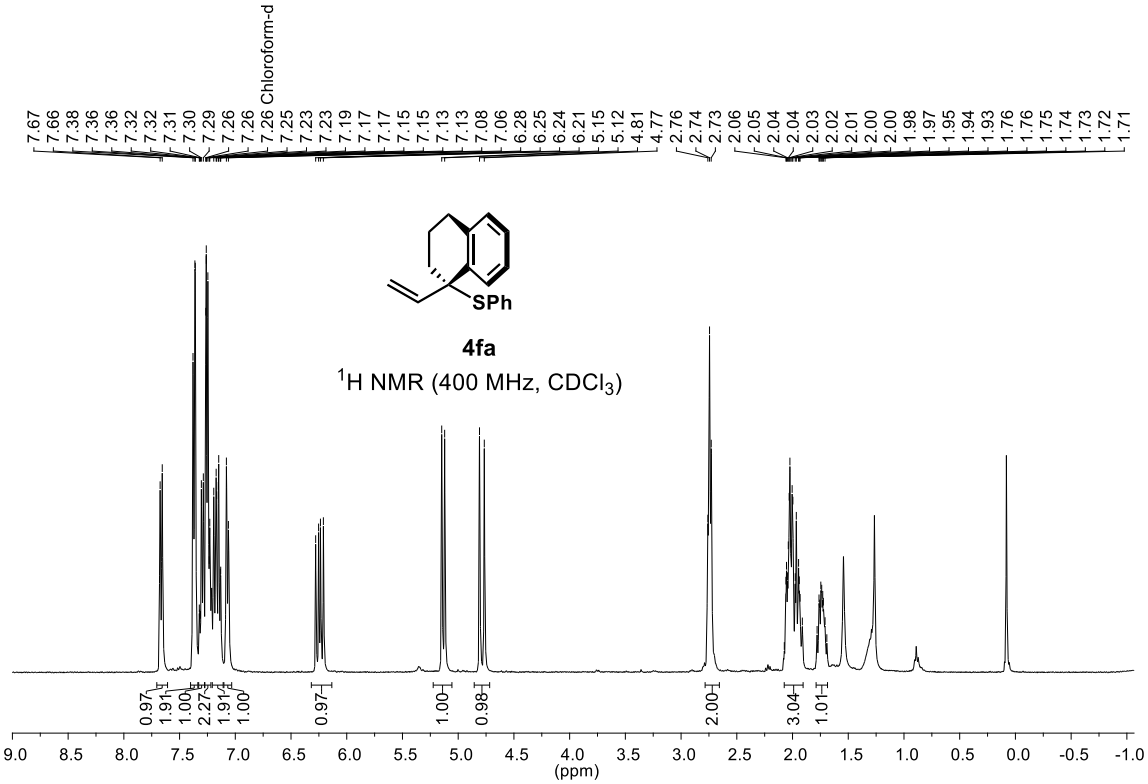

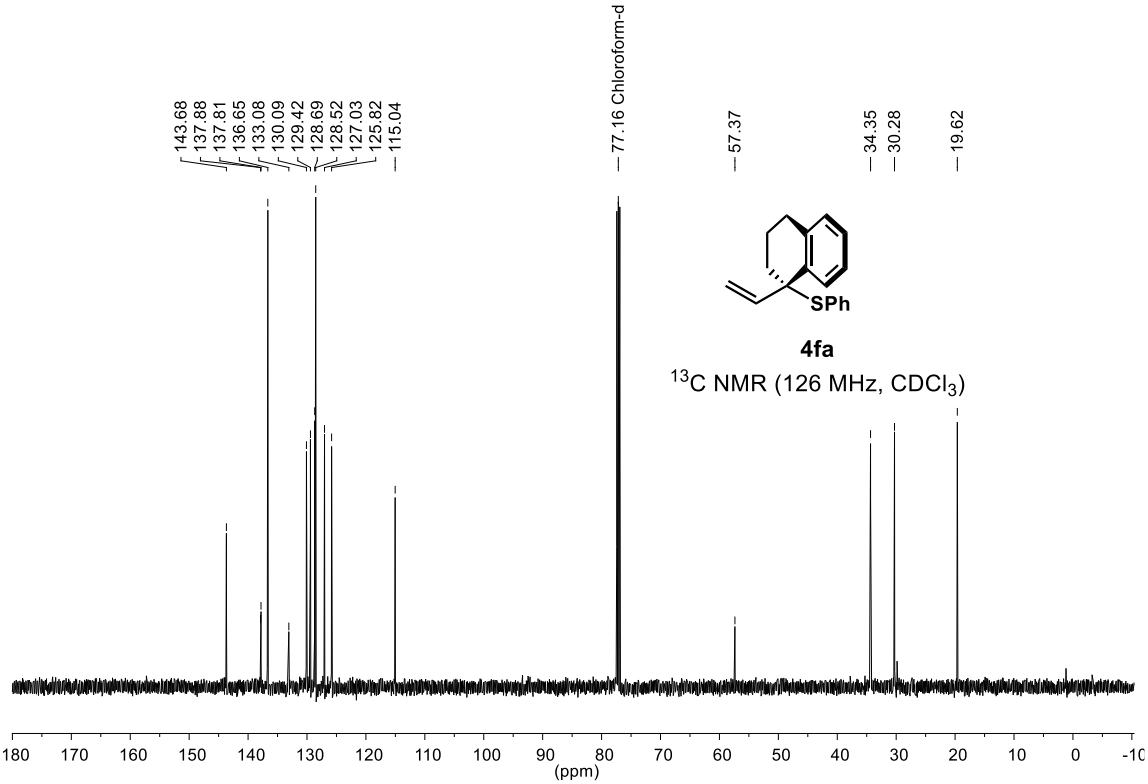

(S)-(2-(naphthalen-2-yl)but-3-en-2-yl)(phenyl)sulfane (**4ha**)

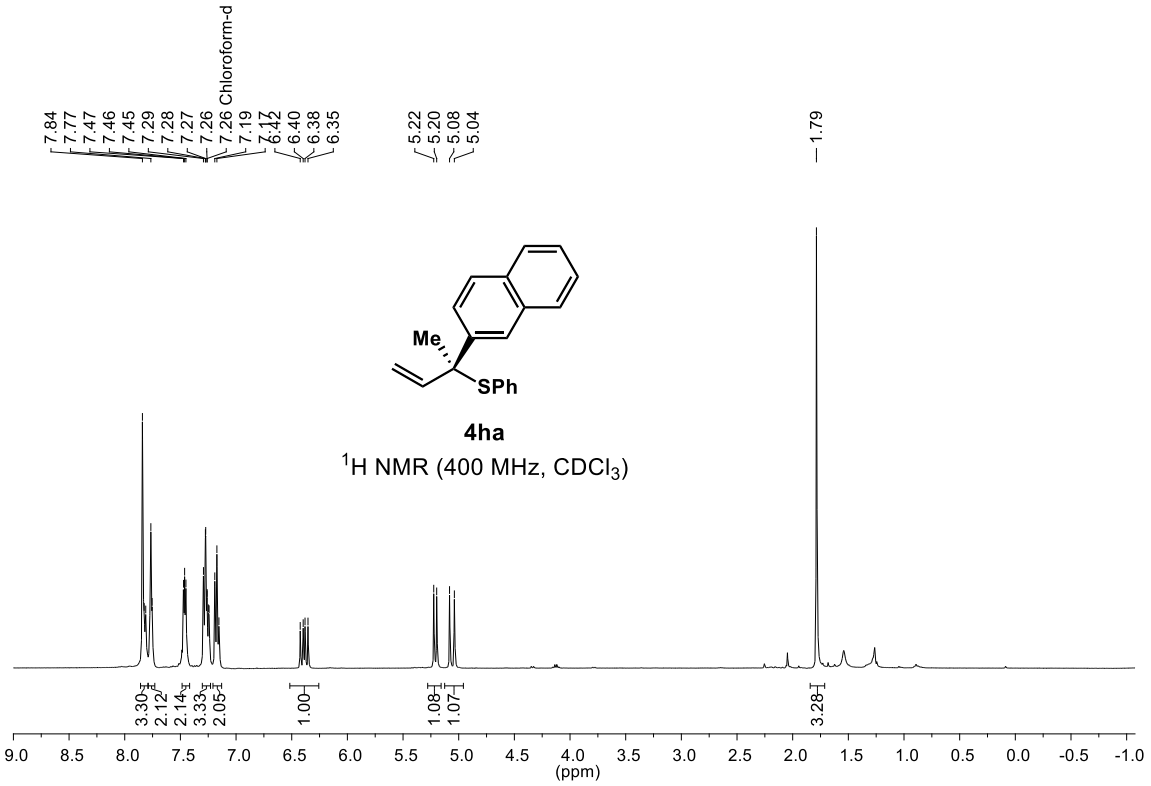

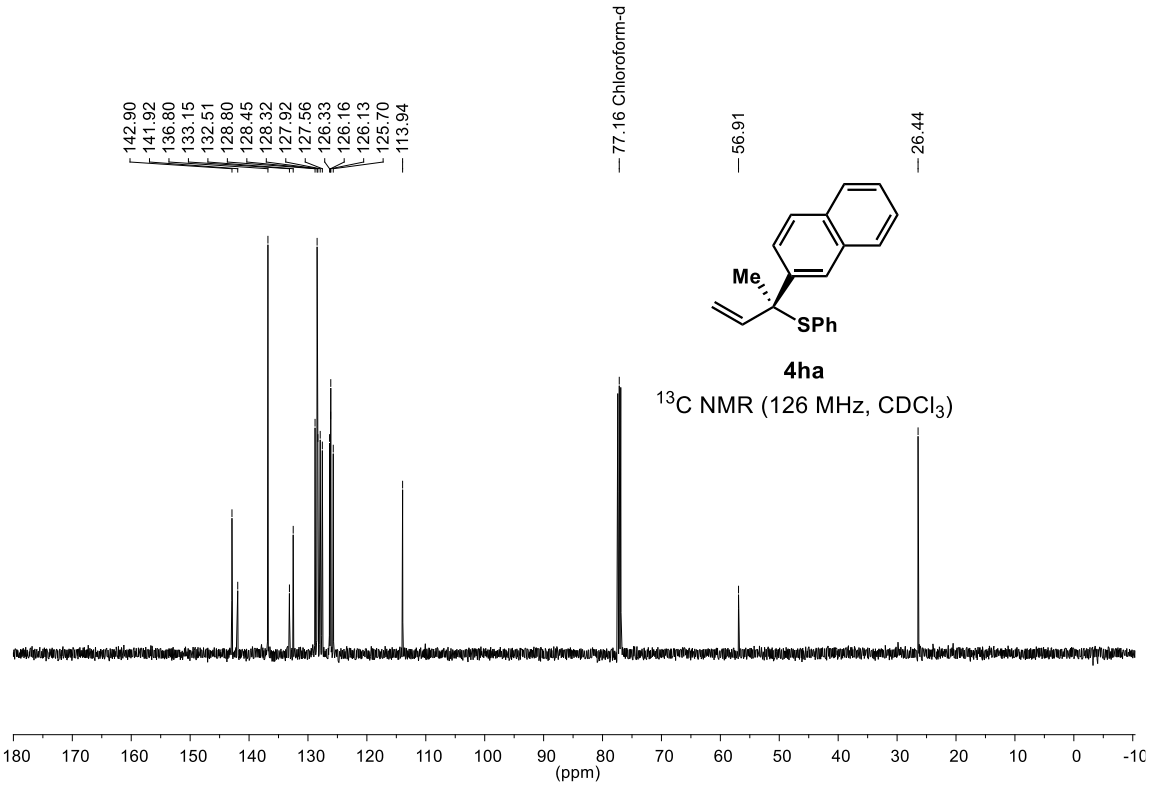

(1-benzyl-2,2-dibromocyclopropyl)benzene (**7e**)

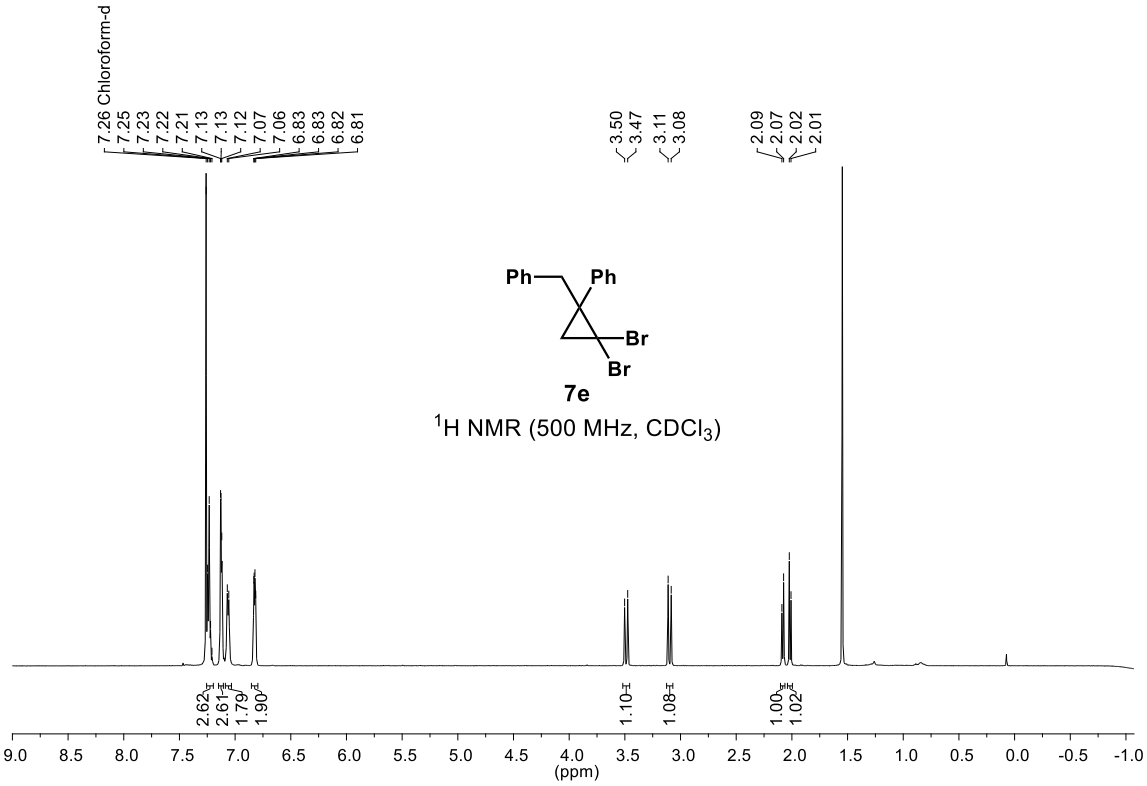

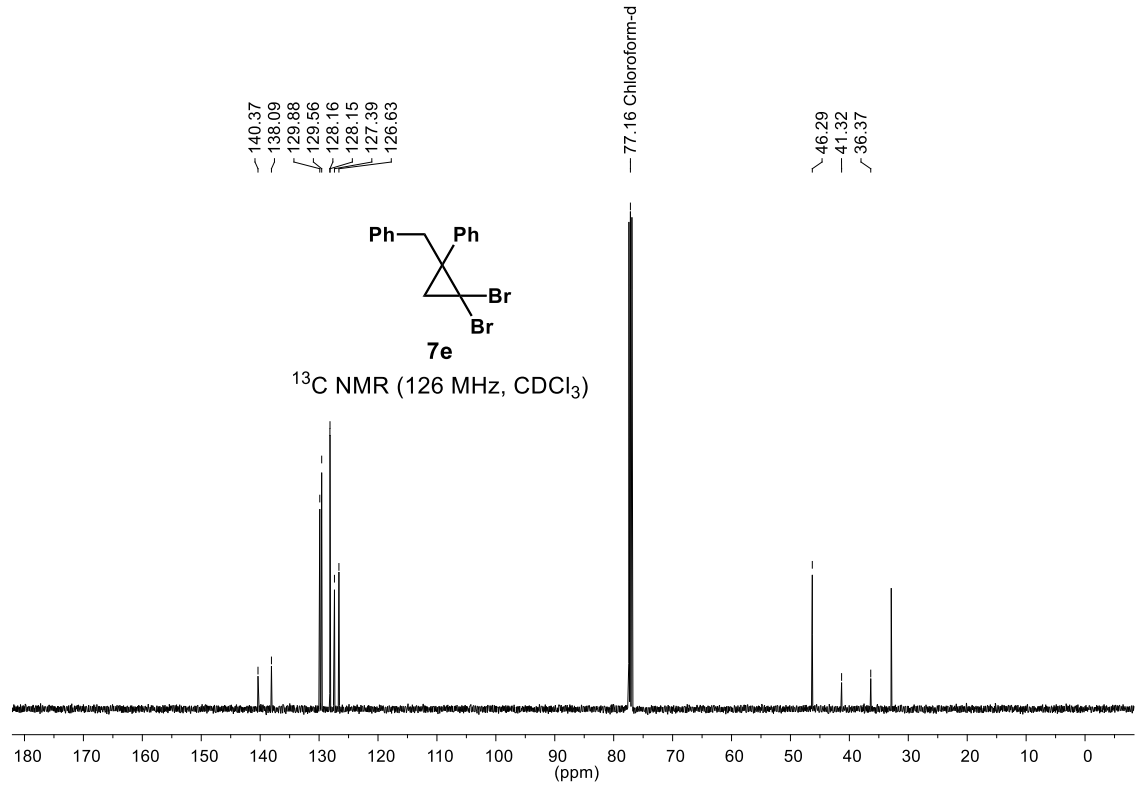

(1-benzyl-2-bromocyclopropyl)benzene (**8e**)

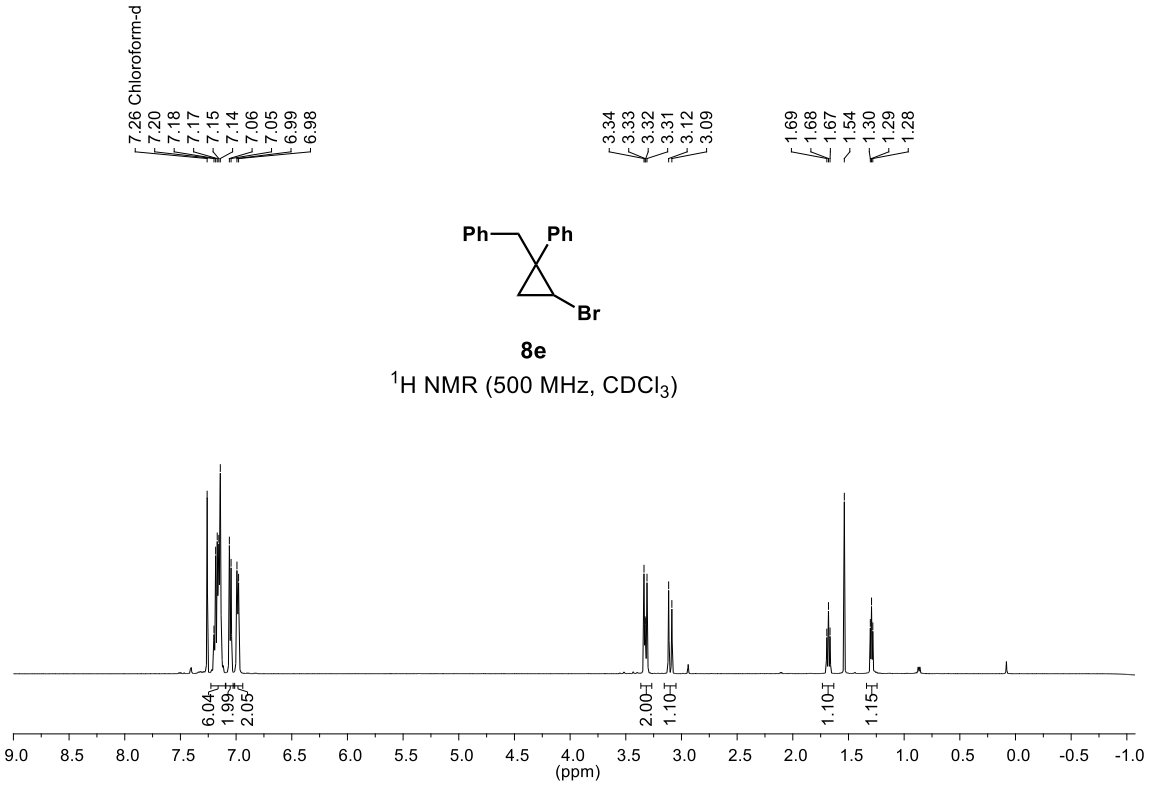

8e

^{1}H NMR (500 MHz, $CDCl_3$)

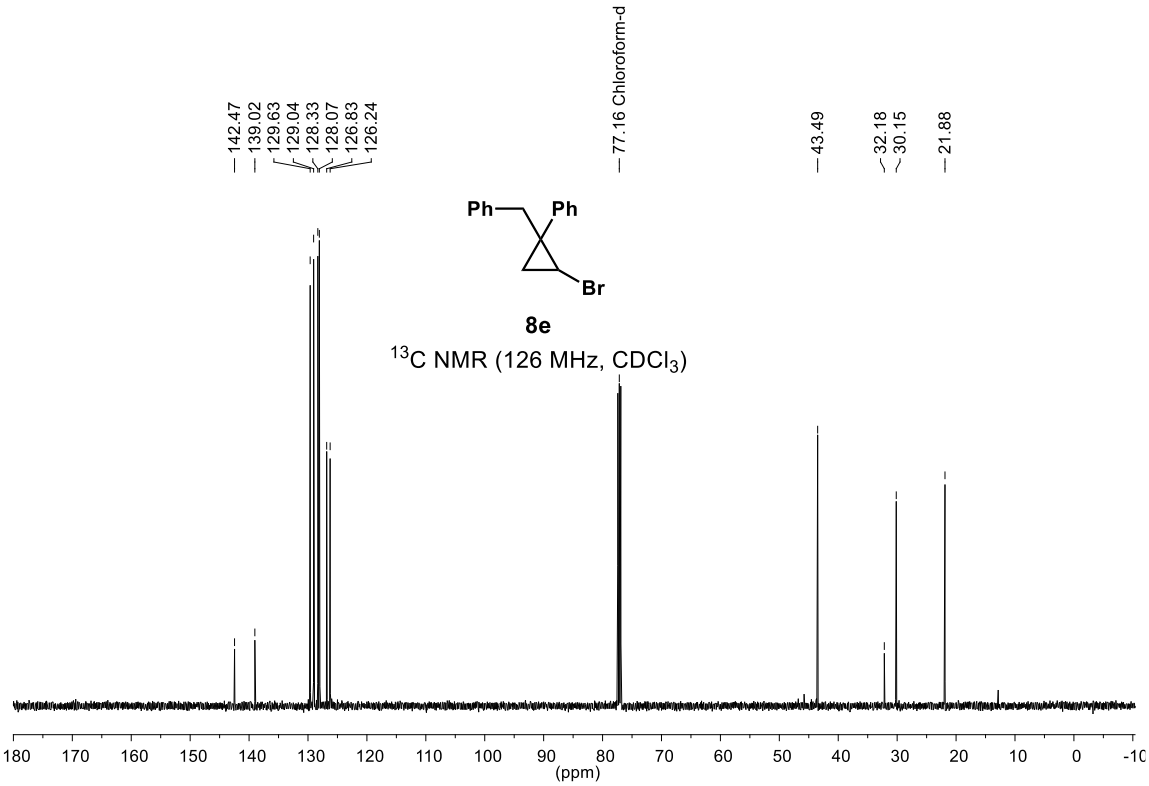

8e

^{13}C NMR (126 MHz, $CDCl_3$)

(1-benzylcycloprop-2-en-1-yl)benzene (**1e**)

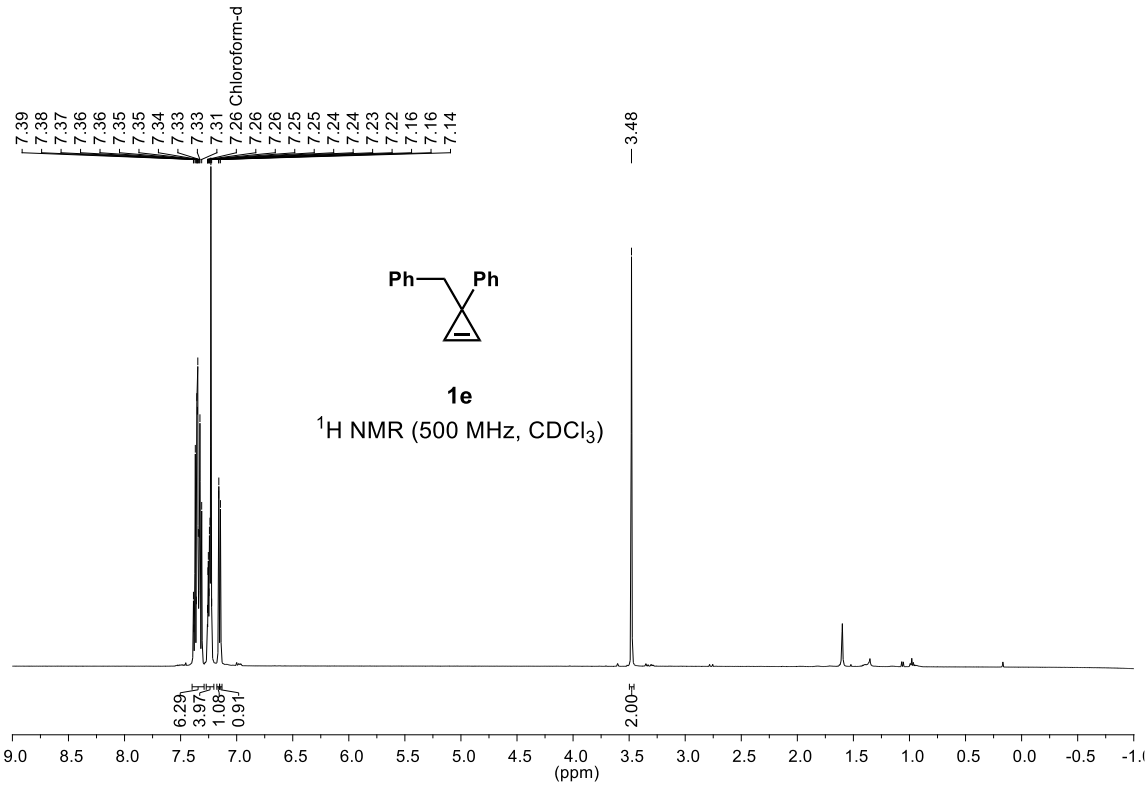

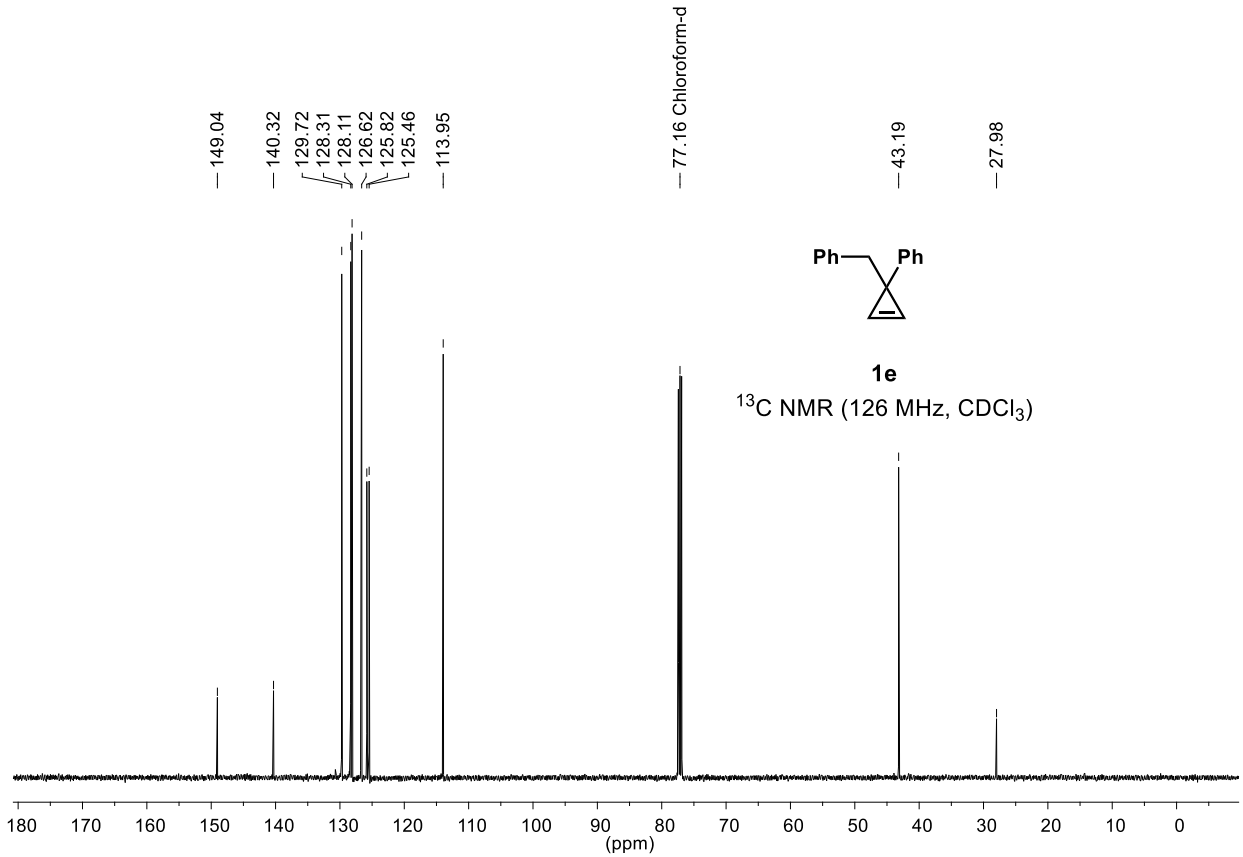

7. SFC Spectra

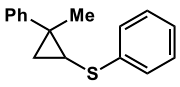

rac-3aa

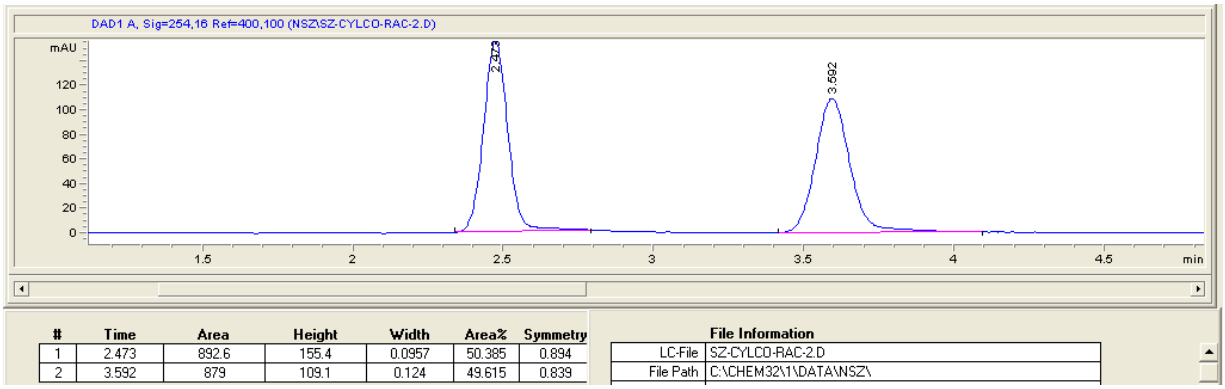

#	Time	Area	Height	Width	Area%	Symmetry
1	2.473	892.6	155.4	0.0957	50.385	0.894
2	3.592	879	109.1	0.124	49.615	0.839

File Information	
LC-File	SZ-CYLCO-RAC-2.D
File Path	C:\CHEM32\1\DATA\NSZ\

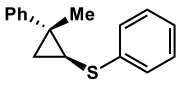

3aa

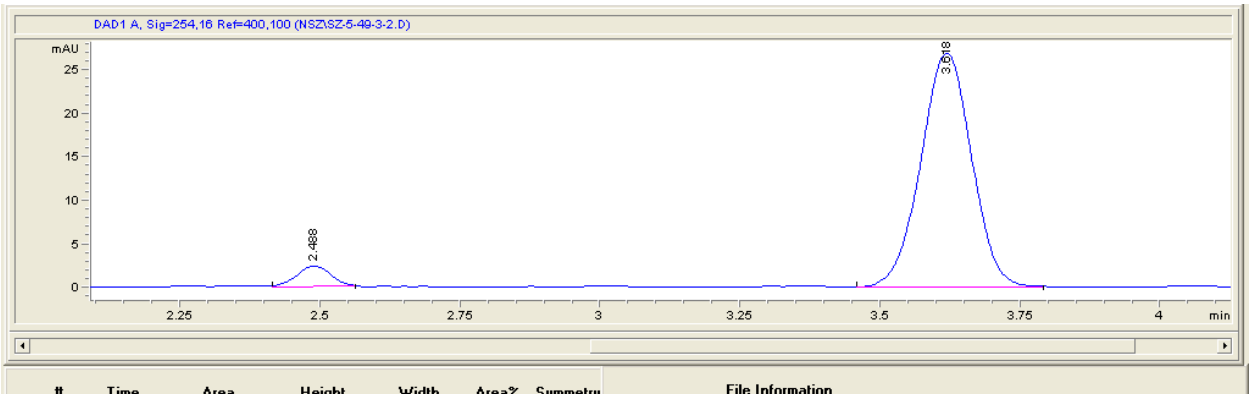

#	Time	Area	Height	Width	Area%	Symmetry
1	2.488	9.8	2.3	0.07	5.396	0.997
2	3.618	172.3	27	0.1064	94.604	0.996

File Information	
LC-File	SZ-5-49-3-2.D
File Path	C:\CHEM32\1\DATA\NSZ\

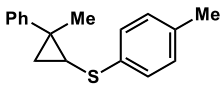

rac-3ab

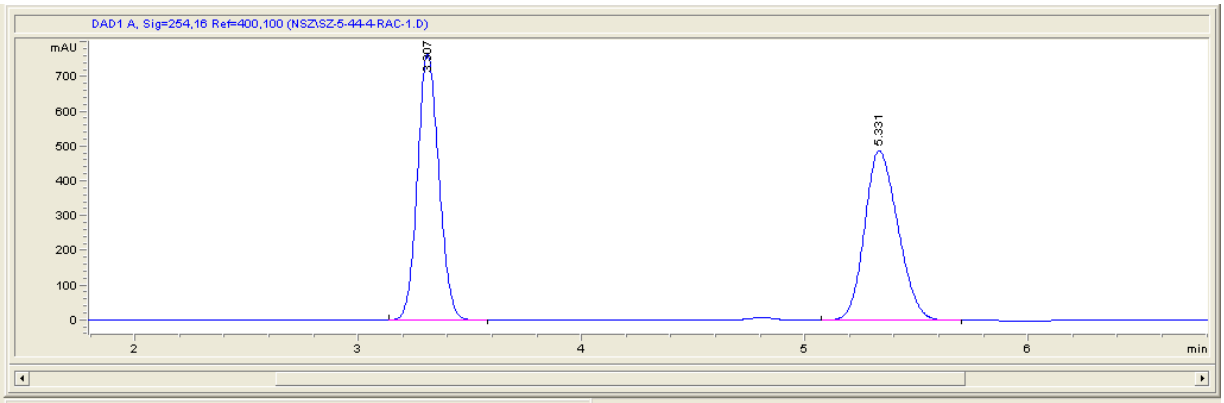

#	Time	Area	Height	Width	Area%	Symmetry
1	3.307	5138.1	768.4	0.103	50.308	0.846
2	5.331	5075.2	488.4	0.1622	49.692	0.755

File Information	
LC-File	SZ-5-44-4-RAC-1.D
File Path	C:\CHEM32\1\DATA\NSZ\

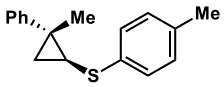

3ab

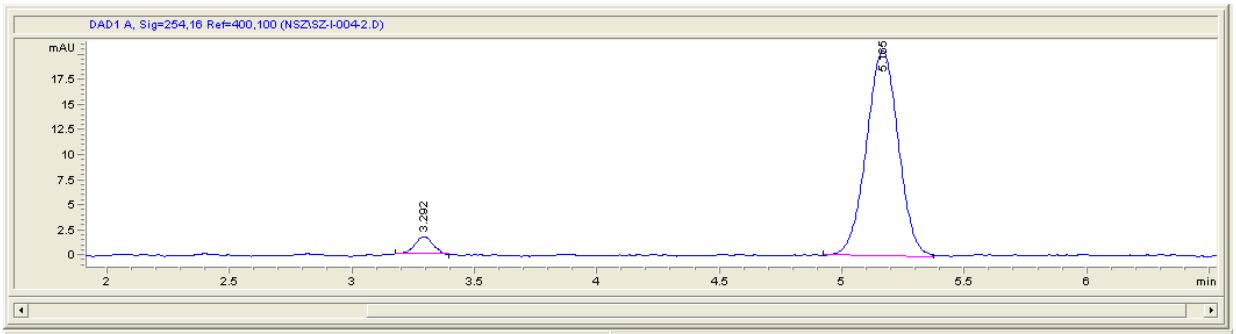

#	Time	Area	Height	Width	Area%	Symmetry
1	3.292	9.4	1.8	0.088	4.803	1.021
2	5.165	186.8	20.5	0.1518	95.197	1.006

File Information	
LC-File	SZ-I-004-2.D
File Path	C:\CHEM32\1\DATA\NSZ\

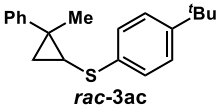

rac-3ac

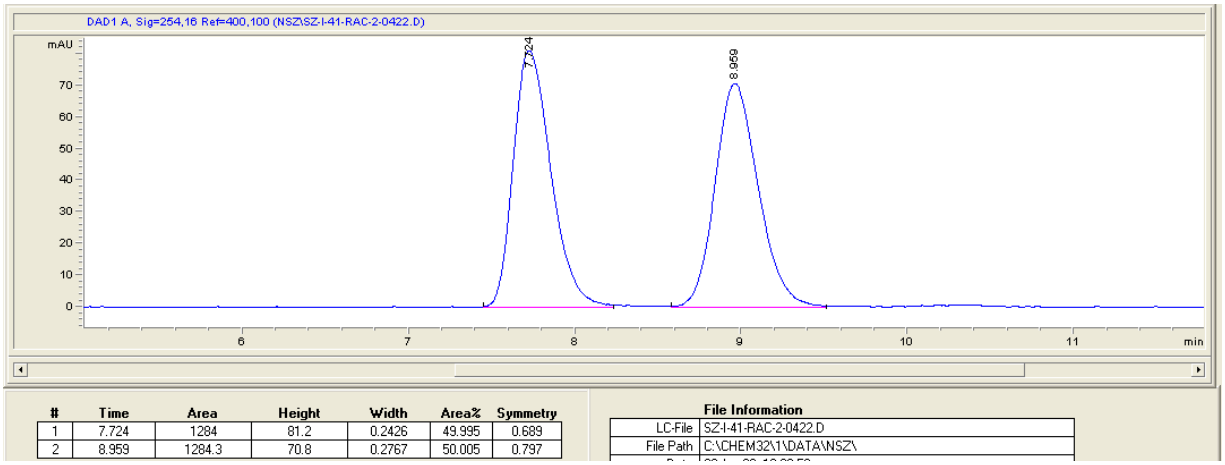

#	Time	Area	Height	Width	Area%	Symmetry
1	7.724	1284	81.2	0.2426	49.995	0.689
2	8.959	1284.3	70.8	0.2767	50.005	0.797

File Information	
LC-File	SZ-I-41-RAC-2-0422.D
File Path	C:\CHEM32\1\DATA\NSZ\

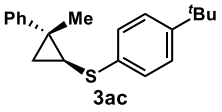

3ac

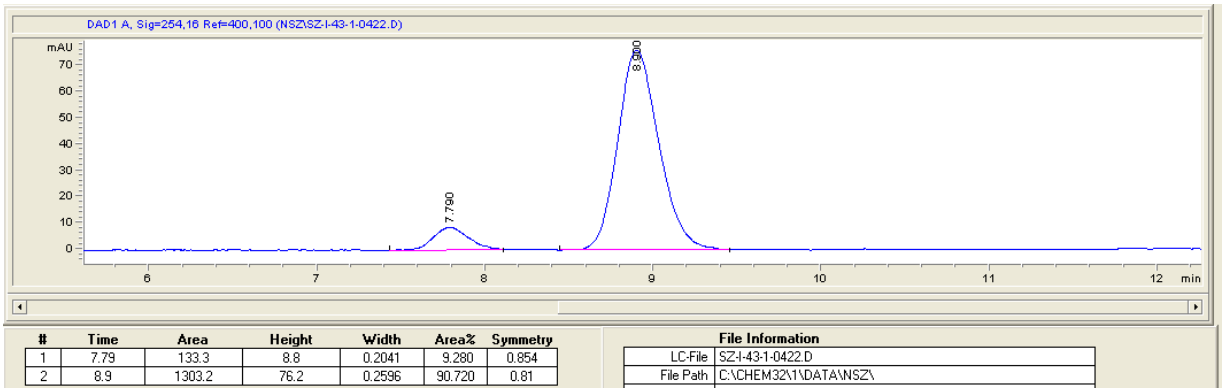

#	Time	Area	Height	Width	Area%	Symmetry
1	7.79	133.3	8.8	0.2041	9.280	0.854
2	8.9	1303.2	76.2	0.2596	90.720	0.81

File Information	
LC-File	SZ-I-43-1-0422.D
File Path	C:\CHEM32\1\DATA\NSZ\

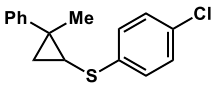

rac-3ad

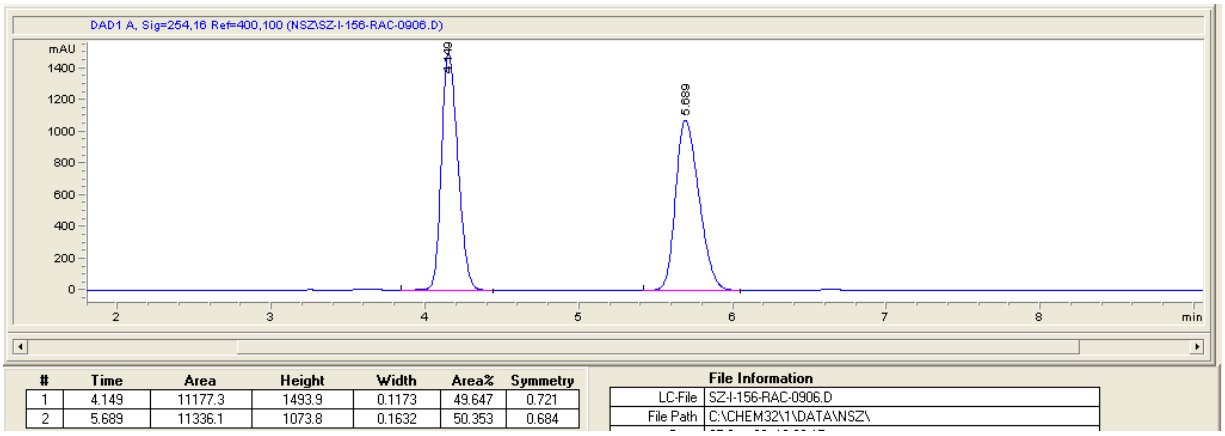

#	Time	Area	Height	Width	Area%	Symmetry
1	4.149	11177.3	1493.9	0.1173	49.647	0.721
2	5.689	11336.1	1073.8	0.1632	50.353	0.684

File Information	
LC-File	SZ-I-156-RAC-0906.D
File Path	C:\CHEM32\1\DATA\NSZ\

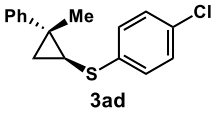

3ad

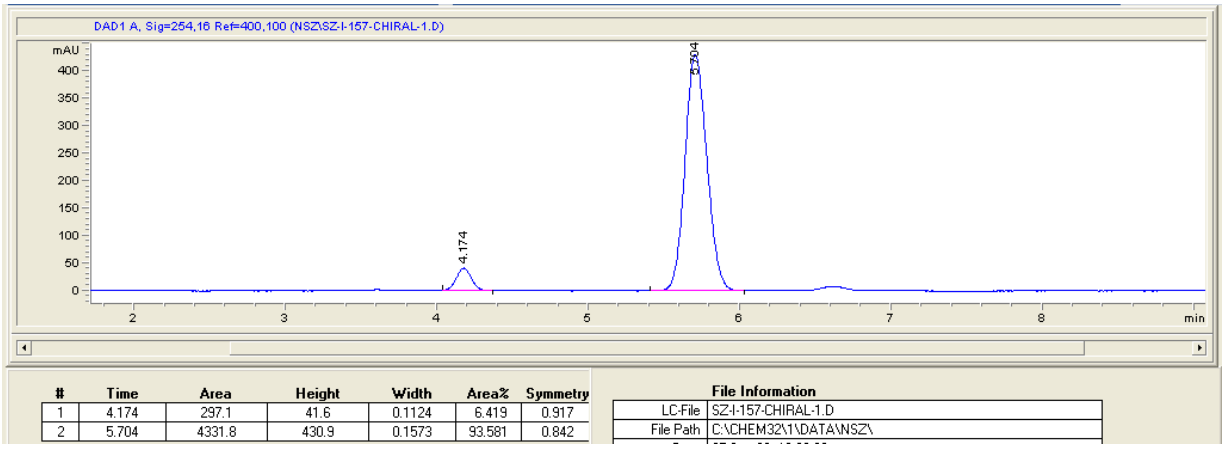

#	Time	Area	Height	Width	Area%	Symmetry
1	4.174	297.1	41.6	0.1124	6.419	0.917
2	5.704	4331.8	430.9	0.1573	93.581	0.842

File Information	
LC-File	SZ-I-157-CHIRAL-1.D
File Path	C:\CHEM32\1\DATA\NSZ\

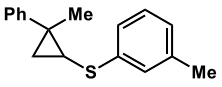

rac-3ae

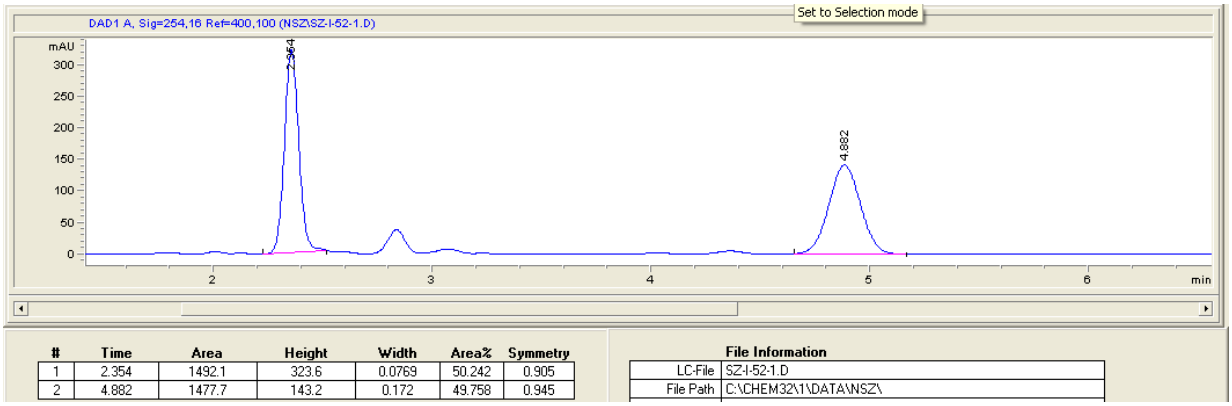

#	Time	Area	Height	Width	Area%	Symmetry
1	2.354	1492.1	323.6	0.0769	50.242	0.905
2	4.882	1477.7	143.2	0.172	49.758	0.945

File Information	
LC-File	SZ-I-52-1.D
File Path	C:\CHEM32\1\DATA\NSZ\

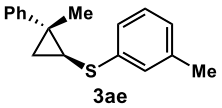

3ae

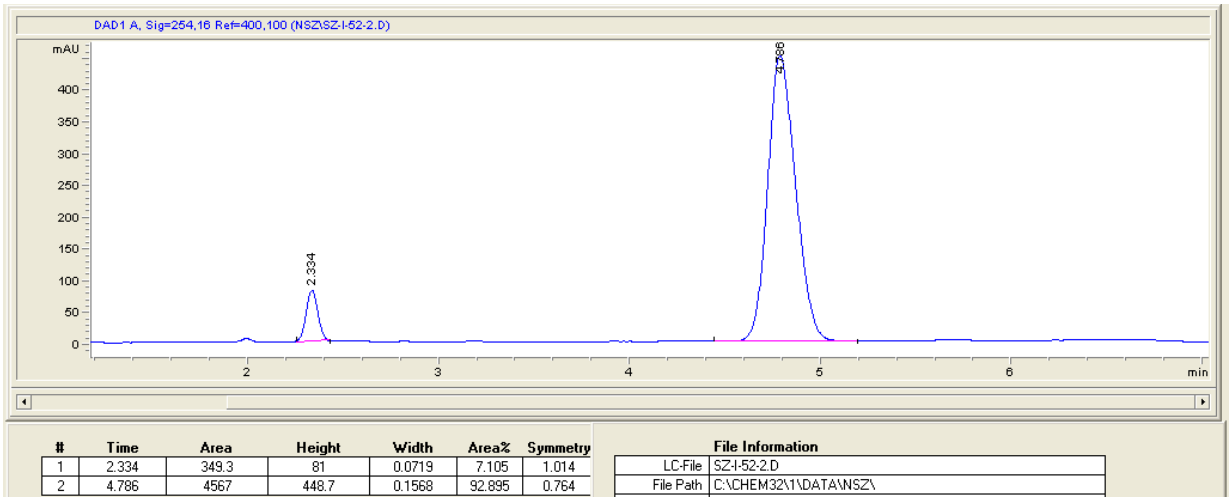

#	Time	Area	Height	Width	Area%	Symmetry
1	2.334	349.3	81	0.0719	7.105	1.014
2	4.786	4567	448.7	0.1568	92.895	0.764

File Information	
LC-File	SZ-I-52-2.D
File Path	C:\CHEM32\1\DATA\NSZ\

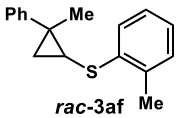

rac-3af

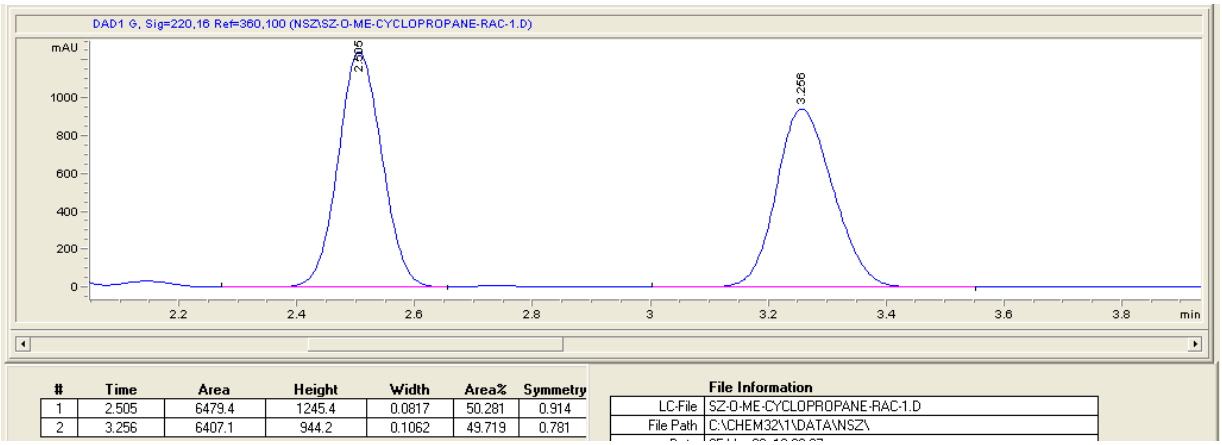

#	Time	Area	Height	Width	Area%	Symmetry
1	2.505	6479.4	1245.4	0.0817	50.281	0.914
2	3.256	6407.1	944.2	0.1062	49.719	0.781

File Information	
LC-File	SZ-O-ME-CYCLOPROPANE-RAC-1.D
File Path	C:\CHEM32\1\DATA\NSZ\

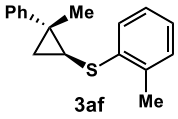

3af

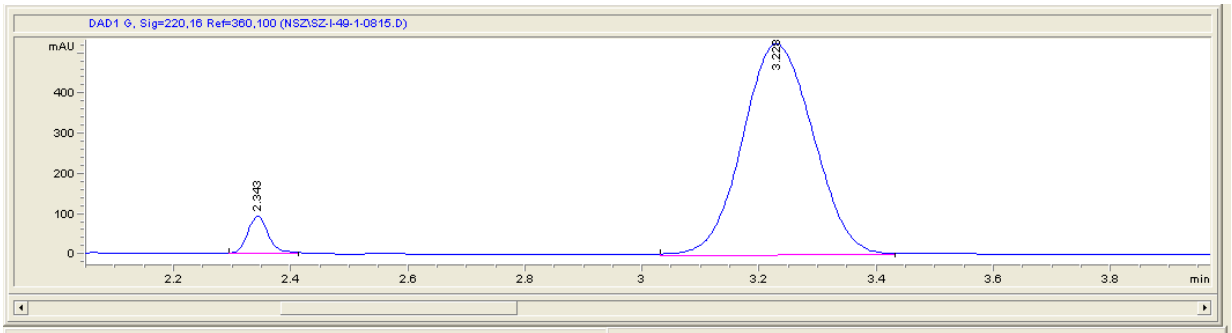

#	Time	Area	Height	Width	Area%	Symmetry
1	2.343	225.4	93.5	0.0402	4.857	0.895
2	3.228	4414.7	525.6	0.14	95.143	0.895

File Information	
LC-File	SZ-I-49-1-0815.D
File Path	C:\CHEM32\1\DATA\NSZ\

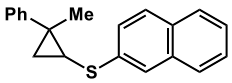

***rac*-3ag**

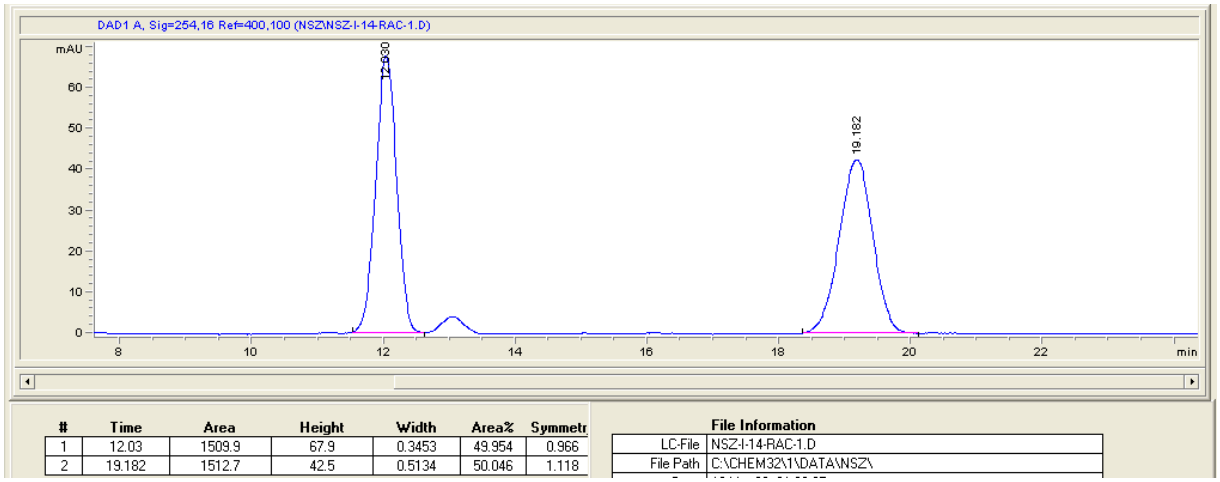

#	Time	Area	Height	Width	Area%	Symmetr
1	12.03	1509.9	67.9	0.3453	49.954	0.966
2	19.182	1512.7	42.5	0.5134	50.046	1.118

File Information	
LC-File	NSZ-I-14-RAC-1.D
File Path	C:\CHEM32\1\DATA\NSZ\

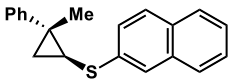

3ag

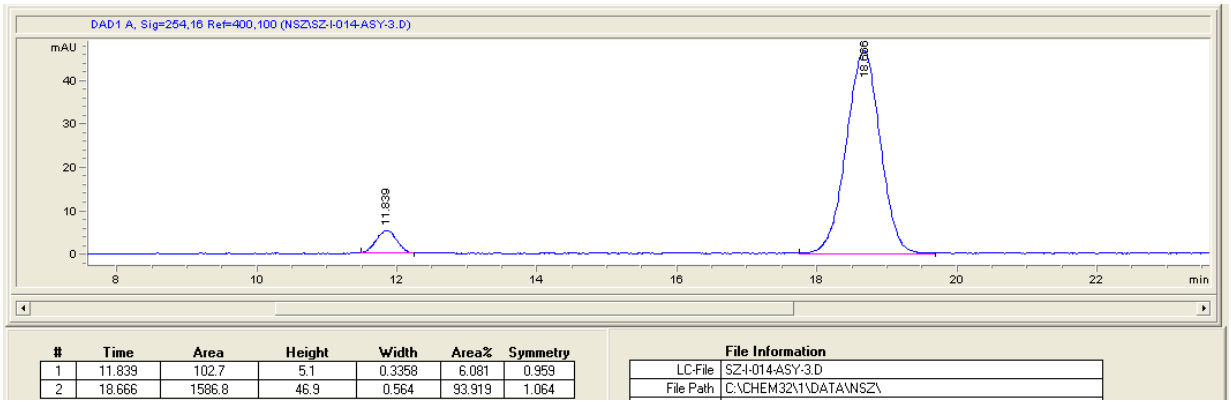

#	Time	Area	Height	Width	Area%	Symmetry
1	11.839	102.7	5.1	0.3358	6.081	0.959
2	18.666	1586.8	46.9	0.564	93.919	1.064

File Information	
LC-File	SZ-I-014-ASY-3.D
File Path	C:\CHEM32\1\DATA\NSZ\

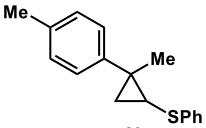

rac-3ba

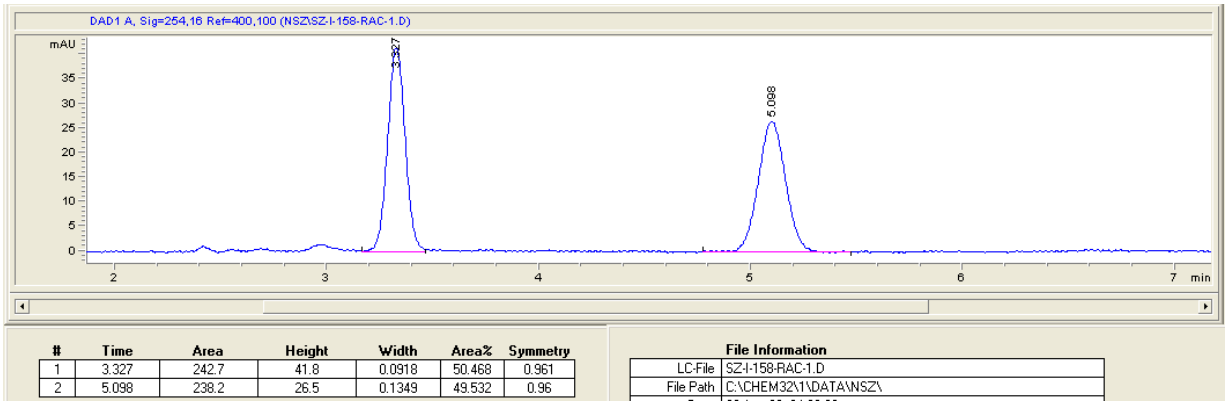

#	Time	Area	Height	Width	Area%	Symmetry
1	3.327	242.7	41.8	0.0918	50.468	0.961
2	5.098	238.2	26.5	0.1349	49.532	0.96

File Information	
LC-File	SZ-I-158-RAC-1.D
File Path	C:\CHEM32\1\DATA\NSZ\

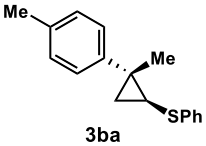

3ba

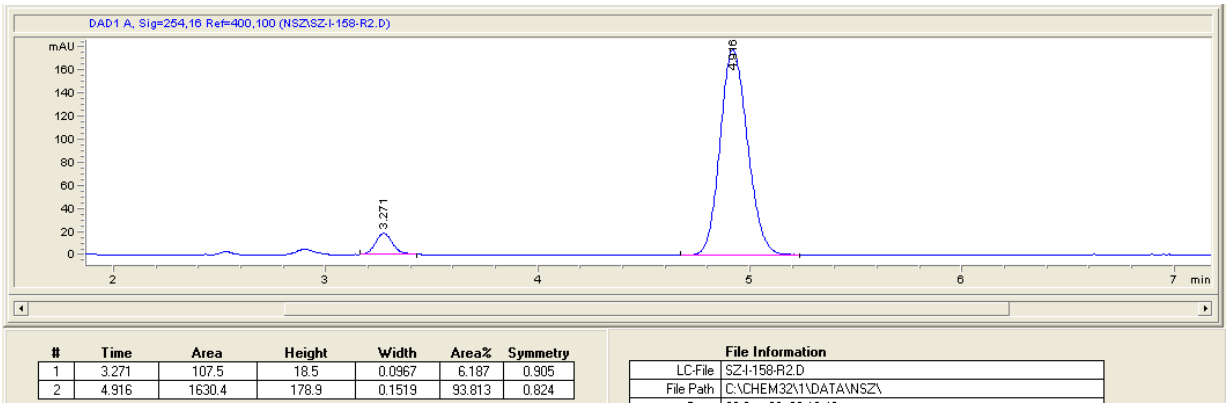

#	Time	Area	Height	Width	Area%	Symmetry
1	3.271	107.5	18.5	0.0967	6.187	0.905
2	4.916	1630.4	178.9	0.1519	93.813	0.824

File Information	
LC-File	SZ-I-158-R2.D
File Path	C:\CHEM32\1\DATA\NSZ\

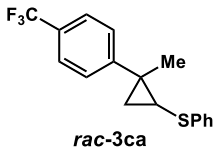

rac-3ca

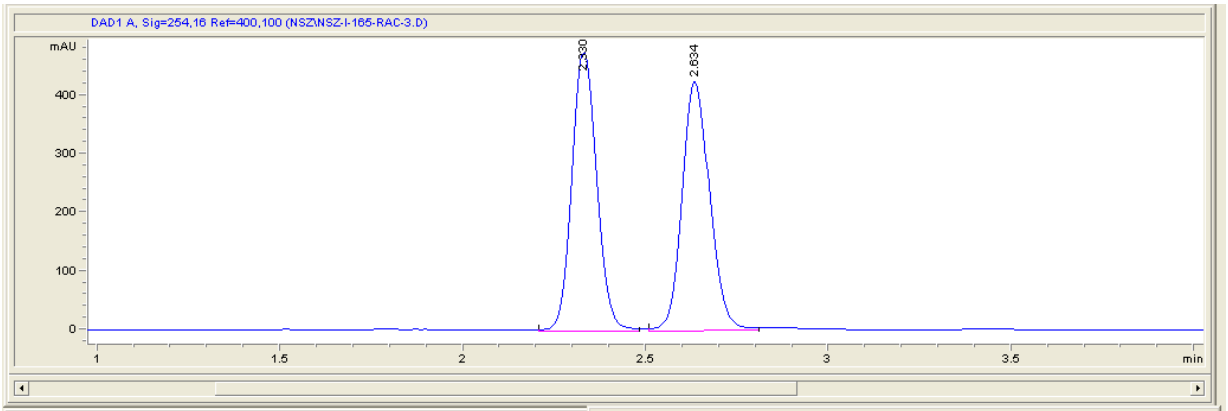

#	Time	Area	Height	Width	Area%	Symmetry
1	2.33	2251.5	476.2	0.0732	49.877	0.866
2	2.634	2262.6	426.2	0.0829	50.123	0.823

File Information	
LC-File	NSZ-I-165-RAC-3.D
File Path	C:\CHEM32\1\DATA\NSZ\

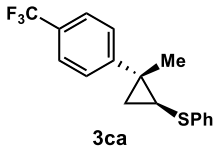

3ca

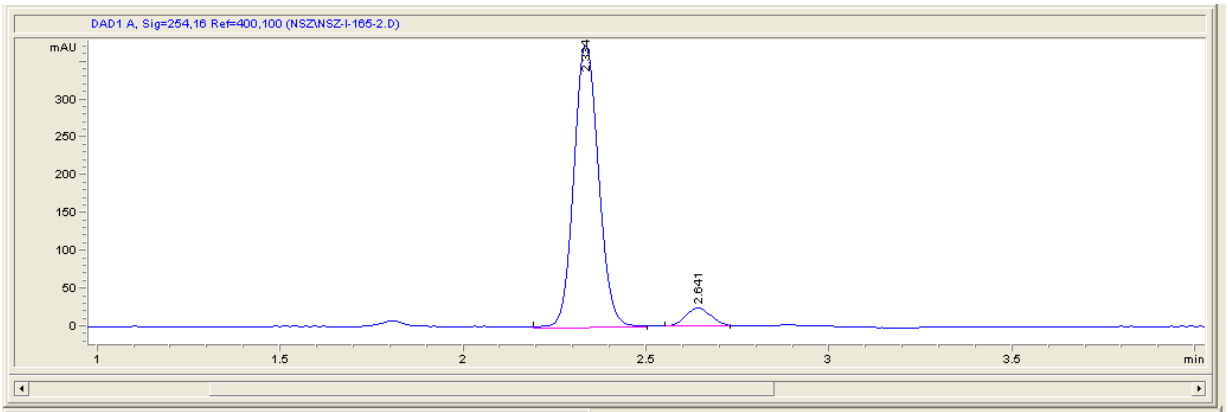

#	Time	Area	Height	Width	Area%	Symmetry
1	2.334	1754.4	373.9	0.0782	93.512	0.885
2	2.641	121.7	24.3	0.0836	6.488	0.938

File Information	
LC-File	NSZ-I-165-2.D
File Path	C:\CHEM32\1\DATA\NSZ\

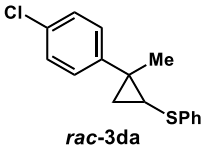

***rac*-3da**

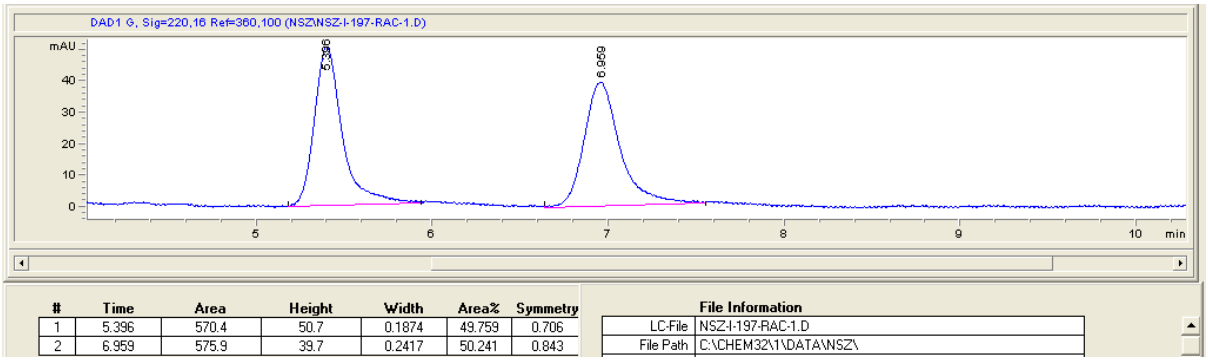

#	Time	Area	Height	Width	Area%	Symmetry
1	5.396	570.4	50.7	0.1874	49.759	0.706
2	6.959	575.9	39.7	0.2417	50.241	0.843

File Information	
LC-File	NSZ-I-197-RAC-1.D
File Path	C:\CHEM32\1\DATA\NSZ\

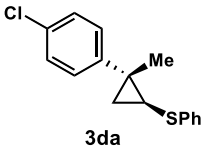

3da

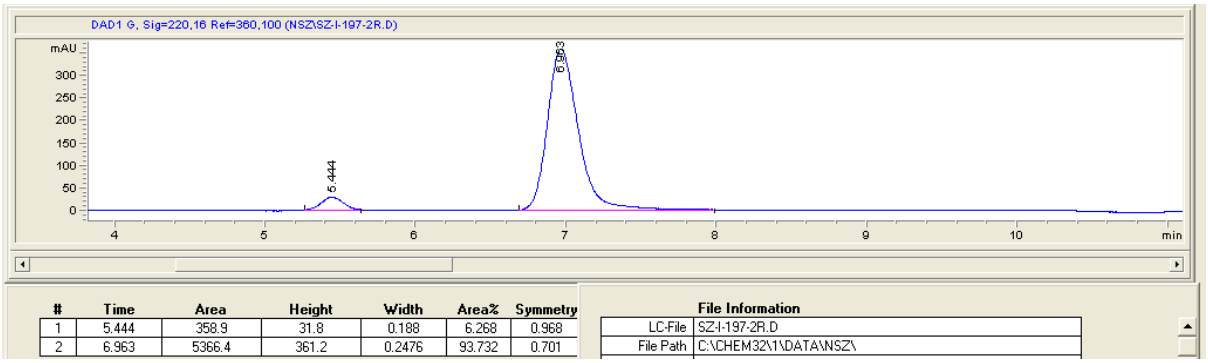

#	Time	Area	Height	Width	Area%	Symmetry
1	5.444	358.9	31.8	0.188	6.268	0.968
2	6.963	5366.4	361.2	0.2476	93.732	0.701

File Information	
LC-File	SZ-I-197-2R.D
File Path	C:\CHEM32\1\DATA\NSZ\

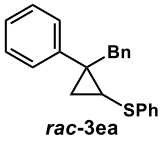

rac-3ea

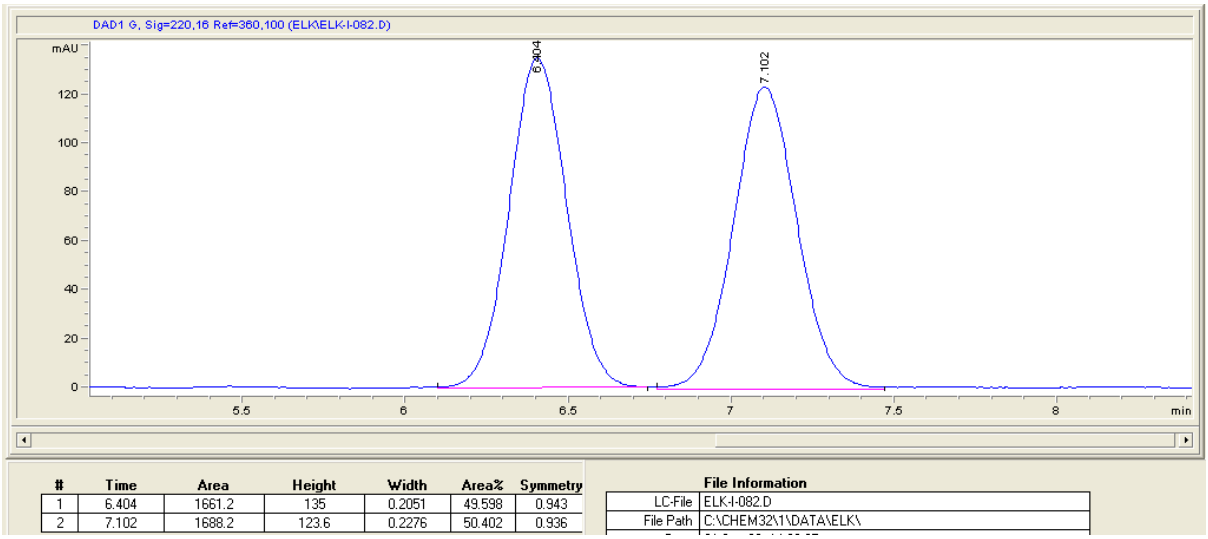

#	Time	Area	Height	Width	Area%	Symmetry
1	6.404	1661.2	135	0.2051	49.598	0.943
2	7.102	1688.2	123.6	0.2276	50.402	0.936

File Information	
LC-File	ELK-I-082.D
File Path	C:\CHEM32\1\DATA\ELK\

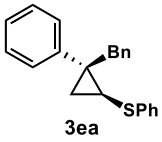

3ea

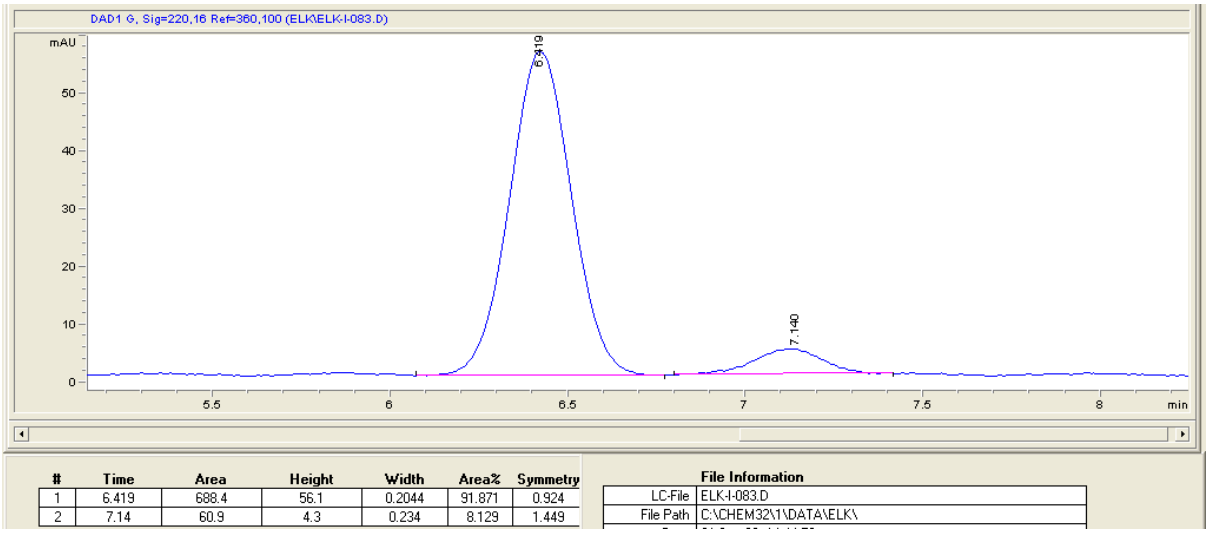

#	Time	Area	Height	Width	Area%	Symmetry
1	6.419	688.4	56.1	0.2044	91.871	0.924
2	7.14	60.9	4.3	0.234	8.129	1.449

File Information	
LC-File	ELK-I-083.D
File Path	C:\CHEM32\1\DATA\ELK\

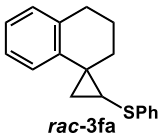

rac-3fa

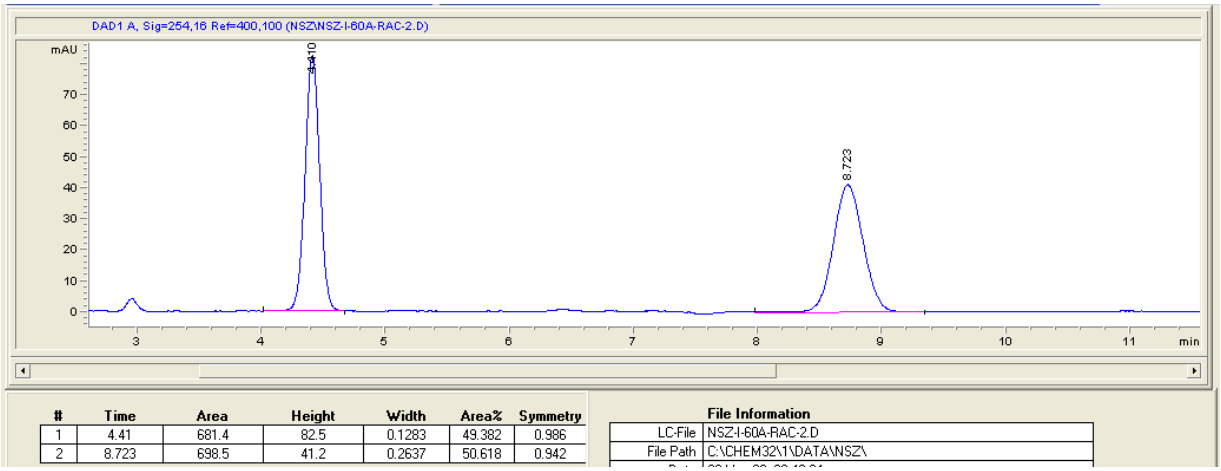

#	Time	Area	Height	Width	Area%	Symmetry
1	4.41	681.4	82.5	0.1283	49.382	0.986
2	8.723	698.5	41.2	0.2637	50.618	0.942

File Information	
LC-File	NSZ-I-60A-RAC-2.D
File Path	C:\CHEM32\1\DATA\NSZ\

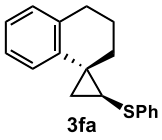

3fa

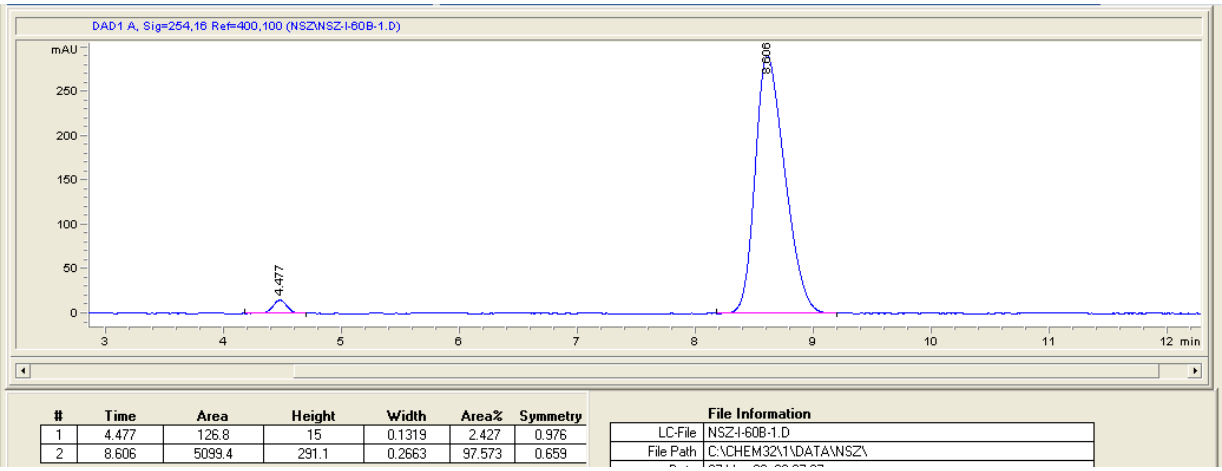

#	Time	Area	Height	Width	Area%	Symmetry
1	4.477	126.8	15	0.1319	2.427	0.976
2	8.606	5099.4	291.1	0.2663	97.573	0.659

File Information	
LC-File	NSZ-I-60B-1.D
File Path	C:\CHEM32\1\DATA\NSZ\

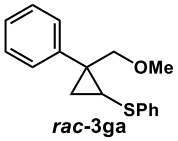

rac-3ga

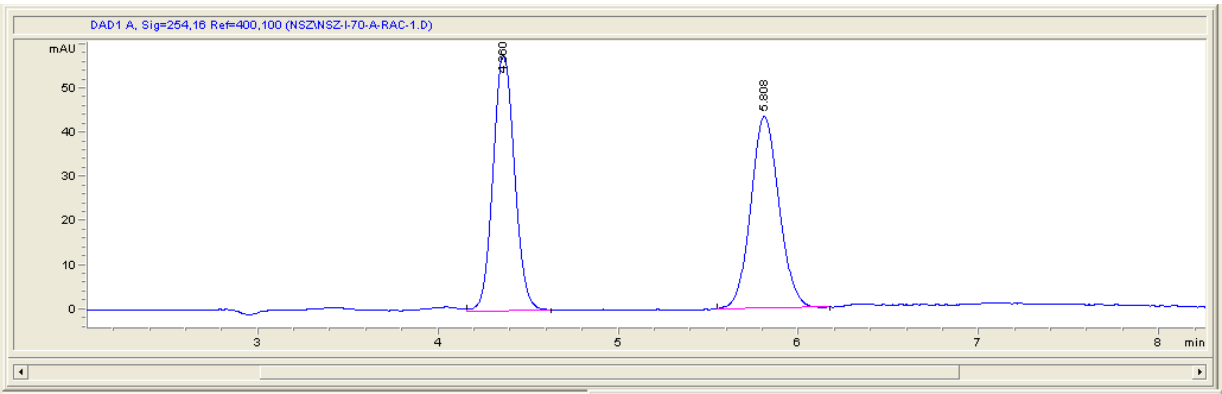

#	Time	Area	Height	Width	Area%	Symmetry
1	4.36	478.3	58.1	0.129	50.031	0.907
2	5.808	477.7	43.5	0.1721	49.969	0.899

File Information	
LC-File	NSZ-I-70-A-RAC-1.D
File Path	C:\CHEM32\1\DATA\NSZ\

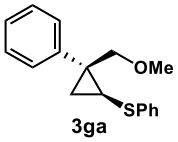

3ga

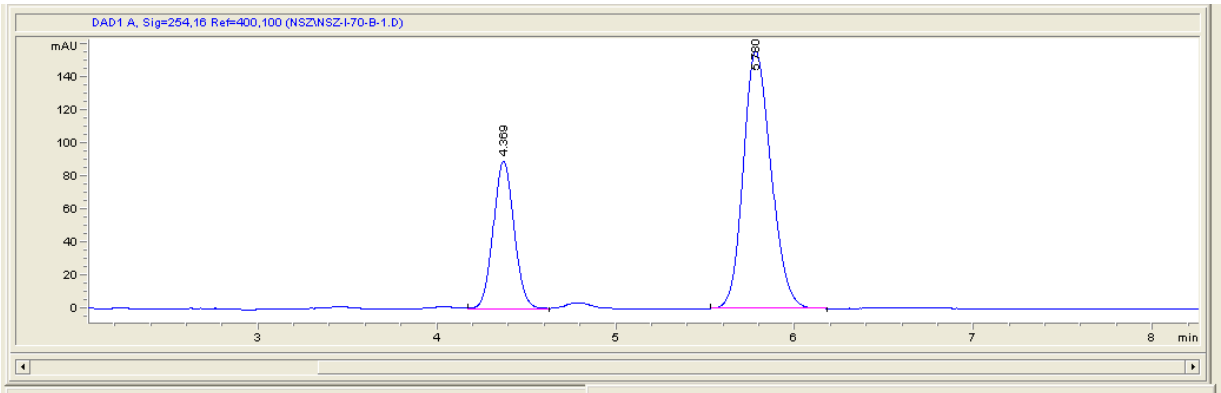

#	Time	Area	Height	Width	Area%	Symmetry
1	4.369	729.4	89.6	0.1269	30.076	0.911
2	5.78	1695.7	155.7	0.1681	69.924	0.795

File Information	
LC-File	NSZ-I-70-B-1.D
File Path	C:\CHEM32\1\DATA\NSZ\

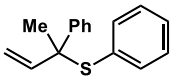

***rac*-4aa**

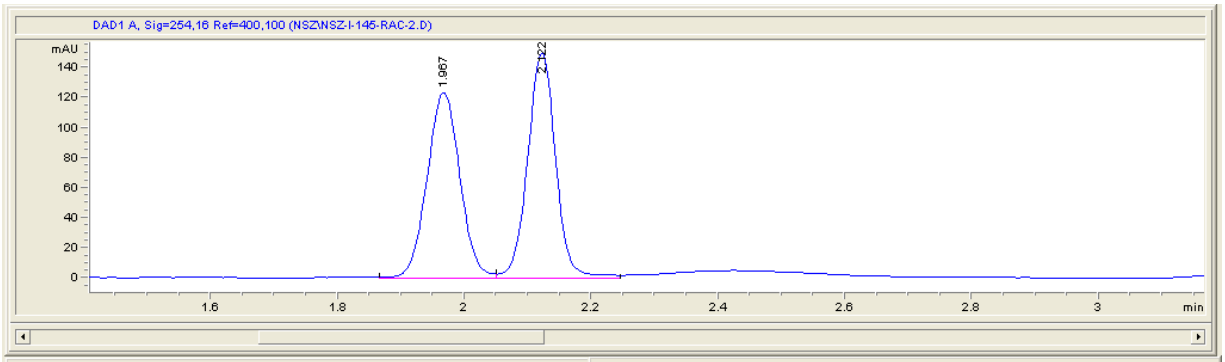

#	Time	Area	Height	Width	Area%	Symmetry
1	1.967	451.9	124.2	0.0564	49.136	0.977
2	2.122	467.8	151.2	0.0481	50.864	0.975

File Information	
LC-File	NSZ-I-145-RAC-2.D
File Path	C:\CHEM32\1\DATA\NSZ\

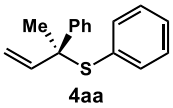

4aa

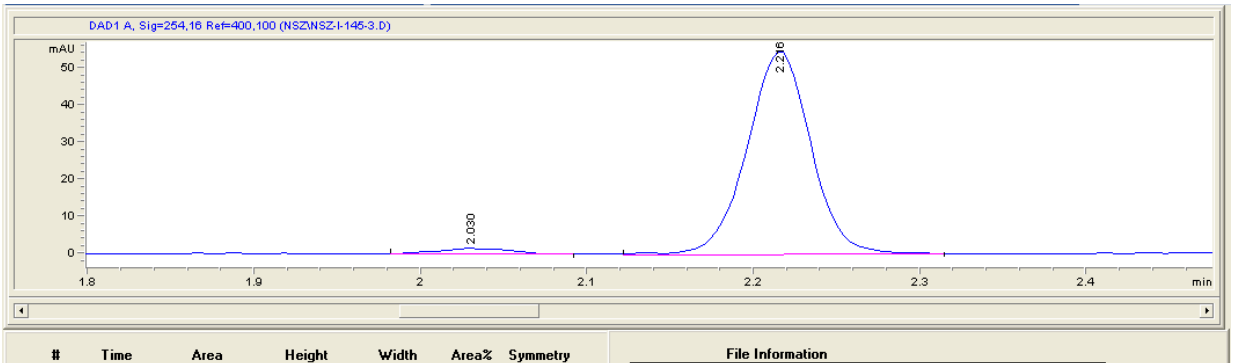

#	Time	Area	Height	Width	Area%	Symmetry
1	2.03	6	1.7	0.0588	3.933	0.821
2	2.216	146.4	54.9	0.0444	96.067	1.044

File Information	
LC-File	NSZ-I-145-3.D
File Path	C:\CHEM32\1\DATA\NSZ\

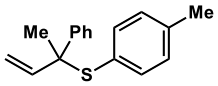

rac-4ab

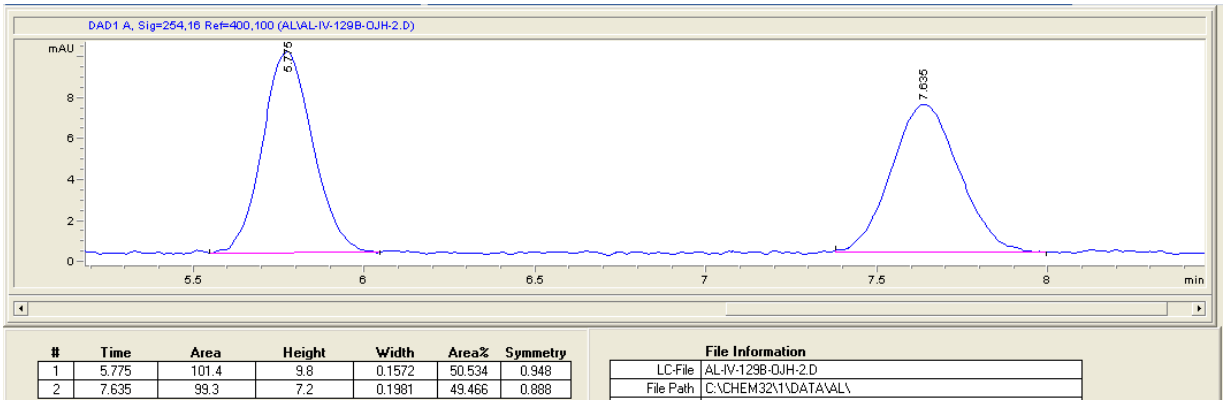

#	Time	Area	Height	Width	Area%	Symmetry
1	5.775	101.4	9.8	0.1572	50.534	0.948
2	7.635	99.3	7.2	0.1981	49.466	0.888

File Information	
LC-File	AL-IV-129B-OJH-2.D
File Path	C:\CHEM32\1\DATA\AL\

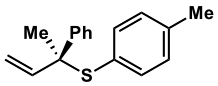

4ab

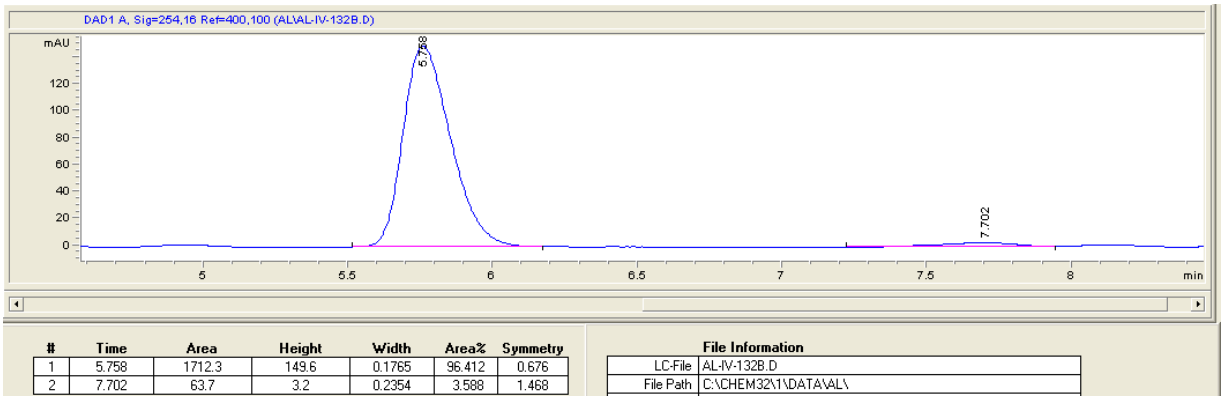

#	Time	Area	Height	Width	Area%	Symmetry
1	5.758	1712.3	149.6	0.1765	96.412	0.676
2	7.702	63.7	3.2	0.2354	3.588	1.468

File Information	
LC-File	AL-IV-132B.D
File Path	C:\CHEM32\1\DATA\AL\

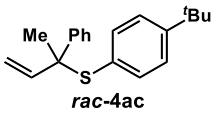

rac-4ac

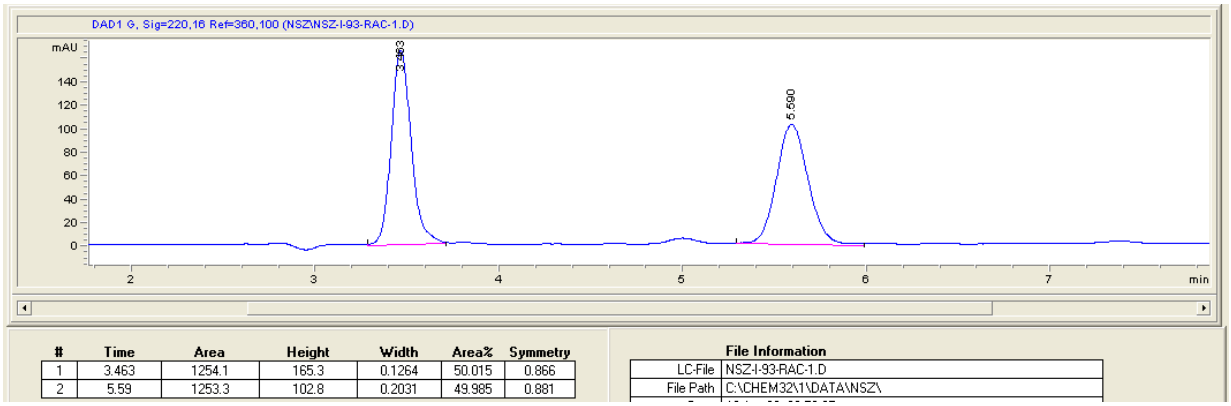

#	Time	Area	Height	Width	Area%	Symmetry
1	3.463	1254.1	165.3	0.1264	50.015	0.866
2	5.59	1253.3	102.8	0.2031	49.985	0.881

File Information	
LC-File	NSZ-I-93-RAC-1.D
File Path	C:\CHEM32\1\DATA\NSZ\

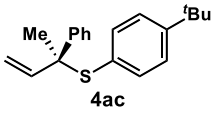

4ac

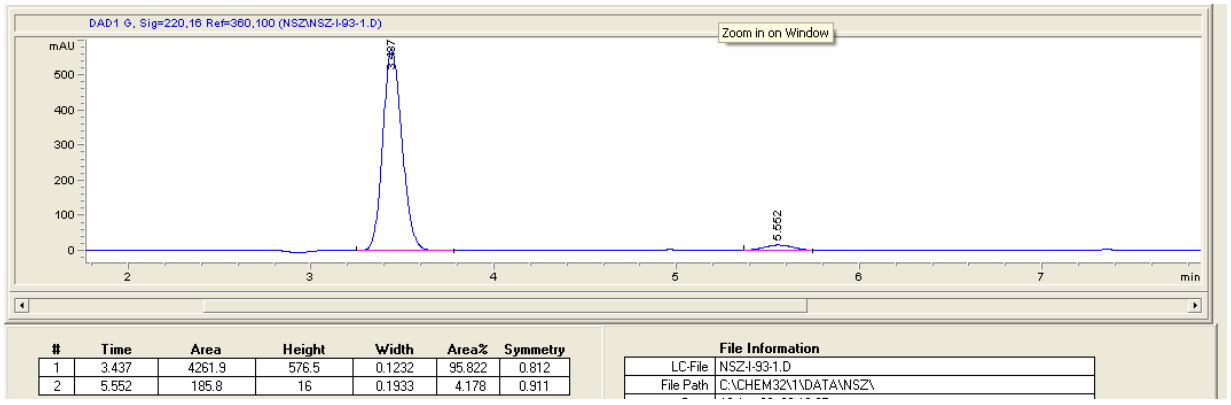

#	Time	Area	Height	Width	Area%	Symmetry
1	3.437	4261.9	576.5	0.1232	95.822	0.812
2	5.552	185.8	16	0.1933	4.178	0.911

File Information	
LC-File	NSZ-I-93-1.D
File Path	C:\CHEM32\1\DATA\NSZ\

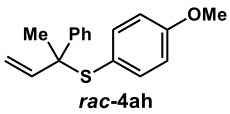

rac-4ah

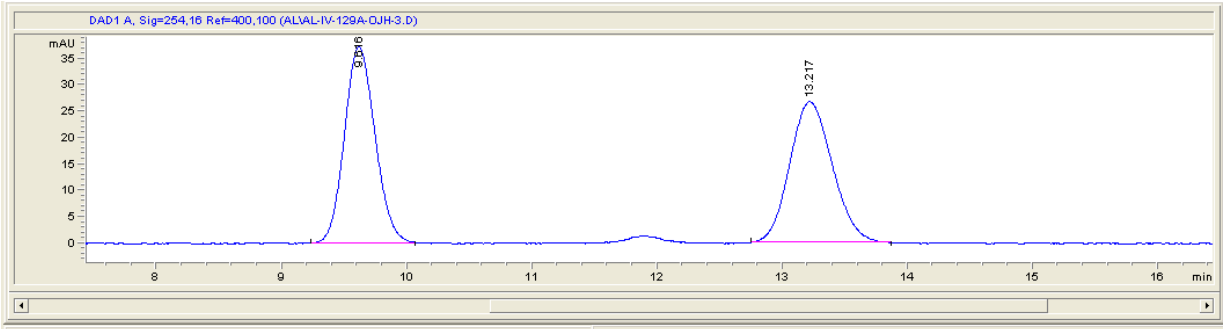

#	Time	Area	Height	Width	Area%	Symmetry
1	9.616	636.4	37.3	0.262	49.980	0.862
2	13.217	636.9	26.8	0.3146	50.020	0.859

File Information	
LC-File	AL-IV-129A-OJH-3.D
File Path	C:\CHEM32\1\DATA\AL\

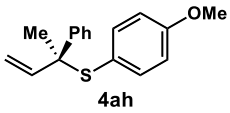

4ah

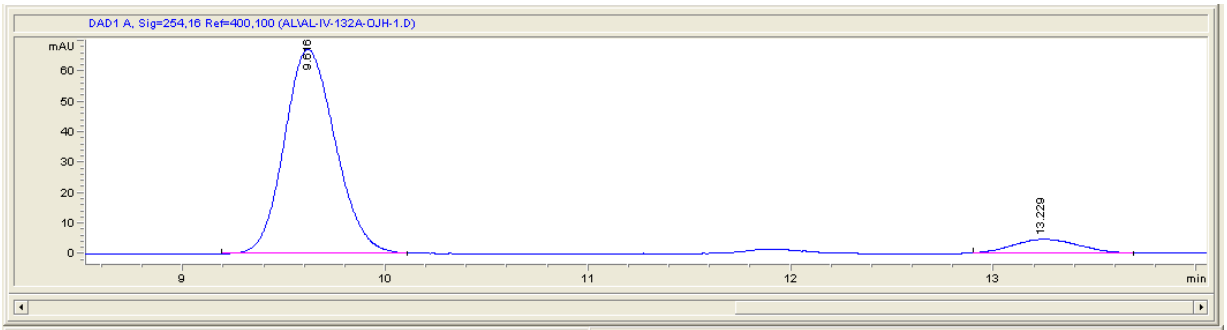

#	Time	Area	Height	Width	Area%	Symmetry
1	9.616	1170.9	67.1	0.2908	91.555	0.84
2	13.229	108	4.6	0.3877	8.445	0.711

File Information	
LC-File	AL-IV-132A-OJH-1.D
File Path	C:\CHEM32\1\DATA\AL\

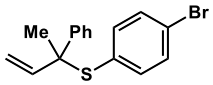

***rac*-4ai**

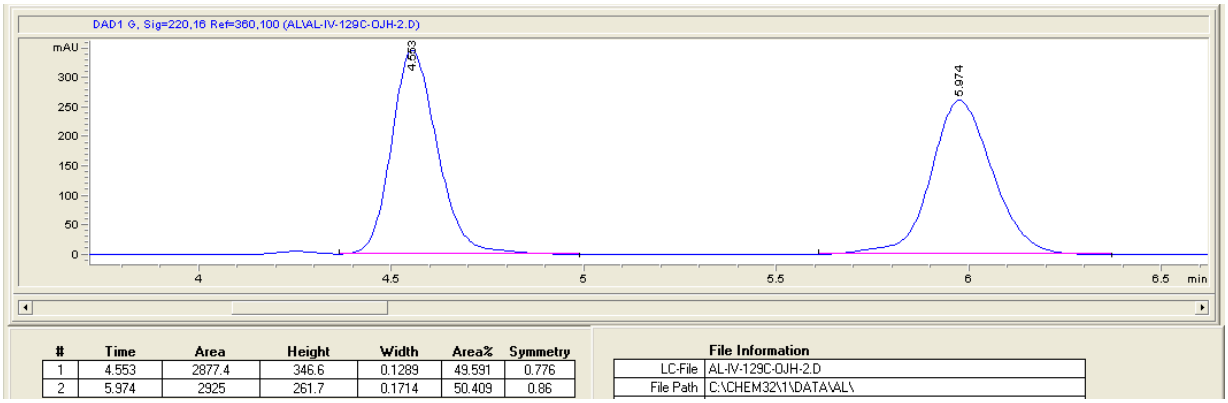

#	Time	Area	Height	Width	Area%	Symmetry
1	4.553	2877.4	346.6	0.1289	49.591	0.776
2	5.974	2925	261.7	0.1714	50.409	0.86

File Information	
LC-File	AL-IV-129C-OJH-2.D
File Path	C:\CHEM32\1\DATA\AL\

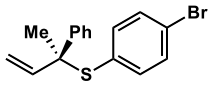

4ai

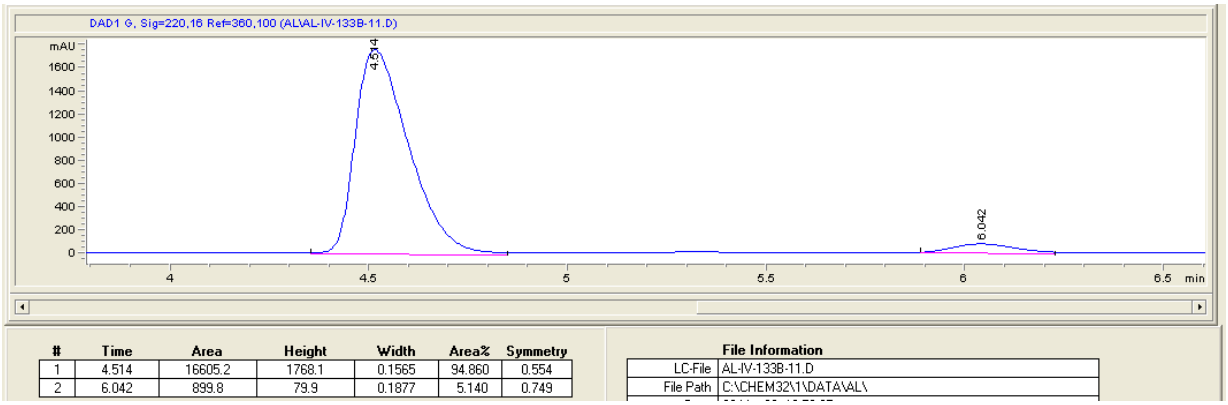

#	Time	Area	Height	Width	Area%	Symmetry
1	4.514	16605.2	1768.1	0.1565	94.860	0.554
2	6.042	899.8	79.9	0.1877	5.140	0.749

File Information	
LC-File	AL-IV-133B-11.D
File Path	C:\CHEM32\1\DATA\AL\

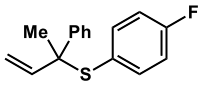

rac-4aj

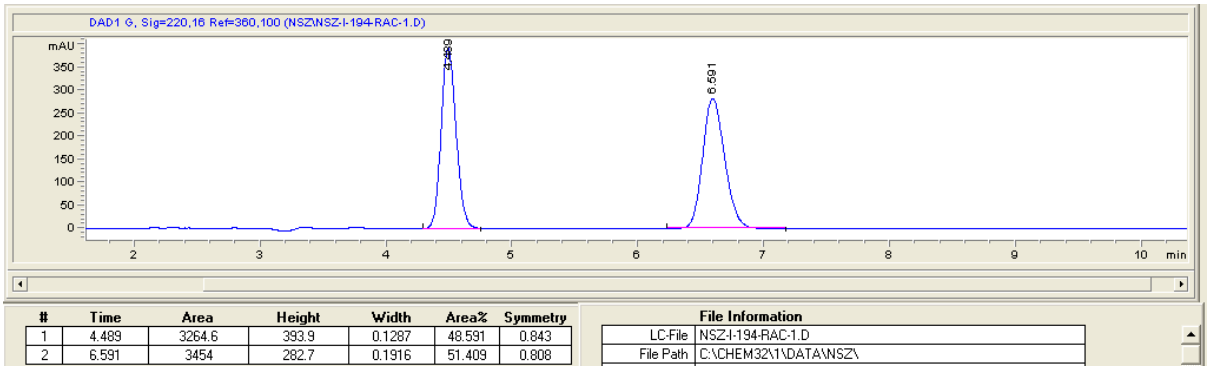

#	Time	Area	Height	Width	Area%	Symmetry
1	4.489	3264.6	393.9	0.1287	48.591	0.843
2	6.591	3454	282.7	0.1916	51.409	0.808

File Information	
LC-File	NSZ-I-194-RAC-1.D
File Path	C:\CHEM32\1\DATA\NSZ\

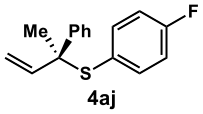

4aj

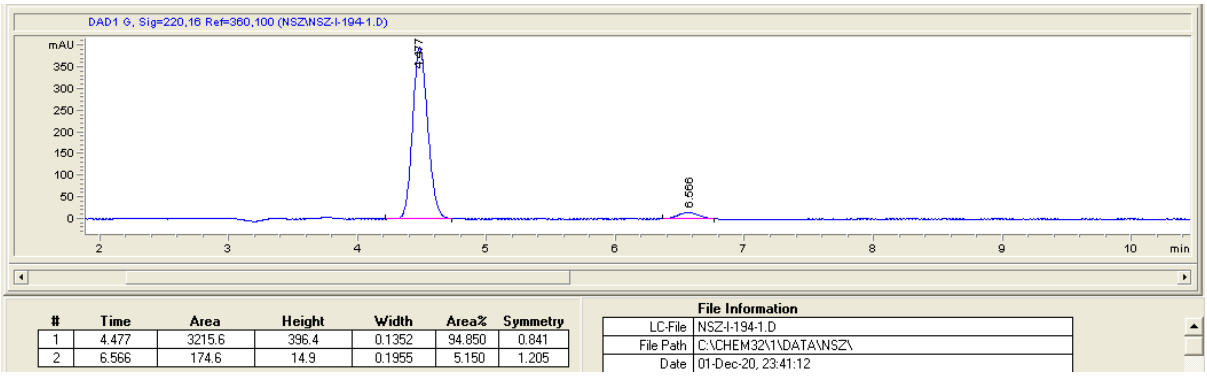

#	Time	Area	Height	Width	Area%	Symmetry
1	4.477	3215.6	396.4	0.1352	94.850	0.841
2	6.566	174.6	14.9	0.1955	5.150	1.205

File Information	
LC-File	NSZ-I-194-1.D
File Path	C:\CHEM32\1\DATA\NSZ\
Date	01-Dec-20, 23:41:12

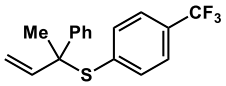

rac-4ak

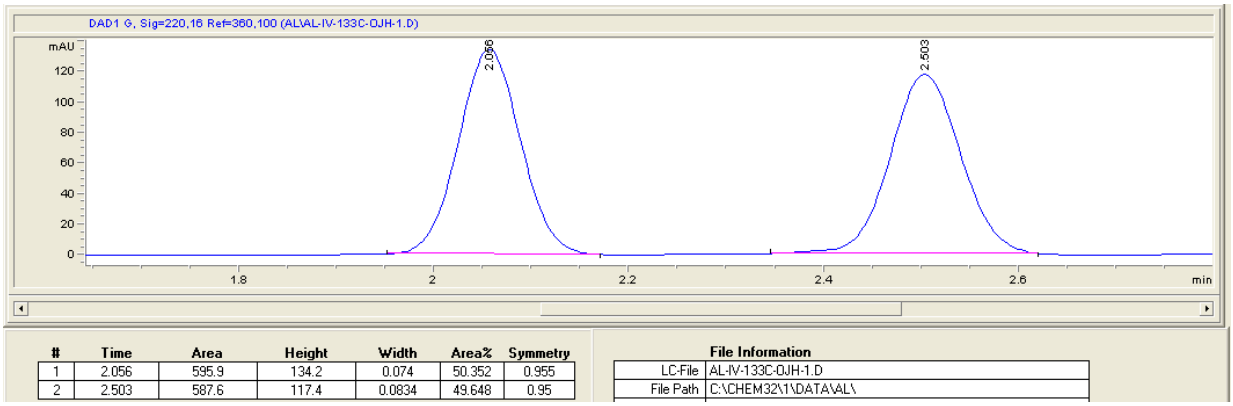

#	Time	Area	Height	Width	Area%	Symmetry
1	2.056	595.9	134.2	0.074	50.352	0.955
2	2.503	587.6	117.4	0.0834	49.648	0.95

File Information	
LC-File	AL-IV-133C-OJH-1.D
File Path	C:\CHEM32\1\DATA\AL\

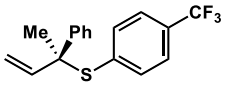

4ak

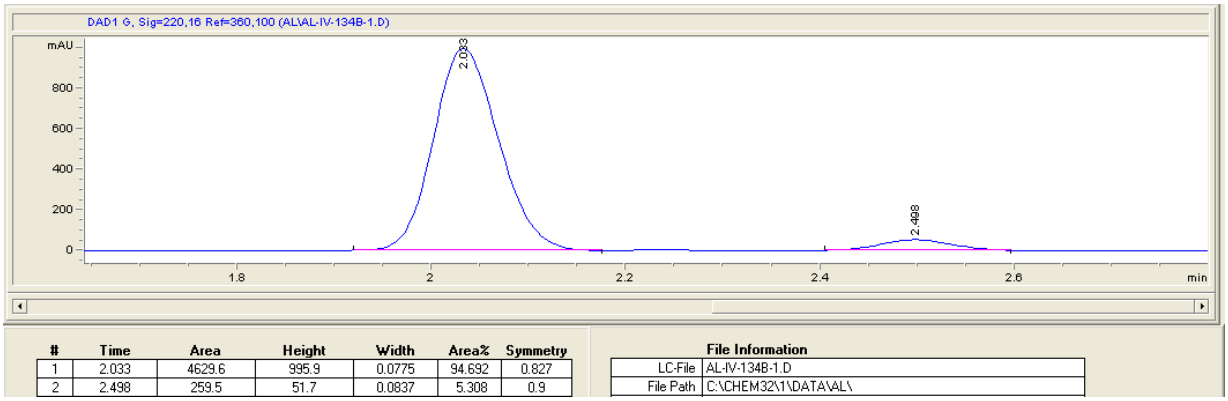

#	Time	Area	Height	Width	Area%	Symmetry
1	2.033	4629.6	995.9	0.0775	94.692	0.827
2	2.498	259.5	51.7	0.0837	5.308	0.9

File Information	
LC-File	AL-IV-134B-1.D
File Path	C:\CHEM32\1\DATA\AL\

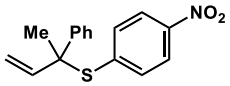

rac-4al

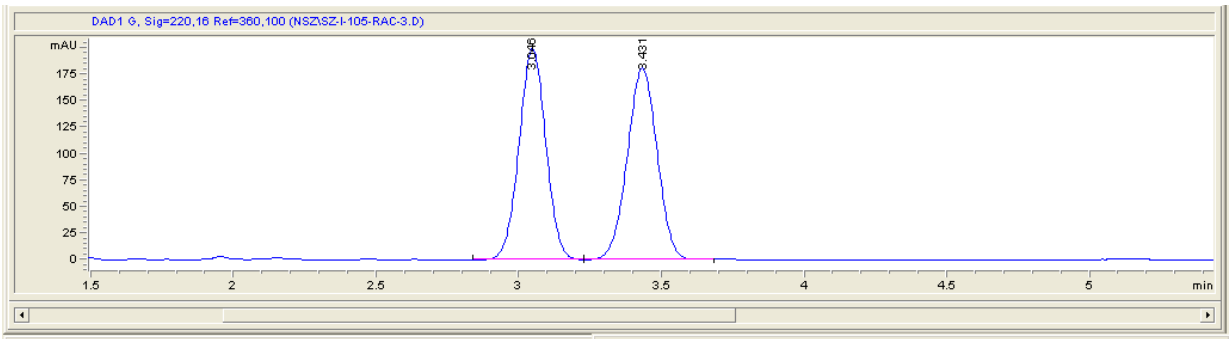

#	Time	Area	Height	Width	Area%	Symmetry
1	3.046	1310.6	199.7	0.1016	49.831	0.971
2	3.431	1319.5	180.9	0.1131	50.169	0.982

File Information	
LC-File	SZ-I-105-RAC-3.D
File Path	C:\CHEM32\1\DATA\NSZ\

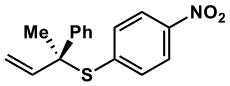

4al

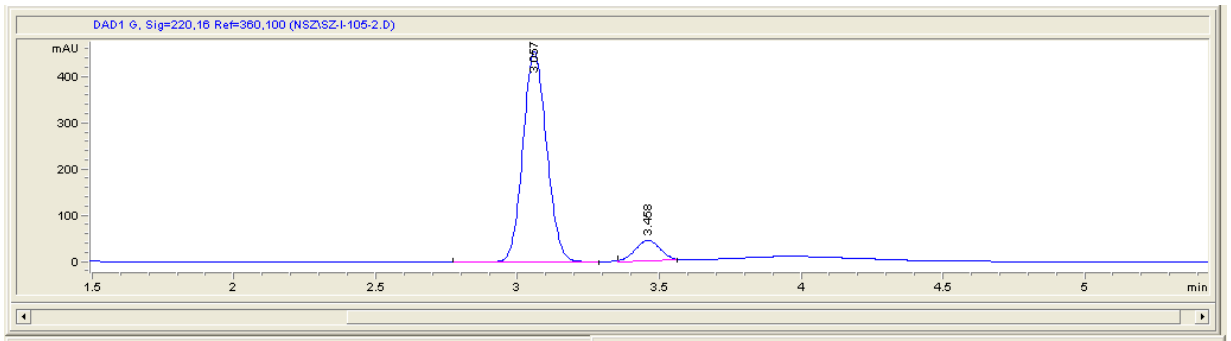

#	Time	Area	Height	Width	Area%	Symmetry
1	3.057	2708.6	456.6	0.0922	90.567	0.873
2	3.458	282.1	44.8	0.105	9.433	1.067

File Information	
LC-File	SZ-I-105-2.D
File Path	C:\CHEM32\1\DATA\NSZ\

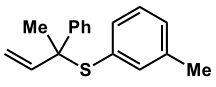

rac-4ae

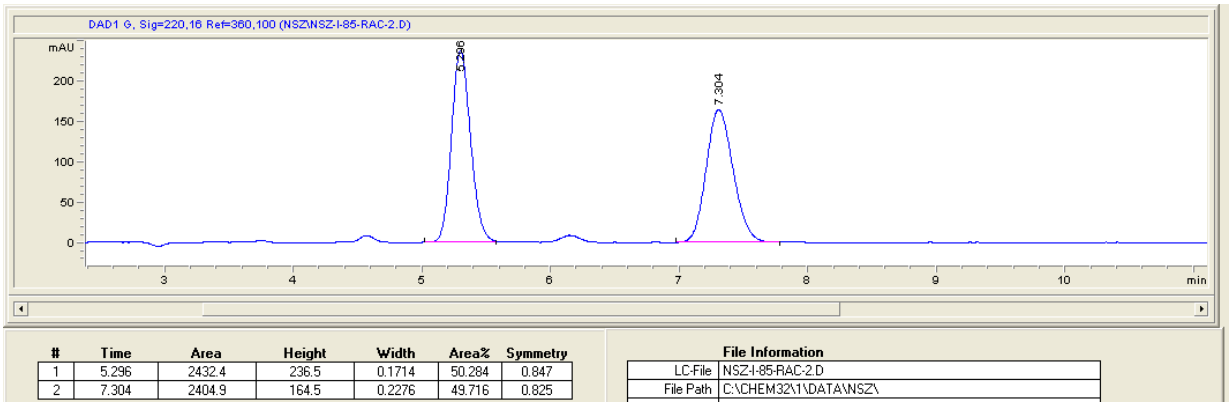

#	Time	Area	Height	Width	Area%	Symmetry
1	5.296	2432.4	236.5	0.1714	50.284	0.847
2	7.304	2404.9	164.5	0.2276	49.716	0.825

File Information	
LC-File	NSZ-I-85-RAC-2.D
File Path	C:\CHEM32\1\DATA\NSZ\

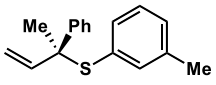

4ae

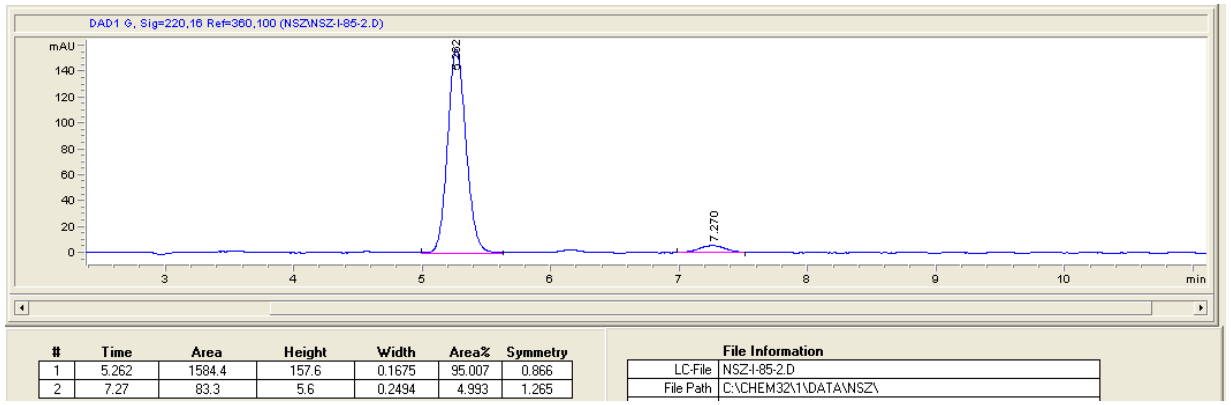

#	Time	Area	Height	Width	Area%	Symmetry
1	5.262	1584.4	157.6	0.1675	95.007	0.866
2	7.27	83.3	5.6	0.2494	4.993	1.265

File Information	
LC-File	NSZ-I-85-2.D
File Path	C:\CHEM32\1\DATA\NSZ\

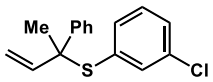

rac-4am

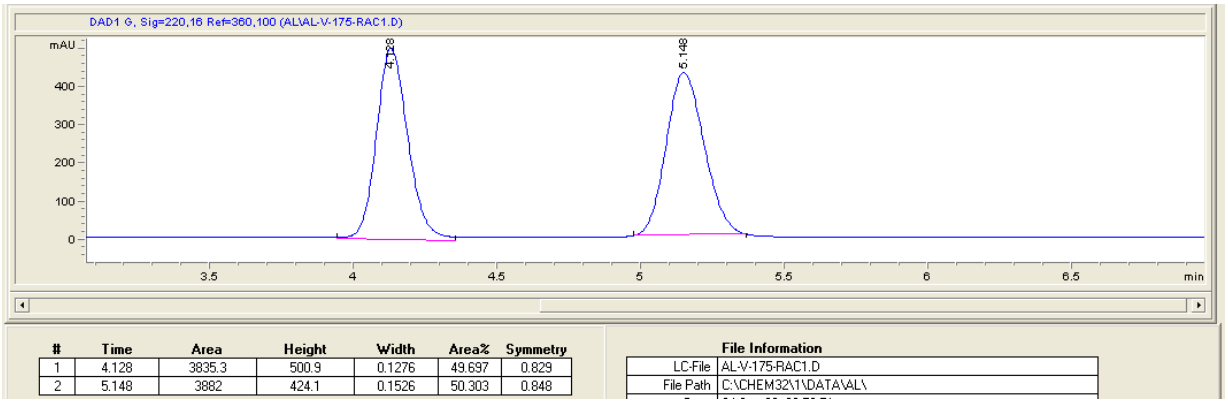

#	Time	Area	Height	Width	Area%	Symmetry
1	4.128	3835.3	500.9	0.1276	49.697	0.829
2	5.148	3882	424.1	0.1526	50.303	0.848

File Information	
LC-File	AL-V-175-RAC1.D
File Path	C:\CHEM32\1\DATA\AL\

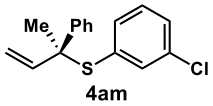

4am

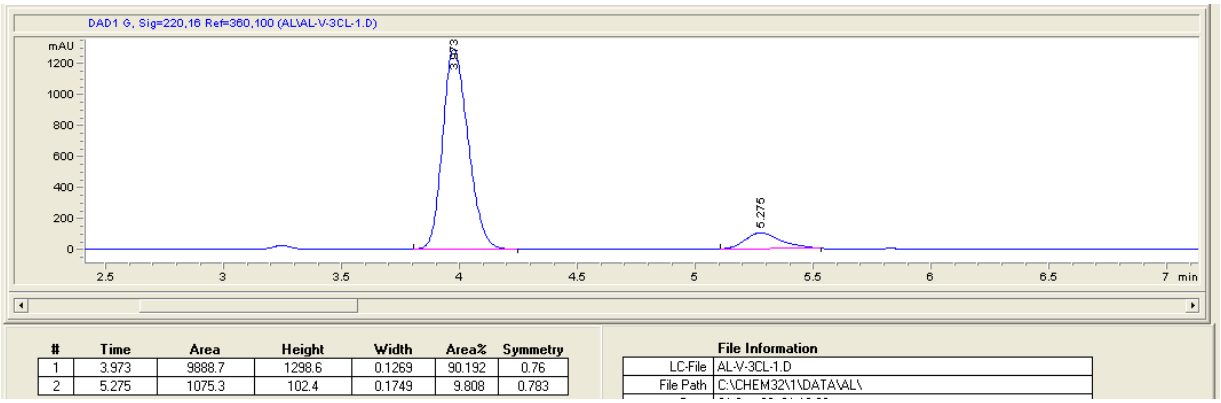

#	Time	Area	Height	Width	Area%	Symmetry
1	3.973	9888.7	1298.6	0.1269	90.192	0.76
2	5.275	1075.3	102.4	0.1749	9.808	0.783

File Information	
LC-File	AL-V-3CL-1.D
File Path	C:\CHEM32\1\DATA\AL\

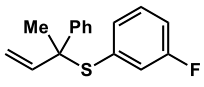

***rac*-4an**

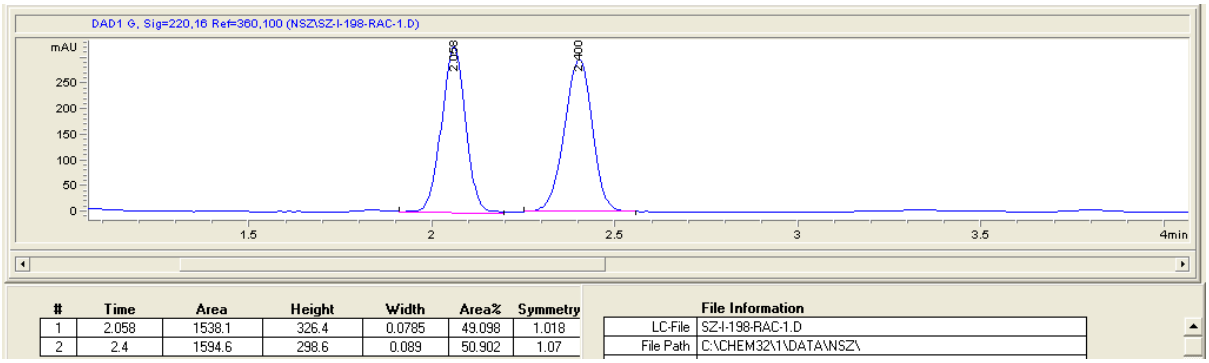

#	Time	Area	Height	Width	Area%	Symmetry
1	2.058	1538.1	326.4	0.0785	49.098	1.018
2	2.4	1594.6	298.6	0.089	50.902	1.07

File Information	
LC-File	SZ-I-198-RAC-1.D
File Path	C:\CHEM32\1\DATA\NSZ\

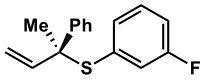

4an

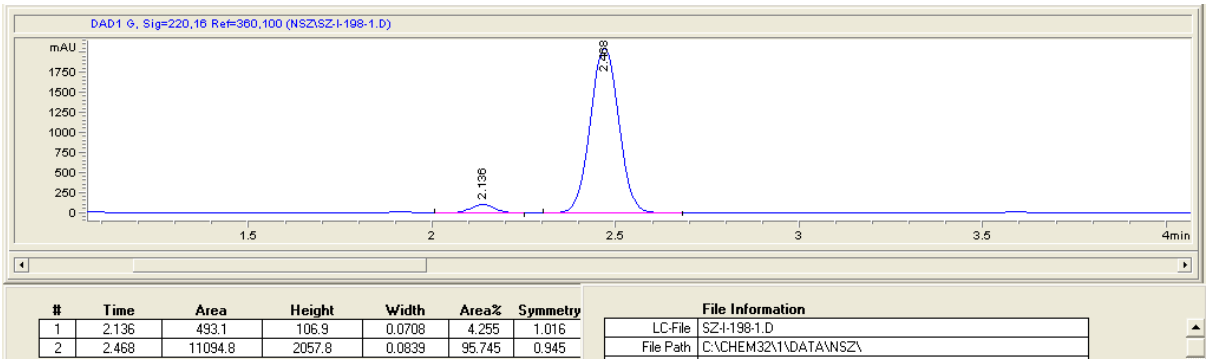

#	Time	Area	Height	Width	Area%	Symmetry
1	2.136	493.1	106.9	0.0708	4.255	1.016
2	2.468	11094.8	2057.8	0.0839	95.745	0.945

File Information	
LC-File	SZ-I-198-1.D
File Path	C:\CHEM32\1\DATA\NSZ\

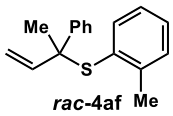

rac-4af

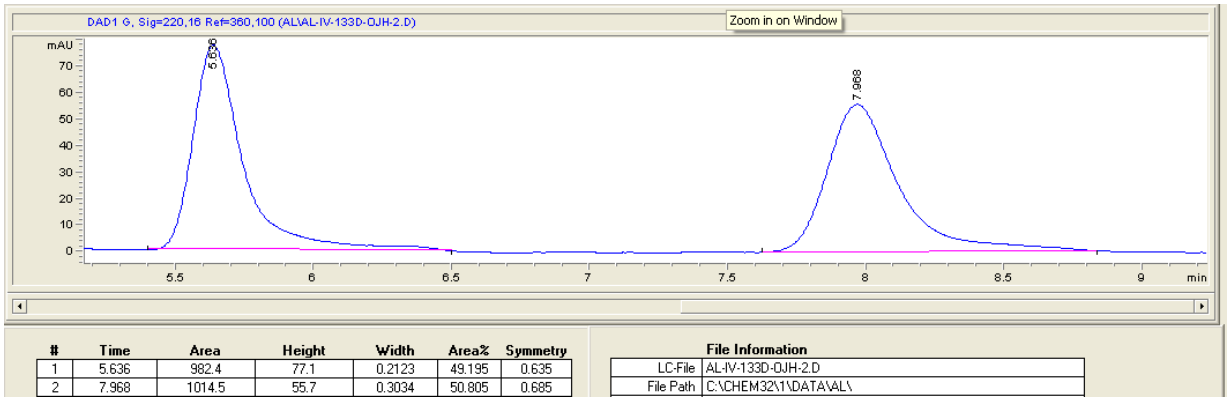

#	Time	Area	Height	Width	Area%	Symmetry
1	5.636	982.4	77.1	0.2123	49.195	0.635
2	7.968	1014.5	55.7	0.3034	50.805	0.685

File Information	
LC-File	AL-IV-133D-OJH-2.D
File Path	C:\CHEM32\1\DATA\AL\

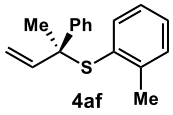

4af

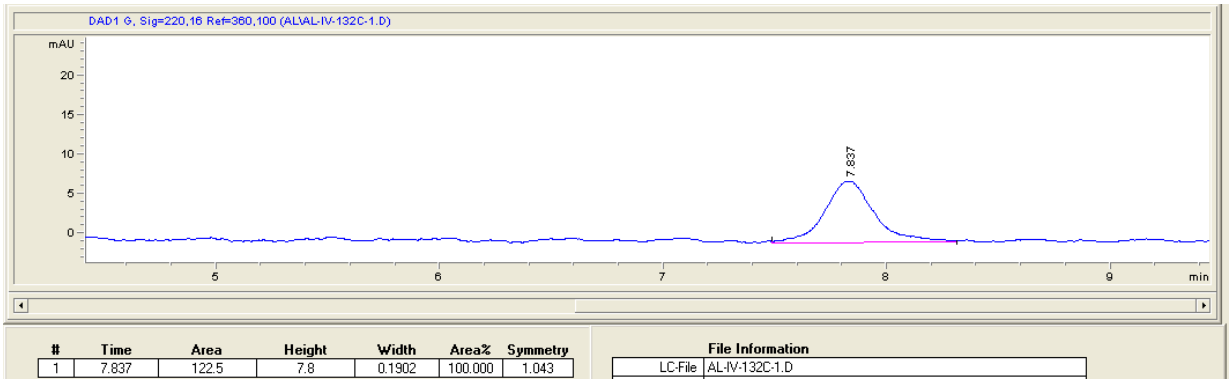

#	Time	Area	Height	Width	Area%	Symmetry
1	7.837	122.5	7.8	0.1902	100.000	1.043

File Information	
LC-File	AL-IV-132C-1.D

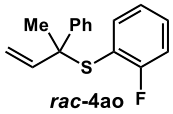

rac-4ao

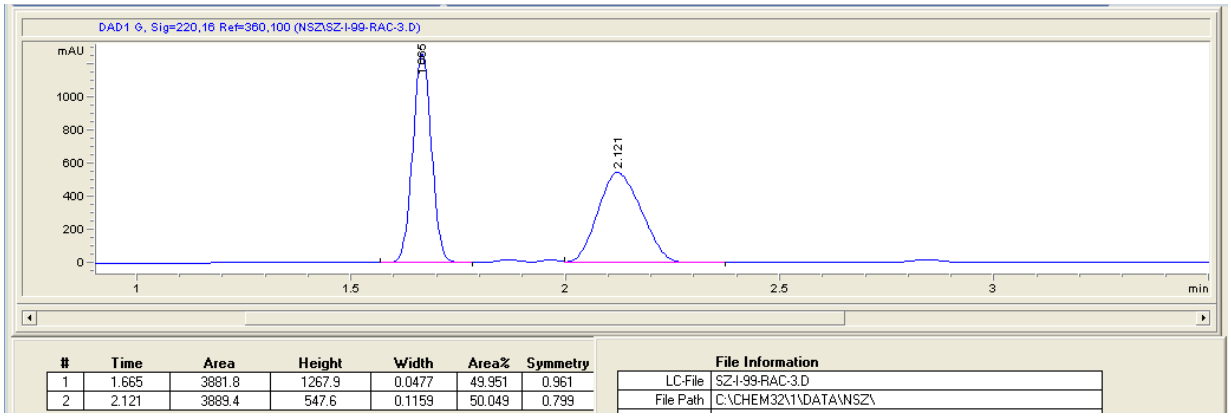

#	Time	Area	Height	Width	Area%	Symmetry
1	1.665	3881.8	1267.9	0.0477	49.951	0.961
2	2.121	3889.4	547.6	0.1159	50.049	0.799

File Information	
LC-File	SZ-I-99-RAC-3.D
File Path	C:\CHEM32\1\DATA\NSZ\

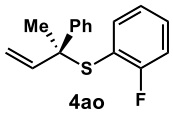

4ao

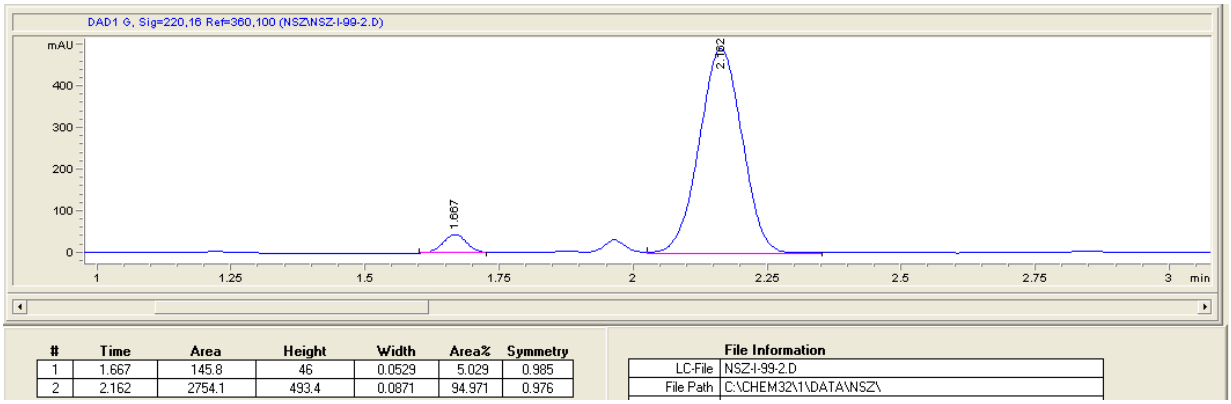

#	Time	Area	Height	Width	Area%	Symmetry
1	1.667	145.8	46	0.0529	5.029	0.985
2	2.162	2754.1	493.4	0.0871	94.971	0.976

File Information	
LC-File	NSZ-I-99-2.D
File Path	C:\CHEM32\1\DATA\NSZ\

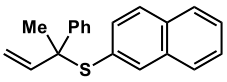

***rac*-4ag**

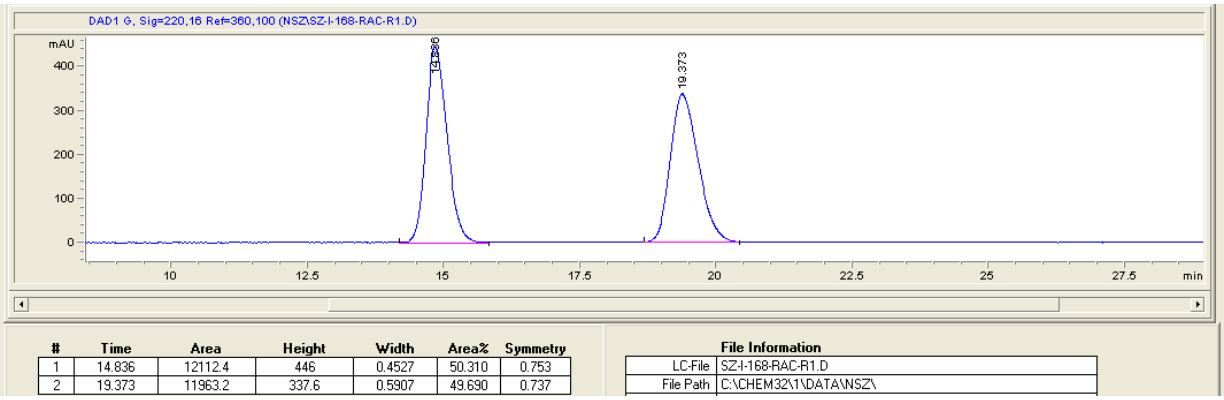

#	Time	Area	Height	Width	Area%	Symmetry
1	14.836	12112.4	446	0.4527	50.310	0.753
2	19.373	11963.2	337.6	0.5907	49.690	0.737

File Information	
LC-File	SZ-I-168-RAC-R1.D
File Path	C:\CHEM32\1\DATA\NSZ\

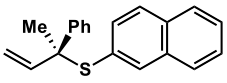

4ag

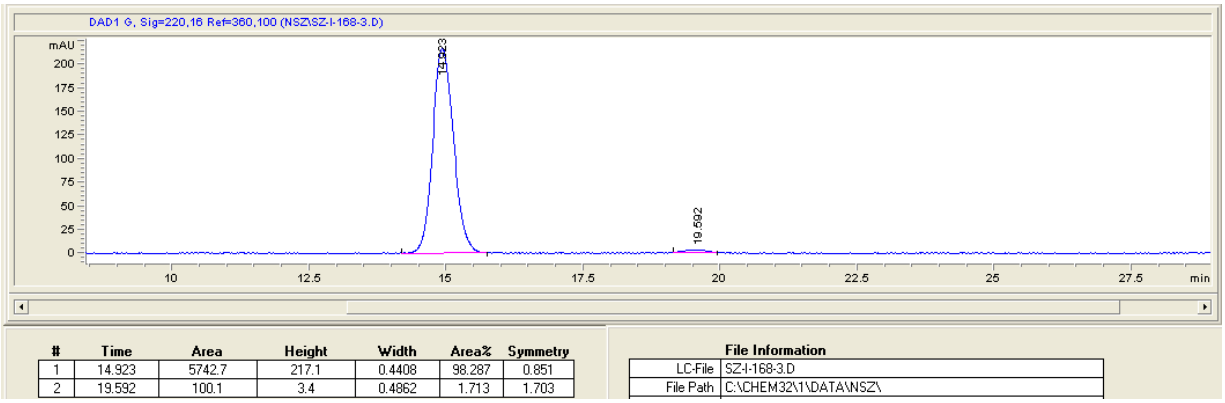

#	Time	Area	Height	Width	Area%	Symmetry
1	14.923	5742.7	217.1	0.4408	98.287	0.851
2	19.592	100.1	3.4	0.4862	1.713	1.703

File Information	
LC-File	SZ-I-168-3.D
File Path	C:\CHEM32\1\DATA\NSZ\

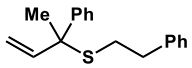

rac-4ap

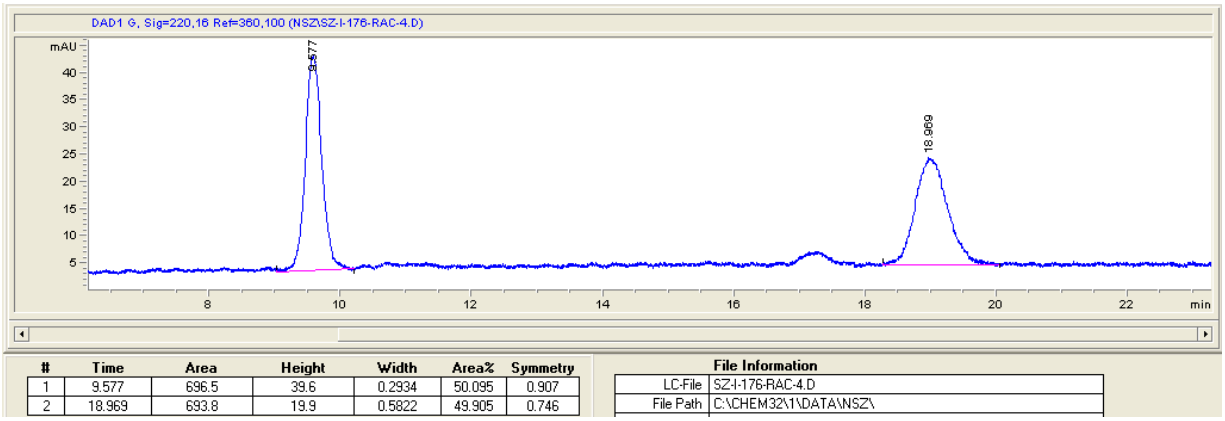

#	Time	Area	Height	Width	Area%	Symmetry
1	9.577	696.5	39.6	0.2934	50.095	0.907
2	18.969	693.8	19.9	0.5822	49.905	0.746

File Information	
LC-File	SZ-I-176-RAC-4.D
File Path	C:\CHEM32\1\DATA\NSZ\

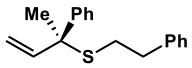

4ap

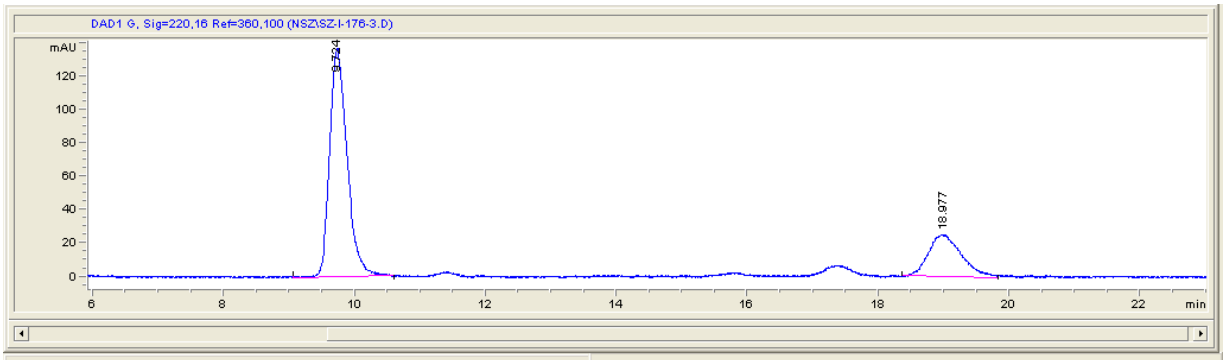

#	Time	Area	Height	Width	Area%	Symmetry
1	9.724	2556.8	137.1	0.3108	74.091	0.694
2	18.977	894.1	25.4	0.5877	25.909	0.741

File Information	
LC-File	SZ-I-176-3.D
File Path	C:\CHEM32\1\DATA\NSZ\

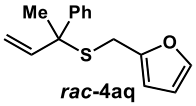

rac-4aq

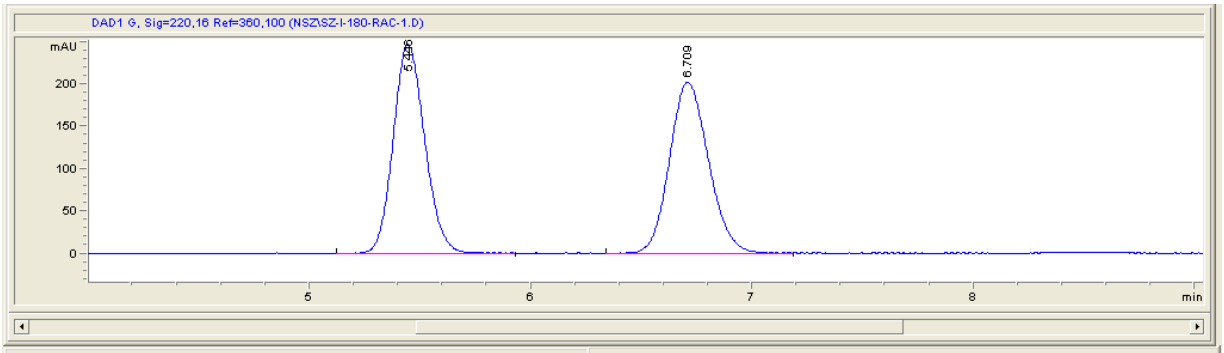

#	Time	Area	Height	Width	Area%	Symmetry
1	5.446	2491.9	247.6	0.1678	49.620	0.863
2	6.709	2530	202.9	0.2079	50.380	0.845

File Information	
LC-File	SZ-I-180-RAC-1.D
File Path	C:\CHEM32\1\DATA\NSZ\

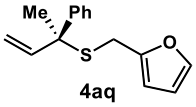

4aq

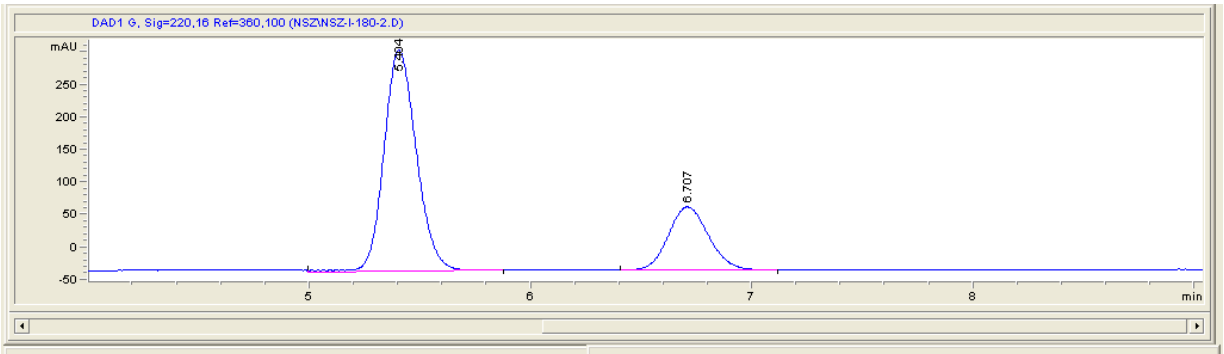

#	Time	Area	Height	Width	Area%	Symmetry
1	5.404	3541.1	341.1	0.1601	74.045	0.84
2	6.707	1241.3	97.4	0.1946	25.955	0.848

File Information	
LC-File	NSZ-I-180-2.D
File Path	C:\CHEM32\1\DATA\NSZ\

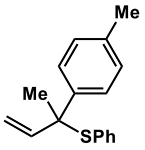

rac-4ba

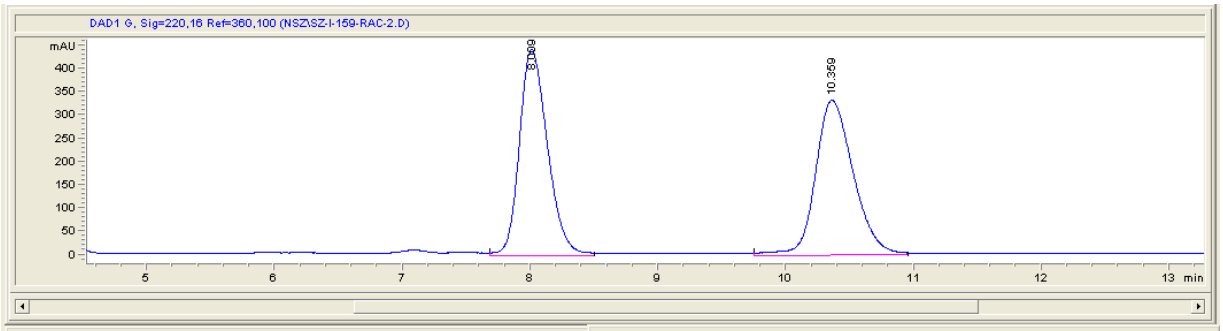

#	Time	Area	Height	Width	Area%	Symmetry
1	8.009	6860.6	445.1	0.2358	49.764	0.732
2	10.359	6925.8	334.3	0.3137	50.236	0.747

File Information	
LC-File	SZ-I-159-RAC-2.D
File Path	C:\CHEM32\1\DATA\NSZ\

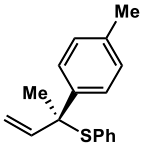

4ba

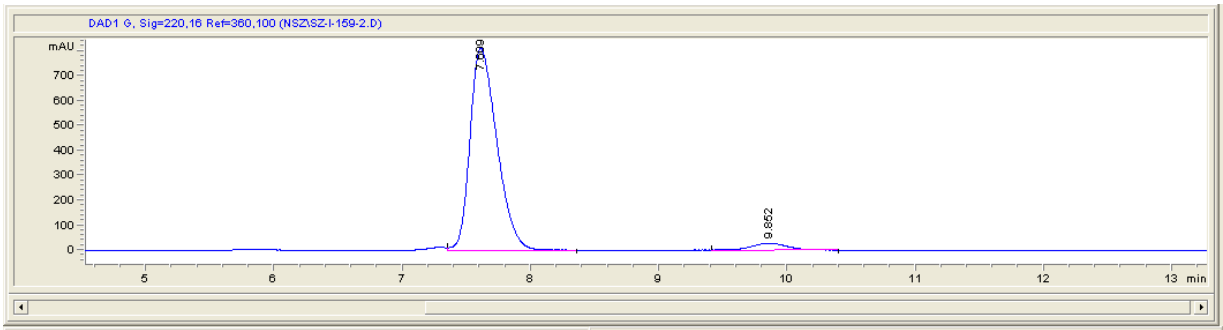

#	Time	Area	Height	Width	Area%	Symmetry
1	7.609	12106.5	816.8	0.2239	94.823	0.63
2	9.852	660.9	29.4	0.2682	5.177	0.914

File Information	
LC-File	SZ-I-159-2.D
File Path	C:\CHEM32\1\DATA\NSZ\

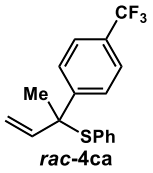

rac-4ca

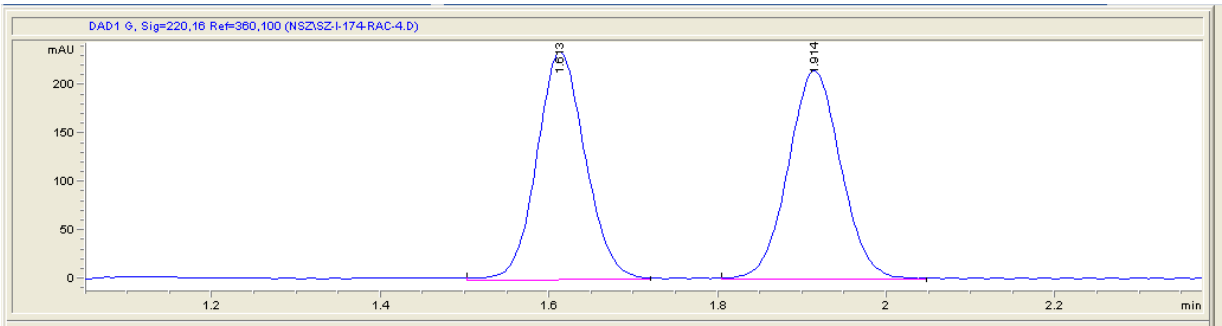

#	Time	Area	Height	Width	Area%	Symmetry
1	1.613	943.8	236.5	0.0665	50.167	0.902
2	1.914	937.5	215.9	0.0724	49.833	0.958

File Information	
LC-File	SZ-I-174-RAC-4.D
File Path	C:\CHEM32\1\DATA\NSZ\

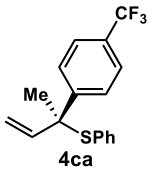

4ca

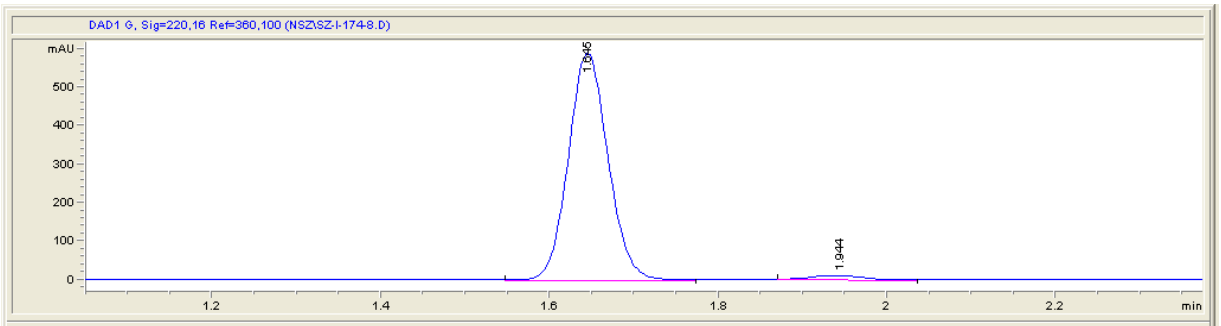

#	Time	Area	Height	Width	Area%	Symmetry
1	1.645	1955.9	593.5	0.0549	96.882	0.901
2	1.944	62.9	12.6	0.0831	3.118	0.801

File Information	
LC-File	SZ-I-174-8.D
File Path	C:\CHEM32\1\DATA\NSZ\

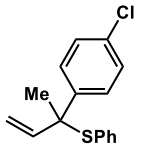

***rac*-4da**

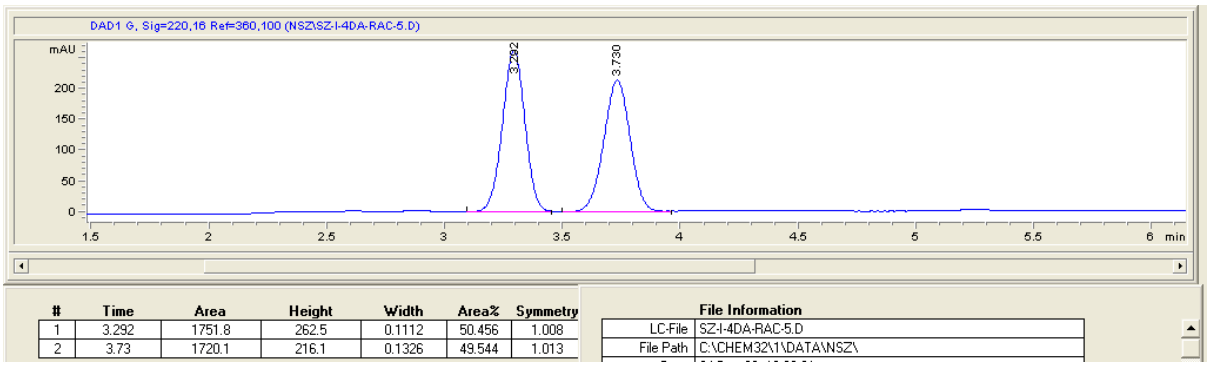

#	Time	Area	Height	Width	Area%	Symmetry
1	3.292	1751.8	262.5	0.1112	50.456	1.008
2	3.73	1720.1	216.1	0.1326	49.544	1.013

File Information	
LC-File	SZ-I-4DA-RAC-5.D
File Path	C:\CHEM32\1\DATA\NSZ\

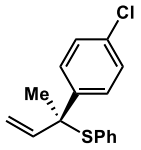

4da

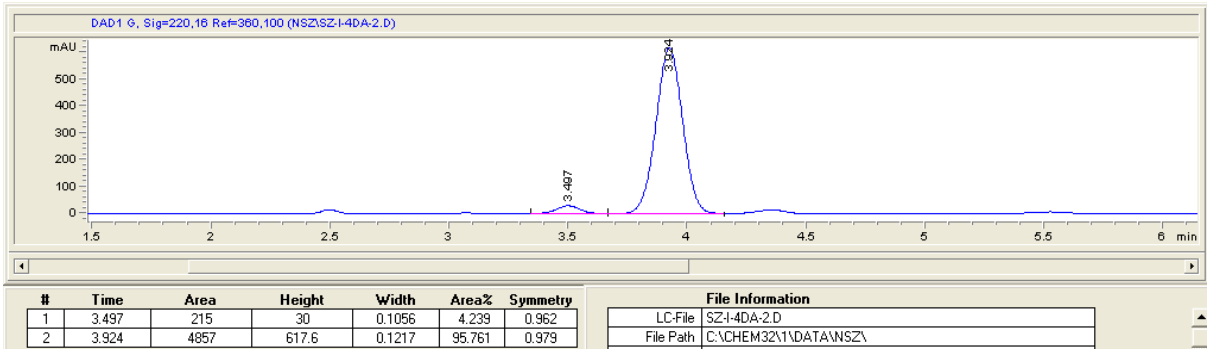

#	Time	Area	Height	Width	Area%	Symmetry
1	3.497	215	30	0.1056	4.239	0.962
2	3.924	4857	617.6	0.1217	95.761	0.979

File Information	
LC-File	SZ-I-4DA-2.D
File Path	C:\CHEM32\1\DATA\NSZ\

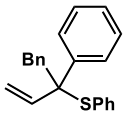

rac-4ea

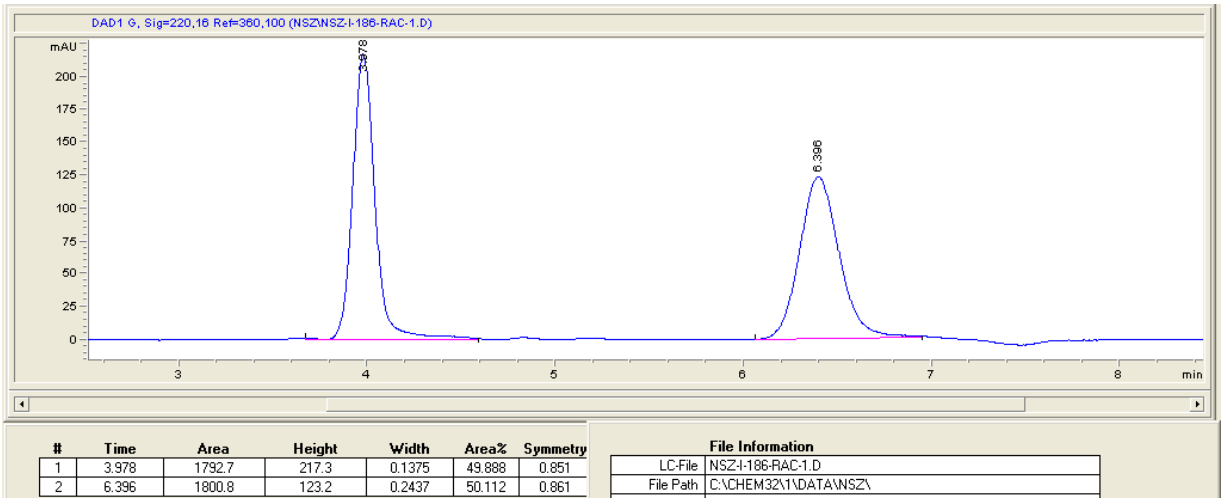

#	Time	Area	Height	Width	Area%	Symmetry
1	3.978	1792.7	217.3	0.1375	49.888	0.851
2	6.396	1800.8	123.2	0.2437	50.112	0.861

File Information	
LC-File	NSZ-I-186-RAC-1.D
File Path	C:\CHEM32\1\DATA\NSZ\

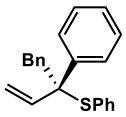

4ea

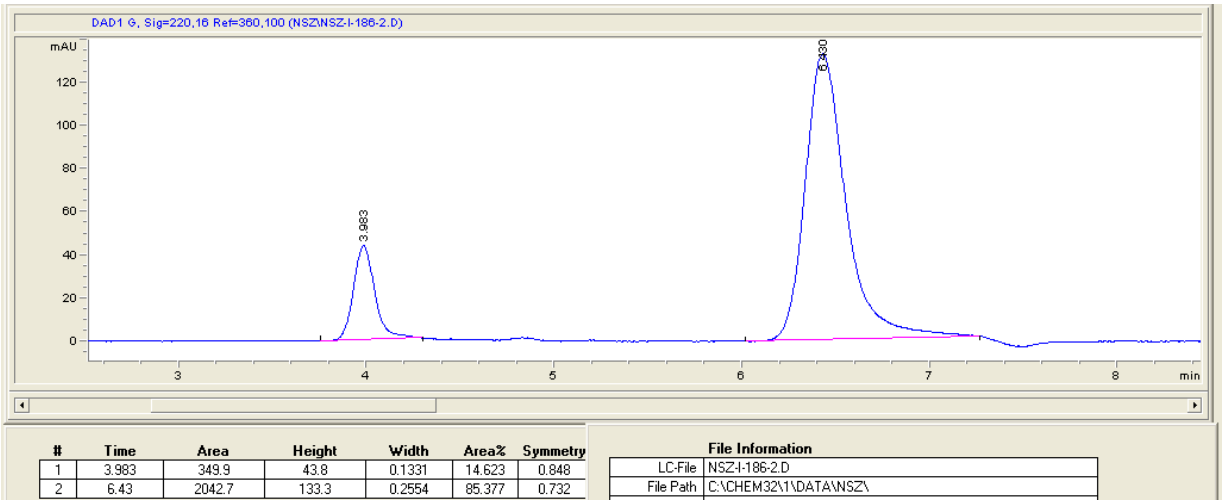

#	Time	Area	Height	Width	Area%	Symmetry
1	3.983	349.9	43.8	0.1331	14.623	0.848
2	6.43	2042.7	133.3	0.2554	85.377	0.732

File Information	
LC-File	NSZ-I-186-2.D
File Path	C:\CHEM32\1\DATA\NSZ\

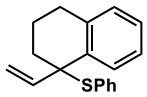

rac-4fa

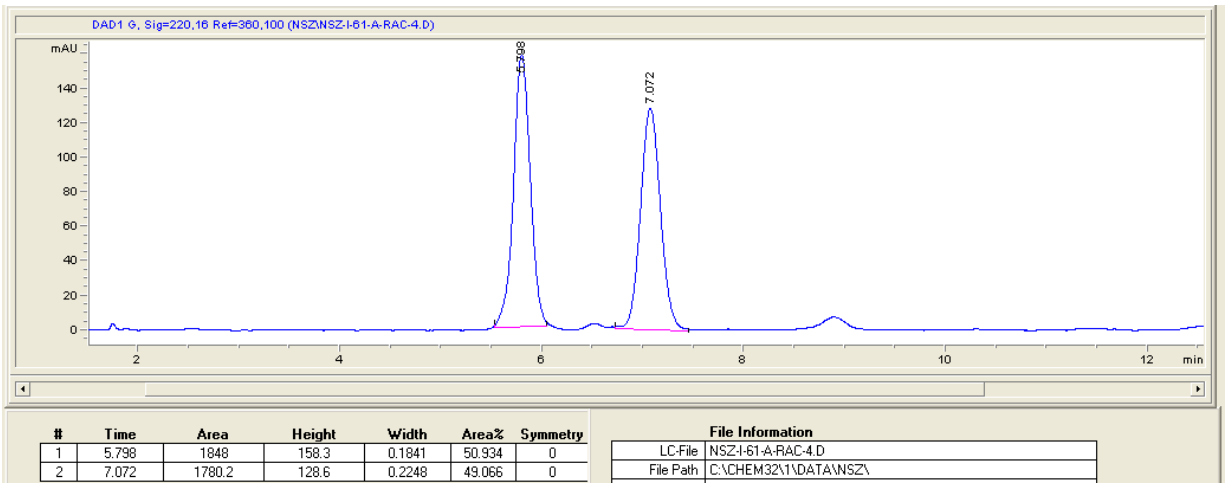

#	Time	Area	Height	Width	Area%	Symmetry
1	5.798	1848	158.3	0.1841	50.934	0
2	7.072	1780.2	128.6	0.2248	49.066	0

File Information	
LC-File	NSZ-I-61-A-RAC-4.D
File Path	C:\CHEM32\1\DATA\NSZ\

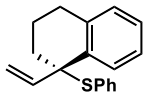

4fa

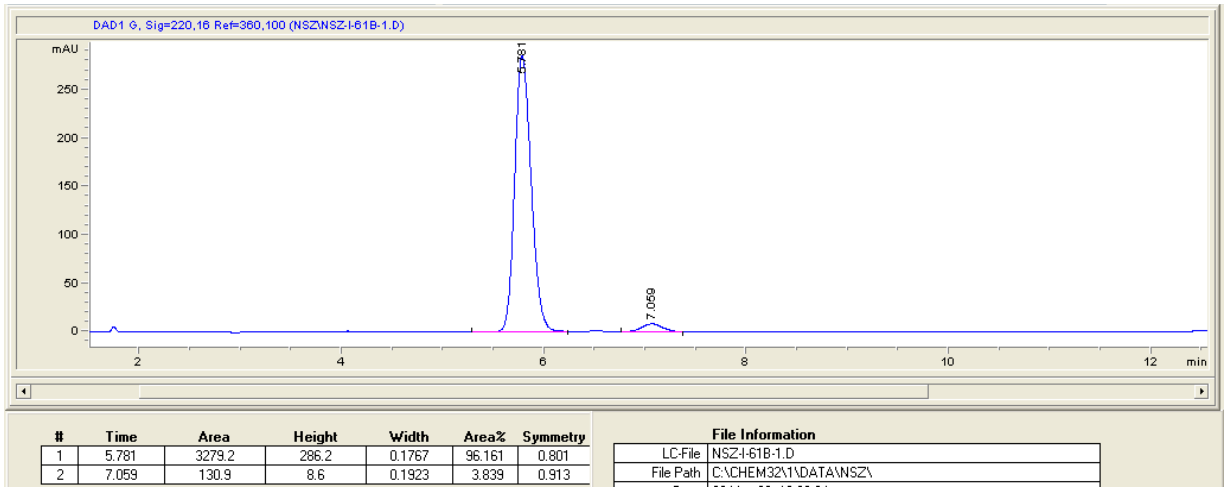

#	Time	Area	Height	Width	Area%	Symmetry
1	5.781	3279.2	286.2	0.1767	96.161	0.801
2	7.059	130.9	8.6	0.1923	3.839	0.913

File Information	
LC-File	NSZ-I-61B-1.D
File Path	C:\CHEM32\1\DATA\NSZ\

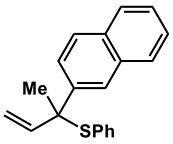

rac-4ha

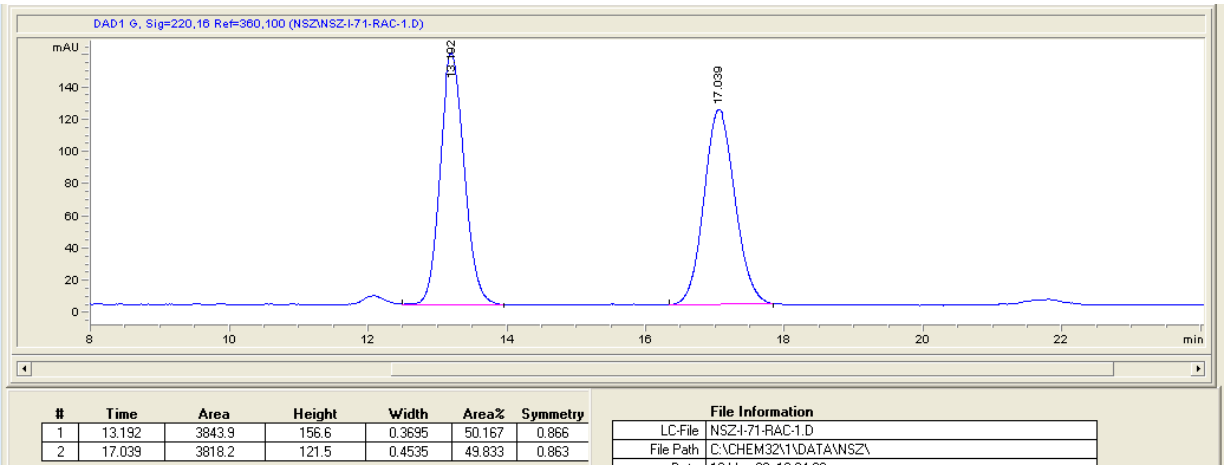

#	Time	Area	Height	Width	Area%	Symmetry
1	13.192	3843.9	156.6	0.3695	50.167	0.866
2	17.039	3818.2	121.5	0.4535	49.833	0.863

File Information	
LC-File	NSZ-I-71-RAC-1.D
File Path	C:\CHEM32\1\DATA\NSZ\

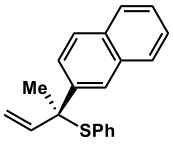

4ha

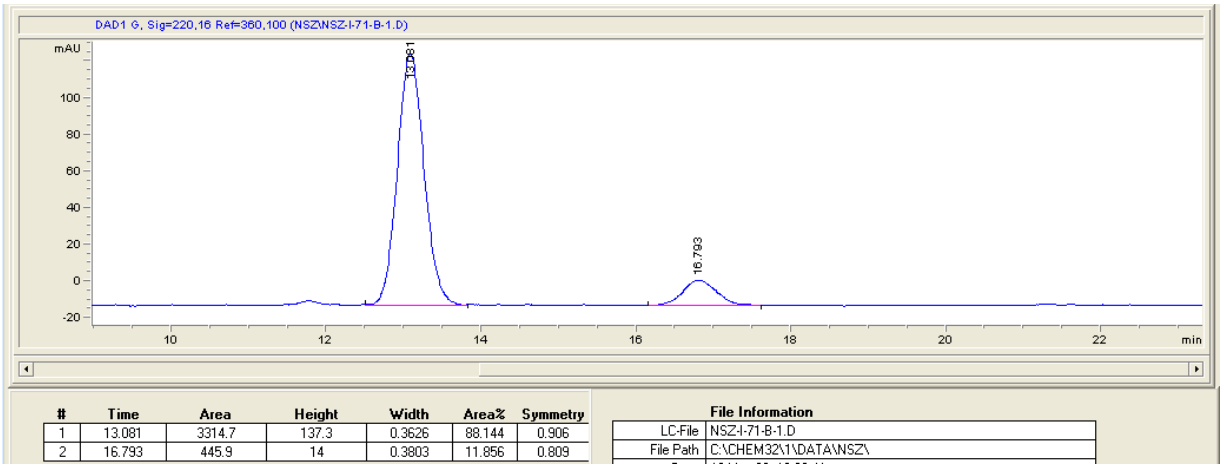

#	Time	Area	Height	Width	Area%	Symmetry
1	13.081	3314.7	137.3	0.3626	88.144	0.906
2	16.793	445.9	14	0.3803	11.856	0.809

File Information	
LC-File	NSZ-I-71-B-1.D
File Path	C:\CHEM32\1\DATA\NSZ\

8. X-ray Crystallography Data for 3ba

X-ray crystallography data for ((1*S*,2*R*)-2-methyl-2-(*p*-tolyl)cyclopropyl)(phenyl)sulfane (3ba)

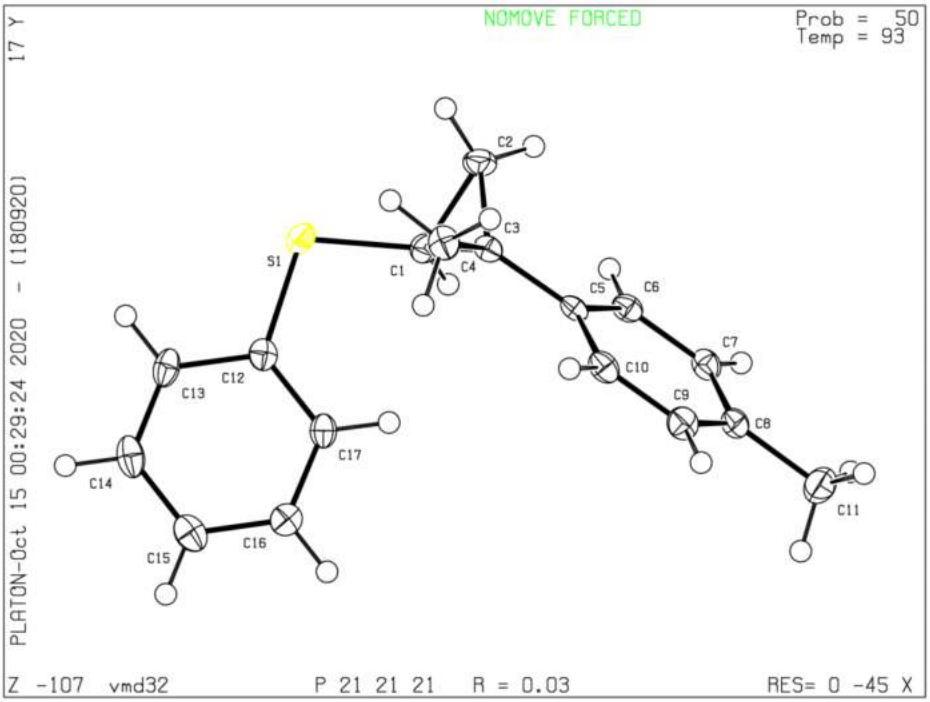

Experimental Summary

A colorless crystal of approximate dimensions 0.032 x 0.229 x 0.280 mm was mounted in a cryoloop and transferred to a Bruker SMART APEX II diffractometer. The APEX2[1] program package was used to determine the unit-cell parameters and for data collection (60 sec/frame scan time). The raw frame data was processed using SAINT[2] and SADABS[3] to yield the reflection data file. Subsequent calculations were carried out using the SHELXTL[4] program package. The diffraction symmetry was *mmm* and the systematic absences were consistent with the orthorhombic space group $P2_12_12_1$ that was later determined to be correct.

The structure was solved by direct methods and refined on F^2 by full-matrix least-squares techniques. The analytical scattering factors[5] for neutral atoms were used throughout the analysis. Hydrogen atoms were included using a riding model.

Least squares analysis yielded wR2 = 0.0781 and Goof = 1.081 for 165 variables refined against 3434 data (0.75 Å), R1 = 0.0326 for those 3191 data with $I > 2.0\sigma(I)$. The absolute structure was assigned by refinement of the Flack parameter[6].

Definitions:

$wR2 = [\Sigma[w(F_o^2-F_c^2)^2] / \Sigma[w(F_o^2)^2]]^{1/2}$

$R1 = \Sigma||F_o|-|F_c|| / \Sigma|F_o|$

$Goof = S = [\Sigma[w(F_o^2-F_c^2)^2] / (n-p)]^{1/2}$ where n is the number of reflections and p is the total number of parameters refined.

The thermal ellipsoid plot is shown at the 50% probability level.

Table 1. Crystal data and structure refinement for 3ba.

Identification code	4ah	
Empirical formula	C17 H18 S	
Formula weight	254.37	
Temperature	93(2) K	
Wavelength	0.71073 Å	
Crystal system	Orthorhombic	
Space group	$P2_12_12_1$	
Unit cell dimensions	a = 6.2171(9) Å	□ = 90°.
	b = 6.2816(9) Å	□ = 90°.
	c = 35.277(5) Å	□ = 90°.
Volume	1377.7(3) $Å^3$	
Z	4	
Density (calculated)	1.226 Mg/m^3	
Absorption coefficient	0.214 mm^{-1}	
F(000)	544	
Crystal color	colorless	
Crystal size	0.280 x 0.229 x 0.032 mm^3	
Theta range for data collection	2.309 to 28.298°	
Index ranges	$-8 \le h \le 8$, $-8 \le k \le 8$, $-46 \le l \le 47$	

Reflections collected	30744
Independent reflections	3434 [R(int) = 0.0458]
Completeness to theta = 25.242°	99.9 %
Absorption correction	Semi-empirical from equivalents
Max. and min. transmission	0.8621 and 0.8226
Refinement method	Full-matrix least-squares on F^2
Data / restraints / parameters	3434 / 0 / 165
Goodness-of-fit on F^2	1.081
Final R indices [I>2sigma(I) = 3191 data]	R1 = 0.0326, wR2 = 0.0760
R indices (all data, 0.75 Å)	R1 = 0.0369, wR2 = 0.0781
Absolute structure parameter	0.04(3)
Largest diff. peak and hole	0.241 and -0.246 e.Å^{-3}

Table 2. Atomic coordinates (x 10^4) and equivalent isotropic displacement parameters (Å^2 x 10^3)

for **3ba**. U(eq) is defined as one third of the trace of the orthogonalized U^{ij} tensor.

	x	y	z	U(eq)
S(1)	9342(1)	2927(1)	3128(1)	21(1)
C(1)	8283(3)	1175(3)	3474(1)	18(1)
C(2)	9892(3)	-19(3)	3712(1)	22(1)
C(3)	8440(3)	1592(3)	3902(1)	16(1)
C(4)	9501(3)	3630(3)	4036(1)	21(1)
C(5)	6565(3)	794(3)	4131(1)	15(1)
C(6)	5667(3)	-1212(3)	4062(1)	17(1)
C(7)	3904(3)	-1940(3)	4269(1)	19(1)
C(8)	2969(3)	-704(3)	4551(1)	20(1)
C(9)	3863(3)	1289(3)	4622(1)	21(1)

C(10)	5625(3)	2027(3)	4416(1)	19(1)
C(11)	1032(3)	-1499(4)	4771(1)	28(1)
C(12)	7299(3)	4873(3)	3071(1)	17(1)
C(13)	7705(3)	6477(3)	2805(1)	21(1)
C(14)	6168(3)	8028(4)	2735(1)	24(1)
C(15)	4226(4)	8018(3)	2931(1)	23(1)
C(16)	3839(3)	6439(3)	3198(1)	21(1)
C(17)	5357(3)	4856(3)	3269(1)	18(1)

Table 3. Bond lengths [Å] and angles [°] for 3ba.

S(1)-C(1)	1.771(2)
S(1)-C(12)	1.774(2)
C(1)-C(2)	1.507(3)
C(1)-C(3)	1.538(3)
C(2)-C(3)	1.513(3)
C(3)-C(5)	1.503(3)
C(3)-C(4)	1.516(3)
C(5)-C(10)	1.399(3)
C(5)-C(6)	1.399(3)
C(6)-C(7)	1.395(3)
C(7)-C(8)	1.388(3)
C(8)-C(9)	1.392(3)
C(8)-C(11)	1.517(3)
C(9)-C(10)	1.393(3)

C(12)-C(17)	1.395(3)
C(12)-C(13)	1.400(3)
C(13)-C(14)	1.387(3)
C(14)-C(15)	1.393(3)
C(15)-C(16)	1.388(3)
C(16)-C(17)	1.394(3)

C(1)-S(1)-C(12)	103.88(9)
C(2)-C(1)-C(3)	59.56(13)
C(2)-C(1)-S(1)	116.60(14)
C(3)-C(1)-S(1)	123.30(14)
C(1)-C(2)-C(3)	61.22(13)
C(5)-C(3)-C(2)	118.51(16)
C(5)-C(3)-C(4)	116.89(16)
C(2)-C(3)-C(4)	116.33(17)
C(5)-C(3)-C(1)	114.90(16)
C(2)-C(3)-C(1)	59.22(13)
C(4)-C(3)-C(1)	118.53(16)
C(10)-C(5)-C(6)	117.16(18)
C(10)-C(5)-C(3)	121.70(17)
C(6)-C(5)-C(3)	121.14(17)
C(7)-C(6)-C(5)	121.21(18)
C(8)-C(7)-C(6)	121.41(19)
C(7)-C(8)-C(9)	117.63(19)
C(7)-C(8)-C(11)	120.93(19)

C(9)-C(8)-C(11)	121.44(19)
C(8)-C(9)-C(10)	121.3(2)
C(9)-C(10)-C(5)	121.3(2)
C(17)-C(12)-C(13)	119.83(19)
C(17)-C(12)-S(1)	123.89(15)
C(13)-C(12)-S(1)	116.27(15)
C(14)-C(13)-C(12)	120.04(19)
C(13)-C(14)-C(15)	120.4(2)
C(16)-C(15)-C(14)	119.4(2)
C(15)-C(16)-C(17)	120.95(19)
C(16)-C(17)-C(12)	119.37(18)

Table 4. Anisotropic displacement parameters ($Å^2$ x 10^3) for 3ba. The anisotropic displacement factor exponent takes the form: $-2\pi^2[h^2 a^{*2} U^{11} + ... + 2 h k a^* b^* U^{12}]$

	U^{11}	U^{22}	U^{33}	U^{23}	U^{13}	U^{12}
S(1)	18(1)	26(1)	19(1)	2(1)	5(1)	0(1)
C(1)	18(1)	18(1)	16(1)	-1(1)	1(1)	0(1)
C(2)	19(1)	18(1)	29(1)	0(1)	2(1)	5(1)
C(3)	16(1)	14(1)	17(1)	0(1)	-3(1)	1(1)
C(4)	22(1)	18(1)	21(1)	-1(1)	-4(1)	-5(1)
C(5)	16(1)	14(1)	14(1)	1(1)	-4(1)	3(1)
C(6)	20(1)	15(1)	17(1)	-2(1)	-2(1)	3(1)
C(7)	20(1)	16(1)	22(1)	2(1)	-4(1)	-2(1)

C(8)	19(1)	24(1)	16(1)	5(1)	-2(1)	1(1)
C(9)	26(1)	22(1)	16(1)	-2(1)	1(1)	2(1)
C(10)	25(1)	14(1)	18(1)	-1(1)	-3(1)	2(1)
C(11)	25(1)	33(1)	25(1)	2(1)	4(1)	-2(1)
C(12)	20(1)	19(1)	12(1)	-2(1)	-3(1)	-3(1)
C(13)	24(1)	26(1)	13(1)	0(1)	1(1)	-9(1)
C(14)	34(1)	21(1)	17(1)	3(1)	-5(1)	-7(1)
C(15)	29(1)	20(1)	21(1)	-1(1)	-7(1)	-2(1)
C(16)	21(1)	22(1)	19(1)	-3(1)	-1(1)	-2(1)
C(17)	23(1)	18(1)	14(1)	0(1)	0(1)	-3(1)

Table 5. Hydrogen coordinates (x 10^4) and isotropic displacement parameters (Å^2 x 10^3) for 3ba.

	x	y	z	U(eq)
H(1A)	7002	330	3392	21
H(2A)	11430	355	3683	27
H(2B)	9611	-1545	3762	27
H(4A)	10727	3961	3872	31
H(4B)	10002	3449	4298	31
H(4C)	8458	4799	4026	31
H(6A)	6270	-2094	3871	21
H(7A)	3331	-3310	4217	23

H(9A)	3258	2163	4814	25
H(10A)	6199	3394	4471	23
H(11A)	716	-2970	4696	41
H(11B)	-214	-596	4714	41
H(11C)	1340	-1445	5043	41
H(13A)	9034	6503	2672	25
H(14A)	6441	9103	2552	29
H(15A)	3175	9083	2883	28
H(16A)	2520	6438	3334	25
H(17A)	5072	3775	3451	22

Table 6. Torsion angles [°] for 3ba.

C(12)-S(1)-C(1)-C(2)	-153.01(15)
C(12)-S(1)-C(1)-C(3)	-83.44(17)
S(1)-C(1)-C(2)-C(3)	114.70(17)
C(1)-C(2)-C(3)-C(5)	103.54(19)
C(1)-C(2)-C(3)-C(4)	-109.00(19)
C(2)-C(1)-C(3)-C(5)	-109.64(18)
S(1)-C(1)-C(3)-C(5)	146.75(15)
S(1)-C(1)-C(3)-C(2)	-103.61(18)
C(2)-C(1)-C(3)-C(4)	105.3(2)
S(1)-C(1)-C(3)-C(4)	1.7(3)
C(2)-C(3)-C(5)-C(10)	156.99(18)
C(4)-C(3)-C(5)-C(10)	9.7(3)
C(1)-C(3)-C(5)-C(10)	-135.95(19)
C(2)-C(3)-C(5)-C(6)	-23.9(3)
C(4)-C(3)-C(5)-C(6)	-171.17(17)
C(1)-C(3)-C(5)-C(6)	43.2(2)
C(10)-C(5)-C(6)-C(7)	0.3(3)
C(3)-C(5)-C(6)-C(7)	-178.90(17)
C(5)-C(6)-C(7)-C(8)	0.1(3)
C(6)-C(7)-C(8)-C(9)	-0.4(3)
C(6)-C(7)-C(8)-C(11)	179.07(18)
C(7)-C(8)-C(9)-C(10)	0.3(3)
C(11)-C(8)-C(9)-C(10)	-179.15(19)

C(8)-C(9)-C(10)-C(5)	0.0(3)
C(6)-C(5)-C(10)-C(9)	-0.3(3)
C(3)-C(5)-C(10)-C(9)	178.82(18)
C(1)-S(1)-C(12)-C(17)	-0.28(19)
C(1)-S(1)-C(12)-C(13)	-179.21(15)
C(17)-C(12)-C(13)-C(14)	-0.8(3)
S(1)-C(12)-C(13)-C(14)	178.16(16)
C(12)-C(13)-C(14)-C(15)	0.8(3)
C(13)-C(14)-C(15)-C(16)	-0.1(3)
C(14)-C(15)-C(16)-C(17)	-0.6(3)
C(15)-C(16)-C(17)-C(12)	0.5(3)
C(13)-C(12)-C(17)-C(16)	0.2(3)
S(1)-C(12)-C(17)-C(16)	-178.73(15)

APPENDIX 2

Supporting Information for Chapter 2

Dynamic Kinetic Resolution of Aldehydes via Intermolecular Hydroacylation

Table of Contents

1. General

Commercial reagents were purchased from Sigma Aldrich, Strem, Alfa Aesar, Acros Organics, Combi-blocks or TCI and used without further purification. 2-phenylpropanal (**1a**) was purchased from Sigma Alrich and distilled before use. Dichloroethane was purchased from Sigma Aldrich, distilled and stored over 3Å MS within a N_2 filled glove box. All experiments were performed in oven-dried or flame-dried glassware under an atmosphere of Ar or in a glove box with a N_2 atmosphere unless otherwise stated. Reactions were monitored using either thin-layer chromatography (TLC; EMD Silica Gel 60 F_{254} plates) or gas chromatography using an Agilent Technologies 7890A GC system equipped with an Agilent Technologies 5975C inert XL EI/CI

MSD. Visualization of the developed plates was performed under UV light (254 nm) or $KMnO_4$ stain. Organic solutions were concentrated under reduced pressure on a Büchi rotary evaporator. Purification and isolation of products were performed via silica gel chromatography (both column and preparative thin-layer chromatography). Column chromatography was performed with Silicycle Silica-P Flash Silica Gel using glass columns. Solvents were purchased from Sigma Aldrich. ^{1}H, ^{2}H, ^{13}C, and ^{19}F spectra were recorded on Bruker AVANCE-600, CRYO-500 or DRX-400 spectrometer. ^{1}H NMR spectra were internally referenced to the residual solvent signal or TMS. ^{2}H and ^{13}C NMR spectra were internally referenced to the residual solvent signal. Data for ^{1}H NMR are reported as follows: chemical shift (δ ppm), multiplicity (s = singlet, d = doublet, t = triplet, q = quartet, m = multiplet), coupling constant (Hz), integration. Data for ^{2}H, ^{13}C and ^{19}F NMR are reported in terms of chemical shift (δ ppm). Infrared (IR) spectra were obtained on a Nicolet iS5 FT-IR spectrometer with an iD5 ATR and are reported in terms of frequency of absorption (cm^{-1}). High resolution mass spectra (HRMS) were obtained on a micromass 70S-250 spectrometer (EI) or an ABI/Sciex QStar Mass Spectrometer (ESI). Enantiomeric excess (*ee*) for enantioselective reactions were determined by chiral SFC analysis using an Agilent Technologies HPLC (1200 series) system and Aurora A5 Fusion.

2. Optimization for DKR Hydroacylation

General procedure for racemic conditions: In a N_2-filled glovebox, Rh source (0.010 mmol, 10 mol %), **L1** (0.010 mmol, 10 mol %) and DCE (0.2 mL) were added to a 1-dram vial with a stir bar. After stirring for 5 min, acrylamide **2a** (0.10 mmol, 1.0 equiv) and aldehyde **1a** (20 μL, 20.1 mg, 0.15 mmol, 1.5 equiv) were added to the vial. The vial was sealed a Teflon-line screw cap and stirred at 80 °C for 24 h. The reaction mixture was then concentrated in vacuo. The diastereoselectivity was determined by ^{1}H NMR analysis of the unpurified reaction mixture. The

product was purified by preparative thin layer chromatography (hexanes/ethyl acetate 5:1) and isolated as a mixture of diastereomers.

[Rh(**L1**)Cl]$_2$ was prepared according to a reported method.[39]

Table S1. Screening conditions for Rh source for racemic condition.

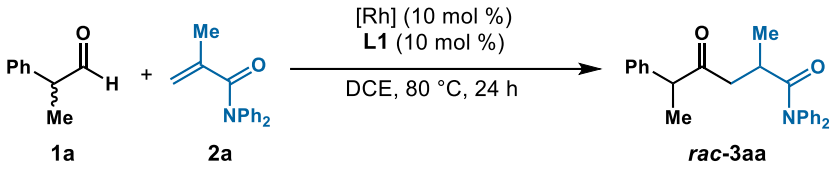

1a **2a** ***rac*-3aa**

entry	[Rh]	deviation	yield (%)	*dr*
1	$Rh(cod)_2SbF_6$	none	n.r.	-
2	$Rh(nbd)_2BF_4$	none	n.r.	-
3	$Rh(nbd)_2BF_4$	catalyst subjected to hydrogenation	67	2:1
4	[Rh(**L1**)Cl]$_2$	5 mol% Rh, no ligand, with 10 mol% $AgBF_4$	80	2:1
5	$[Rh(C_2H_4)_2Cl]_2$	5 mol% Rh, with 10 mol% $AgBF_4$	78	2:1

General procedure for asymmetric conditions: In a N_2-filled glovebox, $Rh(nbd)_2BF_4$ (7.4 mg, 0.020 mmol, 10 mol %), ligand (0.020 mmol, 10 mol %) and solvent (0.2 mL) were added to a 1-dram vial with a stir bar. After stirring at 60 °C for 5 min, the mixture was transferred to a Schlenk tube and washed with solvent (0.4 mL). The tube was sealed and removed from the glovebox and placed on a Schlenk line. The catalyst solution was subjected to two freeze-pump-thaw cycles and backfilled with H_2 gas. After stirring under H_2 atmosphere for 30 min at room temperature, the solvent was completely removed under vacuum. The tube was evacuated and backfilled with Ar. The catalyst was then transferred with solvent (0.4 mL) to a 10-mL Schlenk flask containing 1-$AdNH_2$ (3.0 mg, 0.020 mmol, 10 mol %), acrylamide **2a** (47.4 mg, 0.20 mmol, 1.0 equiv) and aldehyde **1a** (40 μL, 40.2 mg, 0.30 mmol, 1.5 equiv) via cannulation. The flask was sealed with a Teflon-line screw cap and stirred at 60 °C for 24 h. The reaction mixture was then concentrated in vacuo. The diastereoselectivity was determined by ^1H NMR analysis of the unpurified reaction mixture. The product was purified by preparative thin layer chromatography (hexanes/ethyl acetate 5:1) and isolated as a mixture of diastereomers.

Table S2. Screening conditions for asymmetric conditions.

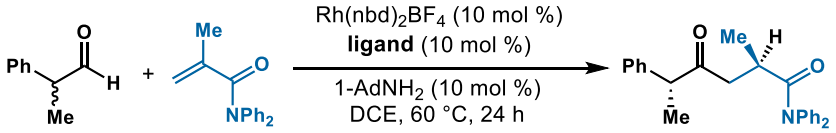

1a **2a** **3aa**

entry	ligand	deviation	yield (%)	*dr*	*ee* (%)
1	Me-DuPhos	none	n.r.	-	-
2	BINAP	none	n.r.	-	-
3	L2	none	n.r.	-	-
4	L2	80 °C	n.r.	-	-
5	L3	none	n.r.	-	-
6	L3	80 °C	37	-	98
7	L4	none	92	12:1	>99
8	L4	40 °C	42	14:1	>99
9	L4	10 mol % DPPA	68	9:1	>99
10	L4	10 mol % benzoic acid	20	9:1	>99
11	L4	10 mol % NaOTf	80	6:1	n.d.
12	L4	20 mol % 1-AdNH$_2$	48	12:1	>99
13	L4	toluene instead of DCE	n.r.	-	-
14	L4	MeNO$_2$ instead of DCE	n.r.	-	-
15	L4	MeCN instead of DCE	n.r.	-	-
16	L4	dioxane instead of DCE	n.r.	-	-
17	L4	THF instead of DCE	68	11:1	99
18	L4	1.0 euiqv **1a**, 1.2 equiv **2a**	58	7:1	99
19	L4	2.0 equiv **1a**, 1.0 equiv **2a**	75	11:1	>99

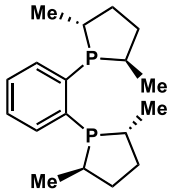

(*R*,*R*)-Me-DuPhos

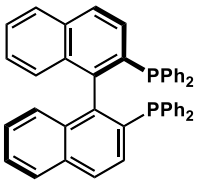

(*R*)-BINAP

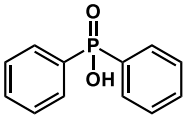

DPPA

3. General Procedure for DKR Hydroacylation

In a N_2-filled glovebox, $Rh(nbd)_2BF_4$ (7.4 mg, 0.020 mmol, 10 mol %), **L4** (9.9 mg, 0.020 mmol, 10 mol %) and DCE (0.2 mL) were added to a 1-dram vial with a stir bar. After stirring at 60 °C for 5 min, the mixture was transferred to a Schlenk tube and washed with DCE (0.4 mL). The tube was sealed and removed from the glovebox and placed on a Schlenk line. The catalyst solution was subjected to two freeze-pump-thaw cycles and backfilled with H_2 gas. After stirring under H_2 atmosphere for 30 min at room temperature, the solvent was completely removed under vacuum. The tube was evacuated and backfilled with Ar. The catalyst was then transferred with DCE (0.4 mL) to a 10-mL Schlenk flask containing 1-$AdNH_2$ (3.0 mg, 0.020 mmol, 10 mol %), acrylamide **2** (47 mg, 0.20 mmol, 1.0 equiv) and aldehyde **1** (40 μL, 40. mg, 0.30 mmol, 1.5 equiv) via cannulation. The flask was sealed with a Teflon-line screw cap and stirred at 60 °C for 24 h. The reaction mixture was then concentrated in vacuo. The diastereoselectivity was determined by ^1H NMR analysis of the unpurified reaction mixture. The product was purified by preparative thin layer chromatography (hexanes/ethyl acetate 5:1) and isolated as a mixture of diastereomers. The product mixture can be further recrystallized from hexanes and PhMe to isolate the major diastereomer **3**.

(2*R*,5*R*)-2-methyl-4-oxo-*N*,*N*,5-triphenylhexanamide (3aa)

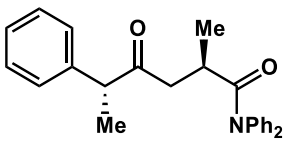

White solid, 92% yield, 12:1 *dr*, >99% *ee*, $[\alpha]^{23}_D$ = -15.3° (c 0.074, DCM). **^{1}H NMR** (600 MHz, $CDCl_3$) δ 7.63 – 7.28 (m, 10H), 7.26 – 7.23 (m, 2H), 7.21 – 7.12 (m, 3H), 3.78 (d, *J* = 7.0 Hz, 1H), 3.12 – 2.98 (m, 2H), 2.24 – 2.16 (m, 1H), 1.38 (d, *J* = 6.9 Hz, 3H), 0.97 (d, *J* = 6.7 Hz, 3H). **^{13}C NMR** (151 MHz, $CDCl_3$) δ 210.0, 176.4, 143.2, 141.1, 129.8, 129.3, 129.0, 128.7, 128.1, 128.1, 127.9, 127.2, 126.8, 126.2, 53.1, 45.6, 33.5, 17.6, 17.5. **IR** (ATR): 2979, 2932, 1704, 1662, 1590, 1489, 1450, 1392, 1268,

967, 754, 655, 623 cm^{-1}. **HRMS** calculated for $C_{25}H_{26}NO_2$ $[M+H]^+$ 372.1964, found 372.1964. **Chiral SFC**: 100 mm CHIRALCEL AD-H, 10% ^{i}PrOH, 2.5 mL/min, 220 nm, 44 °C, nozzle pressure = 200 bar CO_2, t_{R1} (major) = 3.6 min, t_{R2} = 4.5 min, t_{R3} (minor) = 6.0 min, t_{R4} = 15.4 min.

(2*R*,5*R*)-5-(4-methoxyphenyl)-2-methyl-4-oxo-*N*,*N*-diphenylhexanamide (3ba)

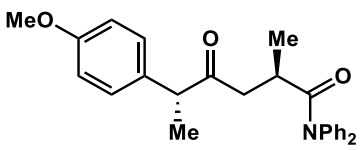

Colorless oil (mixture of diastereomers), 83% yield, 11:1 *dr*, >99% *ee*. **^{1}H NMR** (400 MHz, $CDCl_3$) δ 7.60 – 7.28 (m, 8H), 7.18 (bs, 2H), 7.13 – 7.06 (m, 2H), 6.84 (d, *J* = 8.6 Hz, 2H), 3.78 (s, 3H), 3.72 (q, *J* = 7.0 Hz, 1H), 3.10 – 2.98 (m, 2H), 2.25 – 2.15 (m, 1H), 1.35 (d, *J* = 6.9 Hz, 3H), 0.97 (d, *J* = 6.6 Hz, 3H). **^{13}C NMR** (151 MHz, $CDCl_3$) δ 210.3, 176.4, 158.8, 143.2, 143.2, 133.1, 129.7, 129.2, 129.1, 129.0, 127.9, 126.8, 126.1, 114.4, 55.4, 52.2, 45.5, 33.5, 17.6, 17.5. **IR** (ATR): 2931, 1710, 1663, 1510, 1491, 1394, 1246, 1178, 1032, 908, 757, 728, 701 cm^{-1}. **HRMS** calculated for $C_{26}H_{27}NO_3Na$ $[M+Na]^+$ 424.1889, found 424.1890. **Chiral SFC**: 100 mm CHIRALCEL AD-H, 10% ^{i}PrOH, 2.5 mL/min, 220 nm, 44 °C, nozzle pressure = 200 bar CO_2, t_{R1} (major) = 5.3 min, t_{R2} (minor) = 6.5 min, t_{R3} = 7.5 min, t_{R4} = 12.6 min.

(2*R*,5*R*)-5-(4-chlorophenyl)-2-methyl-4-oxo-*N*,*N*-diphenylhexanamide (3ca)

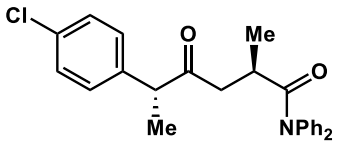

Yellow oil (mixture of diastereomers), 94% yield, 13:1 *dr*, >99% *ee*. **^{1}H NMR** (600 MHz, $CDCl_3$) δ 7.59 – 7.29 (m, 8H), 7.28 (d, *J* = 8.1 Hz, 2H), 7.23 (s, 2H), 7.13 (d, *J* = 8.0 Hz, 2H), 3.76 (q, *J* = 7.0 Hz, 1H), 3.13 – 3.00 (m, 2H), 2.21 – 2.13 (m, 1H), 1.36 (d, *J* = 6.9 Hz, 3H), 0.98 (d, *J* = 6.1 Hz, 3H). **^{13}C NMR** (151 MHz, $CDCl_3$) δ 209.6, 176.2, 143.1, 142.9, 139.4, 133.1, 129.7, 129.4, 129.2, 129.0, 128.9, 127.9, 126.7, 126.2, 52.3, 45.6, 33.5, 17.6, 17.4. **IR** (ATR): 2972, 2929, 1708, 1668, 1590, 1489, 1260, 1103, 795, 673 cm^{-1}. **HRMS** calculated for $C_{25}H_{24}ClNO_2Na$ $[M+Na]^+$ 428.1393, found 428.1408. **Chiral SFC**:

100 mm CHIRALCEL AD-H, 5% ^{i}PrOH, 2.5 mL/min, 220 nm, 44 °C, nozzle pressure = 200 bar CO_2, t_{R1} (major) = 16.3 min, t_{R2} (minor) = 19.5 min, t_{R3} = 21.7 min, t_{R4} = 28.9 min.

(2*R*,5*R*)-5-(4-bromophenyl)-2-methyl-4-oxo-*N*,*N*-diphenylhexanamide (3da)

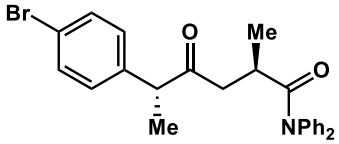

Pale yellow oil (mixture of diastereomers), 65% yield, 10:1 *dr*, >99% *ee*. **^{1}H NMR** (400 MHz, $CDCl_3$) δ 7.54 – 7.29 (m, 10H), 7.26 – 7.11 (m, 3H), 7.08 (d, J = 8.5 Hz, 2H), 3.75 (q, J = 6.9 Hz, 1H), 3.14 – 2.97 (m, 2H), 2.24 – 2.11 (m, 1H), 1.37 (d, J = 7.0 Hz, 3H), 0.99 (d, J = 6.7 Hz, 3H). **^{13}C NMR** (101 MHz, $CDCl_3$) δ 209.4, 176.2, 140.0, 132.1, 132.1, 129.8, 129.8, 129.0, 126.8, 121.2, 52.4, 45.7, 33.5, 17.6, 17.4. **IR** (ATR): 3066, 2971, 2929, 1708, 1667, 1590, 1489, 1451, 1260 cm^{-1}. **HRMS** calculated for $C_{25}H_{24}BrNO_2Na$ $[M+Na]^+$ 472.0888, found 472.0894. **Chiral SFC**: 100 mm CHIRALCEL AD-H, 7% ^{i}PrOH, 2.0 mL/min, 254 nm, 44 °C, nozzle pressure = 200 bar CO_2, t_{R1} (major) = 19.3 min, t_{R2} (minor) = 22.0 min, t_{R3} = 25.0 min, t_{R4} = 30.2 min.

(2*R*,5*R*)-2-methyl-4-oxo-*N*,*N*-diphenyl-5-(4-(trifluoromethyl)phenyl)hexanamide (3ea)

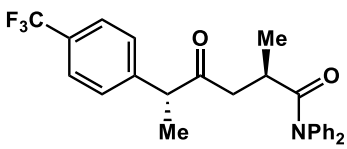

Pale yellow solid (mixture of diastereomers), 93% yield, 11:1 *dr*, >99% *ee*. **^{1}H NMR** (600 MHz, $CDCl_3$) δ 7.57 (d, *J* = 8.0 Hz, 2H), 7.47 (d, *J* = 54.8 Hz, 5H), 7.32 (d, *J* = 8.0 Hz, 4H), 7.25 – 7.12 (m, 3H), 3.86 (q, *J* = 6.9 Hz, 1H), 3.15 – 2.99 (m, 2H), 2.16 (dd, *J* = 17.0, 2.9 Hz, 1H), 1.41 (d, *J* = 7.0 Hz, 3H), 0.99 (d, *J* = 6.8 Hz, 3H). **^{13}C NMR** (151 MHz, $CDCl_3$) δ 209.2, 176.2, 144.9, 143.2, 143.1, 129.8, 129.6 (q, *J* = 32.1 Hz), 129.2, 129.0, 128.5, 128.0, 126.7, 126.2, 126.0 (q, *J* = 3.8 Hz), 124.2 (q, *J* = 272.0 Hz), 52.8, 45.8, 33.5, 17.6, 17.5. **^{19}F NMR** (565 MHz, $CDCl_3$) δ -62.49. **IR** (ATR): 2983, 2936, 1710, 1659, 1490, 1324, 1264, 1127, 1108, 1069, 760, 700, 693 cm^{-1}. **HRMS** calculated for $C_{26}H_{24}F_3NO_2Na$ $[M+Na]^+$ 462.1657, found 462.1675. **Chiral SFC**: 100 mm

CHIRALCEL AD-H, 4% ^{i}PrOH, 1.0 mL/min, 220 nm, 44 °C, nozzle pressure = 200 bar CO_2, t_{R1} (major) = 11.8 min, t_{R2} = 14.3 min, t_{R3} (minor) = 16.3 min, t_{R4} = 17.6 min.

(2*R*,5*R*)-5-(3-methoxyphenyl)-2-methyl-4-oxo-*N*,*N*-diphenylhexanamide (3fa)

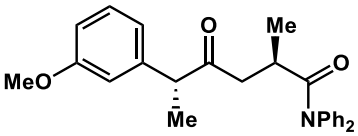

Pale yellow oil (mixture of diastereomers), 78% yield, 10:1 *dr*, >99% *ee*. **^{1}H NMR** (600 MHz, $CDCl_3$) δ 7.64 – 7.26 (m, 8H), 7.22 (dd, *J* = 8.2, 7.5 Hz, 2H), 7.19 – 7.15 (m, 1H), 6.80 – 6.76 (m, 2H), 6.74 – 6.71 (m, 1H), 3.78 (s, 3H), 3.75 (q, *J* = 7.0 Hz, 1H), 3.10 – 2.99 (m, 2H), 2.26 – 2.19 (m, 1H), 1.37 (d, *J* = 6.9 Hz, 3H), 0.98 (d, *J* = 6.7 Hz, 3H). **^{13}C NMR** (151 MHz, $CDCl_3$) δ 209.9, 176.4, 160.1, 143.0, 142.6, 130.0, 129.8, 129.8, 129.3, 129.0, 127.9, 126.8, 126.2, 120.5, 113.8, 112.5, 55.3, 53.1, 45.6, 33.5, 17.6, 17.4. **IR** (ATR): 3060, 2973, 2930, 2850, 1710, 1651, 1597, 1490, 1369, 1296 cm^{-1}. **HRMS** calculated for $C_{26}H_{28}NO_3$ $[M+H]^+$ 402.2069, found 402.2057. **Chiral SFC**: 100 mm CHIRALCEL AD-H, 20% ^{i}PrOH, 1.0 mL/min, 254 nm, 44 °C, nozzle pressure = 200 bar CO_2, t_{R1} (major) = 4.2 min, t_{R2} = 5.9 min, t_{R3} (minor) = 6.4 min, t_{R4} = 12.3 min.

(2*R*,5*R*)-5-(3-chlorophenyl)-2-methyl-4-oxo-*N*,*N*-diphenylhexanamide (3ga)

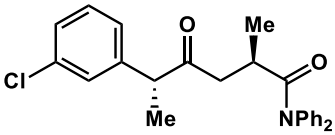

Pale yellow solid (mixture of diastereomers), 92% yield, 11:1 *dr*, >99% *ee*. **^{1}H NMR** (600 MHz, $CDCl_3$) δ 7.62 – 7.29 (m, 8H), 7.25 – 7.21 (m, 4H), 7.19 (s, 1H), 7.08 (d, *J* = 7.0 Hz, 1H), 3.76 (q, *J* = 7.4 Hz, 1H), 3.14 – 2.98 (m, 2H), 2.21 – 2.16 (m, 1H), 1.37 (d, *J* = 7.0 Hz, 3H), 0.99 (d, *J* = 6.5 Hz, 3H). **^{13}C NMR** (151 MHz, $CDCl_3$) δ 209.2, 176.2, 143.1, 142.9, 134.8, 130.3, 130.2, 129.7, 129.2, 129.0, 128.2, 127.9, 127.4, 126.7, 126.3, 126.2, 52.6, 45.7, 33.5, 17.5, 17.4. **IR** (ATR): 2975, 2932, 1713, 1663, 1593, 1490, 1394, 1265, 908, 756, 729, 699, 692 cm^{-1}. **HRMS** calculated for $C_{25}H_{24}ClNO_2Na$ $[M+Na]^+$

428.1393, found 428.1407. **Chiral SFC**: 100 mm CHIRALCEL AD-H, 10% ^{i}PrOH, 2.5 mL/min, 220 nm, 44 °C, nozzle pressure = 200 bar CO_2, t_{R1} (major) = 4.0 min, t_{R2} = 5.6 min, t_{R3} (minor) = 7.0 min, t_{R4} (minor) = 16.8 min.

(2*R*,5*R*)-2-methyl-4-oxo-*N*,*N*-diphenyl-5-(*o*-tolyl)hexanamide (3ha)

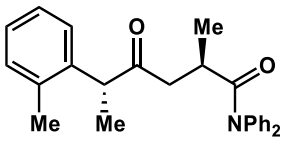

Pale yellow solid (mixture of diastereomers), 39% yield, 5:1 *dr*, 97% *ee*. **^{1}H NMR** (600 MHz, $CDCl_3$) δ 7.60 – 7.27 (m, 9H), 7.26 – 7.21 (m, 2H), 7.19 – 7.15 (m, 2H), 6.99 – 6.92 (m, 1H), 3.99 (q, *J* = 6.9 Hz, 1H), 3.10 – 3.06 (m, 1H), 2.96 (dd, *J* = 17.5, 10.7 Hz, 1H), 2.40 (s, 3H), 2.15 (dd, *J* = 17.7, 3.6 Hz, 1H), 1.33 (d, *J* = 6.9 Hz, 3H), 0.97 (d, *J* = 7.0 Hz, 3H). **^{13}C NMR** (151 MHz, $CDCl_3$) δ 210.6, 176.4, 143.2, 142.9, 139.6, 136.0, 131.0, 129.8, 129.2, 129.0, 127.9, 127.1, 127.1, 126.8, 126.7, 126.2, 49.1, 45.5, 33.6, 20.0, 17.6, 16.8. **IR** (ATR): 2971, 2926, 1710, 1668, 1592, 1490, 1386, 1264, 757, 728, 701, 692 cm^{-1}. **HRMS** calculated for $C_{26}H_{27}NO_2Na$ $[M+Na]^+$ 408.1939, found 408.1919. **Chiral SFC**: 100 mm CHIRALCEL OJ-H, 1% ^{i}PrOH, 2.0 mL/min, 220 nm, 44 °C, nozzle pressure = 200 bar CO_2, t_{R1} (minor) = 15.7 min, t_{R2} (major) = 21.3 min, t_{R3} = 24.8 min, t_{R4} = 27.2 min.

(2*R*,5*R*)-2-methyl-5-(naphthalen-2-yl)-4-oxo-*N*,*N*-diphenylhexanamide (3ia)

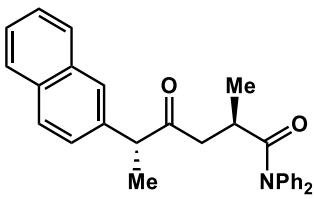

White solid (mixture of diastereomers), 86% yield, 13:1 *dr*, >99% *ee*. **^{1}H NMR** (500 MHz, $CDCl_3$) δ 7.85 – 7.78 (m, 3H), 7.69 (bs, 1H), 7.58 – 7.27 (m, 12H), 7.19 (s, 1H), 3.97 (q, *J* = 6.9 Hz, 1H), 3.13 (dd, *J* = 17.3, 10.6 Hz, 1H), 3.05 (ddd, *J* = 10.4, 6.8, 3.3 Hz, 1H), 2.22 (dd, *J* = 17.3, 3.2 Hz, 1H), 1.48 (d, *J* = 6.9 Hz, 3H), 0.95 (d, *J* = 6.8 Hz, 3H). **^{13}C NMR** (125 MHz, $CDCl_3$) δ 210.1, 176.4, 138.5,

133.7, 132.6, 129.2, 129.2, 128.8, 127.8, 127.8, 127.0, 126.8, 126.4, 126.1, 126.0, 126.0, 53.2, 45.8, 33.6, 17.6, 17.4. **IR** (ATR): 3057, 2974, 2931, 1708, 1664, 1591, 1490, 1452, 1387, 1264 cm^{-1}. **HRMS** calculated for $C_{29}H_{27}NO_2Na$ $[M+Na]^+$ 444.1939, found 444.1938. **Chiral SFC**: 250 mm CHIRALCEL AD-H, 20% ^{i}PrOH, 2.0 mL/min, 254 nm, 44 °C, nozzle pressure = 200 bar CO_2, t_{R1} (major) = 9.2 min, t_{R2} (minor) = 10.3 min, t_{R3} = 11.5 min, t_{R4} = 16.2 min.

(2*R*,5*R*)-5-(benzo[*d*][1,3]dioxol-5-yl)-2-methyl-4-oxo-*N*,*N*-diphenylhexanamide (3ja)

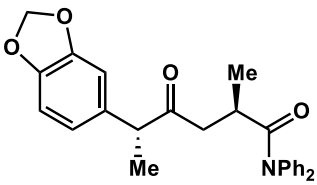

Pale yellow oil (mixture of diastereomers), 82% yield, 8:1 *dr*, >99% *ee*. **^{1}H NMR** (400 MHz, $CDCl_3$) δ 7.63 – 7.27 (m, 8H), 7.25 – 7.14 (m, 2H), 6.74 (d, *J* = 8.4 Hz, 1H), 6.69 – 6.65 (m, 2H), 5.95 – 5.91 (m, 2H), 3.70 (q, *J* = 6.9 Hz, 1H), 3.11 – 2.98 (m, 2H), 2.28 – 2.19 (m, 1H), 1.34 (d, *J* = 6.9 Hz, 3H), 0.99 (d, *J* = 6.7 Hz, 3H). **^{13}C NMR** (101 MHz, $CDCl_3$) δ 210.0, 176.3, 148.1, 146.8, 134.8, 129.2, 126.8, 126.8, 121.4, 108.7, 108.7, 108.2, 101.2, 52.6, 45.5, 33.5, 17.6, 17.5. **IR** (ATR): 2974, 2932, 2898, 1709, 1663, 1591, 1503, 1394 cm^{-1}. **HRMS** calculated for $C_{26}H_{25}NO_4Na$ $[M+Na]^+$ 438.1681, found 438.1682. **Chiral SFC**: 100 mm CHIRALCEL AD-H, 10% ^{i}PrOH, 2.0 mL/min, 254 nm, 44 °C, nozzle pressure = 200 bar CO_2, t_{R1} (major) = 7.3 min, t_{R2} = 8.8 min, t_{R3} (minor) = 11.4 min, t_{R4} = 15.2 min.

(2*S*,5*R*)-4-oxo-*N*,*N*,2,5-tetraphenylhexanamide (3ab)

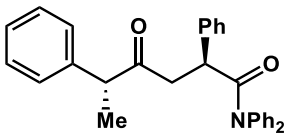

Pale yellow solid (mixture of diastereomers), 83% yield, 9:1 *dr*, >99% *ee*. **^{1}H NMR** (600 MHz, $CDCl_3$) δ 7.37 – 7.24 (m, 8H), 7.23 – 7.12 (m, 10H), 6.91 – 6.86 (m, 2H), 4.24 (dd, *J* = 11.2, 3.6 Hz, 1H), 3.88 (q, *J* = 6.9 Hz, 1H), 3.46 (dd, *J* = 17.8, 11.3 Hz, 1H), 2.36 (dd, *J* = 17.8, 3.5 Hz, 1H), 1.44 (d, *J* = 6.9 Hz, 3H). **^{13}C NMR** (151 MHz,

$CDCl_3$) δ 209.7, 172.7, 143.1, 142.3, 140.8, 138.7, 129.7, 129.4, 129.0, 128.9, 128.7, 128.6, 128.1, 127.9, 127.9, 127.2, 126.5, 126.2, 53.2, 46.9, 46.1, 17.5. **IR** (ATR): 3060, 1027, 2977, 2935, 2908, 1710, 1663, 1596, 1490, 1451 cm^{-1}. **HRMS** calculated for $C_{30}H_{28}NO_2$ $[M+H]^+$ 434.2120, found 434.2125. **Chiral SFC**: 100 mm CHIRALCEL AD-H, 3% ^{i}PrOH, 2.0 mL/min, 254 nm, 44 °C, nozzle pressure = 200 bar CO_2, t_{R1} = 13.6 min, t_{R2} (major) = 16.6 min, t_{R3} (minor) = 20.1 min, t_{R4} = 26.4 min.

(2*R*,5*R*)-2-benzyl-4-oxo-*N*,*N*,5-triphenylhexanamide (3ac)

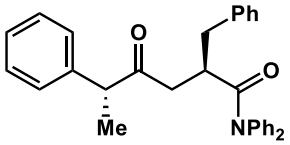

Pale yellow oil (mixture of diastereomers), 91% yield, 9:1 *dr*, 96% *ee*. **^{1}H NMR** (400 MHz, $CDCl_3$) δ 7.35 – 7.13 (m, 18H), 6.82 – 6.67 (m, 2H), 3.30 – 3.17 (m, 1H), 3.02 (dd, *J* = 17.4, 9.8 Hz, 1H), 2.89 (dd, *J* = 13.3, 6.7 Hz, 1H), 2.46 (dd, *J* = 13.2, 8.0 Hz, 1H), 2.31 (dd, *J* = 17.5, 4.4 Hz, 1H), 1.38 (d, *J* = 6.9 Hz, 3H). **^{13}C NMR** (151 MHz, $CDCl_3$) δ 210.0, 174.8, 143.2, 142.7, 140.6, 138.7, 133.2, 129.6, 129.2, 129.0, 128.7, 128.5, 128.4, 128.1, 127.9, 127.2, 126.8, 126.6, 53.2, 43.6, 40.8, 38.7, 17.5. **IR** (ATR): 3027, 2973, 2930, 1708, 1663, 1490, 1394 cm^{-1}. **HRMS** calculated for $C_{31}H_{29}NO_2Na$ $[M+Na]^+$ 470.2096, found 470.2094. **Chiral SFC**: 100 mm CHIRALCEL AD-H, 20% ^{i}PrOH, 2.0 mL/min, 254 nm, 44 °C, nozzle pressure = 200 bar CO_2, t_{R1} (major) = 3.3 min, t_{R2} = 3.9 min, t_{R3} (minor) = 6.8 min, t_{R4} = 15.4 min.

(*R*)-4-oxo-*N*,*N*,5-triphenylhexanamide (3ad)

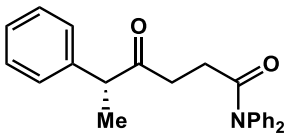

Pale yellow oil (mixture of diastereomers), 45% yield, 79% *ee*. **^{1}H NMR** (400 MHz, $CDCl_3$) δ 7.43 – 7.26 (m, 10H), 7.26 – 7.17 (m, 5H), 3.84 (q, *J* = 7.1 Hz, 1H), 2.91 – 2.78 (m, 1H), 2.62 – 2.47 (m, 2H), 2.38 – 2.24 (m, 1H), 1.41 (d, *J* = 7.0 Hz, 3H). **^{13}C NMR** (151 MHz, $CDCl_3$) δ 210.1, 172.1, 142.8, 140.9, 129.8, 129.1, 129.0, 128.1,

127.6, 127.3, 127.2, 127.2, 126.8, 126.5, 53.1, 36.3, 29.9, 17.5. **IR** (ATR): 3060, 2974, 2930, 1710, 1668, 1594, 1491, 1374, 1271 cm^{-1}. **HRMS** calculated for $C_{24}H_{23}NO_2Na$ $[M+Na]^+$ 380.1627, found 380.1630. **Chiral SFC**: 100 mm CHIRALCEL AD-H, 10% ^{i}PrOH, 2.0 mL/min, 254 nm, 44 °C, nozzle pressure = 200 bar CO_2, t_{R1} (minor) = 8.0 min, t_{R2} (major) = 9.7 min.

(2*R*,5*R*)-2-methyl-1-morpholino-5-phenylhexane-1,4-dione (3ae)

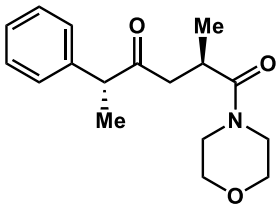

Yellow oil (mixture of diastereomers), 53% yield, 11:1 *dr*, 97% *ee*. **^{1}H NMR** (600 MHz, $CDCl_3$) δ 7.32 (t, *J* = 7.5 Hz, 2H), 7.24 (d, *J* = 7.6 Hz, 1H), 7.22 – 7.18 (m, 2H), 3.78 (q, *J* = 7.0 Hz, 1H), 3.75 – 3.41 (m, 8H), 3.12 (m, 1H), 2.97 (dd, *J* = 17.8, 9.0 Hz, 1H), 2.31 (dd, *J* = 17.8, 4.3 Hz, 1H), 1.35 (d, *J* = 6.8 Hz, 3H), 0.95 (d, *J* = 6.9 Hz, 3H). **^{13}C NMR** (151 MHz, $CDCl_3$) δ 210.0, 174.5, 140.8, 129.1, 128.1, 127.3, 67.1, 66.9, 53.1, 46.3, 45.3, 42.4, 31.0, 17.5, 17.3. **IR** (ATR): 2991, 2930, 2855, 1710, 1635, 1435, 1233, 1113, 1030, 701 cm^{-1}. **HRMS** calculated for $C_{17}H_{23}NO_2Na$ $[M+Na]^+$ 312.1576, found 312.1561. **Chiral SFC**: 100 mm CHIRALCEL AD-H, 6% ^{i}PrOH, 1.0 mL/min, 220 nm, 44 °C, nozzle pressure = 200 bar CO_2, t_{R1} (minor) = 8.0 min, t_{R2} = 9.3 min, t_{R3} = 10.5 min, t_{R4} (major) = 14.2 min.

(2*R*,5*R*)-*N*,*N*-dibenzyl-2-methyl-4-oxo-5-phenylhexanamide (3af)

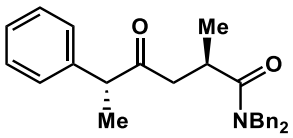

Colorless oil (mixture of diastereomers), 75% yield, 8:1 *dr*, >99% *ee*. **^{1}H NMR** (400 MHz, $CDCl_3$) δ 7.42 – 7.27 (m, 10H), 7.25 – 7.14 (m, 5H), 4.66 – 4.51 (m, 4H), 3.82 (q, *J* = 6.9 Hz, 1H), 3.33 – 3.20 (m, 1H), 3.06 (dd, *J* = 17.5, 9.3 Hz, 1H), 2.34 (dd, *J* = 17.6, 4.4 Hz, 1H), 1.39 (d, *J* = 6.9 Hz, 3H), 0.98 (d, *J* = 6.9 Hz, 3H). **^{13}C NMR** (101 MHz, $CDCl_3$) δ 210.0, 176.6, 140.9, 137.6, 136.9, 129.1, 129.0, 128.7, 128.2, 128.1, 127.7, 127.4,

127.3, 127.1, 53.3, 50.2, 48.3, 46.0, 32.0, 18.0, 17.5. **IR** (ATR): 3027, 2971 2930, 1710, 1636, 1494, 1452, 1223, 730, 697 cm^{-1}. **HRMS** calculated for $C_{27}H_{29}NO_2Na$ $[M+Na]^+$ 422.2096, found 422.2115. **Chiral SFC**: 100 mm CHIRALCEL OJ-H, 1% ^{i}PrOH, 2.0 mL/min, 220 nm, 44 °C, nozzle pressure = 200 bar CO_2, t_{R1} = 10.9 min, t_{R2} (major) = 12.1 min, t_{R3} (minor) = 17.2 min, t_{R4} = 28.9 min.

(2*R*,5*R*)-2-methyl-4-oxo-*N*,5-diphenylhexanamide (3ag)

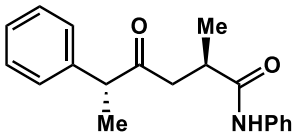

Yellow solid (mixture of diastereomers), 61% yield, 6:1 *dr*, 95% *ee*. **^{1}H NMR** (600 MHz, $CDCl_3$) δ 7.66 (s, 1H), 7.54 – 7.47 (m, 2H), 7.36 – 7.27 (m, 5H), 7.23 – 7.18 (m, 2H), 7.08 (t, *J* = 7.4 Hz, 1H), 3.77 (q, *J* = 6.9 Hz, 1H), 2.93 (dd, *J* = 18.1, 9.4 Hz, 1H), 2.89 – 2.79 (m, 1H), 2.43 (dd, *J* = 18.1, 3.8 Hz, 1H), 1.38 (d, *J* = 7.0 Hz, 3H), 1.10 (d, *J* = 6.9 Hz, 3H). **^{13}C NMR** (151 MHz, $CDCl_3$) δ 210.5, 174.0, 140.5, 138.2, 129.2, 129.1, 128.0, 127.5, 124.2, 120.0, 53.2, 45.4, 37.1, 17.8, 17.4. **IR** (ATR): 3306, 3061, 2972, 2931, 1712, 1667, 1598, 1541, 1493, 1441, 731, 693 cm^{-1}. **HRMS** calculated for $C_{19}H_{21}NO_2Na$ $[M+Na]^+$ 318.1470, found 318.1459. **Chiral SFC**: 100 mm CHIRALCEL AD-H, 6% ^{i}PrOH, 2.0 mL/min, 240 nm, 44 °C, nozzle pressure = 200 bar CO_2, t_{R1} = 11.1 min, t_{R2} = 12.0 min, t_{R3} (minor) = 15.0 min, t_{R2} (major) = 18.6 min.

(2*R*,5*R*)-*N*-methoxy-*N*,2-dimethyl-4-oxo-5-phenylhexanamide (3ah)

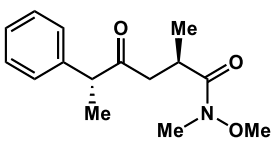

Yellow oil (mixture of diastereomers), 65% yield, 9:1 *dr*, >99% *ee*. **TLC** **R_f** = 0.3 (hexanes/ethyl acetate 5:1). **^{1}H NMR** (500 MHz, $CDCl_3$) δ 7.33 (t, *J* = 7.4 Hz, 2H), 7.27 (d, *J* = 7.7 Hz, 1H), 7.22 (d, *J* = 6.9 Hz, 2H), 3.84 – 3.76 (m, 4H), 3.27 (s, 1H), 3.20 (s, 3H), 2.95 (dd, *J* = 17.9, 9.7 Hz, 1H), 2.30 (dd, *J* = 17.9, 4.4 Hz, 1H), 1.37 (d, *J* = 6.8

Hz, 3H), 0.99 (d, *J* = 7.0 Hz, 3H). **^{13}C NMR** (151 MHz, $CDCl_3$) δ 209.9, 176.6, 140.9, 129.0, 128.0, 127.2, 61.4, 53.0, 44.7, 32.2, 31.4, 17.4, 17.1. **IR** (ATR): 2973, 2933, 1712, 1652, 1453, 1353, 992, 731, 701 cm^{-1}. **HRMS** calculated for $C_{15}H_{22}NO_3$ $[M+H]^+$ 264.1600, found 264.1598. **Chiral SFC**: 100 mm CHIRALCEL AD-H, 4% ^{i}PrOH, 1.0 mL/min, 220 nm, 44 °C, nozzle pressure = 200 bar CO_2, t_{R1} (minor) = 4.6 min, t_{R2} = 6.4 min, t_{R3} = 11.2 min, t_{R4} (major) = 18.6 min.

4. Synthesis of Aldehyde Substrates

General procedure A

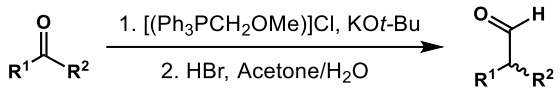

The reaction was performed according to the following procedures.[40a-d]

(Methoxymethyl)-triphenylphosphonium chloride (5.2 mmol, 1.4 equiv) was suspended in anhydrous THF (8 mL) and the mixture was cooled to 0 ℃. Potassium *tert*-butoxide (5.2 mmol, 1.4 equiv) was added under positive pressure and the reaction mixture turned dark red. The reaction was stirred at 0 ℃ for 30 min and the ketone (3.7 mmol, 1.0 equiv) was added dropwise. After stirring overnight, the reaction was quenched with addition of water and extracted with Et_2O (3 × 50 mL). The combined organic solutions were dried over Na_2SO_4, filtered, and concentrated. The resulting oil was purified by flash column chromatography (silica gel, 2.5% EtOAc/Hex) to afford enol ether in mostly 1:1 ratio of *E*/*Z* isomers.

Enol ether was dissolved in a 4:1 mixture of acetone and water (8 mL) and the solution was cooled to 0 ℃. Conc. HBr (48% aqueous solution, 3 mL) was added dropwise, and the mixture was allowed to warm up to room temperature and stirred overnight. The reaction was quenched with sat. $NaHCO_3$ and the solution was extracted with DCM (3 × 20 mL). The combined organic layers

were dried over Na_2SO_4, filtered and concentrated. The resulting oil was purified by flash column chromatography (silica gel, 5% ethyl acetate/hexanes) to afford aldehyde **1**.

2-(4-methoxyphenyl)propanal (1b)

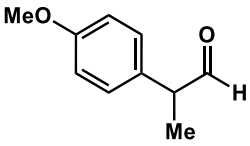

Prepared according to General Procedure A. Colorless oil, 35% yield over two steps. **^{1}H NMR** (400 MHz, $CDCl_3$) δ 9.65 (d, *J* = 1.5 Hz, 1H), 7.17 – 7.09 (m, 2H), 6.95 – 6.87 (m, 2H), 3.81 (s, 3H), 3.58 (qd, *J* = 7.1, 1.5 Hz, 1H), 1.41 (d, *J* = 7.0 Hz, 3H). The ^{1}H NMR spectrum is in accordance with the previous literature.[40a-d]

2-(4-chlorophenyl)propanal (1c)

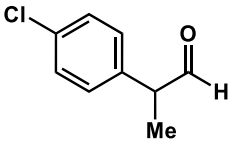

Prepared according to General Procedure A. Colorless oil, 24% yield over two steps. **^{1}H NMR** (400 MHz, $CDCl_3$) δ 9.66 (d, *J* = 1.4 Hz, 1H), 7.39 – 7.31 (m, 2H), 7.19 – 7.11 (m, 2H), 3.62 (qd, *J* = 7.1, 1.4 Hz, 1H), 1.44 (d, *J* = 7.1 Hz, 3H). The ^{1}H NMR spectrum is in accordance with the previous literature.[40a,b]

2-(4-(trifluoromethyl)phenyl)propanal (1e)

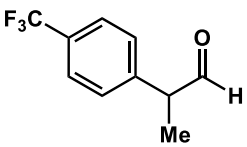

Prepared according to General Procedure A. Colorless oil, 17% yield over two steps.**^{1}H NMR** (400 MHz, $CDCl_3$) δ 9.70 (d, *J* = 1.3 Hz, 1H), 7.65 (d, *J* = 8.0 Hz, 2H), 7.35 (d, *J* = 8.0 Hz, 2H), 3.73 (qd, *J* = 7.1, 1.3 Hz, 1H), 1.49 (d, *J* = 7.1 Hz, 3H). The ^{1}H NMR spectrum is in accordance with the previous literature.[40a,b]

2-(3-chlorophenyl)propanal (1g)

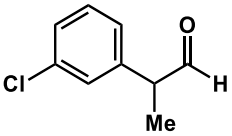

Prepared according to General Procedure A. Colorless oil, 35% yield over two steps. **^{1}H NMR** (400 MHz, $CDCl_3$) δ 9.67 (d, *J* = 1.4 Hz, 1H), 7.37 – 7.27 (m, 2H), 7.22 (dt, *J* = 2.3, 1.0 Hz, 1H), 7.17 – 7.06 (m, 1H), 3.62 (qd, *J* = 7.1, 1.4 Hz, 1H), 1.45 (d, *J* = 7.1 Hz, 3H). The ^{1}H NMR spectrum is in accordance with the previous literature.[40d]

2-(o-tolyl)propanal (1h)

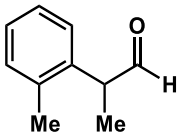

Pale yellow oil, 25% yield over two steps. **^{1}H NMR** (400 MHz, $CDCl_3$) δ 9.67 (d, *J* = 1.2 Hz, 1H), 7.26 – 7.16 (m, 3H), 7.08 – 7.01 (m, 1H), 3.85 (qd, *J* = 7.0, 1.3 Hz, 1H), 2.37 (s, 3H), 1.42 (d, *J* = 7.0 Hz, 3H). The ^{1}H NMR spectrum is in accordance with the previous literature.[40d]

3-methyl-2-phenylbutanal (1k)

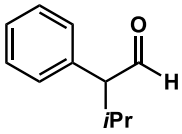

Colorless oil, 73% over two steps. **^{1}H NMR** (400 MHz, $CDCl_3$) δ 9.72 (d, *J* = 3.3 Hz, 1H), 7.41 – 7.35 (m, 2H), 7.34 – 7.27 (m, 1H), 7.24 – 7.17 (m, 3H), 3.21 (dd, *J* = 9.5, 3.3 Hz, 1H), 2.53 – 2.38 (m, 1H), 1.07 (d, *J* = 6.6 Hz, 3H), 0.79 (d, *J* = 6.7 Hz, 3H). The ^{1}H NMR spectrum is in accordance with the previous literature.[40e]

General procedure B:

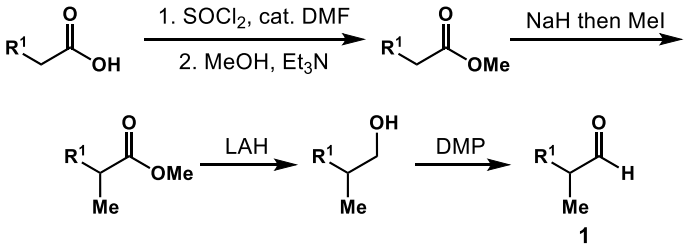

The reaction was performed according to the following procedure.[40a,f]

The carboxylic acid (14 mmol, 1.0 equiv) was dissolved in DCM (14 mL) and thionyl chloride (42 mmol, 3.0 equiv) and DMF (0.14 mmol, 10 mol %) was added to the solution. After stirring at room temperature for 1 h, the solvent was removed in vacuo to give the acid chloride, which was used without further purification. The acid chloride was redissolved in DCM (9.8 mL) and MeOH (4.2 mL). Et_3N (28 mmol, 2.0 equiv) was added dropwise, and the solution was stirred overnight at room temperature. The reaction mixture was concentrated and then dissolved in Et_2O. The mixture was washed with sat. $NaHCO_3$ solution, brine, and then water. The organic layer was dried over $MgSO_4$, and concentrated to give the ester which was used without purification.

NaH (13 mmol, 1.1 equiv) as a 60% dispersion in mineral oil was suspended in DMF (23 mL), the resulting slurry was cooled to 0 °C. The ester (12 mmol, 1.0 equiv) was added dropwise and the reaction was stirred for 5 min. MeI (13 mmol, 1.1 equiv) was added dropwise and the reaction was allowed to warm to room temperature and stirred overnight. The reaction was quenched with sat. NH_4Cl and diluted with Et_2O. The layers were separated, and the aqueous layer was extracted with Et_2O (3 × 50 mL). The combined organic layers were dried over $MgSO_4$, filtered, and concentrated. The resulting oil was purified by flash column chromatography (silica gel, 6% ethyl acetate/hexanes) to afford α-branched ester.

LAH (21 mmol, 2.2 equiv) was suspended in THF (20 mL) and cooled to 0 °C. The carboxylic acid (9.0 mmol, 1.0 equiv) was dissolved in THF (25 mL) and added to the LAH solution. The reaction was allowed to warm up to room temperature and stirred for 1 h. Then, the reaction was cooled to 0 °C again and quenched with dropwise addition of water, then 15% KOH, and then water. The mixture was stirred for 15 min, and white precipitate formed. $MgSO_4$ was added and mixture was filtered through Celite, concentrated to give the alcohol which was used without purification.

Alcohol (5.7 mmol, 1.0 equiv) and pyridine (9.1 mmol, 1.6 equiv) were dissolved in DCM (23 mL) and the solution was cooled to 0 °C. DMP (9.7 mmol, 1.7 equiv) was added in one portion under positive pressure. The reaction was stirred at room temperature for 2.5 h and then quenched by addition of sat. $Na_2S_2O_3$. The mixture was stirred for 15 min and the layers were separated. The aqueous layer was extracted with DCM (3 × 50 mL) and the combined organic layers were dried over MgSO4, filtered and concentrated. The resulting oil was purified by flash column chromatography (15% E_2O/hexanes) to afford the aldehyde **1**.

2-(4-bromophenyl)propanal (1d)

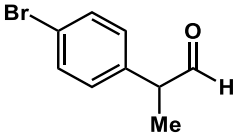

Prepared according to General Procedure B. Pale yellow oil, 5% yield over four steps. **^{1}H NMR** (400 MHz, $CDCl_3$) δ 9.66 (d, *J* = 1.4 Hz, 1H), 7.56 – 7.47 (m, 2H), 7.13 – 7.05 (m, 2H), 3.60 (qd, *J* = 7.1, 1.4 Hz, 1H), 1.44 (d, *J* = 7.1 Hz, 3H). The ^{1}H NMR spectrum is in accordance with the previous literature.[40a,b]

2-(3-methoxyphenyl)propanal (1f)

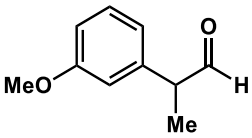

Prepared according to General Procedure B. Colorless oil, 26% yield over four steps. **^{1}H NMR** (400 MHz, $CDCl_3$) δ 9.68 (d, *J* = 1.5 Hz, 1H), 7.30 (t, *J* = 7.9 Hz, 1H), 6.88 – 6.77 (m, 2H), 6.75 (t, *J* = 2.2 Hz, 1H), 3.81 (s, 3H), 3.69 – 3.54 (m, 1H), 1.44 (d, *J* = 7.1 Hz, 3H). The ^{1}H NMR spectrum is in accordance with the previous literature.[40g]

2-(naphthalen-2-yl)propanal (1i)

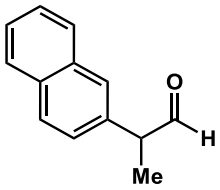

Prepared according to General Procedure B. White solid, 30% yield over four steps.**^{1}H NMR** (400 MHz, $CDCl_3$) δ 9.77 (dd, *J* = 1.4, 0.6 Hz, 1H), 7.90 – 7.79 (m, 3H), 7.68 (s, 1H), 7.53 – 7.44 (m, 2H), 7.32 (dd, *J* = 8.4, 1.8 Hz, 1H), 3.81 (q, *J* = 6.9 Hz, 1H), 1.55 (dd, *J* = 7.0, 0.6 Hz, 3H). The ^{1}H NMR spectrum is in accordance with the previous literature.[40a-d]

2-(benzo[*d*][1,3]dioxol-5-yl)propanal (1j)

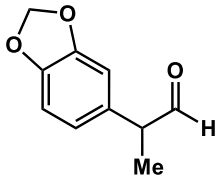

Prepared according to General Procedure B. Colorless oil, 24% yield over four steps. **^{1}H NMR** (400 MHz, $CDCl_3$) δ 9.64 (d, *J* = 1.5 Hz, 1H), 6.81 (dd, *J* = 7.8, 0.6 Hz, 1H), 6.71 – 6.63 (m, 2H), 5.96 (s, 2H), 3.48 (q, *J* = 7.0 Hz, 1H), 1.40 (dd, *J* = 7.1, 1.5 Hz, 3H). The ^{1}H NMR spectrum is in accordance with the previous literature.[40a,b]

2-cyclohexylpropanal (1l)

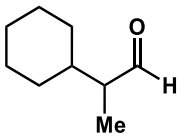

Prepared according to General Procedure B (Esterification was done with LiHMDS (1.0 M in THF) in place of NaH.).[5] Colorless oil, 26% yield over four steps. **^{1}H NMR** (400 MHz, $CDCl_3$) δ 9.66 (d, *J* = 2.3 Hz, 1H), 2.27 – 2.16 (m, 1H), 1.82 – 1.57 (m, 6H), 1.37 – 1.06 (m, 5H), 1.04 (d, *J* = 7.0 Hz, 3H). The ^{1}H NMR spectrum is in accordance with the previous literature.[40c]

5. Synthesis of Acrylamide Substrates

General Procedure C:

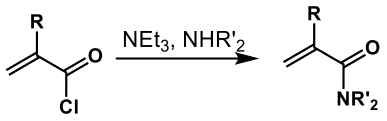

The reaction was performed according to the following procedure.[41a]

Secondary amine (29 mmol, 1.5 equiv), triethylamine (5.3 mL, 3.9 g, 38 mmol, 2.0 equiv) was dissolved in DCM (50 mL) and cooled to 0 °C. Acryloyl chloride (19 mmol, 1.0 equiv) was added dropwise and the reaction was allowed to warm up to room temperature and stirred for 16 h. The reaction was cooled to 0 °C and quenched with sat. NH_4Cl. The layers were separated, and the aqueous layer was extracted with DCM (3 × 30 mL). The combined organic layers were dried over MgSO4, filtered, and concentrated. The resulting oil was purified by flash column chromatography (silica gel, 2–10% ethyl acetate/hexanes). **2a** and **2d** were purified with another recrystallization from hexanes and PhMe at 0 °C to afford the acrylamide.

***N,N*-diphenylmethacrylamide (2a)**

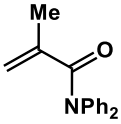

Prepared according to General Procedure C. White solid, 67% yield. **^{1}H NMR** (400 MHz, $CDCl_3$) δ 7.44 – 7.05 (m, 10H), 5.24 (s, 1H), 5.18 (s, 1H), 1.85 (s, 3H). The ^{1}H NMR spectrum is in accordance with the previous literature.[41b]

***N,N*-diphenylacrylamide (2d)**

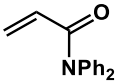

Prepared according to General Procedure C. White solid, 69% yield. **^{1}H NMR** (500 MHz, $CDCl_3$) δ 7.37 (t, *J* = 7.7 Hz, 4H), 7.27 – 7.21 (m, 6H), 6.47 (ddd, *J* = 16.8, 2.0,

0.7 Hz, 1H), 6.27 – 6.13 (m, 1H), 5.63 (ddd, *J* = 10.3, 2.0, 0.7 Hz, 1H). The ^{1}H NMR spectrum is in accordance with the previous literature.[41c]

2-methyl-1-morpholinoprop-2-en-1-one (2e)

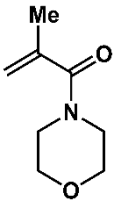

Prepared according to General Procedure C. Yellow oil, 51% yield. **^{1}H NMR** (400 MHz, $CDCl_3$) δ 5.21 (dt, *J* = 2.8, 1.4 Hz, 1H), 5.04 (p, *J* = 1.1 Hz, 1H), 3.78 – 3.52 (m, 8H), 1.95 (dd, *J* = 1.7, 1.1 Hz, 3H). The ^{1}H NMR spectrum is in accordance with the previous literature.[41d]

***N*,*N*-dibenzylmethacrylamide (2f)**

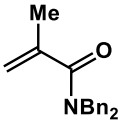

Prepared according to General Procedure C. Brown oil, 57% yield. **^{1}H NMR** (400 MHz, $CDCl_3$) δ 7.32 (m, 6H), 7.17 (m, 4H), 5.18 (dt, *J* = 2.8, 1.3 Hz, 1H), 5.15 (p, *J* = 1.1 Hz, 1H), 4.54 (s, 4H), 2.03 (dd, *J* = 1.7, 1.1 Hz, 3H). The ^{1}H NMR spectrum is in accordance with the previous literature.[41e]

***N*-methoxy-*N*-methylmethacrylamide (2h)**

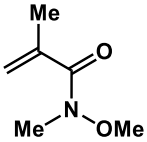

Prepared according to General Procedure C (Pyridine (4 equiv) was used in place of triethylamine.). Colorless oil, 35% yield. **^{1}H NMR** (400 MHz, $CDCl_3$) δ 5.31 – 5.28 (m, 1H), 5.25 – 5.21 (m, 1H), 3.65 (s, 3H), 3.23 (s, 3H), 1.98 – 1.97 (m, 2H). The ^{1}H NMR spectrum is in accordance with the previous literature.[41f]

General Procedure D:

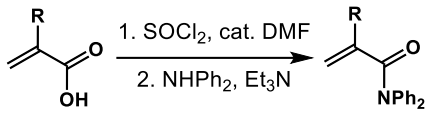

The reaction was performed according to the following procedure.[41a]

The carboxylic acid (9 mmol, 1.0 equiv) was dissolved in DCM (17 mL) and thionyl chloride (1.3 mL, 2.1 g, 18 mmol, 2.0 equiv) and DMF (6.9 µL, 6.5 mg, 0.090 mmol, 10 mol %) were added to the solution. The reaction was allowed to stir at room temperature for 1 h and the solvent was removed in vacuo to give acryloyl chloride as a pale yellow oil, which was used without further purification.

Diphenylamine (2.3 g, 13 mmol, 1.5 equiv) was dissolved in DCM and Et_3N (2.5 mL, 1.8 g, 18 mmol, 2.0 equiv) was added. The solution was cooled to 0 °C. Acryloyl chloride was added dropwise and the color changed from colorless to orange. The reaction was stirred overnight at room temperature and quenched with water. The layers were separated and then extracted with DCM (3 × 40 mL). The combined organic layers were washed with sat. $NaHCO_3$ and brine, dried over $MgSO_4$, filtered and concentrated. The product was purified by flash column chromatography (5% ethyl acetate/hexanes) then recrystallization from hexanes and PhMe at 0 °C to afford the acrylamide **2**.

2-phenyl-*N*,*N*-diphenylacrylamide (2b)

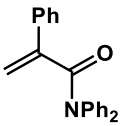

Prepared according to General Procedure D. Yellow solid, 30% yield over two steps. **^{1}H NMR** (400 MHz, $CDCl_3$) δ 7.53 – 6.93 (m, 15 H), 5.63 (s, 1H), 5.55 (s, 1H). The ^{1}H NMR spectrum is in accordance with the previous literature.[41g]

2-benzyl-*N*,*N*-diphenylacrylamide (2c)

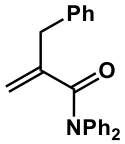

Prepared according to General Procedure D. White solid, 50% yield over two steps. **^{1}H NMR** (400 MHz, $CDCl_3$) δ 7.34 – 7.08 (m, 11H), 6.99 – 6.89 (m, 4H), 5.30 (q, *J* = 0.9 Hz, 1H), 5.15 (td, *J* = 1.6, 0.8 Hz, 1H), 3.49 (s, 2H). The ^{1}H NMR spectrum is in accordance with the previous literature.[41h]

Efforts Towards Other Substituted Acrylamides

The following are acrylamides that were attempted to synthesize using the corresponding procedures.

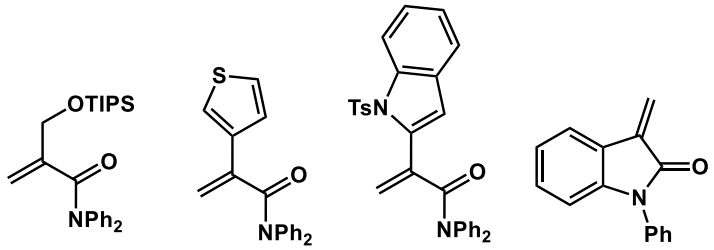

S1 **S2** **S3** **S4**

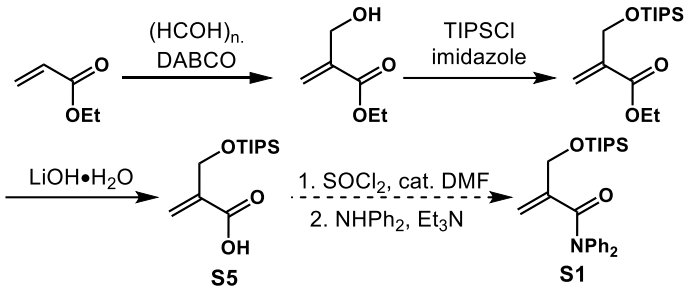

Synthesis of the *N*,*N*-diphenyl-2-(((triisopropylsilyl)oxy)methyl)acrylamide(**S1**) was attempted based on the reported method.[41a] **S5** was successfully prepared and amination was performed

according to General Procedure D. However, **S5** kept polymerizing and purification was not successful.

2-(((triisopropylsilyl)oxy)methyl)acrylic acid (S5)

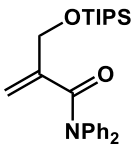

Colorless oil, 34% yield over three steps. **^{1}H NMR** (CDCl3, 400 MHz) δ 11.07 (s, 1H), 6.37 (m, 1H), 6.09 (m, 1H), 4.44 (m, 2H), 1.17 – 1.08 (m, 3H), 1.05 (d, J = 6.8 Hz, 18H). The ^{1}H NMR spectrum is in accordance with the previous literature.[42]

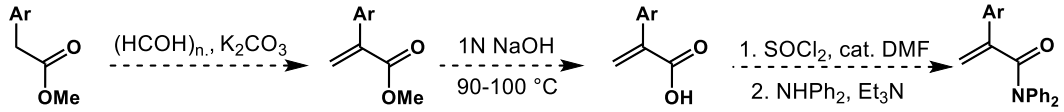

Synthesis of the *N*,*N*-diphenyl-2-(thiophen-3-yl)acrylamide (**S2**) and *N*,*N*-diphenyl-2-(1-tosyl-1H-indol-3-yl)acrylamide (**S3**) was attempted based on the reported method.[41a]

For **S2**, aldol condensation was not successful and the starting acetate degraded, presumably due to its sensitivity to heat. We then prepared **S2** through Pd-catalyzed cross-coupling but no reactivity was observed for hydroacylation with **S2**, likely due to residual amount of Pd in the mixture. Therefore, we decided not to prepare our substrates through cross-couplings.

For **S3**, tosylation was first performed based on reported method to obtain **S6**.[43] Aldol condensation was successful with **S6** and the acrylate (**S7**) was purified. However, **S7** was not stable and dimerized in vacuo overnight.

methyl 2-(1-tosyl-1H-indol-3-yl)acetate (S6)

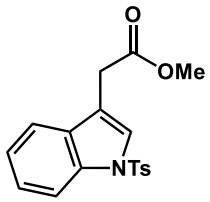

Yellow oil, 50% yield. **^{1}H NMR** (600 MHz, $CDCl_3$) δ 7.97 (d, *J* = 8.3 Hz, 1H), 7.81 – 7.73 (m, 2H), 7.57 (s, 1H), 7.49 (d, *J* = 7.9 Hz, 1H), 7.32 (ddd, *J* = 8.2, 6.6, 1.3 Hz, 1H), 7.23 (m, 3H), 3.71 (s, 3H), 3.70 (s, 2H), 2.34 (s, 3H). The ^{1}H NMR spectrum is in accordance with the previous literature.[43]

methyl 2-(1-tosyl-1H-indol-3-yl)acrylate (S7)

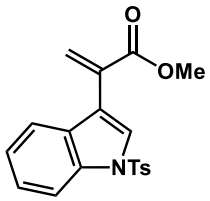

S6 (2.2 g, 6.3 mmol, 1.0 equiv) was dissolved in DMF (42 mL) and paraformaldehyde (380 mg, 13 mmol, 2.0 equiv), K_2CO_3 (860 mg, 6.3 mmol, 1.0 equiv) were added sequentially. The resulting mixture was allowed to stir at 90 °C overnight. The solution was cooled to room temperature and diluted with brine then extracted with hexanes (4 × 100 mL). The combined organic layers were washed with brine and water, dried over $MgSO_4$, filtered and concentrated in vacuo. The product (**S2**) was purified by silica gel column chromatography (10% ethyl acetate/hexanes) to give a yellow oil. Product dimerized in vacuo overnight. Proof of initial success in synthesis: **^{1}H NMR** (400 MHz, $CDCl_3$) δ 8.04 (d, *J* = 8.3 Hz, 1H), 7.95 (s, 1H), 7.78 (d, *J* = 8.0 Hz, 2H), 7.59 (d, *J* = 7.9 Hz, 1H), 7.32 (t, *J* = 7.7 Hz, 1H), 7.24 (t, *J* = 7.6 Hz, 1H), 7.14 (dd, *J* = 8.4, 2.6 Hz, 2H), 6.53 (s, 1H), 6.12 (s, 1H), 3.84 (s, 3H), 2.25 (s, 3H).

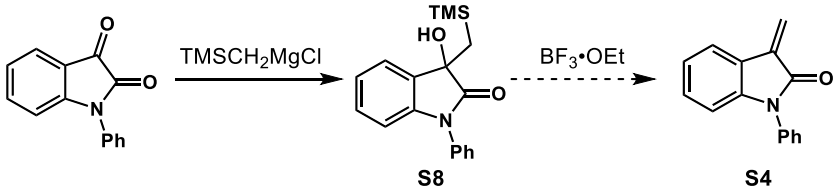

Synthesis of the 3-methylene-1-phenylindolin-2-one (**S4**) was attempted based on the reported method.[44] **S8** was successfully prepared but **S4** was polymerized in vacuo.

3-hydroxy-1-phenyl-3-((trimethylsilyl)methyl)indolin-2-one (S8)

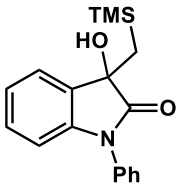

1-phenylisatin (1.5 g, 6.7 mmol, 1.0 equiv) was suspended in Et_2O (25 mL) and the mixture was cooled to -78 °C. Freshly made [(trimethylsilyl)methyl]magnesium chloride (13 mmol, 2.0 equiv, 0.77 M in Et_2O) was added slowly. The mixture was allowed to stir at -78 °C for 15 min and then warmed to room temperature to stir for 18 h. The reaction was quenched with MeOH, and then concentrated in vacuo to give a reddish brown solid. The product (**S1**) was purified through flash column chromatography (20% ethyl acetate/hexanes) to give a pale yellow solid (910 mg, 2.9 mmol, 44%). **^{1}H NMR** (600 MHz, $CDCl_3$) δ 7.57 – 7.50 (m, 2H), 7.46 – 7.42 (m, 3H), 7.40 (td, *J* = 7.3, 1.3 Hz, 1H), 7.28 – 7.22 (m, 1H), 7.12 (td, *J* = 7.5, 1.0 Hz, 1H), 6.86 (d, *J* = 7.9 Hz, 1H), 3.12 (s, 1H), 1.65 (d, *J* = 0.9 Hz, 2H), -0.20 (s, 9H). **^{13}C NMR** (151 MHz, $CDCl_3$) δ 177.8, 143.0, 134.3, 130.9, 129.7, 129.7, 128.1, 126.2, 124.6, 123.7, 110.0, 75.8, 28.8, -0.9. **IR** (ATR): 3336, 2958, 2249, 1705, 1613, 1498, 1200, 728, 701 cm^{-1}. **HRMS** calculated for $C_{18}H_{21}NO_2SiNa$ $[M+Na]^+$ 334.1239, found 334.1249.

3-methylene-1-phenylindolin-2-one (S4)

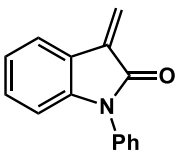

S8 (0.60 g, 1.9 mmol, 1.0 equiv) was dissolved in DCM (39 mL) and the solution was cooled to –78 °C. Boron trifluoride–diethyl ether (1.2 mL, 1.4 g, 9.6 mmol, 5.0 equiv) was added slowly. The mixture was stirred at –78 °C for 2 h, and then at 0 °C for another 1 h. The mixture was poured into saturated aqueous $NaHCO_3$ solution and

extracted with DCM (3 × 50 mL). The combined organic layers were washed again with $NaHCO_3$, dried with $MgSO_4$, filtered and concentrated in vacuo. The product (**S4**) was polymerized under high concentration.

6. Mechanistic Experiments

6.1. NMR Studies for Enamine Formation

In a N_2-filled glovebox, 1-AdNH_2 (7 mol % or 1.0 equiv), **1a** (20 µL, 20 mg, 0.15 mmol, 1.0 equiv), and DCE (0.2 mL) were added to a 1-dram vial. The reaction mixture was stirred at 60 °C for 30 min. The mixture (75 µL) was transferred into an NMR tube, diluted with $CDCl_3$ (0.65 mL), and removed from the glovebox to perform ^{1}H NMR spectroscopy. The selected chemical shift for 1D NOE was 6.61, which proved to be the *E*-enamine. Referenced to TMS.

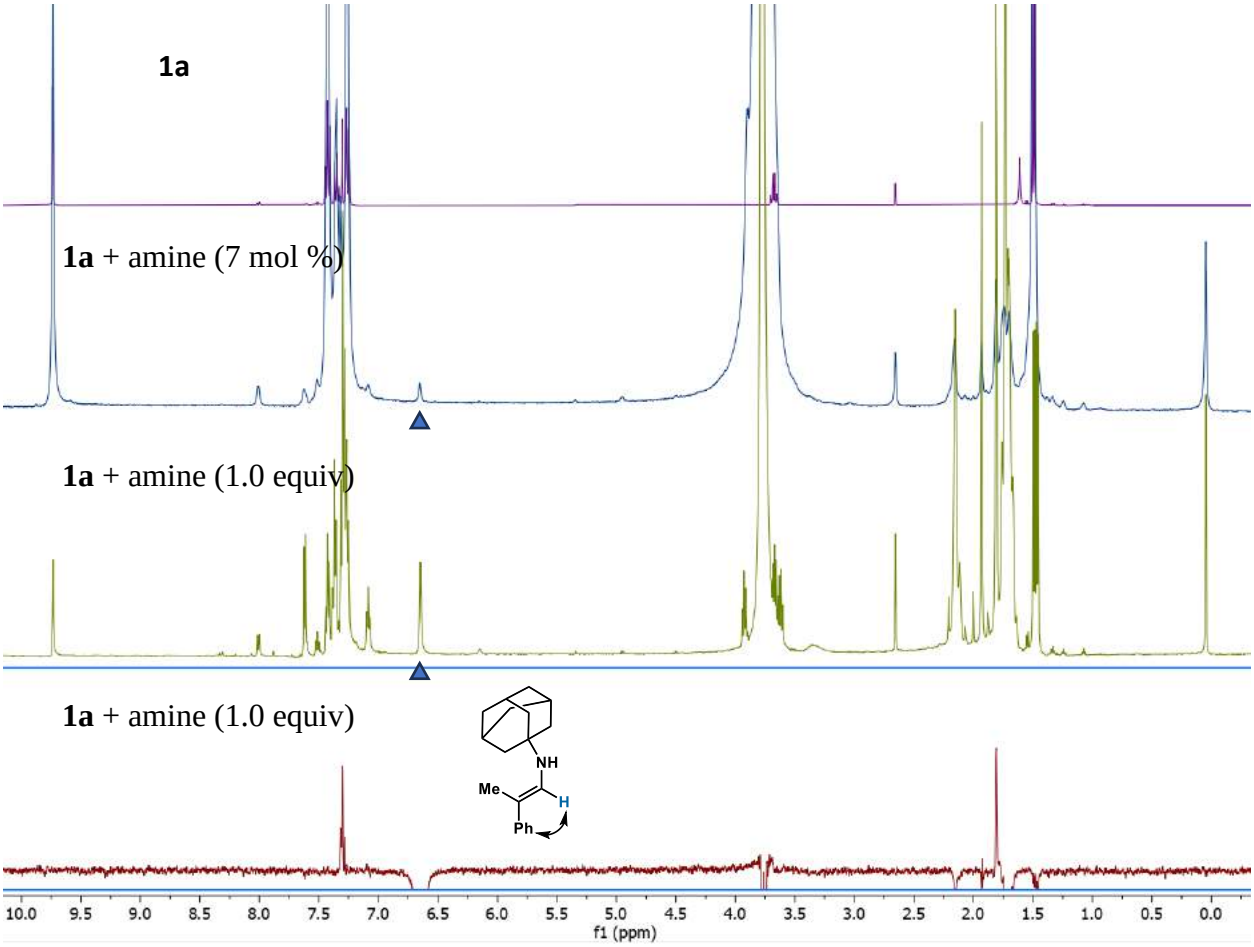

6.2. Racemization Studies

Racemization under reaction condition

All reactions prepared according to "General Procedure for DKR Hydroacylation" with 1,3,5-trimethyoxybenzene as an internal standard and quenched at various time points with exposure to atmosphere. The majority of the reaction mixture was reduced with immediate subjection into $NaBH_4$ (>20 equiv) in MeOH (~20 mL). Reduction was quenched through addition of sat. NH_4Cl and the mixture was extracted with DCM. The combined organic layers were dried over Na_2SO_4, filtered and concentrated. The reduced **1a** was recovered by preparative thin layer chromatography (hexanes/ethyl acetate 5:1) for determination of enantiomeric excess (*ee*). NMR yield and diastereoselectivity of **3aa** were determined by ^1H NMR analysis of the unreduced reaction mixture. Theoretical *ee* of **1a** if under kinetic resolution (KR) were calculated based on product NMR yield and diastereoselectivity assuming no racemization of **1a**.

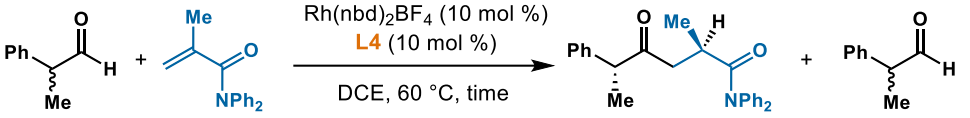

entry	time	deviation	yield (%)	*dr*	theoretical *ee* of 1a for KR (%)	observed 1a *ee* (%)
1	5 min	none	24	9:1	15	12
2	1 h	none	70	8:1	68	38
3	4 h	none	96	3.5:1	>99	42
4	1 h	with 1-$AdNH_2$	53	10:1	82	14

Sample calculation for theoretical *ee* after 5 min:

Results: **3aa** 9:1 *dr*, 24% NMR yield

Theoretical (*R*)-**1a** = starting equiv – major diastereomer yield = 0.75 – 9/10 * 0.24 = 0.534

Theoretical (*S*)-**1a** = starting equiv – minor diastereomer yield = 0.75 – 1/10 * 0.24 = 0.726

Theoretical *ee* = (Theoretical (*S*)-**1a** – Theoretical (*R*)-**1a**) / (Theoretical (*S*)-**1a** + Theoretical (*R*)-**1a**) *100% = (0.726-0.534) / (0.726+0.534) *100% = 15%

Racemization of enantioenriched (*R*)-2-phenylpropanal (1a)

Enantioenriched (*R*)-**1a** was prepared according to the reported methods[40a,f] from (*R*)-2-phenylpropanoic acid (43% yield over two steps). (*R*)-**1a** was reduced to the corresponding alcohol to determine *ee*.

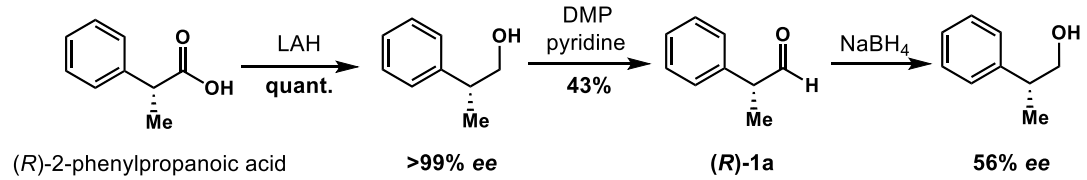

Racemization with 1-AdNH$_2$:

In a N_2-filled glovebox, 1-AdNH$_2$ (4.6 mg, 7 mol %), (*R*)-**1a** (60 µL, 60 mg, 0.45 mmol, 1.0 equiv), and DCE (0.6 mL) were added to a 1-dram vial. The reaction mixture was stirred at 60 ℃ and aliquots (0.1 mL) were taken at various time points and removed from the glove box. The aliquots were reduced with immediate subjection into $NaBH_4$ (>20 equiv) in MeOH (~5 mL). Reduction was quenched with sat. NH_4Cl and the mixture was extracted with DCM. The combined organic layers were dried over Na_2SO_4, filtered and concentrated. The unpurified reaction mixture was used directly to determine *ee*. Background reaction was performed with **1a** (20 µL, 20 mg, 0.15 mmol, 1.0 equiv) in DCE (0.2 mL).

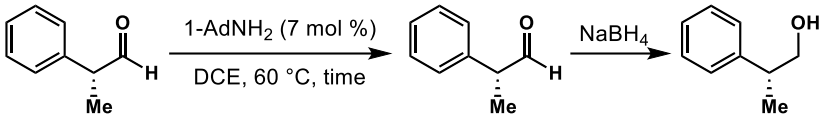

56% *ee* (*R*)-**1a**

time	deviation	*ee* (%)
1 h	none	40
2 h	none	18
3 h	none	14
3.5 h	no amine	56

Racemization with other bases:

In a N_2-filled glovebox, base (7 mol %), (*R*)-**1a** (20 µL, 20 mg, 0.15 mmol, 1.0 equiv), and DCE (0.2 mL) were added to a 1-dram vial. The reaction mixture was stirred at 60 °C for 1 h and then removed from the glove box. Reactions were reduced with immediate subjection into $NaBH_4$ (>20 equiv) in MeOH (~5 mL). Reduction was quenched through addition of sat. NH_4Cl and the mixture was extracted with DCM. The combined organic layers were dried over Na_2SO_4, filtered and concentrated. The unpurified reaction mixture was used directly to determine *ee*.

Racemization with [Rh]:

Reactions were prepared according to "General Procedure for DKR Hydroacylation" without the use of **2a**. After 1 h, reaction was quenched with exposure to atmosphere and reduced with immediate subjection into $NaBH_4$ (>20 equiv) in MeOH (~20 mL). Reduction was quenched through addition of sat. NH_4Cl and the mixture was extracted with DCM. The combined organic layers were dried over Na_2SO_4, filtered and concentrated. The unpurified reaction mixture was used directly to determine *ee*.

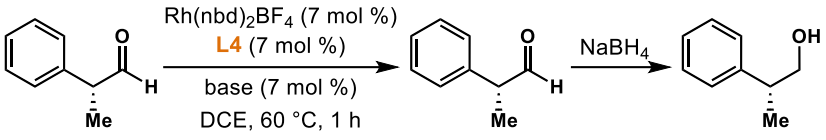

56% *ee* (*R*)-**1a**

base	deviation	*ee* (%)
1-AdNH$_2$	none	7
-	no base	28
1-AdNH$_2$	no Rh	40
2,6-diethylaniline	no Rh	58
diphenylmethanamine	no Rh	38

6.3. Deuterium-Labeling Study

Synthesis of 2-phenylpropanal-1-*d* (*d*-1a)

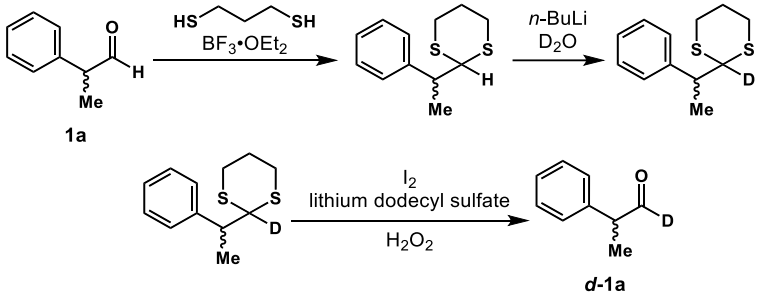

1a ***d*-1a**

The reaction was performed according to the following procedure.[45] 2-phenylpropanal (**1a**) (1.2 g, 8.9 mmol, 1.0 equiv) was dissolved in DCM (15 mL) and propane-1,3-dithiole (0.99 mL, 1.1 g, 9.8 mmol, 1.1 equiv) was added. The solution was cooled down to 0 °C and $BF_3 \cdot OEt_2$ (0.57 mL, 0.64 g, 4.5 mmol, 0.5 equiv) was added dropwise. The reaction was stirred at 0 °C for 1 h and was allowed to warm to room temperature. The mixture was stirred overnight and quenched with sat. $NaHCO_3$ solution and extracted with DCM (3 × 30 mL). The combined organic layers were washed with brine, dried over $MgSO_4$, filtered, and concentrated. The resulting oil was purified by flash column chromatography (silica gel, 3% ethyl acetate/hexanes) to afford the 2-(1-phenylethyl)-1,3-dithiane as a colorless oil (1.7 g, 7.6 mmol, 85%).

2-(1-phenylethyl)-1,3-dithiane (7.6 mmol, 1.0 equiv) was dissolved in dry THF (13 mL) and the solution was cooled to 0 °C. *n*-BuLi (1.4 M in hexanes, 0.63 g, 9.8 mmol, 1.3 equiv) was added dropwise. The solution was allowed to stir at 0 °C for an additional 1 h followed by addition of D_2O (1.2 mL, 1.4 g, 68 mmol, 9.0 equiv). White precipitate formed and the solution was allowed to stir for an additional 20 min at room temperature. The solution was diluted with water and extracted with Et_2O (3 × 70 mL). The combined organic layers were dried over Na_2SO_4, filtered and concentrated in vacuo. ^{1}H NMR shows 100% D incorporation. *d*-dithiane was purified through flash column chromatography (4% ethyl acetate/hexanes) to give a pale yellow oil (1.1 g, 5.1 mmol, 67%). **^{1}H NMR** (400 MHz, $CDCl_3$) δ 7.36 – 7.29 (m, 2H), 7.27 (d, *J* = 1.5 Hz, 2H), 7.25 (d, *J* = 7.3 Hz, 1H), 3.09 (q, *J* = 7.1 Hz, 1H), 2.87 – 2.74 (m, 4H), 2.11 – 2.02 (m, 1H), 1.81 (ddtd, *J* = 14.0, 11.0, 7.6, 4.2 Hz, 1H), 1.48 (d, *J* = 7.1 Hz, 3H).

The reaction was performed according to the following procedure.[46] Lithium dodecyl sulfate (820 mg, 3.0 mmol, 20 mol %) was dissolved in water (50 mL). Under positive pressure was added I_2 (380 mg, 1.5 mmol, 10 mol %), **S7** (3.4 g, 15.1 mmol, 1.0 equiv, washed with 2 mL DCM), and 30% H_2O_2 (6.2 mL, 6.8 g, 60. mmol, 4.0 equiv). The reaction was stirred at room temperature for 2 h and the mixture was cooled to 0 °C. The reaction was quenched with addition of 10% $Na_2S_2O_3$. The solution was stirred at 0 °C for 5 min and then extracted with ethyl acetate (3 × 50 mL). The combined organic layers were washed with water, dried over $MgSO_4$, filtered and concentrated in vacuo. The product (***d*-1a**) was purified by distillation to give a colorless oil (720 mg, 5.3 mmol, 35% yield). ^{1}H NMR shows 98% D incorporation. **^{1}H NMR** (400 MHz, $CDCl_3$) δ 7.43 – 7.35 (m, 2H), 7.34 – 7.28 (m, 1H), 7.24 – 7.19 (m, 2H), 3.63 (q, *J* = 7.1 Hz, 1H), 1.45 (d, *J* = 7.1 Hz, 3H).

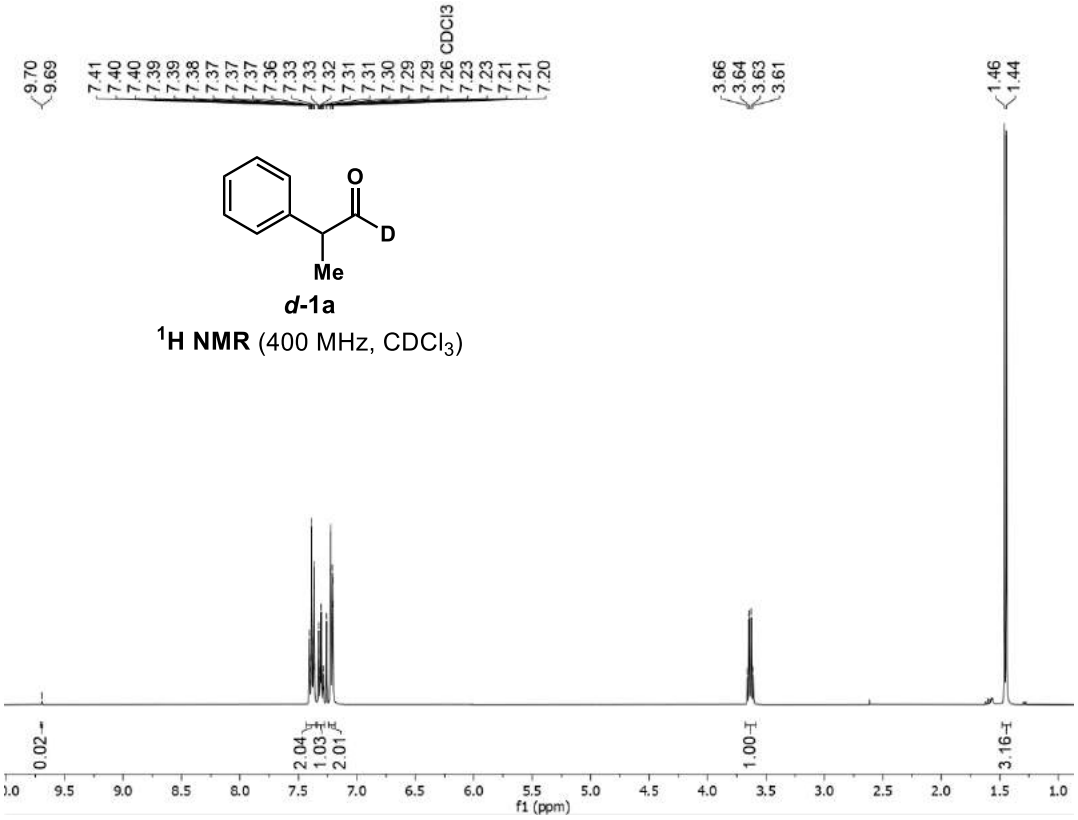

***d*-1a**

^{1}H NMR (400 MHz, $CDCl_3$)

Synthesis of *d*-3aa:

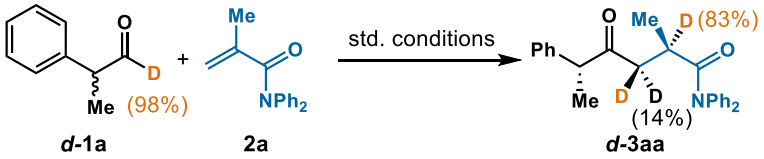

***d*-1a** (1.5 equiv) **2a** ***d*-3aa**

Following the "General Procedure for DKR Hydroacylation", ***d*-1a** was used as the aldehyde coupling partner. The target compound ***d*-3aa** was obtained (83% yield). Deuterium incorporation was determined by ^{1}H and ^{2}H NMR. Percent deuterium (% D) incorporation is depicted as the amount of deuterium in place of one single hydrogen atom at 2.20 and two hydrogen atoms at 3.06.

^{1}H NMR (400 MHz, $CDCl_3$) δ 7.52 – 7.35 (m, 5H), 7.35 – 7.29 (m, 5H), 7.24 – 7.06 (m, 5H), 3.79 (q, *J* = 6.9 Hz, 1H), 3.11 – 3.00 (m, 1.17 H), 2.20 (d, *J* = 17.9 Hz, 0.86H), 1.39 (d, *J* = 6.9 Hz, 3H),

0.98 (d, J = 6.5 Hz, 3H). **HRMS** calculated for $C_{25}H_{24}DNO_2Na$ $[M+Na]^+$ 395.1847, found 395.1841.

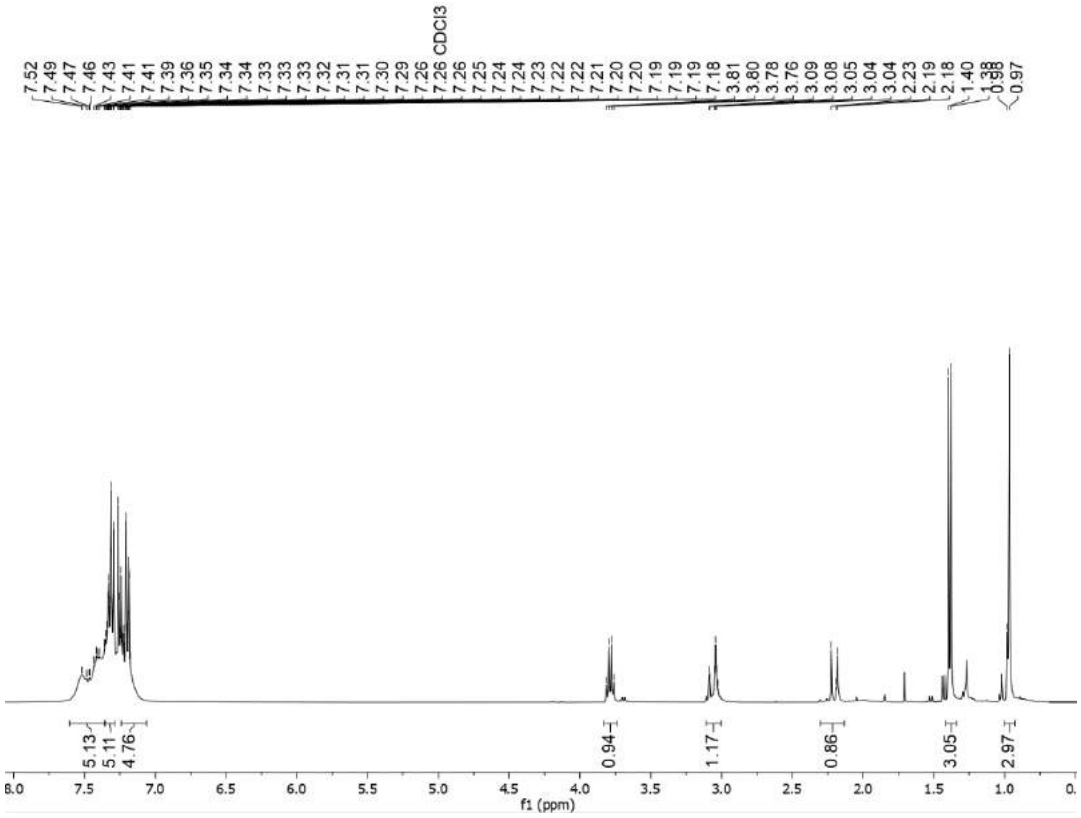

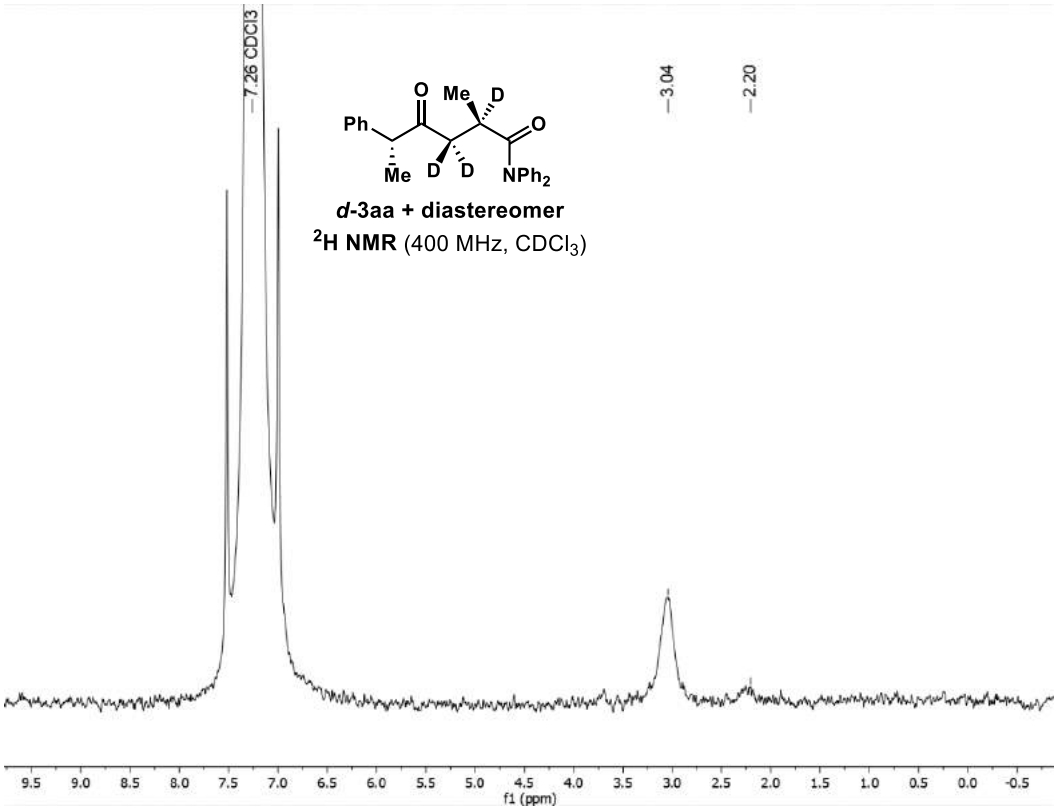

***d*-3aa + diastereomer**

^{2}H NMR (400 MHz, $CDCl_3$)

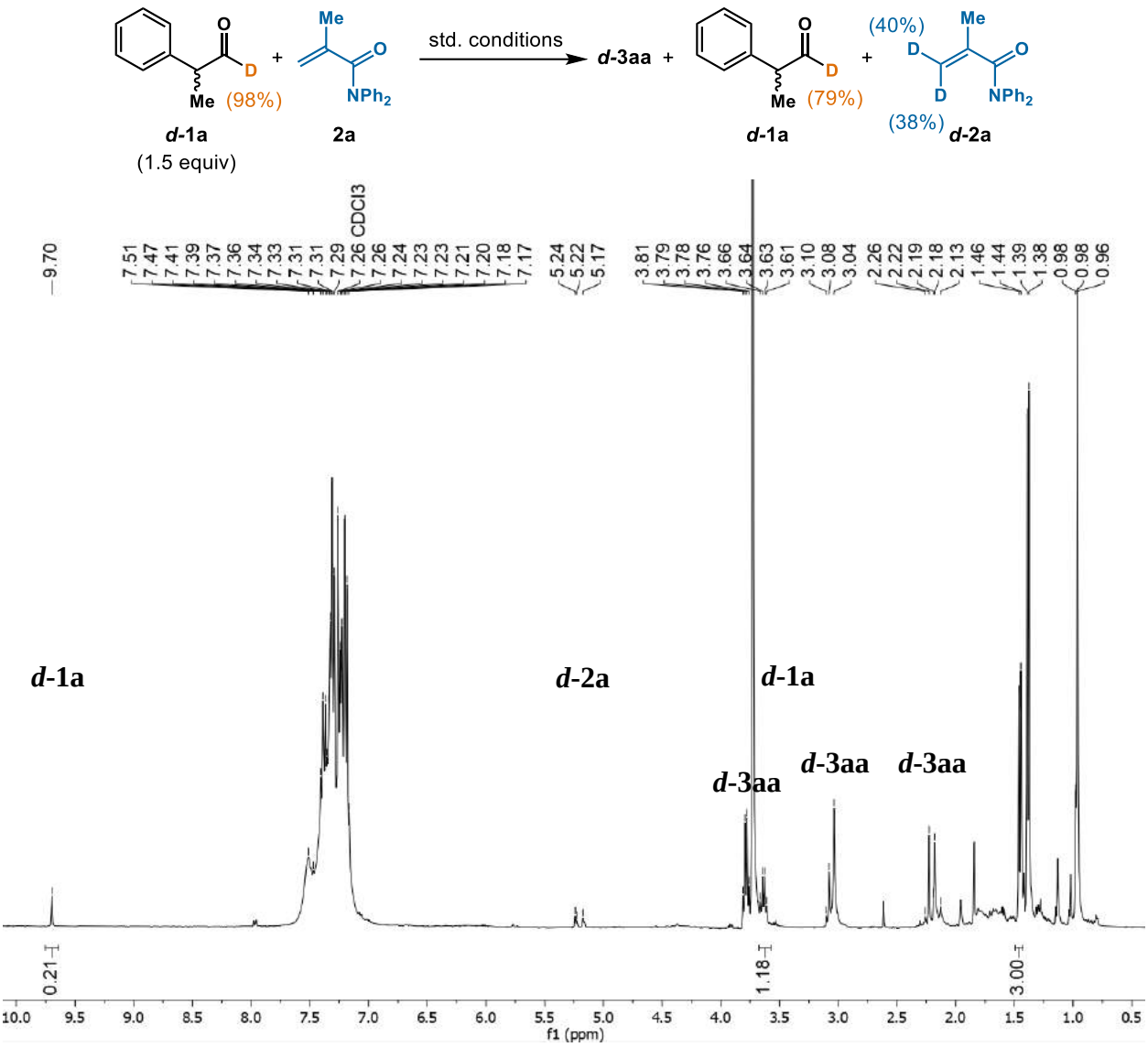

Fig S1. [1]H NMR spectrum for unpurified reaction mixture with important peaks labeled. Peaks of *d*-1a were integrated and the % deuteration went down from 98% to 79% after the reaction.

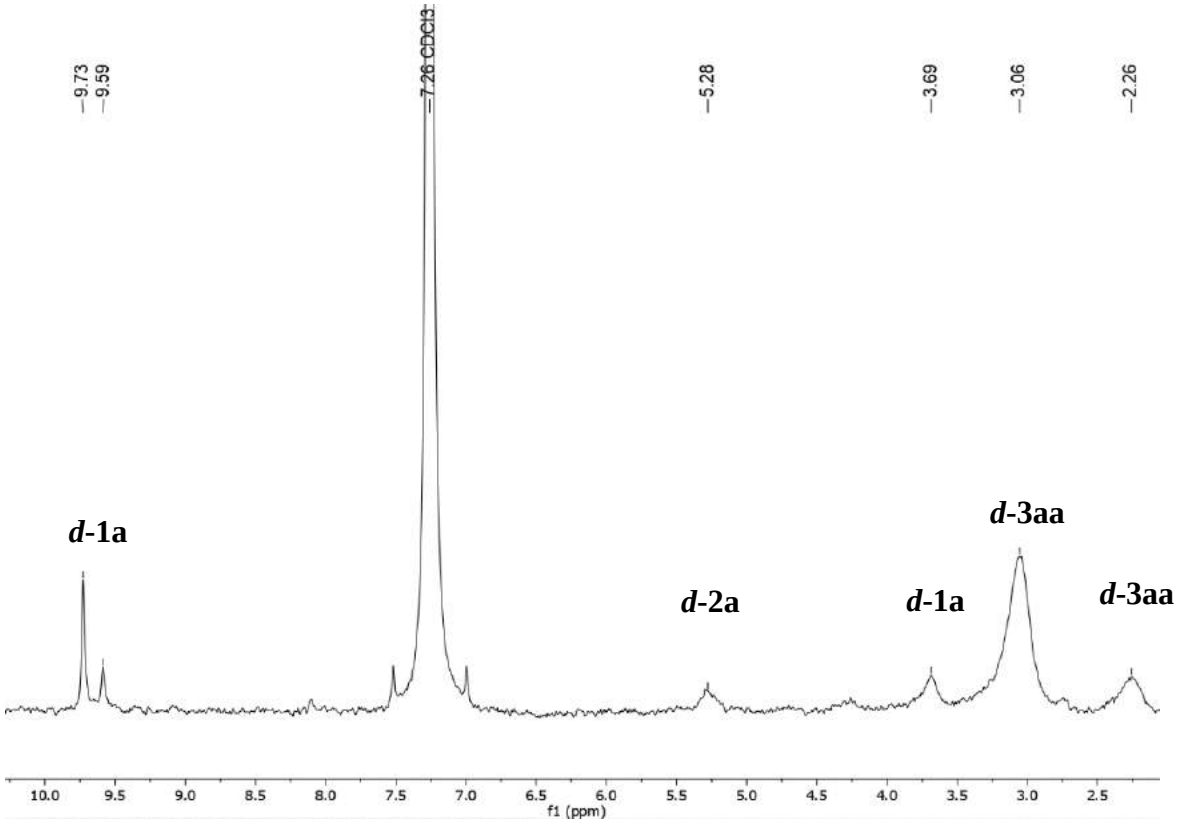

Fig S2. ^{2}H NMR spectrum for unpurified reaction mixture with important peaks labeled.

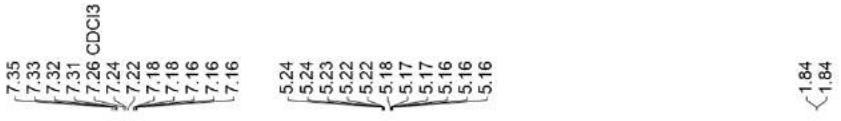

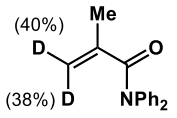

***d*-2a**

^{1}H NMR (400 MHz, $CDCl_3$)

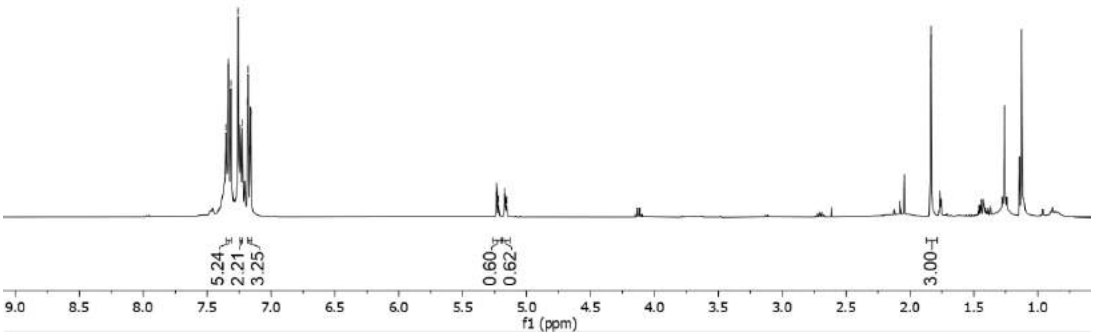

6.4. Competitive KIE

Following the "General Procedure for DKR Hydroacylation", a stock solution (40 µL, 40 mg, 0.30 mmol, 1.5 equiv) of 1:1 mixture of **1a** and ***d*-1a** was used as the aldehyde coupling partner and **2f** (53 mg, 0.15 mmol, 1.0 equiv) was used as the acrylamide accepter. Reactions were quenched after 30 min with exposure to atmosphere. NMR yield was determined by ^{1}H NMR analysis of the unpurified reaction mixture with 1,3,5-trimethyoxybenzene as an internal standard. H/D ratio was determined by ^{1}H NMR analysis of the purified product based on the hydrogen atom at 3.27. KIEs were calculated using the Melander-Saunder equation.[31] The reaction was repeated three times and the reported KIE was the average of the triplicate with 95% confidence.

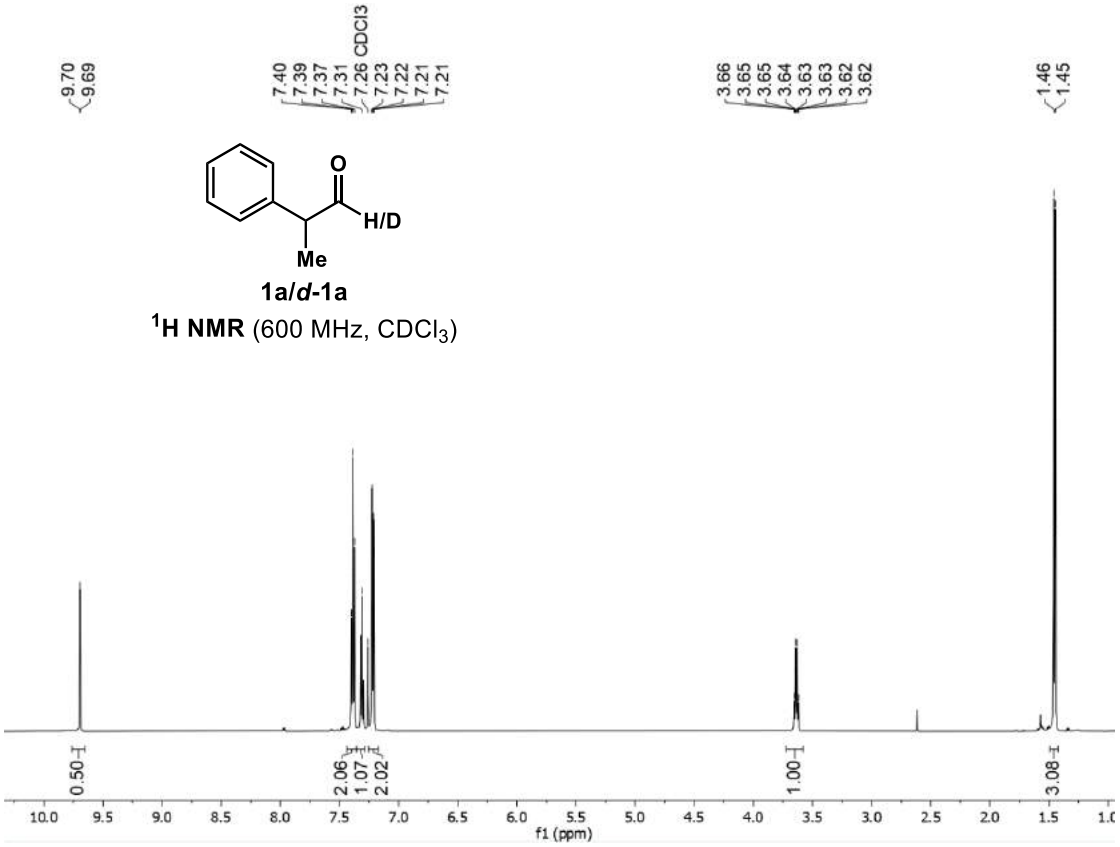

7. X-Ray Crystallographic Data

(2*R*,5*R*)-2-methyl-4-oxo-*N*,*N*,5-triphenylhexanamide (3aa)

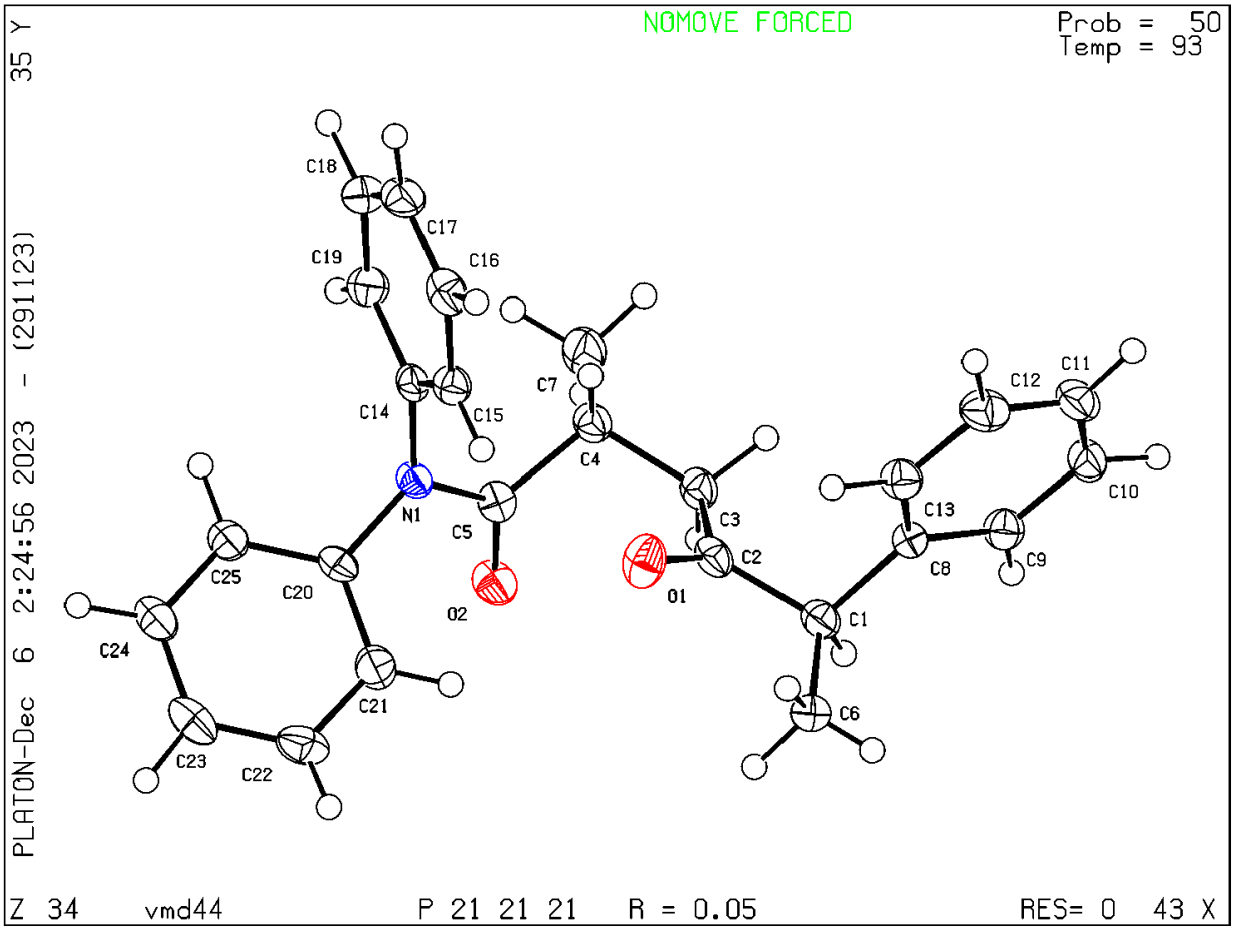

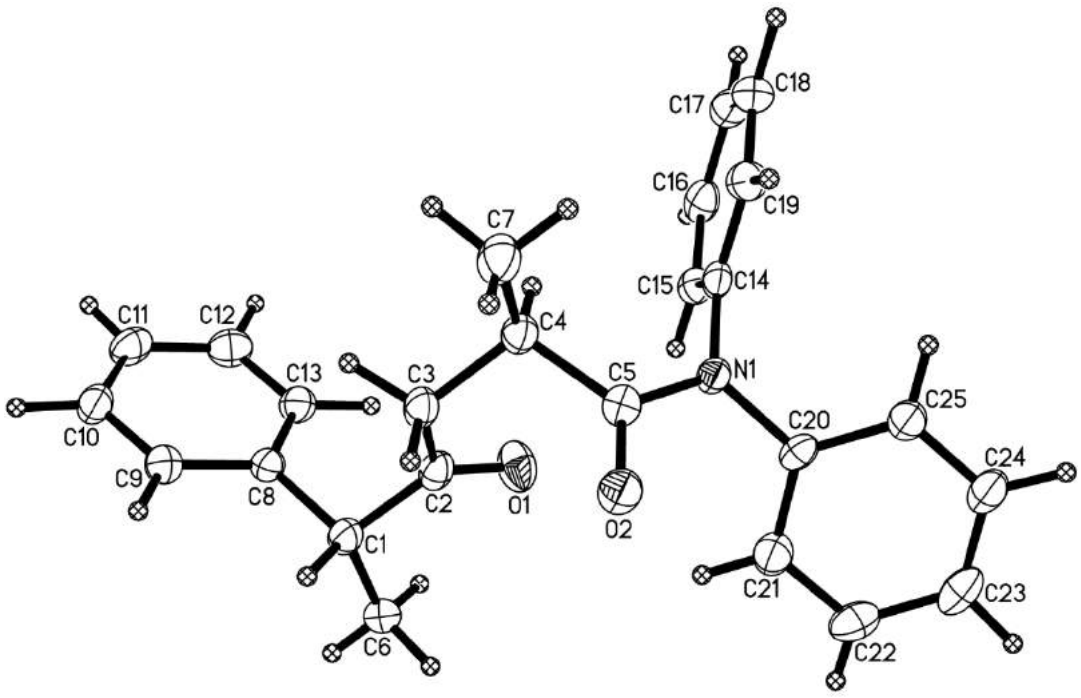

Experimental Summary

A colorless crystal of approximate dimensions 0.180 x 0.195 x 0.307 mm was mounted in a cryoloop and transferred to a Bruker X8 Prospector diffractometer system. The APEX3[1] program package was used to determine the unit-cell parameters and for data collection (10 sec/frame scan time). The raw frame data was processed using SAINT[2] and SADABS[3] to yield the reflection data file. Subsequent calculations were carried out using the SHELXTL[4] program package. The diffraction symmetry was *mmm* and the systematic absences were consistent with the orthorhombic space group $P2_12_12_1$ that was later determined to be correct.

The structure was solved by direct methods and refined on F^2 by full-matrix least-squares techniques. The analytical scattering factors[5] for neutral atoms were used throughout the analysis. Hydrogen atoms were located from a difference-Fourier map and refined (x,y,z and U_{iso}).

Least squares analysis yielded wR2 = 0.1296 and Goof = 1.027 for 353 variables refined against 3753 data (0.83 Å), R1 = 0.0487 for those 3564 data with $I > 2.0\sigma(I)$. The absolute structure was assigned by the synthetic method employed.

Definitions:

$wR2 = [\Sigma[w(F_o^2-F_c^2)^2] / \Sigma[w(F_o^2)^2]]^{1/2}$

$R1 = \Sigma||F_o|-|F_c|| / \Sigma|F_o|$

$Goof = S = [\Sigma[w(F_o^2-F_c^2)^2] / (n-p)]^{1/2}$ where n is the number of reflections and p is the total number of parameters refined.

The thermal ellipsoid plot is shown at the 50% probability level.

Table 1. Crystal data and structure refinement for 3aa.

Identification code	3aa	
Empirical formula	$C_{25}H_{25}NO_2$	
Formula weight	371.46	
Temperature	93(2) K	
Wavelength	1.54178 Å	
Crystal system	Orthorhombic	
Space group	$P2_12_12_1$	
Unit cell dimensions	a = 9.2503(8) Å	a = 90°.
	b = 14.7442(13) Å	b = 90°.
	c = 15.1902(14) Å	g = 90°.
Volume	2071.8(3) $Å^3$	
Z	4	
Density (calculated)	1.191 Mg/m^3	
Absorption coefficient	0.588 mm^{-1}	
F(000)	792	
Crystal color	colorless	
Crystal size	0.307 x 0.195 x 0.180 mm^3	
Theta range for data collection	4.178 to 68.139°	
Index ranges	$-11 \le h \le 11$, $-17 \le k \le 17$, $-18 \le l \le 14$	
Reflections collected	17417	
Independent reflections	3753 [R(int) = 0.0650]	
Completeness to theta = 67.679°	99.8 %	
Absorption correction	Semi-empirical from equivalents	
Max. and min. transmission	0.8643 and 0.7682	
Refinement method	Full-matrix least-squares on F^2	
Data / restraints / parameters	3753 / 0 / 353	
Goodness-of-fit on F^2	1.027	
Final R indices [I>2sigma(I) = 3564 data]	R1 = 0.0487, wR2 = 0.1272	

R indices (all data, 0.83 Å)	R1 = 0.0508, wR2 = 0.1296
Absolute structure parameter	-0.1(3)
Largest diff. peak and hole	0.164 and -0.261 e.Å^{-3}

Table 2. Atomic coordinates (x 10^4) and equivalent isotropic displacement parameters ($Å^2$ x 10^3) for 3aa.

U(eq) is defined as one third of the trace of the orthogonalized U^{ij} tensor.

	x	y	z	U(eq)
O(1)	7619(3)	6227(2)	1779(2)	35(1)
O(2)	4694(3)	6274(2)	533(1)	31(1)
N(1)	4359(3)	5501(2)	1807(2)	21(1)
C(1)	9098(4)	7398(2)	1164(2)	25(1)
C(2)	7680(4)	6994(2)	1491(2)	25(1)
C(3)	6359(4)	7584(2)	1447(2)	25(1)
C(4)	5012(4)	7139(2)	1849(2)	24(1)
C(5)	4678(4)	6274(2)	1342(2)	22(1)
C(6)	10200(4)	6661(2)	945(2)	31(1)
C(7)	3722(4)	7790(3)	1820(3)	35(1)
C(8)	9677(3)	8049(2)	1862(2)	23(1)
C(9)	9965(4)	8950(2)	1652(2)	27(1)
C(10)	10549(4)	9533(2)	2275(2)	29(1)
C(11)	10833(4)	9224(3)	3119(2)	33(1)
C(12)	10543(4)	8326(3)	3333(2)	33(1)
C(13)	9968(4)	7744(2)	2713(2)	26(1)
C(14)	4261(4)	5492(2)	2754(2)	22(1)
C(15)	5445(4)	5231(2)	3258(2)	23(1)
C(16)	5327(4)	5202(2)	4166(2)	28(1)
C(17)	4047(4)	5426(2)	4574(2)	31(1)
C(18)	2866(4)	5681(3)	4076(2)	33(1)
C(19)	2962(4)	5720(2)	3165(2)	28(1)
C(20)	4410(4)	4631(2)	1380(2)	22(1)
C(21)	5577(4)	4407(2)	849(2)	29(1)

C(22)	5677(5)	3536(3)	503(3)	34(1)
C(23)	4630(4)	2892(2)	684(2)	33(1)
C(24)	3460(5)	3124(2)	1197(2)	31(1)
C(25)	3334(4)	3995(2)	1543(2)	26(1)

Table 3. Bond lengths [Å] and angles [°] for 3aa.

O(1)-C(2)	1.215(4)
O(2)-C(5)	1.229(4)
N(1)-C(5)	1.374(4)
N(1)-C(20)	1.438(4)
N(1)-C(14)	1.441(4)
C(1)-C(2)	1.524(5)
C(1)-C(6)	1.527(5)
C(1)-C(8)	1.527(4)
C(1)-H(1A)	1.00(4)
C(2)-C(3)	1.501(5)
C(3)-C(4)	1.535(5)
C(3)-H(3A)	0.97(4)
C(3)-H(3B)	1.05(4)
C(4)-C(5)	1.521(4)
C(4)-C(7)	1.531(5)
C(4)-H(4A)	1.00(4)
C(6)-H(6A)	1.02(4)
C(6)-H(6B)	1.06(5)
C(6)-H(6C)	0.89(4)
C(7)-H(7A)	1.02(5)
C(7)-H(7B)	0.92(5)

C(7)-H(7C)	1.01(5)
C(8)-C(9)	1.392(5)
C(8)-C(13)	1.394(5)
C(9)-C(10)	1.388(5)
C(9)-H(9A)	0.97(4)
C(10)-C(11)	1.386(6)
C(10)-H(10A)	1.04(5)
C(11)-C(12)	1.389(6)
C(11)-H(11A)	0.97(4)
C(12)-C(13)	1.381(5)
C(12)-H(12A)	1.09(5)
C(13)-H(13A)	1.05(5)
C(14)-C(15)	1.390(5)
C(14)-C(19)	1.395(5)
C(15)-C(16)	1.385(5)
C(15)-H(15A)	0.92(4)
C(16)-C(17)	1.377(5)
C(16)-H(16A)	1.05(4)
C(17)-C(18)	1.381(6)
C(17)-H(17A)	0.92(5)
C(18)-C(19)	1.389(5)
C(18)-H(18A)	1.10(4)
C(19)-H(19A)	0.93(4)
C(20)-C(21)	1.388(5)
C(20)-C(25)	1.390(5)
C(21)-C(22)	1.390(5)
C(21)-H(21A)	0.94(4)
C(22)-C(23)	1.385(6)
C(22)-H(22A)	0.86(4)
C(23)-C(24)	1.376(6)

C(23)-H(23A)	0.99(5)
C(24)-C(25)	1.393(5)
C(24)-H(24A)	0.99(5)
C(25)-H(25A)	0.99(4)

C(5)-N(1)-C(20)	120.1(3)
C(5)-N(1)-C(14)	122.3(3)
C(20)-N(1)-C(14)	116.4(2)
C(2)-C(1)-C(6)	111.6(3)
C(2)-C(1)-C(8)	108.7(3)
C(6)-C(1)-C(8)	111.4(3)
C(2)-C(1)-H(1A)	112(2)
C(6)-C(1)-H(1A)	106(2)
C(8)-C(1)-H(1A)	107(2)
O(1)-C(2)-C(3)	121.2(3)
O(1)-C(2)-C(1)	121.4(3)
C(3)-C(2)-C(1)	117.4(3)
C(2)-C(3)-C(4)	113.3(3)
C(2)-C(3)-H(3A)	106(2)
C(4)-C(3)-H(3A)	109(2)
C(2)-C(3)-H(3B)	111(2)
C(4)-C(3)-H(3B)	111(2)
H(3A)-C(3)-H(3B)	105(3)
C(5)-C(4)-C(7)	110.6(3)
C(5)-C(4)-C(3)	108.8(3)
C(7)-C(4)-C(3)	110.7(3)
C(5)-C(4)-H(4A)	108(2)
C(7)-C(4)-H(4A)	109(2)
C(3)-C(4)-H(4A)	109(2)
O(2)-C(5)-N(1)	121.1(3)

O(2)-C(5)-C(4)	120.3(3)
N(1)-C(5)-C(4)	118.6(3)
C(1)-C(6)-H(6A)	108(2)
C(1)-C(6)-H(6B)	114(3)
H(6A)-C(6)-H(6B)	109(4)
C(1)-C(6)-H(6C)	112(2)
H(6A)-C(6)-H(6C)	106(3)
H(6B)-C(6)-H(6C)	107(4)
C(4)-C(7)-H(7A)	113(3)
C(4)-C(7)-H(7B)	111(3)
H(7A)-C(7)-H(7B)	103(4)
C(4)-C(7)-H(7C)	115(3)
H(7A)-C(7)-H(7C)	106(4)
H(7B)-C(7)-H(7C)	109(4)
C(9)-C(8)-C(13)	118.9(3)
C(9)-C(8)-C(1)	120.5(3)
C(13)-C(8)-C(1)	120.6(3)
C(10)-C(9)-C(8)	120.6(3)
C(10)-C(9)-H(9A)	120(2)
C(8)-C(9)-H(9A)	119(2)
C(11)-C(10)-C(9)	120.0(3)
C(11)-C(10)-H(10A)	121(3)
C(9)-C(10)-H(10A)	119(3)
C(10)-C(11)-C(12)	119.6(3)
C(10)-C(11)-H(11A)	124(2)
C(12)-C(11)-H(11A)	117(2)
C(13)-C(12)-C(11)	120.4(3)
C(13)-C(12)-H(12A)	119(2)
C(11)-C(12)-H(12A)	120(2)
C(12)-C(13)-C(8)	120.4(3)

C(12)-C(13)-H(13A)	121(2)
C(8)-C(13)-H(13A)	119(2)
C(15)-C(14)-C(19)	119.9(3)
C(15)-C(14)-N(1)	120.2(3)
C(19)-C(14)-N(1)	119.9(3)
C(16)-C(15)-C(14)	119.7(3)
C(16)-C(15)-H(15A)	124(2)
C(14)-C(15)-H(15A)	116(2)
C(17)-C(16)-C(15)	120.6(3)
C(17)-C(16)-H(16A)	125(2)
C(15)-C(16)-H(16A)	114(2)
C(16)-C(17)-C(18)	119.9(3)
C(16)-C(17)-H(17A)	121(3)
C(18)-C(17)-H(17A)	119(3)
C(17)-C(18)-C(19)	120.5(3)
C(17)-C(18)-H(18A)	125(2)
C(19)-C(18)-H(18A)	114(2)
C(18)-C(19)-C(14)	119.4(3)
C(18)-C(19)-H(19A)	123(2)
C(14)-C(19)-H(19A)	117(2)
C(21)-C(20)-C(25)	120.0(3)
C(21)-C(20)-N(1)	120.0(3)
C(25)-C(20)-N(1)	119.9(3)
C(20)-C(21)-C(22)	119.4(4)
C(20)-C(21)-H(21A)	120(2)
C(22)-C(21)-H(21A)	120(2)
C(23)-C(22)-C(21)	120.8(4)
C(23)-C(22)-H(22A)	122(3)
C(21)-C(22)-H(22A)	117(3)
C(24)-C(23)-C(22)	119.5(3)

C(24)-C(23)-H(23A)	124(3)
C(22)-C(23)-H(23A)	116(3)
C(23)-C(24)-C(25)	120.6(3)
C(23)-C(24)-H(24A)	117(2)
C(25)-C(24)-H(24A)	122(2)
C(20)-C(25)-C(24)	119.7(3)
C(20)-C(25)-H(25A)	121(2)
C(24)-C(25)-H(25A)	119(2)

Table 4. Anisotropic displacement parameters ($Å^2$ x 10^3) for 3aa.

The anisotropic displacement factor exponent takes the form: $-2p^2[h^2 a^{*2}U^{11} + ... + 2 h k a^* b^* U^{12}]$

	U^{11}	U^{22}	U^{33}	U^{23}	U^{13}	U^{12}
O(1)	34(1)	24(1)	46(2)	11(1)	1(1)	0(1)
O(2)	46(2)	27(1)	19(1)	3(1)	-3(1)	-4(1)
N(1)	27(1)	17(1)	18(1)	0(1)	-1(1)	-2(1)
C(1)	34(2)	21(2)	20(2)	-1(1)	0(1)	-3(1)
C(2)	34(2)	21(2)	19(2)	-1(1)	-4(1)	-4(1)
C(3)	32(2)	19(2)	24(2)	2(1)	-1(1)	-3(1)
C(4)	30(2)	20(1)	24(2)	0(1)	0(1)	-2(1)
C(5)	21(2)	21(2)	24(2)	2(1)	-4(1)	2(1)
C(6)	35(2)	29(2)	29(2)	-6(2)	9(2)	-6(2)
C(7)	33(2)	24(2)	48(2)	-1(2)	2(2)	2(2)
C(8)	22(2)	23(2)	23(1)	-3(1)	2(1)	-3(1)
C(9)	28(2)	25(2)	27(2)	1(1)	1(1)	0(1)
C(10)	28(2)	22(2)	37(2)	-5(1)	3(1)	-1(1)

C(11)	31(2)	36(2)	31(2)	-12(2)	-3(2)	-2(2)
C(12)	35(2)	39(2)	24(2)	-2(1)	-3(1)	2(2)
C(13)	30(2)	23(2)	26(2)	1(1)	1(1)	2(1)
C(14)	28(2)	16(1)	22(2)	-1(1)	1(1)	-6(1)
C(15)	27(2)	19(1)	24(2)	2(1)	0(1)	1(1)
C(16)	39(2)	21(2)	25(2)	4(1)	-6(2)	-3(2)
C(17)	48(2)	26(2)	20(2)	1(1)	5(2)	-5(2)
C(18)	37(2)	33(2)	30(2)	-6(2)	10(2)	-5(2)
C(19)	26(2)	30(2)	28(2)	-4(1)	0(1)	0(1)
C(20)	28(2)	20(2)	17(1)	-3(1)	-4(1)	2(1)
C(21)	28(2)	27(2)	33(2)	-3(1)	-1(2)	-1(2)
C(22)	34(2)	36(2)	33(2)	-11(2)	0(2)	10(2)
C(23)	47(2)	21(2)	30(2)	-5(1)	-12(2)	5(2)
C(24)	47(2)	22(2)	23(2)	-1(1)	-3(2)	-4(2)
C(25)	33(2)	23(2)	22(2)	1(1)	-1(1)	-2(1)

Table 5. Hydrogen coordinates (x 10^4) and isotropic displacement parameters ($Å^2$ x 10^3) for 3aa.

	x	y	z	U(eq)
H(1A)	8970(40)	7760(20)	610(20)	15(8)
H(3A)	6190(40)	7700(30)	830(30)	21(9)
H(3B)	6560(50)	8220(30)	1730(30)	29(10)
H(4A)	5220(40)	6970(30)	2470(30)	25(9)
H(6A)	9800(50)	6280(30)	440(30)	32(10)
H(6B)	10450(50)	6230(40)	1480(30)	50(13)
H(6C)	11030(40)	6890(20)	750(20)	15(8)

H(7A)	2790(50)	7510(30)	2050(30)	42(12)
H(7B)	3490(50)	7930(30)	1250(30)	39(12)
H(7C)	3860(50)	8370(30)	2160(30)	41(12)
H(9A)	9800(40)	9160(20)	1060(30)	20(9)
H(10A)	10790(50)	10190(30)	2090(30)	39(12)
H(11A)	11220(40)	9600(30)	3580(30)	30(10)
H(12A)	10720(50)	8080(30)	4000(30)	41(12)
H(13A)	9760(50)	7070(30)	2870(30)	38(11)
H(15A)	6280(40)	5100(20)	2960(20)	13(8)
H(16A)	6260(40)	4980(30)	4490(30)	23(9)
H(17A)	3940(50)	5370(30)	5180(30)	40(12)
H(18A)	1810(50)	5880(30)	4340(30)	35(11)
H(19A)	2180(50)	5840(30)	2800(30)	27(10)
H(21A)	6300(40)	4840(30)	730(20)	20(9)
H(22A)	6440(50)	3410(30)	200(30)	25(10)
H(23A)	4770(50)	2290(30)	410(30)	37(11)
H(24A)	2730(50)	2650(30)	1300(30)	37(11)
H(25A)	2510(40)	4140(20)	1940(30)	25(9)

Table 6. Torsion angles [°] for 3aa.

C(6)-C(1)-C(2)-O(1)	20.1(4)
C(8)-C(1)-C(2)-O(1)	-103.2(3)
C(6)-C(1)-C(2)-C(3)	-160.2(3)
C(8)-C(1)-C(2)-C(3)	76.6(3)
O(1)-C(2)-C(3)-C(4)	3.7(4)
C(1)-C(2)-C(3)-C(4)	-176.1(3)
C(2)-C(3)-C(4)-C(5)	-60.8(3)

C(2)-C(3)-C(4)-C(7)	177.5(3)
C(20)-N(1)-C(5)-O(2)	16.4(5)
C(14)-N(1)-C(5)-O(2)	-176.8(3)
C(20)-N(1)-C(5)-C(4)	-163.7(3)
C(14)-N(1)-C(5)-C(4)	3.0(5)
C(7)-C(4)-C(5)-O(2)	75.9(4)
C(3)-C(4)-C(5)-O(2)	-45.9(4)
C(7)-C(4)-C(5)-N(1)	-103.9(4)
C(3)-C(4)-C(5)-N(1)	134.2(3)
C(2)-C(1)-C(8)-C(9)	-123.4(3)
C(6)-C(1)-C(8)-C(9)	113.2(4)
C(2)-C(1)-C(8)-C(13)	58.6(4)
C(6)-C(1)-C(8)-C(13)	-64.8(4)
C(13)-C(8)-C(9)-C(10)	0.8(5)
C(1)-C(8)-C(9)-C(10)	-177.3(3)
C(8)-C(9)-C(10)-C(11)	-0.8(5)
C(9)-C(10)-C(11)-C(12)	0.6(5)
C(10)-C(11)-C(12)-C(13)	-0.4(6)
C(11)-C(12)-C(13)-C(8)	0.3(6)
C(9)-C(8)-C(13)-C(12)	-0.5(5)
C(1)-C(8)-C(13)-C(12)	177.5(3)
C(5)-N(1)-C(14)-C(15)	-95.9(4)
C(20)-N(1)-C(14)-C(15)	71.3(4)
C(5)-N(1)-C(14)-C(19)	86.1(4)
C(20)-N(1)-C(14)-C(19)	-106.7(3)
C(19)-C(14)-C(15)-C(16)	-0.3(5)
N(1)-C(14)-C(15)-C(16)	-178.3(3)
C(14)-C(15)-C(16)-C(17)	0.3(5)
C(15)-C(16)-C(17)-C(18)	0.1(5)
C(16)-C(17)-C(18)-C(19)	-0.4(6)

C(17)-C(18)-C(19)-C(14)	0.4(6)
C(15)-C(14)-C(19)-C(18)	-0.1(5)
N(1)-C(14)-C(19)-C(18)	178.0(3)
C(5)-N(1)-C(20)-C(21)	46.1(4)
C(14)-N(1)-C(20)-C(21)	-121.4(3)
C(5)-N(1)-C(20)-C(25)	-137.9(3)
C(14)-N(1)-C(20)-C(25)	54.6(4)
C(25)-C(20)-C(21)-C(22)	-1.7(5)
N(1)-C(20)-C(21)-C(22)	174.3(3)
C(20)-C(21)-C(22)-C(23)	-0.1(5)
C(21)-C(22)-C(23)-C(24)	1.4(5)
C(22)-C(23)-C(24)-C(25)	-0.9(5)
C(21)-C(20)-C(25)-C(24)	2.3(5)
N(1)-C(20)-C(25)-C(24)	-173.8(3)
C(23)-C(24)-C(25)-C(20)	-1.0(5)

8. NMR Spectra of Unknown Compounds

(2*R*,5*R*)-2-methyl-4-oxo-*N*,*N*,5-triphenylhexanamide (3aa)

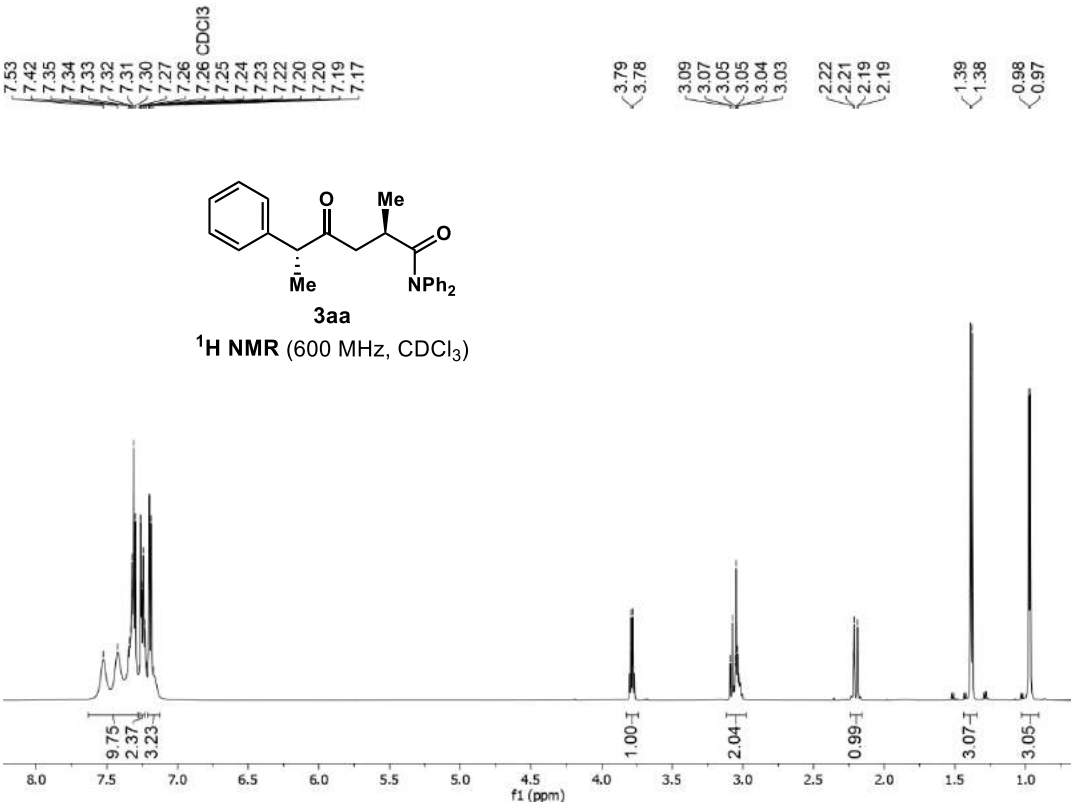

3aa

^{1}H NMR (600 MHz, $CDCl_3$)

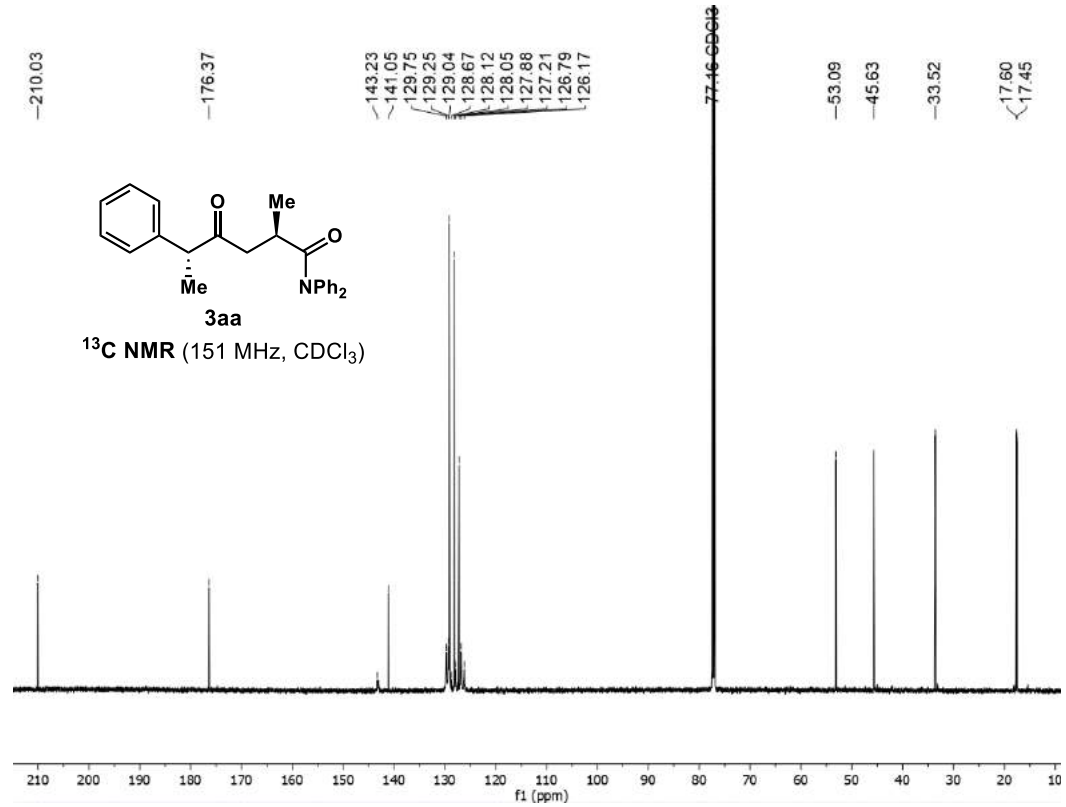

3aa

^{13}C NMR (151 MHz, $CDCl_3$)

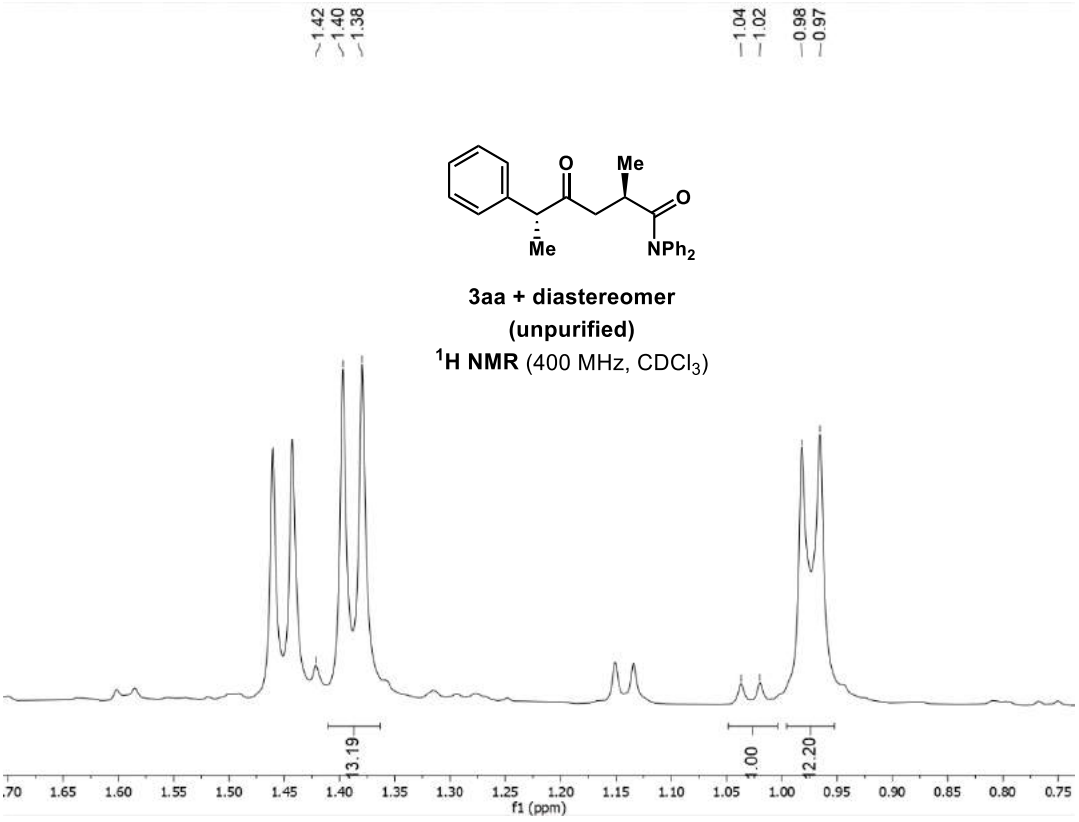

3aa + diastereomer
(unpurified)
^{1}H NMR (400 MHz, $CDCl_3$)

(2*R*,5*R*)-5-(4-methoxyphenyl)-2-methyl-4-oxo-*N*,*N*-diphenylhexanamide (3ba)

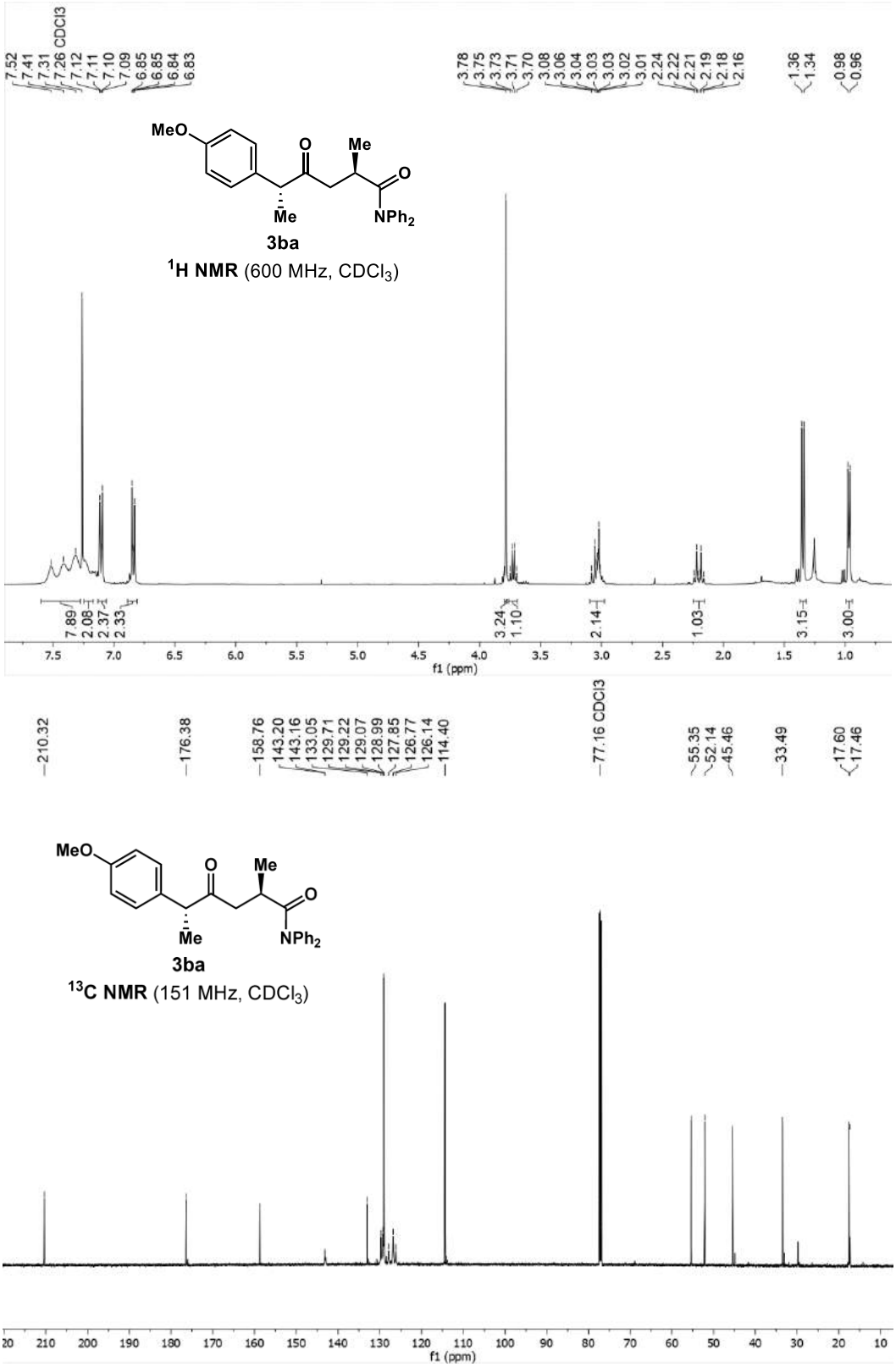

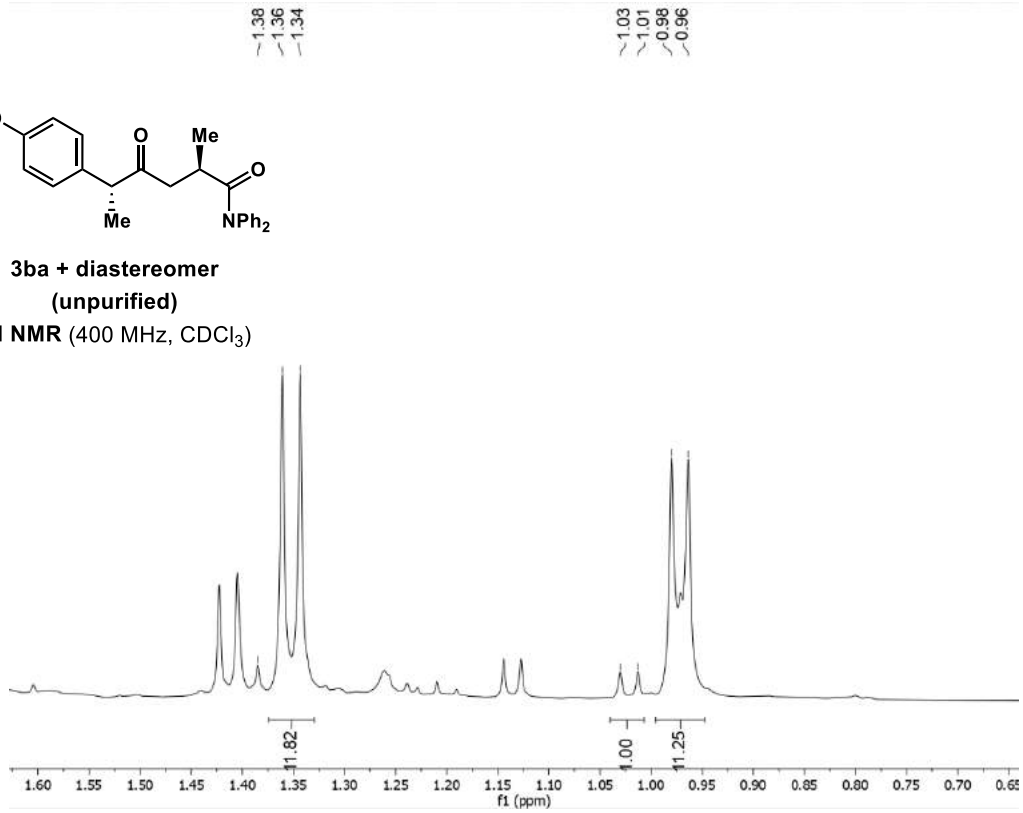

3ba + diastereomer
(unpurified)
^{1}H NMR (400 MHz, $CDCl_3$)

(2*R*,5*R*)-5-(4-chlorophenyl)-2-methyl-4-oxo-*N*,*N*-diphenylhexanamide (3ca)

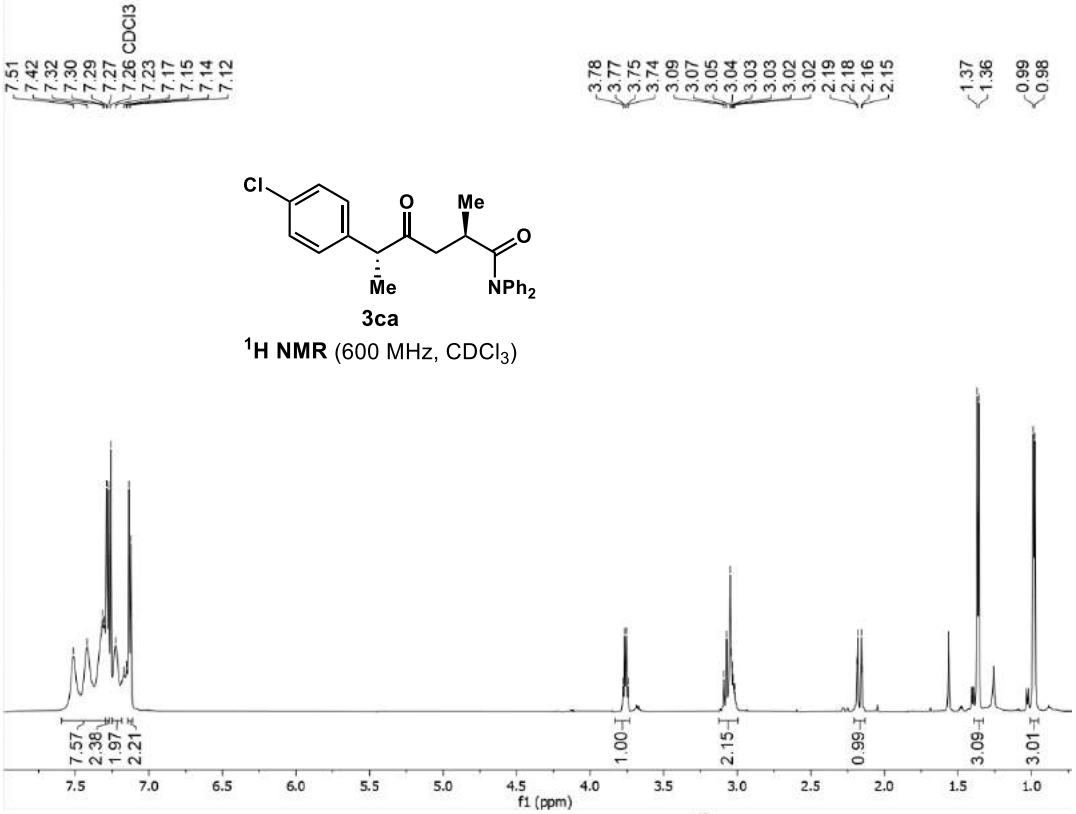

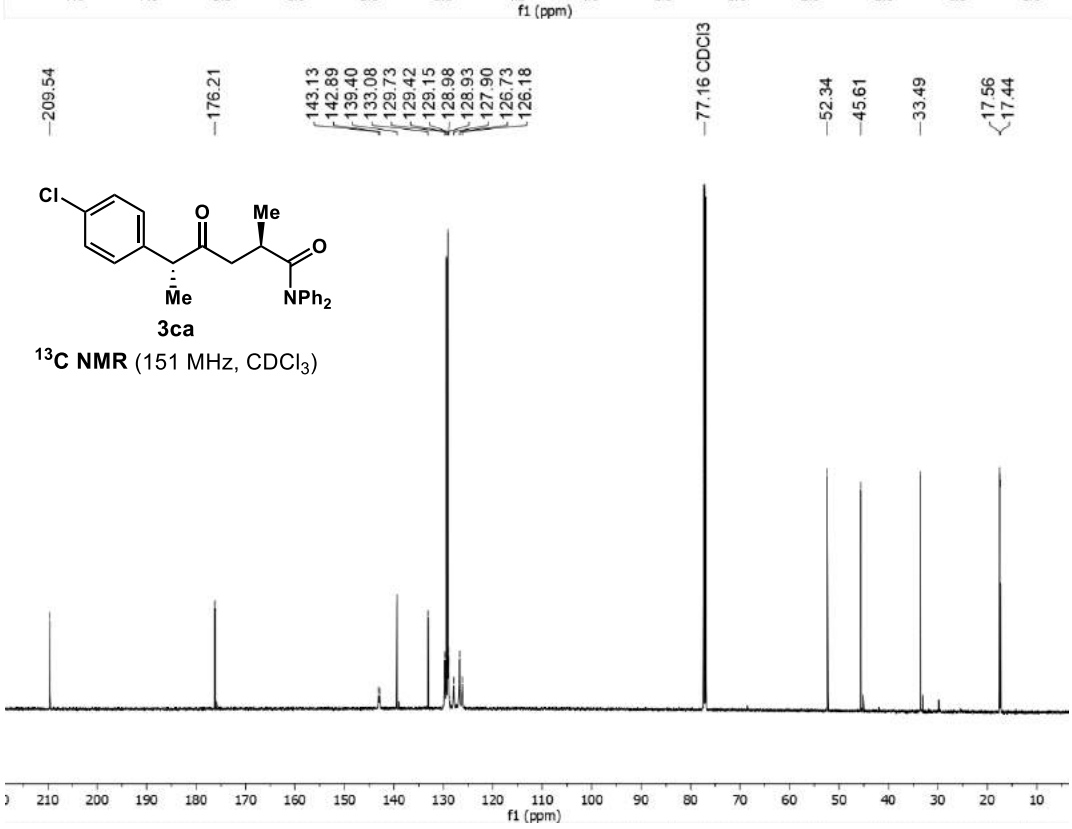

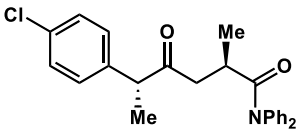

3ca + diastereomer
(unpurified)
^{1}H NMR (400 MHz, $CDCl_3$)

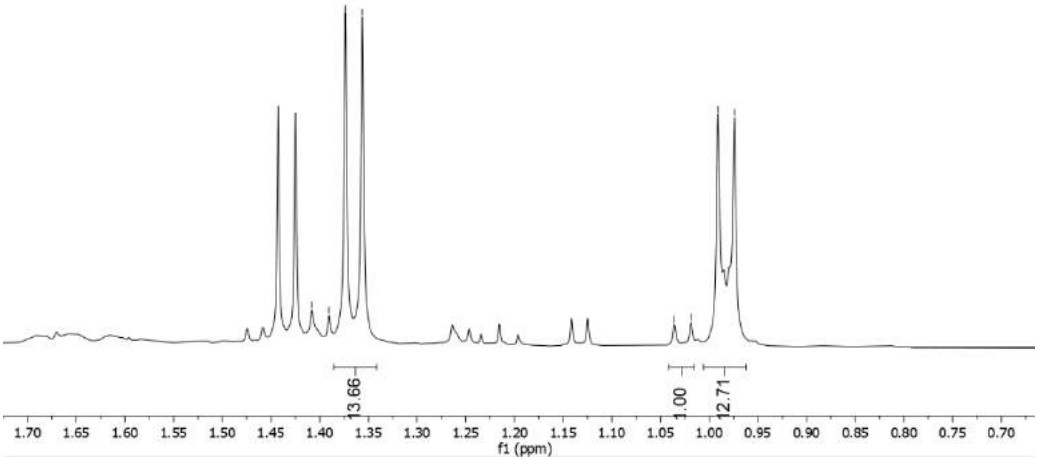

(2*R*,5*R*)-5-(4-bromophenyl)-2-methyl-4-oxo-*N*,*N*-diphenylhexanamide (3da)

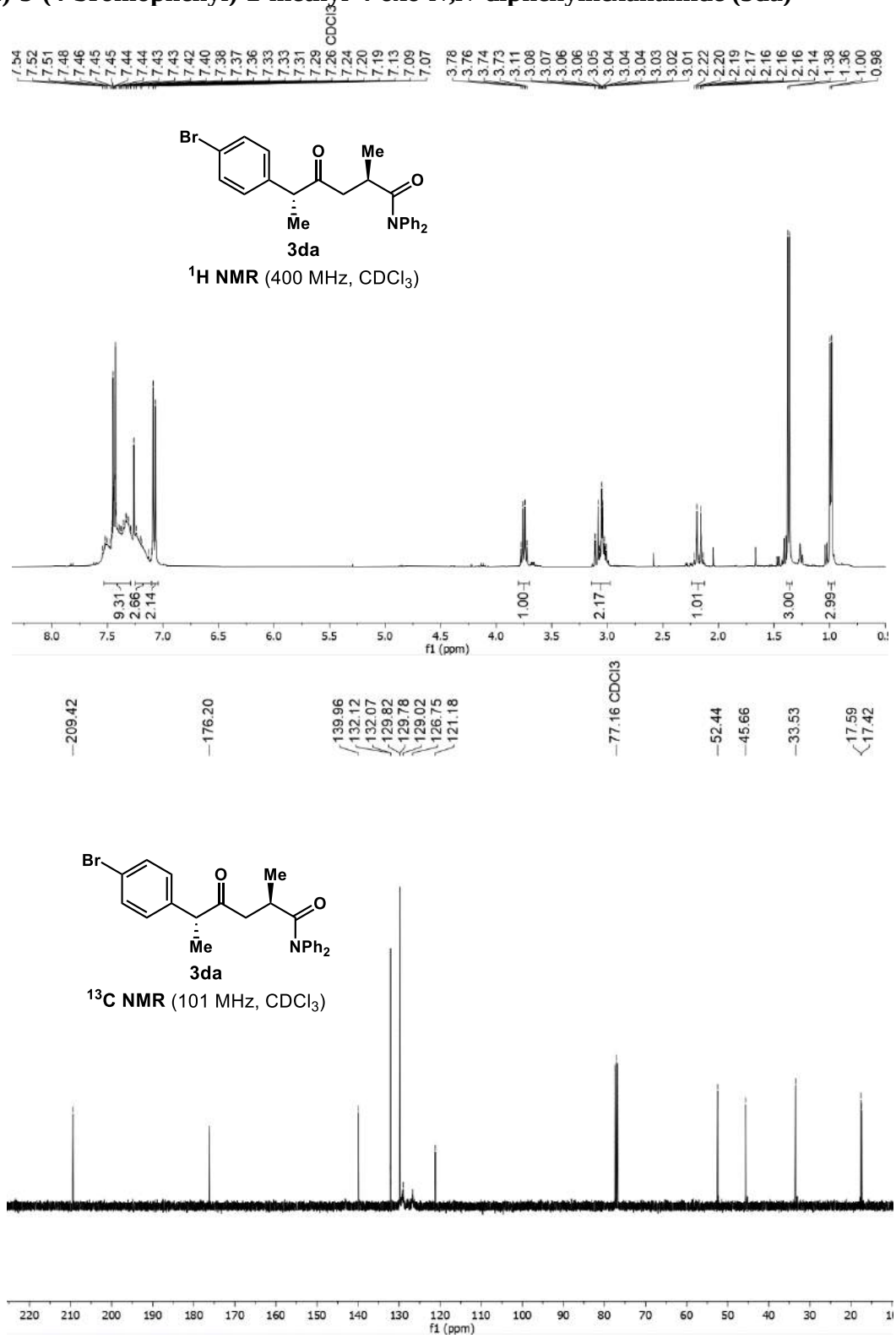

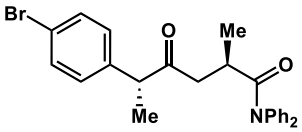

3da + diastereomer
(unpurified)
^{1}H NMR (400 MHz, $CDCl_3$)

(2*R*,5*R*)-2-methyl-4-oxo-*N*,*N*-diphenyl-5-(4-(trifluoromethyl)phenyl)hexanamide (3ea)

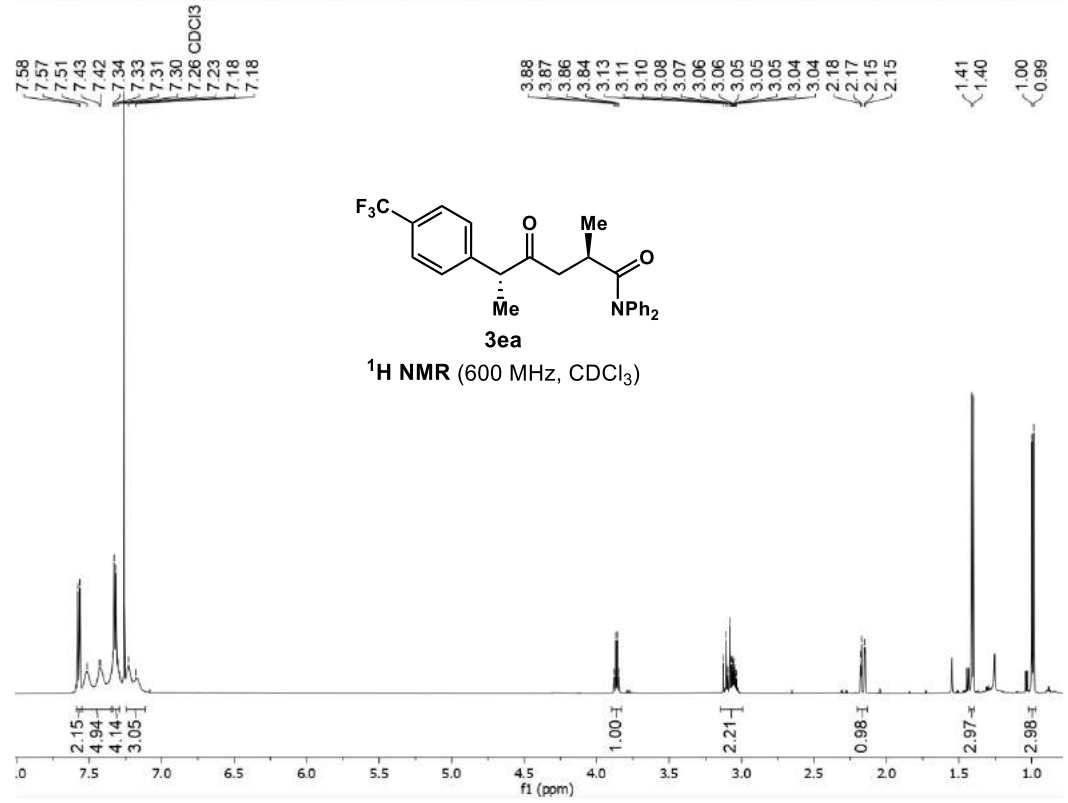

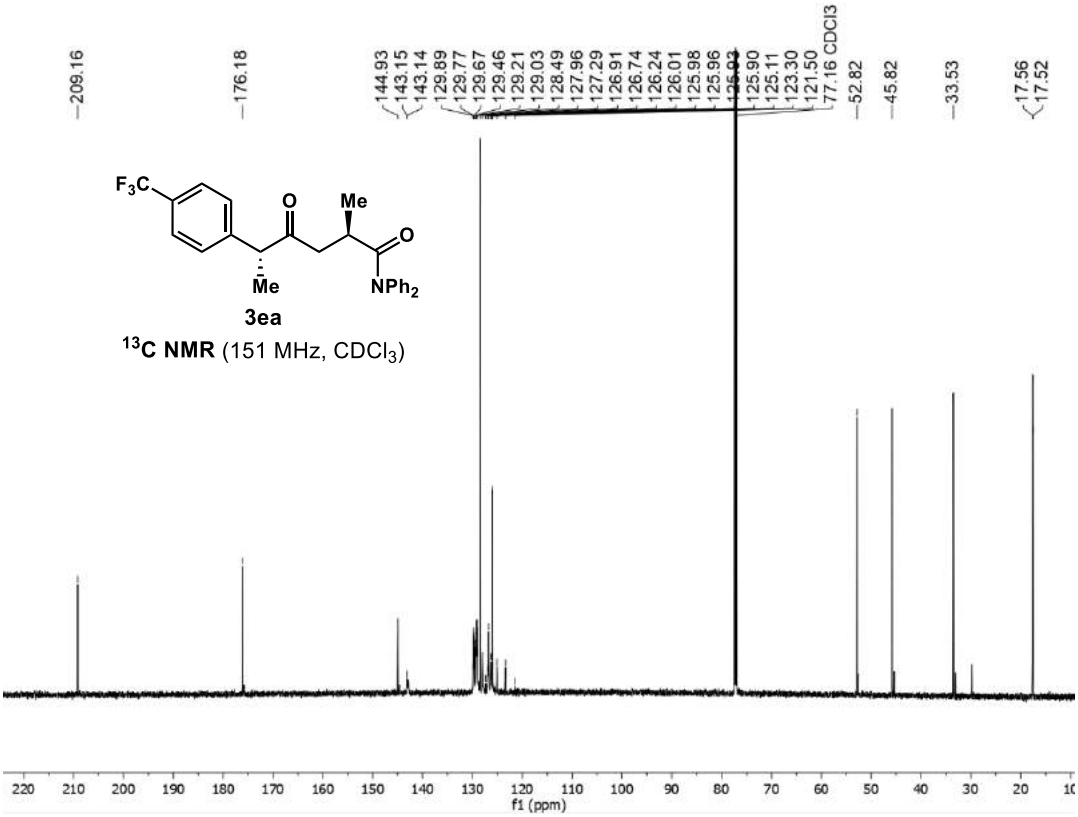

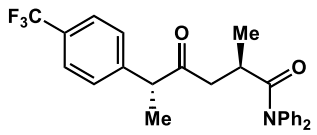

3ea

^{19}F NMR (565 MHz, $CDCl_3$)

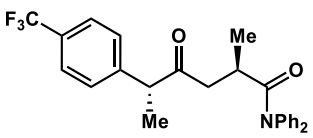

3ea + diastereomer

(unpurified)

^{1}H NMR (400 MHz, $CDCl_3$)

(2*R*,5*R*)-5-(3-methoxyphenyl)-2-methyl-4-oxo-*N*,*N*-diphenylhexanamide (3fa)

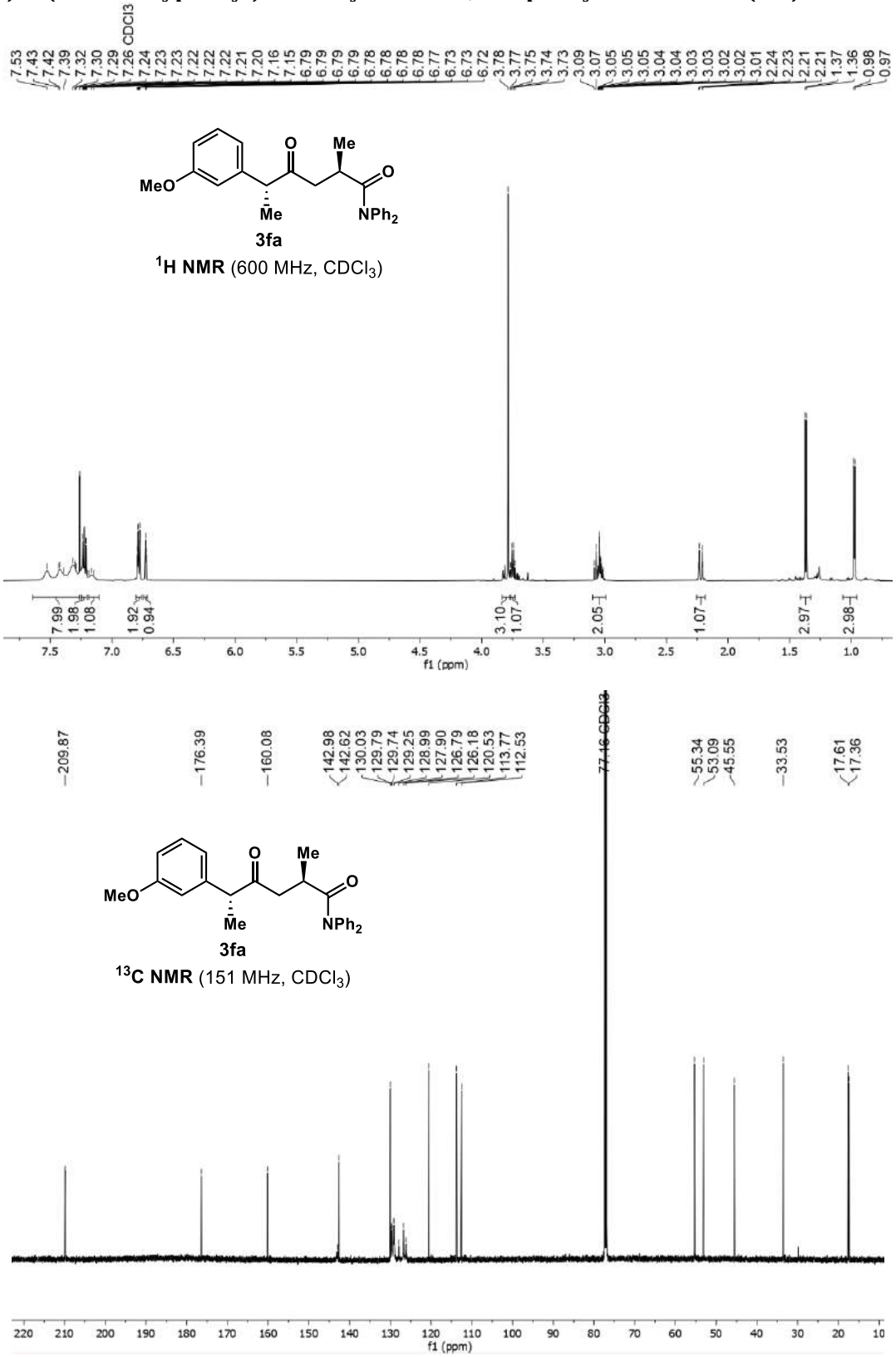

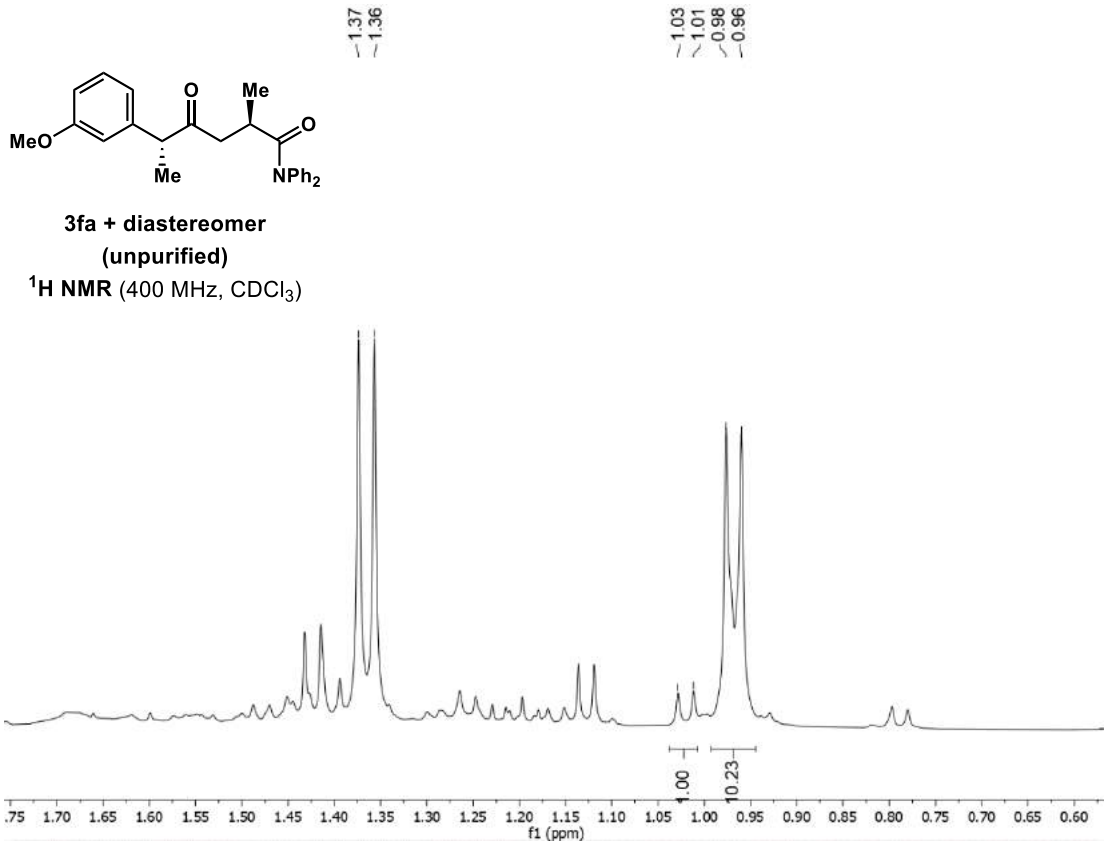

3fa + diastereomer
(unpurified)
^{1}H NMR (400 MHz, $CDCl_3$)

(2*R*,5*R*)-5-(3-chlorophenyl)-2-methyl-4-oxo-*N*,*N*-diphenylhexanamide (3ga)

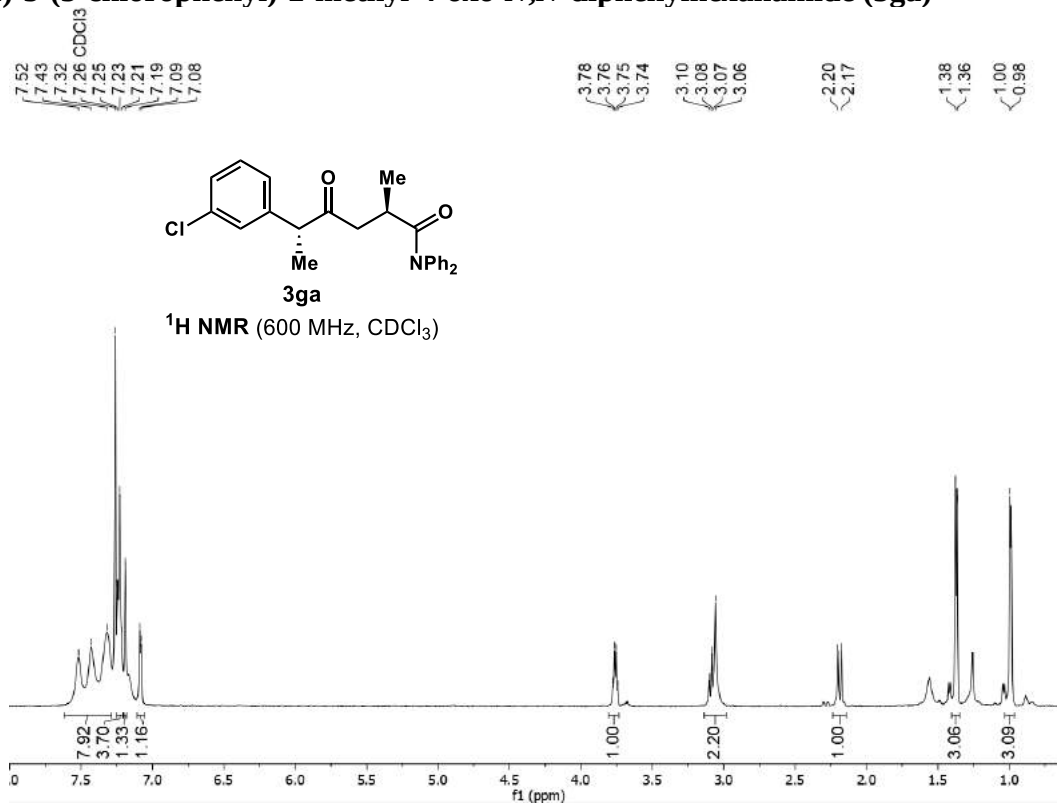

3ga

^{1}H NMR (600 MHz, $CDCl_3$)

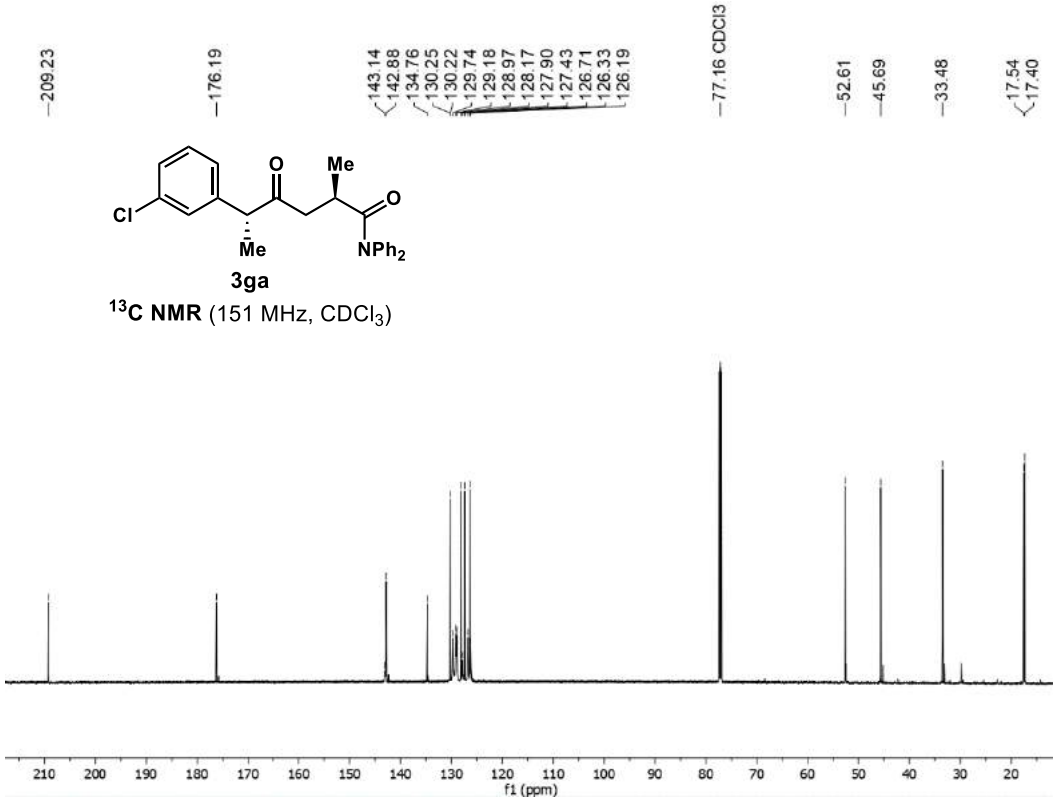

3ga

^{13}C NMR (151 MHz, $CDCl_3$)

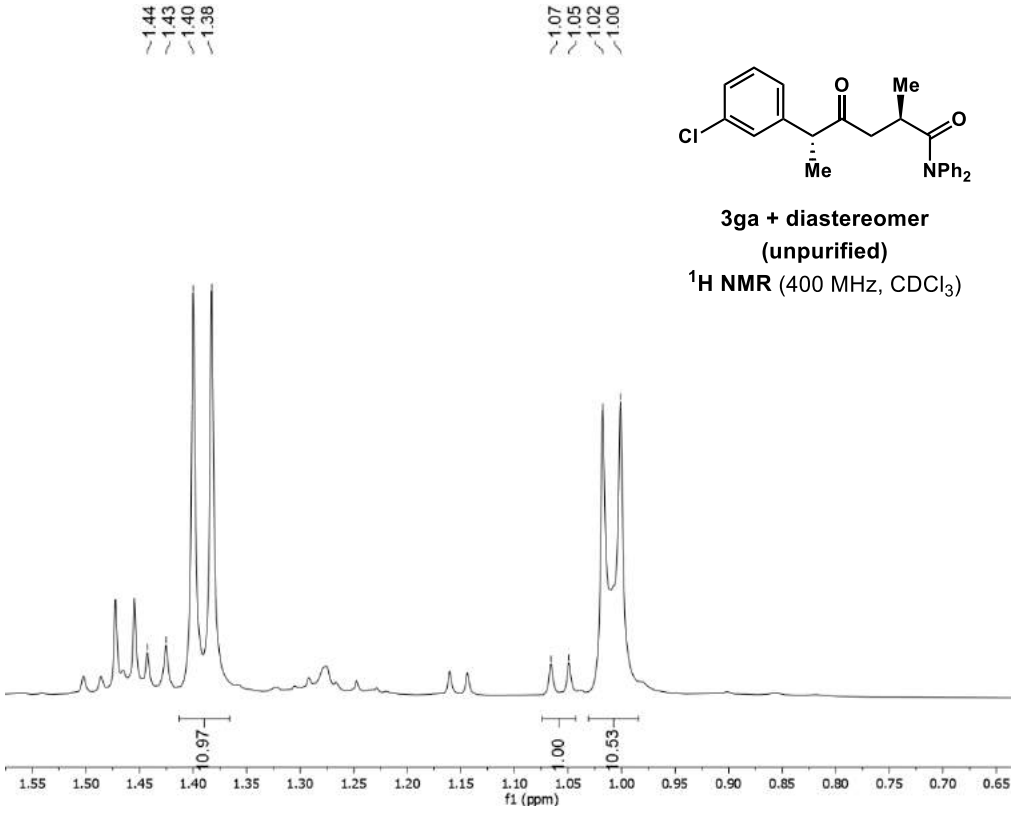

3ga + diastereomer
(unpurified)
^{1}H NMR (400 MHz, $CDCl_3$)

(2*R*,5*R*)-2-methyl-4-oxo-*N*,*N*-diphenyl-5-(*o*-tolyl)hexanamide (3ha)

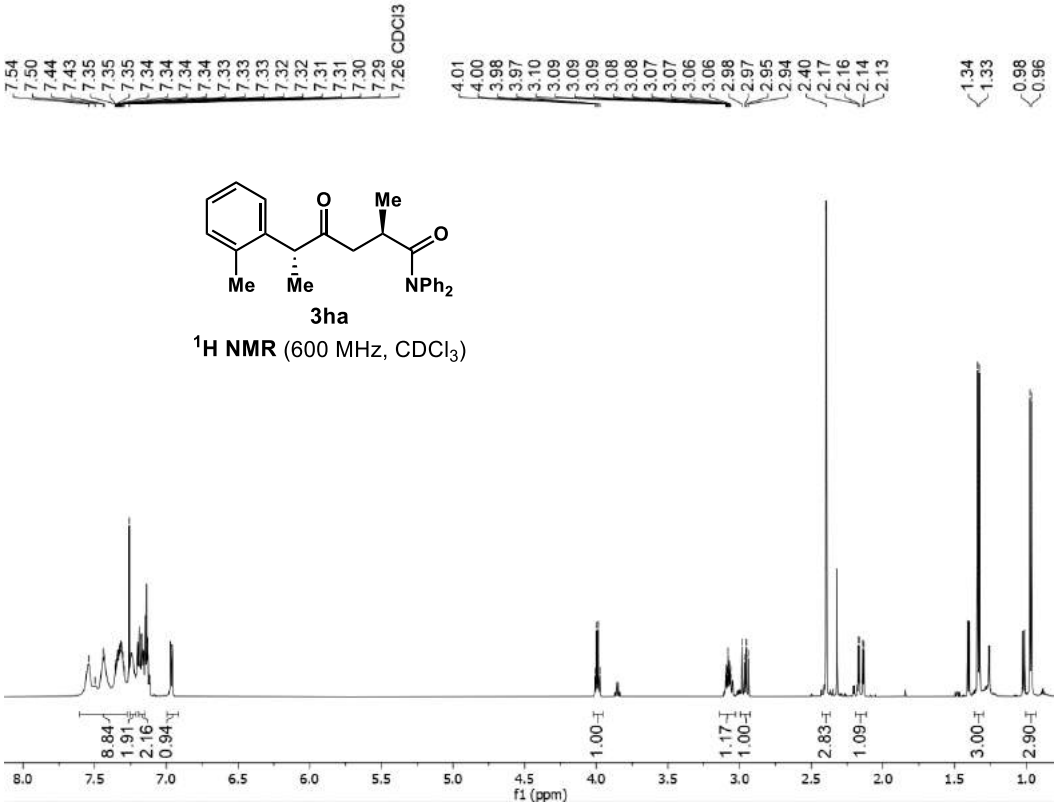

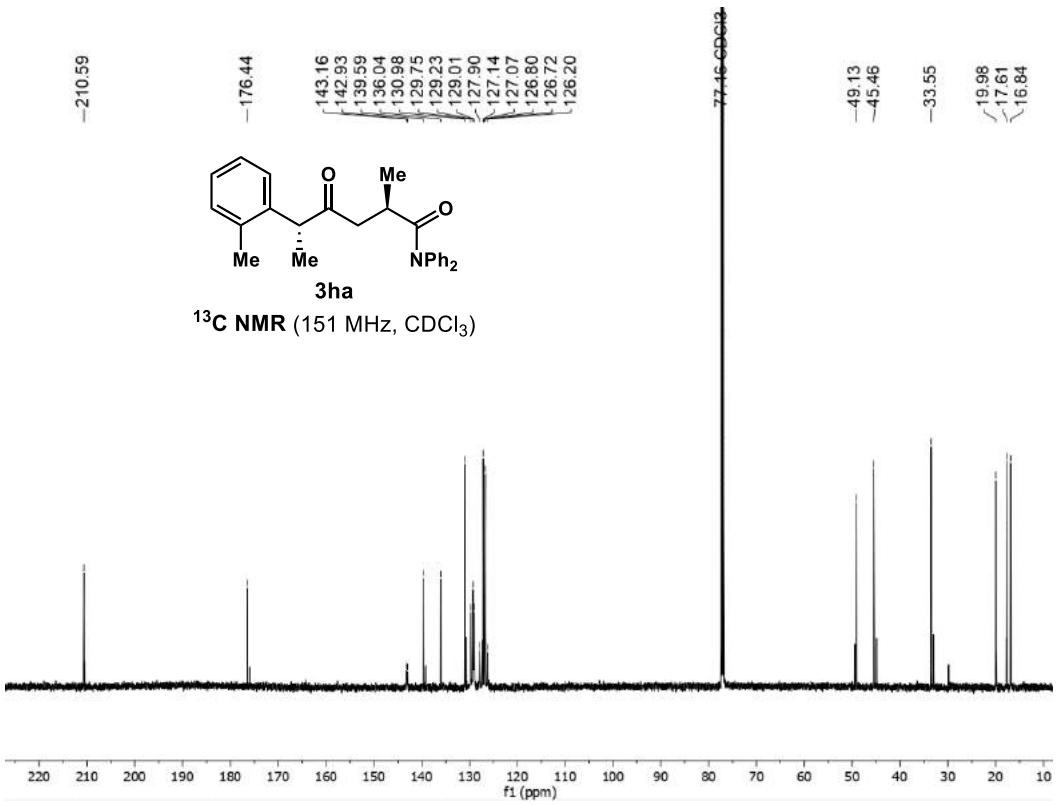

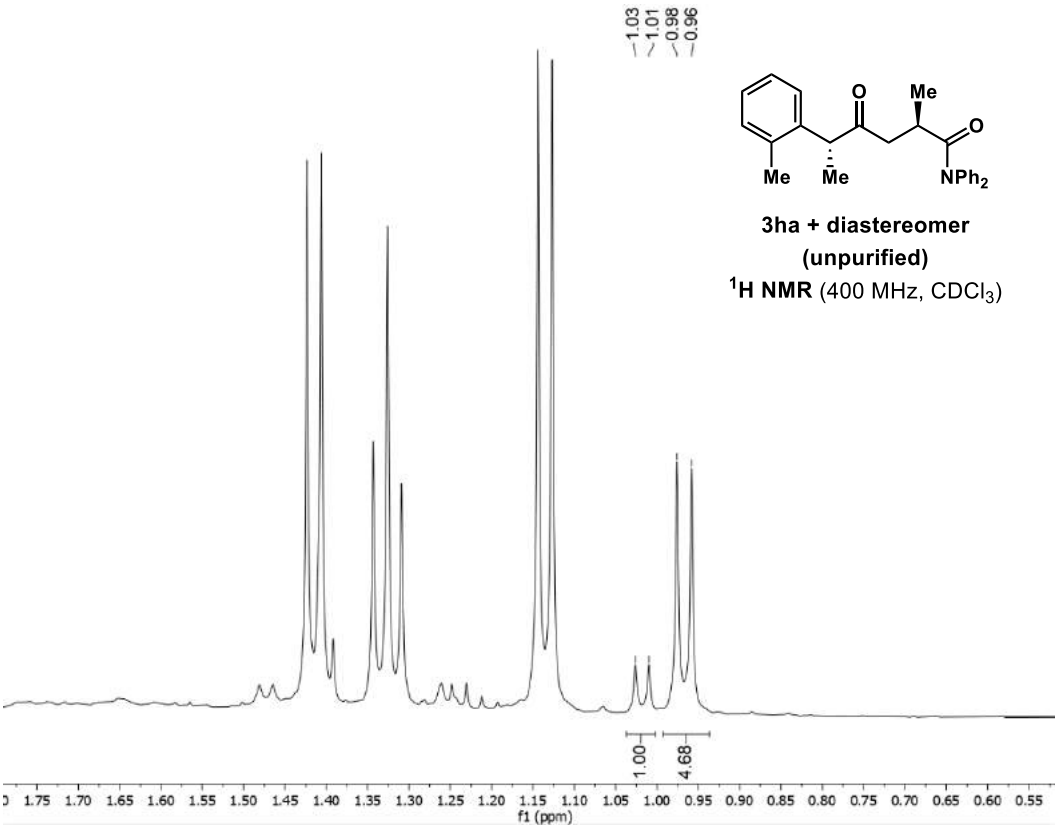

3ha + diastereomer
(unpurified)
^{1}H NMR (400 MHz, $CDCl_3$)

(2*R*,5*R*)-2-methyl-5-(naphthalen-2-yl)-4-oxo-*N*,*N*-diphenylhexanamide (3ia)

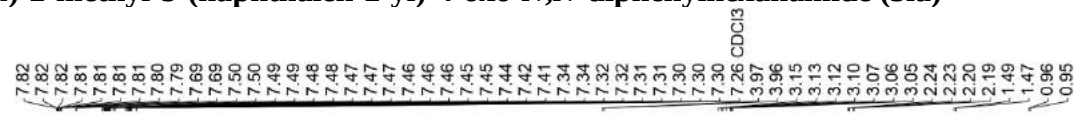

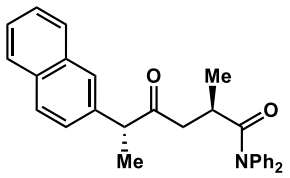

3ia

^{1}H NMR (500 MHz, $CDCl_3$)

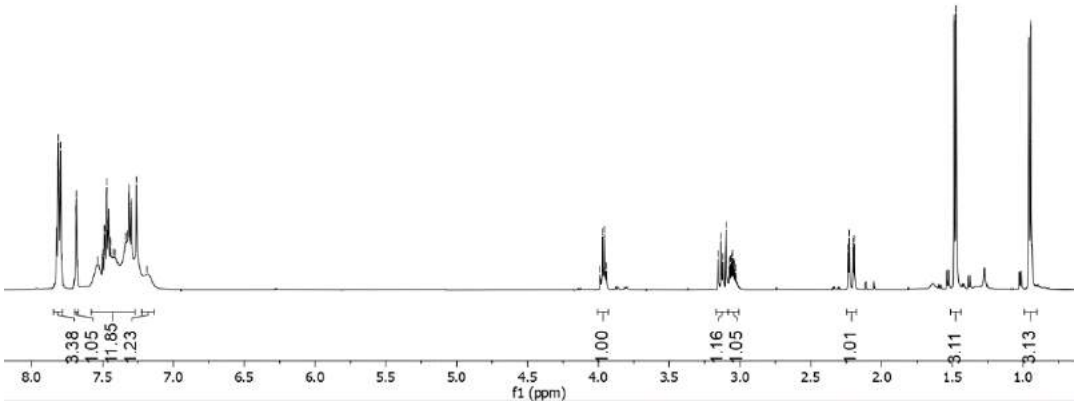

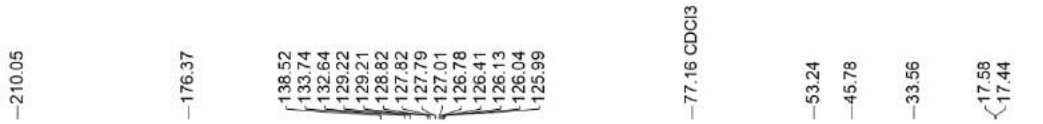

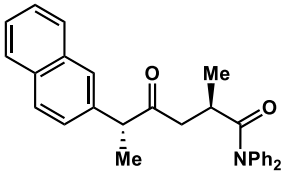

3ia

^{13}C NMR (125 MHz, $CDCl_3$)

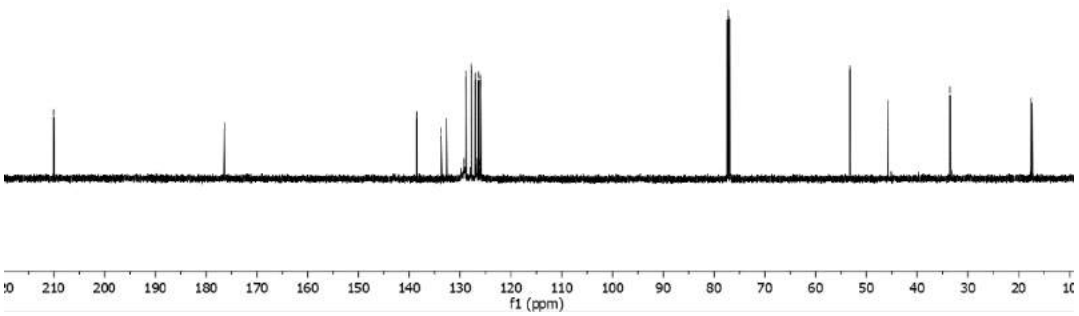

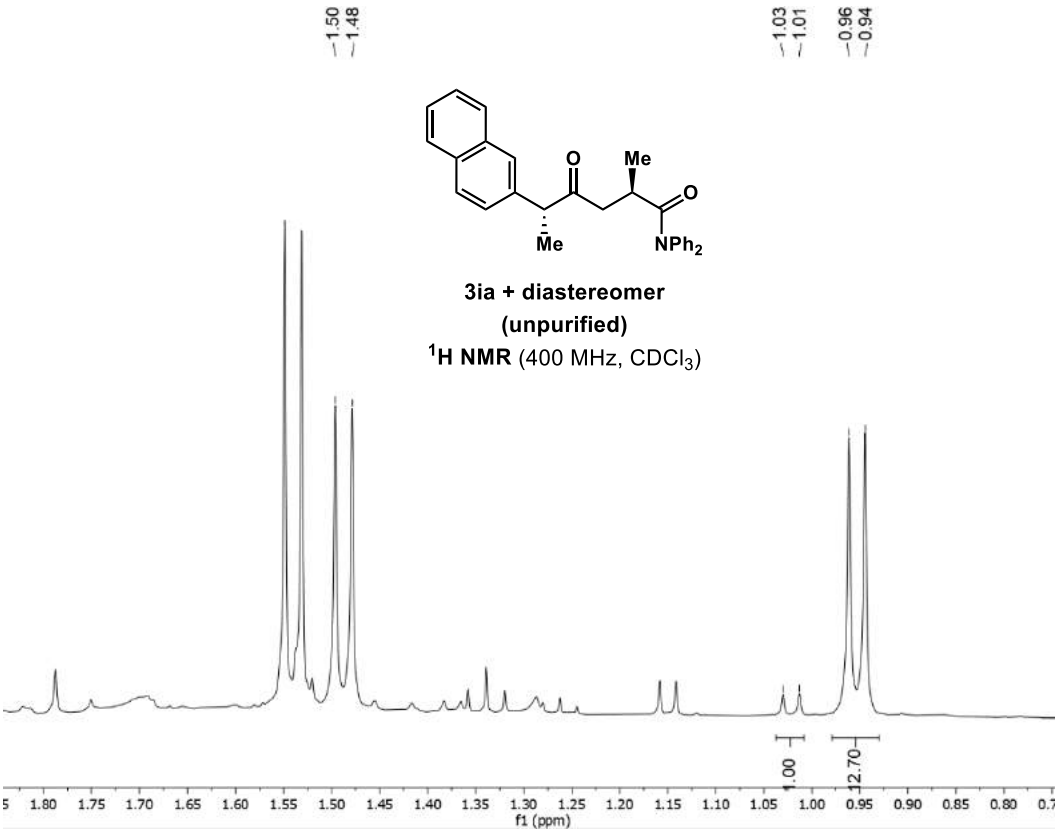

3ia + diastereomer
(unpurified)
^{1}H NMR (400 MHz, $CDCl_3$)

(2*R*,5*R*)-5-(benzo[*d*][1,3]dioxol-5-yl)-2-methyl-4-oxo-*N*,*N*-diphenylhexanamide (3ja)

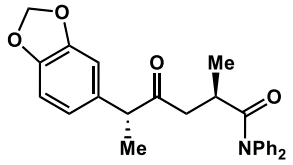

3ja

^{1}H NMR (400 MHz, $CDCl_3$)

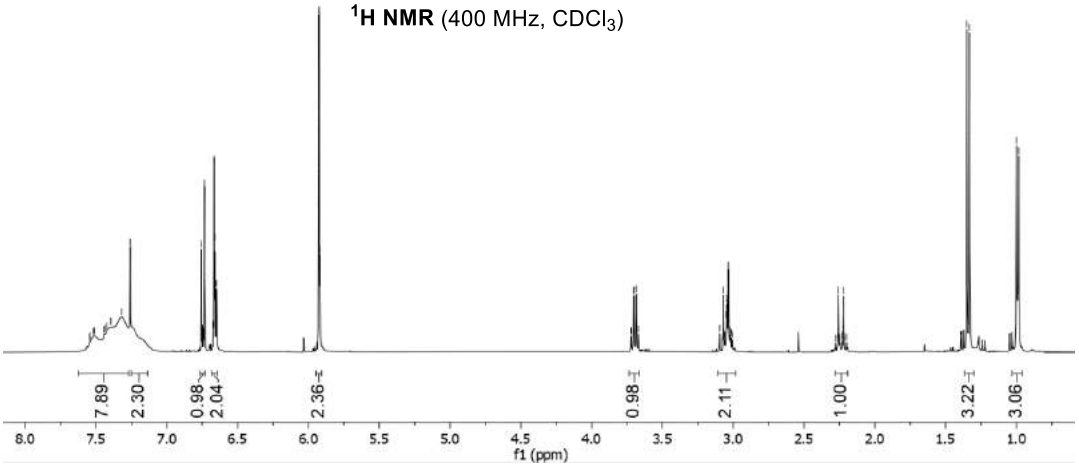

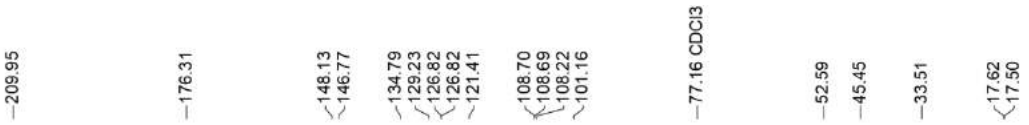

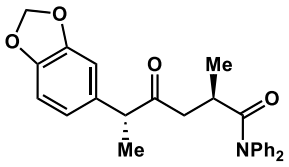

3ja

^{13}C NMR (101 MHz, $CDCl_3$)

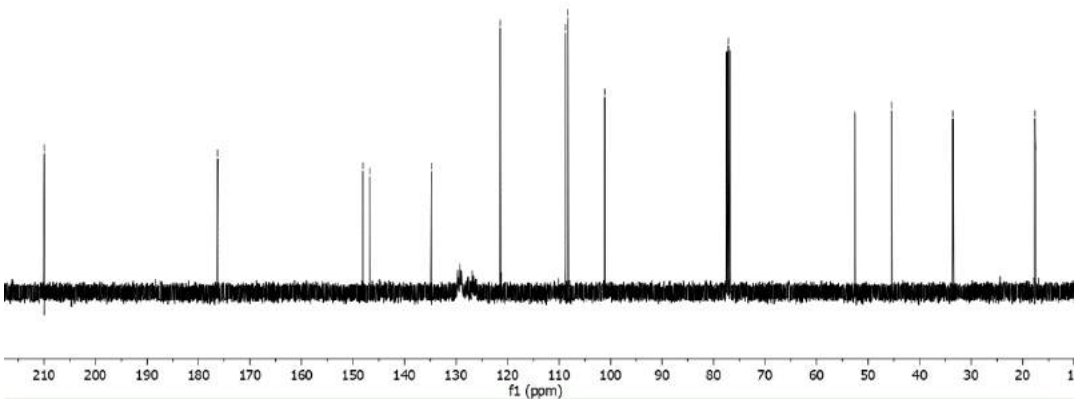

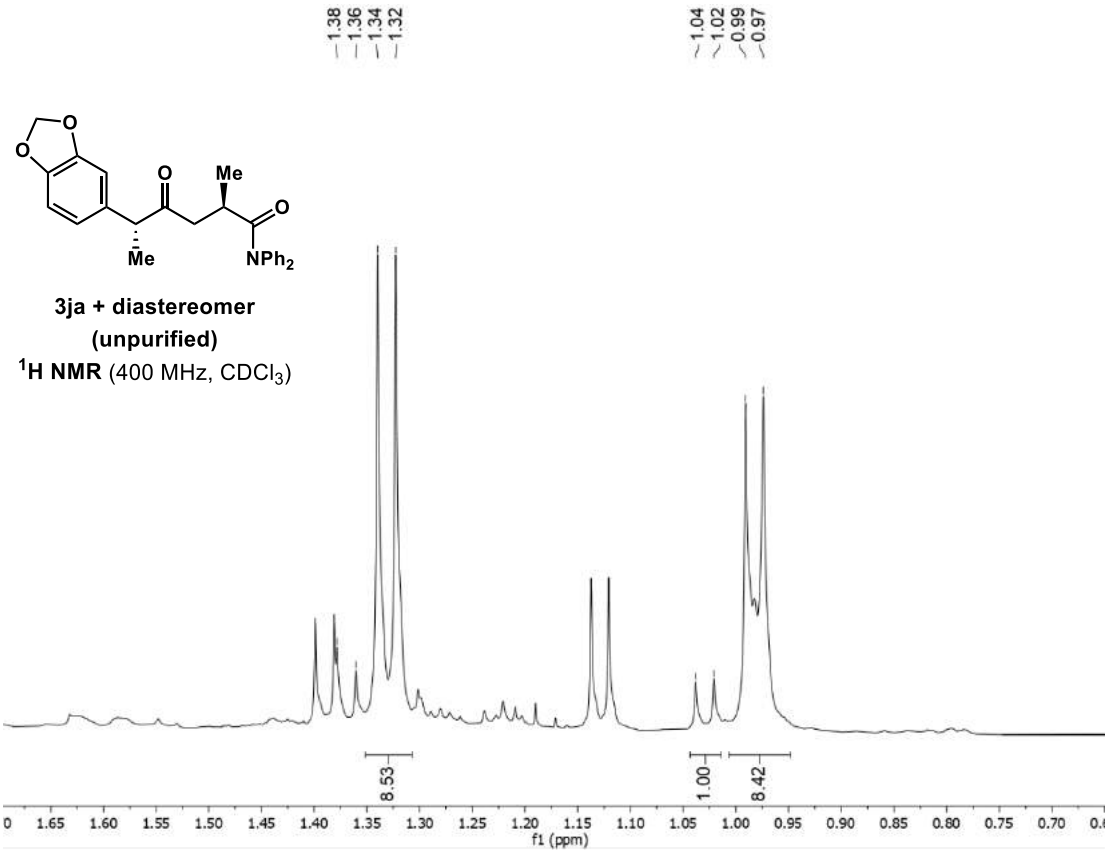

3ja + diastereomer
(unpurified)
^{1}H NMR (400 MHz, $CDCl_3$)

(2*S*,5*R*)-4-oxo-*N*,*N*,2,5-tetraphenylhexanamide (3ab)

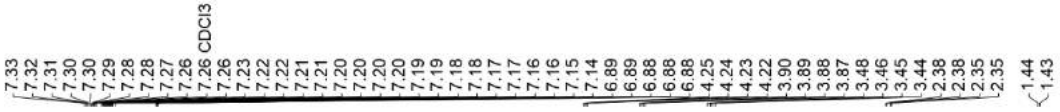

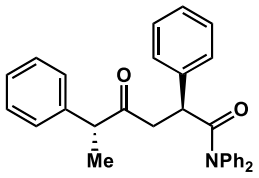

3ab

^{1}H NMR (600 MHz, $CDCl_3$)

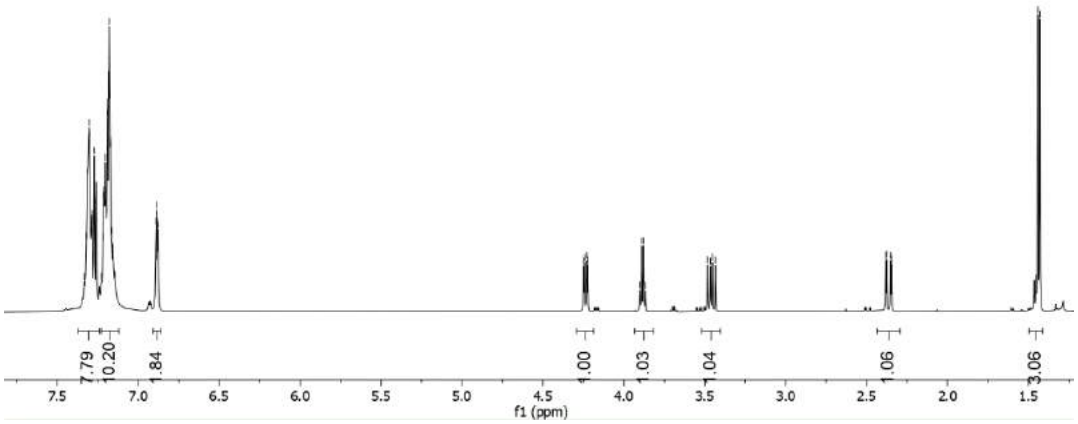

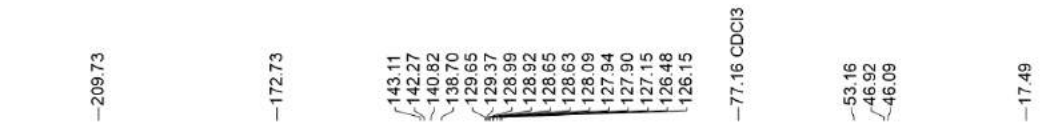

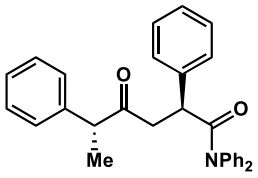

3ab

^{13}C NMR (151 MHz, $CDCl_3$)

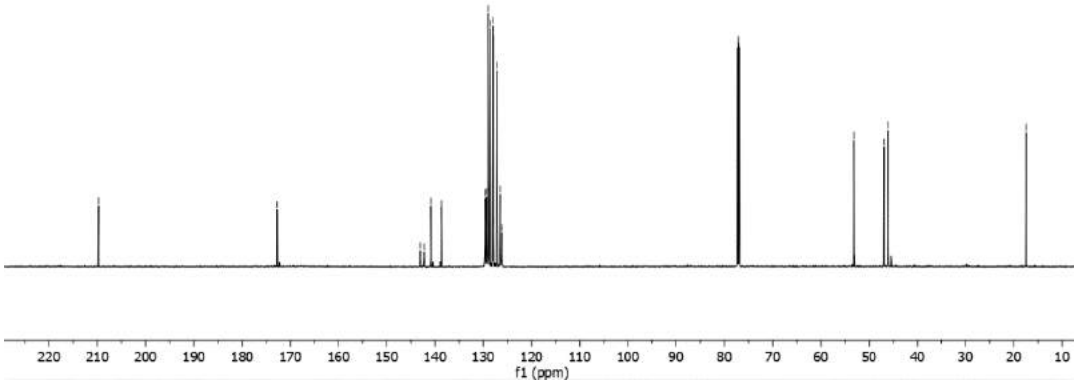

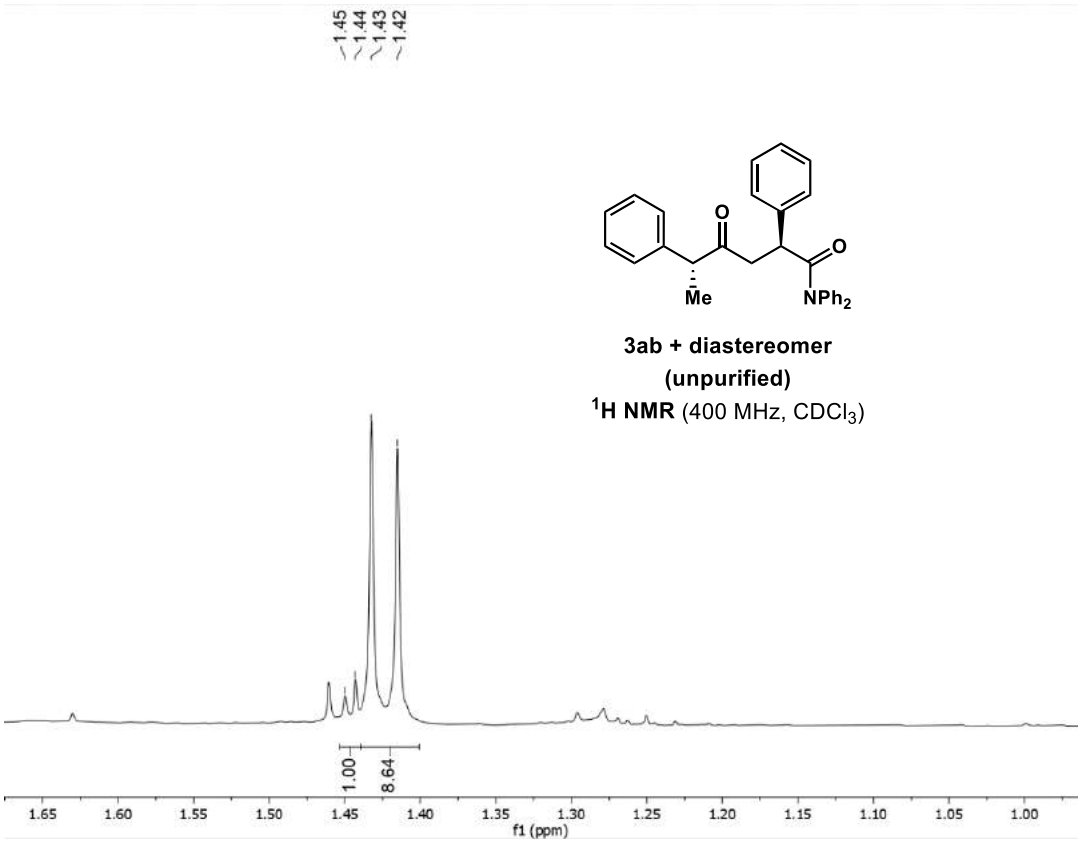

3ab + diastereomer
(unpurified)
^{1}H NMR (400 MHz, $CDCl_3$)

(2*R*,5*R*)-2-benzyl-4-oxo-*N*,*N*,5-triphenylhexanamide (3ac)

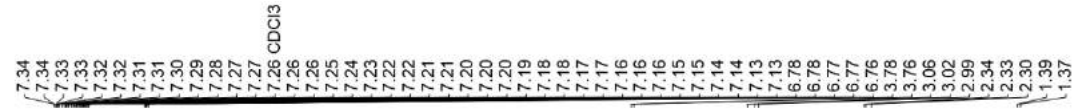

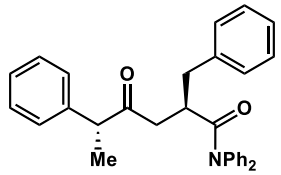

3ac

^{1}H NMR (400 MHz, $CDCl_3$)

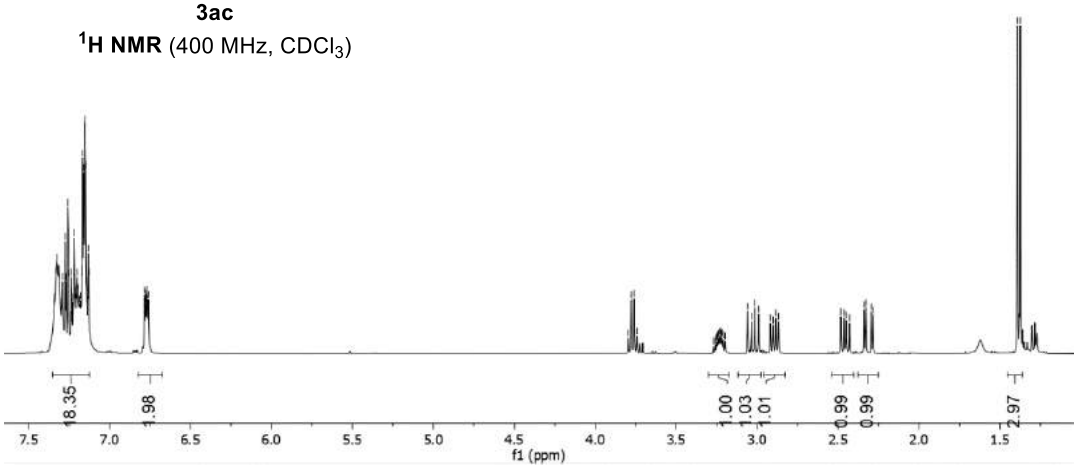

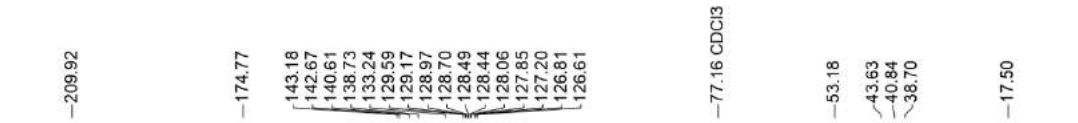

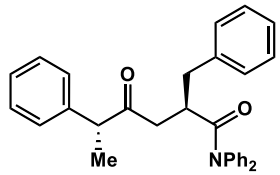

3ac

^{13}C NMR (151 MHz, $CDCl_3$)

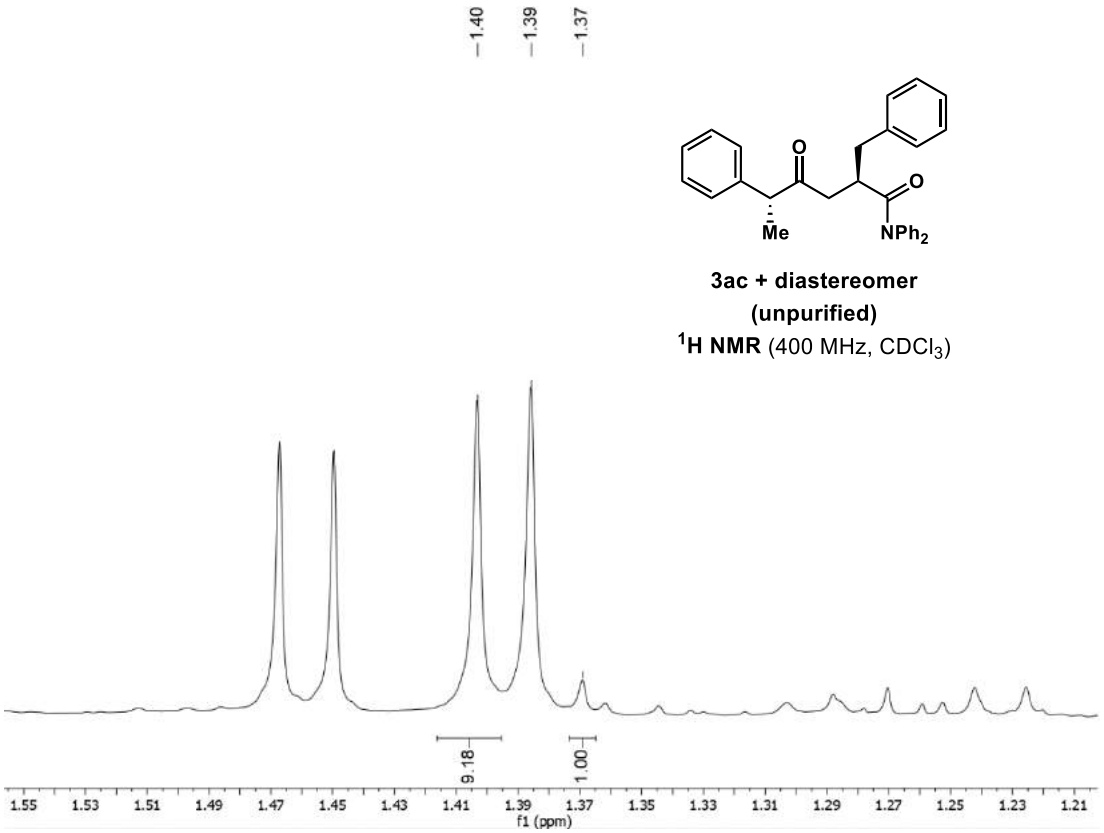

*****Major and minor diastereomer overlap at 1.39 ppm. One peak from each of the doublets was used for determination of *dr*.

(*R*)-4-oxo-*N*,*N*,5-triphenylhexanamide (3ad)

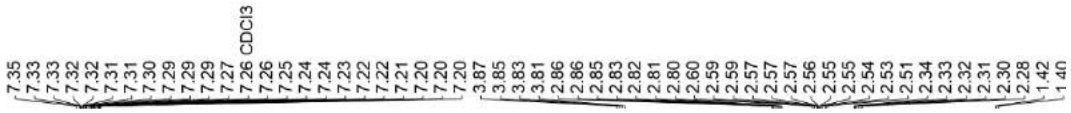

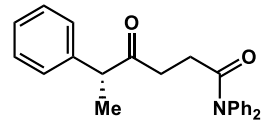

3ad

^{1}H NMR (400 MHz, $CDCl_3$)

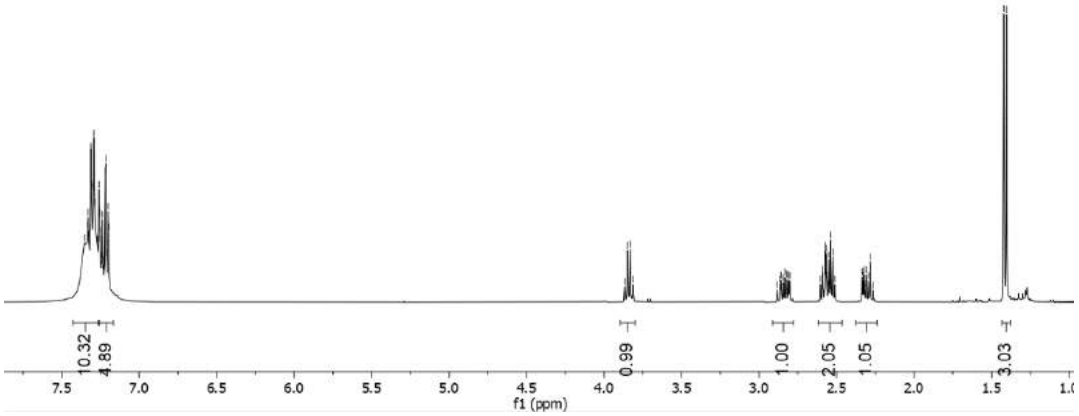

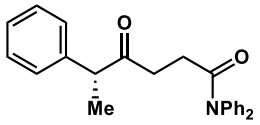

3ad

^{13}C NMR (151 MHz, $CDCl_3$)

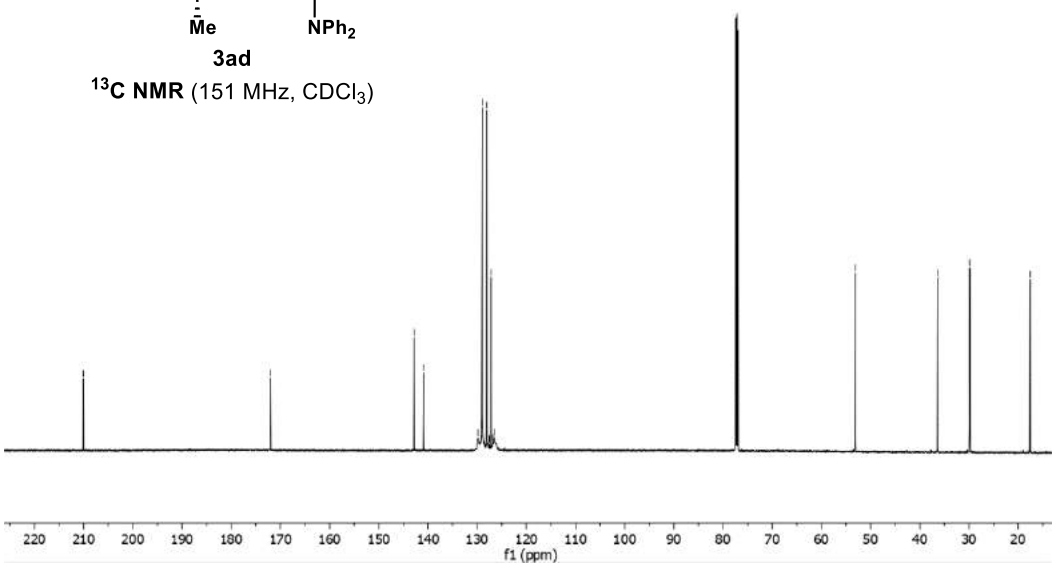

(2*R*,5*R*)-2-methyl-1-morpholino-5-phenylhexane-1,4-dione (3ae)

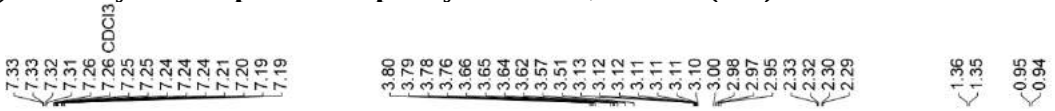

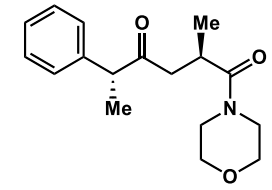

3ae

^{1}H NMR (600 MHz, $CDCl_3$)

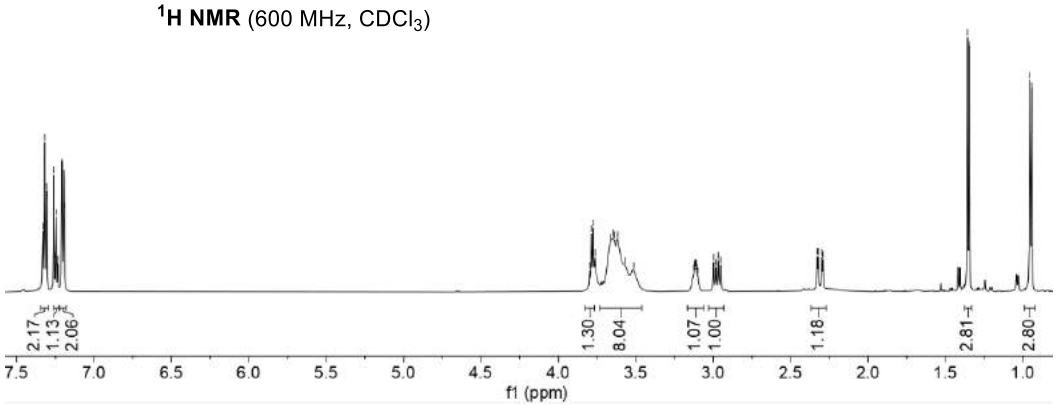

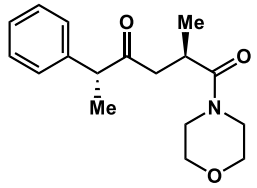

3ae

^{13}C NMR (151 MHz, $CDCl_3$)

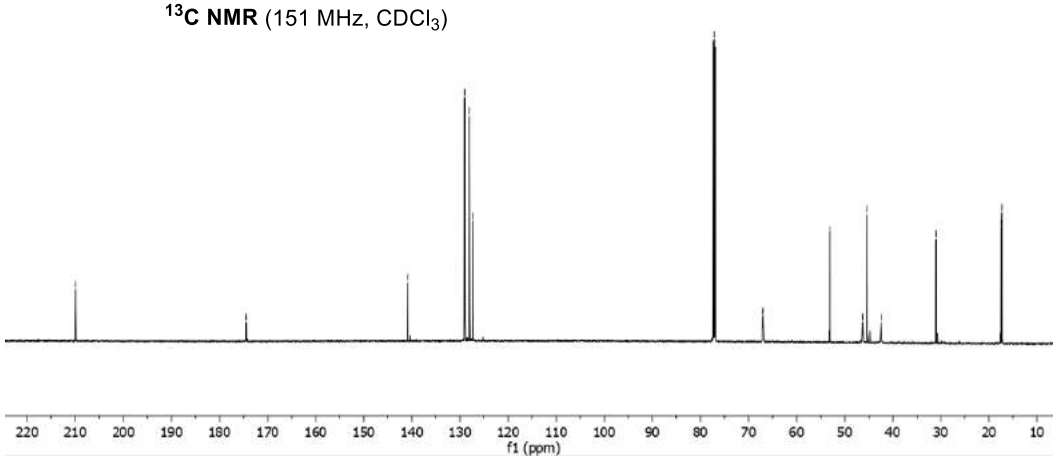

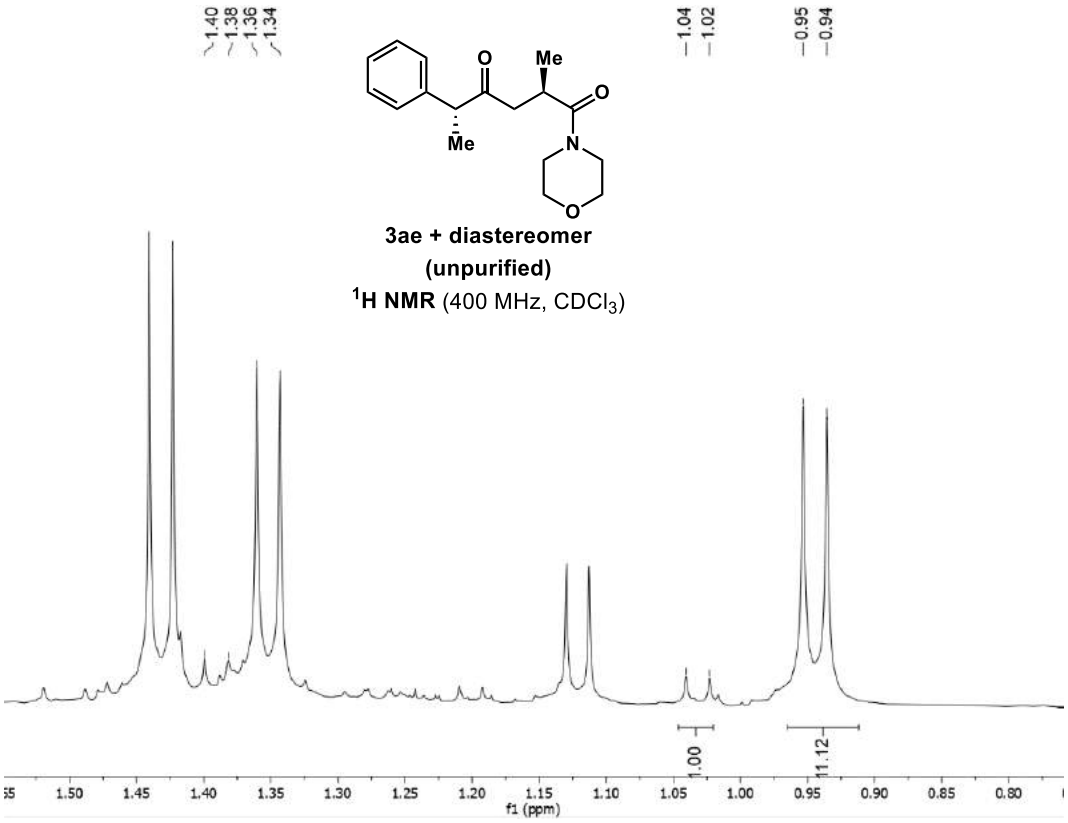

3ae + diastereomer
(unpurified)
^{1}H NMR (400 MHz, $CDCl_3$)

(2*R*,5*R*)-*N*,*N*-dibenzyl-2-methyl-4-oxo-5-phenylhexanamide (3af)

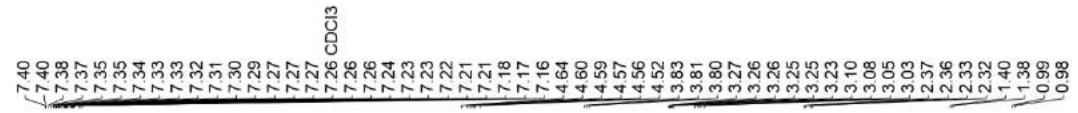

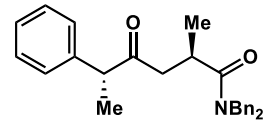

3af

^{1}H NMR (400 MHz, $CDCl_3$)

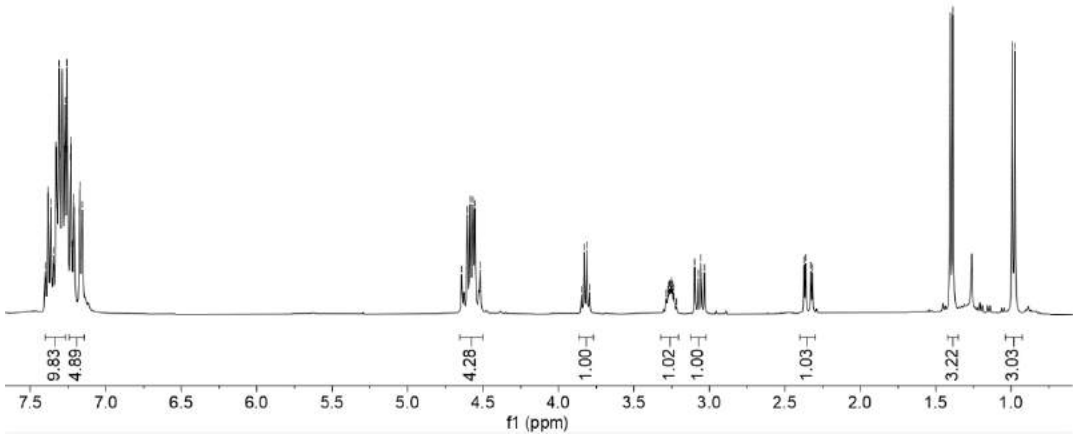

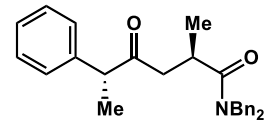

3af

^{13}C NMR (101 MHz, $CDCl_3$)

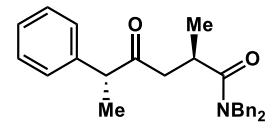

3af + diastereomer
(unpurified)
^{1}H NMR (400 MHz, $CDCl_3$)

(2*R*,5*R*)-2-methyl-4-oxo-*N*,5-diphenylhexanamide (3ag)

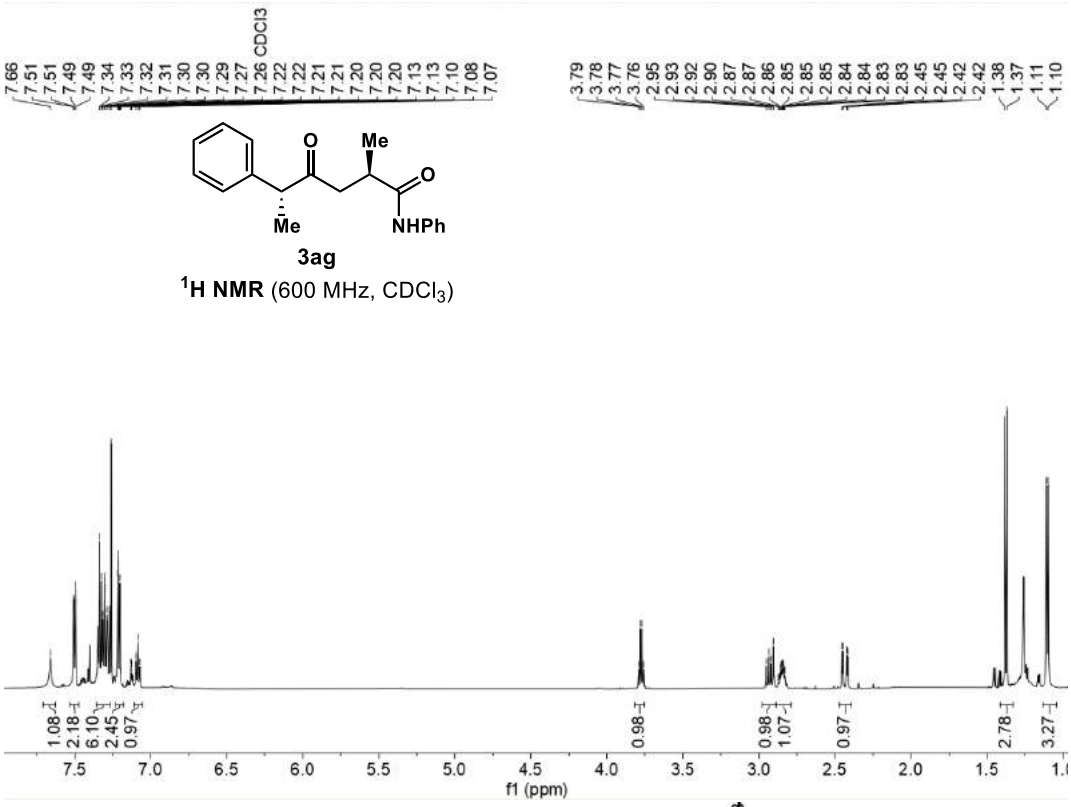

3ag

^{1}H NMR (600 MHz, $CDCl_3$)

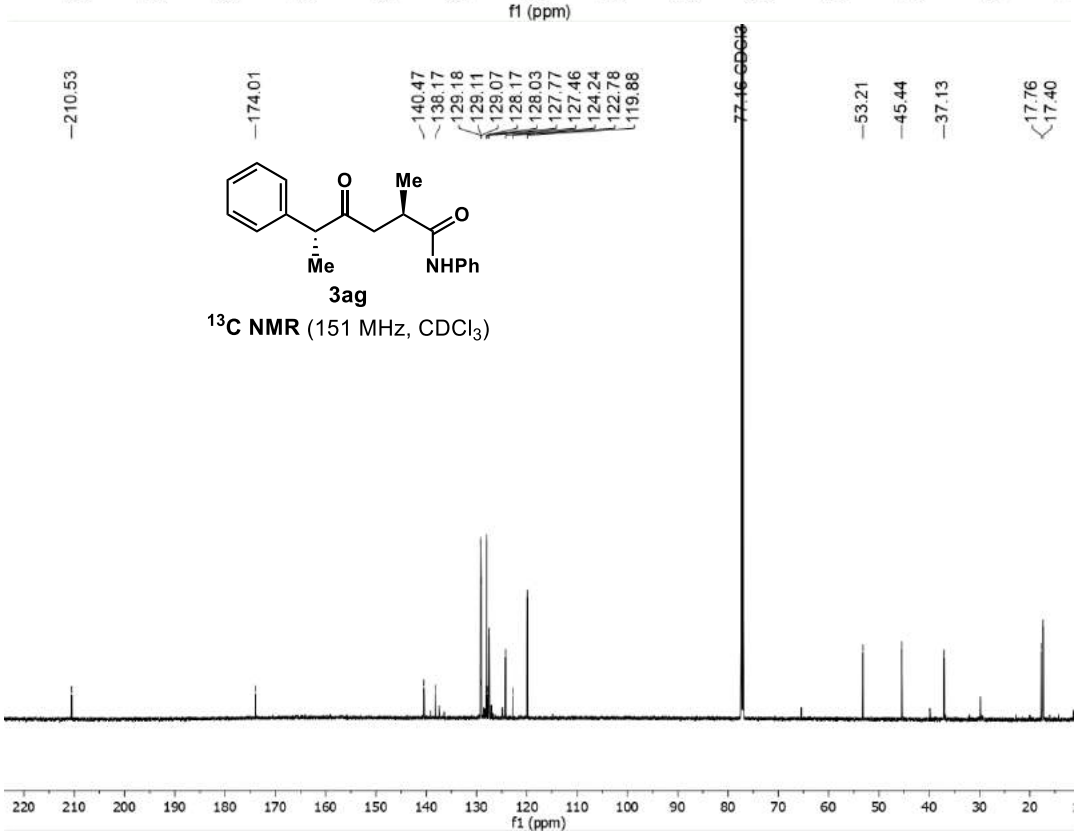

3ag

^{13}C NMR (151 MHz, $CDCl_3$)

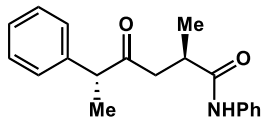

3ag + diastereomer
(unpurified)
^{1}H NMR (400 MHz, $CDCl_3$)

(2*R*,5*R*)-*N*-methoxy-*N*,2-dimethyl-4-oxo-5-phenylhexanamide (3ah)

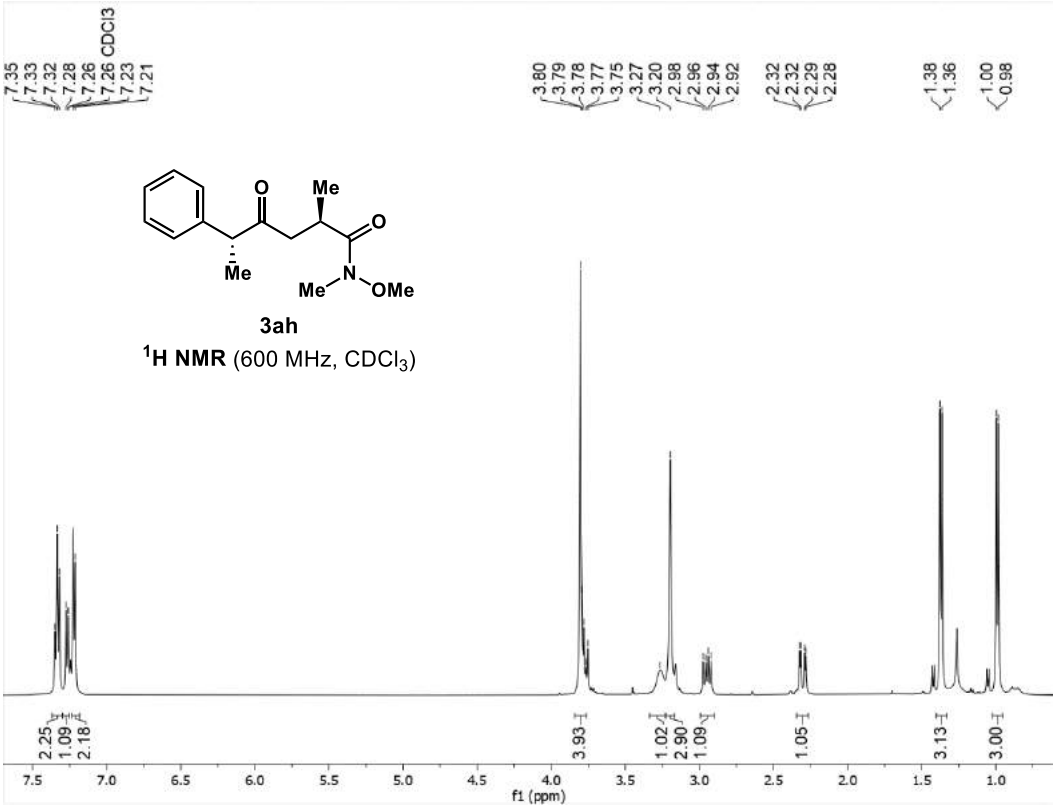

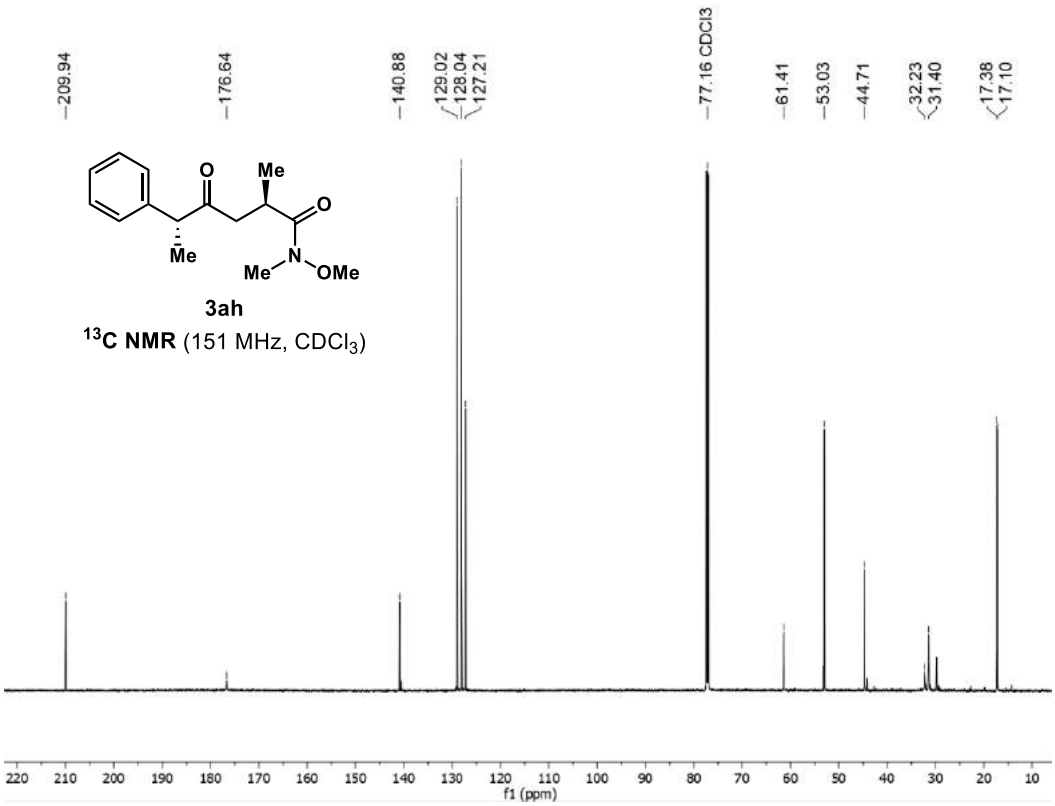

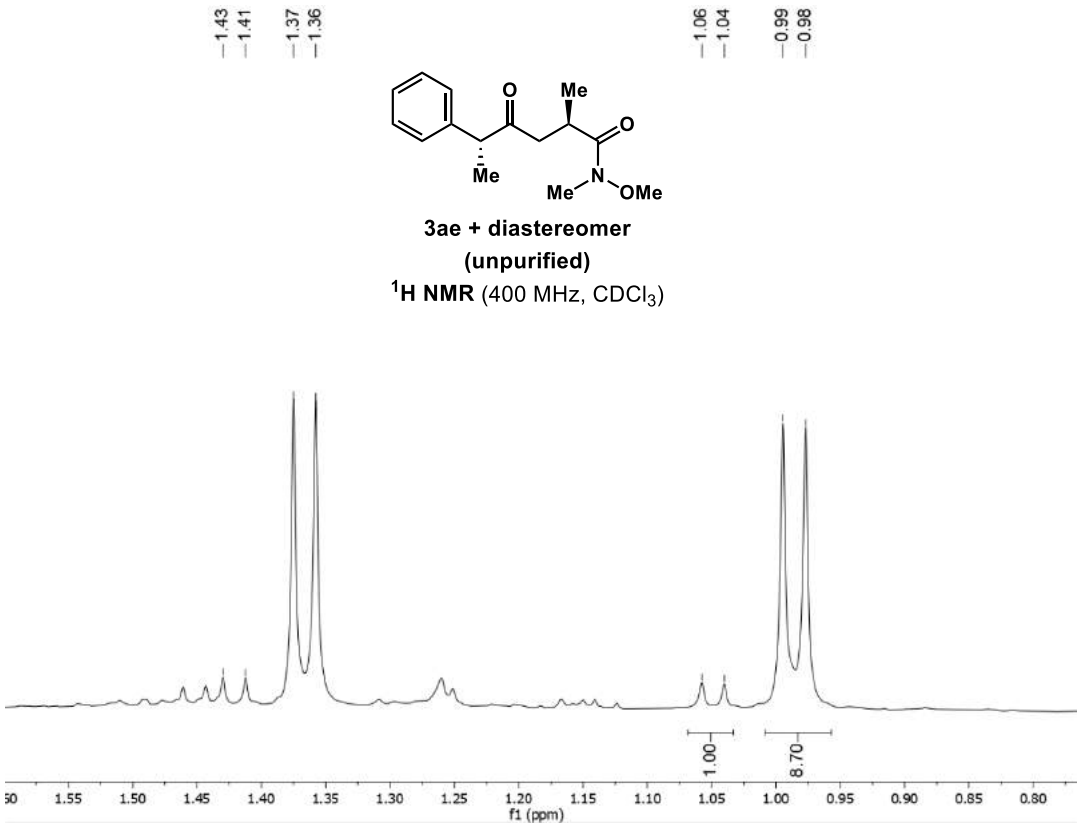

3ae + diastereomer
(unpurified)
^{1}H NMR (400 MHz, $CDCl_3$)

methyl 2-(1-tosyl-1H-indol-3-yl)acrylate (S7) (Proof of Initial Success in Synthesis)

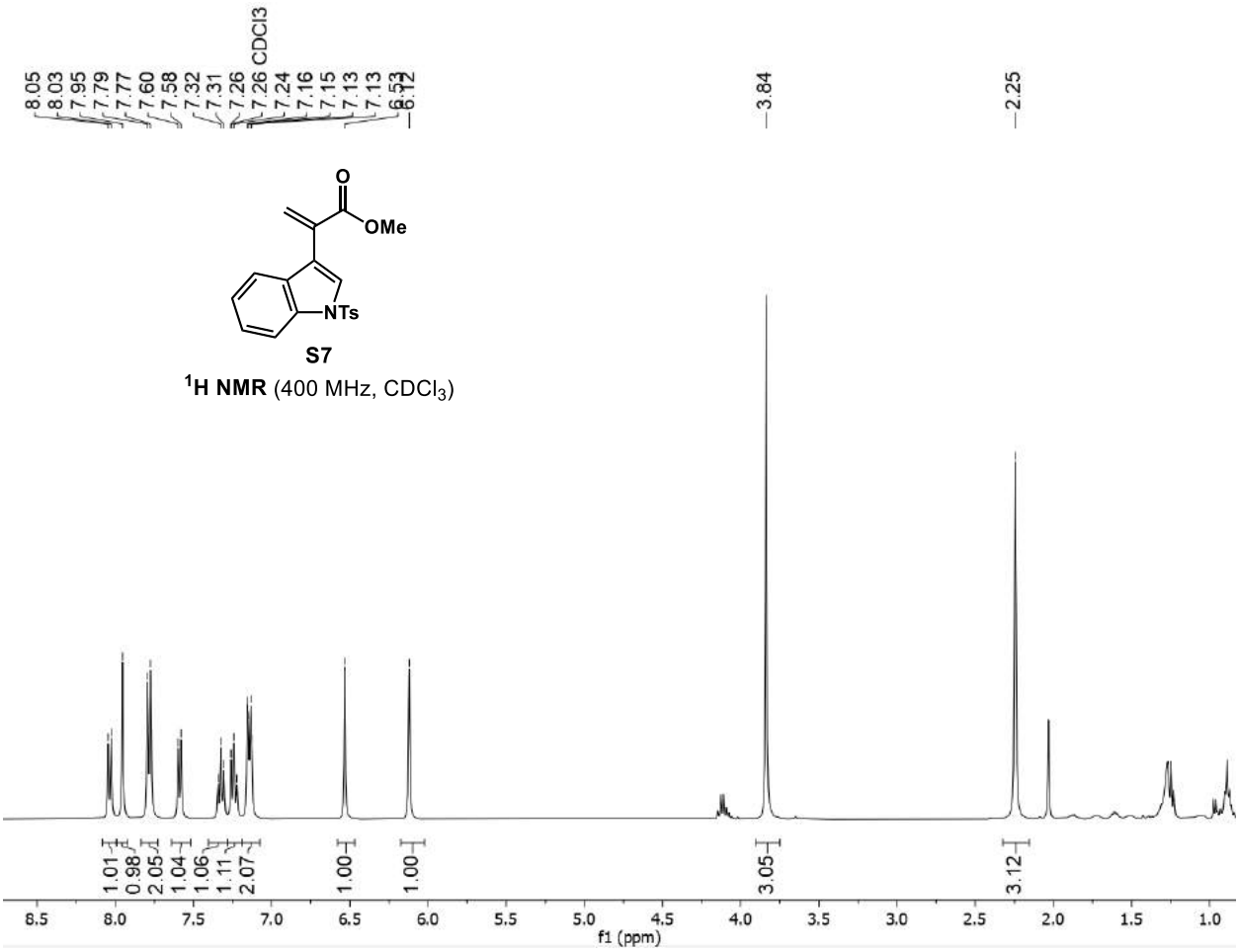

3-hydroxy-1-phenyl-3-((trimethylsilyl)methyl)indolin-2-one (S8)

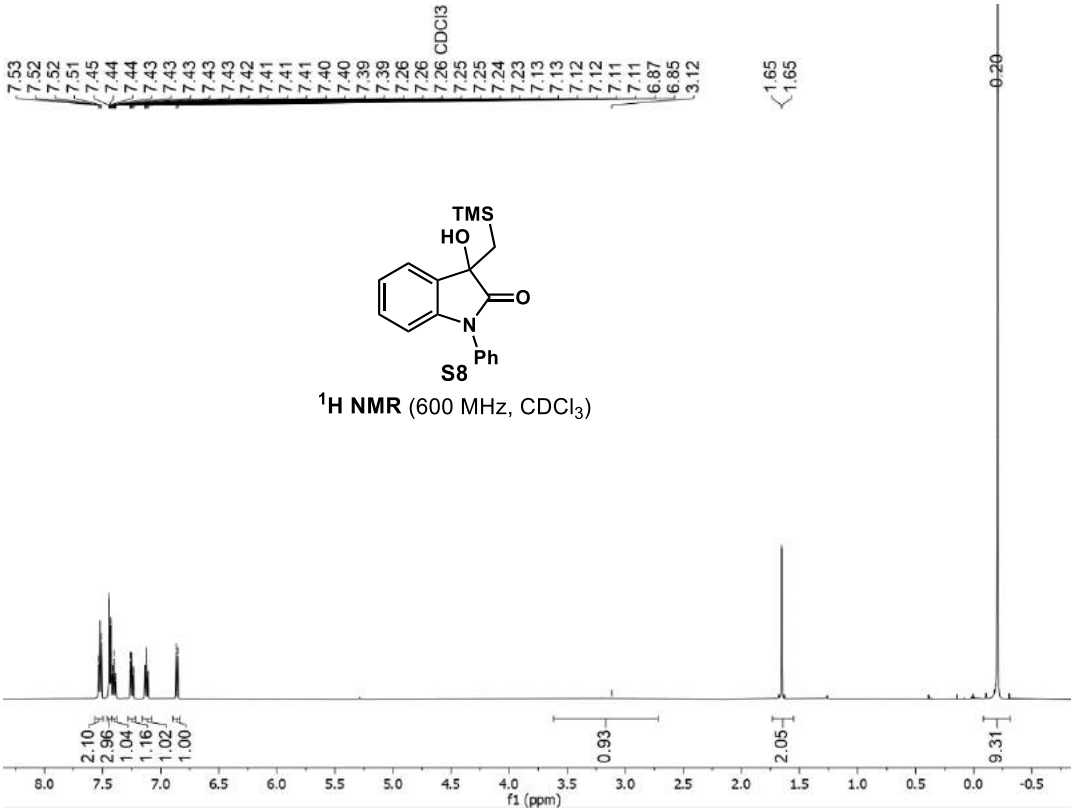

^{1}H NMR (600 MHz, $CDCl_3$)

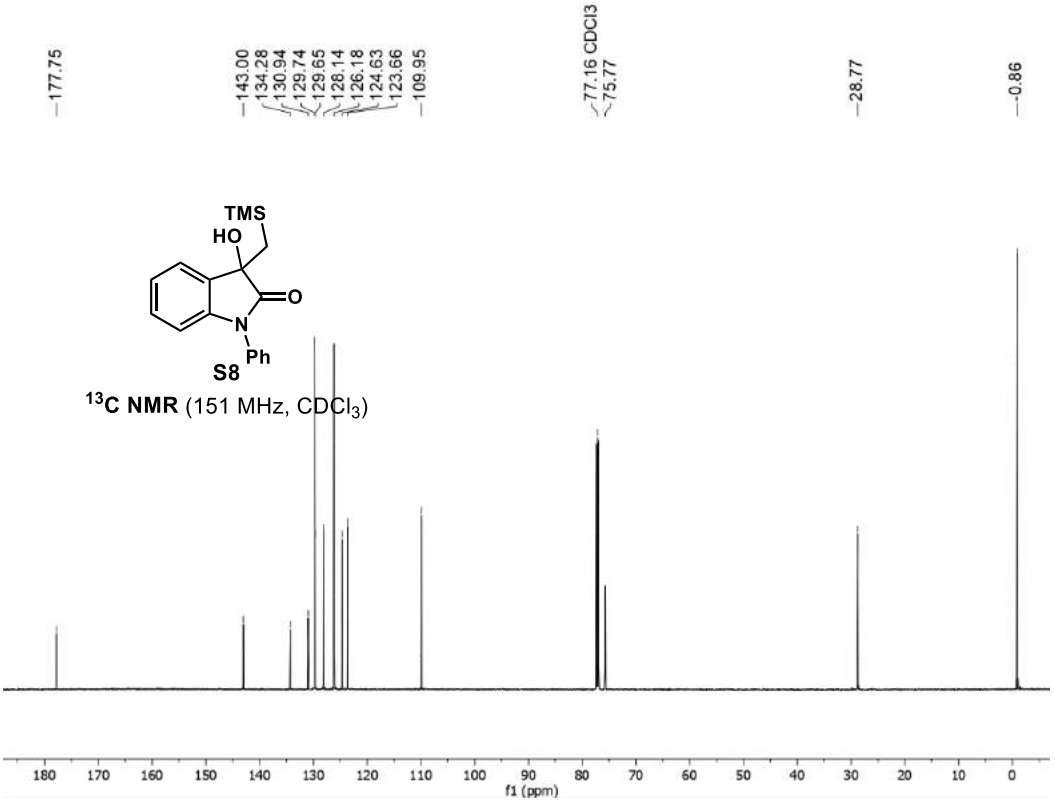

^{13}C NMR (151 MHz, $CDCl_3$)

9. SFC traces

(2R,5R)-2-methyl-4-oxo-N,N,5-triphenylhexanamide (3aa)

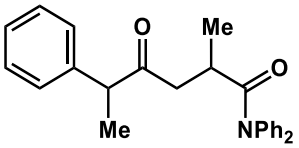

***rac*-3aa**
+ diastereomers

Racemic

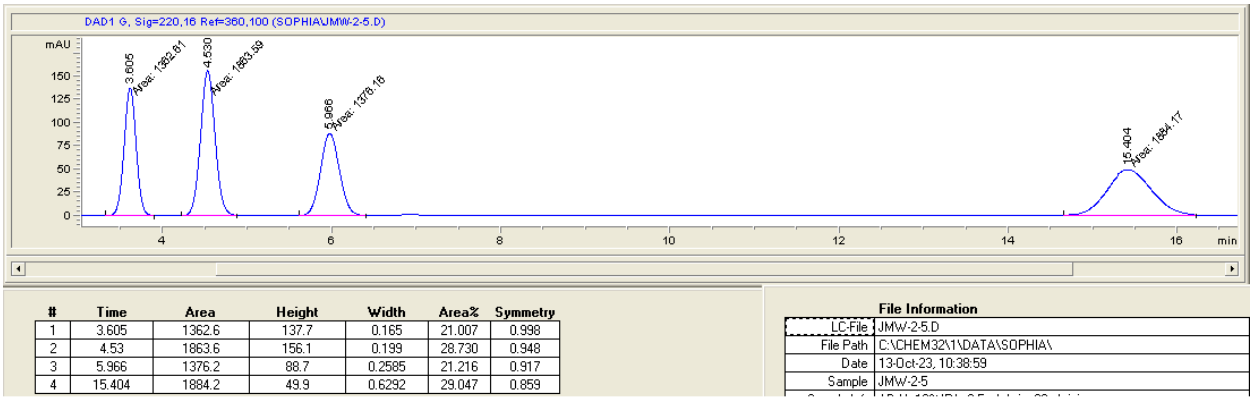

#	Time	Area	Height	Width	Area%	Symmetry
1	3.605	1362.6	137.7	0.165	21.007	0.998
2	4.53	1863.6	156.1	0.199	28.730	0.948
3	5.966	1376.2	88.7	0.2585	21.216	0.917
4	15.404	1884.2	49.9	0.6292	29.047	0.859

File Information

LC-File	JMW-2-5.D
File Path	C:\CHEM32\1\DATA\SOPHIA\
Date	13-Oct-23, 10:38:59
Sample	JMW-2-5

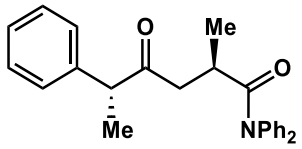

3aa
+ diastereomer

Enantioenriched

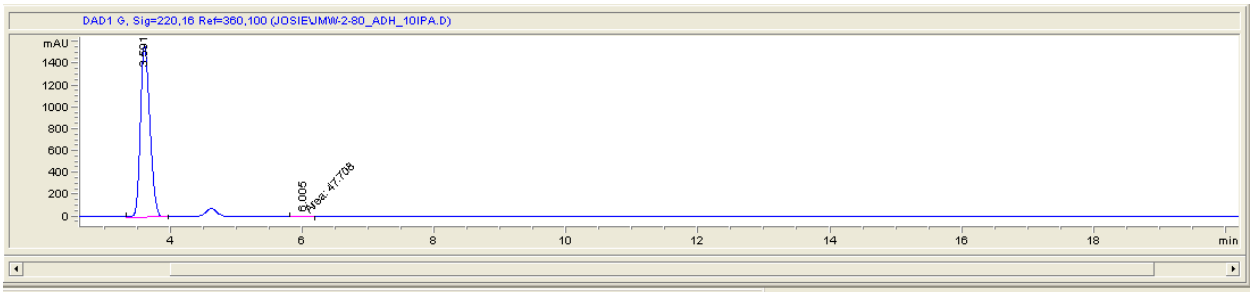

#	Time	Area	Height	Width	Area%	Symmetry
1	3.591	15439.5	1580.9	0.1509	99.692	0.713
2	6.005	47.7	3.5	0.2257	0.308	1.046

File Information

LC-File	JMW-2-80_ADH_10IPA.D
File Path	C:\CHEM32\1\DATA\JOSIE\

(2*R*,5*R*)-5-(4-methoxyphenyl)-2-methyl-4-oxo-*N*,*N*-diphenylhexanamide (3ba)

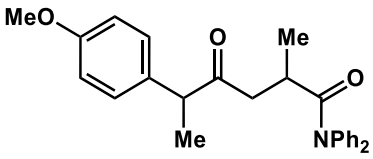

***rac*-3ba**
+ diastereomers

Racemic

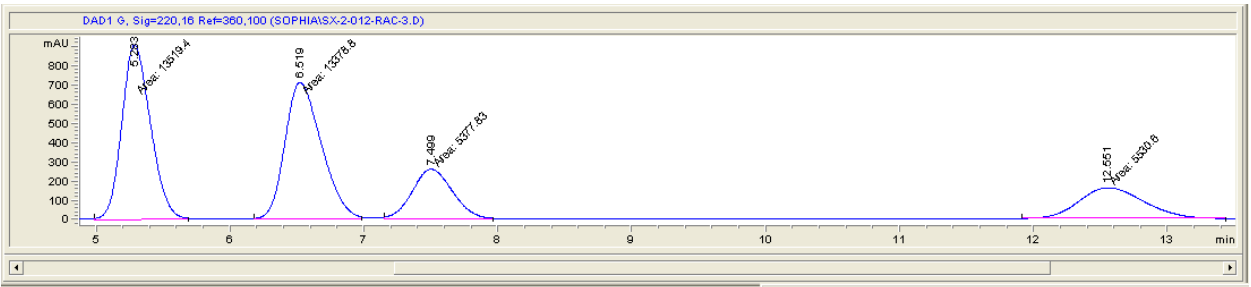

#	Time	Area	Height	Width	Area%	Symmetry
1	5.283	13519.4	906.3	0.2486	35.759	0.782
2	6.519	13378.8	708.6	0.3147	35.387	0.686
3	7.499	5377.8	258	0.3474	14.225	0.876
4	12.551	5530.6	161.3	0.5714	14.629	0.778

File Information	
LC-File	SX-2-012-RAC-3.D
File Path	C:\CHEM32\1\DATA\SOPHIA\
Date	17-Mar-23, 19:21:52
Sample	SX-2-012-rac-3

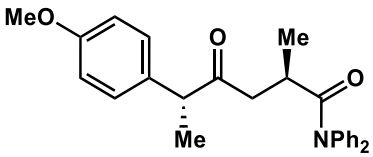

3ba
+ diastereomer

Enantioenriched

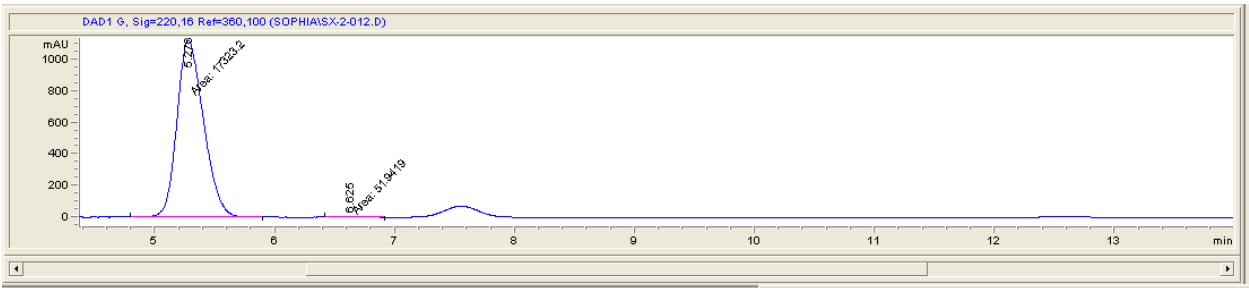

#	Time	Area	Height	Width	Area%	Symmetry
1	5.276	17323.2	1124.1	0.2569	99.701	0.722
2	6.625	51.9	3	0.2866	0.299	0.753

File Information	
LC-File	SX-2-012.D
File Path	C:\CHEM32\1\DATA\SOPHIA\

(2*R*,5*R*)-5-(4-chlorophenyl)-2-methyl-4-oxo-*N*,*N*-diphenylhexanamide (3ca)

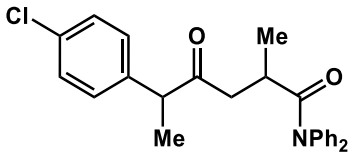

***rac*-3ca**
+ diastereomers

Racemic

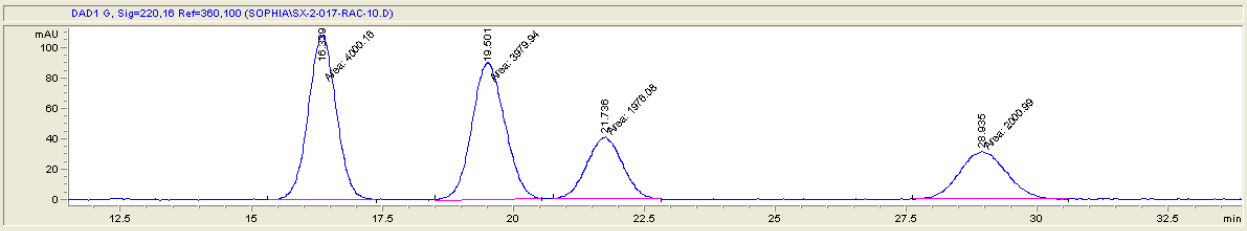

#	Time	Area	Height	Width	Area%	Symmetry
1	16.339	4000.2	107.6	0.6198	33.454	0.979
2	19.501	3979.9	90.5	0.7326	33.285	0.921
3	21.736	1976.1	41	0.8027	16.526	1.019
4	28.935	2001	31.5	1.0596	16.735	0.934

File Information	
LC-File	SX-2-017-RAC-10.D
File Path	C:\CHEM32\1\DATA\SOPHIA\
Date	05-Dec-23, 14:15:15
Sample	SX-2-017-rac-10
Sample Info	AD-H, 5% IPA IN CO2, 2.5 mL/MIN, RT, 20 uL inj

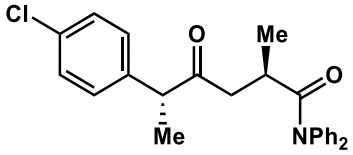

3ca
+ diastereomer

Enantioenriched

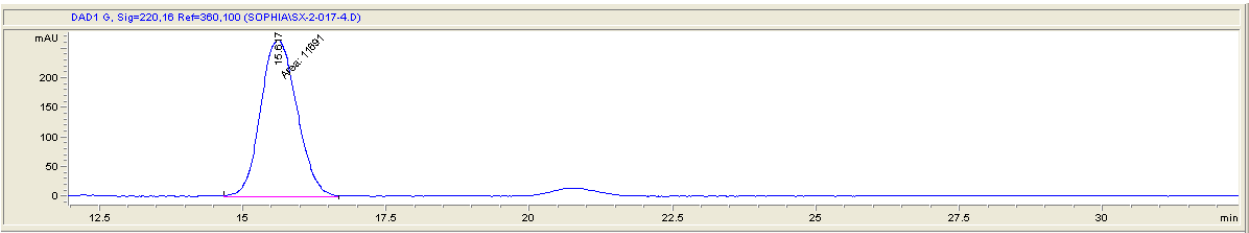

#	Time	Area	Height	Width	Area%	Symmetry
1	15.617	11691	265.7	0.7333	100.000	0.946

File Information	
LC-File	SX-2-017-4.D
File Path	C:\CHEM32\1\DATA\SOPHIA\
Date	05-Dec-23, 14:52:31

(2*R*,5*R*)-5-(4-bromophenyl)-2-methyl-4-oxo-*N*,*N*-diphenylhexanamide (3da)

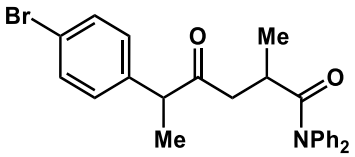

***rac*-3da**
+ diastereomers

Racemic

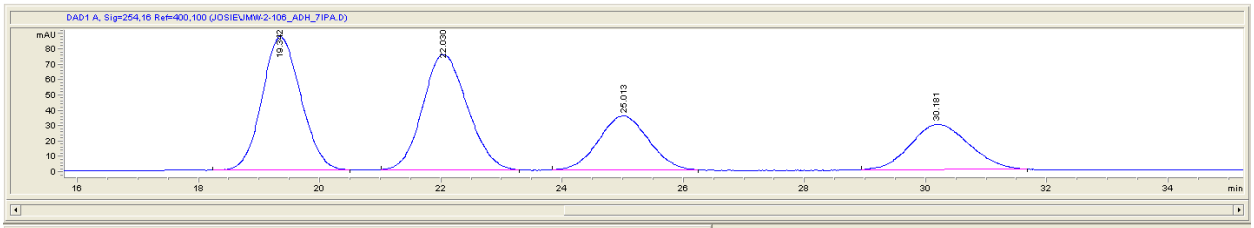

#	Time	Area	Height	Width	Area%	Symmetry
1	19.342	3872.2	87.2	0.555	32.797	0.855
2	22.03	3873.4	75.4	0.6051	32.808	0.835
3	25.013	2040.1	35.4	0.6779	17.280	1.008
4	30.181	2020.7	29.8	0.7949	17.115	0.829

File Information	
LC-File	JMW-2-106_ADH_7IPA.D
File Path	C:\CHEM32\1\DATA\JOSIE\
Date	22-Feb-23, 11:32:47
Sample	JMW-2-106_ADH_7IPA

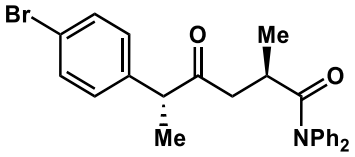

3da
+ diastereomer

Enantioenriched

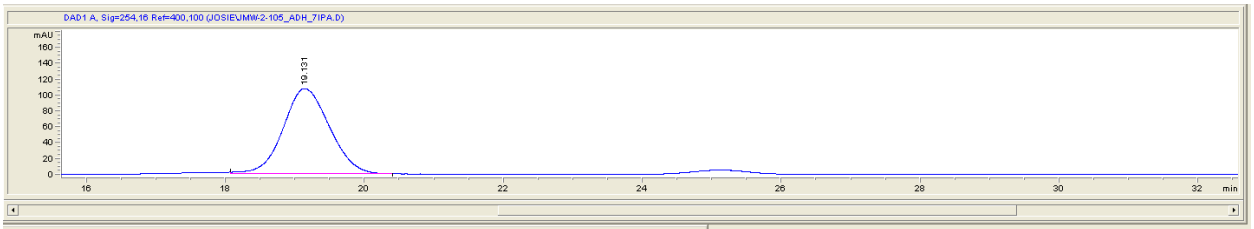

#	Time	Area	Height	Width	Area%	Symmetry
1	19.131	5055.1	108	0.5912	100.000	0.842

File Information	
LC-File	JMW-2-105_ADH_7IPA.D
File Path	C:\CHEM32\1\DATA\JOSIE\
Date	22-Feb-23, 12:13:35

(2*R*,5*R*)-2-methyl-4-oxo-*N*,*N*-diphenyl-5-(4-(trifluoromethyl)phenyl)hexanamide (3ea)

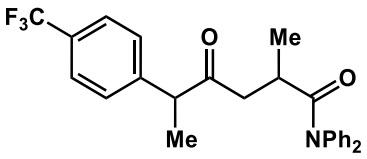

***rac*-3ea**
+ diastereomers

Racemic

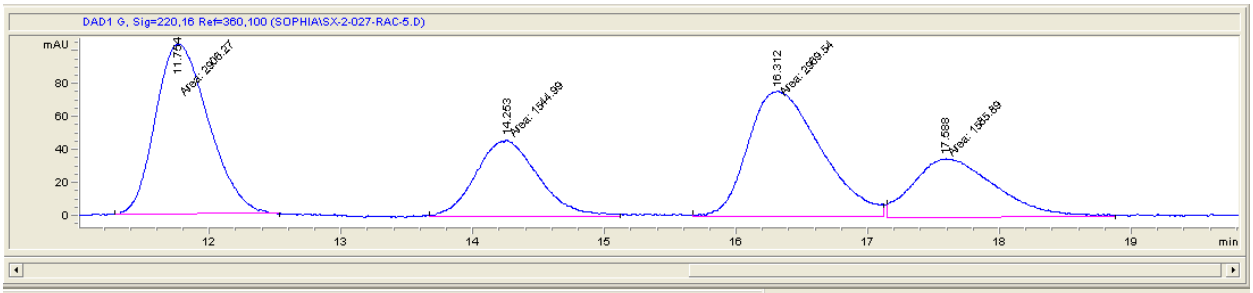

#	Time	Area	Height	Width	Area%	Symmetry
1	11.754	2906.3	103.5	0.4678	32.268	0.702
2	14.253	1545	46.8	0.5501	17.154	0.944
3	16.312	2969.5	76.5	0.6471	32.970	0.679
4	17.588	1585.9	35.9	0.7359	17.608	0.626

File Information	
LC-File	SX-2-027-RAC-5.D
File Path	C:\CHEM32\1\DATA\SOPHIA\
Date	02-May-23, 14:53:26
Sample	SX-2-027-rac-5

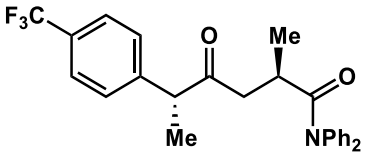

3ea
+ diastereomer

Enantioenriched

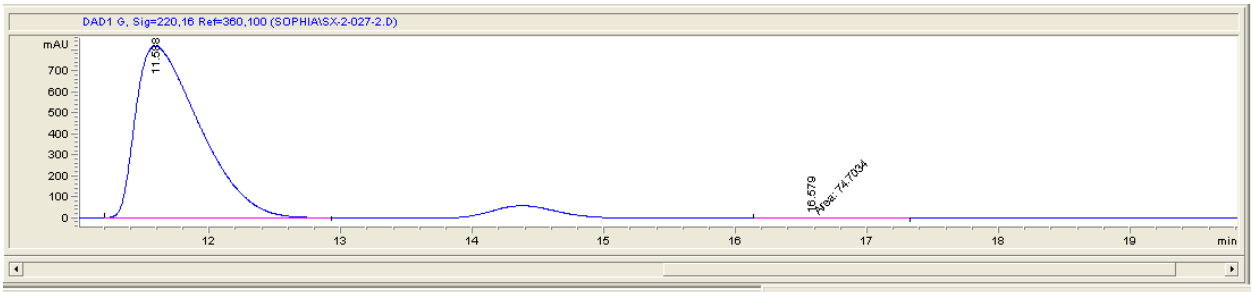

#	Time	Area	Height	Width	Area%	Symmetry
1	11.588	27795.9	820.8	0.4791	99.732	0.419
2	16.579	74.7	2.3	0.5483	0.268	0.362

File Information	
LC-File	SX-2-027-2.D
File Path	C:\CHEM32\1\DATA\SOPHIA\

(2*R*,5*R*)-5-(3-methoxyphenyl)-2-methyl-4-oxo-*N*,*N*-diphenylhexanamide (3fa)

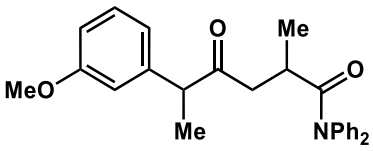

***rac*-3fa**
+ diastereomers

Racemic

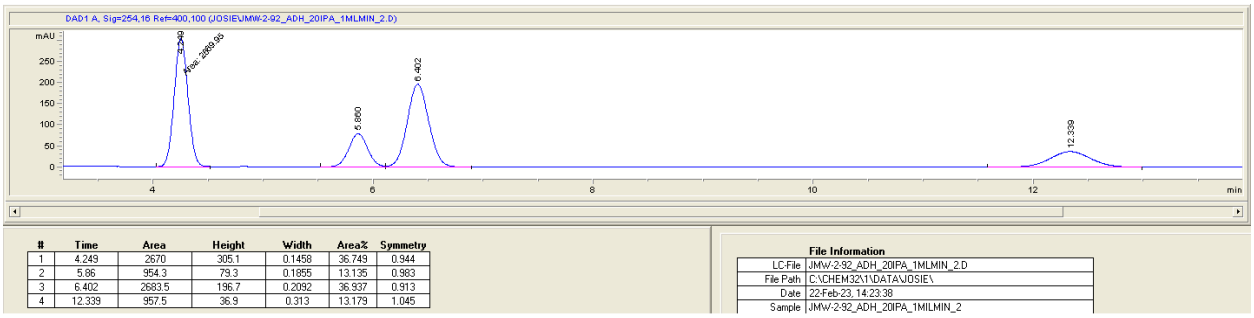

#	Time	Area	Height	Width	Area%	Symmetry
1	4.249	2670	305.1	0.1458	36.749	0.944
2	5.86	954.3	79.3	0.1855	13.135	0.983
3	6.402	2683.5	196.7	0.2092	36.937	0.913
4	12.339	957.5	36.9	0.313	13.179	1.045

File Information	
LC-File	JMW-2-92_ADH_20IPA_1MLMIN_2.D
File Path	C:\CHEM32\1\DATA\JOSIE\
Date	22-Feb-23, 14:23:38
Sample	JMW-2-92_ADH_20IPA_1MLMIN_2

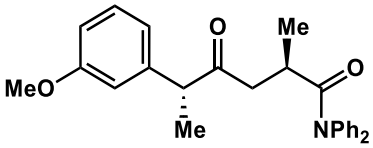

3fa
+ diastereomer

Enantioenriched

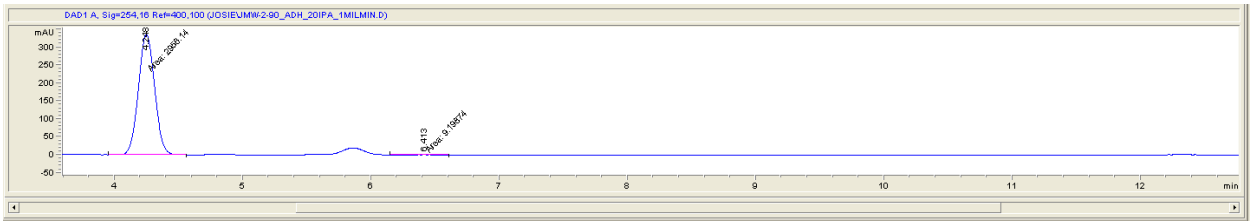

#	Time	Area	Height	Width	Area%	Symmetry
1	4.248	2956.1	336.5	0.1464	99.690	0.936
2	6.413	9.2	7.7E-1	0.1979	0.310	1.302

File Information	
LC-File	JMW-2-90_ADH_20IPA_1MILMIN.D
File Path	C:\CHEM32\1\DATA\JOSIE\

(2*R*,5*R*)-5-(3-chlorophenyl)-2-methyl-4-oxo-*N*,*N*-diphenylhexanamide (3ga)

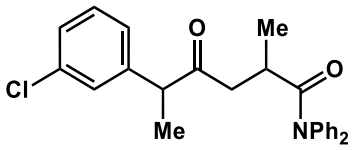

***rac*-3ga**
+ diastereomers

Racemic

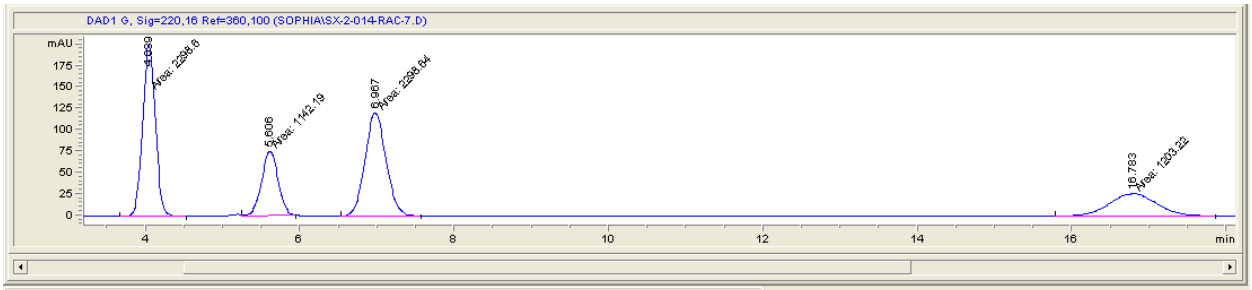

#	Time	Area	Height	Width	Area%	Symmetry
1	4.039	2298.6	200	0.1916	33.108	0.96
2	5.606	1142.2	75.5	0.2521	16.452	1.009
3	6.967	2298.6	120.6	0.3178	33.109	0.889
4	16.783	1203.2	26.8	0.7486	17.331	0.979

File Information

LC-File	SX-2-014-RAC-7.D
File Path	C:\CHEM32\1\DATA\SOPHIA\
Date	07-Apr-23, 17:22:11
Sample	SX-2-014-RAC-7

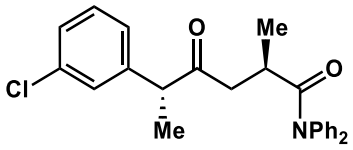

3ga
+ diastereomer

Enantioenriched

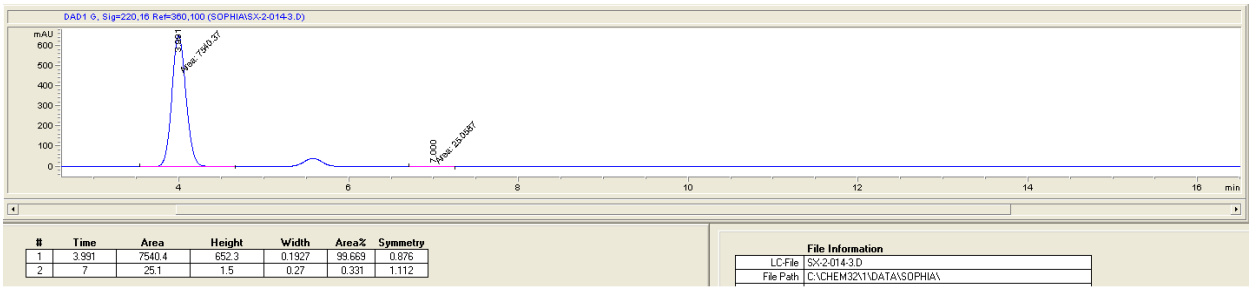

#	Time	Area	Height	Width	Area%	Symmetry
1	3.991	7540.4	652.3	0.1927	99.669	0.876
2	7	25.1	1.5	0.27	0.331	1.112

File Information

LC-File	SX-2-014-3.D
File Path	C:\CHEM32\1\DATA\SOPHIA\

(2*R*,5*R*)-2-methyl-4-oxo-*N*,*N*-diphenyl-5-(*o*-tolyl)hexanamide (3ha)

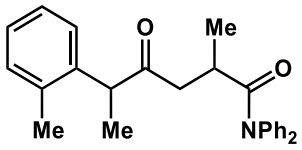

***rac*-3ha**
+ diastereomers

Racemic

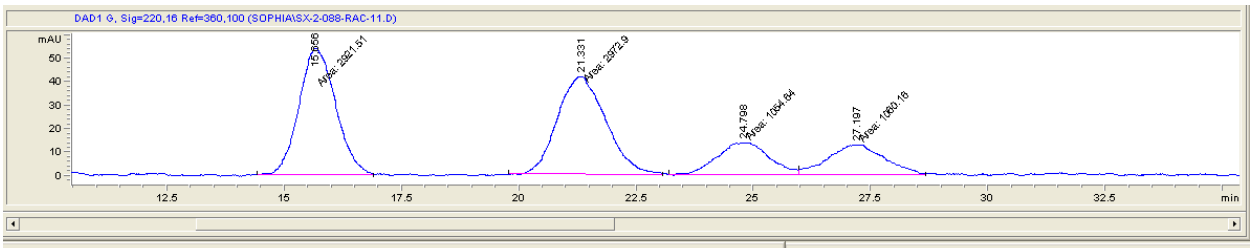

#	Time	Area	Height	Width	Area%	Symmetry
1	15.656	2921.5	53.9	0.9026	36.477	0.812
2	21.331	2972.9	41.5	1.195	37.119	0.956
3	24.798	1054.6	13.7	1.2861	13.168	1.076
4	27.197	1060.2	12.8	1.3772	13.237	1.013

File Information	
LC-File	SX-2-088-RAC-11.D
File Path	C:\CHEM32\1\DATA\SOPHIA\
Date	27-Oct-23, 15:57:39
Sample	SX-2-088-rac-11

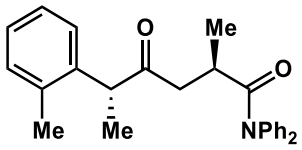

3ha
+ diastereomer

Enantioenriched

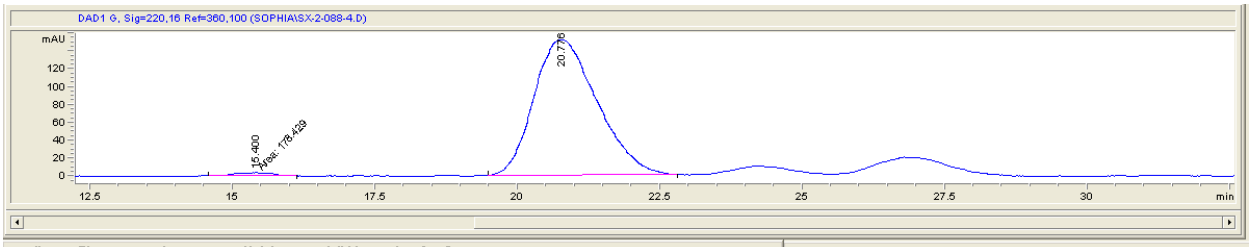

#	Time	Area	Height	Width	Area%	Symmetry
1	15.4	178.4	3.8	0.7845	1.498	1.217
2	20.776	11736.4	152.1	0.9074	98.502	0.778

File Information	
LC-File	SX-2-088-4.D
File Path	C:\CHEM32\1\DATA\SOPHIA\

(2*R*,5*R*)-2-methyl-5-(naphthalen-2-yl)-4-oxo-*N*,*N*-diphenylhexanamide (3ia)

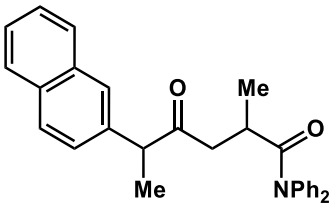

***rac*-3ia**
+ diastereomers

Racemic

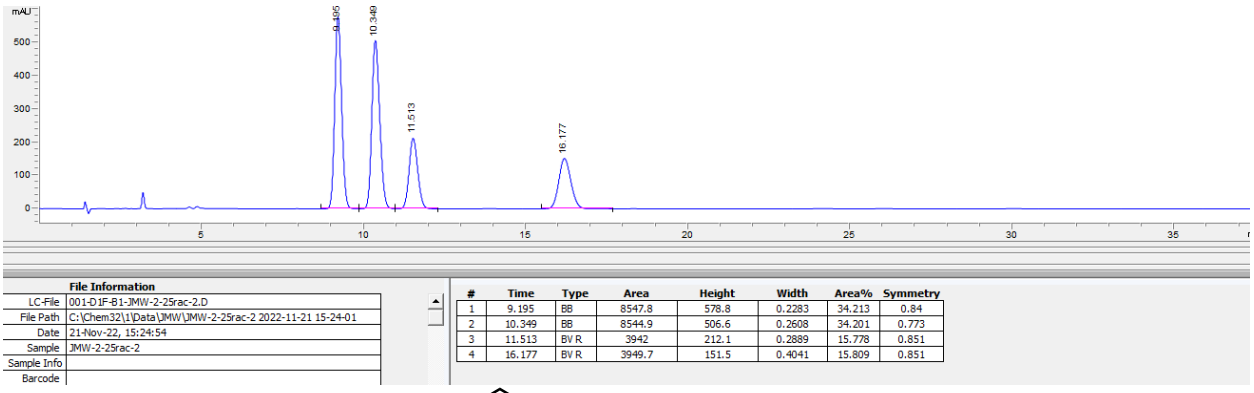

File Information	
LC-File	001-D1F-B1-JMW-2-25rac-2.D
File Path	C:\Chem32\1\Data\JMW\JMW-2-25rac-2 2022-11-21 15-24-01
Date	21-Nov-22, 15:24:54
Sample	JMW-2-25rac-2
Sample Info	
Barcode	

#	Time	Type	Area	Height	Width	Area%	Symmetry
1	9.195	BB	8547.8	578.8	0.2283	34.213	0.84
2	10.349	BB	8544.9	506.6	0.2608	34.201	0.773
3	11.513	BV R	3942	212.1	0.2889	15.778	0.851
4	16.177	BV R	3949.7	151.5	0.4041	15.809	0.851

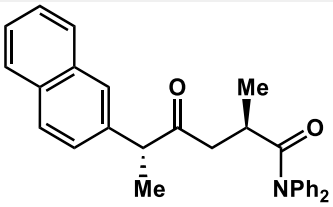

3ia
+ diastereomer

Enantioenriched

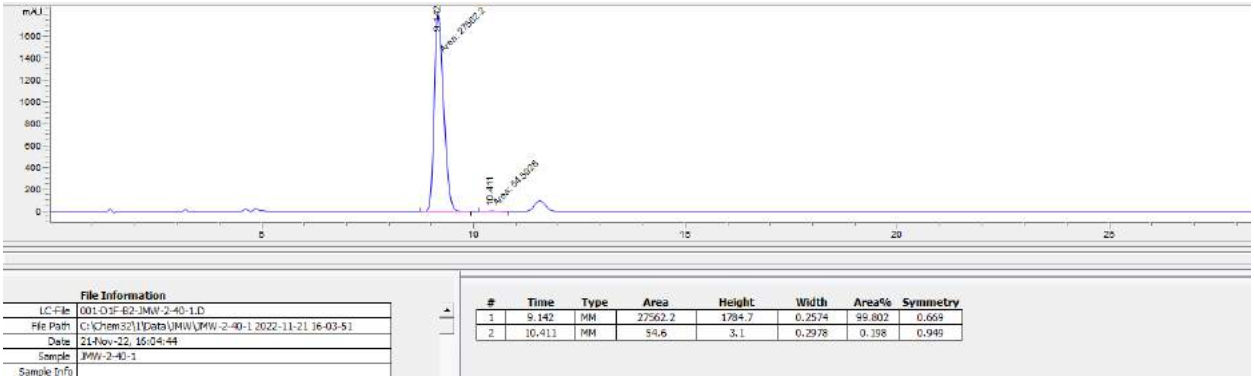

File Information	
LC-File	001-D3F-B2-JMW-2-40-1.D
File Path	C:\Chem32\1\Data\JMW\JMW-2-40-1 2022-11-21 16-03-51
Date	21-Nov-22, 16:04:44
Sample	JMW-2-40-1
Sample Info	

#	Time	Type	Area	Height	Width	Area%	Symmetry
1	9.142	MM	27562.2	1784.7	0.2574	99.802	0.669
2	10.411	MM	54.6	3.1	0.2978	0.198	0.948

(2*R*,5*R*)-5-(benzo[*d*][1,3]dioxol-5-yl)-2-methyl-4-oxo-*N*,*N*-diphenylhexanamide (3ja)

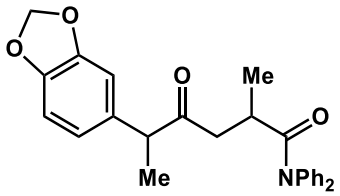

***rac*-3ja**
+ diastereomers

Racemic

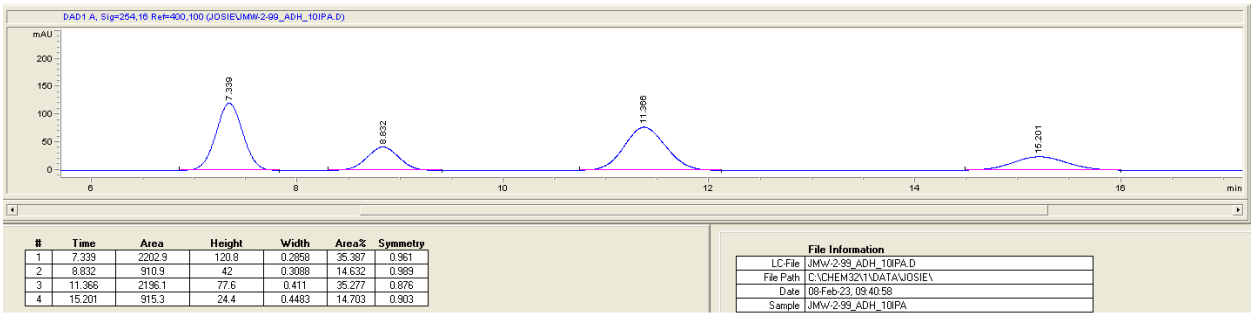

#	Time	Area	Height	Width	Area%	Symmetry
1	7.339	2202.9	120.8	0.2858	35.387	0.961
2	8.832	910.9	42	0.3088	14.632	0.989
3	11.366	2196.1	77.6	0.411	35.277	0.876
4	15.201	915.3	24.4	0.4483	14.703	0.903

File Information	
LC-File	JMW-2-99_ADH_10IPA.D
File Path	C:\CHEM32\1\DATA\JOSIE\
Date	08-Feb-23, 09:40:58
Sample	JMW-2-99_ADH_10IPA

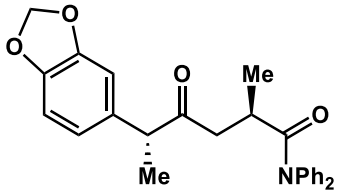

3ja
+ diastereomer

Enantioenriched

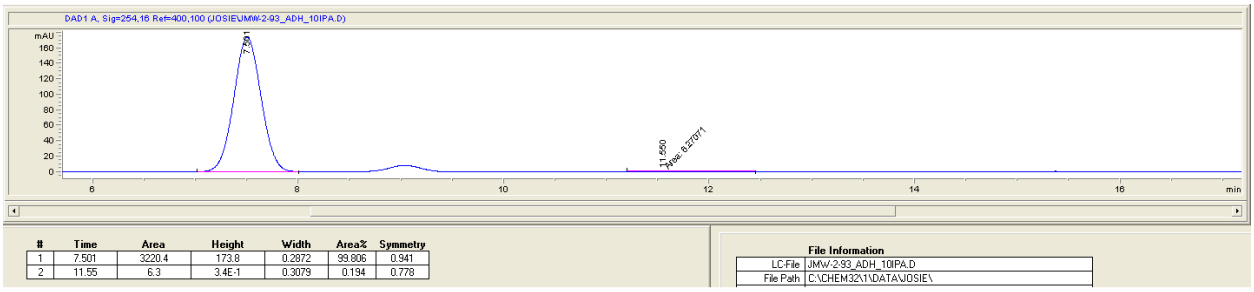

#	Time	Area	Height	Width	Area%	Symmetry
1	7.501	3220.4	173.8	0.2872	99.806	0.941
2	11.55	6.3	3.4E-1	0.3079	0.194	0.778

File Information	
LC-File	JMW-2-93_ADH_10IPA.D
File Path	C:\CHEM32\1\DATA\JOSIE\

(2*S*,5*R*)-4-oxo-*N*,*N*,2,5-tetraphenylhexanamide (3ab)

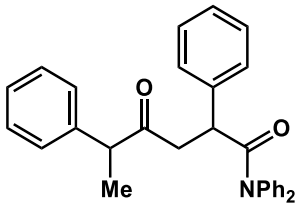

***rac*-3ab**
+ diastereomers

Racemic

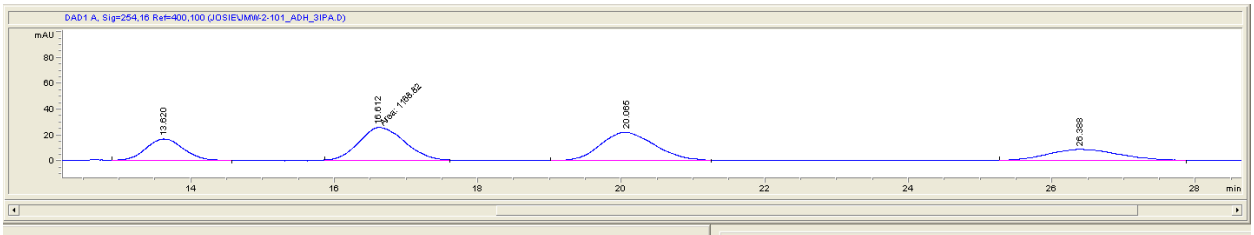

#	Time	Area	Height	Width	Area%	Symmetry
1	13.62	623.5	16.8	0.4378	17.594	0.894
2	16.612	1168.8	25.9	0.7522	32.982	0.763
3	20.065	1148.7	22	0.6149	32.415	0.887
4	26.388	602.8	8.8	0.8049	17.009	0.817

File Information	
LC-File	JMW-2-101_ADH_3IPA.D
File Path	C:\CHEM32\1\DATA\JOSIE\
Date	08-Feb-23, 13:34:44
Sample	JMW-2-101_ADH_3IPA

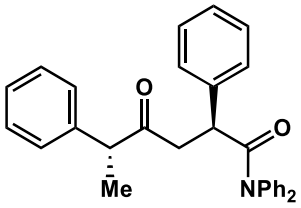

3ab
+ diastereomer

Enantioenriched

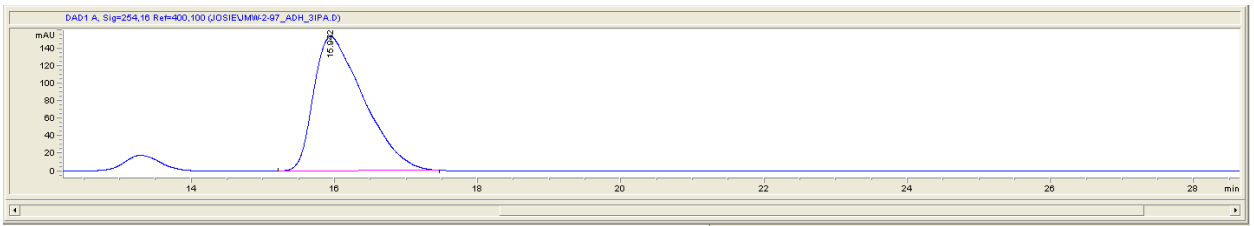

#	Time	Area	Height	Width	Area%	Symmetry
1	15.942	7442.2	153.1	0.6639	100.000	0.483

File Information	
LC-File	JMW-2-97_ADH_3IPA.D
File Path	C:\CHEM32\1\DATA\JOSIE\

(2*R*,5*R*)-2-benzyl-4-oxo-*N*,*N*,5-triphenylhexanamide (3ac)

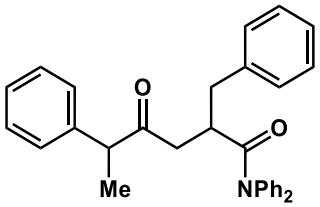

***rac*-3ac**
+ diastereomers

Racemic

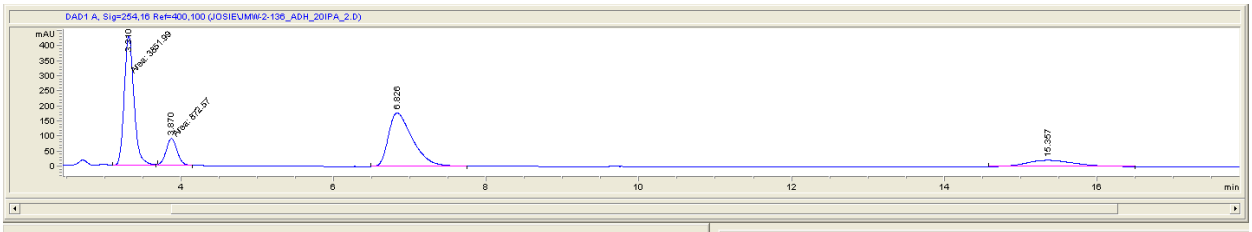

#	Time	Area	Height	Width	Area%	Symmetry
1	3.31	3852	432	0.1486	40.442	0.815
2	3.87	872.6	88.5	0.1644	9.161	0.93
3	6.826	3876	177.6	0.3287	40.694	0.529
4	15.357	924.2	21	0.5205	9.703	0.82

File Information	
LC-File	JMW-2-136_ADH_20IPA_2.D
File Path	C:\CHEM32\1\DATA\JOSIE\
Date	13-Jun-23, 11:45:36
Sample	JMW-2-136_ADH_20IPA_2

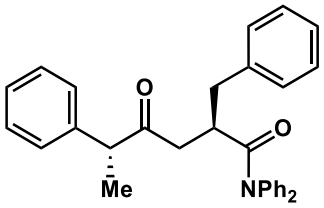

3ac
+ diastereomer

Enantioenriched

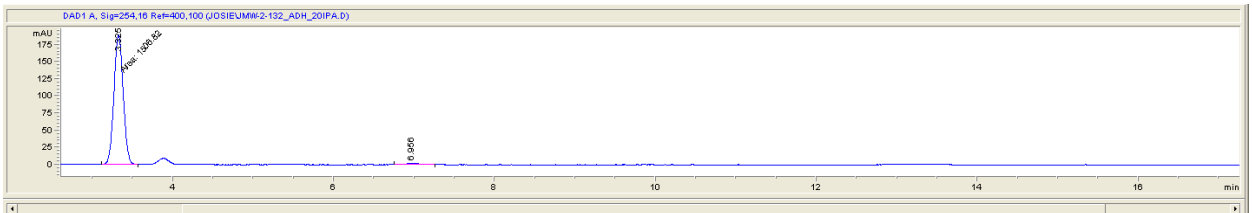

#	Time	Area	Height	Width	Area%	Symmetry
1	3.325	1506.8	189.1	0.1328	98.281	0.947
2	6.956	26.3	1.6	0.1982	1.719	0.659

File Information	
LC-File	JMW-2-132_ADH_20IPA.D
File Path	C:\CHEM32\1\DATA\JOSIE\

(*R*)-4-oxo-*N*,*N*,5-triphenylhexanamide (3ad)

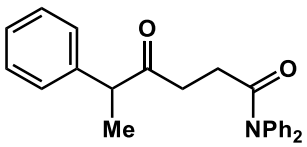

rac-3ad

Racemic

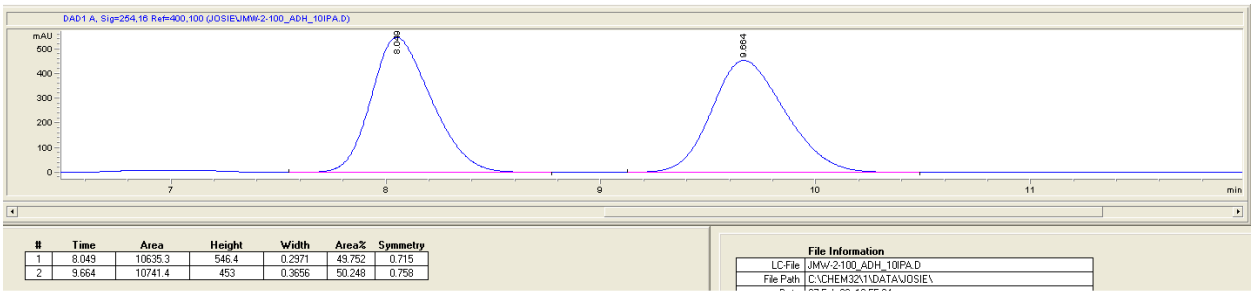

#	Time	Area	Height	Width	Area%	Symmetry
1	8.049	10635.3	546.4	0.2971	49.752	0.715
2	9.664	10741.4	453	0.3656	50.248	0.758

File Information

LC-File	JMW-2-100_ADH_10IPA.D
File Path	C:\CHEM32\1\DATA\JOSIE\

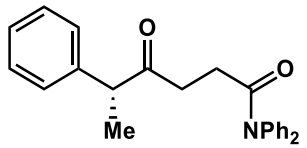

3ad

Enantioenriched

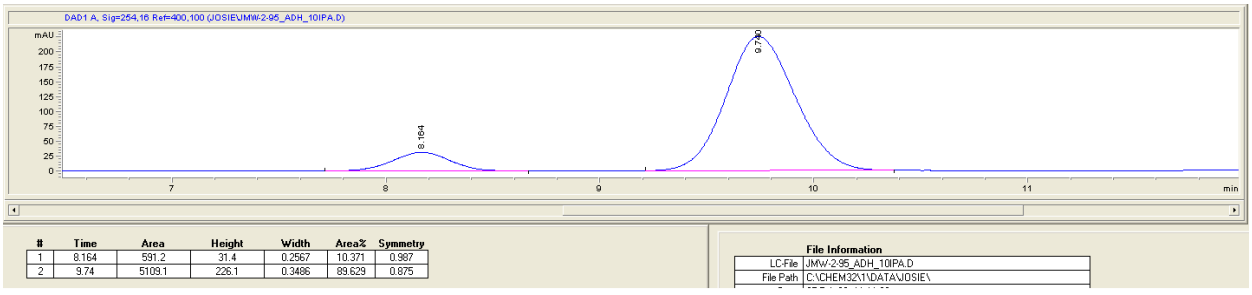

#	Time	Area	Height	Width	Area%	Symmetry
1	8.164	591.2	31.4	0.2567	10.371	0.987
2	9.74	5109.1	226.1	0.3486	89.629	0.875

File Information

LC-File	JMW-2-95_ADH_10IPA.D
File Path	C:\CHEM32\1\DATA\JOSIE\

(2*R*,5*R*)-2-methyl-1-morpholino-5-phenylhexane-1,4-dione (3ae)

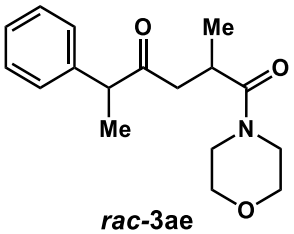

***rac*-3ae**
+ diastereomers

Racemic

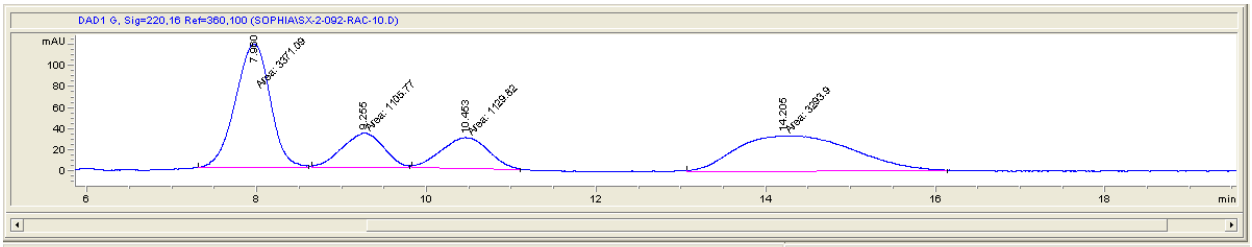

#	Time	Area	Height	Width	Area%	Symmetry
1	7.96	3371.1	117.6	0.4776	37.875	1.108
2	9.255	1105.8	32.4	0.5685	12.424	1.076
3	10.453	1129.8	29.3	0.6428	12.694	1.008
4	14.205	3293.9	34.3	1.6022	37.008	0.682

File Information	
LC-File	SX-2-092-RAC-10.D
File Path	C:\CHEM32\1\DATA\SOPHIA\
Date	26-Oct-23, 14:19:58
Sample	SX-2-092-rac-10
Sample Info	AD-H, 6% IPA, 1.0 mL/min, 20 uL injec

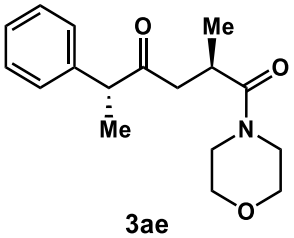

3ae
+ diastereomer

Enantioenriched

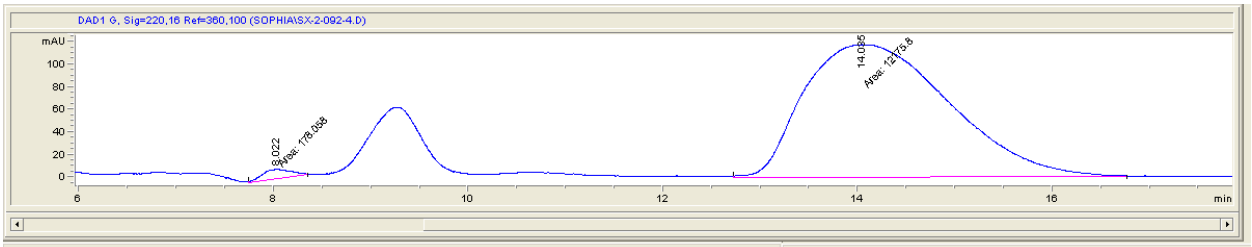

#	Time	Area	Height	Width	Area%	Symmetry
1	8.022	178.1	8.5	0.3507	1.441	1.002
2	14.035	12175.8	117.3	1.73	98.559	0.636

File Information	
LC-File	SX-2-092-4.D
File Path	C:\CHEM32\1\DATA\SOPHIA\

(2*R*,5*R*)-*N*,*N*-dibenzyl-2-methyl-4-oxo-5-phenylhexanamide (3af)

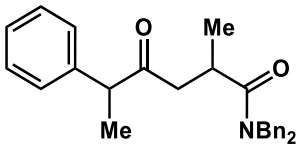

***rac*-3af**
+ diastereomers

Racemic

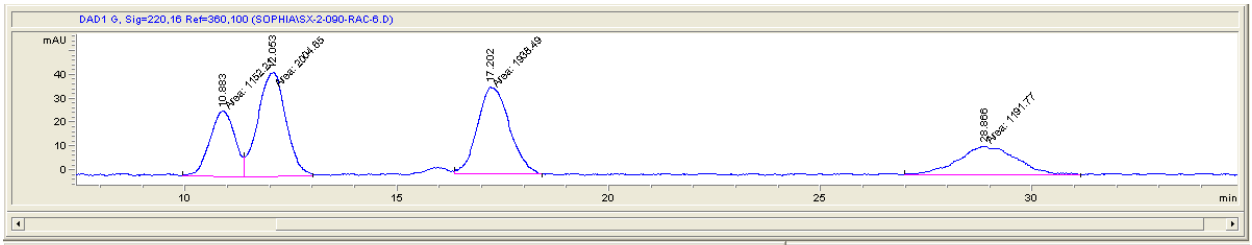

#	Time	Area	Height	Width	Area%	Symmetry
1	10.883	1152.2	27.5	0.6974	18.326	1.116
2	12.053	2004.7	43.7	0.7644	31.885	1.091
3	17.202	1938.5	36.8	0.8786	30.833	0.734
4	28.866	1191.8	12.2	1.6273	18.956	0.864

File Information	
LC-File	SX-2-090-RAC-6.D
File Path	C:\CHEM32\1\DATA\SOPHIA\
Date	27-Oct-23, 13:03:05
Sample	SX-2-090-RAC-6
Sample Info	OJ-H, 1% IPA, 2.0 mL/min, 20 uL injec

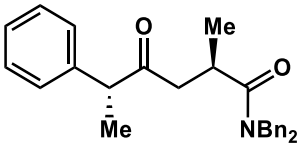

3af
+ diastereomer

Enantioenriched

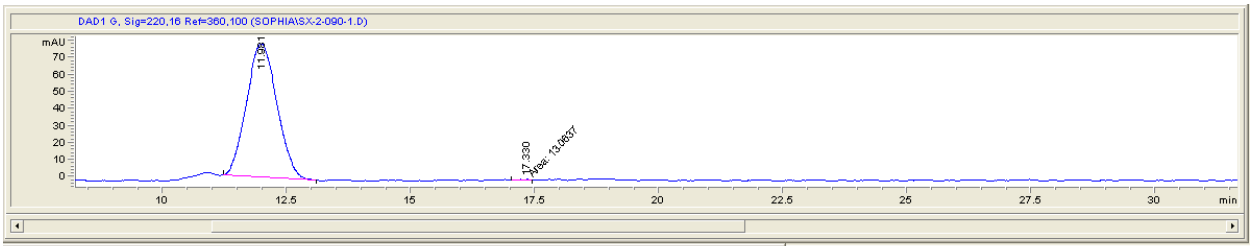

#	Time	Area	Height	Width	Area%	Symmetry
1	11.981	3330.3	78.5	0.5279	99.609	0.954
2	17.33	13.1	8.9E-1	0.2453	0.391	2.759

File Information	
LC-File	SX-2-090-1.D
File Path	C:\CHEM32\1\DATA\SOPHIA\

(2*R*,5*R*)-*N*,*N*-dibenzyl-2-methyl-4-oxo-5-phenylhexanamide (3ag)

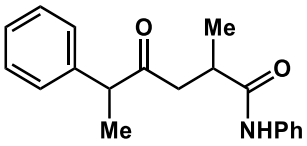

***rac*-3ag**
+ diastereomers

Racemic

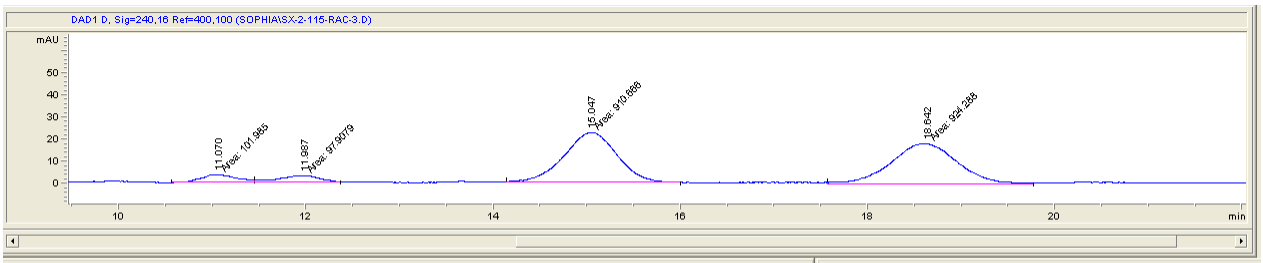

#	Time	Area	Height	Width	Area%	Symmetry
1	11.07	102	3.7	0.4582	5.012	1.008
2	11.987	97.9	3.2	0.5103	4.812	1.527
3	15.047	910.7	22.7	0.6684	44.754	1.062
4	18.642	924.3	18.5	0.8325	45.423	1.195

File Information	
LC-File	SX-2-115-RAC-3.D
File Path	C:\CHEM32\1\DATA\SOPHIA\
Date	01-Nov-23, 17:35:01
Sample	SX-2-115-rac-3.D
Sample Info	AD-H, 6% IPA, 2.0 mL/min, 20 uL injec

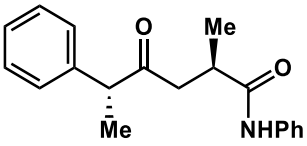

3ag
+ diastereomer

Enantioenriched

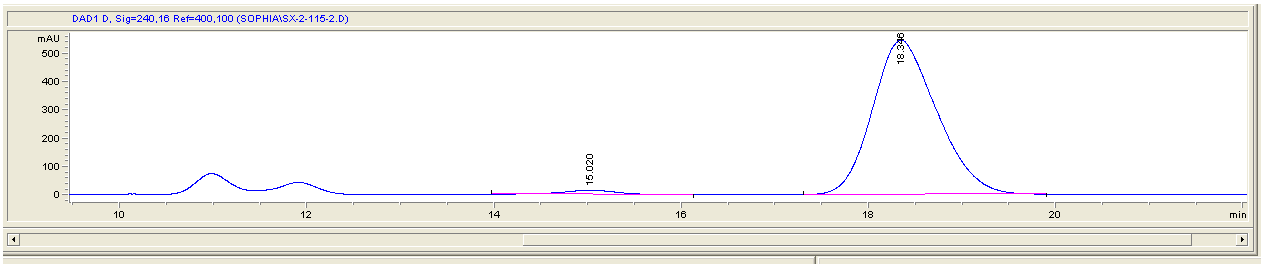

#	Time	Area	Height	Width	Area%	Symmetry
1	15.02	663.1	15.3	0.517	2.478	1.166
2	18.346	26093.1	545	0.6926	97.522	0.772

File Information	
LC-File	SX-2-115-2.D
File Path	C:\CHEM32\1\DATA\SOPHIA\
Date	01-Nov-23, 17:09:27

(2*R*,5*R*)-*N*-methoxy-*N*,2-dimethyl-4-oxo-5-phenylhexanamide (3ah)

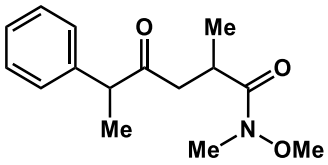

***rac*-3ah**
+ diastereomers

Racemic

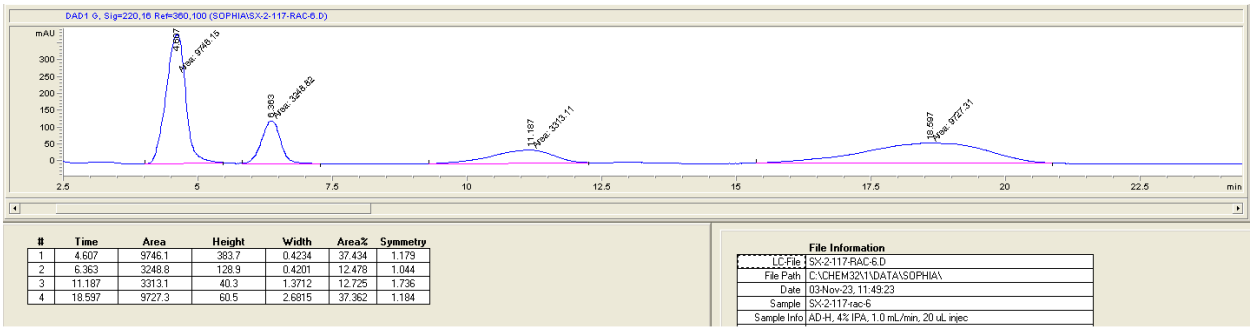

#	Time	Area	Height	Width	Area%	Symmetry
1	4.607	9746.1	383.7	0.4234	37.434	1.179
2	6.363	3248.8	128.9	0.4201	12.478	1.044
3	11.187	3313.1	40.3	1.3712	12.725	1.736
4	18.597	9727.3	60.5	2.6815	37.362	1.184

File Information	
LC-File	SX-2-117-RAC-6.D
File Path	C:\CHEM32\1\DATA\SOPHIA\
Date	03-Nov-23, 11:49:23
Sample	SX-2-117-rac-6
Sample Info	AD-H, 4% IPA, 1.0 mL/min, 20 uL injec

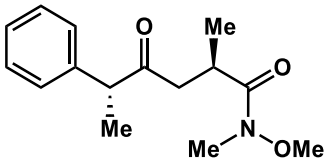

3ah
+ diastereomer

Enantioenriched

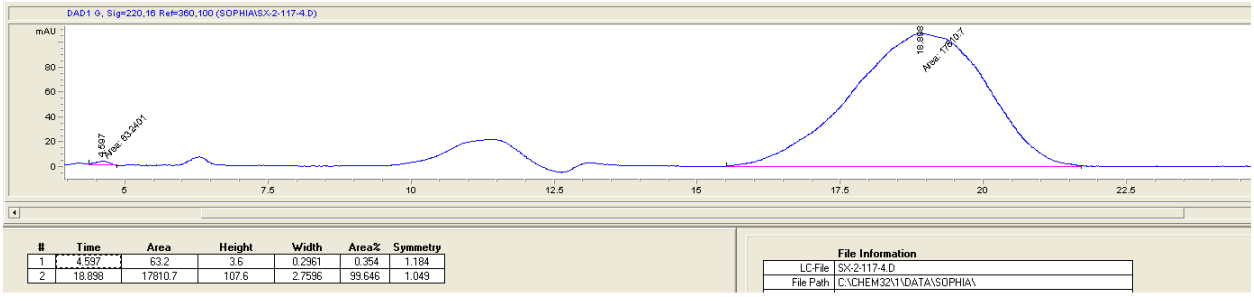

#	Time	Area	Height	Width	Area%	Symmetry
1	4.597	63.2	3.6	0.2961	0.354	1.184
2	18.898	17810.7	107.6	2.7596	99.646	1.049

File Information	
LC-File	SX-2-117-4.D
File Path	C:\CHEM32\1\DATA\SOPHIA\

APPENDIX 3

Supporting Information for Chapter 3

Regio- and Enantioselective Hydroacylation of Azetines

Table of Contents

1. General

Commercial reagents were purchased from Sigma Aldrich, Strem, Alfa Aesar, Acros Organics, Combi-Blocks, or TCI and were used without further purification, unless otherwise stated. 1,2-Dichloroethane was purified using an Innovative Technologies Pure Solv system, degassed by three freeze-pump-thaw cycles, and stored within a N_2-filled glove box. Solvents were purchased from Fisher. All experiments were performed in oven-dried or flame-dried glassware. Reactions

were monitored using either thin-layer chromatography (TLC) or gas chromatography using an Agilent Technologies 7890A GC system equipped with an Agilent Technologies 5975C inert XL EI/CI MSD. Visualization of the developed plates was performed under UV light (254 nm), $KMnO_4$ stain, or iodine stain. Organic solutions were concentrated under reduced pressure on a Büchi rotary evaporator. Column chromatography was performed with Silicycle Silica-P Flash Silica Gel using glass columns. ^1H, ^{13}C and ^{19}F NMR spectra were recorded on Bruker AVANCE600, CRYO500 or DRX400 spectrometers. ^1H NMR spectra were internally referenced to the residual solvent signal. ^{13}C NMR spectra were internally referenced to the residual solvent signal. Data for ^1H NMR are reported as follows: chemical shift (δ ppm), multiplicity (s = singlet, d = doublet, t = triplet, q = quartet, m = multiplet), coupling constant (Hz), integration. Data for ^{13}C NMR are reported in terms of chemical shift (δ ppm). Infrared (IR) spectra were obtained on a Nicolet iS5 FT-IR spectrometer with an iD5 ATR and are reported in terms of frequency of absorption (cm^{-1}). High resolution mass spectra (HRMS) were obtained on a micromass 70S-250 spectrometer (EI) or an ABI/Sciex QStar Mass Spectrometer (ESI). Enantiomeric ratio for enantioselective reactions was determined by chiral SFC analysis using an Agilent Technologies HPLC (1200 series) system and Aurora A5 Fusion.

2. Azetine Hydroacylation General Procedures and Compound Characterization

2.1 General Procedure A

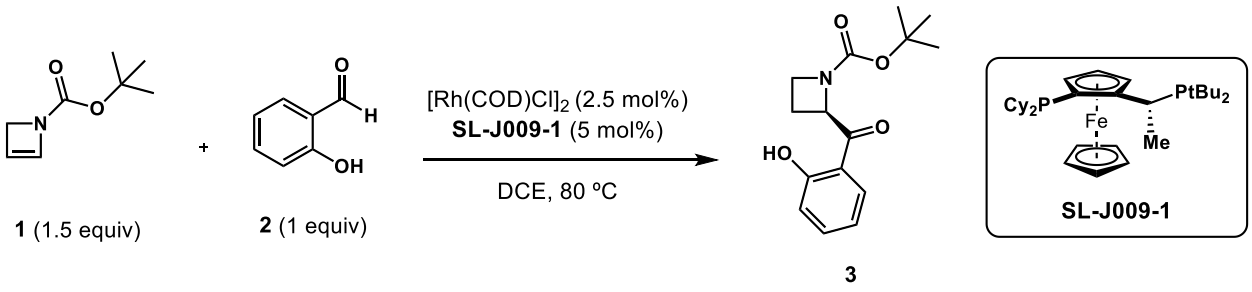

General Procedure A:

In an N_2-filled glove box, $[Rh(COD)Cl]_2$ (1.2 mg, 0.0025 mmol), **SL-J009-1** (2.8 mg, 0.0050 mmol), and DCE (0.20 mL) were added to a 1-dram vial without a stir bar. The resulting mixture was allowed to sit for 10 minutes at room temperature. Aldehyde **2a** (12 mg, 0.10 mmol) was added followed by 2-Azetine **1** (23 mg, 0.15 ml, 1M in DCE) to initiate the reaction. The mixture was heated to 80 ˚C and kept at that temperature until no starting material was observed by TLC

or GC-MS. The regioselectivity was determined by ^{1}H NMR analysis of the crude mixture. Isolated yields were obtained by preparative thin-layer chromatography (25% Ethyl Acetate in Hexanes).

2.2 Gram-Scale Procedure

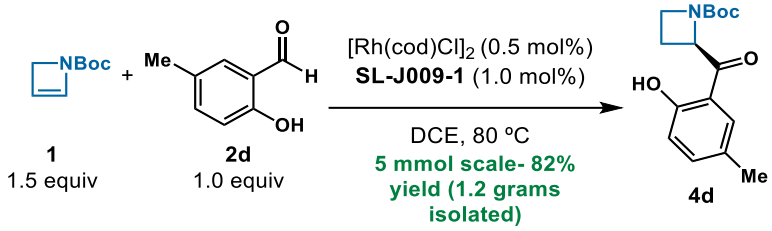

Gram-Scale Procedure:

In an N_2-filled glove box, $[Rh(COD)Cl]_2$ (12.3 mg, 0.025 mmol), **SL-J009-1** (27.7 mg, 0.050 mmol), and DCE (10 mL) were added to a 25 mL Schlenk flask without a stir bar. The resulting mixture was allowed to sit for 10 minutes at room temperature. Aldehyde **2d** (681 mg, 5.00 mmol) was added followed by 2-Azetine **1** (1.16 g, 7.50 ml, 1M in DCE) to initiate the reaction. The mixture was heated in an oil bath at 80 ˚C outside of the glovebox until no starting material was observed by TLC or GC-MS. The regioselectivity was determined by ^{1}H NMR analysis of the crude mixture. The crude mixture was purified by column chromatography on silica gel (25% ethyl acetate in hexanes) to yield the desired product. 1.20 grams isolated, 82% yield.

2.3 Compound Characterization for 3a-3m

tert-butyl (R)-2-(2-hydroxybenzoyl)azetidine-1-carboxylate (3a)

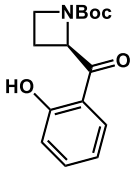

White solid, 97% yield, 99:1 *er*, >20:1 *rr*, $[\alpha]^{24}_D$ = +165.1 (*c* 0.5, $CHCl_3$). **^{1}H NMR** (400 MHz, $CDCl_3$) δ 12.01 (s, 1H), 7.55 – 7.46 (m, 2H), 7.02 (d, *J* = 8.2 Hz, 1H), 6.93 – 6.84 (m, 1H), 5.57 (dd, *J* = 9.6, 5.6 Hz, 1H), 4.06 – 3.93 (m, 2H), 2.69 (dtd, *J* = 11.2, 9.2, 6.3 Hz, 1H), 2.20 (ddt, *J* = 11.3, 8.8, 5.6 Hz, 1H), 1.41 (s, 9H). **^{13}C NMR** (126 MHz, $CDCl_3$) δ 201.4, 163.1, 155.9, 136.9, 129.0, 119.2, 119.0, 117.0, 80.3, 63.0, 46.8, 28.4, 21.9. **IR** (ATR): 3068, 2974, 2897, 1667, 1646, 1453, 1428, 1151, 757, 745, 678 cm^{-1}. **HRMS** calculated for $C_{15}H_{19}NO_4Na$ $[M+Na]^+$ 300.1212, found 300.1223. **Chiral SFC:** 100 mm CHIRALCEL AD-

H, 5% ^{i}PrOH, 2.0 mL/min, 332 nm, 44 °C, nozzle pressure = 200 bar CO_2, t_{R1} (major) = 4.7 min, t_{R2} (minor) = 9.9 min.

tert-butyl (R)-2-(2-hydroxy-3-methylbenzoyl)azetidine-1-carboxylate (3b)

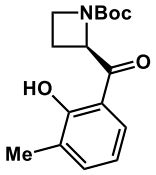

White solid, 99% yield, 98:2 *er*, >20:1 *rr*, $[\alpha]^{24}_{D}$ = +156.1 (*c* 0.5, $CHCl_3$). **^{1}H NMR** (400 MHz, $CDCl_3$) δ 12.31 (s, 1H), 7.36 (t, *J* = 7.4 Hz, 2H), 6.79 (t, *J* = 7.7 Hz, 1H), 5.57 (dd, *J* = 9.6, 5.6 Hz, 1H), 4.05 – 3.92 (m, 2H), 2.74 – 2.63 (m, 1H), 2.26 (s, 3H), 2.17 (ddt, *J* = 11.3, 8.8, 5.6 Hz, 1H), 1.41 (s, 9H). **^{13}C NMR** (126 MHz, $CDCl_3$) δ 201.5, 161.5, 155.9, 137.6, 128.1, 126.5, 118.6, 116.1, 80.2, 63.2, 46.8, 28.4, 22.0, 15.7. **IR** (ATR): 2974, 2360, 1699, 1643, 1427, 1390, 1365, 1275, 1246, 1141, 750. **HRMS** calculated for $C_{16}H_{21}NO_4Na$ $[M+Na]^+$ 314.1368, found 314.1357. **Chiral HPLC:** 250 mm CHIRALCEL IA, 5% ^{i}PrOH, 2.0 mL/min, 254 nm, t_{R1} (major) = 4.3 min, t_{R2} (minor) = 7.9 min.

tert-butyl (R)-2-(2-hydroxy-4-isopropylbenzoyl)azetidine-1-carboxylate (3c)

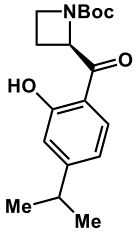

White solid, 99% yield, 93:7 *er*, >20:1 *rr*, $[\alpha]^{24}_{D}$ = +88.2 (*c* 0.5, $CHCl_3$). **^{1}H NMR** (400 MHz, $CDCl_3$) δ 12.04 (s, 1H), 7.44 (d, *J* = 8.3 Hz, 1H), 6.87 (d, *J* = 1.3 Hz, 1H), 6.75 (dd, *J* = 8.3, 1.5 Hz, 1H), 5.54 (dd, *J* = 9.6, 5.6 Hz, 1H), 4.06 – 3.89 (m, 2H), 2.88 (dt, *J* = 13.8, 6.9 Hz, 1H), 2.78 – 2.57 (m, 1H), 2.18 (ddt, *J* = 11.2, 8.9, 5.6 Hz, 1H), 1.40 (s, 9H), 1.23 (d, *J* = 6.9 Hz, 6H). **^{13}C NMR** (126 MHz, $CDCl_3$) δ 200.7, 163.4, 159.3, 155.9, 129.0, 118.1, 116.3, 115.0, 80.2, 63.0, 46.9, 34.6, 28.4, 23.4, 21.9. **IR** (ATR): 2965, 1699, 1640, 1390, 1364, 1240, 1213, 1182, 1141, 772, 734, 715. **HRMS** calculated for $C_{18}H_{25}NO_4Na$ $[M+Na]^+$ 342.1681, found 342.1683. **Chiral SFC:** 100 mm CHIRALCEL AD-H, 3% ^{i}PrOH, 2.0 mL/min, 265 nm, 44 °C, nozzle pressure = 200 bar CO_2, t_{R1} (major) = 6.6 min, t_{R2} (minor) = 15.0 min.

tert-butyl (R)-2-(2-hydroxy-5-methylbenzoyl)azetidine-1-carboxylate (3d)

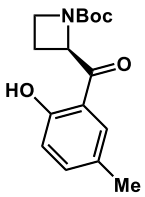

White solid, 79% yield, >99:1 *er*, >20:1 *rr*, $[\alpha]^{24}_{D}$ = +109.1 (*c* 0.1, $CHCl_3$). **^{1}H NMR** (600 MHz, $CDCl_3$) δ 11.87 (s, 1H), 7.34 – 7.27 (m, 2H), 6.93 (d, *J* = 8.4 Hz, 1H), 5.57 (dd, *J* = 9.4, 5.6 Hz, 1H), 4.06 – 3.99 (m, 1H), 3.97 (dt, *J* = 13.9, 7.0 Hz, 1H), 2.74 – 2.66 (m, 1H), 2.29 (s, 3H), 2.22 – 2.15 (m, 1H), 1.41 (s, 9H).

^{13}C NMR (151 MHz, $CDCl_3$) δ 201.2, 161.0, 155.9, 138.0, 128.6, 128.3, 118.7, 116.7, 80.3, 63.0, 47.1, 28.4, 22.0, 20.7. **IR** (ATR): 2971, 1667, 1650, 1615, 1451, 1436, 1307, 1234, 1219, 1159, 944, 824, 762, 661, 597. **HRMS** calculated for $C_{16}H_{21}NO_4Na$ $[M+Na]^+$ 314.1368, found 314.1375. **Chiral SFC:** 100 mm CHIRALCEL AD-H, 5% ^{i}PrOH, 4.0 mL/min, 220 nm, 44 °C, nozzle pressure = 200 bar CO_2, t_{R1} (major) = 1.9 min, t_{R2} (minor) = 4.7 min.

tert-butyl (R)-2-(2-hydroxy-3-methoxybenzoyl)azetidine-1-carboxylate (3e)

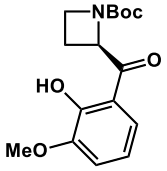

White solid, 99% yield, 99:1 *er*, >20:1 *rr*, $[\alpha]^{24}_D$ = +102.6 (*c* 0.7, $CHCl_3$). **^{1}H NMR** (600 MHz, $CDCl_3$) δ 12.26 (s, 1H), 7.12 (d, *J* = 8.2 Hz, 1H), 7.06 (d, *J* = 7.9 Hz, 1H), 6.84 (t, *J* = 8.1 Hz, 1H), 5.55 (dd, *J* = 9.6, 5.6 Hz, 1H), 4.01 (dd, *J* = 14.8, 8.1 Hz, 1H), 3.95 (td, *J* = 8.4, 5.8 Hz, 1H), 3.90 (s, 3H), 2.73 – 2.64 (m, 1H), 2.18 (ddd, *J* = 14.3, 11.2, 5.6 Hz, 1H), 1.40 (s, 9H). **^{13}C NMR** (151 MHz, $CDCl_3$) δ 201.7, 153.3, 149.2, 120.0, 118.7, 117.3, 116.9, 80.2, 63.3, 56.2, 47.1, 31.0, 28.3, 21.9. **IR** (ATR): 2973, 1697, 1644, 1455, 1390, 1363, 1250, 1140, 1087, 962, 919, 737, 594. **HRMS** calculated for $C_{16}H_{21}NO_5Na$ $[M+Na]^+$ 330.1317, found 330.1315. **Chiral SFC:** 100 mm CHIRALCEL AD-H, 3% ^{i}PrOH, 3.0 mL/min, 332 nm, 44 °C, nozzle pressure = 200 bar CO_2, t_{R1} (major) = 11.0 min, t_{R2} (minor) = 22.0 min.

tert-butyl (R)-2-(3-allyl-2-hydroxybenzoyl)azetidine-1-carboxylate (3f)

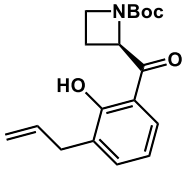

White solid, 90% yield, 99:1 *er*, >20:1 *rr*, $[\alpha]^{24}_D$ = +119.2 (*c* 0.6, $CHCl_3$). **^{1}H NMR** (400 MHz, $CDCl_3$) δ 12.36 (s, 1H), 7.45 – 7.31 (m, 2H), 6.83 (t, *J* = 7.7 Hz, 1H), 6.00 (ddt, *J* = 23.0, 10.6, 6.6 Hz, 1H), 5.57 (dd, *J* = 9.6, 5.6 Hz, 1H), 5.10 (dd, *J* = 7.0, 1.4 Hz, 1H), 5.07 (s, 1H), 4.08 – 3.90 (m, 2H), 3.43 (d, *J* = 6.6 Hz, 2H), 2.76 – 2.61 (m, 1H), 2.18 (ddt, *J* = 11.3, 8.8, 5.6 Hz, 1H), 1.41 (s, 9H). **^{13}C NMR** (126 MHz, $CDCl_3$) δ 201.5, 161.1, 155.9, 136.8, 136.0, 130.0, 127.0, 118.8, 116.4, 116.3, 80.2, 63.2, 47.0, 33.6, 28.4, 22.0. **IR** (ATR): 2975, 2916, 1698, 1639, 1613, 1431, 1390, 1365, 1276, 1239, 1142, 1045, 913, 751, 610. **HRMS** calculated for $C_{18}H_{23}NO_4Na$ $[M+Na]^+$ 340.1525, found 340.1527. **Chiral SFC:** 100 mm CHIRALCEL AD-H, 3% ^{i}PrOH, 2.0 mL/min, 265 nm, 44 °C, nozzle pressure = 200 bar CO_2, t_{R1} (major) = 15.1 min, t_{R2} (minor) = 22.4 min.

tert-butyl (R)-2-(2-hydroxy-5-(4,4,5,5-tetramethyl-1,3,2-dioxaborolan-2-yl)benzoyl) azetidine-1-carboxylate (3g)

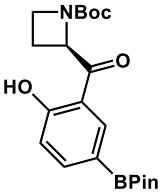

Yellow solid, 88% yield, 99:1 *er*, >20:1 *rr*, $[\alpha]^{24}_D$ = +156.4 (*c* 0.3, $CHCl_3$). **^{1}H NMR** (500 MHz, $CDCl_3$) δ 12.30 (s, 1H), 7.99 (s, 1H), 7.90 (d, *J* = 8.3 Hz, 1H), 6.99 (d, *J* = 8.4 Hz, 1H), 5.71 (dd, *J* = 9.6, 5.7 Hz, 1H), 4.08 – 3.91 (m, 2H), 2.83 – 2.68 (m, 1H), 2.26 – 2.12 (m, 1H), 1.39 (s, 9H), 1.33 (s, 12H). **^{13}C NMR** (151 MHz, $CDCl_3$) δ 201.8, 165.4, 143.0, 136.5, 118.2, 116.7, 84.1, 80.2, 62.8, 46.9, 31.0, 28.3, 24.9, 24.9, 21.9. **IR** (ATR): 2977, 1703, 1645, 1587, 1363, 1270, 1245, 1141, 1094, 965, 772, 731, 689. **HRMS** calculated for $C_{21}H_{30}BNO_6Na$ $[M+Na]^+$ 425.2100, found 425.2108. **Chiral SFC:** 100 mm CHIRALCEL AD-H, 3% ^{i}PrOH, 2.0 mL/min, 332 nm, 44 °C, nozzle pressure = 200 bar CO_2, t_{R1} (minor) = 3.1 min, t_{R2} (major) = 4.0 min.

tert-butyl (R)-2-(5-chloro-2-hydroxybenzoyl)azetidine-1-carboxylate (3h)

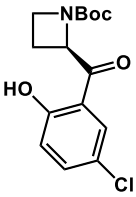

White solid, 65% yield, 98:2 *er*, >20:1 *rr*, $[\alpha]^{24}_D$ = +81.4 (*c* 0.6, $CHCl_3$). **^{1}H NMR** (400 MHz, $CDCl_3$) δ 11.91 (s, 1H), 7.49 (d, *J* = 2.5 Hz, 1H), 7.43 (dd, *J* = 8.9, 2.5 Hz, 1H), 6.98 (d, *J* = 8.9 Hz, 1H), 5.51 (dd, *J* = 9.6, 5.6 Hz, 1H), 4.06 – 3.94 (m, 2H), 2.71 (dtd, *J* = 11.2, 9.0, 6.3 Hz, 1H), 2.20 (ddt, *J* = 11.3, 8.8, 5.7 Hz, 1H), 1.41 (s, 9H). **^{13}C NMR** (126 MHz, $CDCl_3$) δ 200.8, 161.6, 155.8, 136.8, 128.2, 123.9, 120.6, 117.6, 80.5, 62.8, 46.9, 28.4, 21.8. **IR** (ATR): 2977, 2780, 1674, 1646, 1598, 1478, 1457, 1440, 1425, 1388, 1364, 1269, 1156, 1121, 827, 675. **HRMS** calculated for $C_{15}H_{18}ClNO_4Na$ $[M+Na]^+$ 334.0822, found 334.0831. **Chiral SFC:** 100 mm CHIRALCEL AD-H, 5% ^{i}PrOH, 3.0 mL/min, 332 nm, 44 °C, nozzle pressure = 200 bar CO_2, t_{R1} (major) = 2.3 min, t_{R2} (minor) = 4.4 min.

tert-butyl (R)-2-(5-bromo-2-hydroxybenzoyl)azetidine-1-carboxylate (3i)

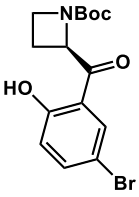

White solid, 69% yield, 92:8 *er*, >20:1 *rr*, $[\alpha]^{24}_D$ = +82.1 (*c* 0.05, $CHCl_3$). **^{1}H NMR** (400 MHz, $CDCl_3$) δ 11.93 (s, 1H), 7.63 (d, *J* = 2.4 Hz, 1H), 7.56 (dd, *J* = 8.9, 2.3 Hz, 1H), 6.93 (d, *J* = 8.9 Hz, 1H), 5.51 (dd, *J* = 9.6, 5.6 Hz, 1H), 4.05 – 3.94 (m, 2H), 2.76 – 2.66 (m, 1H), 2.20 (ddt, *J* = 11.3, 8.8, 5.7 Hz, 1H), 1.41 (s, 9H). **^{13}C NMR** (126 MHz, $CDCl_3$) δ 200.7, 162.0, 155.7, 139.6, 131.3, 121.0, 118.3, 110.8, 80.5, 62.8, 47.4, 28.4, 21.8. **IR** (ATR): 2974, 2776, 1675, 1646, 1592, 1477, 1457, 1440, 1423, 1364, 1268, 1177, 1156, 1118, 825, 661, 625. **HRMS** calculated for $C_{15}H_{18}BrNO_4Na$ $[M+Na]^+$ 378.0317, found 378.0302. **Chiral**

SFC: 100 mm CHIRALCEL AD-H, 5% ^{i}PrOH, 3.0 mL/min, 332 nm, 44 °C, nozzle pressure = 200 bar CO_2, t_{R1} (major) = 2.6 min, t_{R2} (minor) = 4.9 min.

tert-butyl (R)-2-(2-hydroxy-5-(trifluoromethyl)benzoyl)azetidine-1-carboxylate (3j)

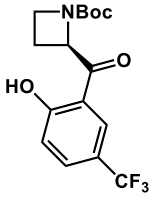

White solid, 67% yield, 79:21 *er*, >20:1 *rr*, $[\alpha]^{24}_D$ = +57.1 (*c* 0.03, $CHCl_3$). **^{1}H NMR** (400 MHz, $CDCl_3$) δ 12.31 (s, 1H), 7.81 (s, 1H), 7.72 (dd, *J* = 8.8, 1.8 Hz, 1H), 7.13 (d, *J* = 8.8 Hz, 1H), 5.59 (dd, *J* = 9.6, 5.7 Hz, 1H), 4.09 – 3.90 (m, 2H), 2.74 (dtd, *J* = 15.6, 9.1, 6.4 Hz, 1H), 2.23 (ddt, *J* = 11.4, 8.7, 5.8 Hz, 1H), 1.41 (s, 9H). **^{13}C NMR** (126 MHz, $CDCl_3$) δ 201.2, 165.3, 133.2 (apparent d, *J* = 3.1 Hz), 126.5 (q, *J* = 4.0 Hz), 123.7 (q, *J* = 542.8 Hz), 121.6 (q, *J* = 33.8 Hz), 119.8 (2C), 116.4, 80.5, 62.7, 47.3, 28.3, 21.7. **^{19}F NMR** (565 MHz, $CDCl_3$) δ -61.9. **IR** (ATR): 2985, 2743, 1678, 1645, 1614, 1440, 1368, 1323, 1313, 1277, 1182, 1154, 1112, 1077, 1061, 839, 662, 623. **HRMS** calculated for $C_{16}H_{18}F_3NO_4Na$ $[M+Na]^+$ 368.1086, found 368.1086. **Chiral HPLC:** 250 mm CHIRALCEL IA, 5% ^{i}PrOH, 2.0 mL/min, 254 nm, t_{R1} (minor) = 4.7 min, t_{R2} (major) = 8.3 min.

tert-butyl (R)-2-(3-fluoro-2-hydroxybenzoyl)azetidine-1-carboxylate (3k)

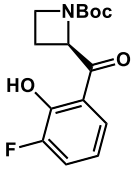

White solid, 61% yield, 97:3 *er*, >20:1 *rr*, $[\alpha]^{24}_D$ = +107.8 (*c* 0.3, $CHCl_3$). **^{1}H NMR** (600 MHz, $CDCl_3$) δ 12.02 (s, 1H), 7.31 (dd, *J* = 15.9, 8.6 Hz, 2H), 6.84 (d, *J* = 4.1 Hz, 1H), 5.54 (dd, *J* = 8.6, 5.8 Hz, 1H), 4.06 – 3.93 (m, 2H), 2.75 – 2.64 (m, 1H), 2.27 – 2.12 (m, 1H), 1.41 (s, 9H). **^{13}C NMR** (151 MHz, $CDCl_3$) δ 201.5, 152.7, 151.5, 151.3 (d, *J* = 76.9 Hz), 124.0 (d, *J* = 3.9 Hz), 122.3 (d, *J* = 17.3 Hz), 118.7 (d, *J* = 3.1 Hz), 118.6 (d, *J* = 6.5 Hz), 80.5, 63.1, 46.7, 28.3, 21.78. **^{19}F NMR** (565 MHz, $CDCl_3$) δ -135.2. **IR** (ATR): 2975, 1697, 1652, 1588, 1506, 1454, 1390, 1364, 1276, 1245, 1140, 1098, 972, 929, 743, 598. **HRMS** calculated for $C_{15}H_{18}FNO_4Na$ $[M+Na]^+$ 318.1118, found 318.1104. **Chiral SFC:** 100 mm CHIRALCEL AD-H, 3% ^{i}PrOH, 3.0 mL/min, 332 nm, 44 °C, nozzle pressure = 200 bar CO_2, t_{R1} (major) = 5.7 min, t_{R2} (minor) = 15.5 min.

tert-butyl (R)-2-(2-hydroxy-5-(methoxycarbonyl)benzoyl)azetidine-1-carboxylate (3l)

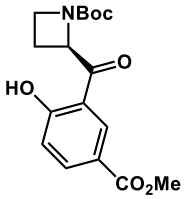

White solid, 84% yield, 92:8 *er*, >20:1 *rr*, $[\alpha]^{24}_D$ = +92.9 (*c* 0.4, $CHCl_3$). **^{1}H NMR** (600 MHz, $CDCl_3$) δ 12.43 (s, 1H), 8.28 (s, 1H), 8.14 (d, *J* = 8.6 Hz, 1H), 7.05 (d, *J* = 8.6 Hz, 1H), 5.66 (dd, *J* = 8.9, 6.0 Hz, 1H), 4.07 – 3.97 (m, 2H), 3.91 (s, 3H), 2.82 – 2.73 (m, 1H), 2.26 – 2.14 (m, 1H), 1.41 (s, 9H) ppm. **^{13}C NMR** (151 MHz, $CDCl_3$) δ 201.7, 166.6, 165.9, 155.8, 137.6, 131.6, 121.4, 119.1, 116.5, 80.4, 62.8, 52.4, 46.74, 28.4, 21.9 ppm. **IR** (ATR): 2974, 1721, 1679, 1634, 1598, 1463, 1447, 1433, 1269, 1158, 1117, 948, 853, 769, 668. **HRMS** calculated for $C_{17}H_{21}NO_6Na$ $[M+Na]^+$ 358.1266, found 358.1257. **Chiral SFC:** 100 mm CHIRALCEL AD-H, 2% ^{i}PrOH, 2.0 mL/min, 240 nm, 44 °C, nozzle pressure = 200 bar CO_2, t_{R1} (major) = 18.6 min, t_{R2} (minor) = 21.4 min.

di-tert-butyl 2,2'-(5-(tert-butyl)-2-hydroxyisophthaloyl)(2R,2'R)-bis(azetidine-1-carboxylate) (3m)

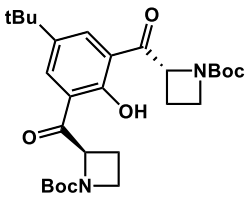

Yellow solid, 76% yield, XX:X *er*, >20:1 *rr*, $[\alpha]^{24}_D$ = +61.9 (*c* 0.6, $CHCl_3$). **^{1}H NMR** (400 MHz, $CDCl_3$) δ 12.86 (s, 1H), 7.99 (s, 2H), 5.56 (dd, *J* = 8.3, 5.4 Hz, 2H), 4.09 – 3.69 (m, 4H), 2.82 – 2.58 (m, 2H), 2.25 – 2.06 (m, 2H), 1.42 (s, 18H), 1.31 (s, 9H). **^{13}C NMR** (151 MHz, $CDCl_3$) 199.1, 160.9, 155.9, 142.2, 133.4, 80.1, 65.9, 46.3, 34.5, 31.3, 28.5, 25.5, 21.7 ppm. **IR** (ATR): 2970, 1699, 1651, 1598, 1450, 1390, 1364, 1289, 1245, 1142, 1090, 1050, 971, 920, 860, 772, 865. **HRMS** calculated for $C_{28}H_{40}N_2O_7Na$ $[M+Na]^+$ 517.2914, found 517.2921. **Chiral SFC:** 150 mm CHIRALCEL AD-H, 2% ^{i}PrOH, 2.0 mL/min, 220 nm, 44 °C, nozzle pressure = 200 bar CO_2.

2.4 General Procedure B

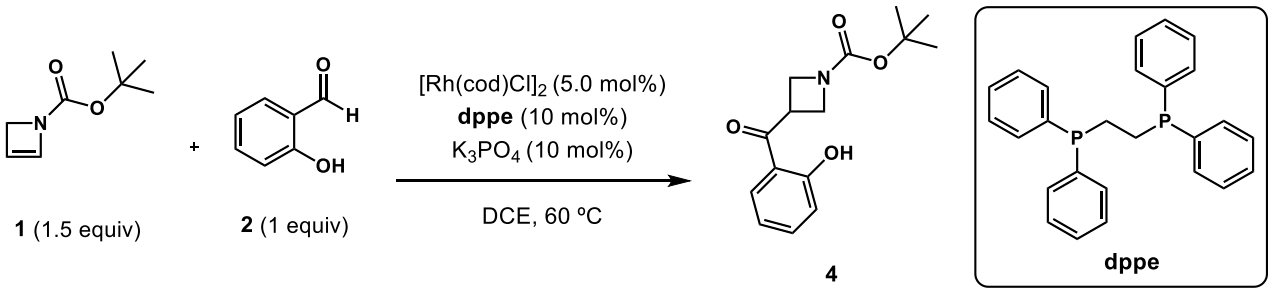

General Procedure B:

In an N_2-filled glove box, $[Rh(COD)Cl]_2$ (2.5 mg, 0.0050 mmol), dppe (4.0 mg, 0.010 mmol), and DCE (0.20 mL) were added to a 1-dram vial without a stir bar. The resulting mixture was allowed to sit for 10 minutes at room temperature. Aldehyde **2** (12 mg, 0.10 mmol) was added followed by

K_3PO_4 (2.1 mg, 0.010 mmol) and 2-Azetine **1** (23 mg, 0.15 ml, 1M in DCE) to initiate the reaction. The mixture was heated to 60 ˚C and kept at that temperature until no starting material was observed by TLC or GC-MS. The regioselectivity was determined by ^{1}H NMR analysis of the crude mixture. Isolated yields were obtained by preparative thin-layer chromatography.[1]

2.5 Compound Characterization for 4a-4l

tert-butyl 3-(2-hydroxybenzoyl)azetidine-1-carboxylate (4a)

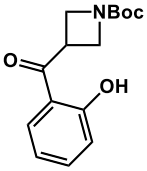

White solid, 98% yield, >20:1 *rr*. **^{1}H NMR** (500 MHz, $CDCl_3$) δ 12.04 (s, 1H), 7.53 – 7.47 (m, 1H), 7.40 (dd, *J* = 8.0, 1.4 Hz, 1H), 7.02 (d, *J* = 8.4 Hz, 1H), 6.90 (t, *J* = 7.6 Hz, 1H), 4.32 – 4.15 (m, 5H), 1.44 (s, 9H) ppm. **^{13}C NMR** (126 MHz, $CDCl_3$) δ 203.2, 163.0, 156.3, 137.0, 129.4, 119.4, 119.1, 117.9, 80.1, 51.1, 35.6, 28.5 ppm. **IR** (ATR): 2962, 1694, 1635, 1392, 1360, 1151, 1107, 762, 687 cm^{-1}. **HRMS** calculated for $C_{15}H_{19}NO_4Na$ $[M+Na]^+$ 300.1212, found 300.1222.

tert-butyl 3-(2-hydroxy-3-methylbenzoyl)azetidine-1-carboxylate (4b)

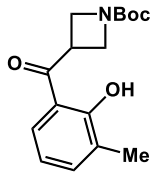

White solid, 48% yield, >20:1 *rr*. **^{1}H NMR** (600 MHz, $CDCl_3$) δ 12.35 (s, 1H), 7.37 – 7.34 (m, 1H), 7.26 – 7.24 (m, 1H), 6.82 – 6.78 (m, 1H), 4.28 – 4.14 (m, 5H), 2.27 (s, 3H), 1.44 (s, 9H) ppm. **^{13}C NMR** (151 MHz, $CDCl_3$) δ 203.4, 161.5, 156.3, 137.7, 128.2, 127.0, 118.7, 117.1, 80.0, 51.0, 35.7, 28.5, 15.7 ppm. **IR** (ATR): 2975, 2929, 1698, 1634, 1403, 1380, 1365, 1348, 1269, 1245, 1132, 1083, 770, 751, 732 cm^{-1}. **HRMS** calculated for $C_{16}H_{21}NO_4Na$ $[M+Na]^+$ 314.1368, found 314.1353.

tert-butyl 3-(2-hydroxy-4-isopropylbenzoyl)azetidine-1-carboxylate (4c)

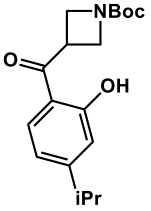

Colorless oil, 73% yield, >20:1 *rr*. **^{1}H NMR** (600 MHz, $CDCl_3$) δ 12.07 (s, 1H), 7.32 (d, *J* = 8.3 Hz, 1H), 6.87 (d, *J* = 1.3 Hz, 1H), 6.77 (dd, *J* = 8.3, 1.5 Hz, 1H), 4.30 – 4.10 (m, 5H), 2.89 (dt, *J* = 13.8, 6.9 Hz, 1H), 1.44 (s, 9H), 1.24 (d, *J* = 6.9 Hz, 6H) ppm. **^{13}C NMR** (151 MHz, $CDCl_3$) δ 202.5, 163.3, 159.5, 156.29, 129.5, 118.3, 116.4, 116.0, 80.1, 51.1, 35.5, 34.6, 28.5, 23.4 ppm. **IR** (ATR): 2960, 2933, 1689, 1633, 1406, 1382, 1243, 1156, 1113, 1054, 808, 772, 732 cm^{-1}. **HRMS** calculated for $C_{18}H_{25}NO_4Na$ $[M+Na]^+$ 342.1681, found 342.1668.

tert-butyl 3-(2-hydroxy-5-methylbenzoyl)azetidine-1-carboxylate (4d)

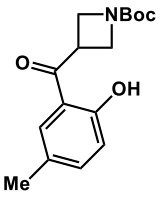

Colorless oil, 84% yield, >20:1 *rr*. **^{1}H NMR** (400 MHz, $CDCl_3$) δ 11.87 (s, 1H), 7.30 (dd, *J* = 8.5, 1.8 Hz, 1H), 7.16 (s, 1H), 6.92 (d, *J* = 8.5 Hz, 1H), 4.33 – 4.07 (m, 5H), 2.29 (s, 3H), 1.44 (s, 9H) ppm. **^{13}C NMR** (125 MHz, $CDCl_3$) δ 203.0, 161.0, 156.3, 138.1, 129.1, 128.5, 118.8, 117.6, 80.1, 51.0, 35.5, 28.5, 20.7 ppm. **IR** (ATR): 2975, 1698, 1639, 1393, 1364, 1277, 1245, 1133, 956, 784, 771, 734 cm^{-1}. **HRMS** calculated for $C_{16}H_{21}NO_4Na$ $[M+Na]^+$ 314.1368, found 314.1364.

tert-butyl 3-(2-hydroxy-3-methoxybenzoyl)azetidine-1-carboxylate (4e)

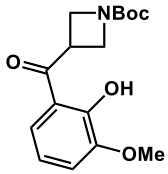

Yellow oil, 55% yield, >20:1 *rr*. **^{1}H NMR** (500 MHz, $CDCl_3$) δ 12.27 (s, 1H), 7.07 (d, *J* = 7.9 Hz, 1H), 7.01 (dd, *J* = 8.2, 1.1 Hz, 1H), 6.85 (t, *J* = 8.1 Hz, 1H), 4.29 – 4.13 (m, 5H), 3.91 (s, 3H), 1.44 (s, 9H) ppm. **^{13}C NMR** (151 MHz, $CDCl_3$) δ 203.5, 156.3, 153.4, 149.4, 120.5, 118.9, 118.0, 117.4, 80.1, 56.4, 51.0, 36.0, 28.5 ppm. **IR** (ATR): 2975, 1694, 1638, 1455, 1437, 1403, 1355, 1251, 1133, 1088, 966, 771, 735 cm^{-1}. **HRMS** calculated for $C_{16}H_{21}NO_5Na$ $[M+Na]^+$ 330.1317, found 330.1310.

tert-butyl 3-(2-hydroxy-6-methoxybenzoyl)azetidine-1-carboxylate (4f)

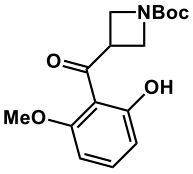

Colorless oil, 40% yield, >20:1 *rr*. **^{1}H NMR** (500 MHz, $CDCl_3$) δ 12.91 (s, 1H), 7.37 (t, *J* = 8.3 Hz, 1H), 6.60 (d, *J* = 8.2 Hz, 1H), 6.37 (d, *J* = 8.1 Hz, 1H), 4.26 – 4.06 (m, 5H), 3.88 (s, 3H), 1.45 (s, 9H) ppm. **^{13}C NMR** (151 MHz, $CDCl_3$) δ 203.5, 165.2, 161.0, 156.5, 136.9, 111.3, 110.0, 101.2, 101.2, 79.8, 56.1, 41.3, 28.5 ppm. **IR** (ATR): 2924, 1698, 1622, 1601, 1457, 1392, 1363, 1158, 1092, 773, 747 cm^{-1}. **HRMS** calculated for $C_{16}H_{21}NO_5Na$ $[M+Na]^+$ 330.1317, found 330.1306.

tert-butyl 3-(5-chloro-2-hydroxybenzoyl)azetidine-1-carboxylate (4g)

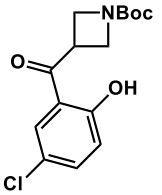

White solid, 60% yield, >20:1 *rr*. **^{1}H NMR** (600 MHz, $CDCl_3$) δ 11.95 (s, 1H), 7.44 (dd, *J* = 8.9, 1.6 Hz, 1H), 7.35 (s, 1H), 6.99 (d, *J* = 8.9 Hz, 1H), 4.31 – 4.07 (m, 5H), 1.45 (s, 9H) ppm. **^{13}C NMR** (151 MHz, $CDCl_3$) δ 202.4, 161.5, 156.2, 137.0, 128.6, 124.1, 120.8, 118.5, 80.3, 50.9, 35.6, 28.5 ppm. **IR** (ATR): 3058, 2928, 2930, 2895, 1685, 1640, 1475, 1401, 1347, 1272, 1184, 1169, 1138, 953, 901, 837, 797, 774, 751, 647 cm^{-1}. **HRMS** calculated for $C_{15}H_{18}ClNO_4Na$ $[M+Na]^+$ 334.0822, found 334.1811.

tert-butyl 3-(5-bromo-2-hydroxybenzoyl)azetidine-1-carboxylate (4h)

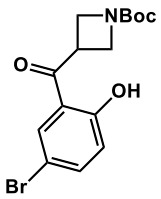

White solid, 55% yield, >20:1 *rr*. **^{1}H NMR** (400 MHz, $CDCl_3$) δ 11.97 (s, 1H), 7.57 (dd, *J* = 8.9, 2.3 Hz, 1H), 7.50 (d, *J* = 2.3 Hz, 1H), 6.94 (d, *J* = 8.9 Hz, 1H), 4.28 – 4.09 (m, 5H), 1.45 (s, 9H) ppm. **^{13}C NMR** (151 MHz, $CDCl_3$) δ 202.4, 161.9, 156.2, 139.7, 131.7, 121.1, 119.1, 110.9, 80.3, 51.0, 35.6, 28.5 ppm. **IR** (ATR): 2964, 2923, 1682, 1638, 1474, 1405, 1345, 1298, 1271, 1169, 1138, 950, 898, 838, 796, 772, 755, 626 cm^{-1}. **HRMS** calculated for $C_{15}H_{18}BrNO_4Na$ $[M+Na]^+$ 378.0317, found 378.0324.

tert-butyl 3-(2-hydroxy-5-(trifluoromethyl)benzoyl)azetidine-1-carboxylate (4i)

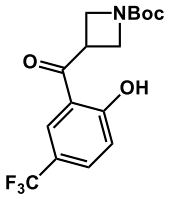

White solid, 30% yield, >20:1 *rr*. **^{1}H NMR** (500 MHz, $CDCl_3$) δ 12.34 (s, 1H), 7.72 (d, *J* = 8.8 Hz, 1H), 7.67 (s, 1H), 7.14 (d, *J* = 8.8 Hz, 1H), 4.28 – 4.21 (m, 5H), 1.45 (s, 9H) ppm. **^{13}C NMR** (151 MHz, $CDCl_3$) δ 202.9, 165.3, 156.2, 133.4 (q, *J* = 3.1 Hz), 126.9 (q, *J* = 4.0 Hz), 123.7 (q, *J* = 271.5 Hz), 121.9 (q, *J* = 33.7 Hz), 120.1, 117.3, 80.3, 50.9, 35.6, 28.5 ppm. **^{19}F NMR** (565 MHz, $CDCl_3$) δ -61.95 ppm. **IR** (ATR): 2977, 1695, 1647, 1394, 1363, 1322, 1279, 1161, 1119, 1080 cm^{-1}. **HRMS** calculated for $C_{16}H_{18}F_3NO_4Na$ $[M+Na]^+$ 368.1086, found 368.1103.

tert-butyl 3-(3-fluoro-2-hydroxybenzoyl)azetidine-1-carboxylate (4j)

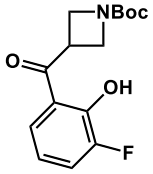

White solid, 52% yield, >20:1 *rr*. **^{1}H NMR** (600 MHz, $CDCl_3$) δ 12.05 (s, 1H), 7.35 – 7.29 (m, 1H), 7.20 (dt, *J* = 8.1, 1.4 Hz, 1H), 6.86 (td, *J* = 8.1, 4.5 Hz, 1H), 4.29 – 4.08 (m, 5H), 1.44 (s, 9H) ppm. **^{13}C NMR** (151 MHz, $CDCl_3$) δ 203.3, 156.2, 152.1 (d, *J* = 248.8 Hz), 151.6 (d, *J* = 12.7 Hz), 124.4 (d, *J* = 3.8 Hz), 122.5 (d, *J* = 17.3 Hz), 119.7 (d, *J* = 3.0 Hz), 118.7 (d, *J* = 6.6 Hz), 80.2, 50.9, 36.0, 28.5 ppm. **^{19}F NMR** (565 MHz, $CDCl_3$) δ -135.16 (dd, *J* = 10.4, 4.5 Hz) ppm. **IR** (ATR): 2976, 2894, 1698, 1651, 1453, 1393, 1364, 1349, 1271, 1246, 1134, 1071, 851, 770, 746 cm^{-1}. **HRMS** calculated for $C_{15}H_{18}FNO_4Na$ $[M+Na]^+$ 318.1118, found 318.1104.

tert-butyl 3-(3-hydroxy-[1,1'-biphenyl]-4-carbonyl)azetidine-1-carboxylate (4k)

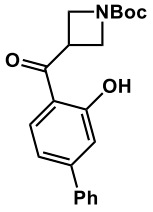

White solid, 24% yield, >20:1 *rr*. **^{1}H NMR** (500 MHz, $CDCl_3$) δ 12.14 (s, 1H), 7.63 – 7.60 (m, 2H), 7.50 – 7.39 (m, 4H), 7.25 (d, *J* = 1.7 Hz, 1H), 7.15 (dd, *J* = 8.3, 1.7 Hz, 1H), 4.33 – 4.17 (m, 5H), 1.46 (s, 9H) ppm. **^{13}C NMR** (151 MHz, $CDCl_3$) δ 202.7, 163.3, 156.3, 149.8, 139.3, 129.9, 129.1, 129.0, 127.4, 118.4, 117.0, 116.7, 80.1, 51.1, 35.6, 28.5 ppm. **IR** (ATR): 2929, 1699, 1630, 1393, 1362, 1247, 1195, 1158, 1133, 949, 751, 685 cm^{-1}. **HRMS** calculated for $C_{21}H_{23}NO_4Na$ $[M+Na]^+$ 376.1525, found 376.1508.

tert-butyl 3-(2-hydroxy-5-(methoxycarbonyl)benzoyl)azetidine-1-carboxylate (4l)

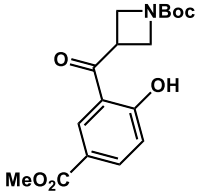

Colorless oil, 46% yield, >20:1 *rr*. **^{1}H NMR** (500 MHz, $CDCl_3$) δ 12.44 (s, 1H), 8.19 – 8.12 (m, 2H), 7.05 (d, *J* = 8.5 Hz, 1H), 4.26 (t, *J* = 4.6 Hz, 5H), 3.91 (s, 3H), 1.45 (s, 9H) ppm. **^{13}C NMR** (151 MHz, $CDCl_3$) δ 203.4, 166.5, 165.8, 156.2, 137.7, 132.0, 121.5, 119.3, 117.4, 80.2, 52.4, 35.6, 28.5 ppm. **IR** (ATR): 2926, 1709, 1688, 1392, 1365, 1122, 1088, 767 cm^{-1}. **HRMS** calculated for $C_{17}H_{21}NO_6Na$ $[M+Na]^+$ 358.1266, found 358.1253.

3. Azetine Synthesis

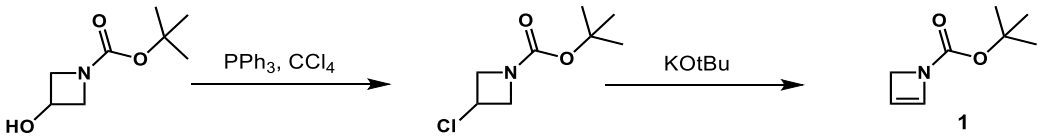

tert-butyl azete-1(2H)-carboxylate (1)

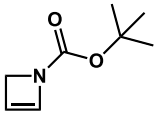

Synthesized according to reported procedures from commercially available tert-butyl 3-chloroazetidine-1-carboxylate.[1] Further purified via fractional distillation under reduced pressure to afford a colorless oil. Upon purification, azetine **1** was stored as a 1M solution in DCE. The solution was stored in a dark freezer for up to a month. ^{1}H and ^{13}C NMR spectra of the product are in agreement with previously reported data.[1] **H NMR** (500 MHz, $CDCl_3$) δ 6.56 (s, 1H), 5.51 (s, 1H), 4.38 (s, 2H), 1.46 (s, 9H) ppm. **^{13}C NMR** (126 MHz, $CDCl_3$) δ 151.9, 138.7, 111.8, 80.3, 58.4, 28.4 ppm.

4. Azetidine Derivatization

4.1 Sodium Borohydride Reduction

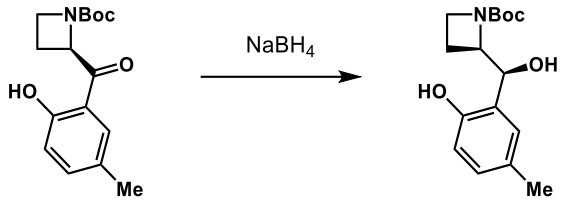

4d **6**

The procedure for the synthesis of compound **6** was adapted from a previously published method.[2] To a round bottom flask containing a stir bar was added **4d** (29 mg, 0.10 mmol, 1 equiv) and absolute ethanol (10 mL). This mixture was stirred at room temperature under a nitrogen atmosphere until **4d** was completely dissolved. $NaBH_4$ (4.2 mg, 0.11 mmol, 1.1 equiv) was then added. The reaction was monitored for completion by TLC. Upon complete consumption of starting material, the mixture was concentrated, and the residue was redissolved in DCM. The organic mixture was washed with water (x3), dried with magnesium sulfate, filtered, and concentrated. The crude material was purified by column chromatography (30% ethyl acetate in hexanes) to afford **6** in 99% yield.

tert-butyl (R)-2-((S)-hydroxy(2-hydroxy-5-methylphenyl)methyl)azetidine-1-carboxylate (6)

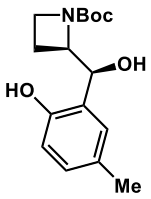

White solid, 99% yield, >20:1 *dr*. **^{1}H NMR** (500 MHz, $CDCl_3$) δ 8.66 (s, 1H), 6.97 (d, *J* = 8.2 Hz, 1H), 6.76 (d, *J* = 8.3 Hz, 2H), 4.84 (d, *J* = 9.0 Hz, 1H), 4.61 (q, *J* = 8.1 Hz, 1H), 3.91 – 3.71 (m, 2H), 2.23 (s, 3H), 2.01 (dt, *J* = 16.5, 7.9 Hz, 1H), 1.95 – 1.83 (m, 1H), 1.48 (s, 9H) ppm. **^{13}C NMR** (125 MHz, $CDCl_3$) δ 158.3, 154.6, 130.1, 129.0, 128.5, 121.2, 117.4, 81.5, 81.2, 65.8, 46.3, 28.5, 20.6, 19.1 ppm. **IR** (ATR): 3218, 2971, 2912, 1644, 1500, 1410, 1366, 1245, 1152, 828, 773 cm^{-1}. **HRMS** calculated for $C_{16}H_{23}NO_4Na$ $[M+Na]^+$ 316.1525, found 316.1524.

4.2 Methyl Grignard Addition

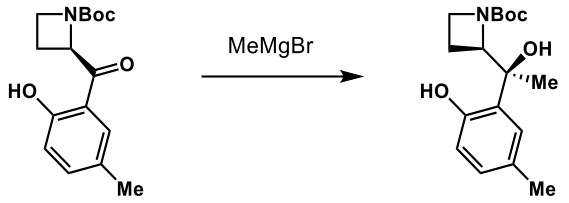

4d **7**

The procedure for the synthesis of compound **7** was adapted from a previously published method.[3] To a solution of **4d** (29.0 mg, 0.10 mmol, 1 equiv) in THF (2 mL) at 0 ˚C was added MeMgBr (0.40 mL, 0.60 mmol, 1.5 M in diethyl ether, 6 equiv). The mixture was stirred at 0 ˚C until no starting material was observed by TLC. Upon completion, the mixture was quenched with saturated aqueous NH_4Cl and extracted with ethyl acetate (x3). The organic layers were combined, washed with water (x1), and brine (x1). The resulting solution was dried with $MgSO_4$, filtered, and concentrated. The crude compound was purified by flash column chromatography on silica gel (30% ethyl acetate in hexanes) to afford **7** in 67% yield and 7:1 *dr*.

tert-butyl (R)-2-((S)-1-hydroxy-1-(2-hydroxy-5-methylphenyl)ethyl)azetidine-1-carboxylate (7)

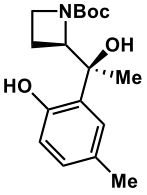

White solid, 67% yield, 7:1 *dr*. **^{1}H NMR** (600 MHz, $CDCl_3$) δ 9.30 (s, 1H), 6.94 (dd, *J* = 8.2, 1.6 Hz, 1H), 6.76 (d, *J* = 8.2 Hz, 1H), 6.68 (s, 1H), 4.56 (t, *J* = 7.5 Hz, 1H), 3.82 (dd, *J* = 16.6, 8.3 Hz, 1H), 3.71 (dd, *J* = 15.9, 7.7 Hz, 1H), 3.67 (s, 1H), 2.23 (s, 3H), 2.15 (dd, *J* = 15.3, 7.7 Hz, 2H), 1.63 (s, 3H), 1.48 (s, 9H) ppm. **^{13}C NMR** (151 MHz, $CDCl_3$) δ 158.9, 154.3, 129.6, 128.4, 126.6, 124.9, 117.9, 80.9, 79.93, 70.3, 47.9, 28.9, 28.5, 20.8, 18.6 ppm. **IR** (ATR): 3436, 3284, 2923, 2853, 1627, 1450, 1432, 1146, 821, 771 cm^{-1}. **HRMS** calculated for $C_{17}H_{25}NO_4Na$ $[M+Na]^+$ 330.1681, found 330.1665.

4.3 Boc Deprotection

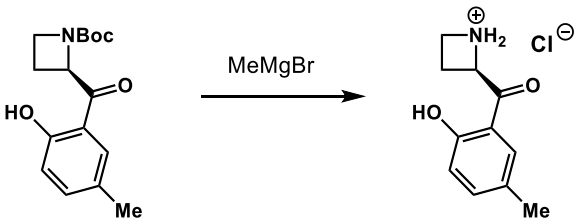

4d **8**

To a round bottom flask containing azetidine **4d** (50 mg, 0.17 mmol, 1.0 equiv) was added 4M HCl in 1,4-dioxane (0.43 mL, 1.70 mmol, 10 equiv). This mixture was stirred for 1 hour at room temperature under air. The reaction mixture was concentrated to dryness under reduced pressure to give azetidine **8**.

(R)-2-(2-hydroxy-5-methylbenzoyl)azetidin-1-ium chloride (8)

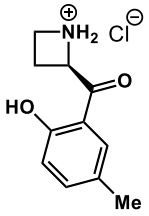

White solid, 99% yield. **^{1}H NMR** (500 MHz, D_2O) δ 7.51 (d, *J* = 8.5 Hz, 1H), 7.47 (s, 1H), 7.00 (d, *J* = 8.5 Hz, 1H), 4.28 (dd, *J* = 18.4, 9.5 Hz, 1H), 4.04 (dd, *J* = 16.6, 10.2 Hz, 1H), 3.15 (dd, *J* = 17.5, 10.7 Hz, 1H), 2.68 (dd, *J* = 20.3, 10.2 Hz, 1H), 2.31 (s, 3H) ppm (proton alpha to ketone proposed to be overlapping with D_2O peak) ppm. **^{13}C NMR** (125 MHz, D_2O) δ 215.5, 158.4, 139.2, 130.4, 129.6, 117.9, 116.1, 43.6, 30.3, 24.0, 19.4 ppm. **IR** (ATR): 2921, 1644, 1495, 1288, 1224, 1169, 831, 729 cm^{-1}. **HRMS** calculated for $C_{11}H_{14}NO_2$ $[M]^+$ 192.1024, found 192.1025.

4.4 Phenol to Aryl Triflate

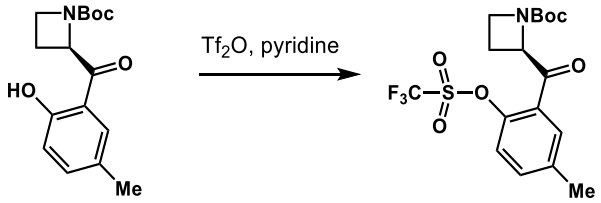

4d **9**

The procedure for the synthesis of compound **9** was adapted from a previously published method.[4] Azetidine **4d** (44 mg, 0.15 mmol, 1 equiv) was added to a round bottom flask containing a stir bar followed by DCM (6.0 ml) and pyridine (1.0 mL, 0.75 mmol, 5 equiv). This solution was cooled to 0 ˚C and trifluoromethanesulfonic anhydride (1.7 mL, 0.30 mmol, 2 equiv) was added dropwise. Following addition, the mixture was warmed to room temperature and stirred for 12 hours. Upon completion, the solution was washed with brine (x3). The organic layer was dried with sodium sulfate, filtered, and concentrated. The crude compound was purified by column chromatography on silica gel (20% ethyl acetate in hexanes) to afford **9** in 46% yield.

tert-butyl (R)-2-(5-methyl-2-(((trifluoromethyl)sulfonyl)oxy)benzoyl)azetidine-1-carboxylate (9)

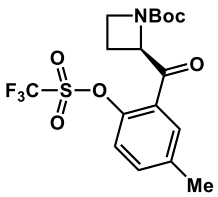

White solid, 46% yield. **^{1}H NMR** (600 MHz, $CDCl_3$) δ 7.62 (s, 1H), 7.42 (d, *J* = 8.1 Hz, 1H), 7.30 – 7.25 (m, 1H), 5.36 (dd, *J* = 9.2, 5.3 Hz, 1H), 4.06 (dd, *J* = 15.1, 8.0 Hz, 1H), 3.95 (dd, *J* = 14.0, 8.3 Hz, 1H), 2.64 – 2.56 (m, 1H), 2.45 (s, 3H), 2.27 (tt, *J* = 10.7, 5.4 Hz, 1H), 1.41 (s, 9H) ppm. **^{13}C NMR** (151 MHz, $CDCl_3$) δ 195.9, 155.7, 145.1, 139.0, 134.5, 131.1, 130.0, 122.3, 118.7 (q, *J* = 320.8 Hz), 80.3, 64.9, 46.9, 29.8, 28.4, 21.0 ppm. **^{19}F NMR** (565 MHz, $CDCl_3$) δ -73.07 ppm. **IR** (ATR): 2981, 2889, 1694, 1418, 1382, 1206, 1139, 1120, 884, 607 cm^{-1}. **HRMS** calculated for $C_{17}H_{20}F_3NO_6SNa$ $[M+Na]^+$ 446.0861, found 446.0865.

5. Mechanistic Studies for Azetine Hydroacylation

5.1 Deuterium-Labeling Studies

Synthesis of *d*-2a:

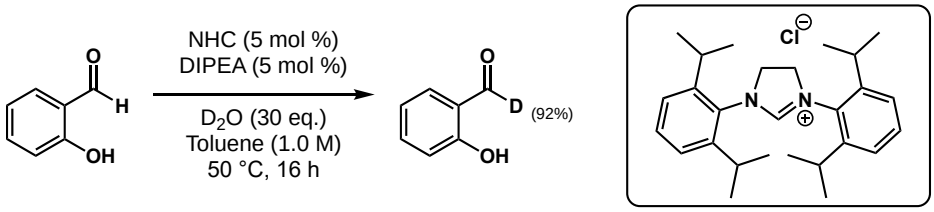

Deuteration reactions were run in 5 mL vials with a screw cap septa and stirred at 1000 rpm. A dry, argon flushed 5 mL vial equipped with a magnetic stir bar was charged with NHC (23.5 mg, 0.055 mmol, 0.05 eq.), flushed with argon followed by the addition of 500 µL (1 M) anhydrous toluene. DIPEA (10 µL, 0.055 mmol, 0.05 eq.), D_2O (600 µL, 33 mmol, 30 eq.) and then salicylaldehyde (117 µL, 1.1 mmol) was added. The reaction vial was closed with a screw cap then wrapped with teflon tape and electrical tape and the mixture was stirred at 50 ˚C for 24 h. After the reaction, an aliquot (50 µL) was taken for **^{1}H NMR** measurements. Crude residue was purified by preparatory TLC using Hex:Et_2O (90:10) combination to give colorless liquid.

Deuterium incorporation = 92% (crude: 93%), Reaction yield = 54% (68 mg). NMR spectra are given on pages xx-xx.

^{1}H NMR (400 MHz, $CDCl_3$) δ 9.92 (s, 1H), 7.59-7.52 (m, 2H), 7.05-6.99 (m, 2H).

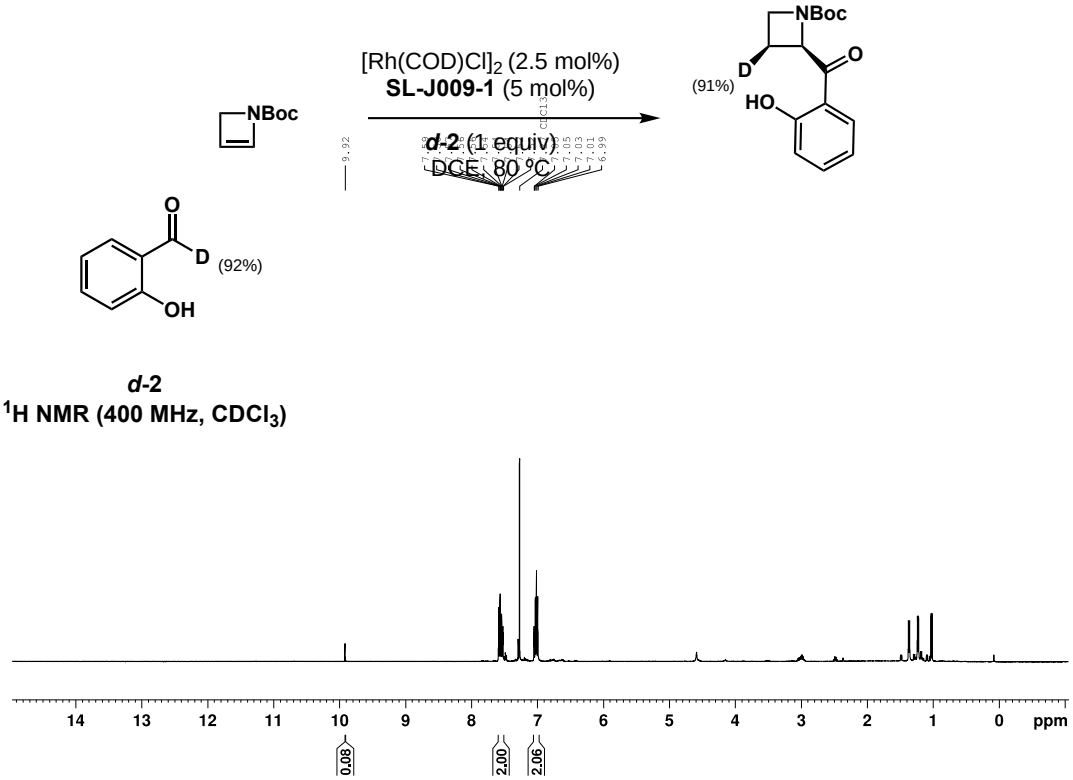

Synthesis of *d*-3a:

Following **General Procedure A**, ***d*-2a** was used as the aldehyde partner. White solid, 85% yield, >20:1 *rr*. **^{1}H NMR** (400 mHz, $CDCl_3$) δ 12.03 (s, 1H), 7.55 – 7.48 (m, 2H), 7.03 (d, *J* = 8.4 Hz, 1H), 6.92 – 6.88 (m, 1H), 5.58 (dd, *J* = 9.6, 5.6 Hz, 1H), 4.15 – 3.95 (m, 2H), 2.69 (dtd, *J* = 11.4, 9.1, 6.8 Hz, 1H), 2.22 (m, 1H), 1.42 (s, 9H). Deuterium incorporation was determined by ^{1}H NMR. Percent deuterium (% D) incorporation is depicted as the amount of deuterium in place of a single hydrogen atom at that site.

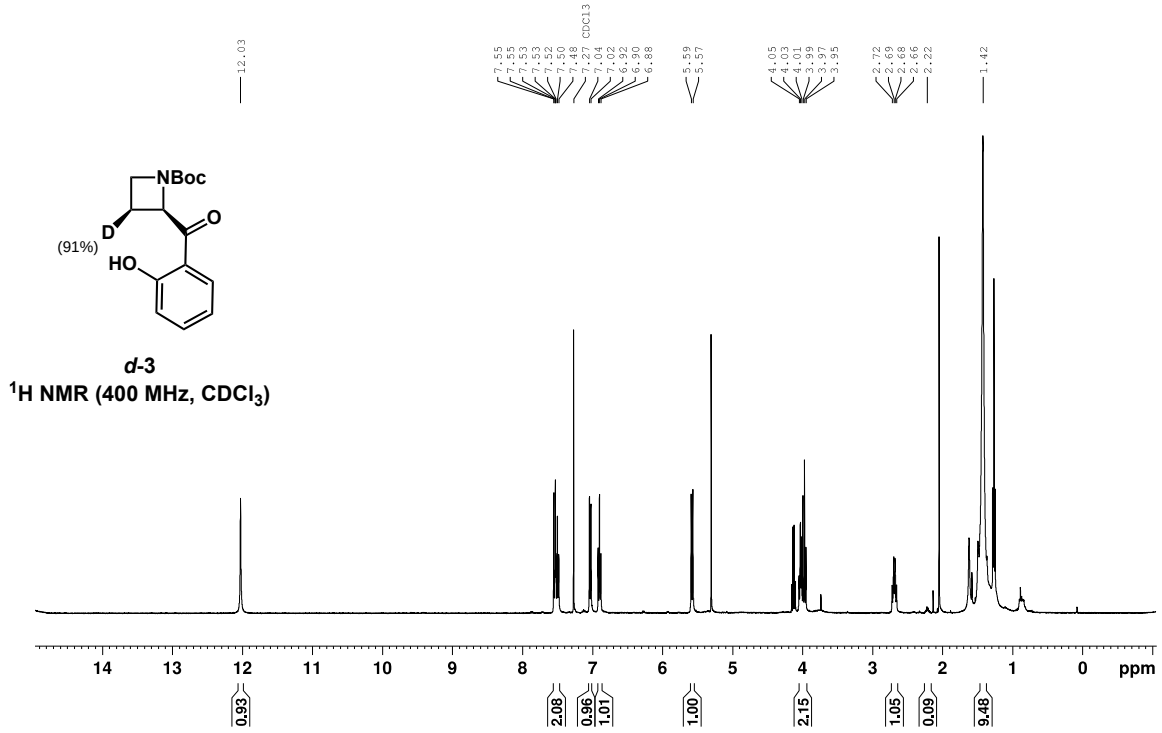

5.2 Initial Rate Kinetic Isotope Effect (KIE) Studies

Parallel KIE Studies

In a N_2-filled glovebox, a 0.1 M solution of catalyst was prepared by combining $[Rh(COD)Cl]_2$ (53.9 mg, 0.109 mmol), **dppe** (86.9 mg, 0.22 mmol), and DCE (1.1 mL) in a 1-dram vial. 10 side-by-side reactions were charged with triphenylmethane (1.0 mg, 4.0 µmol). Catalyst solution (0.10 mL, 10 mol% Rh) was added to each vial, followed by K_3PO_4 (2.1 mg, 9.8 µmol), Aldehyde **2a** (12 mg, 0.10 mmol) or ***d*-2a** (12 mg, 0.10 mmol), and 2-Azetine **1a** (23 mg, 0.15 ml, 1M in DCE) to initiate the reaction. The mixture was stirred at 60 ˚C, with one reaction vial containing **2a** and one reaction vial containing ***d*-2a,** stopped every 20 minutes and quenched with 2 mL of ethyl acetate. No further catalysis occurs after dilution with ethyl acetate. The appearance of **3a** or ***d*-3a** was monitored by internally referenced GC-FID analysis.

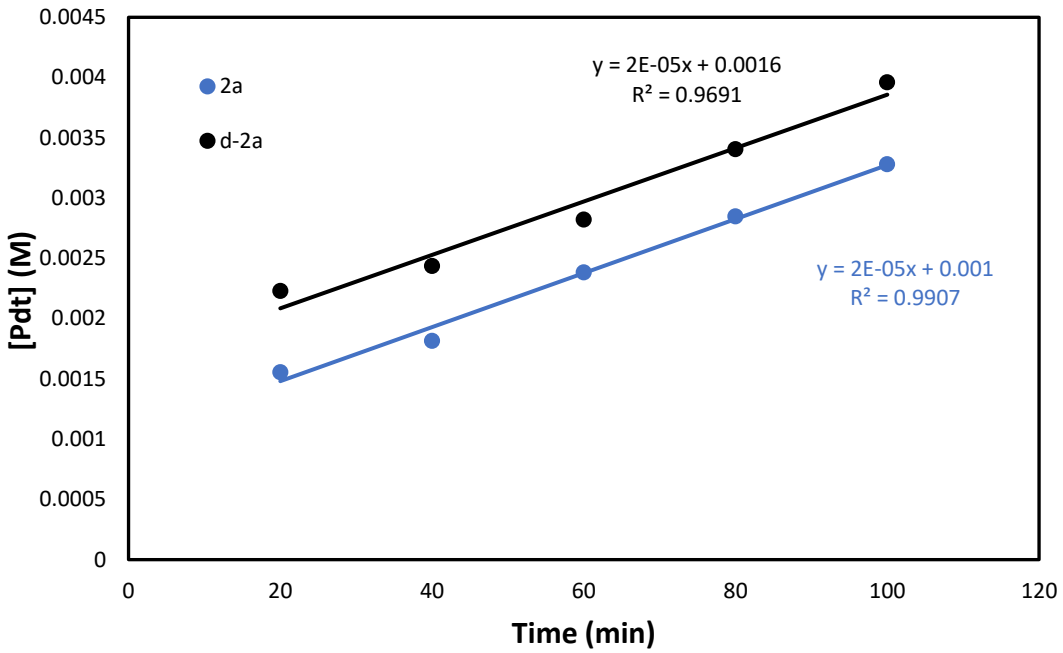

adjusted initial rate of deuterium species (considering 9% of 2a in d-2a):

$2 \times 10^{-5} = 0.91\ K_D + 0.09 \times (2 \times 10^{-5})$

$K_D = 2 \times 10^{-5}$

Calculation of KIE: $K_H/K_D = (2 \times 10^{-5})/(2 \times 10^{-5}) = 1$

Figure S13. Initial Rate KIE for 3-acyl

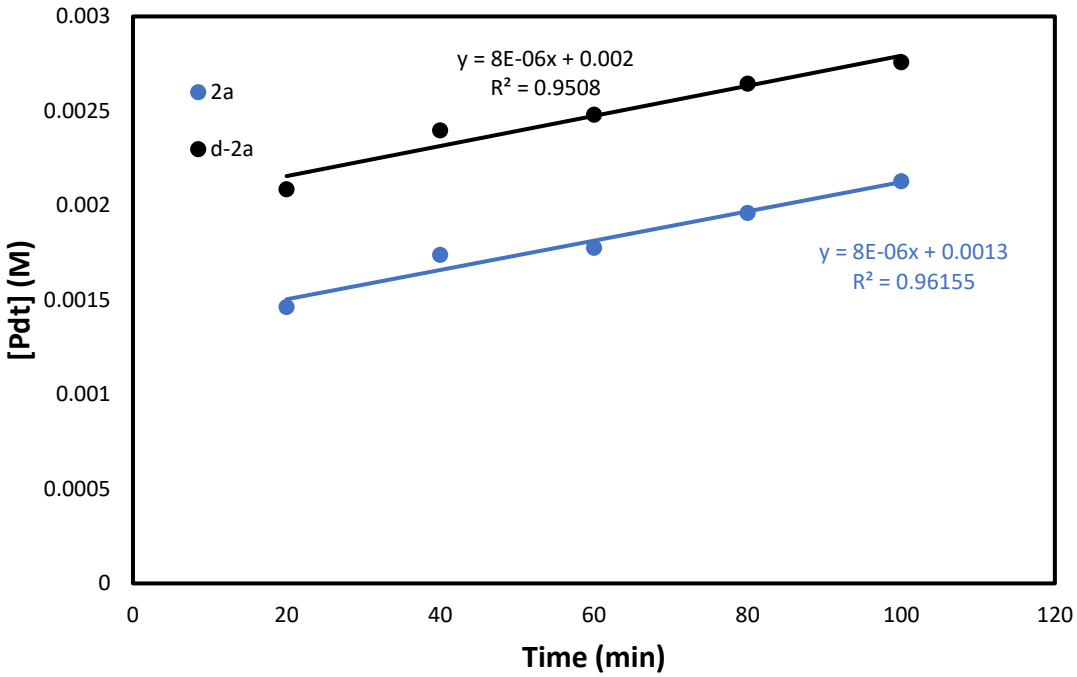

adjusted initial rate of deuterium species (considering 9% of 2a in d-2a):

$8 \times 10^{-6} = 0.91\ K_D + 0.09 \times (8 \times 10^{-6})$

$K_D = 8 \times 10^{-6}$
Calculation of KIE: $K_H/K_D = (8 \times 10^{-6})/(8 \times 10^{-6}) = 1$
Figure S13. Initial Rate KIE for 3-acyl

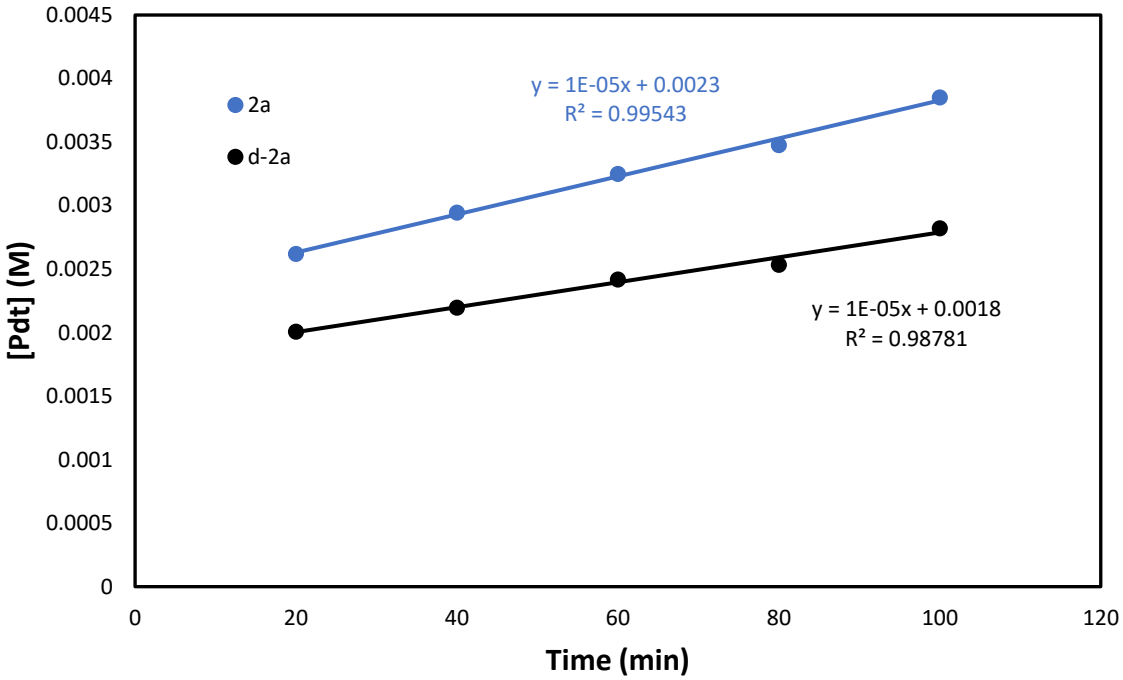

adjusted initial rate of deuterium species (considering 9% of 2a in d-2a):
$1 \times 10^{-5} = 0.91\ K_D + 0.09 \times (1 \times 10^{-5})$
$K_D = 1 \times 10^{-5}$
Calculation of KIE: $K_H/K_D = (1 \times 10^{-5})/(1 \times 10^{-5}) = 1$
Figure S13. Initial Rate KIE for 3-acyl

Competition KIE Studies

In a N_2-filled glovebox, a 0.1 M solution of catalyst was prepared by combining $[Rh(COD)Cl]_2$ (4.8 mg, 0.010 mmol), **SL-J009-1** (10.8 mg, 0.020 mmol), and DCE (0.10 mL) in a 1-dram vial. 3 side-by-side reactions were charged with 1,3,5-trimethoxybenzene (1.0 mg, 5.9 µmol). Catalyst solution (0.025 mL, 2.5 mol% Rh) was added to the vial, followed by Aldehyde **2a** (12 mg, 0.10 mmol) and ***d*-2a** (12 mg, 0.10 mmol), and 2-Azetine **1a** (23 mg, 0.15 ml, 1M in DCE) was added to initiate the reaction. The mixture was stirred at 80 ˚C, with one reaction vial stopped every 5 minutes and quenched with 2 mL of ethyl acetate. No further catalysis occurs after dilution with

ethyl acetate. The mixture was transferred to an NMR tube and an ^{1}H NMR spectrum was taken where the appearance of **3aa** or ***d*-3aa** was monitored by comparing the integration of key protons of the product (2.69 ppm) for **3aa** or (2.22 ppm) for ***d*-3aa**, to the internal standard (3.75 ppm).

Table S1. Competitive Kinetic Isotope Effect Data for 2-Acyl Hydroacylation

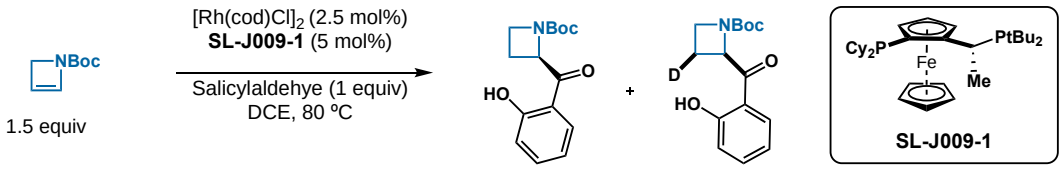

Entry	% Conversion	% yield 3aa	% yield *d*-3aa	K_H/K_D
1	5	3.6	2	1.8
2	15	10	5	2.0
3	20	13	7	1.8
4	23	15	8	1.8
5	34	22	12	1.8
6	38	25	13	1.9
7	39	26	14	1.8
8	40	28	14	1.9
9	51	33	18	1.8

6. References

(1) Hodgson, D. M.; Pearson, C. I.; Kazmi, M. Generation and Electrophile Trapping of *N* -Boc-2-Lithio-2-Azetine: Synthesis of 2-Substituted 2-Azetines. *Org. Lett.* **2014**, *16* (3), 856–859. https://doi.org/10.1021/ol403626k.

(2) Yang, Y.; Xing, D. Iridium-Catalysed Branched-Selective Hydroacylation of 1,3-Dienes with Salicylaldehydes. *Chem. Commun.* **2021**, *57* (60), 7378–7381. https://doi.org/10.1039/D1CC01872H.

(3) Delany, P. K.; Hodgson, D. M. Synthesis and Homologation of an Azetidin-2-Yl Boronic Ester with α-Lithioalkyl Triisopropylbenzoates. *Org. Lett.* **2019**, *21* (24), 9981–9984. https://doi.org/10.1021/acs.orglett.9b03901.

(4) Chen, Y.-J.; Xu, H.-B.; Liu, H.; Dong, L. Highly-Selective Synthesis of Functionalized Spirobenzofuranones and Diketones. *Org. Chem. Front.* **2022**, *9* (17), 4633–4639. https://doi.org/10.1039/D2QO00677D.

7. NMR Spectra of Unknown Compounds

tert-butyl (R)-2-(2-hydroxybenzoyl)azetidine-1-carboxylate (3a)

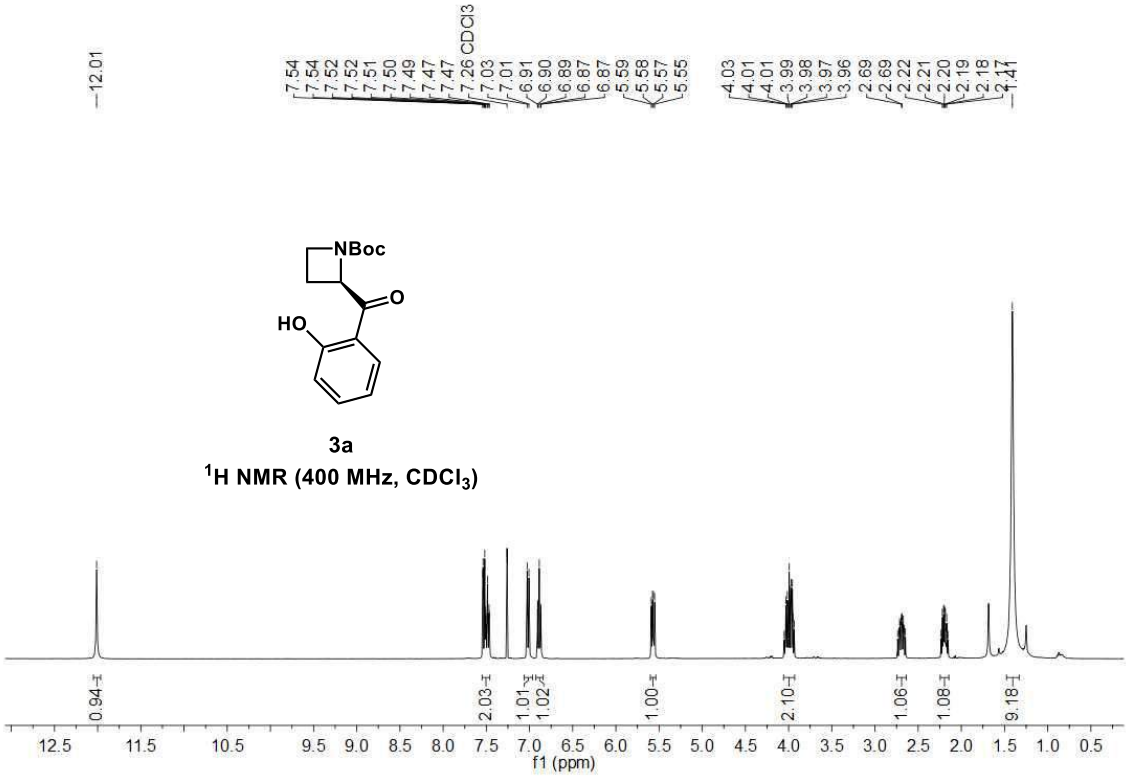

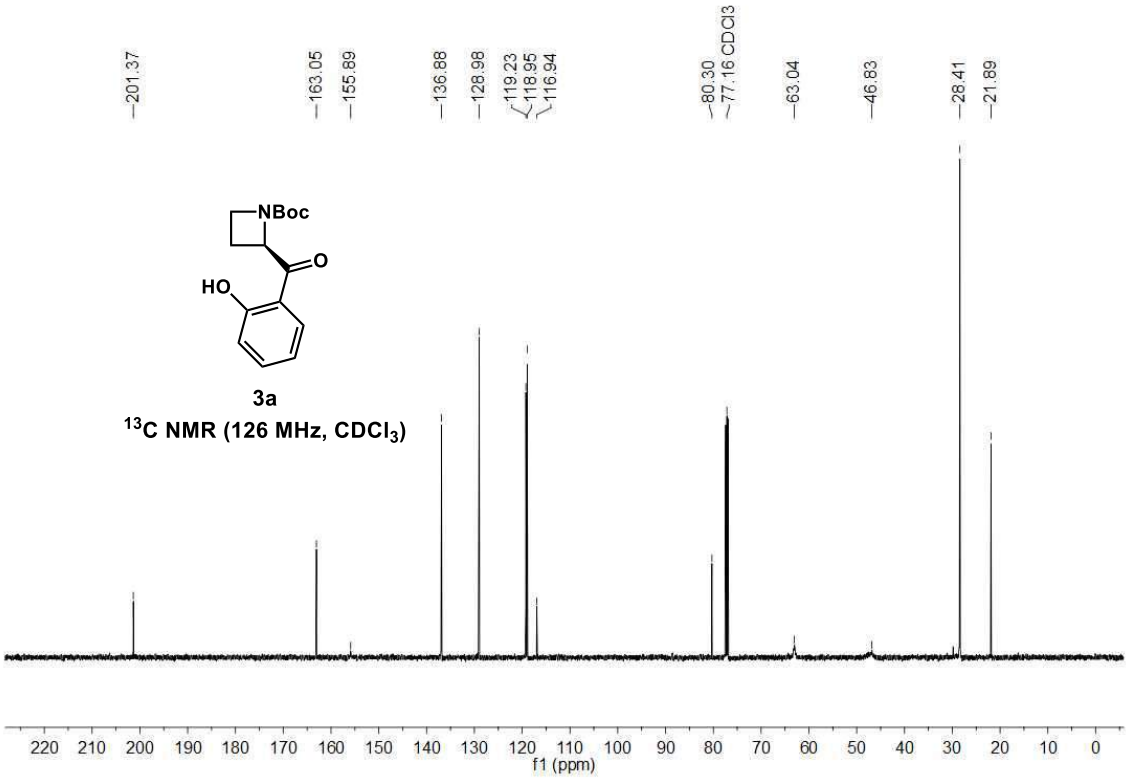

tert-butyl (R)-2-(2-hydroxy-3-methylbenzoyl)azetidine-1-carboxylate (3b)

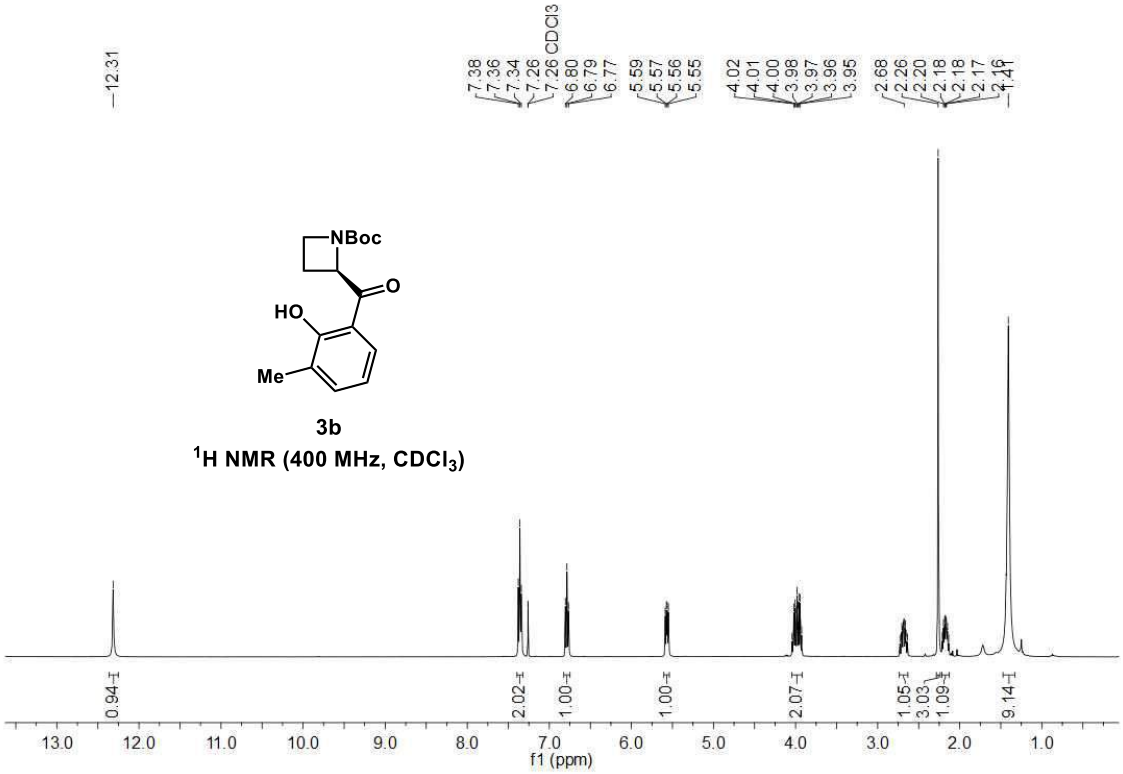

3b

^{1}H NMR (400 MHz, $CDCl_3$)

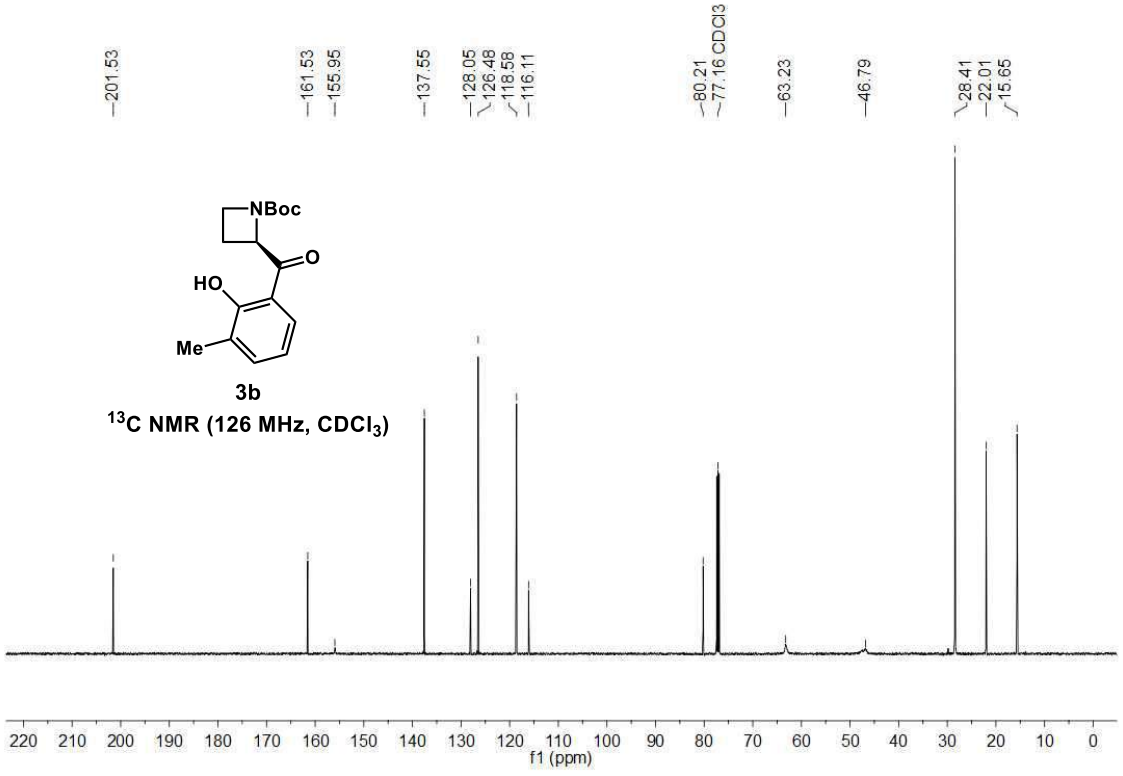

3b

^{13}C NMR (126 MHz, $CDCl_3$)

tert-butyl (R)-2-(2-hydroxy-4-isopropylbenzoyl)azetidine-1-carboxylate (3c)

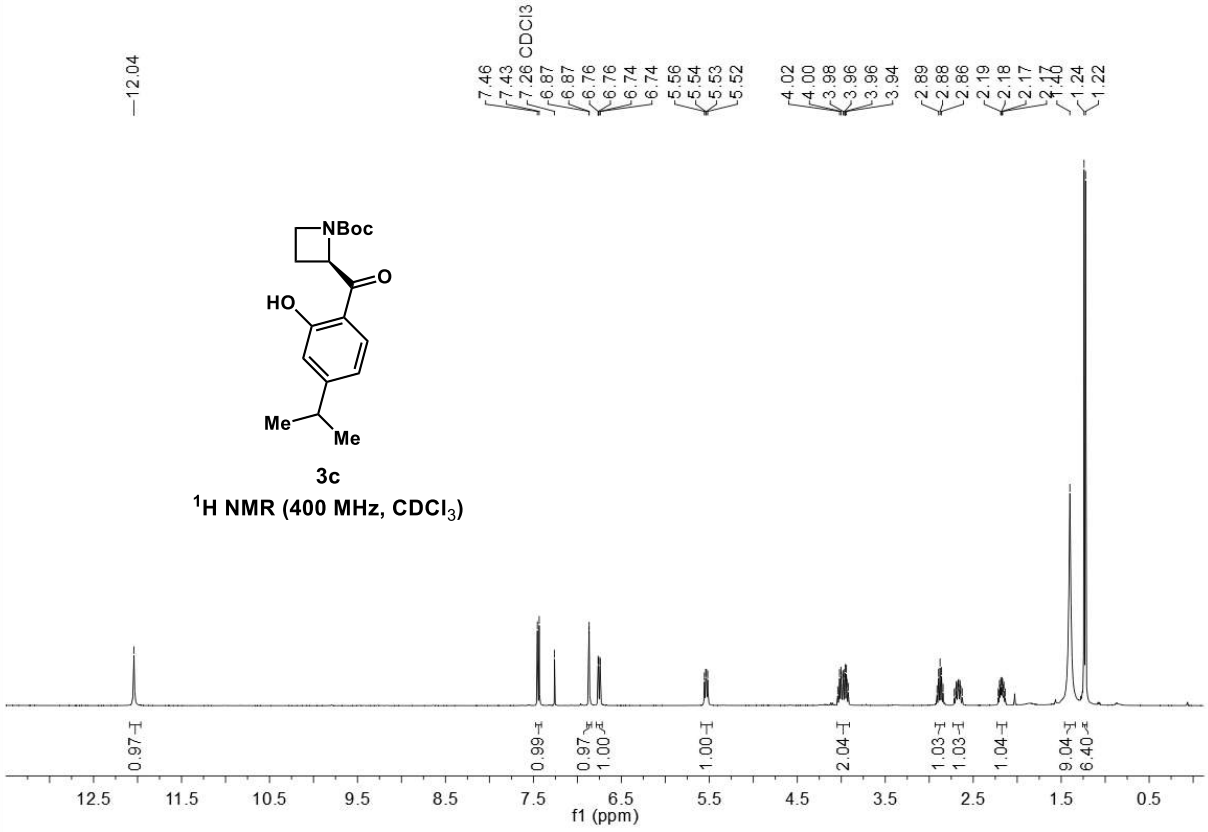

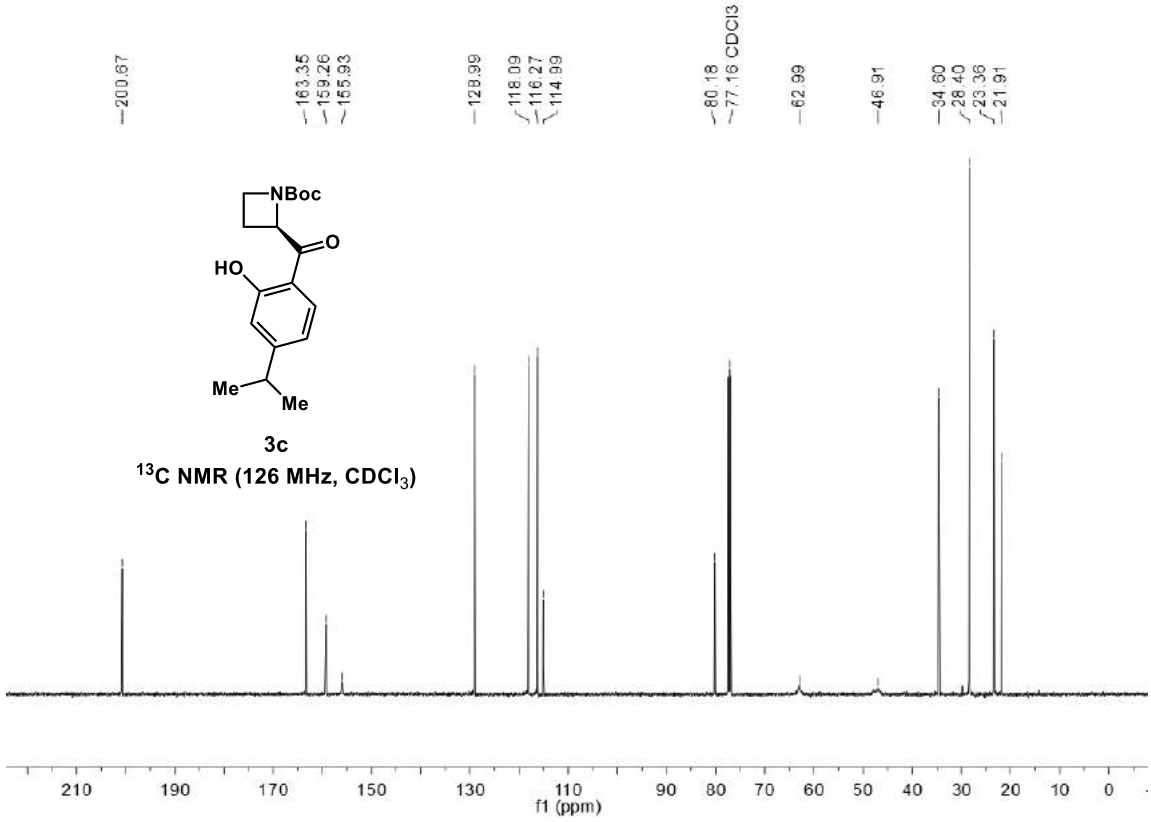

tert-butyl (R)-2-(2-hydroxy-5-methylbenzoyl)azetidine-1-carboxylate (3d)

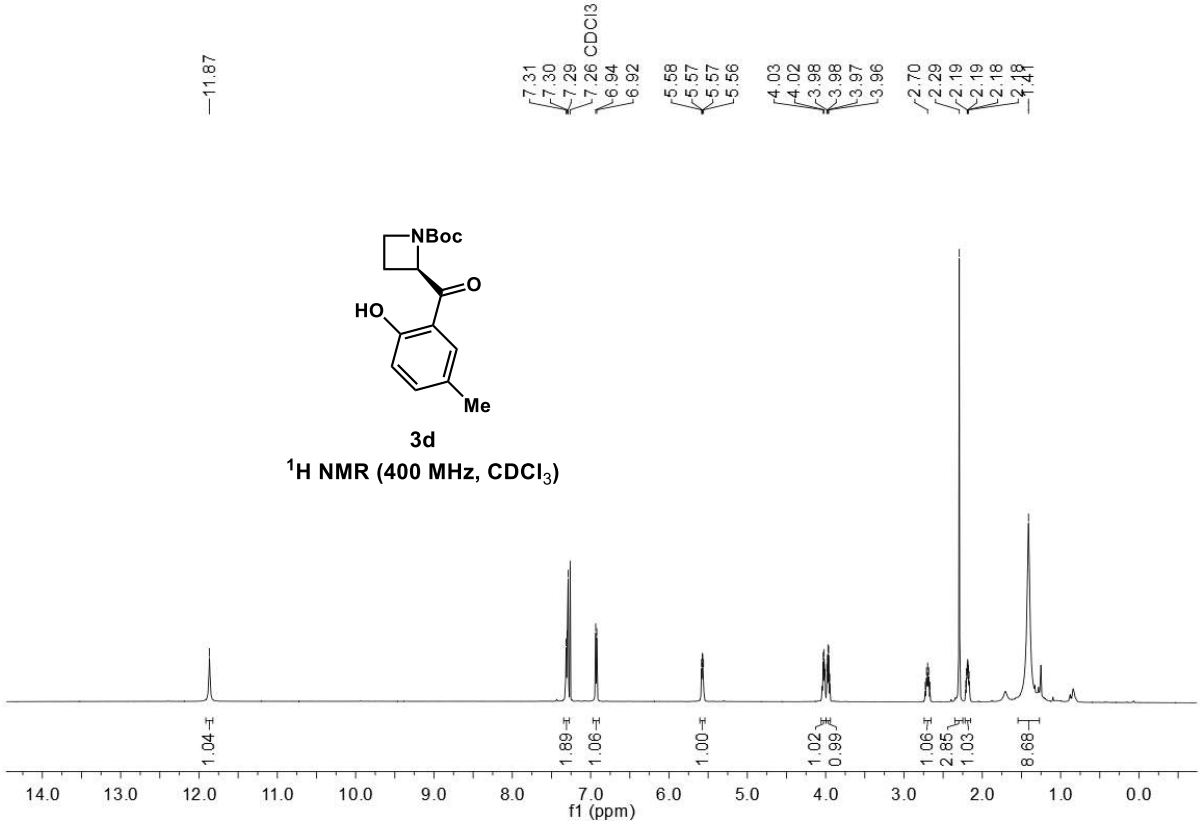

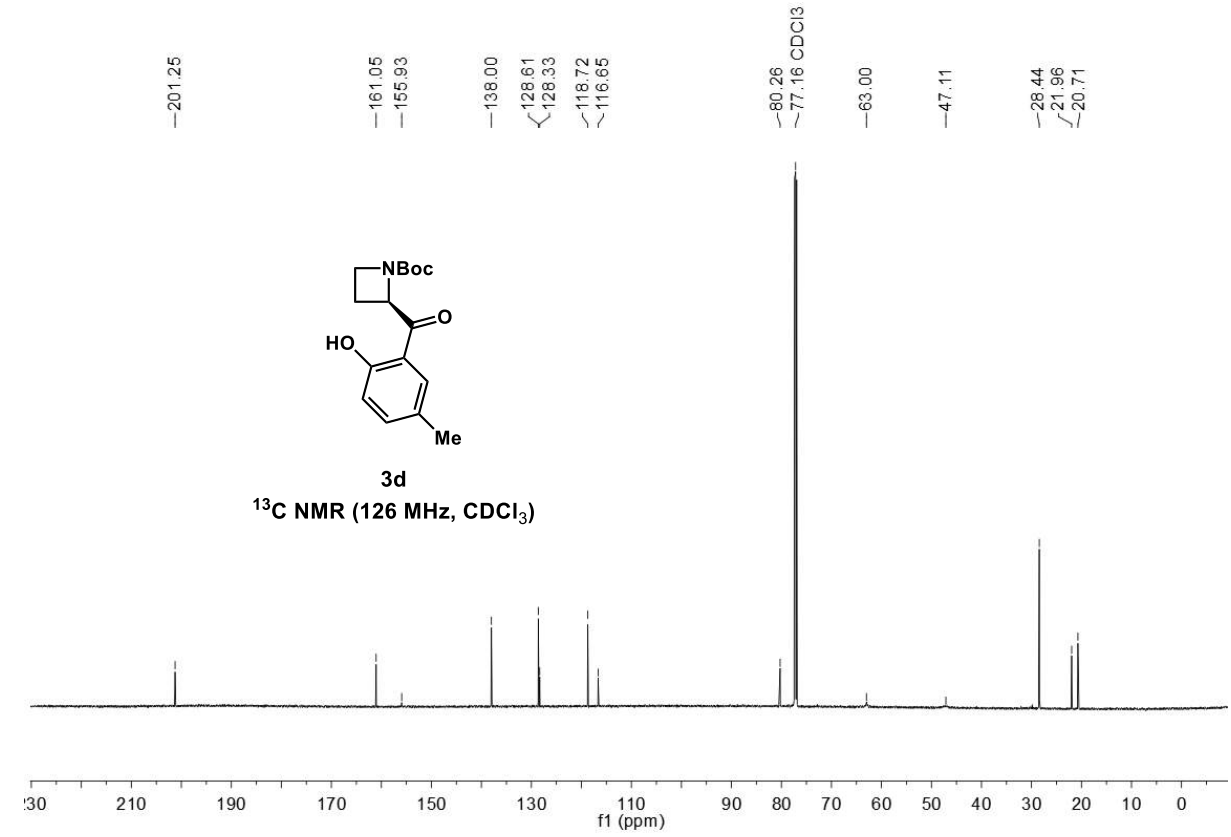

tert-butyl (R)-2-(2-hydroxy-3-methoxybenzoyl)azetidine-1-carboxylate (3e)

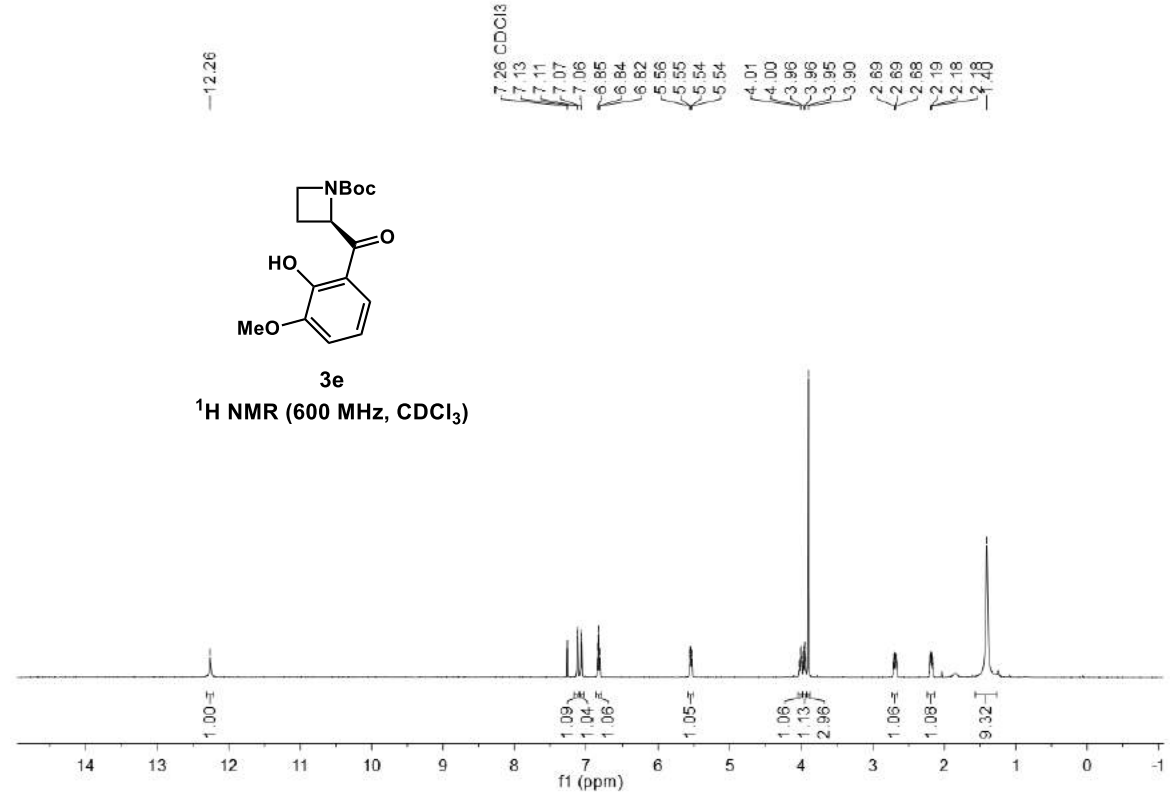

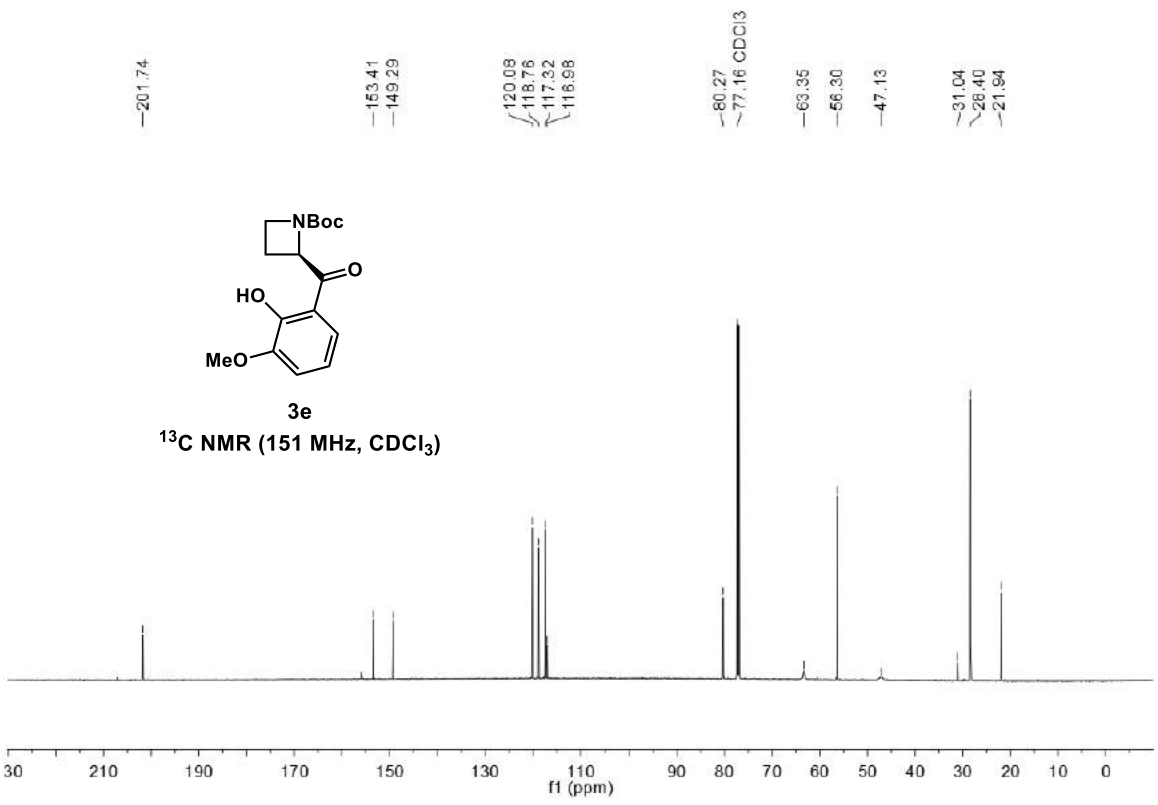

tert-butyl (R)-2-(3-allyl-2-hydroxybenzoyl)azetidine-1-carboxylate (3f)

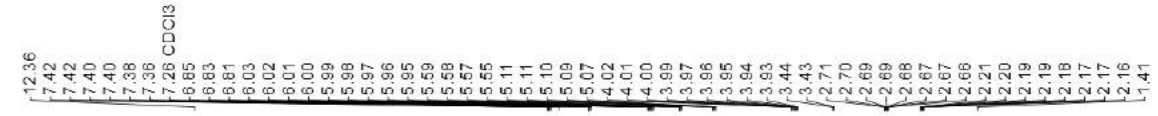

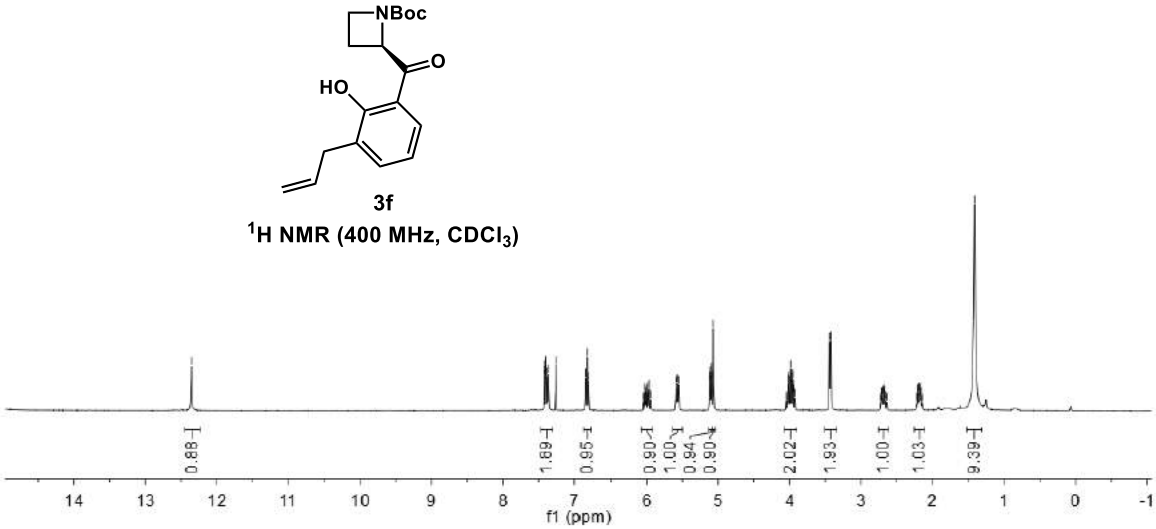

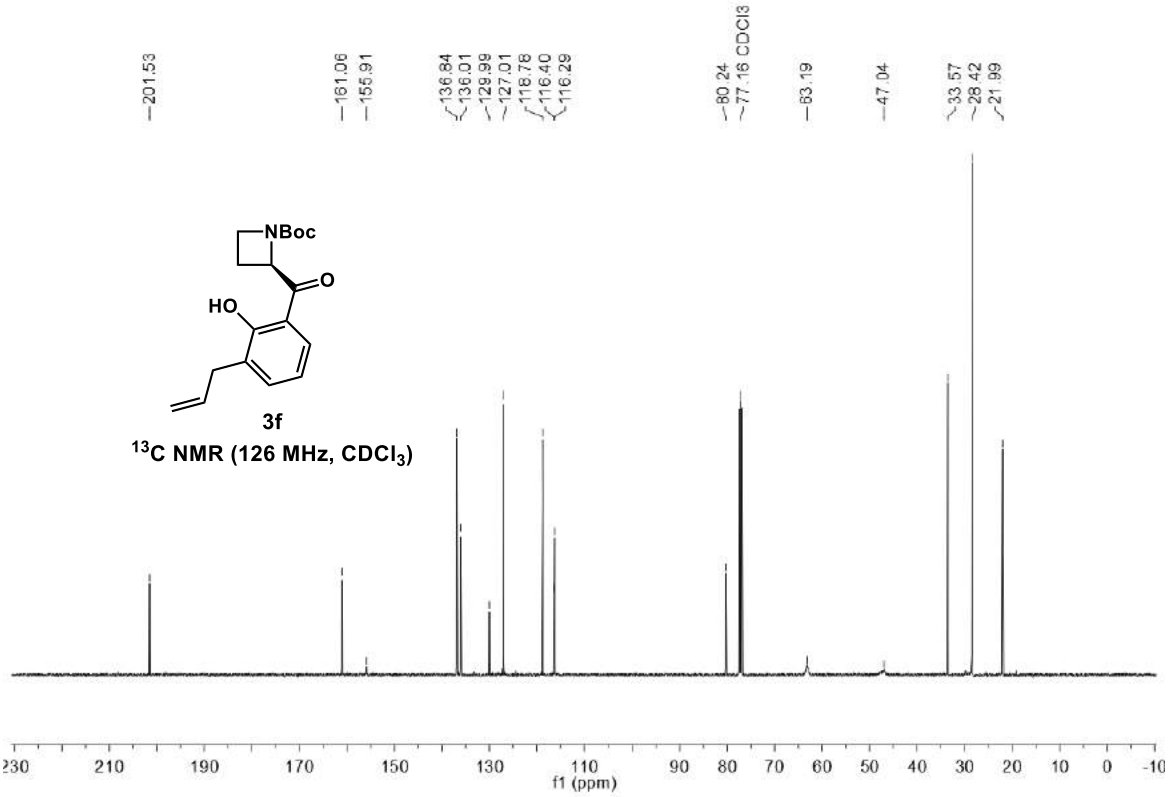

tert-butyl(R)-2-(2-hydroxy-5-(4,4,5,5-tetramethyl-1,3,2-dioxaborolan-2-yl)benzoyl) azetidine-1-carboxylate (3g)

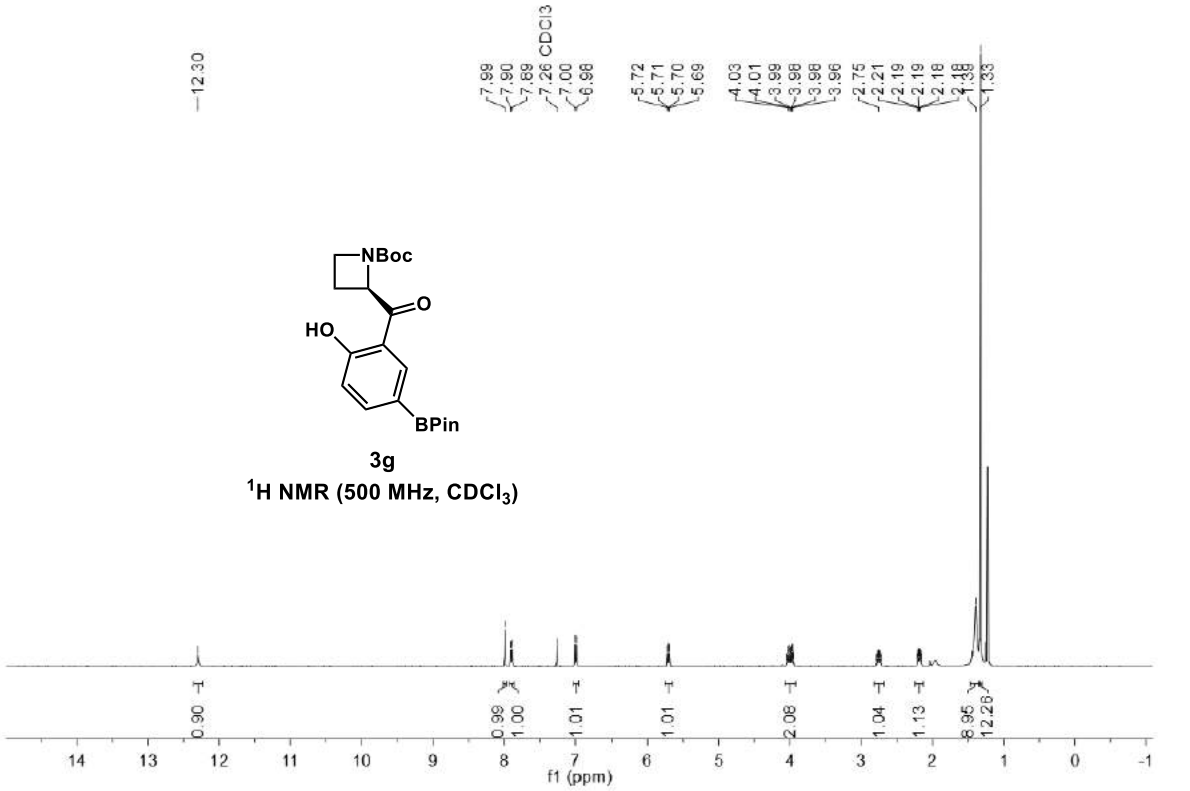

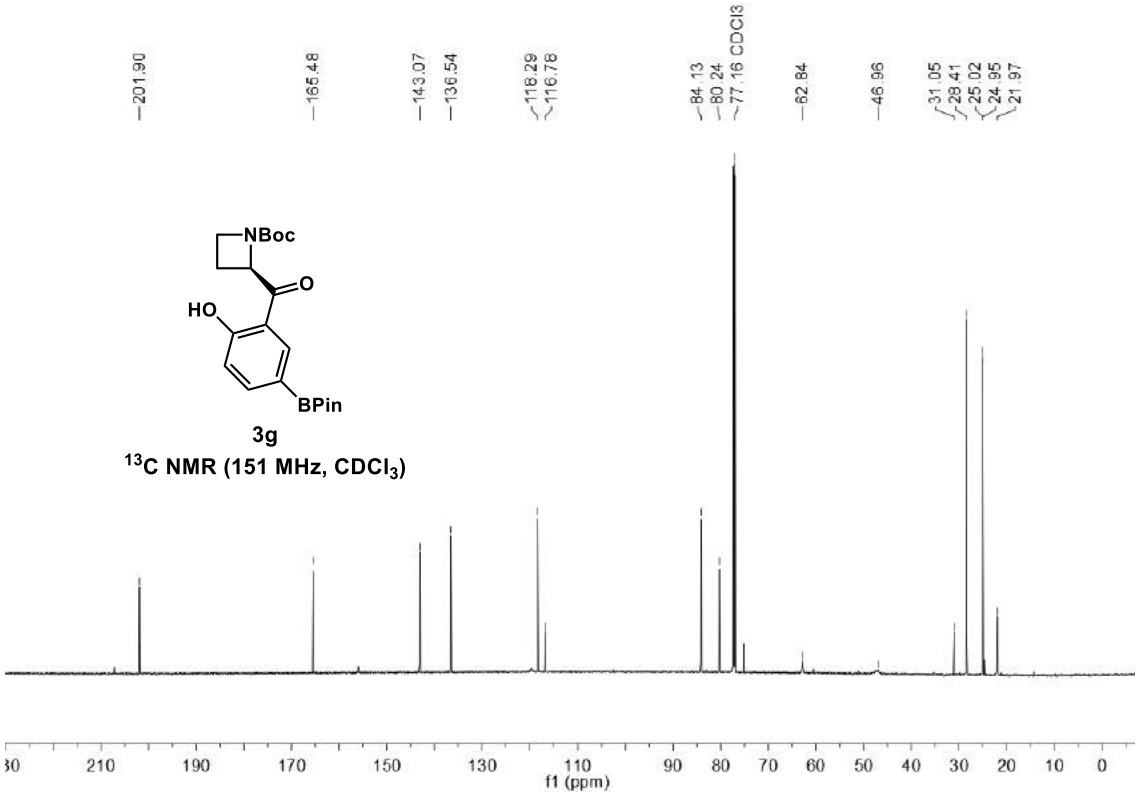

tert-butyl (R)-2-(5-chloro-2-hydroxybenzoyl)azetidine-1-carboxylate (3h)

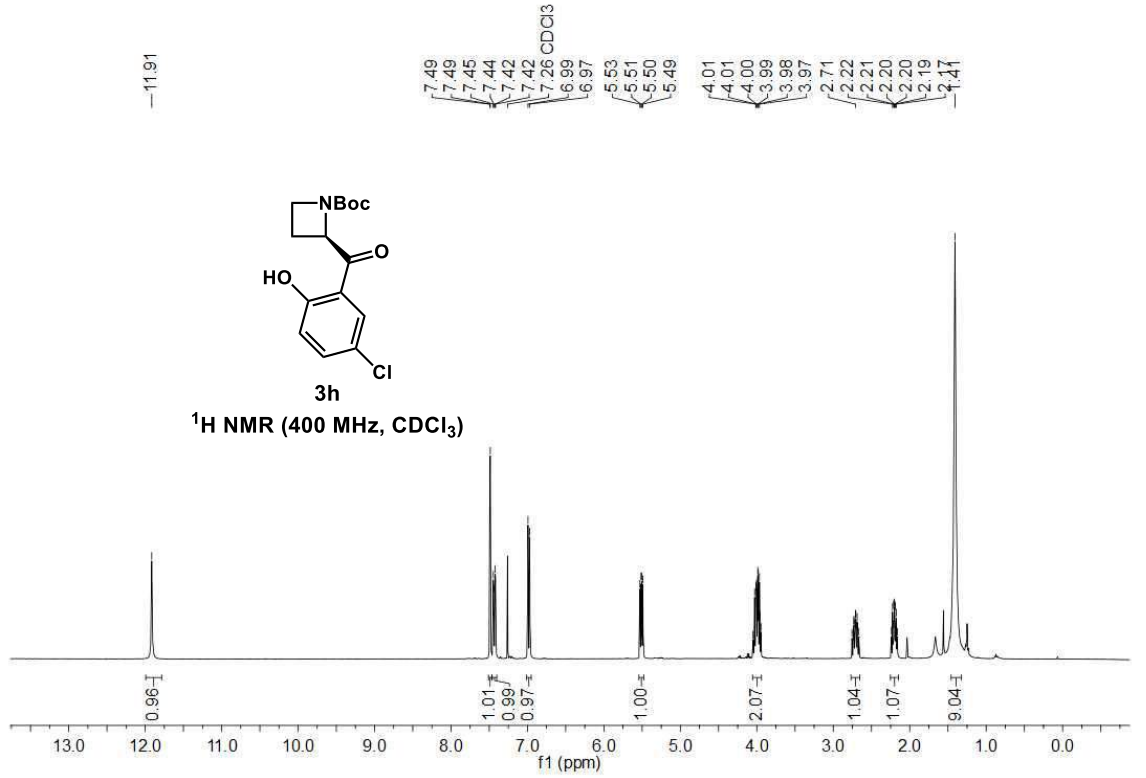

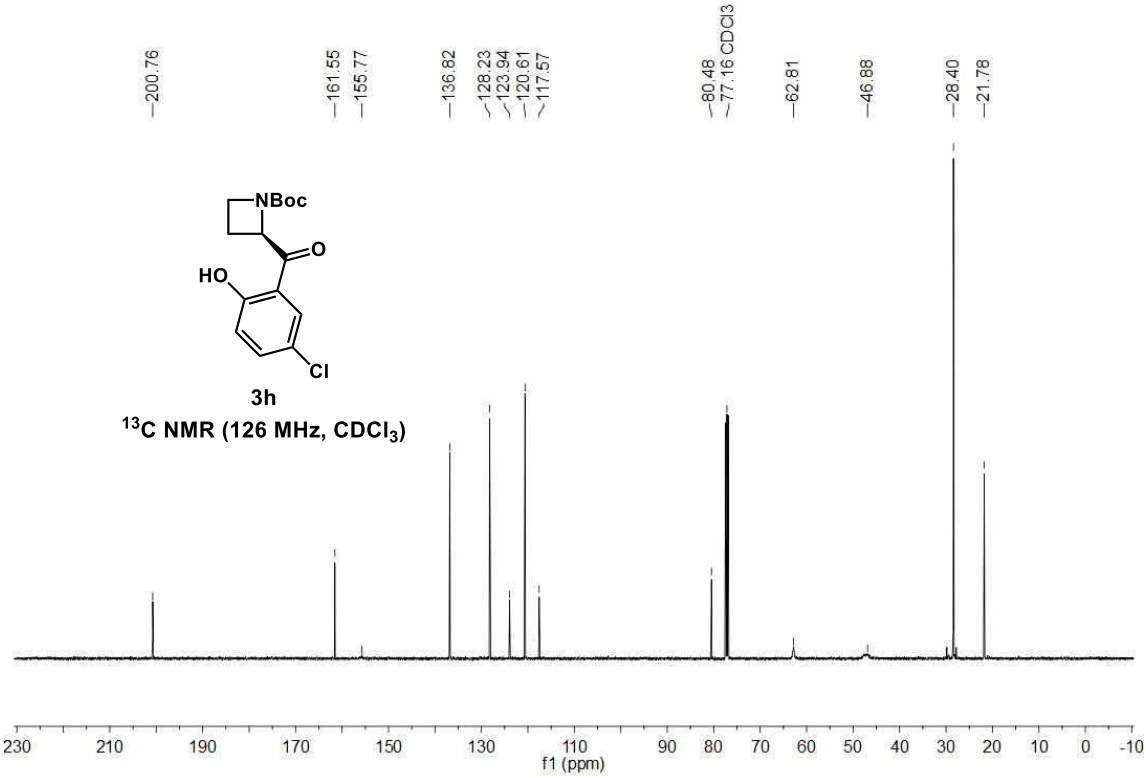

tert-butyl (R)-2-(5-bromo-2-hydroxybenzoyl)azetidine-1-carboxylate (3i)

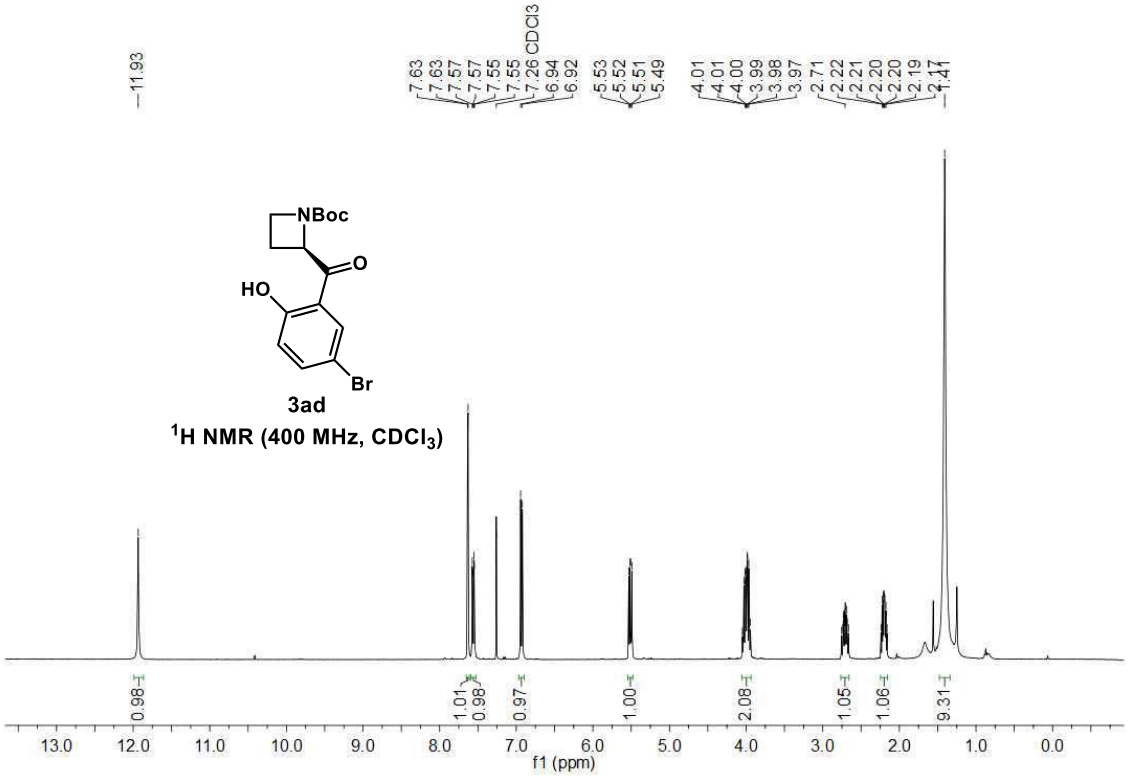

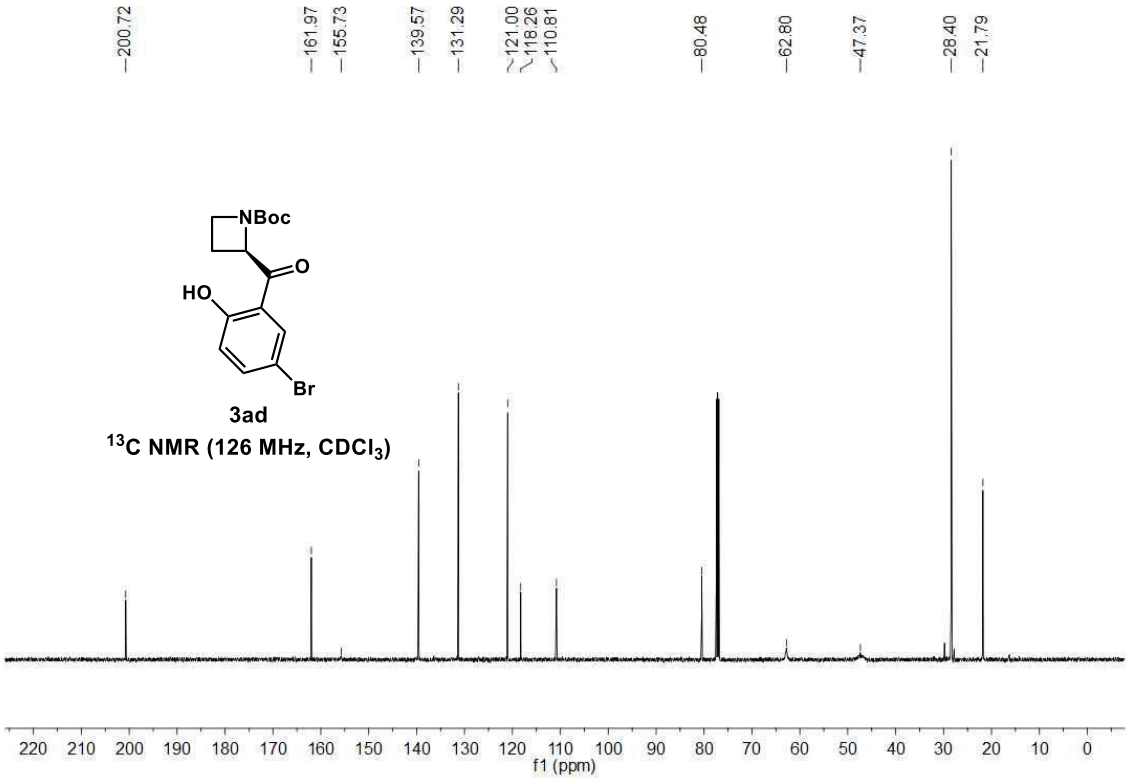

tert-butyl (R)-2-(2-hydroxy-5-(trifluoromethyl)benzoyl)azetidine-1-carboxylate (3j)

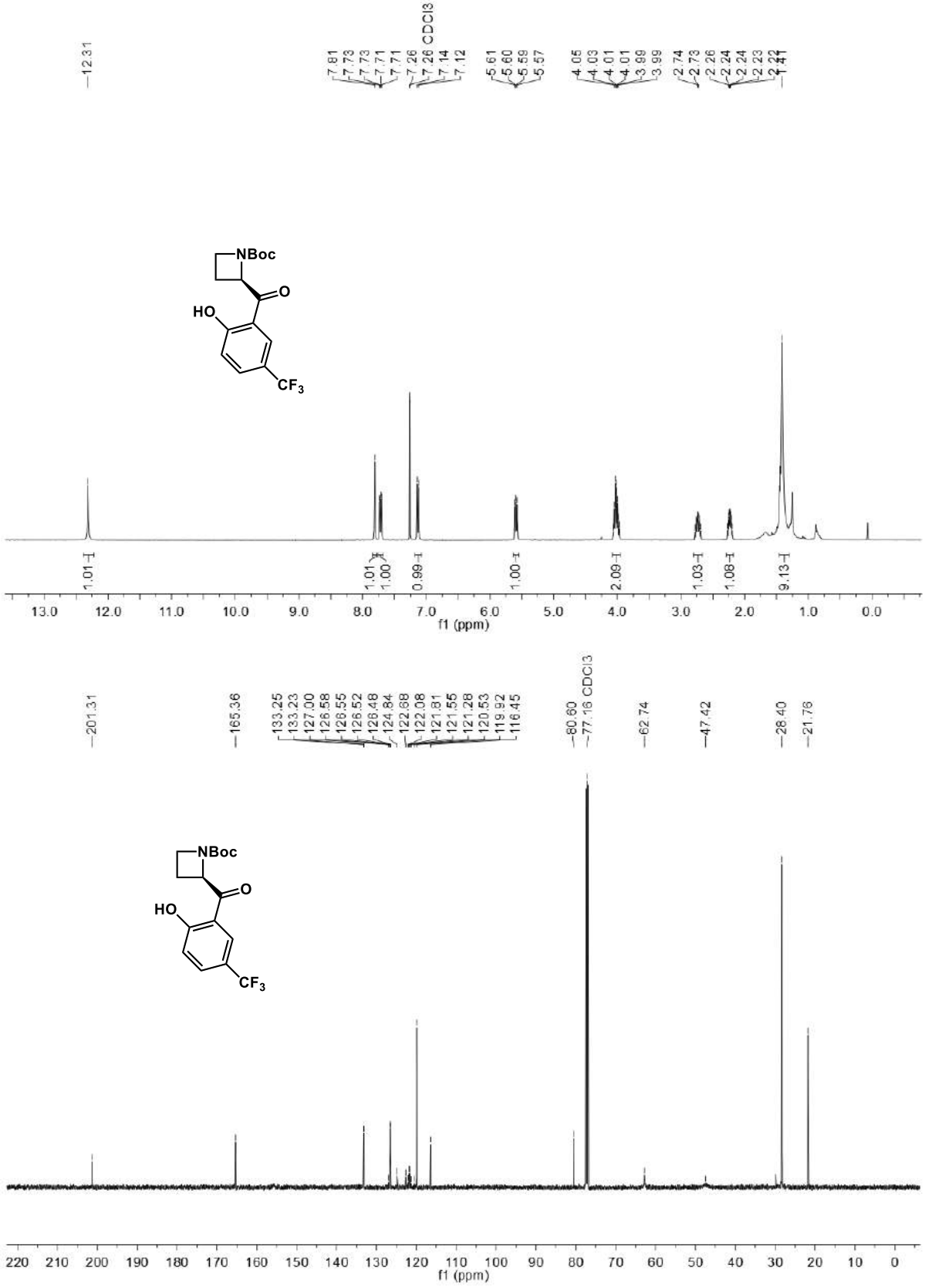

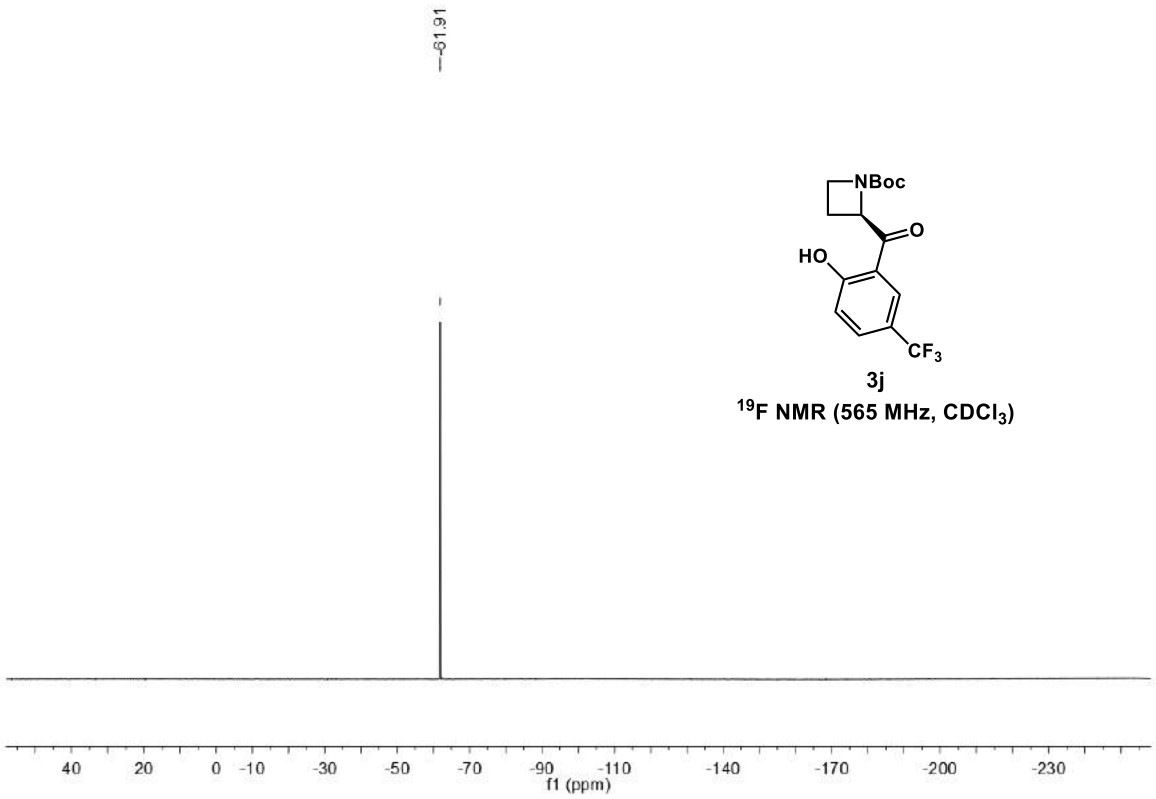

3j

^{19}F NMR (565 MHz, $CDCl_3$)

tert-butyl (R)-2-(3-fluoro-2-hydroxybenzoyl)azetidine-1-carboxylate (3k)

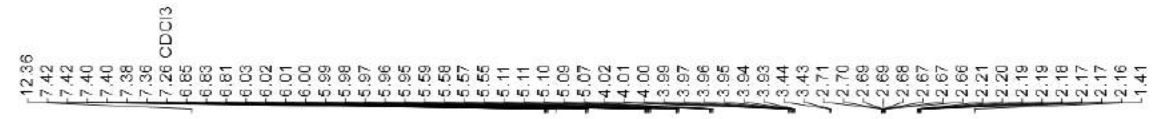

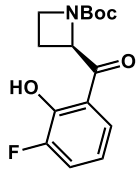

3k

^{1}H NMR (600 MHz, $CDCl_3$)

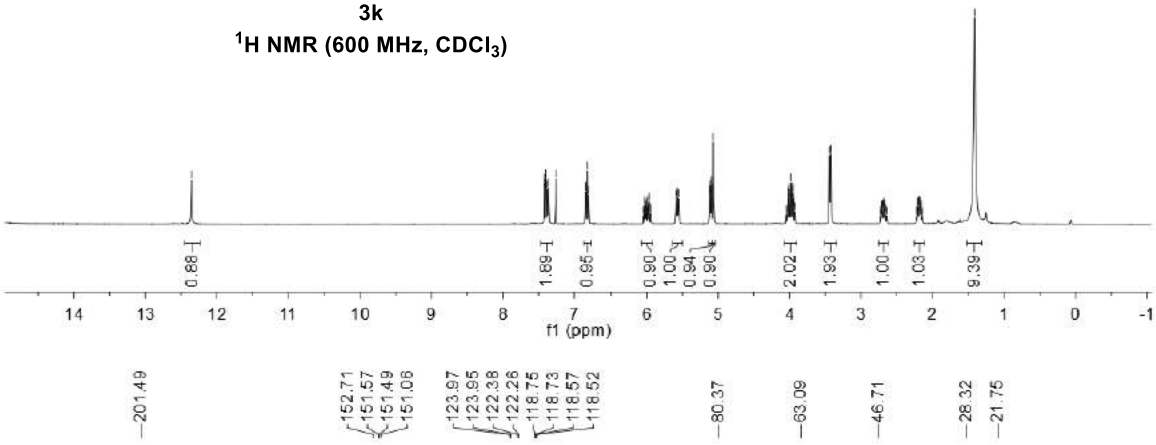

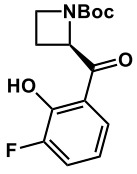

3k

^{13}C NMR (MHz, $CDCl_3$)

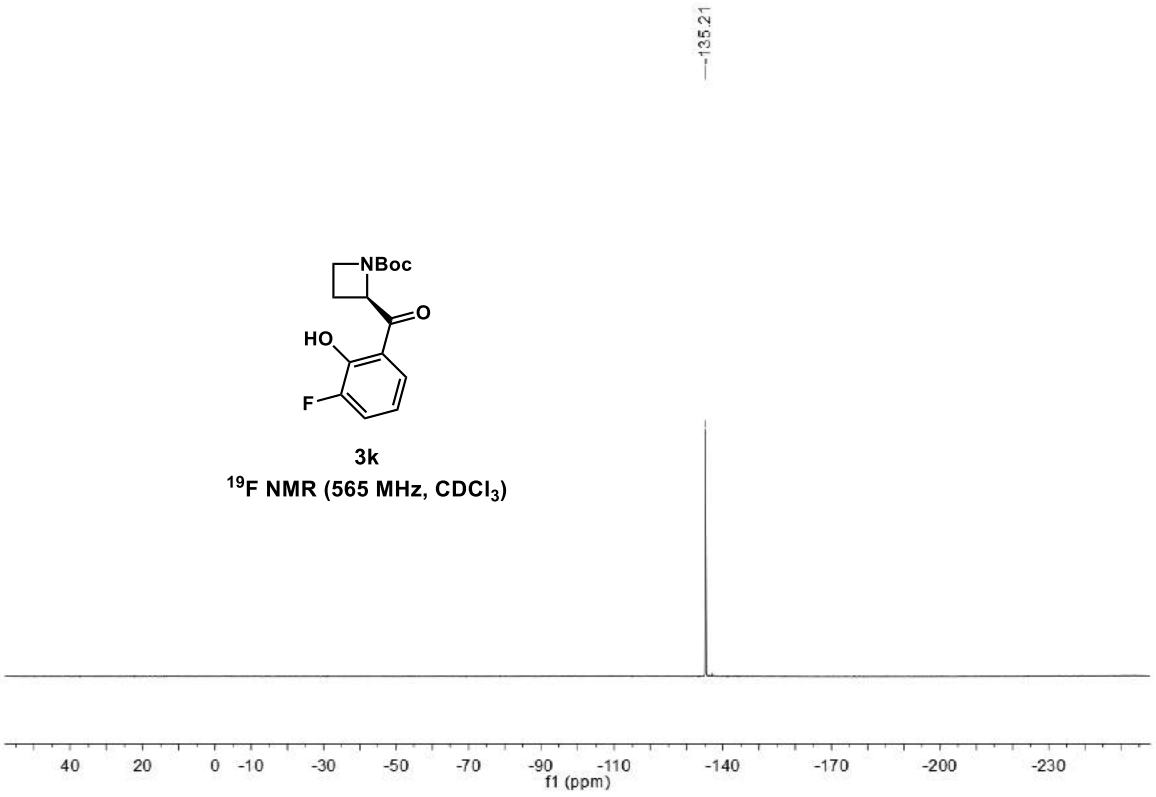

3k

^{19}F NMR (565 MHz, $CDCl_3$)

tert-butyl (R)-2-(2-hydroxy-5-(methoxycarbonyl)benzoyl)azetidine-1-carboxylate (3l)

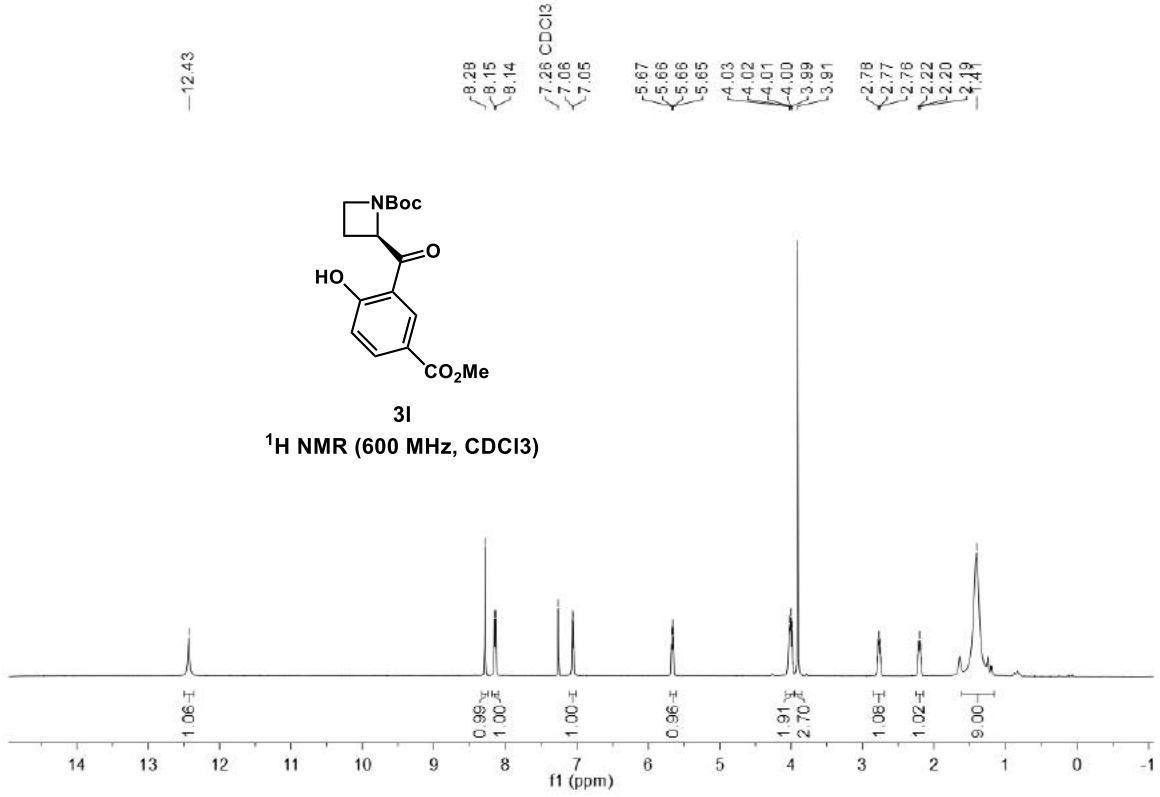

3l

^{1}H NMR (600 MHz, CDCl3)

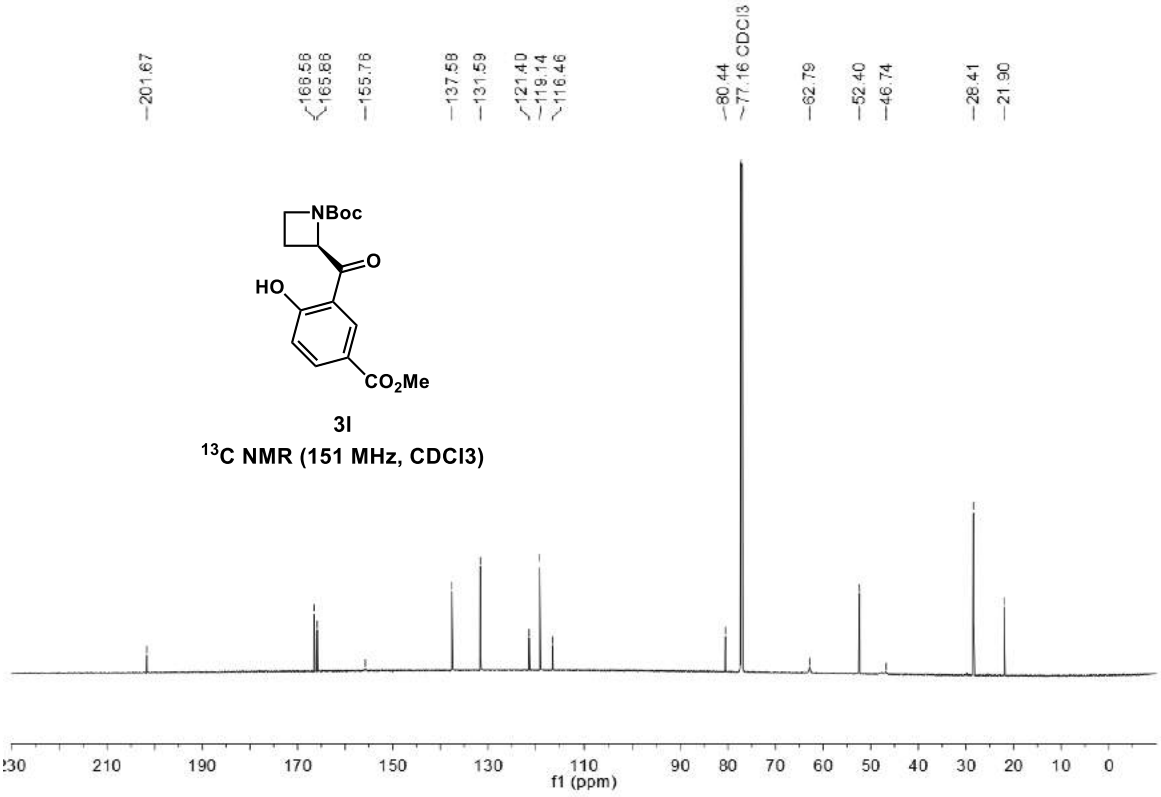

3l

^{13}C NMR (151 MHz, CDCl3)

di-tert-butyl 2,2'-(5-(tert-butyl)-2-hydroxyisophthaloyl)(2R,2'R)-bis(azetidine-1-carboxylate) (3m)

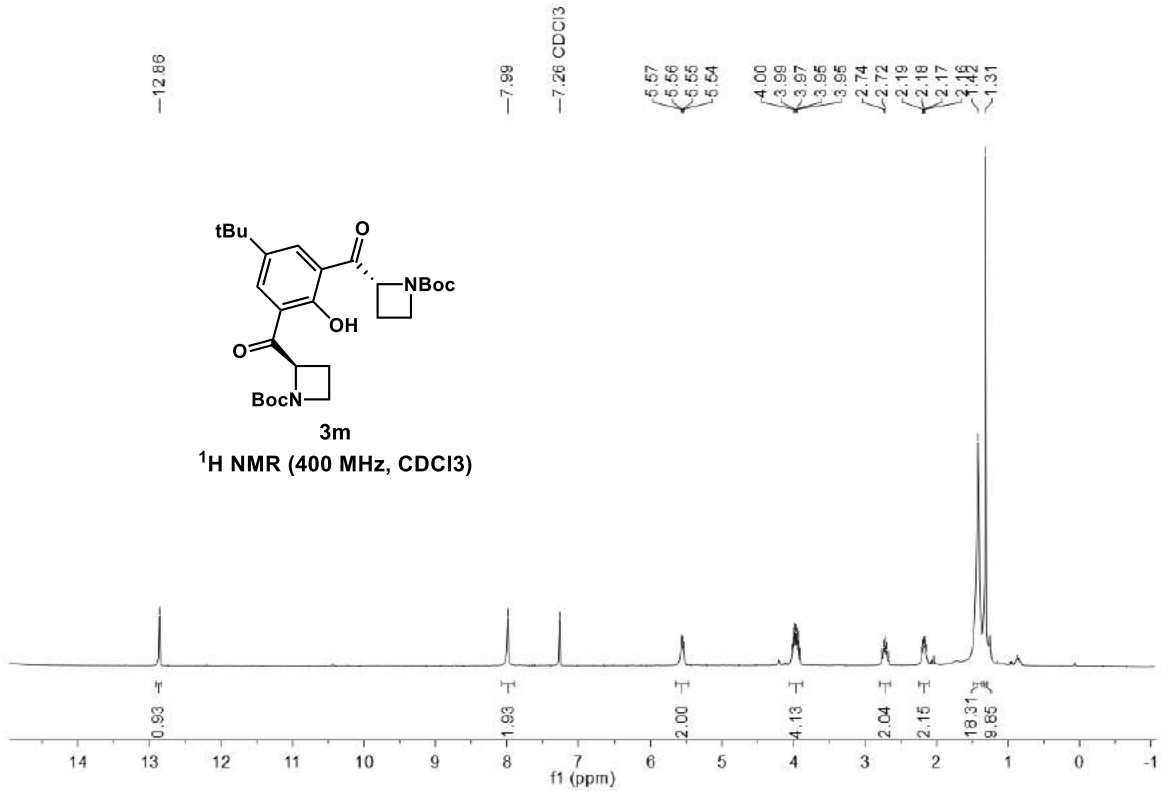

3m

^{1}H NMR (400 MHz, CDCl3)

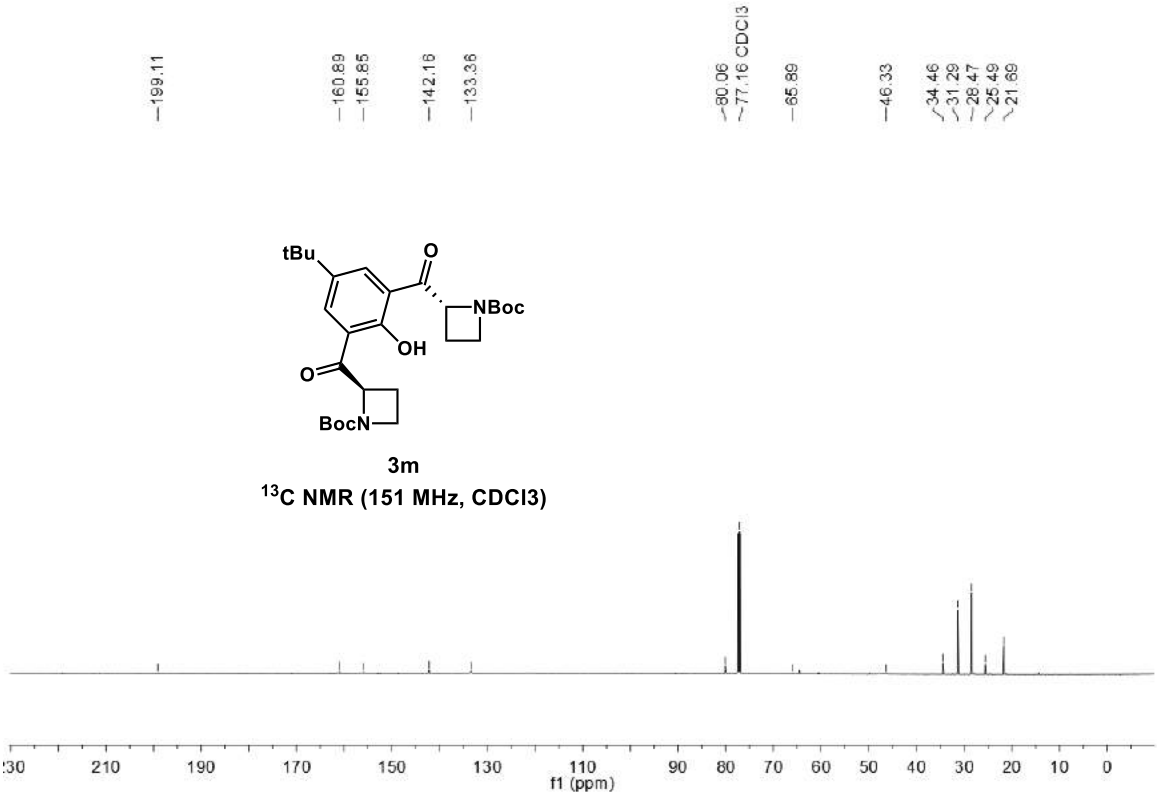

3m

^{13}C NMR (151 MHz, CDCl3)

tert-butyl 3-(2-hydroxybenzoyl)azetidine-1-carboxylate (4a)

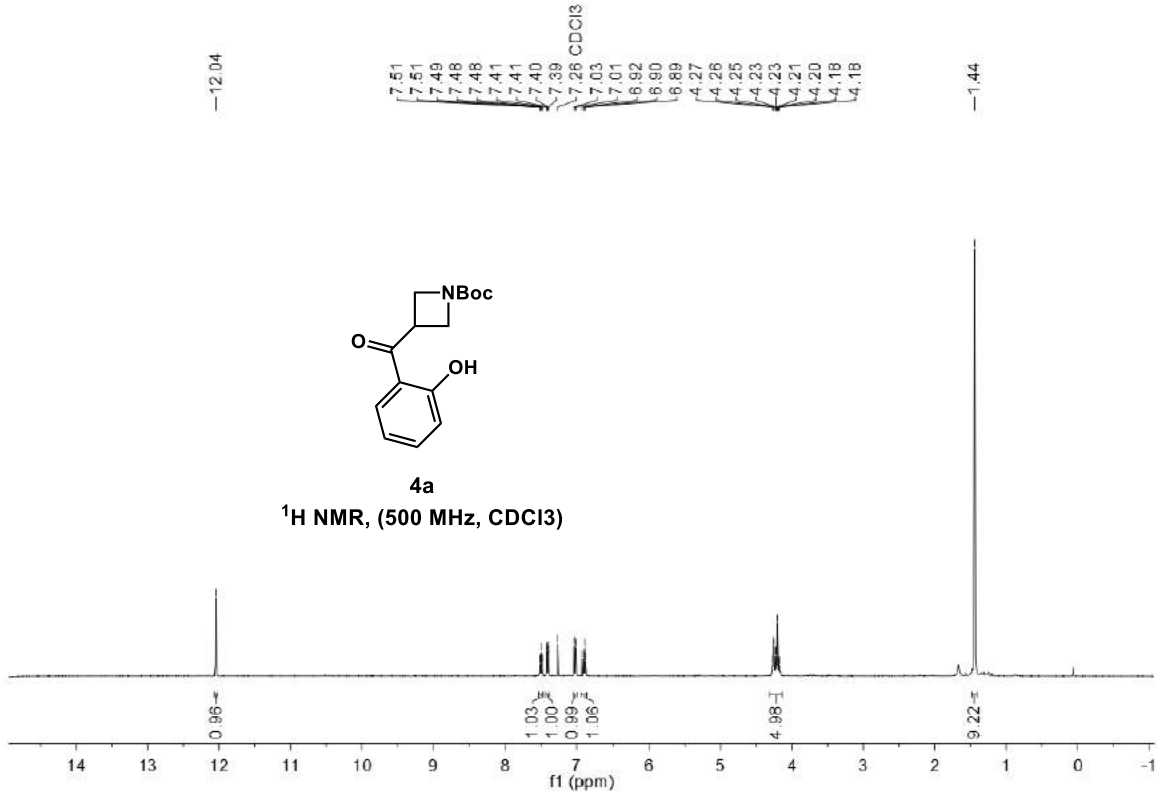

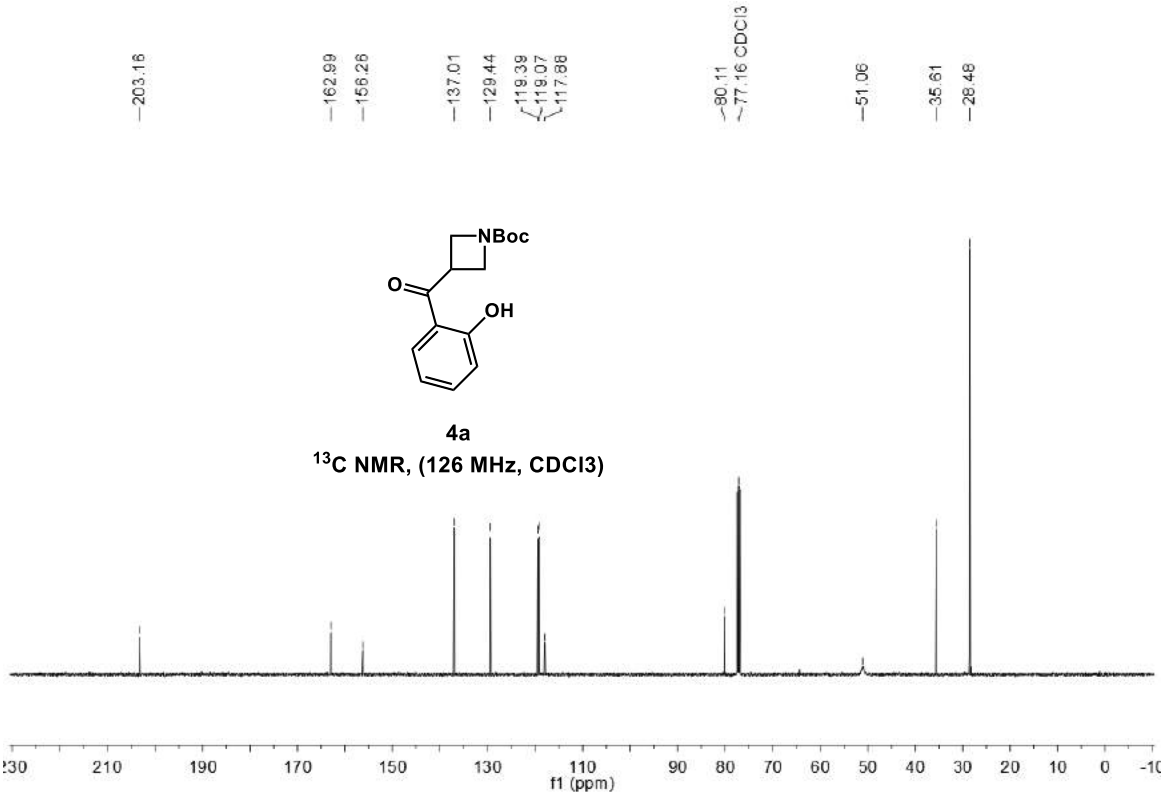

tert-butyl 3-(2-hydroxy-3-methylbenzoyl)azetidine-1-carboxylate (4b)

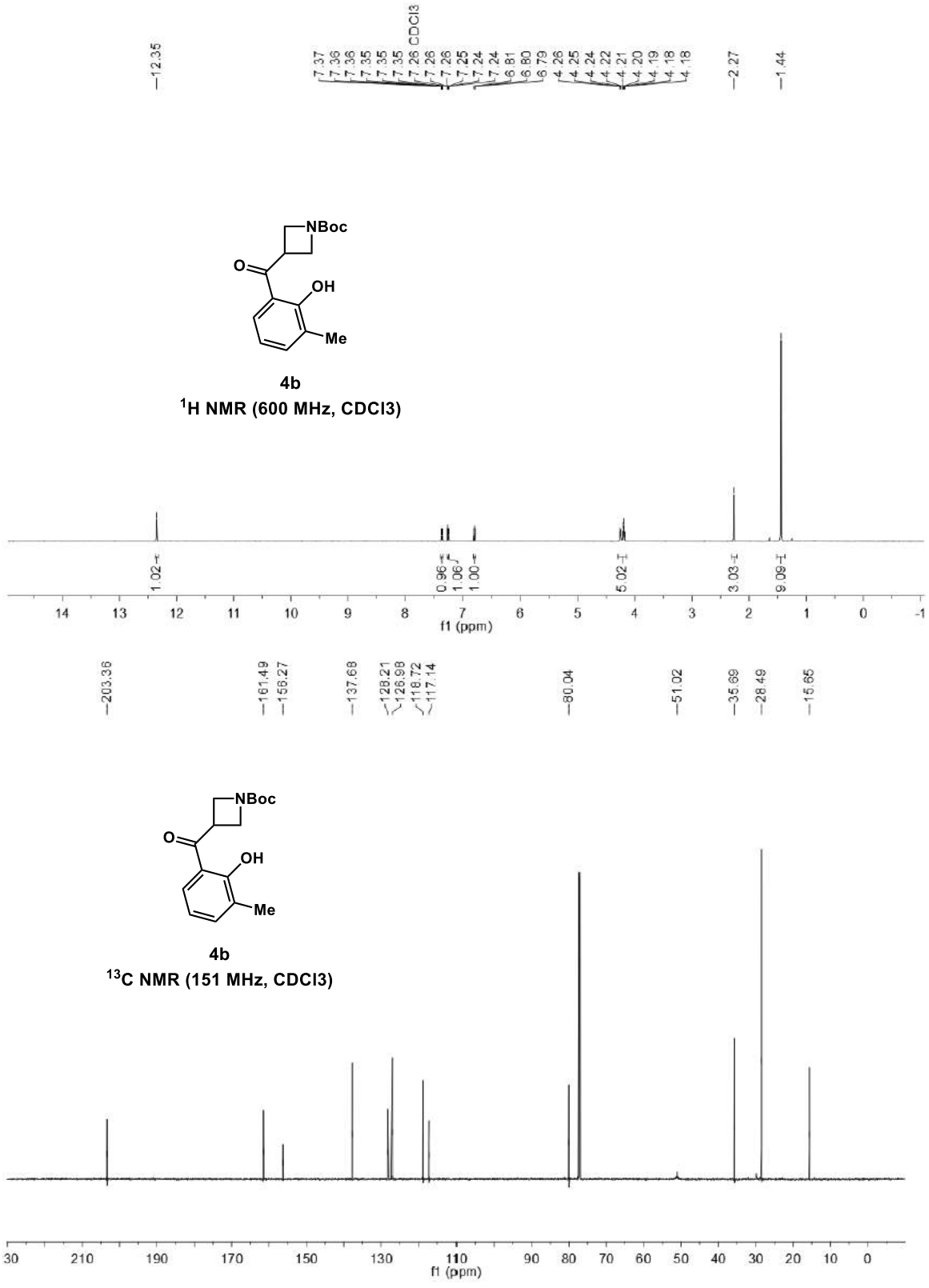

tert-butyl 3-(2-hydroxy-4-isopropylbenzoyl)azetidine-1-carboxylate (4c)

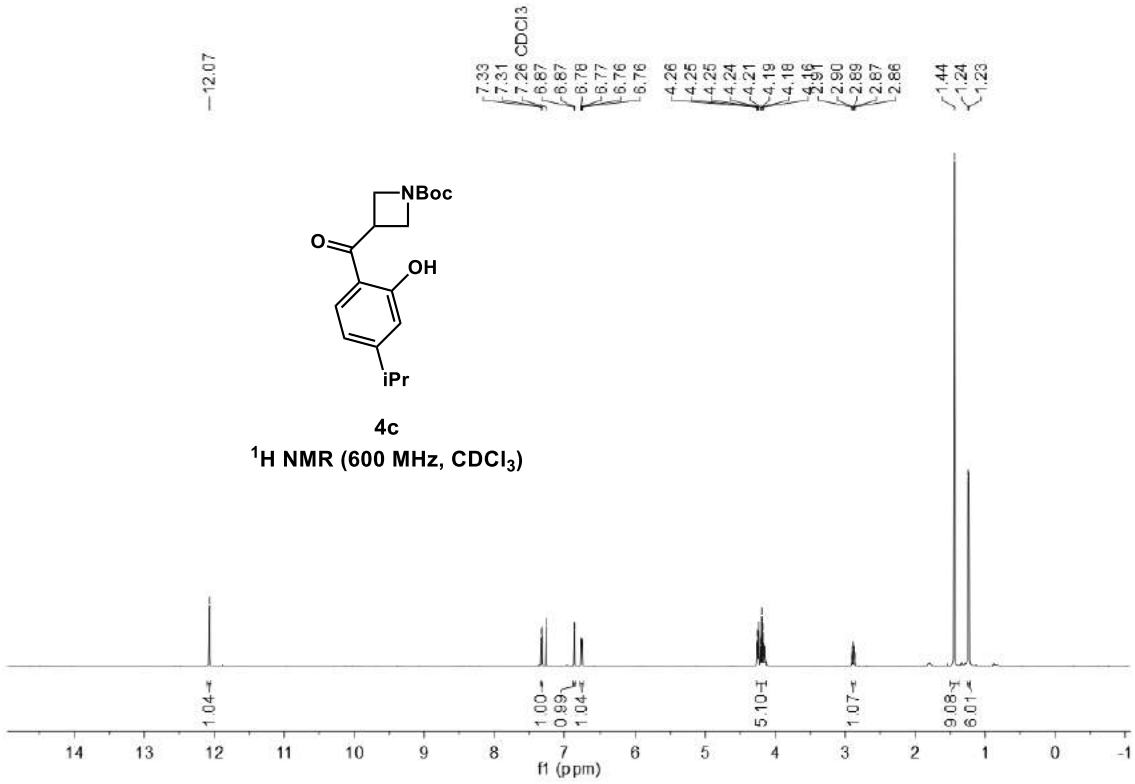

4c

^{1}H NMR (600 MHz, $CDCl_3$)

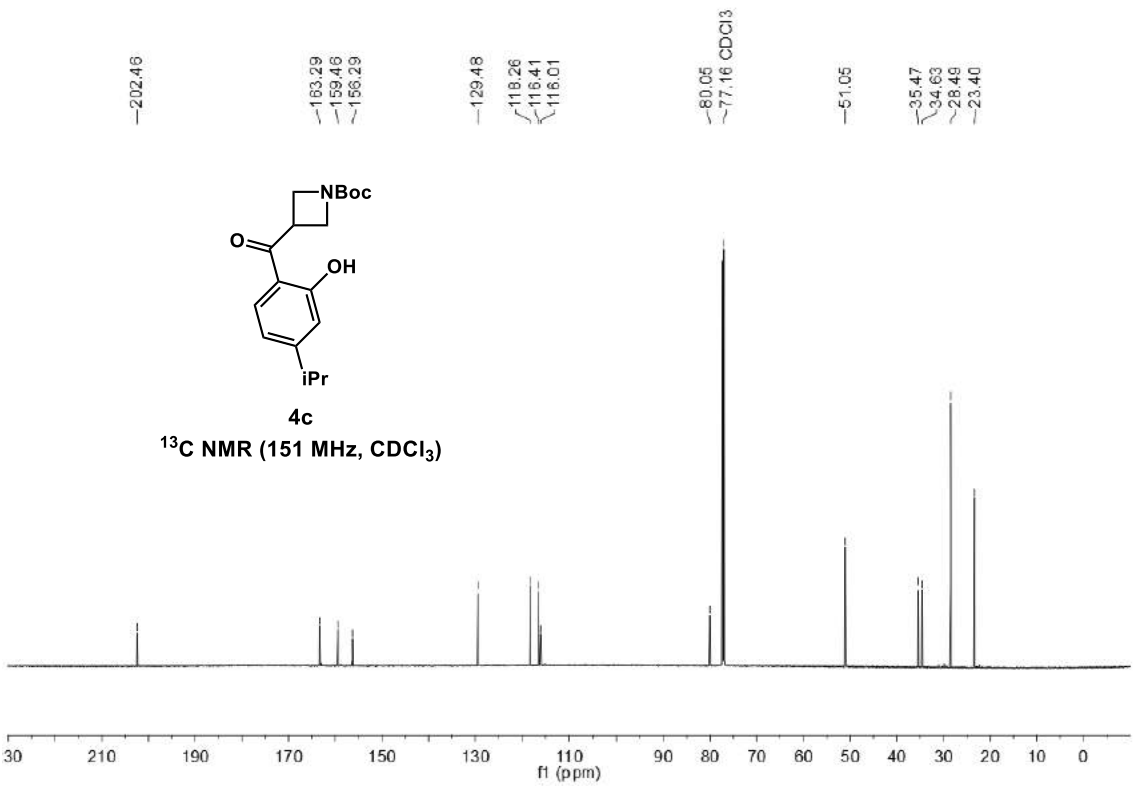

4c

^{13}C NMR (151 MHz, $CDCl_3$)

tert-butyl 3-(2-hydroxy-5-methylbenzoyl)azetidine-1-carboxylate (4d)

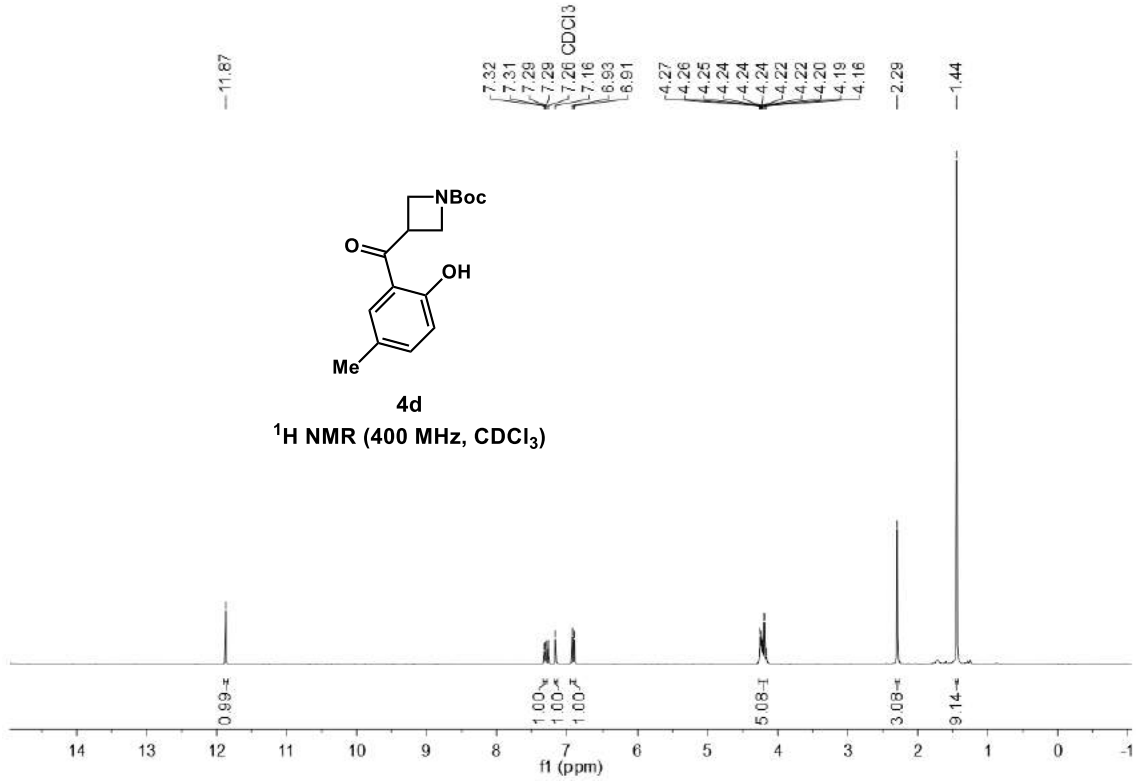

4d

^{1}H NMR (400 MHz, $CDCl_3$)

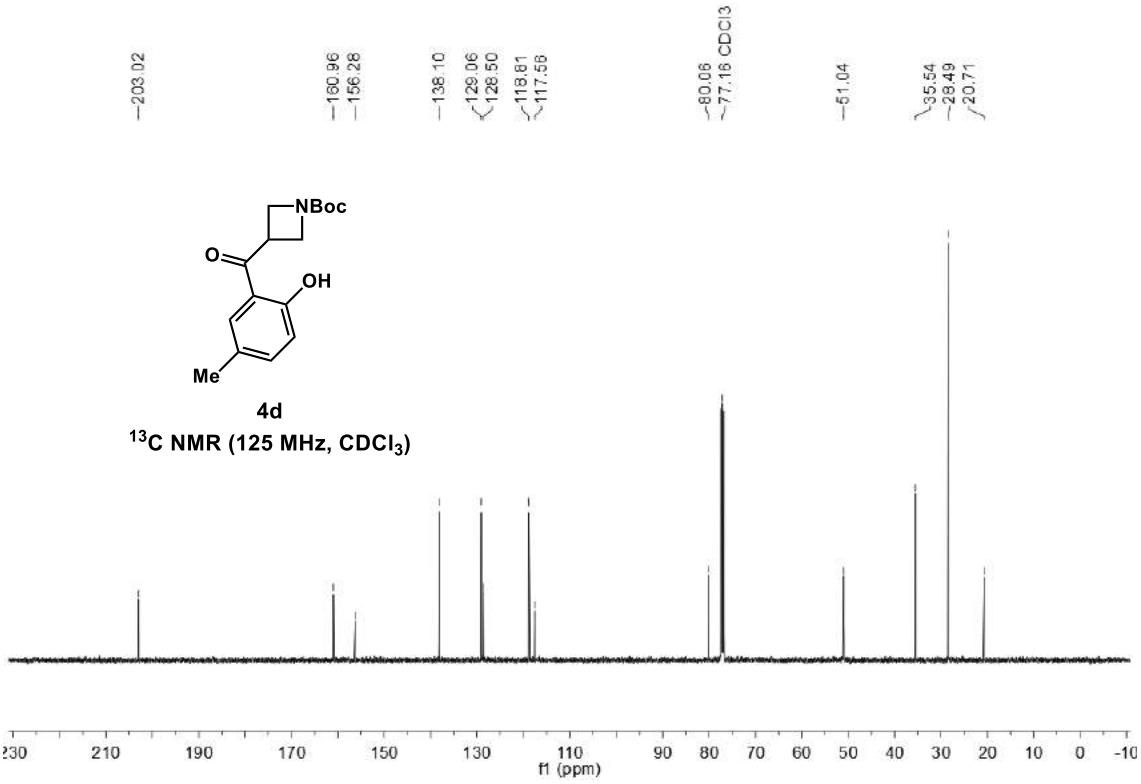

4d

^{13}C NMR (125 MHz, $CDCl_3$)

tert-butyl 3-(2-hydroxy-3-methoxybenzoyl)azetidine-1-carboxylate (4e)

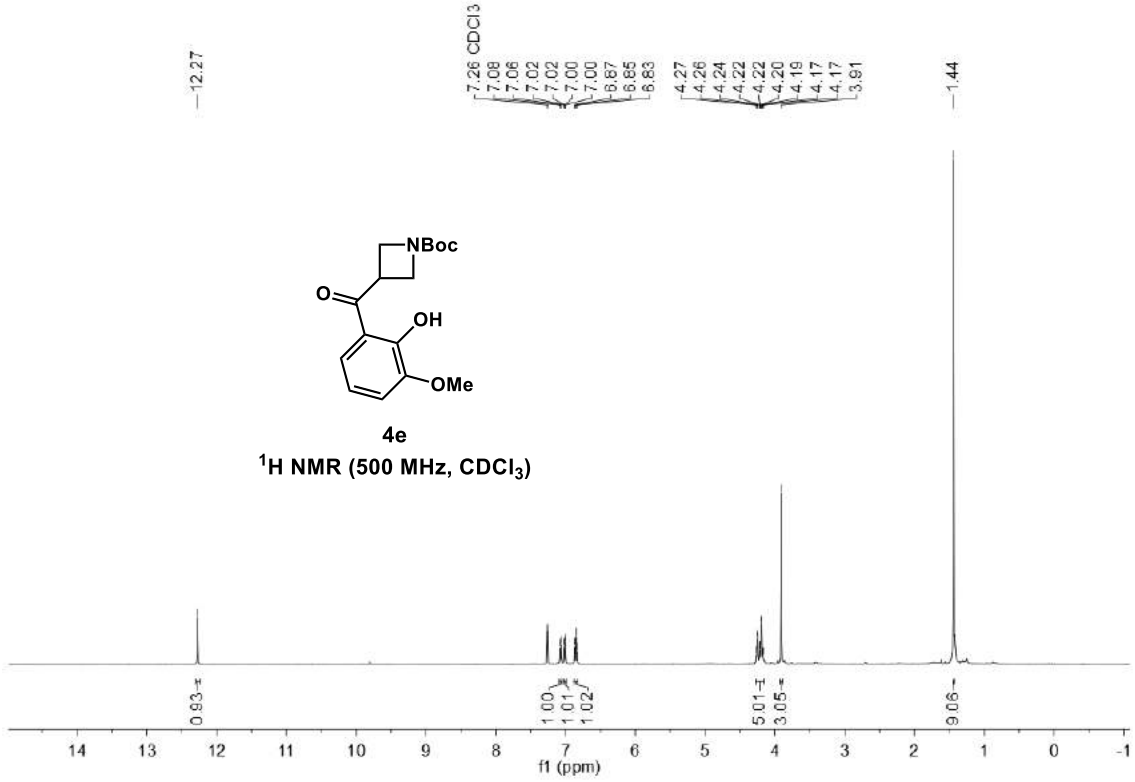

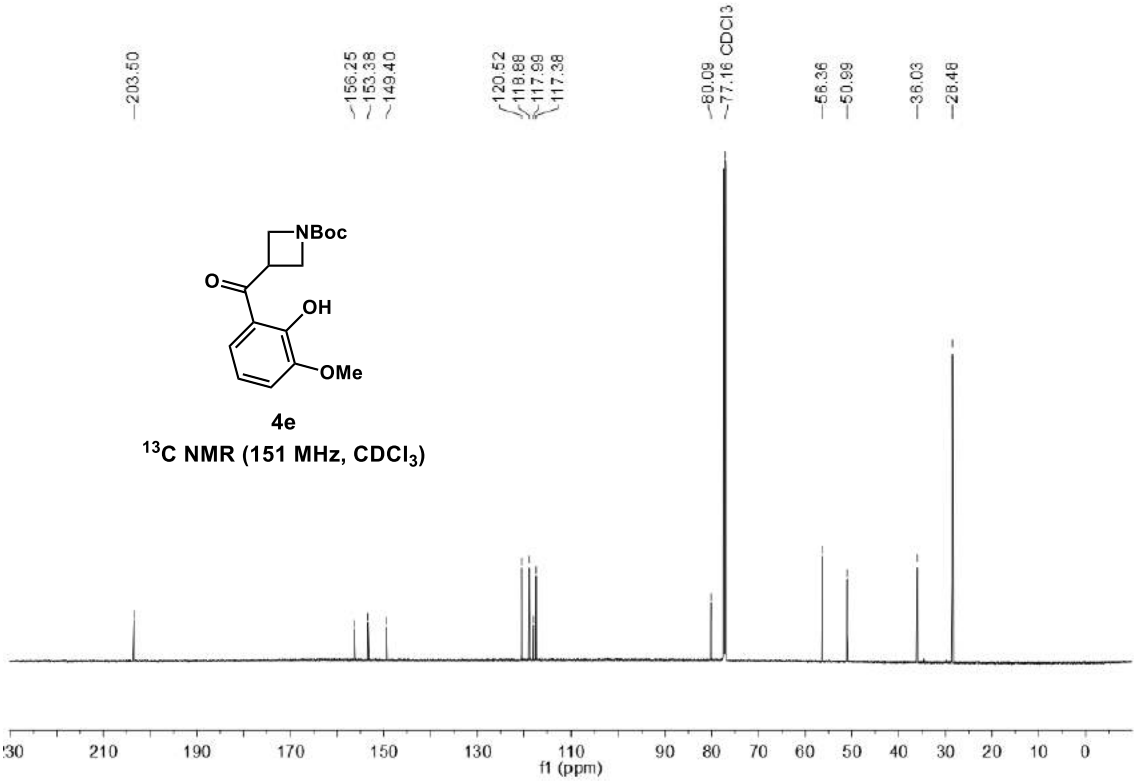

tert-butyl 3-(2-hydroxy-6-methoxybenzoyl)azetidine-1-carboxylate (4f)

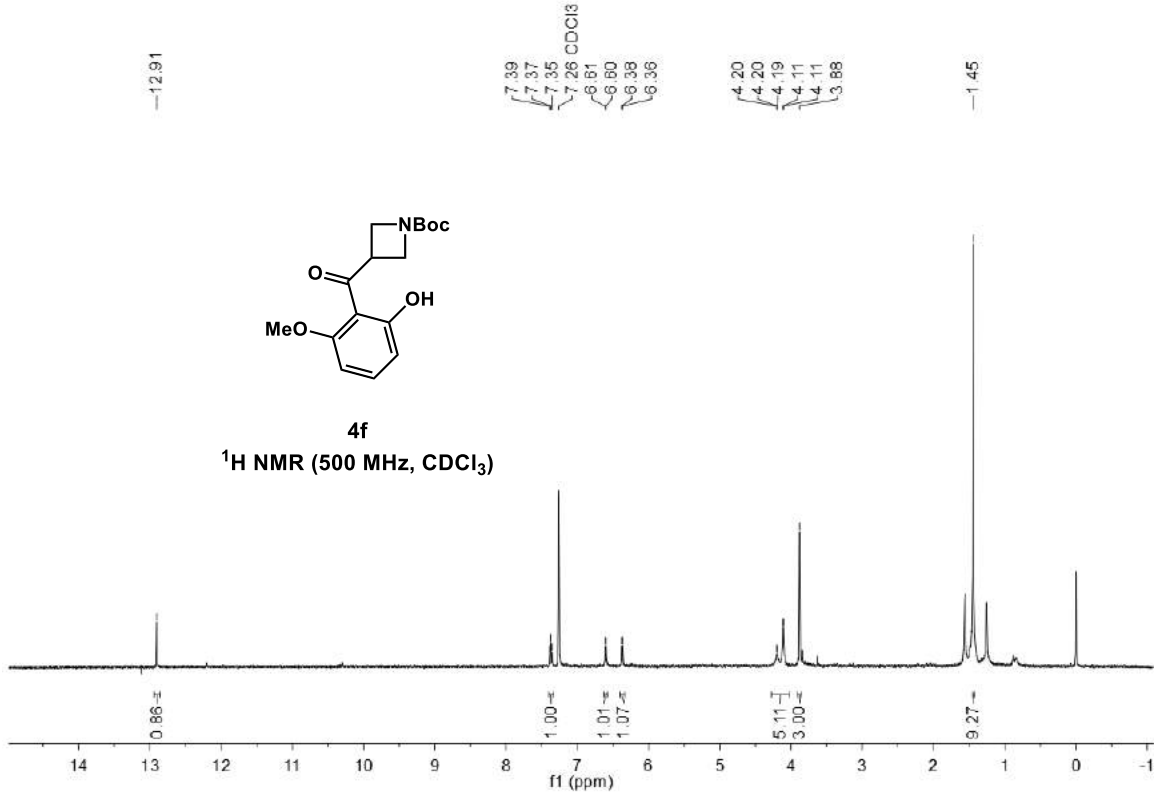

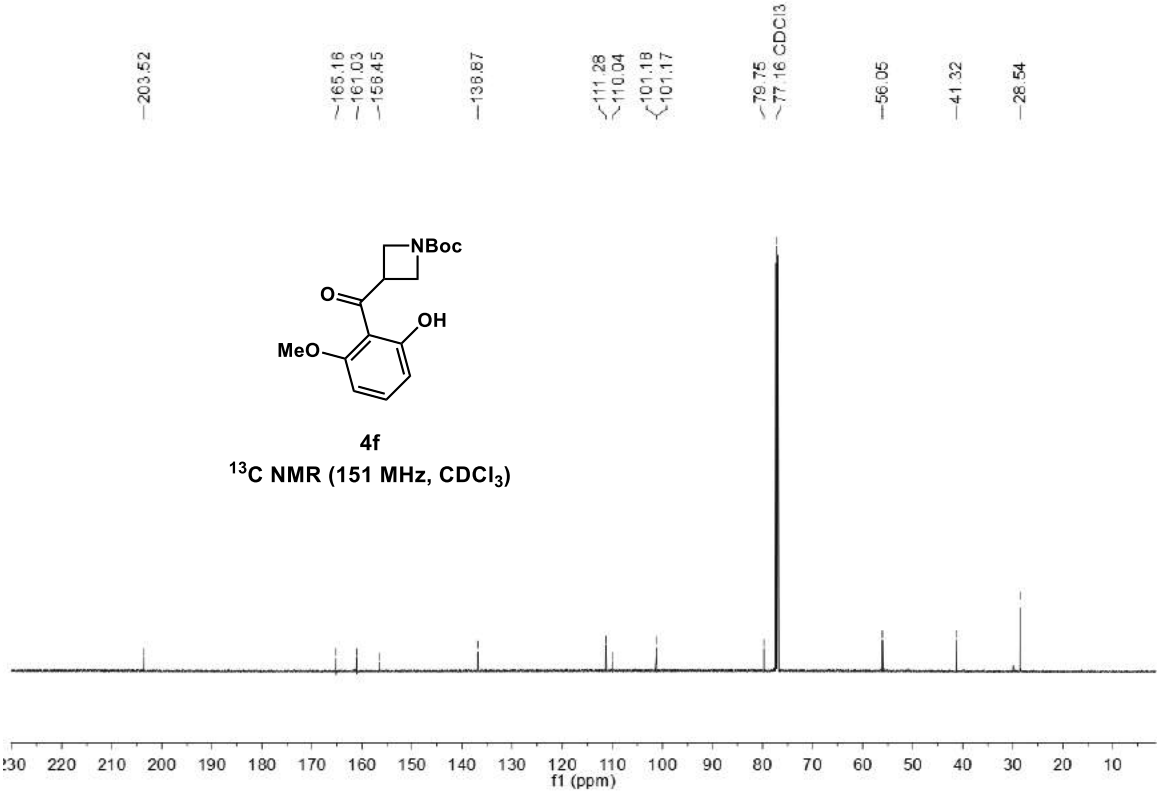

tert-butyl 3-(5-chloro-2-hydroxybenzoyl)azetidine-1-carboxylate (4g)

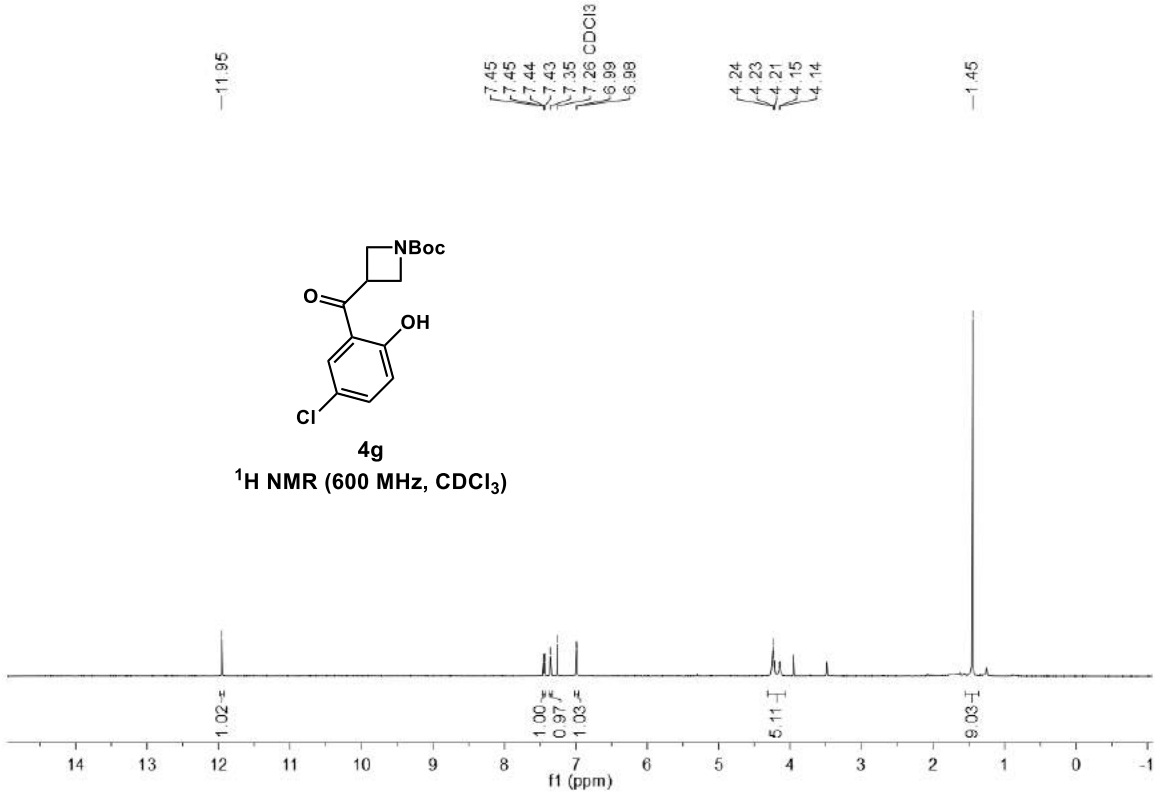

4g

^{1}H NMR (600 MHz, $CDCl_3$)

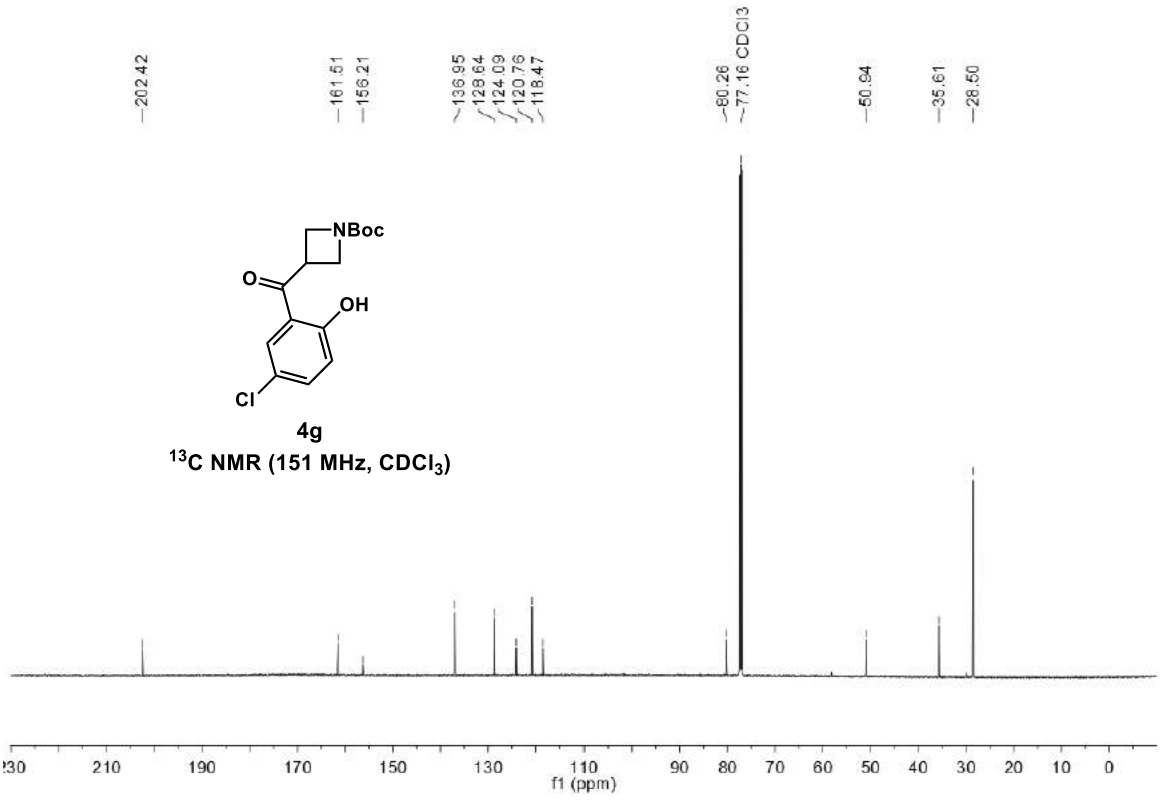

4g

^{13}C NMR (151 MHz, $CDCl_3$)

tert-butyl 3-(5-bromo-2-hydroxybenzoyl)azetidine-1-carboxylate (4h)

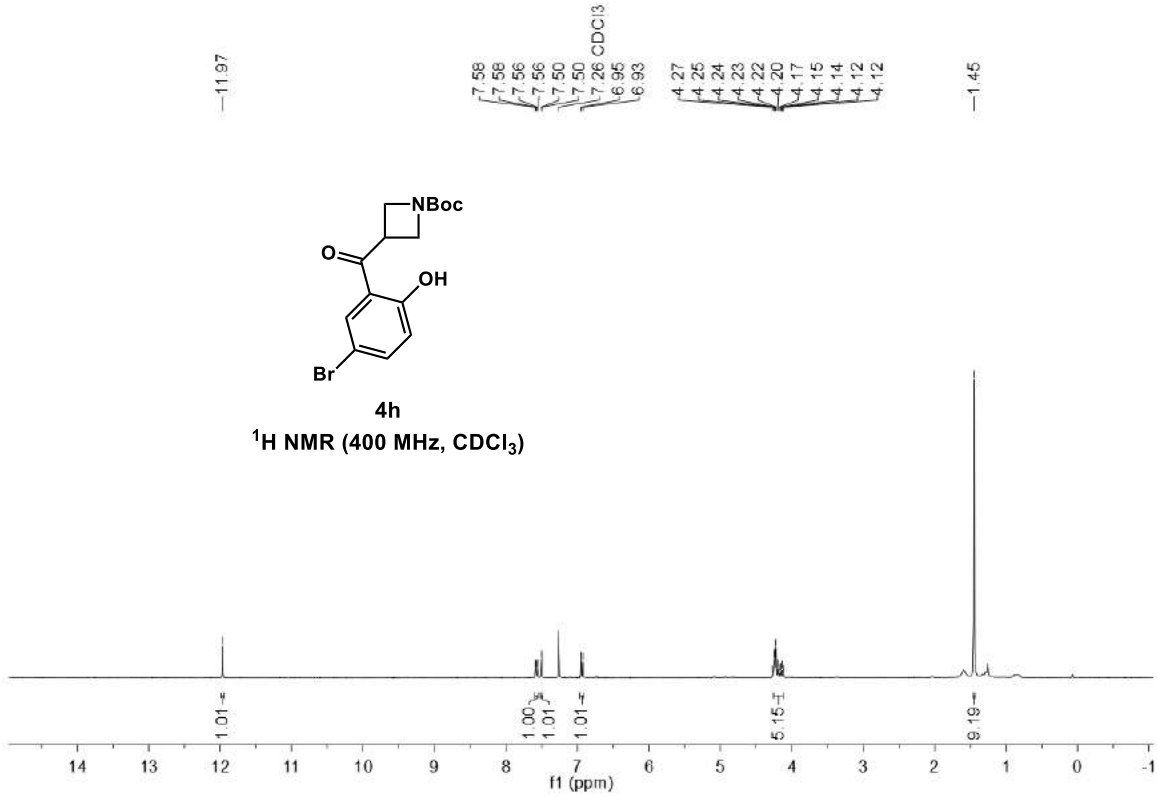

4h

^{1}H NMR (400 MHz, $CDCl_3$)

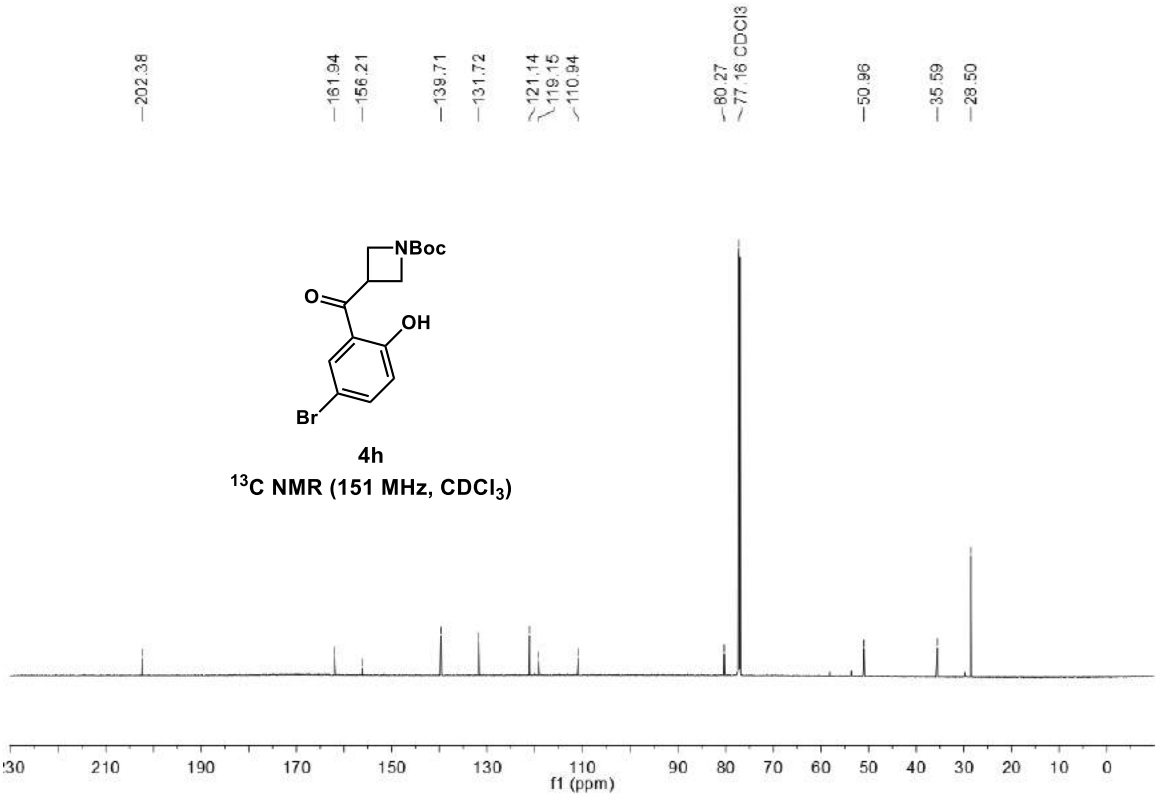

4h

^{13}C NMR (151 MHz, $CDCl_3$)

tert-butyl 3-(2-hydroxy-5-(trifluoromethyl)benzoyl)azetidine-1-carboxylate (4i)

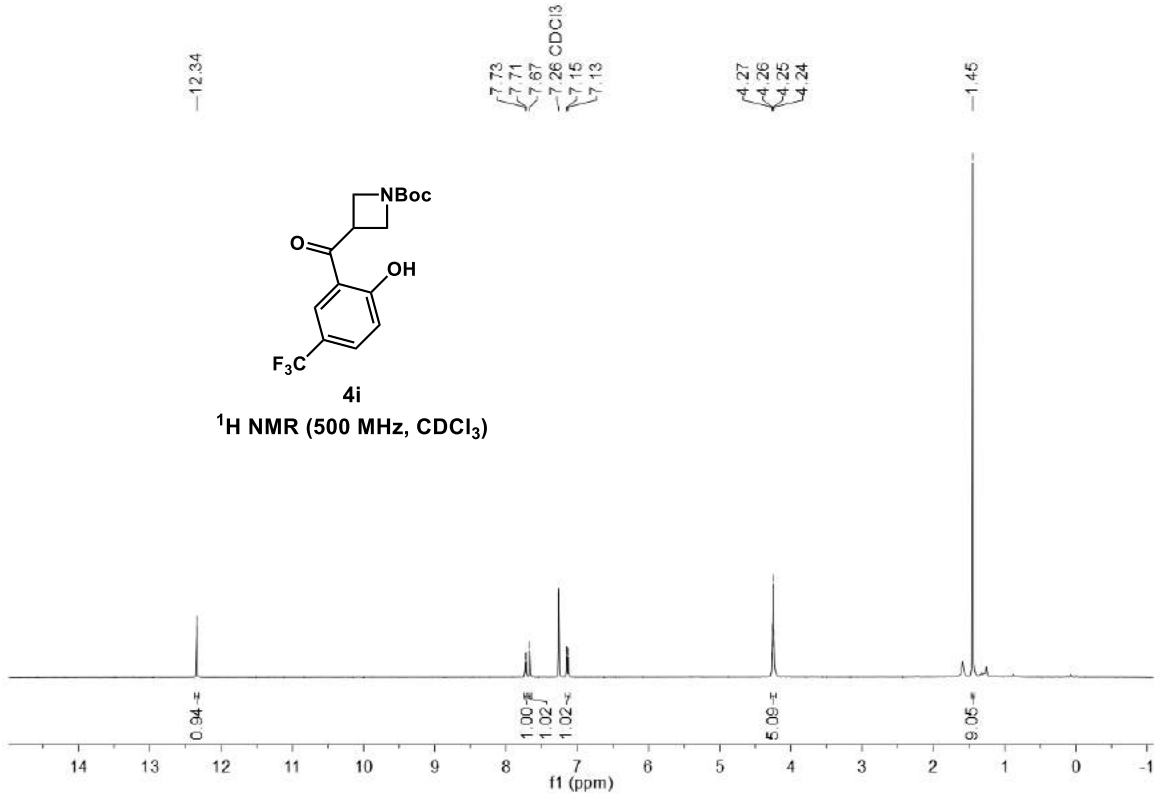

4i

^{1}H NMR (500 MHz, $CDCl_3$)

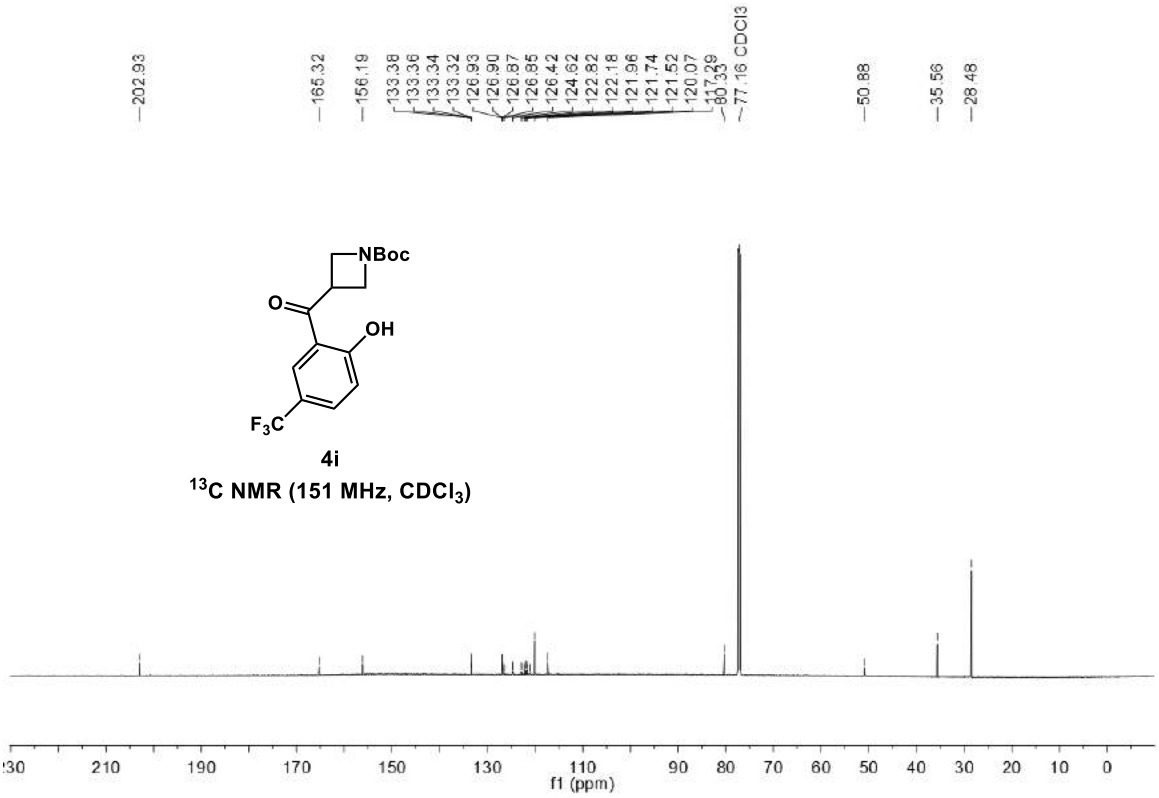

4i

^{13}C NMR (151 MHz, $CDCl_3$)

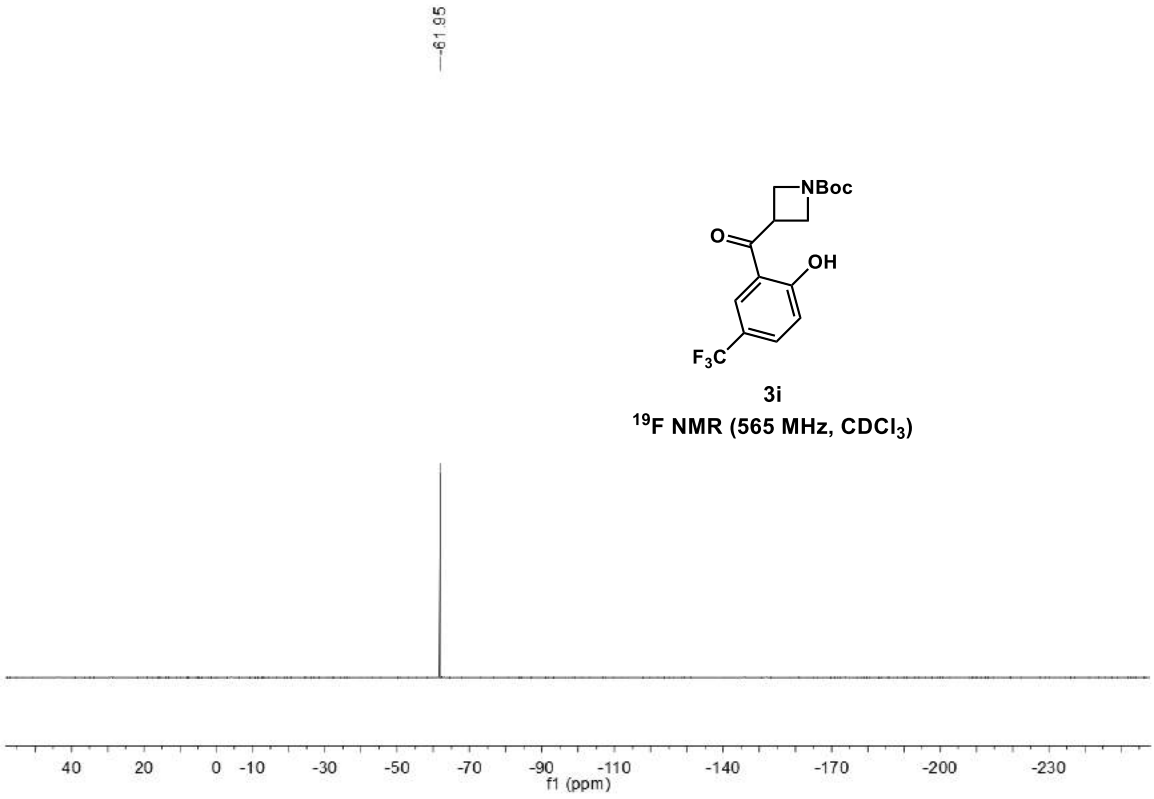

3i

^{19}F NMR (565 MHz, $CDCl_3$)

tert-butyl 3-(3-fluoro-2-hydroxybenzoyl)azetidine-1-carboxylate (4j)

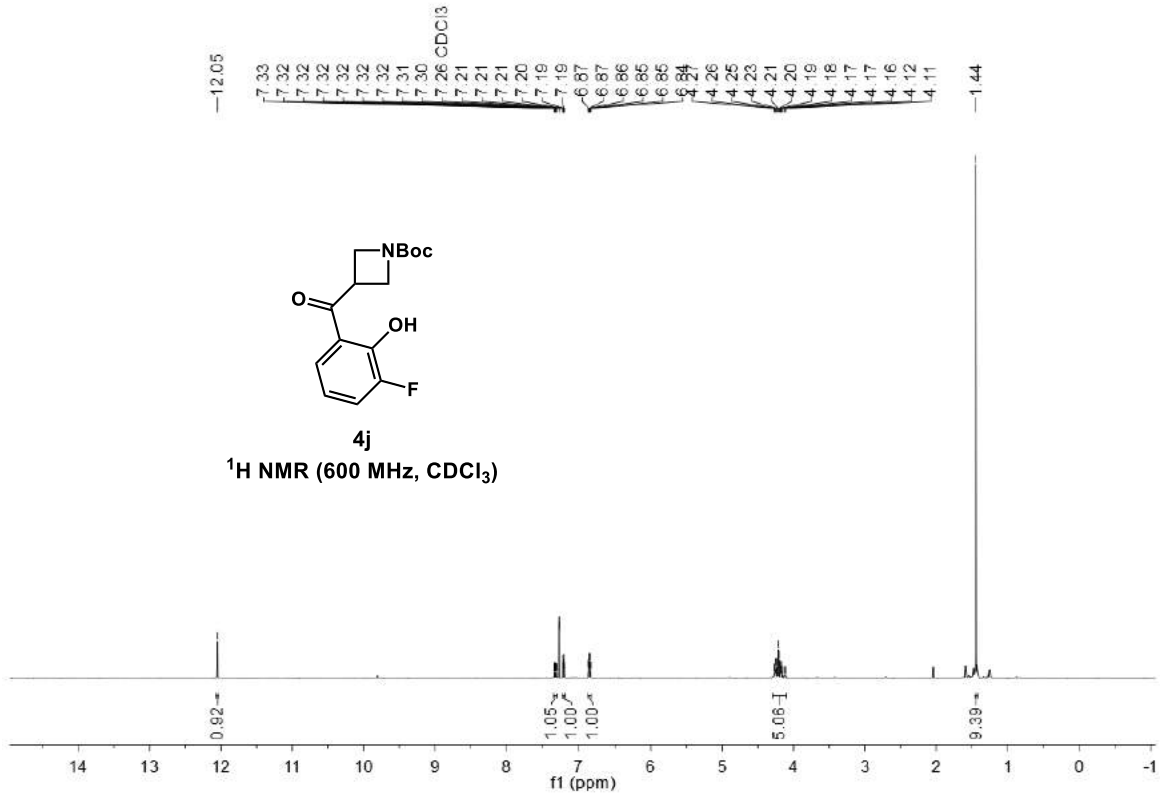

4j

^{1}H NMR (600 MHz, $CDCl_3$)

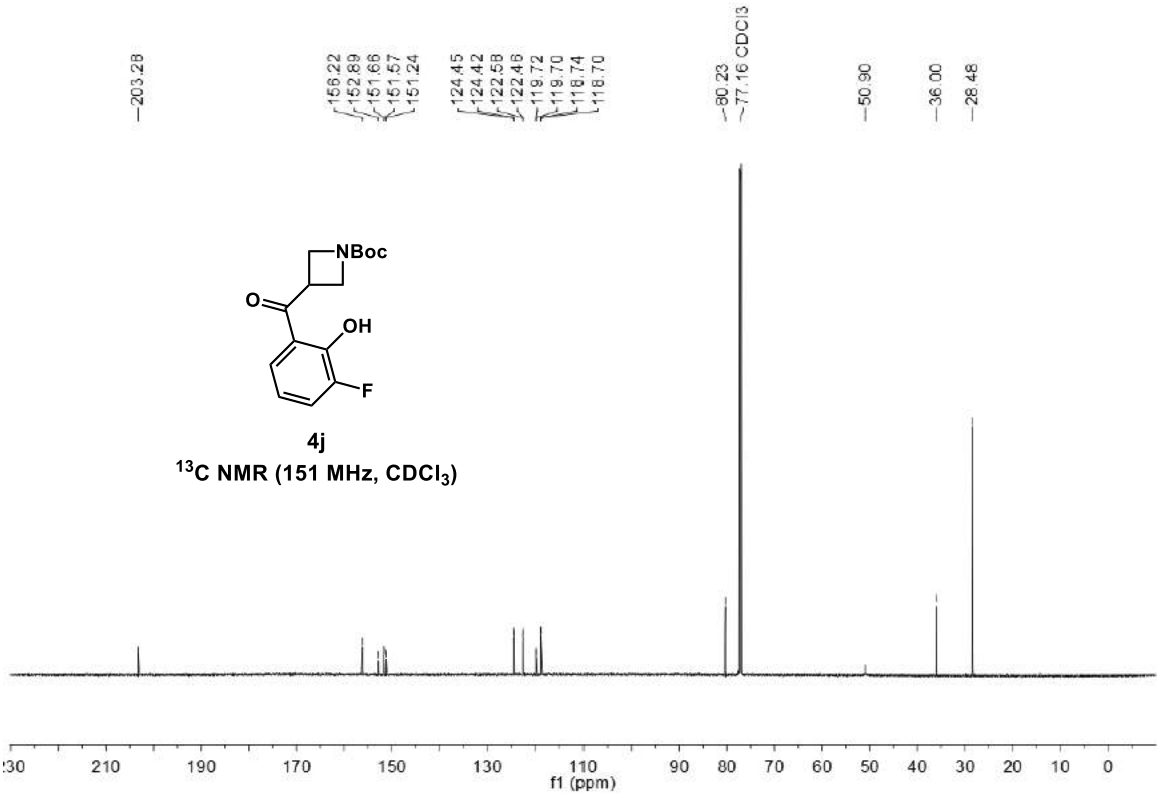

4j

^{13}C NMR (151 MHz, $CDCl_3$)

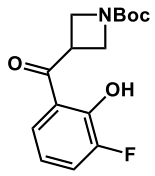

4j

^{19}F NMR (565 MHz, $CDCl_3$)

tert-butyl 3-(3-hydroxy-[1,1'-biphenyl]-4-carbonyl)azetidine-1-carboxylate (4k)

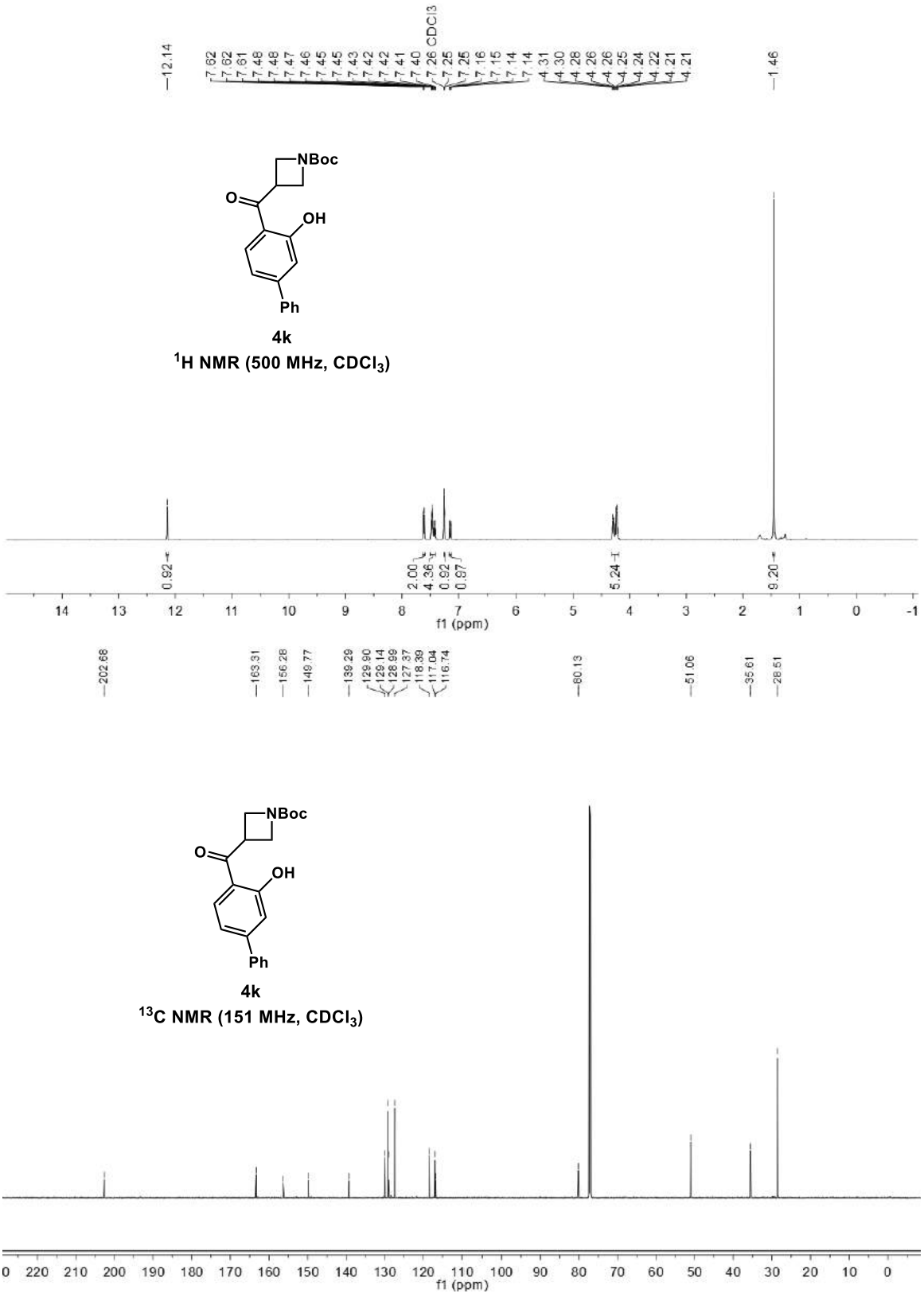

tert-butyl 3-(2-hydroxy-5-(methoxycarbonyl)benzoyl)azetidine-1-carboxylate (4l)

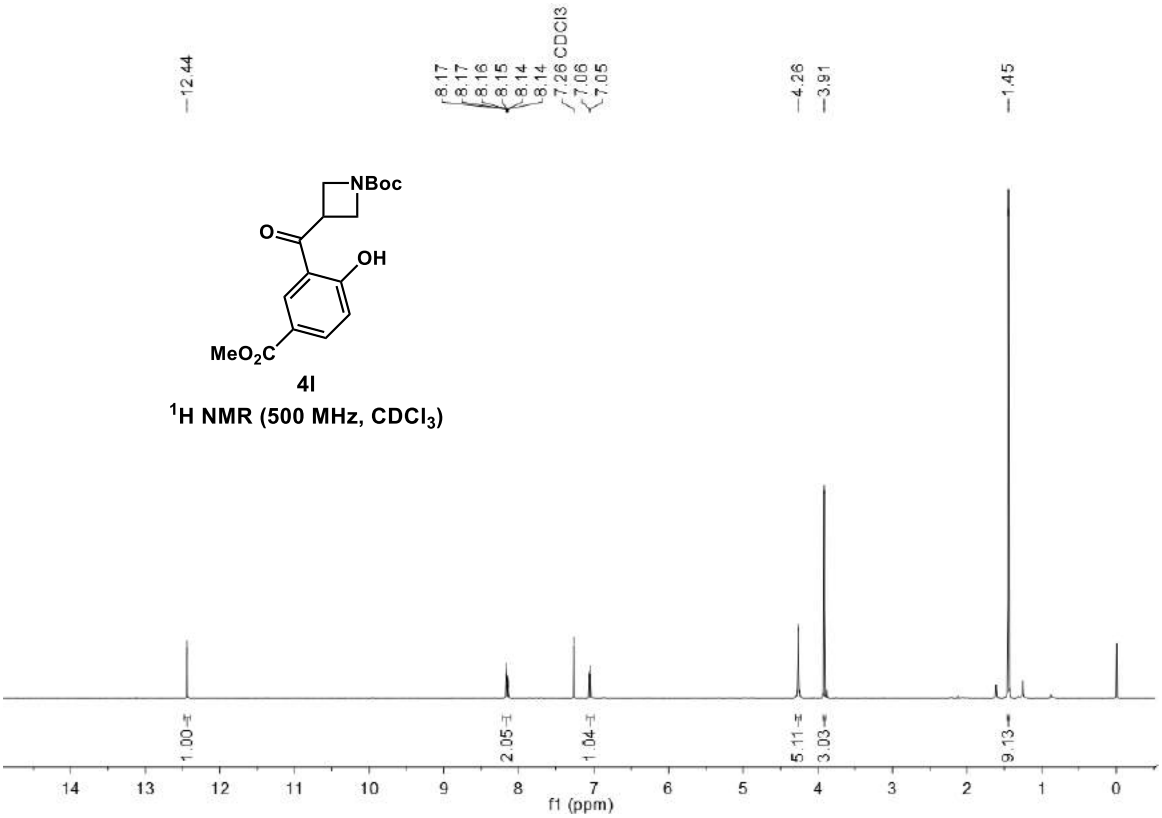

4l

^{1}H NMR (500 MHz, $CDCl_3$)

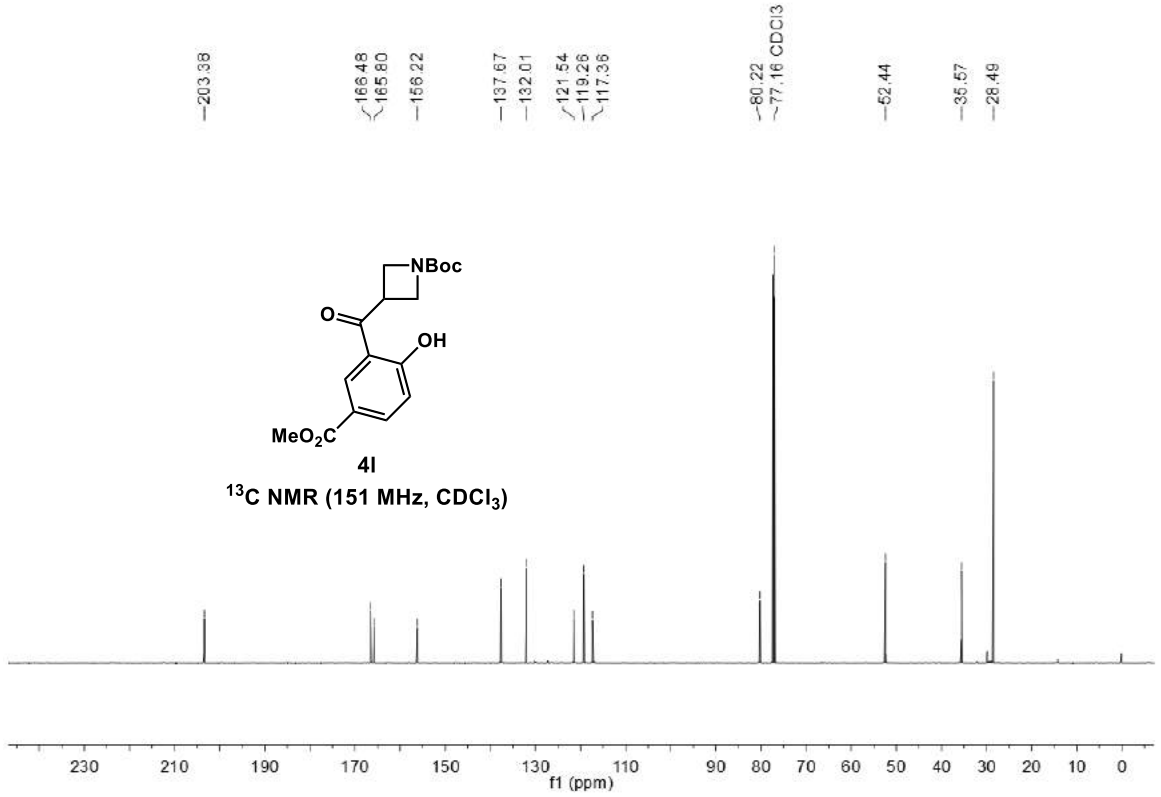

4l

^{13}C NMR (151 MHz, $CDCl_3$)

tert-butyl azete-1(2H)-carboxylate (1)

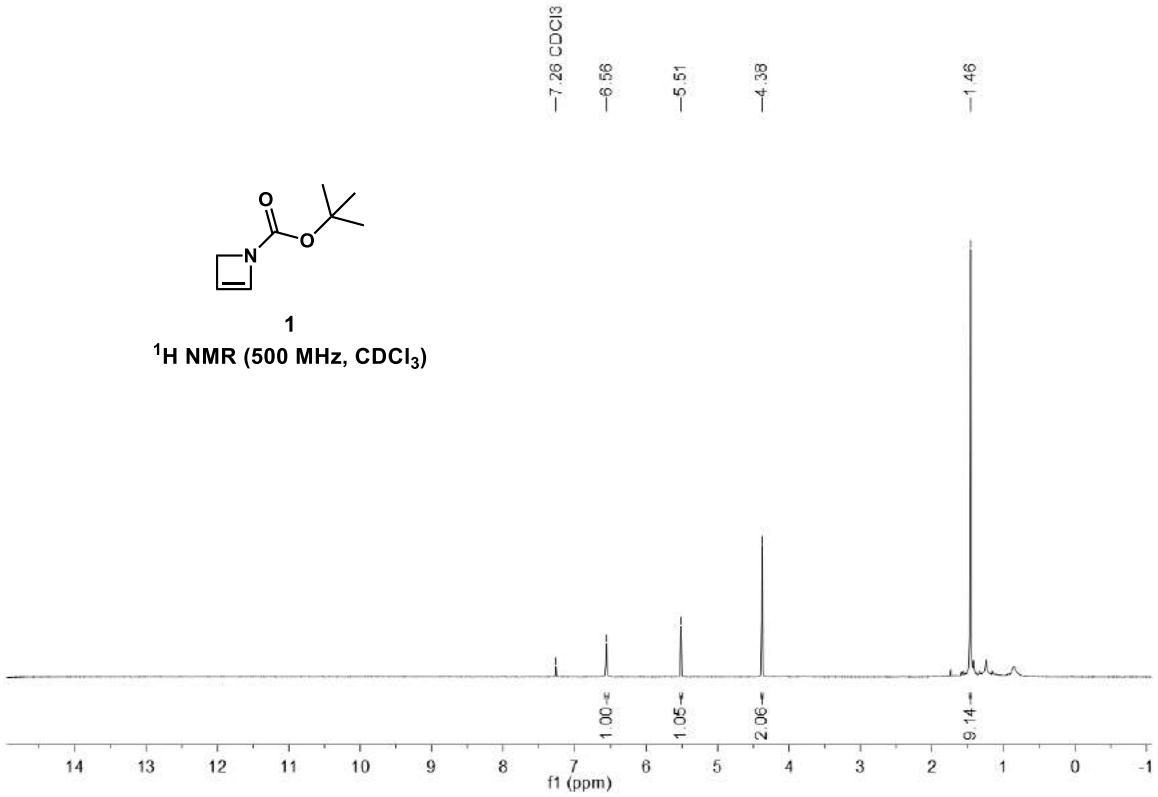

1

^{1}H NMR (500 MHz, $CDCl_3$)

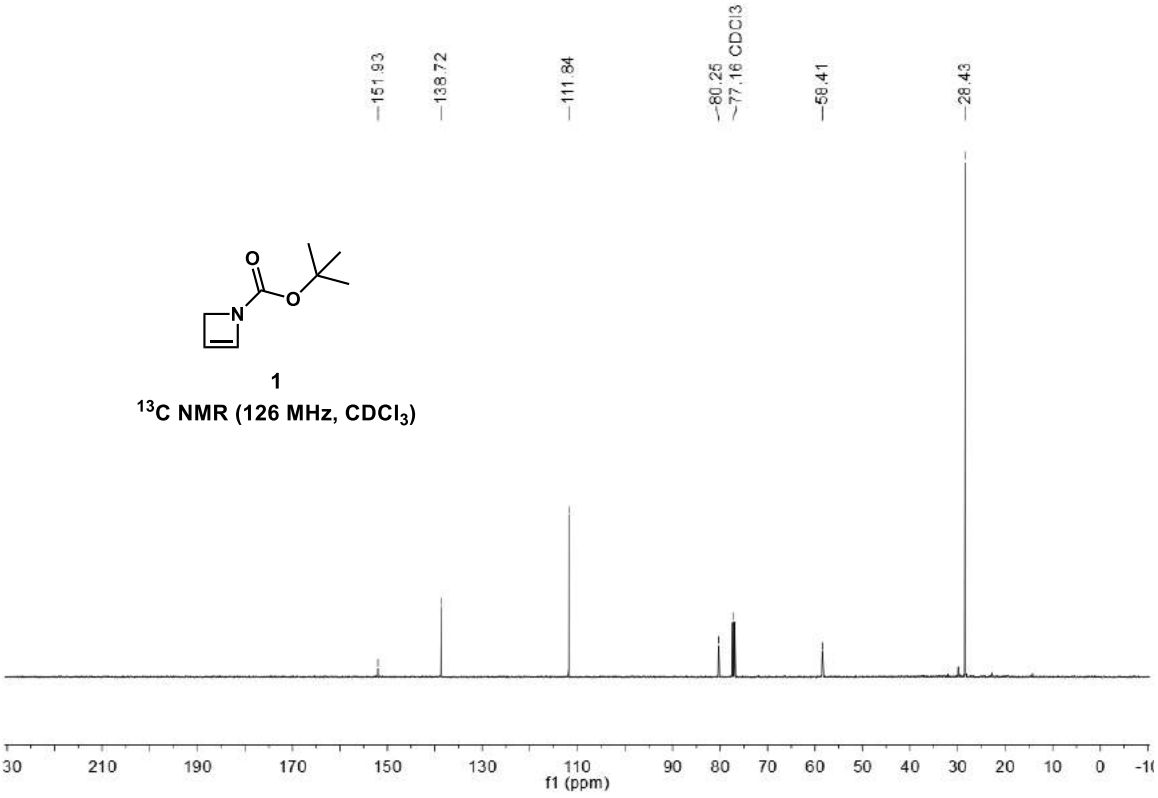

1

^{13}C NMR (126 MHz, $CDCl_3$)

tert-butyl (R)-2-((S)-hydroxy(2-hydroxy-5-methylphenyl)methyl)azetidine-1-carboxylate (6)

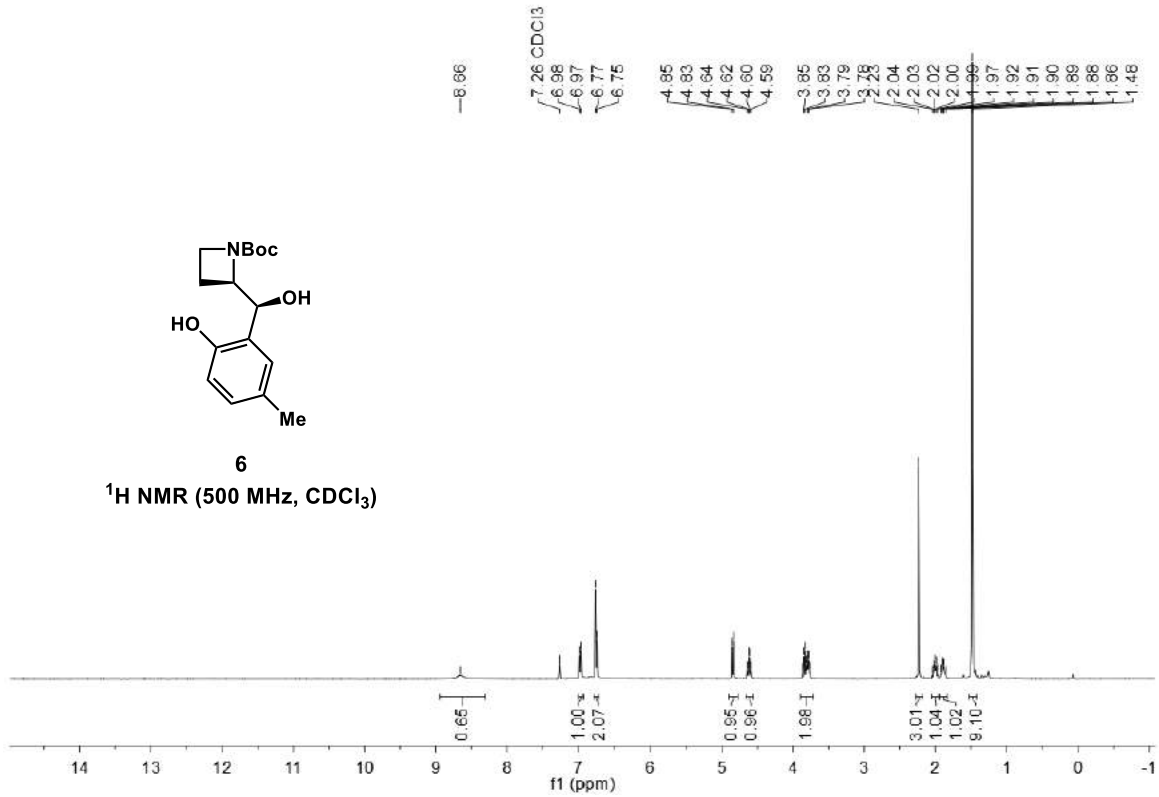

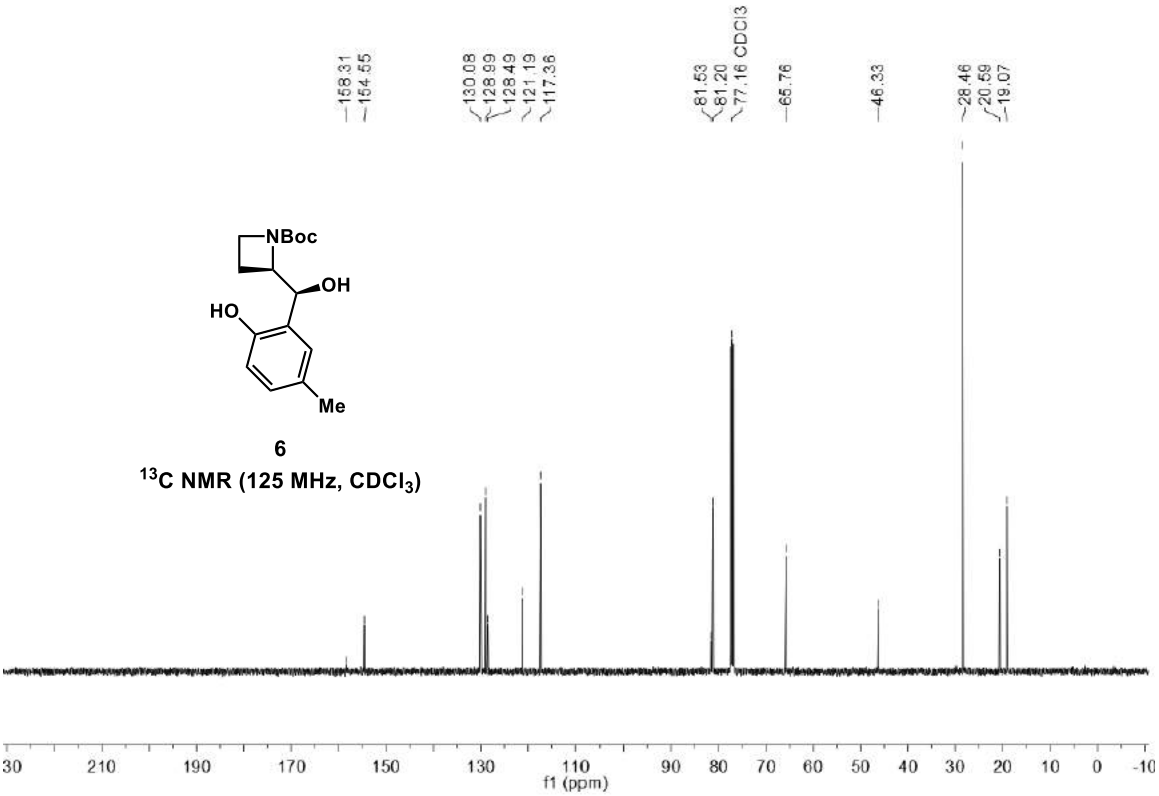

tert-butyl (R)-2-((S)-1-hydroxy-1-(2-hydroxy-5-methylphenyl)ethyl)azetidine-1-carboxylate (7)

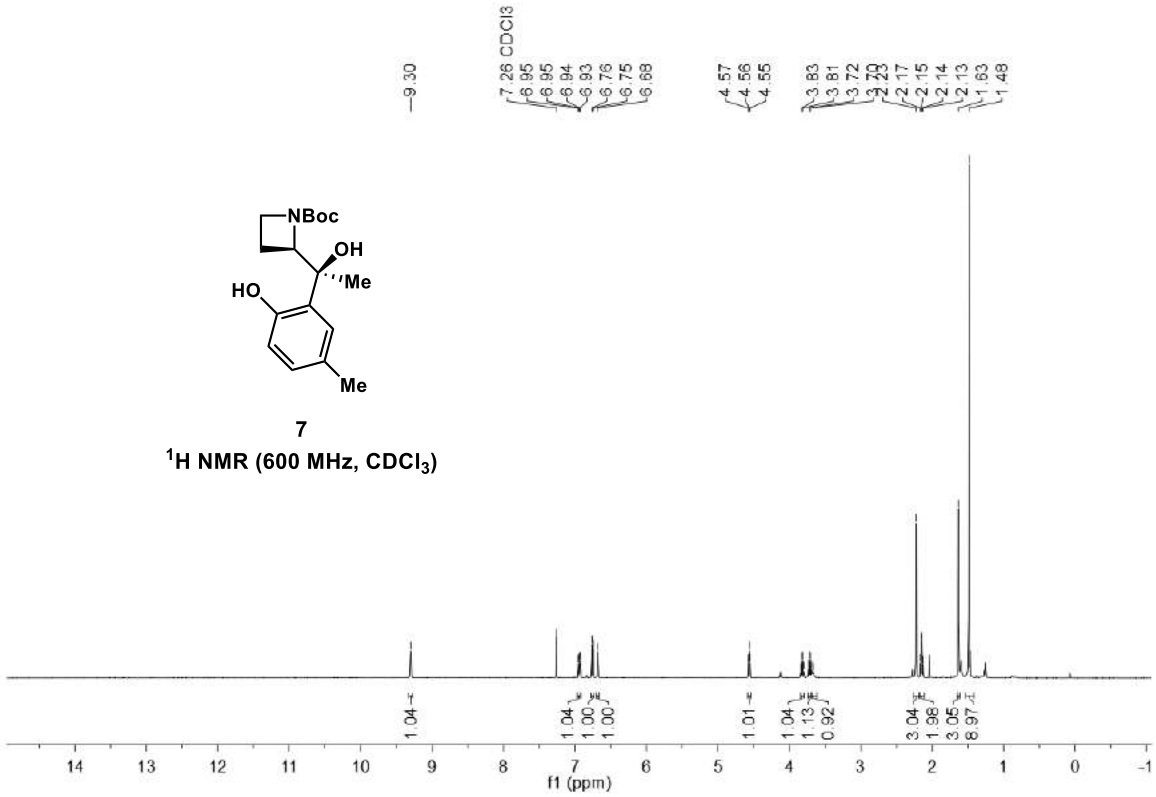

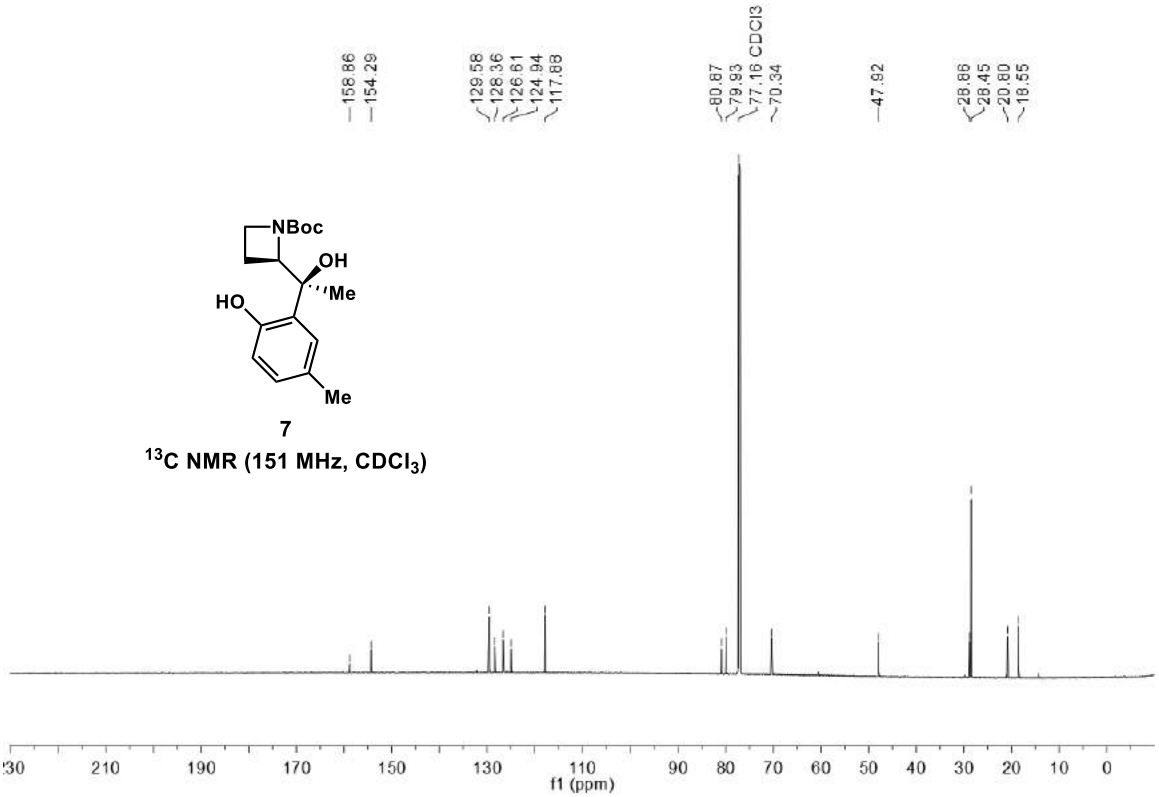

(R)-2-(2-hydroxy-5-methylbenzoyl)azetidin-1-ium chloride (8)

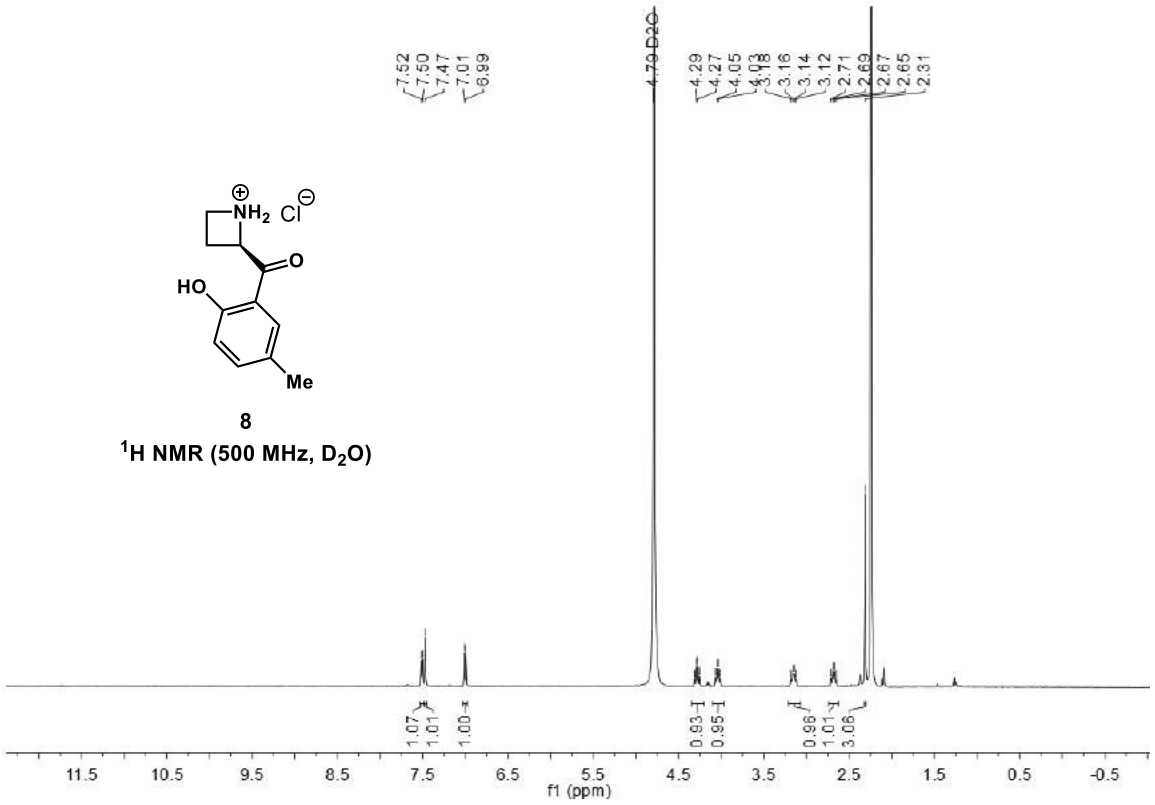

8

^{1}H NMR (500 MHz, D_2O)

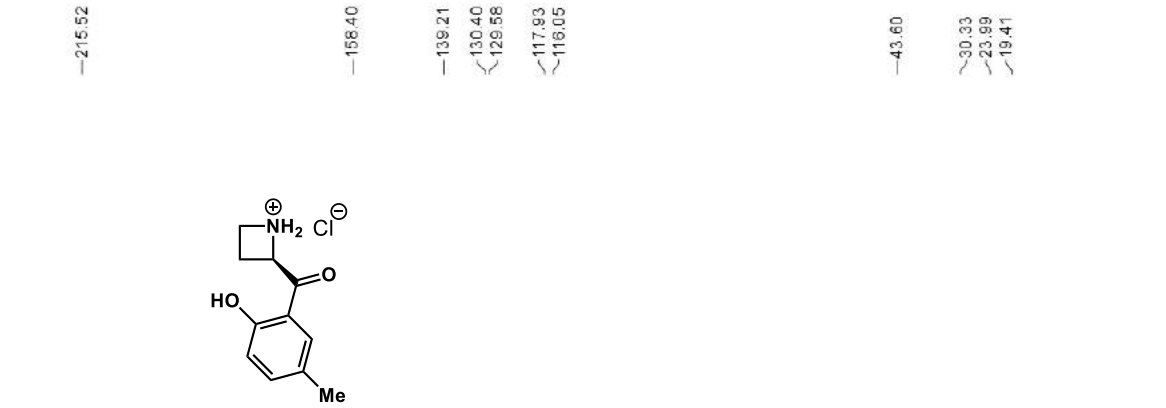

8

^{13}C NMR (125 MHz, D_2O)

tert-butyl (R)-2-(5-methyl-2-(((trifluoromethyl)sulfonyl)oxy)benzoyl)azetidine-1-carboxylate (9)

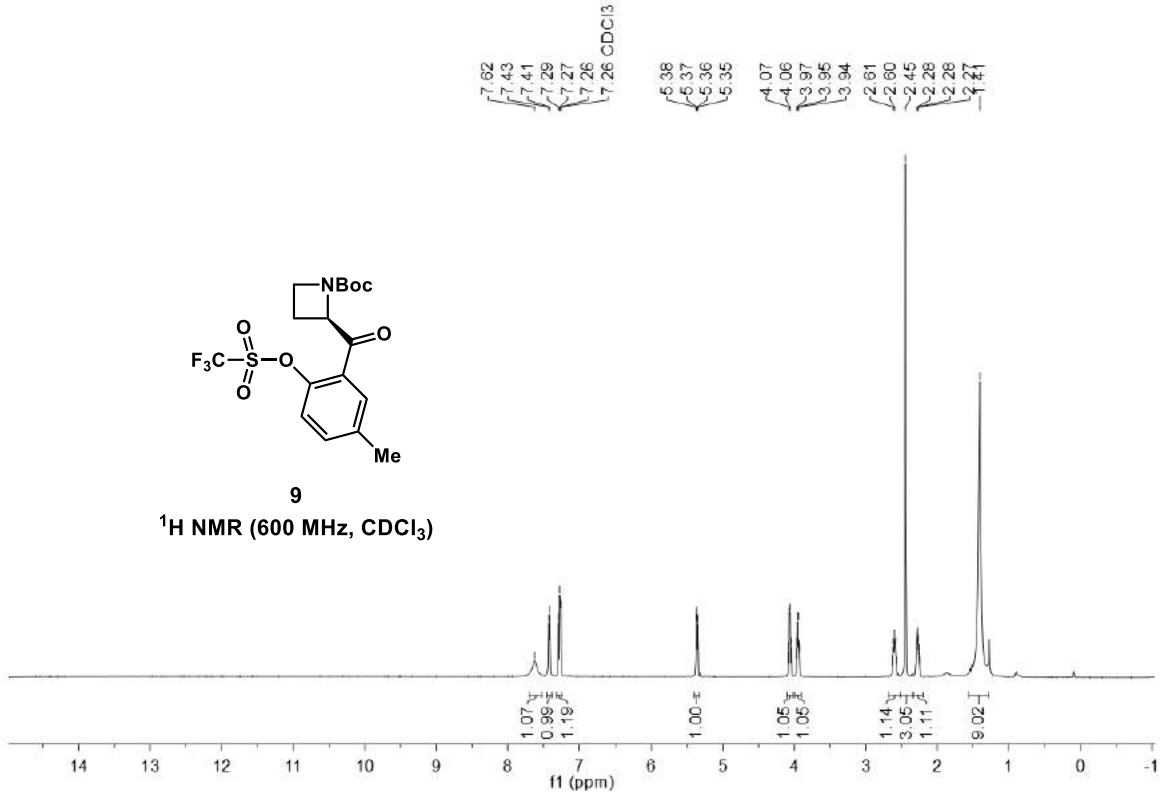

9

^{1}H NMR (600 MHz, $CDCl_3$)

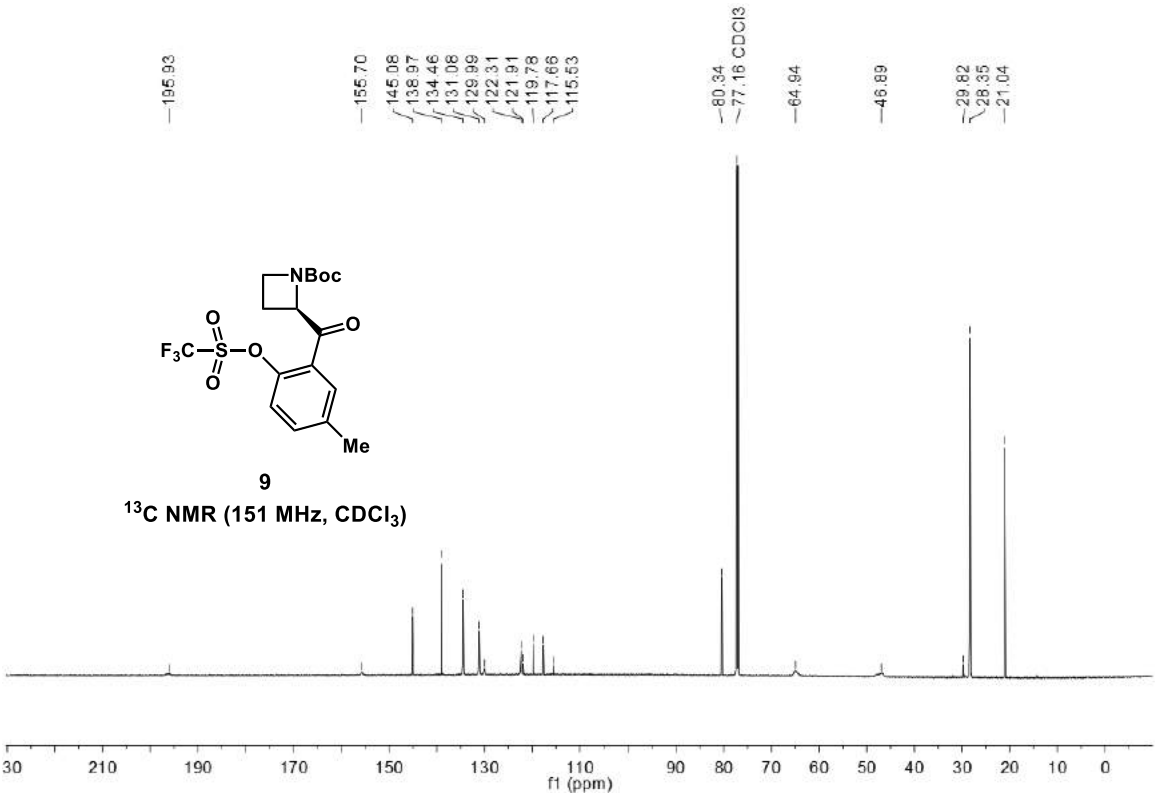

9

^{13}C NMR (151 MHz, $CDCl_3$)

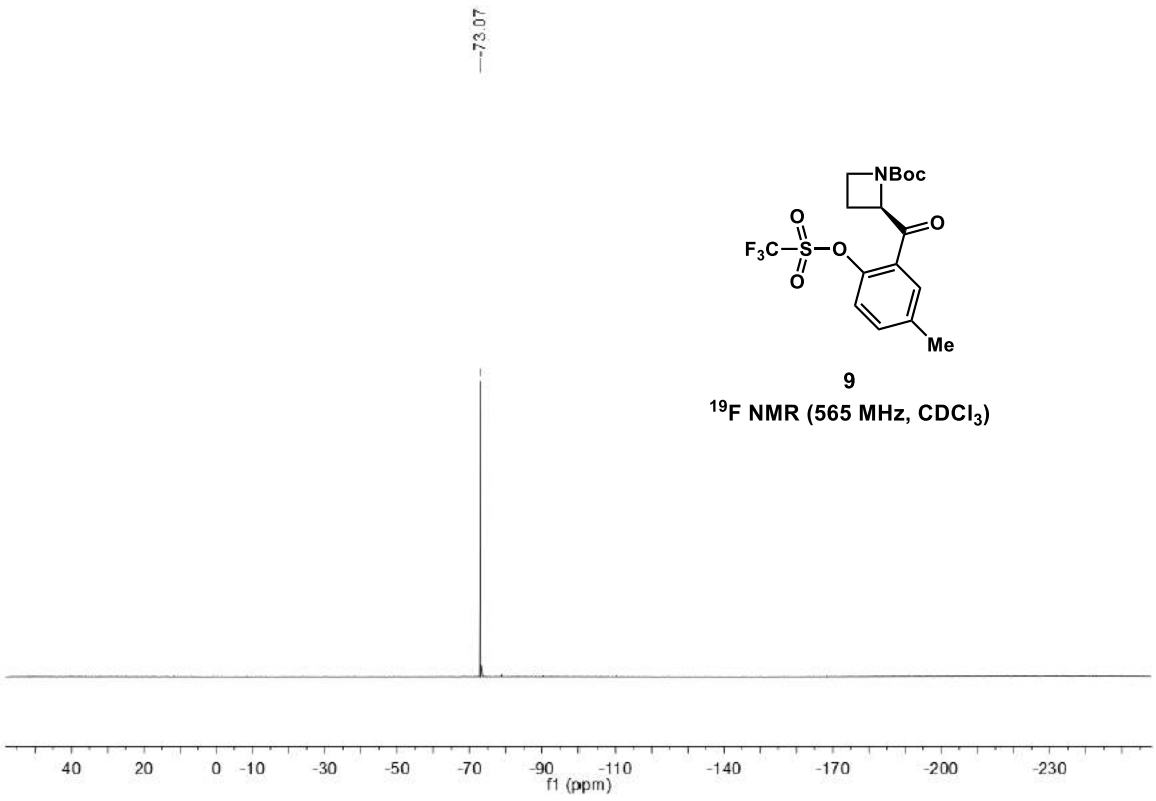

9

^{19}F NMR (565 MHz, $CDCl_3$)

8. SFC Spectra

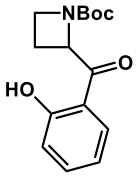

***rac*-3a**

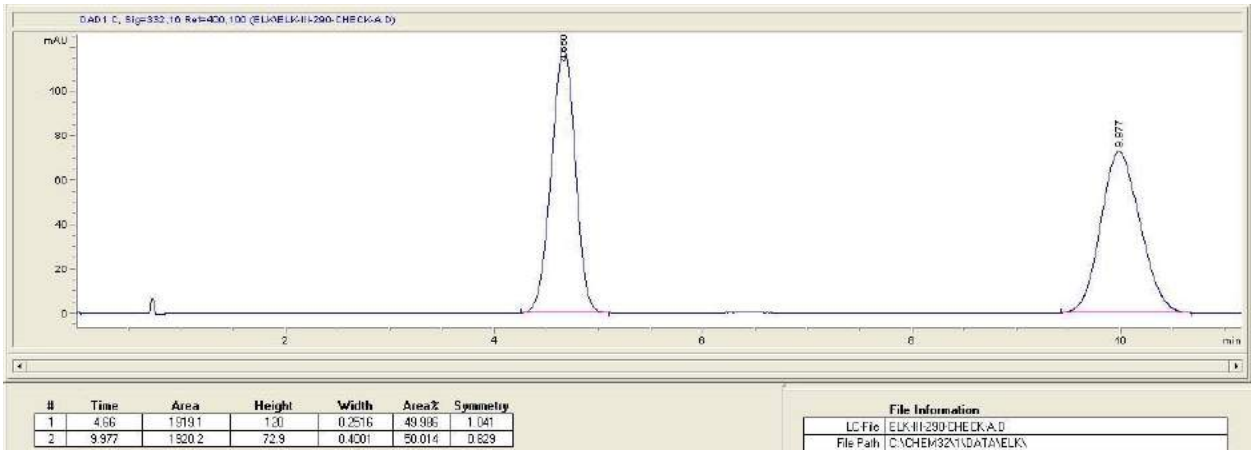

#	Time	Area	Height	Width	Area%	Symmetry
1	4.66	1519.1	1.20	0.2516	49.986	1.041
2	9.977	1520.2	72.9	0.4001	50.014	0.829

File Information	
LC File	ELK-III-290 CHECK-A.D
File Path	C:\CHEM32\1\DATA\ELK\

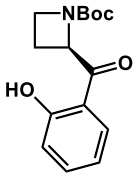

3a

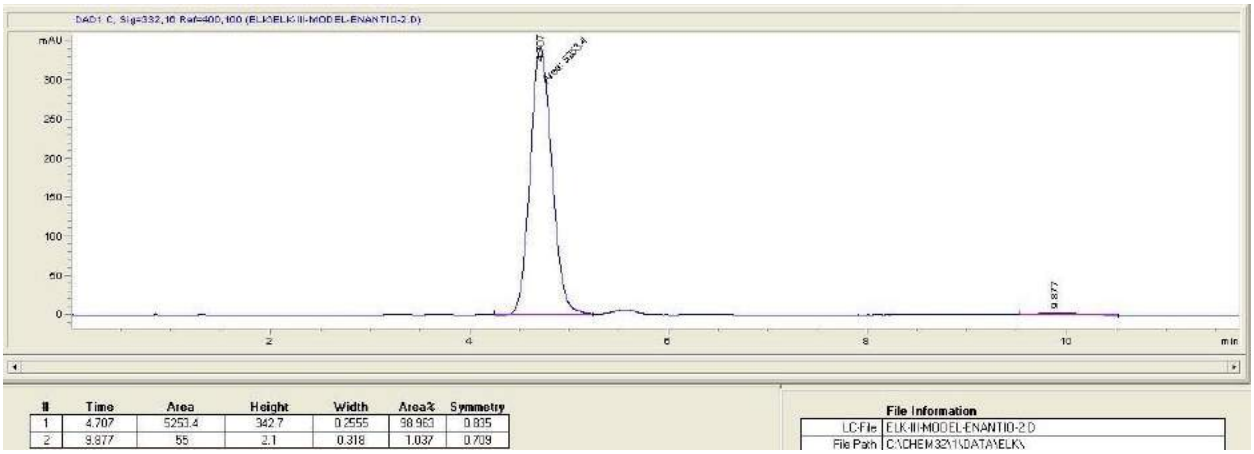

#	Time	Area	Height	Width	Area%	Symmetry
1	4.707	5253.4	342.7	0.2555	98.963	0.835
2	9.877	55	2.1	0.318	1.037	0.709

File Information	
LC File	ELK-III-MODEL-ENANTIO-2.D
File Path	C:\CHEM32\1\DATA\ELK\

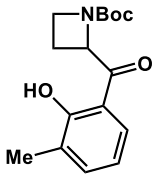

***rac*-3b**

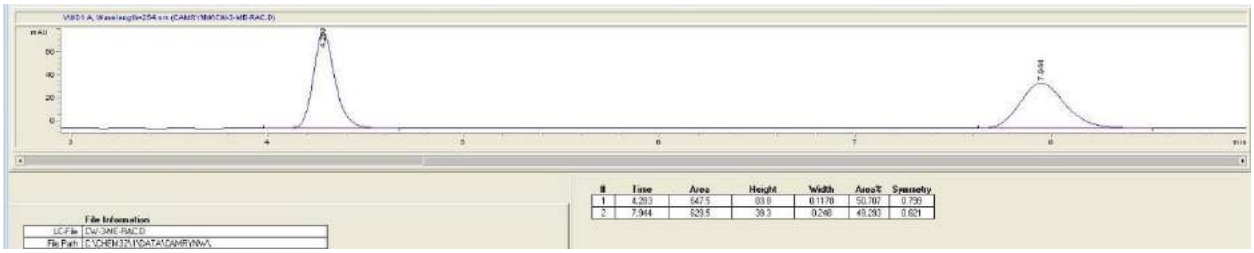

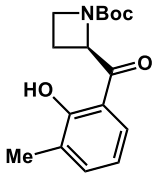

3b

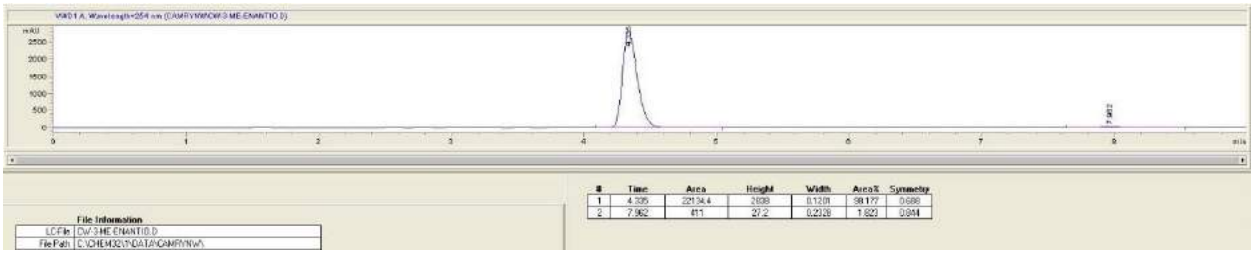

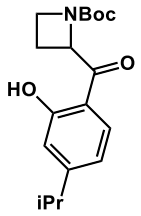

***rac*-3c**

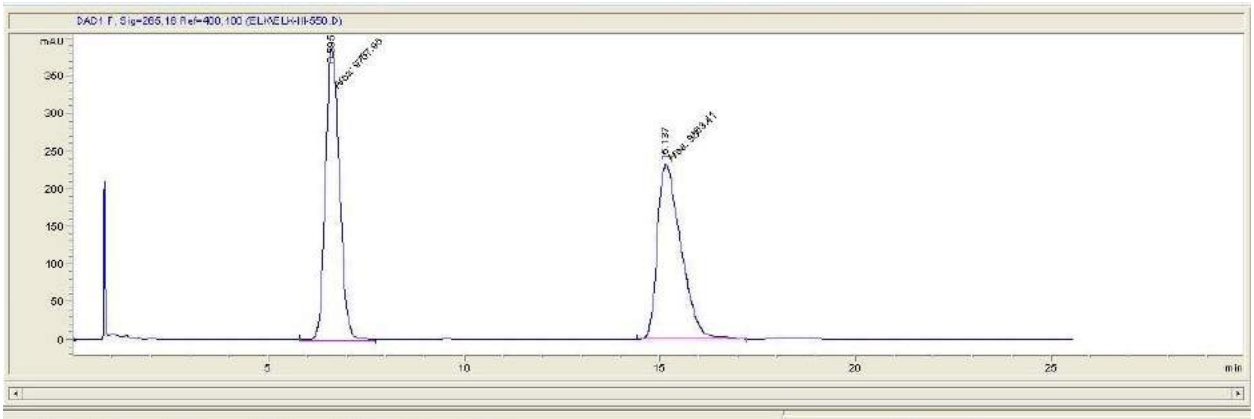

#	Time	Area	Height	Width	Area%	Symmetry
1	6.595	9758	386.8	0.4209	49.757	0.767
2	15.137	9863.4	232.9	0.7058	50.243	0.543

File Information

LC File	ELK-III-550.D
File Path	C:\CHEM32\1\DATA\ELK\

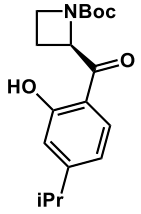

3c

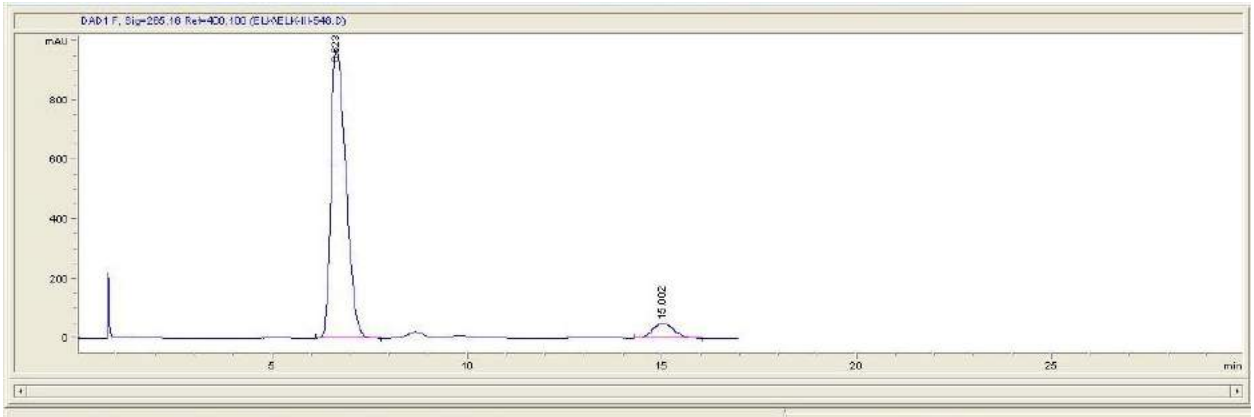

#	Time	Area	Height	Width	Area%	Symmetry
1	6.623	25786.5	971.1	0.4108	92.994	0.529
2	15.002	1942.6	50.4	0.482	7.006	0.906

File Information

LC File	ELK-III-548.D
File Path	C:\CHEM32\1\DATA\ELK\

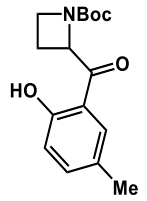

rac-3d

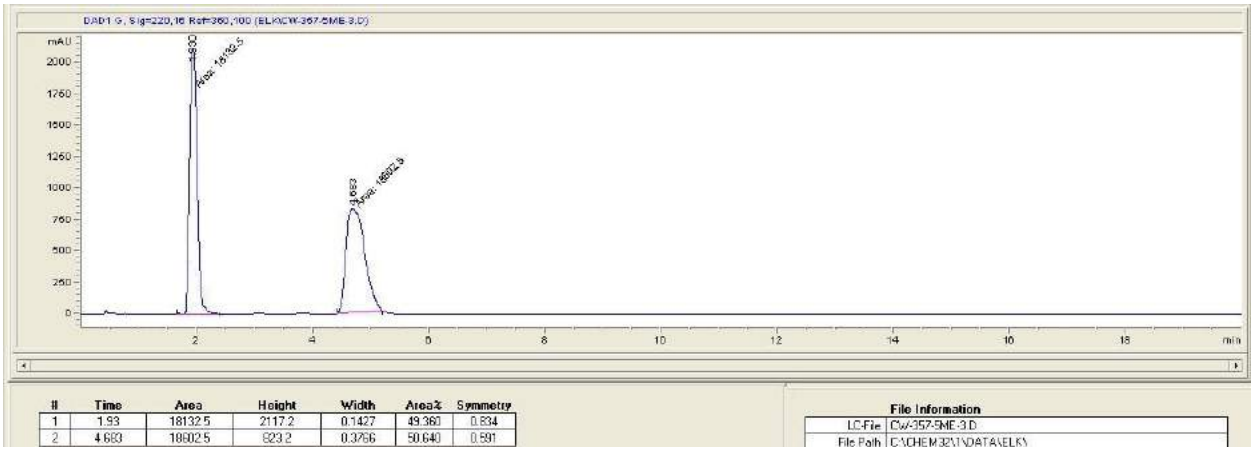

#	Time	Area	Height	Width	Area%	Symmetry
1	1.93	18132.5	2117.2	0.1427	49.360	0.834
2	4.663	18602.5	823.2	0.3766	50.640	0.891

File Information	
LC-File	CW-357-5ME-3.D
File Path	C:\CHEM32\1\DATA\ELK\

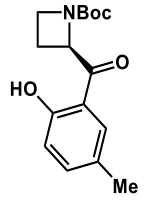

3d

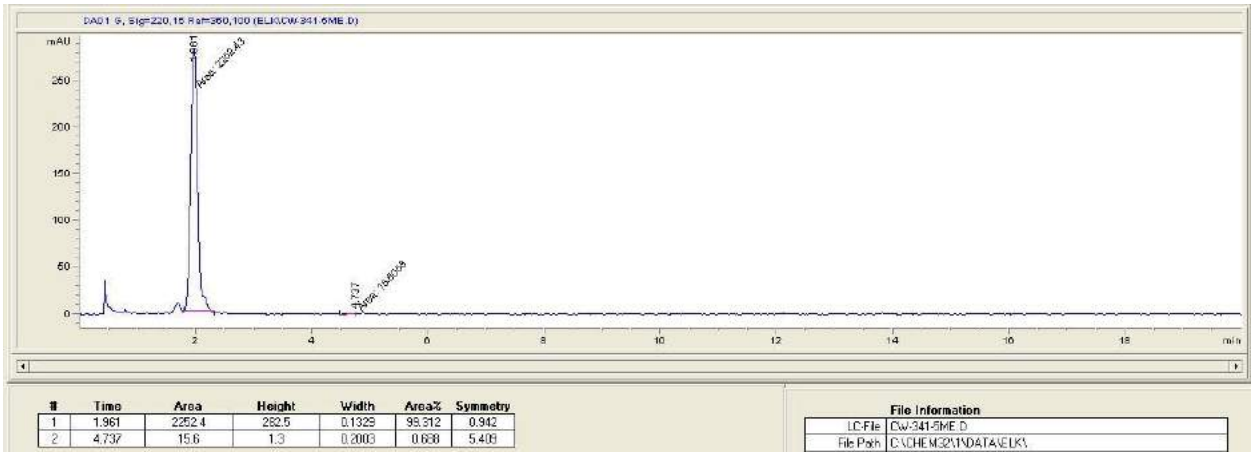

#	Time	Area	Height	Width	Area%	Symmetry
1	1.961	2252.4	282.5	0.1329	99.312	0.942
2	4.737	15.6	1.3	0.2003	0.688	5.409

File Information	
LC-File	CW-341-5ME.D
File Path	C:\CHEM32\1\DATA\ELK\

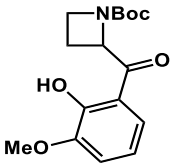

***rac*-3e**

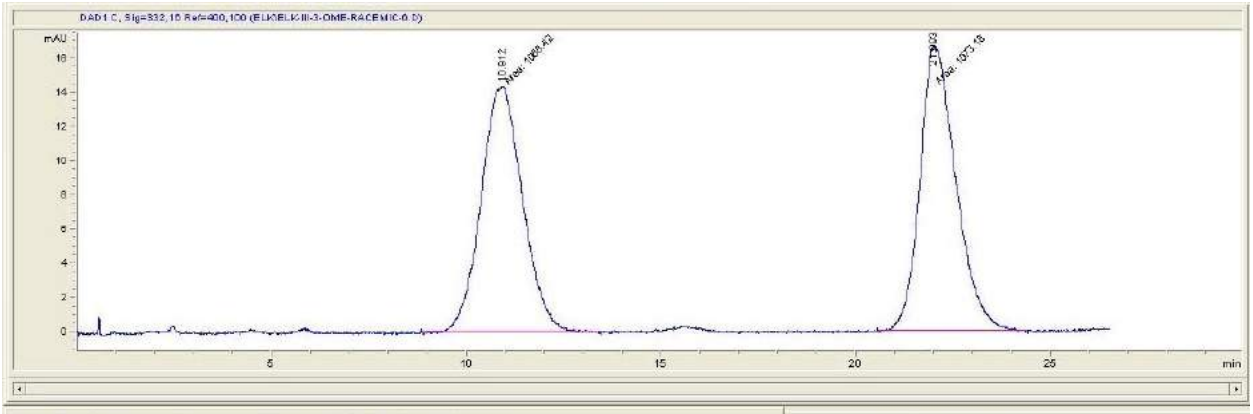

#	Time	Area	Height	Width	Area%	Symmetry
1	10.912	1066.4	14.4	1.2382	49.842	0.993
2	21.993	1073.2	16.6	1.0762	50.158	0.618

File Information

LC File	ELK-III-3-OME-RACEMIC-6.D
File Path	C:\CHEM32\1\DATA\ELK\

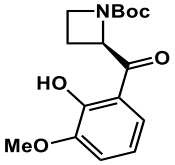

3e

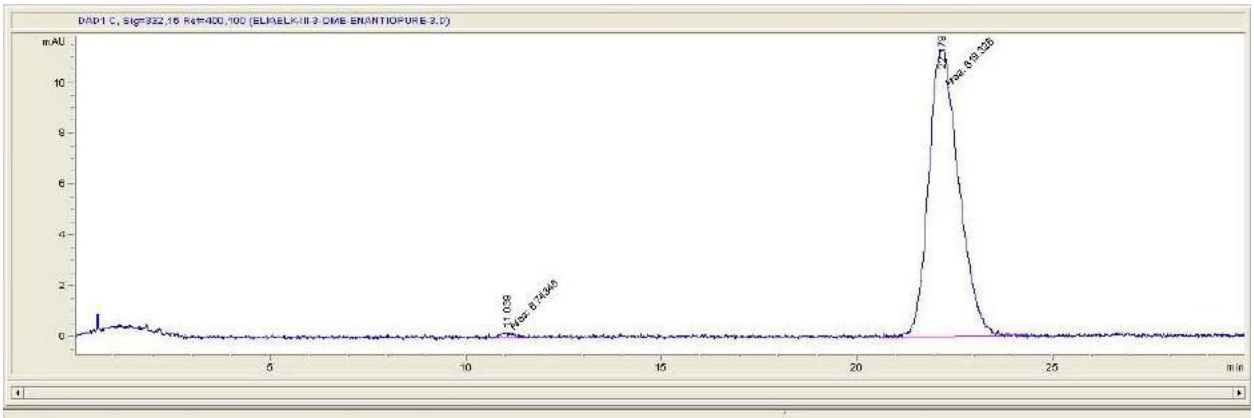

#	Time	Area	Height	Width	Area%	Symmetry
1	11.039	6.7	2.4E-1	0.4776	1.077	0.912
2	22.178	619.3	11.3	0.9095	98.923	0.844

File Information

LC File	ELK-III-3-OME-ENANTIOPURE-3.D
File Path	C:\CHEM32\1\DATA\ELK\

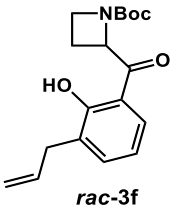

***rac*-3f**

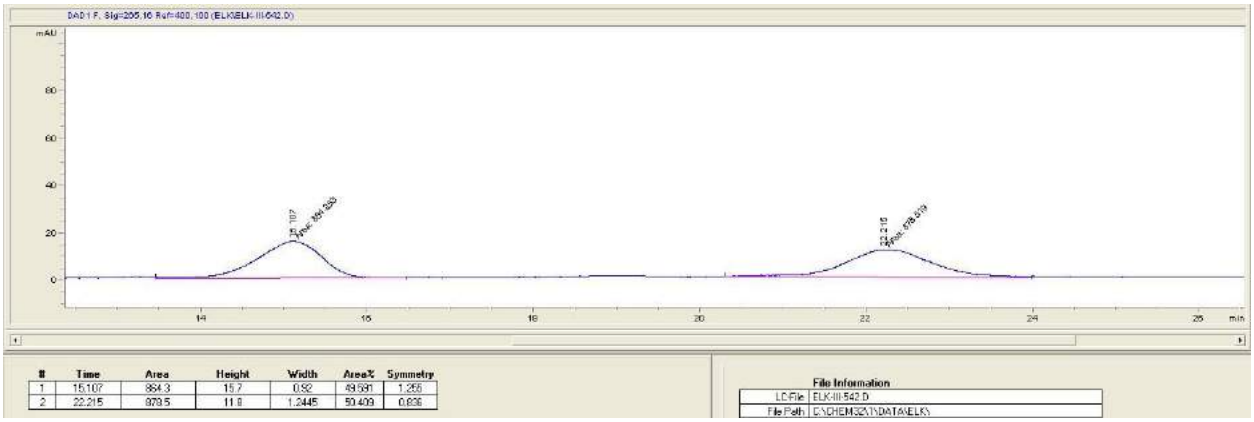

#	Time	Area	Height	Width	Area%	Symmetry
1	15.107	864.3	15.7	0.92	49.591	1.266
2	22.215	878.5	11.8	1.2445	50.409	0.836

File Information	
LC-File	ELK-III-542.D
File Path	C:\CHEM32\1\DATA\ELK\

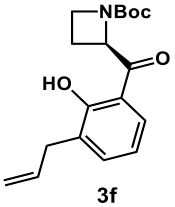

3f

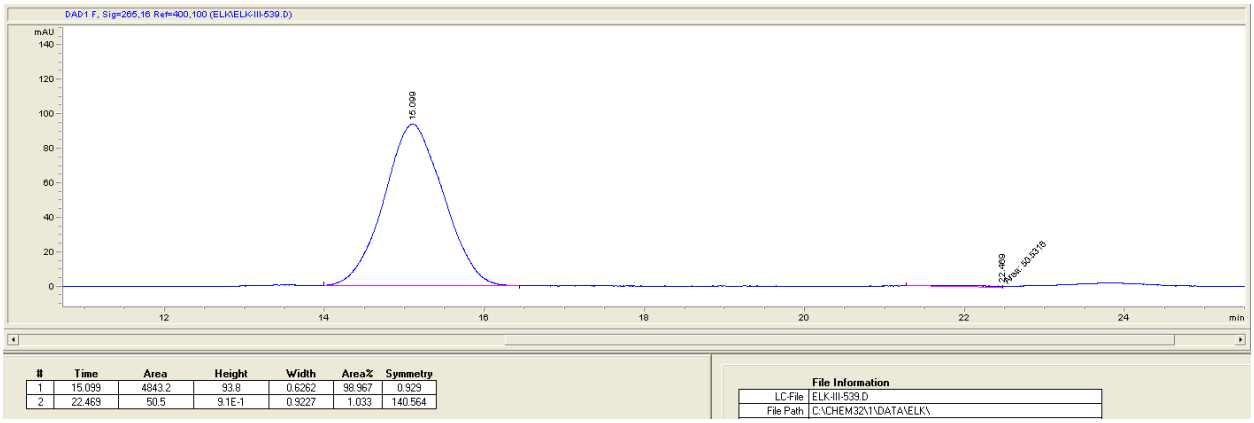

#	Time	Area	Height	Width	Area%	Symmetry
1	15.099	4843.2	93.8	0.8262	98.967	0.929
2	22.469	50.5	9.1E-1	0.9227	1.033	140.564

File Information	
LC-File	ELK-III-539.D
File Path	C:\CHEM32\1\DATA\ELK\

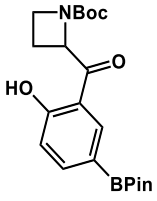

***rac*-3g**

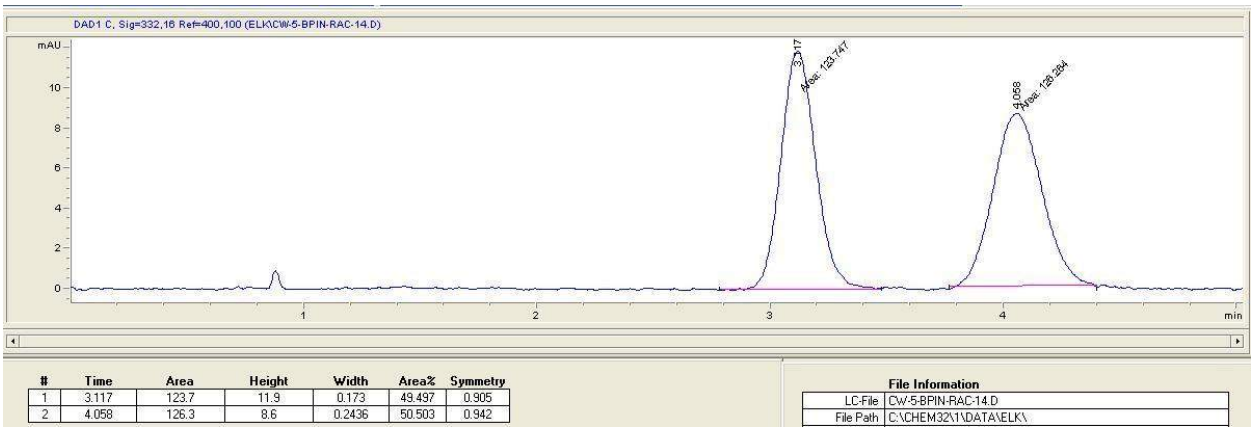

#	Time	Area	Height	Width	Area%	Symmetry
1	3.117	123.7	11.9	0.173	49.497	0.905
2	4.058	126.3	8.6	0.2436	50.503	0.942

File Information	
LC-File	CW-5-BPIN-RAC-14.D
File Path	C:\CHEM32\1\DATA\ELK\

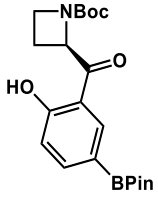

3g

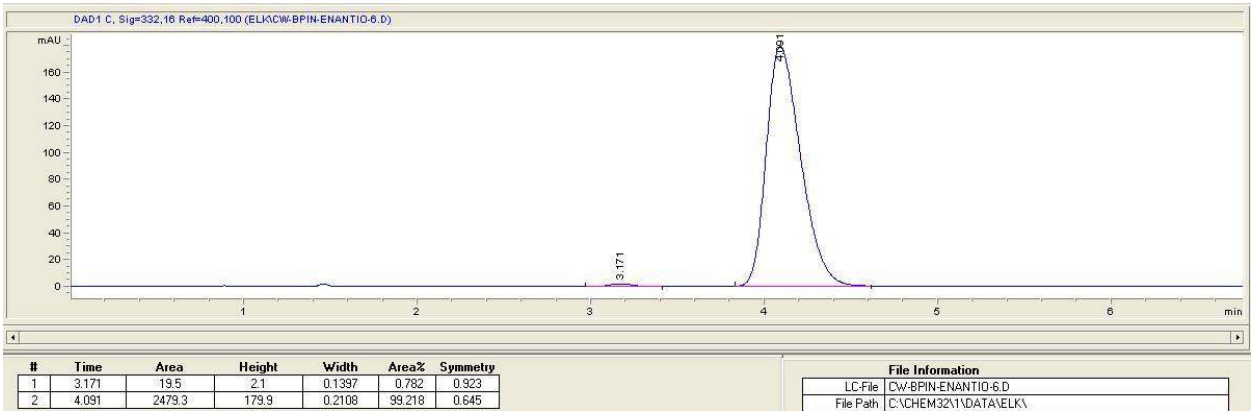

#	Time	Area	Height	Width	Area%	Symmetry
1	3.171	19.5	2.1	0.1397	0.782	0.923
2	4.091	2479.3	179.9	0.2108	99.218	0.645

File Information	
LC-File	CW-BPIN-ENANTIO-6.D
File Path	C:\CHEM32\1\DATA\ELK\

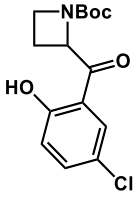

***rac*-3h**

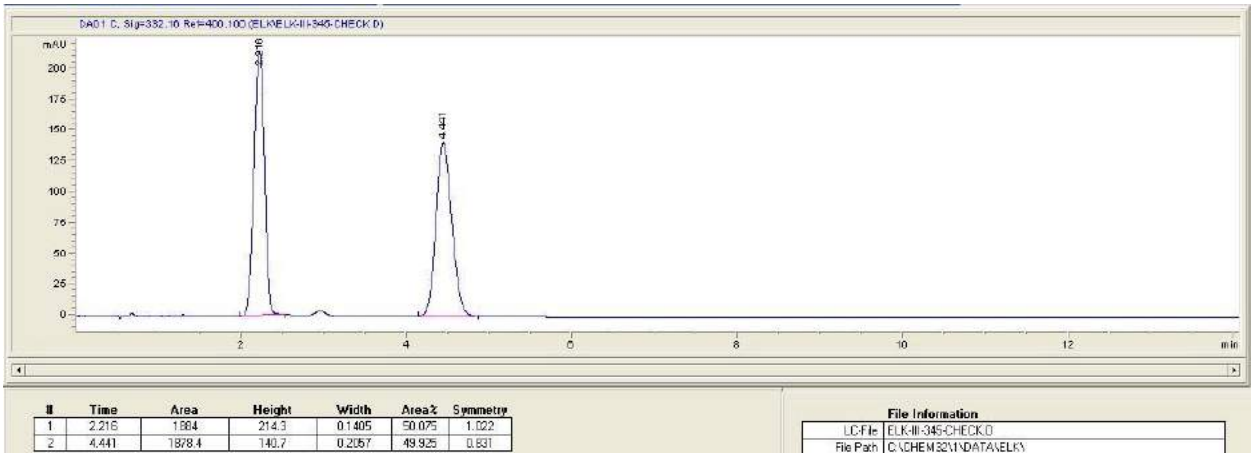
mAU
2.216
4.441
min
Time Area Height Width Area% Symmetry
1 2.216 1984 214.3 0.1405 50.075 1.022
2 4.441 1978.4 140.7 0.2057 49.925 0.831
File Information
LC-File ELK-III-345-CHECK.D
File Path C:\CHEM32\1\DATA\ELK\

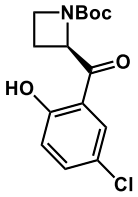
NBoc
O
HO
Cl

3h

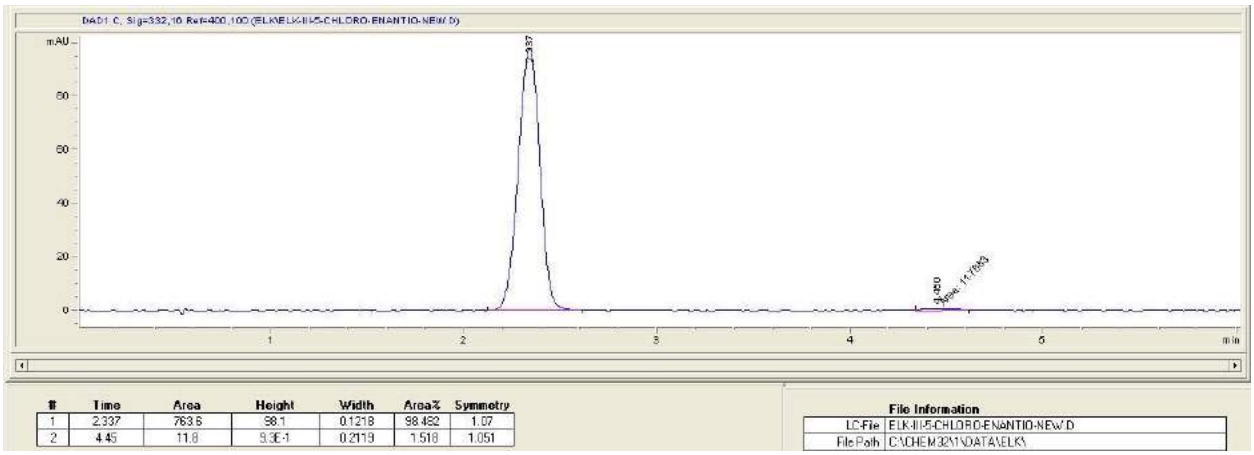
mAU
2.337
min
Time Area Height Width Area% Symmetry
1 2.337 763.6 98.1 0.1218 98.482 1.07
2 4.45 11.8 9.3E-1 0.2119 1.518 1.051
File Information
LC-File ELK-III-5-CHLORO-ENANTIO-NEW.D
File Path C:\CHEM32\1\DATA\ELK\

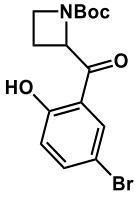
NBoc
O
HO
Br

***rac*-3i**

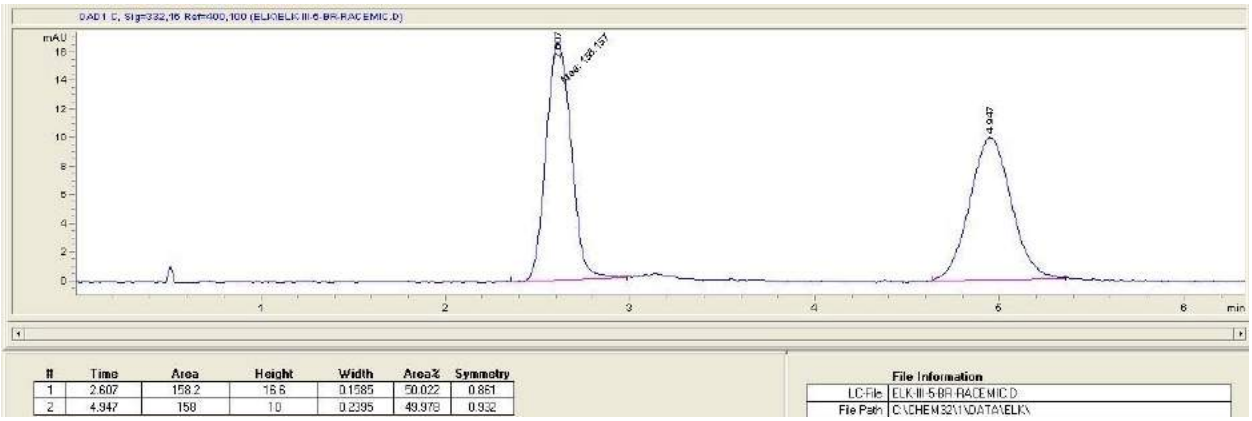

#	Time	Area	Height	Width	Area%	Symmetry
1	2.607	158.2	16.6	0.1585	50.022	0.861
2	4.947	158	10	0.2395	49.978	0.932

File Information	
LC-File	ELK-III-5-BR-RACEMIC.D
File Path	C:\CHEM32\1\DATA\ELK\

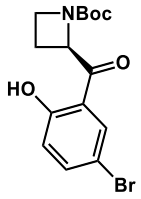

3i

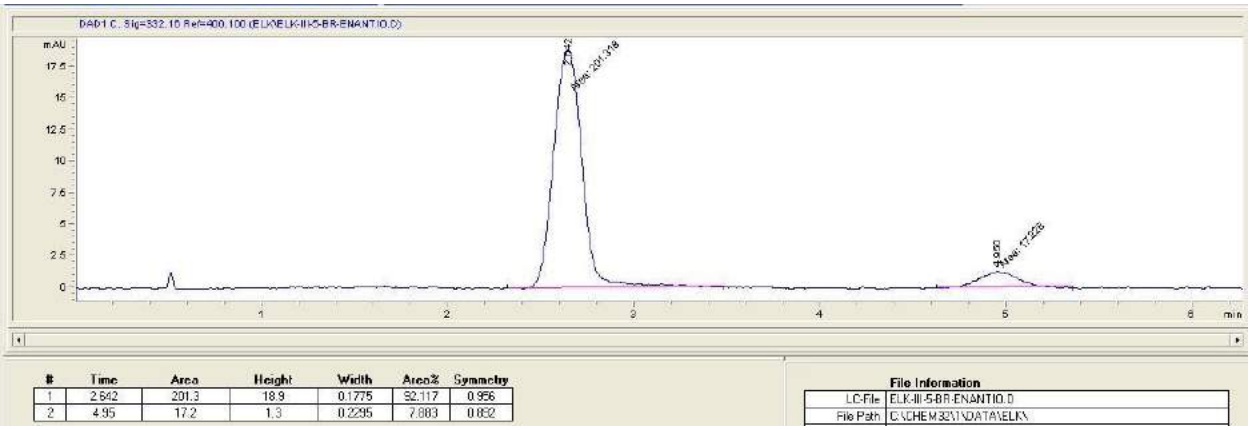

#	Time	Area	Height	Width	Area%	Symmetry
1	2.642	201.3	18.9	0.1775	92.117	0.956
2	4.95	17.2	1.3	0.2295	7.883	0.852

File Information	
LC-File	ELK-III-5-BR-ENANTIO.D
File Path	C:\CHEM32\1\DATA\ELK\

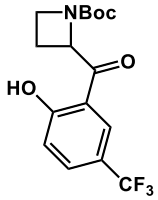

***rac*-3j**

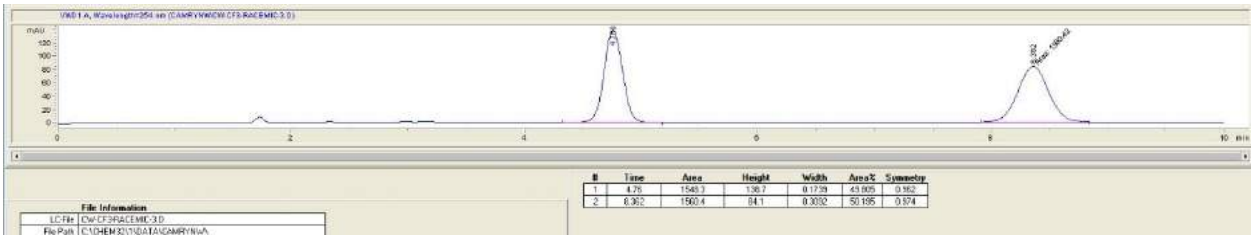

#	Time	Area	Height	Width	Area%	Symmetry
1	4.76	1548.9	136.7	0.1739	49.805	0.162
2	8.302	1560.4	84.1	0.3092	50.195	0.974

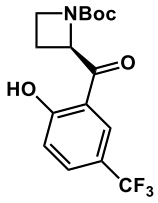

3j

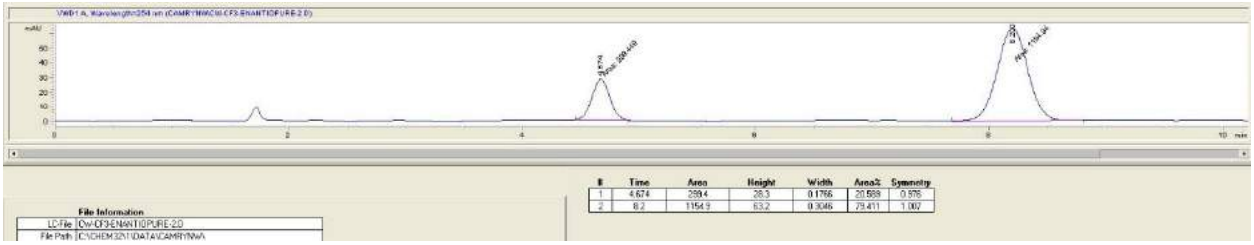

#	Time	Area	Height	Width	Area%	Symmetry
1	4.674	259.4	28.3	0.1766	20.589	0.976
2	8.2	1154.9	63.2	0.3046	79.411	1.007

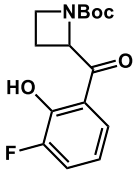

***rac*-3k**

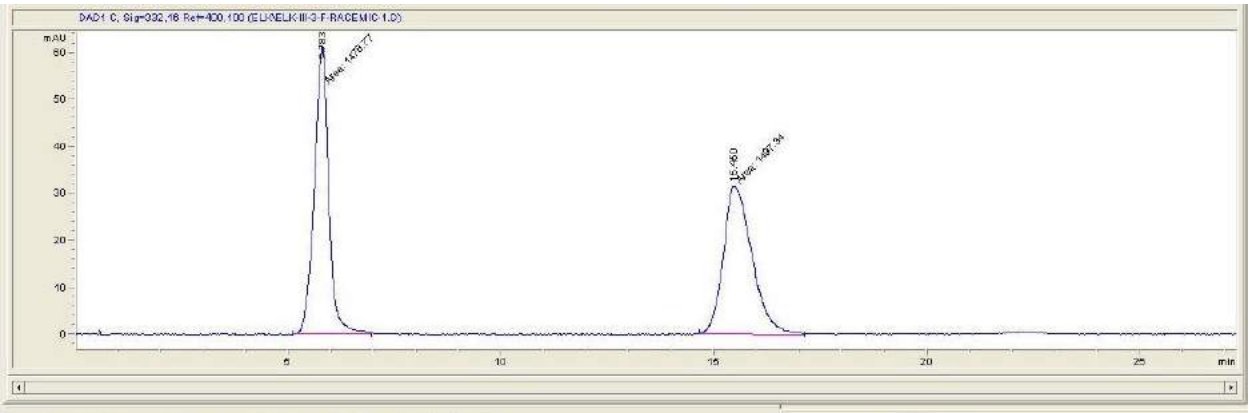

#	Time	Area	Height	Width	Area%	Symmetry
1	5.783	1476.8	61.3	0.4018	49.654	1.171
2	15.45	1497.3	31.6	0.7892	50.346	0.591

File Information	
LC File	ELK-III-3-F-RACEMIC-1.D
File Path	D:\CHEM32\1\DATA\ELK\

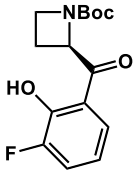

3k

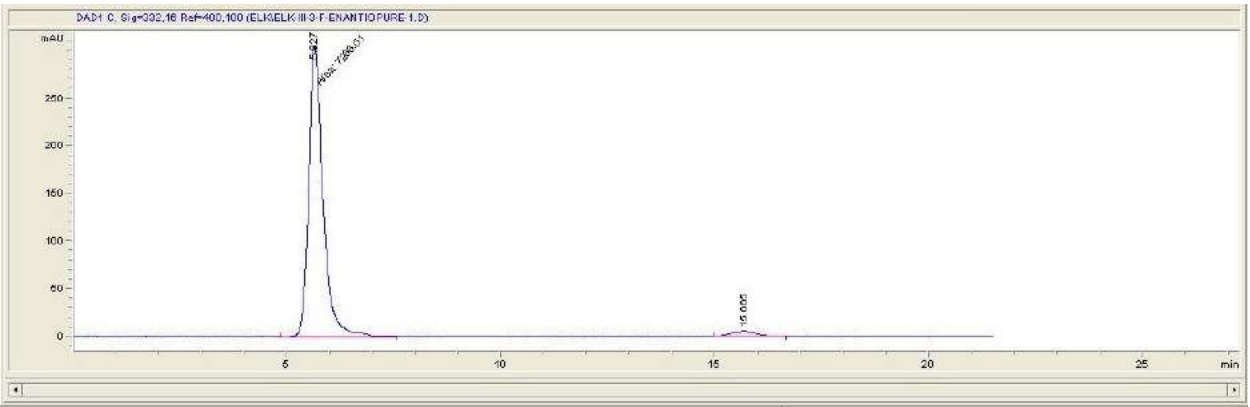

#	Time	Area	Height	Width	Area%	Symmetry
1	5.627	7286	306	0.3958	96.925	0.613
2	15.885	230.5	5.4	0.5001	3.075	1.028

File Information	
LC File	ELK-III-3-F-ENANTIOPURE-1.D
File Path	D:\CHEM32\1\DATA\ELK\

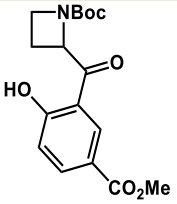

***rac*-3l**

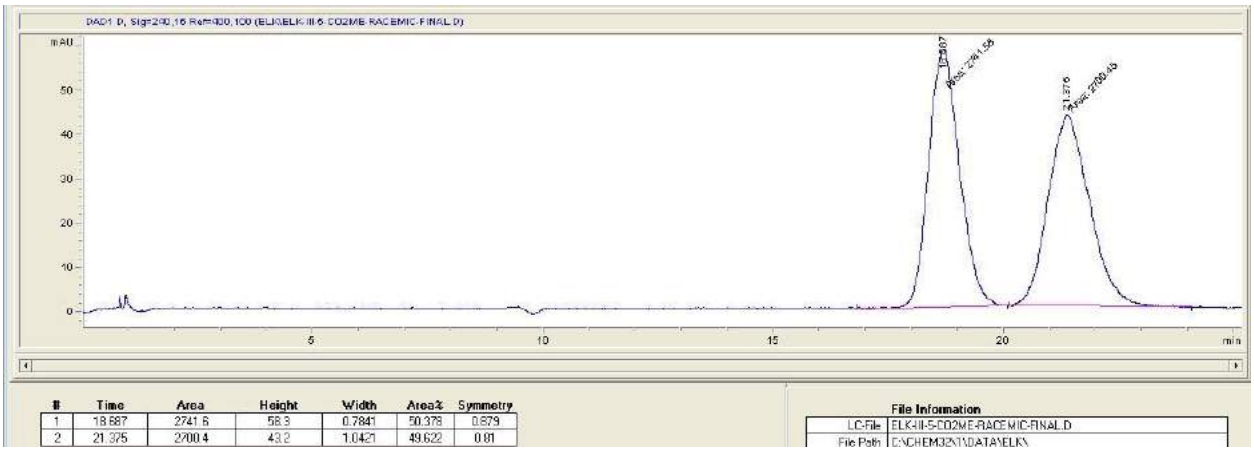

#	Time	Area	Height	Width	Area%	Symmetry
1	18.887	2741.6	58.3	0.7841	50.378	0.879
2	21.375	2700.4	43.2	1.0421	49.622	0.81

File Information	
LC-File	ELK-III-5-CO2ME-RACEMIC-FINAL.D
File Path	C:\CHEM32\1\DATA\ELK\

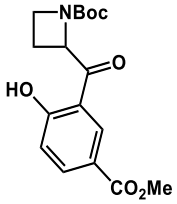

***rac*-3l**

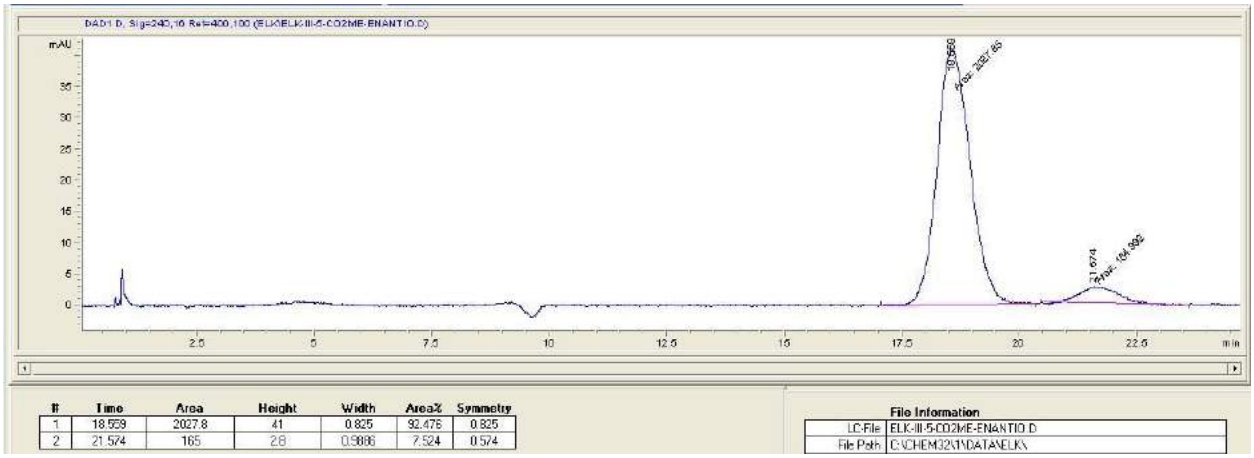

#	Time	Area	Height	Width	Area%	Symmetry
1	18.559	2027.8	41	0.825	92.476	0.825
2	21.574	165	2.8	0.9886	7.524	0.574

File Information	
LC-File	ELK-III-5-CO2ME-ENANTIO.D
File Path	C:\CHEM32\1\DATA\ELK\

9. X-ray Crystallography Data for 7

A colorless crystal of approximate dimensions 0.138 x 0.258 x 0.283 mm was mounted in a cryoloop and transferred to a Bruker X8 Prospector APEX II diffractometer system. The APEX3[1] program package was used to determine the unit-cell parameters and for data collection (15 sec/frame scan time). The raw frame data was processed using SAINT[2] and SADABS[3] to yield the reflection data file. Subsequent calculations were carried out using the SHELXTL[4] program package. The systematic absences were consistent with the monoclinic space groups $P2_1$ and $P2_1/m$. It was later determined that space group $P2_1$ was correct.

The structure was solved by direct methods and refined on F^2 by full-matrix least-squares techniques. The analytical scattering factors[5] for neutral atoms were used throughout the analysis. Hydrogen atoms H(1) and H(2) were located from a difference-map and refined (xyz and U_{iso}). The remaining hydrogen atoms were included using a riding model.

Least-squares analysis yielded wR2 = 0.0734 and Goof = 1.047 for 212 variables refined against 3041 data (0.83 Å), R1 = 0.0283 for those 3023 data with $I > 2.0\sigma(I)$. The absolute structure was assigned by refinement of the Flack parameter[6].

References:

1. APEX3 Version 2018.1-0, Bruker AXS, Inc.; Madison, WI 2018.

2. SAINT Version 8.38a, Bruker AXS, Inc.; Madison, WI 2013.

3. Sheldrick, G. M. SADABS, Version 2014/5, Bruker AXS, Inc.; Madison, WI 2014.

4. Sheldrick, G. M. SHELXTL, Version 2014/7, Bruker AXS, Inc.; Madison, WI 2014.

5. International Tables for Crystallography 1992, Vol. C., Dordrecht: Kluwer Academic Publishers.

6. Parsons, S., Flack, H. D., Wagner, T. Acta Cryst. B69, 249-259, 2013.

Definitions:

$wR2 = [\Sigma[w(F_o^2-F_c^2)^2] / \Sigma[w(F_o^2)^2]]^{1/2}$

$R1 = \Sigma||F_o|-|F_c|| / \Sigma|F_o|$

$Goof = S = [\Sigma[w(F_o^2-F_c^2)^2] / (n-p)]^{1/2}$ where n is the number of reflections and p is the total number of parameters refined.

The thermal ellipsoid plot is shown at the 50% probability level.

Table 1. Crystal data and structure refinement for vmd45.

Identification code	vmd45 (Erin Kuker)	
Empirical formula	$C_{17}\ H_{25}\ N\ O_4$	
Formula weight	307.38	
Temperature	93(2) K	
Wavelength	1.54178 Å	
Crystal system	Monoclinic	
Space group	$P2_1$	
Unit cell dimensions	a = 8.35900(10) Å	α = 90°.
	b = 11.0425(2) Å	β = 94.9670(6)°.
	c = 9.1481(2) Å	γ = 90°.
Volume	841.24(3) Å^3	
Z	2	
Density (calculated)	1.213 Mg/m^3	
Absorption coefficient	0.697 mm^{-1}	
F(000)	332	
Crystal color	colorless	
Crystal size	0.283 x 0.258 x 0.138 mm^3	
Theta range for data collection	4.852 to 68.321°	
Index ranges	$-10 \le h \le 9$, $-13 \le k \le 13$, $-10 \le l \le 10$	
Reflections collected	17066	
Independent reflections	3041 [R(int) = 0.0471]	
Completeness to theta = 67.679°	99.9 %	
Absorption correction	Semi-empirical from equivalents	
Max. and min. transmission	0.8643 and 0.7943	
Refinement method	Full-matrix least-squares on F^2	
Data / restraints / parameters	3041 / 1 / 212	
Goodness-of-fit on F^2	1.047	
Final R indices [I>2sigma(I) = 3023 data]	R1 = 0.0283, wR2 = 0.0733	
R indices (all data, 0.83 Å)	R1 = 0.0285, wR2 = 0.0734	
Absolute structure parameter	-0.04(8)	
Largest diff. peak and hole	0.164 and -0.151 e.Å^{-3}	

Table 2. Atomic coordinates (x 10^4) and equivalent isotropic displacement parameters ($Å^2$ x 10^3) for vmd45. U(eq) is defined as one third of the trace of the orthogonalized U^{ij} tensor.

	x	y	z	U(eq)
O(1)	8410(2)	4452(1)	6019(2)	17(1)
O(2)	3925(2)	5848(1)	4241(2)	22(1)
O(3)	9024(1)	5936(1)	2197(1)	16(1)
O(4)	11120(2)	6973(1)	3387(1)	15(1)
N(1)	8928(2)	6479(1)	4525(2)	14(1)
C(1)	9172(2)	7250(2)	5831(2)	16(1)
C(2)	7415(2)	6988(2)	6143(2)	18(1)
C(3)	7253(2)	6147(2)	4780(2)	14(1)
C(4)	7006(2)	4794(2)	5120(2)	15(1)
C(5)	6834(2)	4020(2)	3724(2)	18(1)
C(6)	5496(2)	4618(2)	5951(2)	14(1)
C(7)	3999(2)	5117(2)	5448(2)	16(1)
C(8)	2638(2)	4841(2)	6165(2)	18(1)
C(9)	2745(2)	4080(2)	7373(2)	19(1)
C(10)	4207(2)	3585(2)	7909(2)	19(1)
C(11)	5556(2)	3871(2)	7177(2)	16(1)
C(12)	4366(3)	2753(2)	9220(3)	30(1)
C(13)	9771(2)	6489(2)	3362(2)	12(1)
C(14)	9884(2)	5601(2)	905(2)	17(1)
C(15)	10459(3)	6719(2)	148(2)	26(1)
C(16)	11252(3)	4745(2)	1378(2)	23(1)
C(17)	8579(3)	4962(2)	-66(2)	23(1)

Table 3. Bond lengths [Å] and angles [°] for vmd45.

O(1)-C(4)	1.425(2)
O(2)-C(7)	1.365(2)
O(3)-C(13)	1.336(2)
O(3)-C(14)	1.483(2)
O(4)-C(13)	1.246(2)
N(1)-C(13)	1.325(2)
N(1)-C(1)	1.467(2)
N(1)-C(3)	1.485(2)
C(1)-C(2)	1.547(3)
C(2)-C(3)	1.551(3)
C(3)-C(4)	1.544(3)
C(4)-C(5)	1.533(3)
C(4)-C(6)	1.541(2)
C(6)-C(11)	1.390(3)
C(6)-C(7)	1.407(3)
C(7)-C(8)	1.395(3)
C(8)-C(9)	1.385(3)
C(9)-C(10)	1.389(3)
C(10)-C(11)	1.397(3)
C(10)-C(12)	1.507(3)
C(14)-C(15)	1.515(3)
C(14)-C(16)	1.517(3)
C(14)-C(17)	1.519(3)
C(13)-O(3)-C(14)	121.64(14)
C(13)-N(1)-C(1)	127.09(15)
C(13)-N(1)-C(3)	134.56(16)
C(1)-N(1)-C(3)	94.67(14)
N(1)-C(1)-C(2)	88.56(14)
C(1)-C(2)-C(3)	88.95(13)
N(1)-C(3)-C(4)	114.54(14)
N(1)-C(3)-C(2)	87.75(13)
C(4)-C(3)-C(2)	114.89(16)
O(1)-C(4)-C(5)	110.25(15)

O(1)-C(4)-C(6)	110.56(15)
C(5)-C(4)-C(6)	108.62(15)
O(1)-C(4)-C(3)	104.73(14)
C(5)-C(4)-C(3)	112.09(16)
C(6)-C(4)-C(3)	110.57(15)
C(11)-C(6)-C(7)	117.73(16)
C(11)-C(6)-C(4)	119.93(16)
C(7)-C(6)-C(4)	122.16(17)
O(2)-C(7)-C(8)	121.81(17)
O(2)-C(7)-C(6)	118.23(16)
C(8)-C(7)-C(6)	119.95(18)
C(9)-C(8)-C(7)	120.52(18)
C(8)-C(9)-C(10)	121.04(18)
C(9)-C(10)-C(11)	117.61(19)
C(9)-C(10)-C(12)	122.38(19)
C(11)-C(10)-C(12)	120.00(18)
C(6)-C(11)-C(10)	123.15(18)
O(4)-C(13)-N(1)	122.14(17)
O(4)-C(13)-O(3)	124.77(16)
N(1)-C(13)-O(3)	113.09(15)
O(3)-C(14)-C(15)	110.84(16)
O(3)-C(14)-C(16)	109.49(16)
C(15)-C(14)-C(16)	112.15(17)
O(3)-C(14)-C(17)	102.07(15)
C(15)-C(14)-C(17)	110.57(17)
C(16)-C(14)-C(17)	111.27(17)

Table 4. Anisotropic displacement parameters ($Å^2$ x 10^3) for vmd45. The anisotropic displacement factor exponent takes the form: $-2\pi^2[h^2 a^{*2}U^{11} + ... + 2 h k a^* b^* U^{12}]$

	U^{11}	U^{22}	U^{33}	U^{23}	U^{13}	U^{12}
O(1)	11(1)	14(1)	24(1)	3(1)	0(1)	1(1)
O(2)	12(1)	26(1)	27(1)	8(1)	-1(1)	4(1)
O(3)	14(1)	19(1)	14(1)	-3(1)	2(1)	-2(1)
O(4)	11(1)	14(1)	20(1)	-1(1)	1(1)	-1(1)
N(1)	12(1)	14(1)	15(1)	-2(1)	1(1)	-2(1)
C(1)	19(1)	15(1)	15(1)	-3(1)	1(1)	-1(1)
C(2)	19(1)	15(1)	22(1)	-2(1)	7(1)	1(1)
C(3)	9(1)	14(1)	19(1)	1(1)	3(1)	0(1)
C(4)	11(1)	14(1)	20(1)	-1(1)	0(1)	0(1)
C(5)	16(1)	17(1)	22(1)	-2(1)	2(1)	-1(1)
C(6)	12(1)	13(1)	18(1)	-3(1)	0(1)	-2(1)
C(7)	14(1)	14(1)	19(1)	-2(1)	-1(1)	-1(1)
C(8)	12(1)	18(1)	25(1)	-4(1)	0(1)	1(1)
C(9)	15(1)	21(1)	23(1)	-6(1)	7(1)	-4(1)
C(10)	20(1)	20(1)	19(1)	-1(1)	4(1)	-4(1)
C(11)	12(1)	16(1)	21(1)	-1(1)	0(1)	0(1)
C(12)	24(1)	36(1)	30(1)	11(1)	6(1)	-2(1)
C(13)	10(1)	10(1)	17(1)	1(1)	0(1)	2(1)
C(14)	21(1)	18(1)	14(1)	-2(1)	4(1)	2(1)
C(15)	36(1)	22(1)	22(1)	3(1)	7(1)	-3(1)
C(16)	27(1)	22(1)	21(1)	-5(1)	0(1)	6(1)
C(17)	26(1)	24(1)	19(1)	-5(1)	-1(1)	0(1)

Table 5. Hydrogen coordinates (x 10^4) and isotropic displacement parameters ($Å^2$ x 10^3) for vmd45.

	x	y	z	U(eq)
H(1)	8450(30)	3690(30)	6080(30)	32(8)
H(2)	3000(40)	6160(30)	4020(30)	43(8)
H(1A)	9381	8110	5610	20
H(1B)	9980	6934	6591	20
H(2A)	6708	7708	6053	22
H(2B)	7313	6560	7082	22
H(3A)	6454	6456	3991	17
H(5A)	6696	3168	3989	28
H(5B)	7801	4105	3198	28
H(5C)	5896	4291	3092	28
H(8A)	1629	5178	5821	22
H(9A)	1805	3895	7842	23
H(11A)	6563	3538	7534	20
H(12A)	3297	2575	9531	45
H(12B)	5019	3146	10026	45
H(12C)	4883	1997	8956	45
H(15A)	11283	7128	797	40
H(15B)	9552	7270	-80	40
H(15C)	10913	6483	-762	40
H(16A)	12073	5180	2002	35
H(16B)	11724	4434	509	35
H(16C)	10841	4068	1930	35
H(17A)	8217	4245	443	34
H(17B)	9008	4715	-984	34
H(17C)	7672	5514	-283	34

Table 6. Torsion angles [°] for vmd45.

C(13)-N(1)-C(1)-C(2)	158.81(18)
C(3)-N(1)-C(1)-C(2)	-1.99(14)
N(1)-C(1)-C(2)-C(3)	1.90(14)
C(13)-N(1)-C(3)-C(4)	87.2(3)
C(1)-N(1)-C(3)-C(4)	-114.44(16)
C(13)-N(1)-C(3)-C(2)	-156.4(2)
C(1)-N(1)-C(3)-C(2)	1.98(14)
C(1)-C(2)-C(3)-N(1)	-1.87(13)
C(1)-C(2)-C(3)-C(4)	114.23(16)
N(1)-C(3)-C(4)-O(1)	38.3(2)
C(2)-C(3)-C(4)-O(1)	-61.18(18)
N(1)-C(3)-C(4)-C(5)	-81.3(2)
C(2)-C(3)-C(4)-C(5)	179.28(14)
N(1)-C(3)-C(4)-C(6)	157.38(15)
C(2)-C(3)-C(4)-C(6)	57.9(2)
O(1)-C(4)-C(6)-C(11)	-18.7(2)
C(5)-C(4)-C(6)-C(11)	102.4(2)
C(3)-C(4)-C(6)-C(11)	-134.24(18)
O(1)-C(4)-C(6)-C(7)	166.31(17)
C(5)-C(4)-C(6)-C(7)	-72.6(2)
C(3)-C(4)-C(6)-C(7)	50.8(2)
C(11)-C(6)-C(7)-O(2)	-179.70(17)
C(4)-C(6)-C(7)-O(2)	-4.6(3)
C(11)-C(6)-C(7)-C(8)	-0.9(3)
C(4)-C(6)-C(7)-C(8)	174.16(18)
O(2)-C(7)-C(8)-C(9)	178.90(17)
C(6)-C(7)-C(8)-C(9)	0.2(3)
C(7)-C(8)-C(9)-C(10)	0.7(3)
C(8)-C(9)-C(10)-C(11)	-0.7(3)
C(8)-C(9)-C(10)-C(12)	-179.9(2)
C(7)-C(6)-C(11)-C(10)	0.9(3)
C(4)-C(6)-C(11)-C(10)	-174.32(17)
C(9)-C(10)-C(11)-C(6)	-0.1(3)
C(12)-C(10)-C(11)-C(6)	179.2(2)

C(1)-N(1)-C(13)-O(4)	17.1(3)
C(3)-N(1)-C(13)-O(4)	169.70(18)
C(1)-N(1)-C(13)-O(3)	-162.82(16)
C(3)-N(1)-C(13)-O(3)	-10.2(3)
C(14)-O(3)-C(13)-O(4)	14.1(3)
C(14)-O(3)-C(13)-N(1)	-166.02(15)
C(13)-O(3)-C(14)-C(15)	-64.7(2)
C(13)-O(3)-C(14)-C(16)	59.5(2)
C(13)-O(3)-C(14)-C(17)	177.50(16)

Table 7. Hydrogen bonds for vmd45 [Å and °].

D-H...A	d(D-H)	d(H...A)	d(D...A)	<(DHA)
O(1)-H(1)...O(4)#1	0.84(4)	1.99(4)	2.813(2)	167(3)
O(2)-H(2)...O(4)#2	0.85(3)	1.86(4)	2.7078(18)	173(3)

Symmetry transformations used to generate equivalent atoms:

#1 -x+2,y-1/2,-z+1 #2 x-1,y,z